INFORMATION TO USERS

This material was produced from a microfilm copy of the original document. While the most advanced technological means to photograph and reproduce this document have been used, the quality is heavily dependent upon the quality of the original submitted.

The following explanation of techniques is provided to help you understand markings or patterns which may appear on this reproduction.

1. The sign or "target" for pages apparently lacking from the document photographed is "Missing Page(s)". If it was possible to obtain the missing page(s) or section, they are spliced into the film along with adjacent pages. This may have necessitated cutting thru an image and duplicating adjacent pages to insure you complete continuity.

2. When an image on the film is obliterated with a large round black mark, it is an indication that the photographer suspected that the copy may have moved during exposure and thus cause a blurred image. You will find a good image of the page in the adjacent frame.

3. When a map, drawing or chart, etc., was part of the material being photographed the photographer followed a definite method in "sectioning" the material. It is customary to begin photoing at the upper left hand corner of a large sheet and to continue photoing from left to right in equal sections with a small overlap. If necessary, sectioning is continued again — beginning below the first row and continuing on until complete.

4. The majority of users indicate that the textual content is of greatest value, however, a somewhat higher quality reproduction could be made from "photographs" if essential to the understanding of the dissertation. Silver prints of "photographs" may be ordered at additional charge by writing the Order Department, giving the catalog number, title, author and specific pages you wish reproduced.

5. PLEASE NOTE: Some pages may have indistinct print. Filmed as received.

Xerox University Microfilms
300 North Zeeb Road
Ann Arbor, Michigan 48106

Downloaded from SHAREOK. Persistent Handle URL: https://hdl.handle.net/11244/3606

74-3997

BLOMQUIST, Carl Alfred, 1935-
HEAT TRANSFER FROM NATURAL FLAMES FOR LIQUID FUELS IN CIRCULAR PANS.

The University of Oklahoma, Ph.D., 1973
Engineering, chemical

University Microfilms, A XEROX Company, Ann Arbor, Michigan

THIS DISSERTATION HAS BEEN MICROFILMED EXACTLY AS RECEIVED.

THE UNIVERSITY OF OKLAHOMA

GRADUATE COLLEGE

HEAT TRANSFER FROM NATURAL FLAMES FOR LIQUID FUELS IN CIRCULAR PANS

A DISSERTATION

SUBMITTED TO THE GRADUATE FACULTY

in partial fulfillment of the requirements for the

degree of

DOCTOR OF PHILOSOPHY

BY

CARL ALFRED BLOMQUIST

Norman, Oklahoma

1973

HEAT TRANSFER FROM NATURAL FLAMES FOR

LIQUID FUELS IN CIRCULAR PANS

APPROVED BY

DISSERTATION COMMITTEE

ABSTRACT

In this study free-burning, buoyant, diffusion flames from fires of liquid fuels in cylindrical pans were studied. The fuels were acetone, benzene, cyclohexane, n-hexane, Jet-A, JP-4, and methanol. The burner diameters were 24, 18, and 12 inches. An insulated water-cooled probe was used to obtain total heat transfer data and a narrow-angle and wide-angle radiometer were used to measure external radiative fluxes.

These natural flames consist of a series of necks and bulges that constantly changes size and shape. Time averaged photographs revealed shapes varying from conical to cylindrical. For single component fuels the flame height (maximum fixible height on the time-averaged photographs) was found to be a function of the 0.6 power of the Froude number, based on the equivalent diameter of the burner and the fuel vapor density. A simple multiplying factor that accounts for the volumetric combustion air allows the flame height data to be correlated with a single equation.

Radiative fluxes calculated with emission and extinction coefficients obtained from narrow-angle radiometer data were excessive. The use of existing emission and extinction coefficients obtained from small laminar flames resulted in optically thick flames. Based on a cylindrical flame shape mean

beam lengths were computed and found to be in good agreement with existing prediction methods. These lengths were used with the wide angle radiometer data to obtain emission and extinction coefficients. These calculations revealed that the coefficients need to be treated as sets instead of unique values and that two or three sets of values can be obtained for flames from the same fuel. Convective heat fluxes were found to be in reasonable agreement with existing data. Convective heat transfer coefficients calculated from these fluxes showed considerable scatter. This can be attributed to the temperature variations inside the flame that cannot be determined from the external optical temperature measurements. These coefficients are several orders at magnitude higher than values predicted from existing correlations for gases. The heat transfer to small targets inside large flames was found to be somewhat insensitive to the flame shape, but targets external to the flame are more dependent on the size and shape of the flame.

ACKNOWLEDGMENTS

It is difficult to remember everyone who contributed to my graduate program but the following deserve special recognition and thanks: To my committee chairman, Dr. C. M. Sliepcevich, for his guidance, encouragement and financial support, without which I would not have been able to attend graduate school. To Dr. J. Reed Welker for the many hours spent listening to my problems, for the advice and encouragement he rendered, and for handling the number of details associated with this dissertation during my absence. To Dr. C. P. Colver for serving on my committee and for providing the opportunity for me to attend The University of Oklahoma. To Dr. T. J. Love and Dr. F. M. Townsend for serving as members of my committee. To Ms. Bobbie Everidge, Mrs. Carlotta Wood, Miss Ann Haynes, Miss Suzy Wallace, and Mrs. Ruth Kempton for typing the dissertation. To Mr. Steve Presson for preparing the figures. To Argonne National Laboratory for the use of their computing facilities. To my fellow graduate students, especially to Mr. Dan Neskora, for their support and assistance.

Words cannot convey my feelings of gratitude to my wife, Cecelia, for her encouragement and for the difficult

job of transforming the hand-written material of my special problem and dissertation into a typed copy. I also want to thank my daughters, Annette, Rita and Cheryl for their acceptance of my inaccessibility and lack of attention that occasionally occurred during my studies.

Carl A. Blomquist

TABLE OF CONTENTS

		Page
LIST OF TABLES		x
LIST OF ILLUSTRATIONS		xvii
Chapter I		
I.	INTRODUCTION	1
II.	FLAME CHARACTERISTICS	5
	Flame Shape and Size	5
	Prediction of Flame Height and Fuel Burning Rate	10
	Flame Temperature	52
	Summary of Flame Temperature	62
	Soot Formation	64
III.	FLAME HEAT TRANSFER	74
	Energy Transfer Mechanism in a Flame	74
	Method for Obtaining Heat Flux from Flames	75
	Review of Flame Total Heat Flux Data	78
	Remarks on Flame Heat Transfer	138
IV.	FACILITIES AND EQUIPMENT	139
	Building	139
	Probe	143
	Burners and Fuel Supply System	155
	Burn Table	155
	Camera and Film	158
	Radiometers and Flame Temperature Sensors	167
	Instrumentation	170
V.	EXPERIMENTAL PROCEDURE	176
VI.	RESULTS FOR FLAME SHAPE, SIZE, SOOT ACCUMULATION, TEMPERATURE AND FUEL BURNING RATE	181

Chapter Page

Flame Shape and Size 181
Soot Accumulation 219
Flame Temperature 219
Fuel Burning Rate 220
Flame Height Correlation 221
Burning Rate Correlation 241

VII. GEOMETRY OF RADIATIVE TRANSFER BETWEEN FLAME AND OBJECT 252

Target Surrounded by a Flame 252
Target External to a Flame 261

VIII. HEAT TRANSFER RESULTS 271

Determination of Flame Emission and Extinction Coefficients from Narrow Angle Radiometer Data 271
Radiant Flux Calculations Using Radiometer 72804 Data 278
Heat Transfer Results Using Data from Radiometer 72804 287
Radiant Heat Flux for Cylindrical Shaped Flames Using the Data of Neill, Pfenning and Tsai 296
Application of Configuration Factor and Mean Path Length to Obtain Emission and Extinction Coefficients from Radiometer 81510 Data 304
Heat Transfer Results Using Temperature Data from Small Cylinder 328

IX. CONCLUSIONS AND RECOMMENDATIONS 338

Conclusions 338
Recommendations 342

NOMENCLATURE 344

BIBLIOGRAPHY 356

APPENDICES 364

A: DEVELOPMENT OF EQUATION OF TRANSFER 365

B: FUEL PROPERTIES 372

APPENDICES

		Page
C:	TABULAR SUMMARY OF DATA	376
D:	CHARACTERISTICS OF FUEL SYSTEM	449
	General	449
	Dimensional Information	450
	Fuel Pan Equilibrium Time	456
	Equivalent Length of Fuel and Dynamic Fuel Pan Level	461
E:	COMPUTER PROGRAMS	466

LIST OF TABLES

Table		Page
II-1.	Typical Values of Spalding's Transfer Number	14
II-2.	Values of v_∞ from Burgess, Strasser and Grumer (15)	27
II-3.	Comparison of Flame Temperature Calculated by Shimy's (61) Equation with Theoretical Flame Temperature	55
II-4.	Flame Temperatures from Rasbash, Rogowski and Stark (57)	56
II-5.	JP-4 Fuel Flame Temperatures from Gordon and McMillan (31)	61
II-6.	Optical Flame Temperature from Welker (80)	61
II-7.	Optical Flame Temperatures from Neill (50)	62
II-8.	Flame Temperatures from Deshpande (24)	63
III-1.	Bader's Heat Flux Meter Data	80
III-2.	Neill's Initial Total Heat Transfer Rates (Btu/hr-ft^2)	82
III-3.	Deshpande's Total Heat Transfer Rates (Btu/hr-ft^2)	83
III-4.	Absorption Coefficient and Emittance of Flames from Rasbash, et al. (57)	106
III-5.	Absorption Coefficients and Maximum Linear Burning Rates of Liquid Fuels from Burgess, et al. (15)	107
III-6.	Neill's Data for the Extinction Coefficients and Maximum Heat Flux for Flames from a 2" Wide Channel Burner	108

Table		Page
III-7.	Mean Values of "a" for Several Soots as Given by Siddall and McGrath (62) . . .	114
III-8.	Comparison of Experimental and Theoretical Values of $k_2\lambda^{-a}$	117
III-9.	Neill's Radiant Flux Data for Methanol Flames	126
III-10.	Neill's Calculated Radiant Flux for Laminous Flames	126
III-11.	Deshpande's Calculated Radiative Heat Flux Values for Flames	127
III-12.	Comparison of Convection Correlations . .	134
III-13.	Convective Heat Flux for Methanol Flames from Neill's Data	136
III-14.	Neill's Convective Heat Flux for Luminous Flames	136
III-15.	Convective Flux for Flames from Deshpande	137
IV-1.	Additional Instrumentation	174
VI-1.	Flame Size and Projected Area for Acetone	204
VI-2.	Flame Size and Projected Area for Benzene	206
VI-3.	Flame Size and Projected Area for Cyclo-hexane	208
VI-4.	Flame Size and Projected Area for n-Hexane	210
VI-5.	Flame Size and Projected Area for Jet A .	212
VI-6.	Flame Size and Projected Area for JP-4 . .	215
VI-7.	Flame Size and Projected Area for Methanol	217
VI-8.	Mean Thickness of Soot Accumulation on Probe	220
VI-9.	Acetone Burning Rate, H/D_e, and Froude Number	234

Table		Page
VI-10.	Benzene Burning Rate, H/D_e, and Froude Number	235
VI-11.	Cyclohexane Burning Rate, H/D_e, and Froude Number	236
VI-12.	n-Hexane Burning Rate, H/D_e, and Froude Number	237
VI-13.	Jet A Burning Rate, H/D_e, and Froude Number	238
VI-14.	JP-4 Burning Rate, H/D_e, and Froude Number	239
VI-15.	Methanol Burning Rate, H/D_e, and Froude Number	240
VI-16.	Heat Transfer Rates from Fuel Pan Bottom and Side	248
VI-17.	Heat Transfer Rates from Radiation and by Fuel	249
VIII-1.	Emission and Extinction Coefficients Obtained from Radiometer 72804 Data	278
VIII-2.	Radiant Heat Fluxes for Acetone Calculated with Radiometer 72804 Emission and Extinction Coefficients	280
VIII-3.	Radiant Heat Fluxes for Benzene Calculated with Radiometer 72804 Emission and Extinction Coefficients	281
VIII-4.	Radiant Heat Fluxes for Cyclohexane Calculated with Radiometer 72804 Emission and Extinction Coefficients	282
VIII-5.	Radiant Heat Fluxes for n-Hexane Calculated with Radiometer 72804 Emission and Extinction Coefficients	283
VIII-6.	Radiant Heat Fluxes for Jet A Calculated with Radiometer 72804 Emission and Extinction Coefficients	284
VIII-7.	Radient Heat Fluxes for JP-4 Calculated with Radiometer 72804 Emission and Extinction Coefficients	285

Table		Page
VIII-8.	Radiant Heat Fluxes for Methanol Calculated with Emission and Extinction Coefficients from Neill (50)	286
VIII-9.	Heat Transfer Results for Acetone Using Flame Radiant Flux Calculated with Radiometer 72804 Data	289
VIII-10.	Heat Transfer Results for Benzene Using Flame Radiant Flux Calculated with Radiometer 72804 Data	290
VIII-11.	Heat Transfer Results for Cyclohexane Using Flame Radiant Flux Calculated with Radiometer 72804 Data	291
VIII-12.	Heat Transfer Results for n-Hexane Using Flame Radiant Flux Calculated with Radiometer 72804 Data	292
VIII-13.	Heat Transfer Results for Jet A Using Flame Radiant Flux Calculated with Radiometer 72804 Data	293
VIII-14.	Heat Transfer Results for JP-4 Using Flame Radiant Flux Calculated with Radiometer 72804 Data	294
VIII-15.	Heat Transfer Results for Methanol Using Flame Radiant Flux Calculated with Data from Neill (50)	295
VIII-16.	Radiant Heat Flux for a Cylindrical-Shaped Acetone Flame Using Extinction and Emission Coefficients from Tsai (79), Pfenning (54), and Neill (50)	297
VIII-17.	Radiant Heat Flux for a Cylindrical-Shaped Benzene Flame Using Extinction and Emission Coefficients from Tsai (79) and Neill (50)	298
VIII-18.	Radiant Heat Flux for a Cylindrical-Shaped Cyclohexane Flame Using Extinction and Emission Coefficients from Tsai (79) and and Neill (50)	299
VIII-19.	Radiant Heat Flux for a Cylindrical-Shaped n-Hexane Flame Using Extinction and Emission Coefficients from Tsai (79) and Neill (50)	300

Table		Page
VIII-20.	Radiant Heat Flux for a Cylindrical-Shaped JP-4 Flame Using Extinction and Emission Coefficients from Neill (50) .	301
VIII-21.	Radiant Heat Flux for a Cylindrical-Shaped Methanol Flame Using Extinction and Emission Coefficients from Tsai (79) . .	302
VIII-22.	Configuration Factor and Mean Path Length Data for a Cylindrical-Shaped Acetone Flame	306
VIII-23.	Configuration Factor and Mean Path Length Data for a Cylindrical-Shaped Benzene Flame	307
VIII-24.	Configuration Factor and Mean Path Length Data for a Cylindrical-Shaped Cyclohexane Flame	308
VIII-25.	Configuration Factor and Mean Path Length Data for a Cylindrical-Shaped n-Hexane Flame	309
VIII-26.	Configuration Factor and Mean Path Length Data for a Cylindrical-Shaped Jet A Flame	310
VIII-27.	Configuration Factor and Mean Path Length Data for a Cylindrical-Shaped JP-4 Flame	311
VIII-28.	Configuration Factor and Mean Path Length Data for a Cylindrical-Shaped Methanol Flame	312
VIII-29.	Emission and Extinction Coefficients Obtained from Radiometer 81510 Data . .	317
VIII-30.	Heat Transfer Results for Acetone Using Flame Radiant Flux Calculated with Radiometer 81510 Data	318
VIII-31.	Heat Transfer Results for Benzene Using Flame Radiant Flux Calculated with Radiometer 81510 Data	319
VIII-32.	Heat Transfer Results for Cyclohexane Using Flame Radiant Flux Calculated with Radiometer 81510 Data	320

Table		Page
VIII-33.	Heat Transfer Results for n-Hexane Using Flame Radiant Flux Calculated with Radiometer 81510 Data	321
VIII-34.	Heat Transfer Results for Jet A Using Flame Radiant Flux Calculated with Radiometer 81510 Data	322
VIII-35.	Heat Transfer Results for JP-4 Using Flame Radiant Flux Calculated with Radiometer 81510 Data	323
VIII-36.	Heat Transfer Results for Methanol Using Flame Radiant Flux Calculated with Radiometer 81510 Data	324
VIII-37.	Coefficients for Free Convection Correlation for Flames	328
VIII-38.	Heat Transfer Results for Acetone Using Temperature Data from Small Cylinder . .	330
VIII-39.	Heat Transfer Results for Benzene Using Temperature Data from Small Cylinder . .	331
VIII-40.	Heat Transfer Results for Cyclohexane Using Temperature Data from Small Cylinder . .	332
VIII-41.	Heat Transfer Results for n-Hexane Using Temperature Data from Small Cylinder . .	333
VIII-42.	Heat Transfer Results for Jet A Using Temperature Data from Small Cylinder . .	334
VIII-43.	Heat Transfer Results for JP-4 Using Temperature Data from Small Cylinder . .	335
VIII-44.	Heat Transfer Results for Methanol Using Temperature Data from Small Cylinder . .	336
B-1.	Physical Constants of Fuels	373
B-2.	Transport Properties of Fuels	374
B-3.	Physical Properties of Air	375
C-1.	Experimental Data for Acetone Flames . . .	377
C-2.	Experimental Data for Benzene Flames . . .	386

Table		Page
C-3.	Experimental Data for Cyclohexane Flames .	395
C-4.	Experimental Data for n-Hexane Flames . . .	404
C-5.	Experimental Data for Jet A Flames	413
C-6.	Experimental Data for JP-4 Flames	427
C-7.	Experimental Data for Methanol Flames . . .	439
D-1.	Fuel Line Components	450
D-2.	Measured Dimensions and Volume for the 24 Inch Diameter Fuel Pan	453
D-3.	Measured Dimensions and Volume for the 18 Inch Diameter Fuel Pan	454
D-4.	Measured Dimensions and Volume for the 12 Inch Diameter Fuel Pan	455
D-5.	Comparison of Predicted and Measured Fuel Depth for 24 Inch Diameter Fuel Pan . . .	457
D-6.	Coefficients for Equation D-6	461
D-7.	Comparison of Measured and Calculated Change in Fuel Pan Level	465

LIST OF ILLUSTRATIONS

Figure		Page
II-1.	Shape of Flames Immediately Above the Liquid Surface from Rasbash, et al. (57)	6
II-2.	Cinerecord of Flames of a Petrol Fire, Showing Upward Movement of Flame (Time After Ignition 8 min, 40 sec, Film Speed 28.9 Frames per Second) from Rasbash, et al. (57)	9
II-3.	Flame Profiles (Thick Lines--Flame Continuous for More than 90 Percent of Time; Thin Lines--Flame Continuous for Less than 90 Percent of Time), From Rasbash, et al. (57)	9
II-4.	Series of One Thousandth Second Exposure Time Photographs of an Acetone Pool Flame from Pfenning (54)	11
II-5.	Bader's Data for the Temperature Distribution in JP-4 Fuel Fires 5 Minutes after Ignition	59
II-6.	Thermocouple Spacing Using by Gordon and McMillan (31)	60
III-1.	Probe Heat Fluxes	76
III-2.	Geometry for Intensity Variation Through a Flame	100
IV-1.	Low Velocity Wind Tunnel	140
IV-2.	Burn Table and Associated Equipment Located in Static Test Room	141
IV-3.	Instruments and Equipment Located in Observation Room	142
IV-4.	Probe Assembly	144

Figure		Page
IV-5.	Probe Outer Shell	145
IV-6.	a. Top Insulating Spacer b. Bottom Insulating Spacer	146
IV-7.	a. Top Cap. b. Spacer Rod	147
IV-8.	a. Outer Pipe of Bayonet Exchanger b. Inner Pipe of Bayonet Exchanger . . .	148
IV-9.	Lower Insulating Spacer Retainer	149
IV-10.	Bayonet Exchanger Support Bar	150
IV-11.	Probe Support Plate	151
IV-12.	a. Lower Support Leg b. Upper Support Leg	152
IV-13.	Photograph of Probe Assembly and Radiometer Supports	153
IV-14.	Burner	156
IV-15.	Schematic Diagram of Fuel Level Control System	157
IV-16.	Plan View of Burn Table	159
IV-17.	Elevation View of Burn Table	160
IV-18.	Assembly of Pinhole Camera	161
IV-19.	Body of Pinhole Camera	162
IV-20.	Foil Holder for Pinhole Camera	163
IV-21.	Back for Pinhole Camera.	164
IV-22.	a. Shutter Connecting Bar for Pinhole Camera b. Shutter for Pinhole Camera	165
IV-23.	Photograph of Pinhole Camera and Polaroid Film Holder	166
IV-24.	Calibration Curve for Radiometer 81510 . .	168
IV-25.	Calibration Curve for Radiometer 72804 With a 7° View Restrictor	169

Figure		Page
IV-26.	Radiometer Mounting Bracket	171
IV-27.	Radiometer and Thermocouple Locations . .	172
IV-28.	Temperature Sensing Cylinder	173
VI-1.	24 Inch Diameter Acetone Flame	182
VI-2.	18 Inch Diameter Acetone Flame	183
VI-3.	12 Inch Diameter Acetone Flame	184
VI-4.	24 Inch Diameter Benzene Flame	185
VI-5.	18 Inch Diameter Benzene Flame	186
VI-6.	12 Inch Diameter Benzene Flame	187
VI-7.	24 Inch Diameter Cyclohexane Flame	188
VI-8.	18 Inch Diameter Cyclohexane Flame	189
VI-9.	12 Inch Diameter Cyclohexane Flame	190
VI-10.	24 Inch Diameter n-Hexane Flame	191
VI-11.	18 Inch Diameter n-Hexane Flame	192
VI-12.	12 Inch Diameter n-Hexane Flame	193
VI-13.	24 Inch Diameter Jet-A Flame	194
VI-14.	18 Inch Diameter Jet-A Flame	195
VI-15.	12 Inch Diameter Jet-A Flame	196
VI-16.	24 Inch Diameter JP-4 Flame	197
VI-17.	18 Inch Diameter JP-4 Flame	198
VI-18.	12 Inch Diameter JP-4 Flame	199
VI-19.	24 Inch Diameter Methanol Flame	200
VI-20.	18 Inch Diameter Methanol Flame	201
VI-21.	12 Inch Diameter Methanol Flame	202
VI-22.	Tank Gauge Level as a Function of Time for Acetone	227

Figure		Page
VI-23.	Tank Gauge Level as a Function of Time for Benzene	228
VI-24.	Tank Gauge Level as a Function of Time for Cyclohexane	229
VI-25.	Tank Gauge Level as a Function of Time for n-Hexane	230
VI-26.	Tank Gauge Level as a Function of Time for Jet A	231
VI-27.	Tank Gauge Level as a Function of Time for JP-4	232
VI-28.	Tank Gauge Level as a Function of Time for Methanol	233
VI-29.	H/D_e as a Function of Froude Number	242
VI-30.	Modified Dimensionless Flame Height as a Function of Froude Number	243
VI-31.	Burner and Fuel Heat Rates	244
VII-1.	System Geometry for Cylindrical Target Surrounded by a Flame of Circular Cross-Section	254
VII-2.	System Geometry Between an External Target and a Flame of Circular Cross-Section	262
VIII-1.	Radiometer 72804 Heat Flux versus Flame Path Length for Acetone	272
VIII-2.	Radiometer 72804 Heat Flux versus Flame Path Length for Benzene	273
VIII-3.	Radiometer 72804 Heat Flux versus Flame Path Length for Cyclohexane	274
VIII-4.	Radiometer 72804 Heat Flux versus Flame Path Length for n-Hexane	275
VIII-5.	Radiometer 72804 Heat Flux versus Flame Path Length for Jet A	276
VIII-6.	Radiometer 72804 Heat Flux versus Flame Path Length for JP-4	277

Figure		Page
VIII-7.	Heat Flux versus Mean Path Length for Acetone and JP-4	314
VIII-8.	Heat Flux versus Mean Path Length for Benzene, n-Hexane and Methanol	315
VIII-9.	Heat Flux versus Mean Path Length for Cyclohexane and Jet A	316
VIII-10.	Local Nusselt Number for Probe as a Function of Rayleigh Number	327
VIII-11.	Nusselt Number for Small Cylinder as a Function of Rayleigh Number	337
A-1.	Elemental Volume for Derivation of Transport Equation	365
D-1.	Pertinent Dimensions of Fuel System . . .	450
D-2.	Fuel Tank Level Difference as a Function of Time with H_R as a Parameter for the 24 Inch Diameter Burner	453
D-3.	Line Resistance as a Function of Breather Rod Height Above Bottom of Fuel Pan . .	454
D-4.	Fuel Tank Level as a Function of Time . .	455

CHAPTER I

INTRODUCTION

Ever since man discovered fire, he has been interested in its use. At first he used fires for warmth but eventually discovered that food tasted better when cooked. Early man also looked upon fire as sort of a religion and the Greek philosophers even placed fire among the four elements. Man's ability to make and use fires was an essential factor in his evolution and the development of civilizations. Still, appreciation of the benefits of fire has seldom been unmixed with fear of its destructive effects. Fires are well represented among the great disasters that have befallen man. Each disaster provided a stimulus for research into the nature, control, prevention, and extinguishment of fires. Due to the complexity of fire, this research is still continuing and will continue for many additional years.

Everyone has a concept of a fire or a flame, but how do you define them? Fire is a general term for combustion of a fuel and can be defined as a chemical reaction in which rapid oxidation takes place and heat and light are produced. A flame is the phenomenon exhibited when a gas or vapor is

actively undergoing combustion. A flame can also be considered as a thermal wave which travels at sub-sonic velocities, accompanied by exothermic chemical reactions.

Flames can be classified in a number of ways. A "premixed" flame is one where the fuel and oxidizer are mixed together before combustion. In a "diffusion" flame the fuel and oxygen are combined by molecular and eddy diffusion in the combustion zone. A flame is described as "buoyant" when the forces causing it to rise from its source are largely due to the buoyancy of the hot gases. "Jet" flames result when the fuel flow rate is such that its initial momentum is large compared to the buoyancy forces of the hot gases. A "luminous" flame has a yellow-orange color caused by glowing soot particles that are formed because of incomplete combustion of hydrocarbon fuels. A "non-luminous" flame burns with an almost transparent blue flame. A "controlled" fire results when the flow rate of the fuel is regulated. A "natural," "free-burning," or "uncontrolled" fire is one where the fuel burning rate depends only on the fuel and environmental conditions. Gas fires are "controlled" and fires from liquid and solid fuels are usually "uncontrolled." A "laminar" flame is one that burns without spatial movement of the flame boundaries, and a "turbulent" flame flickers or moves with respect to time and position. In this study free-burning, buoyant, diffusion flames from fires of liquid fuels in cylindrical pans were studied.

Over the years an extensive amount of fire research has been conducted and hundreds of papers published. The bulk of this work has been on small premixed or jet diffusion flames and on solid-fuel fires. The incentive for solid-fuel fire studies has been the large losses from forest fires and burning buildings. Most of the studies with small flames used gaseous fuels. These studies were concerned with reaction kinetics, burning velocities, flame stability, spectroscopic analyses and measurement of temperature profiles. Additional details on this work can be found in Gaydon (30), Lewis and Von Elbe (41), and the combustion literature. Studies on natural fires of liquid fuels are fewer in number than the other types of fires. The University of Oklahoma Research Institute has conducted a number of such studies, some of which are Welker (80), Shahrokhi (60), Hood (33), Huffman (38), Tsai (79), Neill (50), Deshpande (24), and Pfenning (54).

Given a specific fuel, burner size and shape, one would like to know the following:

1. Reaction kinetics
2. Flame shape
3. Flame size
4. Fuel burning rate
5. Air flow rate
6. Flame temperature
7. Soot formation
8. Flame emission coefficient

9. Flame extinction coefficient
10. Flame radiant heat transfer
11. Flame convective heat transfer
12. Flame emittance

This study is concerned primarily with Items 2, 3, 10, and 11, with emphasis placed on obtaining prediction methods that will be easy to use without sacrificing accuracy. Items 4, 6, 7, 8, 9, and 12 will also be briefly discussed.

The liquid fuels used were acetone, benzene, cyclohexane, n-hexane, Jet-A, JP-4, and methanol. Acetone, benzene, and methanol were obtained from McKesson and Robbins Chemical Company. Cyclohexane and n-hexane were obtained from Phillips Petroleum Co. Jet-A was obtained from the local airport which was supplied by Continental Oil Company. The JP-4 was furnished by Tinker Air Force Base. These fuels were selected for contractual purposes, availability, cost and physical properties. Pan sizes of 12, 18, and 24 inch inside diameter were used with each fuel.

CHAPTER II

FLAME CHARACTERISTICS

Flame Shape and Size

What is the shape of a free-burning flame and what height does it attain? These are questions that require answers in order to calculate the radiant heat-transfer from a flame. Rasbash, Rogowski and Stark (57) aptly described the flame shape for alcohol and hydrocarbon liquid flames. They state that the main part of the flames had the shape of a cylindrical column, whose diameter was usually less than that of the vessel; this column of flame rose from a region of thin flame moving inwards from the vessel edge. A number of characteristic shapes were discernible for this region of thin flames and are shown in Figure II-1. All the fuels produced the flame shape shown in Figure II-1A as a thin zone of flame sloped downwards from the edge towards the center of the vessel and from this zone several flame surfaces and ridges branched off, either upwards directly into the flame column or downwards to touch the liquid surface over an appreciable area before passing upwards into the main flame column. This shape remained characteristic of the alcohol fire for the entire

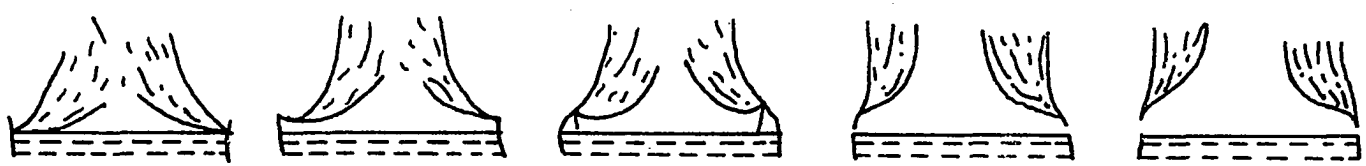


Figure II-1. Shape of Flames Immediately Above the Liquid Surface.

burning time. The flames for benzol and petrol began to lift from the liquid surface about 7 to 10 sec after ignition, and with the kerosene fire about 15 to 20 sec after ignition. The flames of these hydrocarbon liquids then passed through the shape shown in Figure II-1B in which the flame progressed inwards from the vessel edge parallel to the liquid surface before breaking up into ridges. At this stage none of the downward moving ridges touched the liquid surface. The flames then passed into the shape shown in Figure II-1C in which they were bent over the vessel like an inverted saucer. The petrol and kerosene fires maintained the shape shown in Figure II-1C throughout the tests. The benzol fires, however, passed into the phase shown in Figure II-1D, in which the thin flame zone passed almost straight upwards from the vessel edge. For occasional short periods, the flames bulged outwards as shown in Figure II-1E.

All the flames showed a marked pulsation which was due to two causes. First, the zone of the flame near the edge of the vessel vibrated with a frequency of about two to three per second. Secondly, the columns of flames tended to move upwards as alternating necks and bulges. The bulges usually became more pronounced as they proceeded up the flame; after traveling a certain distance they would break up.

When the hydrocarbon flames reached the stage shown in Figure II-1B, a rippling began to appear on the surface, usually accompanied by bubbles. With benzol, the bubbling

also became vigorous although not as vigorous as with the benzol. With kerosene, the bubbles were very small (up to about 0.5 mm) except at thermocouples placed near the surface where the bubbling was usually quite vigorous. No bubbling or rippling at the surface was observed during the alcohol fires.

The shape and volume of the flames were determined from a large number of measurements of the flame projected image, obtained from motion pictures taken at about 30 frames per second. No measurements were made on those parts of the flames which according to photographs, had become detached from the rising column of flames. An example of consecutive photographs in part of a film is shown in Figure II-2.

Figure II-3 shows the mean contours of the flames for burning times of 2, 5 and 8 minutes. The parts of the flames represented by thin lines are those where, in more than 10 percent of the readings, there was no flame present and may be taken as representing those parts of the flame where disintegration of the main column of flame occurred. This figure also shows that, in most cases, there was a tendency for a neck to be formed some 10 to 20 cm above the liquid surface.

Neill (50) assumed the flame shape to be circular and obtained the flame dimensions from photographs taken from a fixed camera position. Exposure times of 1/5 or 1/10 second were used to obtain an average size flame column. A negative of a dimensioned grid was placed over the flame photograph and



Figure II-2. Cinerecord of Flames of a Petrol Fire, Showing Upward Movement of Flame (Time After Ignition 8 min 40 sec, Film Speed 28.9 Frames per Second) from Rasbash, et al. (57).

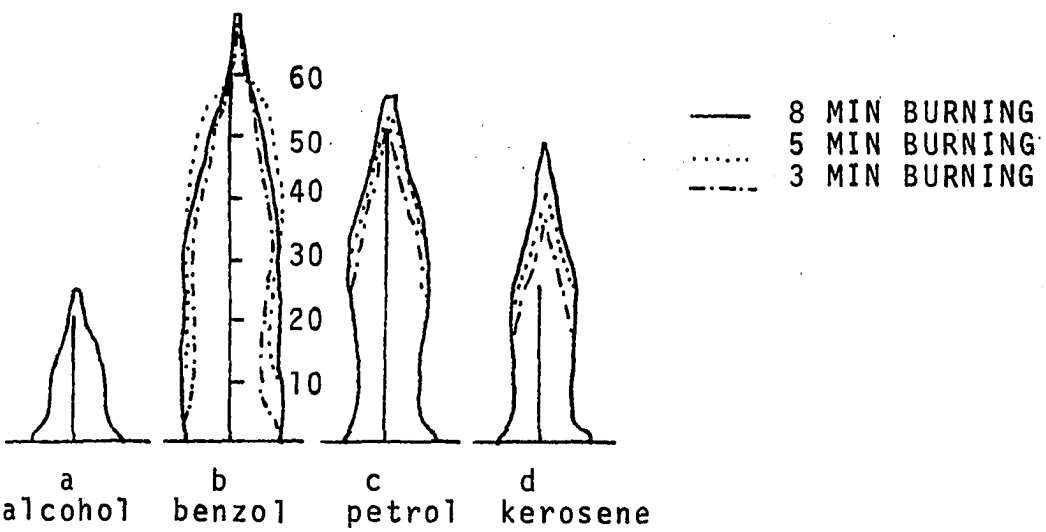


Figure II-3. Flame Profiles (Thick Lines Flame Continuous for More Than 90 Percent of Time; Thin Lines Flame Continuous for Less Than 90 Percent of Time).

the dimensions of the flame were adjusted by eye to encompass a rectangular area equivalent to the area of the flame on the photograph.

Even though the literature contains numerous references to the use of photographs to obtain flame dimensions, there has not been any standard technique developed for determining the shape or size of a flame. Figure II-4, from Pfenning (54) shows the variations in the shape of a turbulent buoyant diffusion flame of acetone burning from a 30 centimeter pool as a series of one millisecond exposure photographs. Pfenning states that due to the turbulent nature of this flame, the time of exposure of the photograph determines the estimated flame size.

Prediction of Flame Height and Fuel Burning Rate

Wohl, Gazley, and Kapp (82) assumed that the fuel stream rises in the form of a cylindrical jet in free space; the fuel and air diffuse laterally against each other; the burning zone is infinitesimally thin and occurs at the places of stoichiometric air-fuel ratio; the maximum flame height is reached when the burning zone closes in on the axis; the diffusion process between the fuel and air occurs at constant molecular diffusivity and constant velocity of flow. The diffusion process is treated as the diffusion of one hypothetical gas through a fictitious medium. The mole fraction of the hypothetical gas is zero at stoichiometric composition,

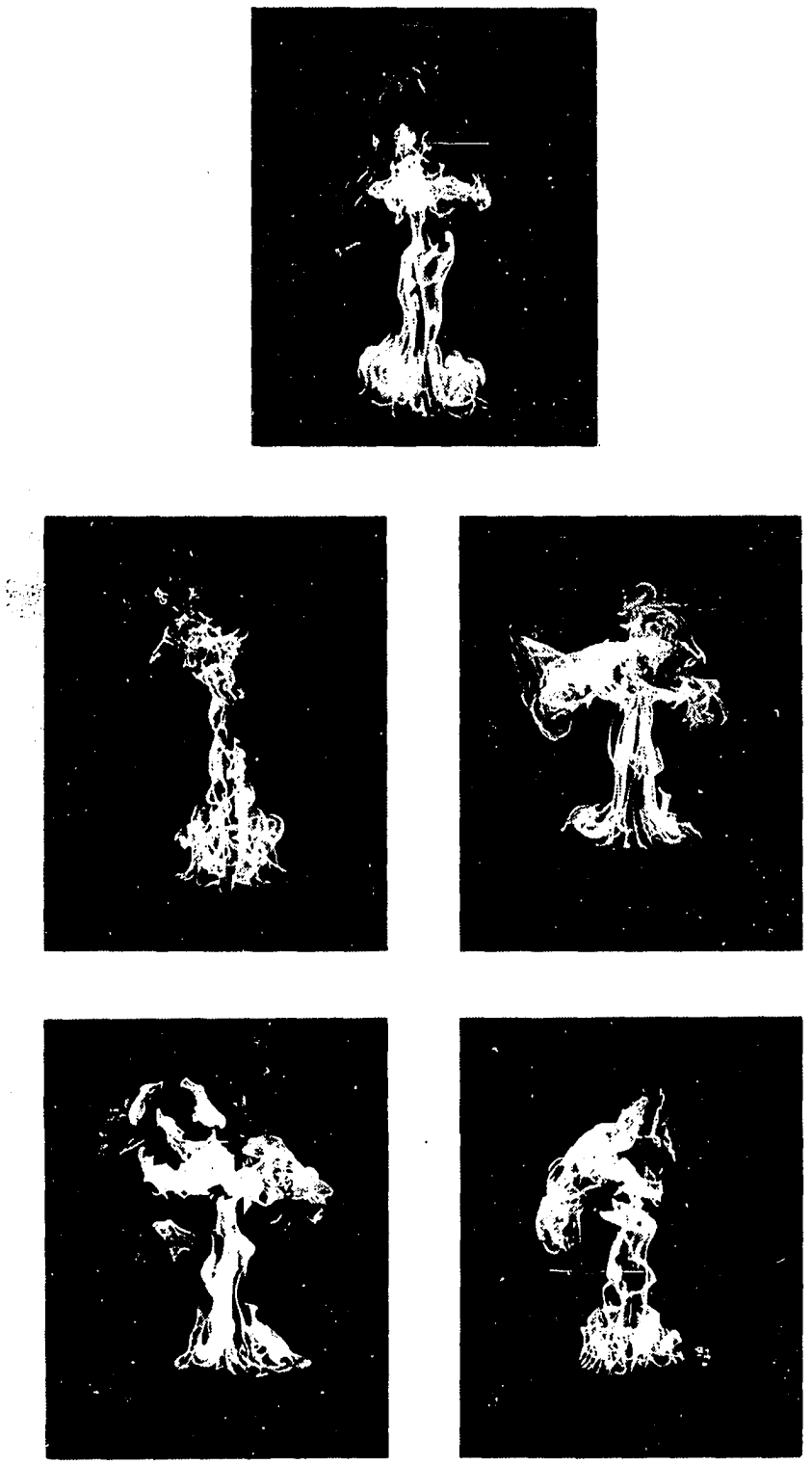


Figure II-4. Series of One Thousandth Second Exposure Time Photogrpahs of an Acetone Pool Flame From Pfenning (54).

i.e., in the burning zone, it is positive where fuel is in excess, i.e., inside the burning zone of the diffusion flame, and negative where air is in excess, i.e., outside the burning zone. With these assumptions, the following approximate equation for the flame height was obtained

$$H = \frac{Q_g \, C_f}{4\pi \, \underline{D} \, C_{fs}} \qquad \text{(II-1)}$$

where C_f = mole fraction of fuel

C_{fs} = stoichiometric mole fraction of fuel

$\underline{D}$ = diffusivity, ft^2/hr

H = flame height, ft

Q_g = volume flow rate of fuel gas, ft^3/hr

Spalding (64) applied mass and heat transfer theory to the combustion of solid and liquid fuels and some of the conclusions reached were:

1. The rate of matter transfer from a fuel or liquid surface of a given shape in a given stream of gas depends only on a dimensionless term called the Transfer Number, B_s.
2. There are many different forms of the Transfer Number since differential equations can be formed from the fundamental balance equations by elimination and substitution. The number of fundamental equations is equal to the number of participating chemical elements, plus one for heat.
3. Since there can only be one value of the normal gas velocity of the surface, each of the many forms of the Transfer Number must have the same numerical value.

4. For liquid fuels, vaporization is an important component process and the Transfer Number, B_s, formed from a heat balance equation is

$$B_s = \frac{H_c \, m_{o_{2a}}}{Q_s \, r} + \frac{C_p(T_a - T_s)}{Q_s} \qquad \text{(II-2)}$$

where C_p = specific heat, Btu/lbm-°F

H_c = net heating value of fuel, Btu/lbm

$m_{o_{2a}}$ = mass concentration of oxygen in air

r = mass of oxygen required for combustion of a unit mass of fuel

Q_s = heat reaching fuel surface from flame per pound of fuel vaporized, Btu/lbm

T_a = temperature of air, °F

T_s = temperature of fuel surface, °F

In this derivation the heats of hydrocarbon decomposition have been ignored, and the existence of reactions involving intermediate reaction products has also been neglected. The value of T_s is not precisely known, but it is always sufficiently accurate to insert the boiling temperature of the fuel. Table II-1 gives typical values for the Transfer Number for the following conditions:

1. Combustion in atmospheric air, $(T_a - T_s) = 0$, Q_s = latent heat of fuel; CO formation neglected.
2. Same as condition 1 except Q_s = latent heat and sensible heat to raise fuel from 15°C to its boiling point.

TABLE II-1

TYPICAL VALUES OF SPALDING'S TRANSFER NUMBER

Fuel	B_s	
	Condition 1	Condition 2
n-Hexane	9.00	6.39
n-Heptane	9.15	5.45
Benzene	7.74	6.09
Cyclohexane	8.25	6.22
Methanol	2.67	2.37

Spalding also concludes that the natural convection combustion rate from a vertical flat plate or sphere, for Transfer Numbers from 0.25 to 3, may be expressed by the empirical equation

$$\frac{M_s C_{pa} X}{K_a} = 0.45(B_s)^{0.75} \left(\frac{gX^3}{\alpha_a^2}\right)^{0.25} \qquad \text{(II-3)}$$

where α_a = air thermal diffusivity, ft^2/hr

K_a = air thermal conductivity, Btu-ft/hr-ft^2-°F

M_s = fuel burning rate per unit surface area, $lbm/ft^2/hr$

X = characteristic dimension, take as plate height or sphere diameter, ft

Spalding assumes the physical properties are those of air at room temperature for Equation II-3.

Rasbash, Rogowski, and Stark (57) used Equation II-3 to predict a burning rate of 62 g/min for their ethanol fire.

This value is in good agreement with the experimental value of 56 g/min. The authors state that Equation II-3 predicts that the rate of burning per unit area will decrease as the linear dimension of the burning surface increases. This is contrary to the behavior generally observed with liquids burning in open vessels, a fact which is no doubt due to the importance of radiation to the surface in this type of fire.

Blinov and Khudyakov (12) burned gasoline, tractor kerosene, diesel oil, and solar oil in cylindrical pans of diameters 0.37 cm to 22.9 meters. Flame photographs indicate that as pan diameter increases the flame structure, for any of the fuels, changes from a conical steady flame (1.1 cm pans) to a pulsating-tip flame, of maximum frequency about 18-20 cycles per second (3 cm pans). Further increase in pan diameter reduces the pulsations, but the unstable portion of the flame shifts downward until, for a 15 cm pan, the entire flame is changing continuously in structure everywhere, and with 1.3 meter pans the random turbulent motion is fully established. Hottel (35) plotted the linear burning rate data of Blinov and Khudyakov against pan diameter, and found the same general structure for all the fuels. The burning rate first decreases with increasing pan diameter, with an almost constant product of the two. This is the laminar flow regime, with Reynolds number (based on properties of the non-burning fuel vapor and the product of the pan diameter and linear burning rate) less than about 20. With further increase in pan diameter the

burning reaches a minimum value and then rises rapidly in the range of Reynolds number from 20 to 200, and finally levels off again at a pan diameter of about 1 meter or a Reynolds number of about 500. Above that value the burning is turbulent and the burning velocity is substantially uninfluenced by pan diameter or fuel type. The burning rate keeps pace with the fuel vaporization rate, which is heat transfer-controlled. Hottel proposed that the net heat transfer rate to the surface is given by

$$\frac{4Q_b}{\pi D^2} = \frac{K_c(T_f - T_b)}{D} + U(T_f - T_b) + \sigma F(T_f^4 - T_b^4)(1 - e^{-\kappa D}) \qquad \text{(II-4)}$$

where F = configuration factor

K_c = conduction coefficient, Btu/hr-ft^2-°F/ft

Q_b = heat transferred to fuel, Btu/hr

T_b = temperature of fuel surface, °R

T_f = flame temperature, °R

U = overall coefficient of heat transfer, Btu/hr-ft^2-°F

κ = mean absorption coefficient, in^{-1}

σ = Stefan-Boltzmann constant, 0.1714 (10^{-8}) Btu/hr-ft^2-°R^4

At small diameters the first term on the right will be large and cause the burning rate to be high. At large diameters the first term will have disappeared completely, the second will be constant, and the third and dominant term will be constant because κD is large. At intermediate diameters the third term

will be low because of the thinness of the flame but the pan will be too large for the first term to be significant; hence a minimum rate. Calculations based on the gasoline results indicate that on the basis of U = 1 Btu/hr-ft^2-°F, F = 1/4, and D large enough to make the flame opaque, the burning rate corresponds to radiation and convection from a flame at about 1600°F.

Flame height to diameter ratio was also plotted against pan diameter. A continuous decrease in this ratio occurs out to the turbulent regime where it becomes constant at a value of about 1.7 for the one fuel adequately studied (gasoline). The quantity vD^2/H, which is the ratio of the volumetric burning rate to the flame height, is substantially constant for the laminar regime. Here v is the liquid fuel regression rate and H is the flame height.

Equation II-4 is referred to by many authors, but none of them has examined this equation very closely. The term $K_c(T_f - T_b)/D$ has the form of conduction heat transfer. The temperature difference is between the flame and the fuel surface. The characteristic dimension should be the distance between the point where T_f occurs and the fuel surface. This distance is undefinable. Similarly the thermal conductivity is that of the medium where conduction occurs. Once again this cannot be defined. Therefore, the conduction term is ambiguous. The convection term $U(T_f-T_b)$ is appropriate but U should be replaced by a convection coefficient at the surface

of the fuel. The radiative term $F(T_f^4 - T_b^4)(1 - e^{-\kappa D})$ assumes that the absorptance of the fuel is equal to the emittance of the flame and is expressed by $(1 - e^{-\kappa D})$. The burner diameter appears as the radiation path length in the emittance term. This is valid only if the flame has a hemispherical shape and the receptor is at the center of the base of the hemisphere. In spite of these assumptions, Equation II-4 has been acclaimed to adequately represent the form of the burning rate data.

Fons (29) states that the heat transfer-mass transfer analogy yields the relation

$$\frac{M_s D}{\mu_a} = C_1 B_E^m \left(\frac{\rho_a g D^3}{\mu_a^2}\right)^{n_1} \qquad \text{(II-5)}$$

which holds for all burning regimes depending on the value of n_1. In this equation the Emmons' form of the heat ratio, B_E, is used. This ratio is given by the following expression

$$B_E = \frac{h_{ab} - h_a + H_c m_{o2a/r}}{H_v + h_{1b} - h_1} \qquad \text{(II-6)}$$

where h_a = enthalpy of air, Btu/lbm

h_{ab} = enthalpy of air at fuel boiling point temperature, Btu/lbm

h_1 = enthalpy of fuel, Btu/lbm

h_{1b} = enthalpy of fuel at its boiling point, Btu/lbm

H_v = heat of vaporization of fuel, Btu/lbm

ρ_a = air density, lb/ft^3

μ_a = viscosity of air, lbm/ft-sec

Equations II-5 and II-6 are similar to those given by Spalding (Equations II-3 and II-2). Fons measured the burning rate of n-hexane and cyclohexane using 10 circular, water cooled pans with diameters from 0.22 to 11.94 inches. The fuel surface was brought to within 0.220 inches of the burner lip. Values of $(M_s D/\mu_a)$ for both fuels were plotted against $(\rho_a g D^3/\mu_a{}^2)$ which is a modified Grashof number. The results indicate that the value of n is Equation II-5 increases with the diameter of the burner from 0.25 for the 3-inch pan to about 1.0 for the 12-inch pan. Since neither rippling nor boiling of the liquid surface was observed in any of the tests, the increase of the exponent n_1 with pan diameter cannot be attributed to a change in roughness of the evaporating surface. Equation II-5 is based on the theory that heat transfer is by conduction and convection only through the vapor zone. Since radiation becomes important for larger burner diameters, this influence may account for the increased value of n_1. Hottel's analysis (35) shows that the rate of burning does not change with pan diameters greater than 3 feet. For this case, the value of n_1 would be 1/3. Fons does not give a value for m but gives a value of B_E = 6.25 for n-hexane and B_E = 5.65 for cyclohexane. The use of these values would have a slight effect on the plotted burning rate data.

Fons also measured the fuel temperature at 1/16 and 11/16 inches below the surface of the liquid. These temperatures increased with burning time and pan diameter. For the 11 to 16 minute test duration, the temperature nearest the surface never reached the boiling temperature of the fuel. The temperature at the 11/16-inch depth was 45-50°F lower than the temperature at the 1/16-inch depth.

Thomas, Webster, and Raftery (74) used a simple dimensional analysis of the flow for any one fuel-air system to arrive at the functional equation

$$\frac{H}{D} = f\left(\frac{Q_g^2}{gD^5}\right) \qquad \text{(II-7)}$$

Experiments were conducted with cribs of wood (spruce) on a square base. Mean flame heights were obtained from photographs; the flames had a short period of fluctuation in height so that the heights recorded photographically were averaged over a period considerably longer than the few seconds for a single fluctuation. Values of H/D were plotted on log-log paper against $(Q_g\rho_g)^2/D^5$. The term $\rho_g Q_g$ is the mass rate of fuel consumption and ρ_g is the density of the cold fuel gas. The resulting straight line is represented by the following dimensional equation in cgs units

$$\frac{H}{D} = 4.4\left(\frac{\rho_g^2 Q_g^2}{D^5}\right)^{0.3} \qquad \text{(II-8)}$$

This equation does not predict a constant H/D ratio for large values of Q_g^2/D^5. Therefore, extrapolation of the data to higher flow rates or smaller burners will over-estimate the flame height.

Emmons (27) burned acetone and methyl alcohol in open pools from 1/4 to 10 inches in diameter. The pans were mounted flush with the burn table and the curves of linear burning velocity versus pan diameter are in agreement with the results of Blinov and Khudyakov (12) for pan sizes above 4 inches, but for the smaller pan sizes the liquid burning rate decreased with pan diameter instead of increasing. This disagreement was resolved when the pans were placed on the top of the table. For this condition the burning rate increased with the decreasing pan diameters below 4 inches. One might suppose that radiation directly from the flames to the exposed rim with subsequent heat conduction to the liquid to be responsible for the increased rate of burning. However, placing a radiation shield over the exposed rim had no effect on the burning rate. Emmons concluded that the heat transfer path from flames to the liquid is

1. Radiation from flames to the whole table top.
2. Convection transfer from table top to inducted air.
3. Convection transfer from inducted air to pan rim.
4. Conduction through the rim to the fluid.

This four-step mechanism takes the place of the simple conduction term assumed by Hottel (35).

Tests were conducted where lampblack from a kerosene fire was coated on the inside of the pans and then acetone and methyl alcohol were burned. The result was about a 7 percent increase in the burning rate. Studies were made on the burning rate of methyl alcohol with the pans partially filled with fuel. Observed burning rates decreased as the fuel level decreased.

Emmons postulated that the liquid burning rate can be obtained from the following heat balance

$$\frac{\pi D^2}{4} \rho_l \, 60 v H_v = Q_r + Q_c + Q_{cd} - Q_o - Q_l \qquad \text{(II-9)}$$

where Q_c = convective heat transferred from flame to fuel, Btu/hr

Q_{cd} = convective heat transferred from air to pan Btu/hr

Q_l = sensible heat gain by fuel, Btu/hr

Q_o = heat loss from fuel to pan bottom, Btu/hr

ρ_l = density of liquid fuel, lbm/ft^3

v = liquid regression rate, ft/min

H_v = latent heat of vaporization, Btu/lbm

The author further defines a burning velocity corrected for pan heating as

$$v_c = v \, H_{VE}/H_v \qquad \text{(II-10)}$$

where H_{VE} = effective heat of vaporization, Btu/lbm defined as

$$H_{VE} = H_v + C_{pl}(T_s - T_l) + C_{po}(\Delta T_o)\ w_o/w_l \qquad \text{(II-11)}$$

C_{po} = specific heat of fuel pan, Btu/lbm -°F

ΔT_o = temperature rise of fuel pan, °F

w_l = mass of fuel, lbm

w_o = mass of fuel pan, lbm

Emmons used Equation II-10 to correct the methanol burning velocity obtained with partially filled fuel pans. In computing H_{VE}, it was assumed that the pan temperature reached the fuel boiling point temperature. The corrected burning velocity increased steeply for pans less than 1/4 full. The author believes that the heat capacity of small pans is too great to ever be heated to the fuel boiling point and this is the primary reason for the rapid rise of the corrected burning velocity. Pan temperature was measured while burning acetone and for pans less than about 1 inch in diameter the temperature was below the fuel boiling point, but for pans larger than 2 inches, the temperature was about 7°C above the fuel boiling point.

The fuel cannot lose heat to the bottom of the pan, since measured pan temperatures are above the fuel boiling point for acetone. Heat input to the pan sides by air convection is feasible, but the possibility of reradiation or conduction from the surface the pan is mounted on should also

be considered. The most likely cause of pan temperatures higher than fuel temperatures is that the pan absorbed radiant energy transmitted through the fuel, a conclusion supported by the fact that burning rates increased when the bottom of the pan was blackened.

Burgess, Grumer and Wolfard (14) measured the burning rate of methyl alcohol, unsymmetrical dimethylhydrazine, benzene, n-hexane, liquid n-butane and liquid hydrogen in a quiet ambient atmosphere. Open trays up to 8 feet in diameter were used and the liquid level was nearly flush with the rim. They found that Equation II-4 conforms to measured burning rates under the following simple assumptions: the flame temperature, shape factor, and extinction coefficient are constant for diameters beyond perhaps 12 inches, and the conduction and convection terms are negligible. Curves of linear regression rate versus tray diameter were constructed by assuming a value of the ultimate burning rate and comparing it with the burning rate at the 1 foot diameter. The ratio of these rates was then equated to $(1 - e^{-\kappa D})$ to calculate κ. The curves, therefore, represent predicted evaporation rates from the tray due exclusively to radiative heat transfer. These calculated curves and the experimental points are generally in good agreement except for benzene. The burning rate of this fuel is usually susceptible to any casual environmental disturbance that ruffles the flame and increases its capacity. The authors plotted the maximum predicted burning rate against the ratio

of the heat of combustion to the heat required to vaporize the fuel, i.e., the heat of vaporization at the boiling point plus the integrated heat capacity of the fuel from ambient temperature to the boiling point. The resulting curve was linear.

Magnus (44) measured the burning rates and temperatures in the fuel and in and above the flame zone for ethanol and gasoline. Tanks from 12 to 120 cm diameter with a height to diameter ratio of 4/3 were used with different initial fuel levels. The conclusions from these tests were:

1. Ambient air temperature, humidity and barometric pressure have no significant effect on the fuel burning rate, whereas wind velocities of less than 0.5 m/sec exerted a perceptible influence on the burning rate.
2. The burning rate per unit area increases with tank diameter.
3. The effect of freeboard height on the burning rate is a function of the tank height to diameter ratio and fuel composition. For small freeboard height ethanol burns slower than gasoline, but for freeboard heights greater than one-half the tank height, ethanol burns more rapidly than gasoline.
4. The effect of heat conduction from tank freeboard wall to the fuel is only perceptible very close to the tank wall at the fuel surface.
5. The maximum flame temperature and the fuel burning rate decrease with increasing freeboard height.

6. The fuel is heated only in a thin layer beneath the surface with ethanol, the surface temperature remains essentially constant.
7. The maximum flame temperature occurs at approximately the same distance above the liquid surface.
8. The maximum temperature profile for gasoline is 10 to 15 percent higher than for ethanol.

Burgess, Strasser, and Grumer (15) measured the burning rate of liquid hydrogen, LNG, butane, methanol, benzene, hexane, xylene, unsymmetrical dimethyl hydrazine, and diethylenetriamine. The noncryogenic fuels were burned in trays of 7-240 cm diameter and about 8 cm depth, particular attention being given to flush filling of the trays at the smallest diameters. Liquid hydrogen was burned in stainless-steel dewars of 7-33 cm diameter and LNG in insulated trays or within a diked area which had been precooled with liquid nitrogen. Almost all tests were conducted outdoors in winds of less than 1 ft/sec average velocity.

The linear burning rate was found to increase with an increase in the initial fuel temperature. Steady burning rates in the near absence of wind were plotted against tray diameter and the curves represent the empirical expression

$$v = v_\infty \ (1 - e^{-\kappa D}) \qquad \text{(II-12)}$$

where v_∞ = linear burning rate for an infinite flame size, ft/min

Two values of "v" for each fuel were used to evaluate "v_∞" and "κ" in the above equation and Table II-2 lists these values of v_∞.

TABLE II-2

VALUES OF v_∞ FROM BURGESS, STRASSER AND GRUMER (15)

Fuel	v_∞, cm/min	v_∞, ft/min
Hexane	0.73	0.024
Butane	0.79	0.026
Benzene	0.60	0.020
Xylene	0.58	0.019
Methanol	0.17	0.006
UDMH	0.38	0.012
Hydrogen	1.4	0.046
LNG	0.66	0.022

Values of v_∞ for the nine fuels were plotted against the ratio of the net heat of combustion to the sensible heat of vaporization and the resulting straight line can be represented by

$$v_\infty = \frac{0.0076\ H_c}{H_v + C_{pl}(T_s - T_l)} \text{ cm/min} \qquad \text{(II-13)}$$

It was confirmed that linear burning rates increase at tray diameters below 5 to 10 cm. Flames at very small diameters are simple laminar diffusion flames, and heat transfer to the liquid is demonstrably an edge effect of no interest in large-scale experiments. Conductive heat transfer becomes negligible at large diameters by virtue of being an edge effect.

It is not so easy to dispose of convective heat transfer, especially with the slower burning flames. A steep temperature gradient was noted at the interface between liquid and vapor phases in both methanol and benzene flames. The presence of soot particles above the benzene pool is also suggestive of convection. The strong absorption of flame radiation by methanol vapor dictates that the flame stand very close to the liquid surface, which again favors convection as the heat transfer mode. On the other hand, convection can be ruled out for the faster burning butane and hydrogen flames since there was no sharp rise in temperature as a thermocouple emerged from the liquid phase into the vapor zone. Since the burning rate curves tended toward an asymptotic value at large tray diameters, the authors conclude that the rate of radiative feedback from the flame to the pool of liquid is the rate controlling process.

Spalding (65) questions the dominance of radiative heat transfer for the results given by Burgess, Strasser and Grumer (15). He states that at large Grashof numbers, the exponent of the Grashof number in Equation II-3 changes from 0.25 to 1/3 and the coefficient multiplying it is reduced by the ratio (0.14/0.54). For large fuel surface dimensions, Equation II-3 must be similarly changed, and the result is

$$V_\infty = [0.117\ B_s^{3/4}\ \rho_a^{2/3}(gK_a/C_{pa})^{1/3}]/60\ \rho_l \qquad \text{(II-14)}$$

where $V_\infty = M_s/60\rho_l$ = linear burning rate for an infinite flame size, ft/min

ρ_a = density of air, lbm/ft^3

ρ_l = liquid fuel density, lbm/ft^3

Using Equation II-2 and neglecting the second term in the numerator, the following equation is obtained

$$v_\infty \left(\frac{H_v + \int_{T_l}^{T_s} C_{pl}\, dT}{H_c} \right) = \left(\frac{0.117\, m_{o_{2a}}\, \rho_a}{B_s^{1/4}\, r\, 60\, \rho_l} \right) \left(\frac{g k_a}{\rho_a C_{pa}} \right)^{1/3} \qquad \text{(II-15)}$$

For hydrocarbons burning freely in air, $B_s \simeq 5$, $\rho_l \simeq 49.9$ and $r \simeq 3.48$. Using these values and air physical properties at room temperature, Equation II-15 becomes

$$v_\infty \left(\frac{H_v + \int_{T_l}^{T_s} C_{pl}\, dT}{H_c} \right) \simeq 9.48\ (10^{-5})\ \text{ft/min} = 0.003\ \text{cm/min} \qquad \text{(II-16)}$$

The value on the right-hand side of this equation is of the same order of magnitude as the value of 0.0076 cm/min given by Burgess, et al. (15).

Spalding concludes:

1. An application of the established theory of natural-convection burning, modified to take account of the transition to turbulence at large Grashof numbers, correctly predicts that the burning rate of liquid-fuel trays will be independent of tray diameter.

2. The use of heat-transfer data obtained in turbulent natural convection to supply the numerical constant in the burning-rate equation predict burning rates of the same order of magnitude as the experimental rates.
3. A replot of the original experimental data in the terms suggested by Equation II-14 appears to be well worthwhile; only if systematic deviations from that equation are exhibited should new mechanisms for the process be sought.
4. The burning rates predicted by Equation II-16 are about one-half the experimental ones. It may be that the difference is caused by the radiative heat flux. However, a more precise estimate of the convection controlled burning rate is needed which does not rely on the crude extrapolation from laminar to turbulent conditions that was used.

Burgess and Grumer (13) state that convection may be important in diffusion flames of slow-burning fuels such as methanol, in wind driven flames, and in some kinds of decomposition flames. However, with faster-burning diffusion flames, such as those supported by liquid hydrocarbons, there are numerous reported observations that are at odds with Spalding's concept. First it should be pointed out that flames above large liquid pools do not resemble the shapes obtained by Spalding, but conform to the flame shapes reported by Rasbash, et al. (57), i.e., with a thick vapor zone interposed between the luminous zone and the liquid surface. The various fuel vapors differ considerably in their absorptions of flame

radiation, and the vapors immediately above the liuqid are not necessarily very hot. Methanol absorbed its own flame radiation almost completely within a 3 mm path length of liquid while benzene is rather transparent to its own flame radiation.

With Equation II-15 the rate constant ranges from 0.0027 cm/min for benzene to 0.008 cm/min for methanol. Experimental data show that Equation II-15 predicts much lower burning rates at larger diameters than actually obtained.

Burgess and Grumer were also skeptical of the importance of turbulence in the vapor flow above hydrocarbon pools. With butane and hexane the flame tips were rumpled, luminous and fluctuating, but these were located some distance downstream from the liquid surface. The sides of the flames in proximity to the fuel surface were smooth, transparent and remarkably steady.

Agoston (2) treated the burning of liquid pools in a manner analogous to that used in the convective evaporation of drops and the combustion of fuel drops. The following equation is proposed for the liquid burning rate

$$v_l = \frac{a_3}{d^{n_3}} + \frac{a_2 a_3}{d^{n_3 - 3p}} + a_4 + a_2 a_4 d^{3p} \qquad \text{(II-17)}$$

where a_2, a_3, a_4 = constants

d = burner diameter, mm

n_3 = constant

p = exponent

v_l = linear burning rate, mm/min

This equation is for a burning liquid pool under non-turbulent natural convection conditions. The author refers to the data of Blinov and Khudyakov (12) and states that because the observed values of v_l contain the undetermined influence of heat conduction through the pan wall, of flame radiation, and possibly of pan rim aerodynamic effects superimposed upon the diffusive-convective mechanism, the data cannot be used to evaluate the constants in the above equation. Equation II-17 predicts increasing values of v_l for large values of d whereas Blinov and Khudyakov's data show v_l to become constant. Agoston concludes that a transition from laminar to turbulent convection could account for such a change. Equations such as II-17 are of dubious value since there is no easy way of evaluating the constants.

In a later paper Thomas (72) presented the following equation for the flame height from wood cribs.

$$H/D = 4.4[M_l^2(10^6)/D^5]^{0.30} \text{ (in cgs units)} \qquad \text{(II-18)}$$

This equation is identical to Equation II-8 except for the 10^6 term in the numerator, since $M_l = \rho_g Q_g$. Since numerical data are not given, this difference cannot be explained. For the purpose of plotting results on a dimensionless scale, the author uses an air density of 1.3 (10^{-3}) gm/cm^3 and transforms Equation II-18 into the following

$$H/D = 42 \left[M_s/\rho_a (gD)^{1/2}\right]^{0.61} \qquad \text{(II-19)}$$

Putman and Speich (56) conducted a study to establish modeling laws for partially and fully merged flames using gaseous fuels. The basic requirement was that the fuel jets produce turbulent diffusion flames which are buoyancy controlled. This requirement can be satisfied by keeping the fuel flow Reynolds number in excess of 5000, and the Froude number at a low value. The authors found that the height of buoyancy controlled flames could be expressed by

$$H/D = 29 \ (Q_g^2/gD^5)^{1/5} \qquad \text{(II-20)}$$

Thomas, Baldwin, and Heselden (73) burned ethyl alcohol in a 91 cm diameter vertical-sided steel tray surrounded by a circular asbestos wood board (276 cm diameter), covered with aluminum foil, in the plane of the top of the tray. With the fuel surface 11-14 cm below the tray edge, the mean burning rate was 19 g/sec and the mean flame height was 150 cm. With the fuel surface of 2.5-4 cm below the tray edge, the mean burning rate was 17 g/sec and the mean flame height was 170 cm. Previous correlations predict that the flame height should increase with increasing burning rates. The authors do not comment on this measured reverse effect.

Steward (68) stated that the height of a fire is a rather ambiguous quantity, and will be taken as the height at

which a certain fixed quantity of air has been entrained. It is necessary to take experimental data to determine this fixed quantity of entrained air for a meaningful physical height such as the visible fire height. In order to analyze a flame, a model consisting of a two-dimensional linear fire with a finite base from which fuel is rising, was postulated with the following assumptions:

1. Turbulent flow fully developed and molecular processes neglected.
2. Transverse forces small compared with those in the vertical direction.
3. Mixing in the vertical direction neglected.
4. No horizontal pressure variation.
5. Ambient fluid is of uniform density.
6. The heat capacities of the air, jet, and fuel are equal and independent of temperature. The molecular weight of the jet, air, and fuel are equal and the jet fluid and air are perfect gases.
7. Normalized density and velocity profiles are independent of height.
8. The rate of entrainment is proportional to the local velocity of the jet.
9. The entrained air mixes with the fuel and burns to stoichiometric completion instantaneously.
10. Radiation from the flame is neglected.

The author states that the neglect of radiation is probably the worst assumption of all, however, its inclusion would make an analytical solution impossible. The height of a buoyancy controlled flame above a circular source is given by

$$H/D = \left(\frac{1875\ Q^2\ (r + \omega\rho_a/\rho_g)^2\ \omega^3}{256\ \pi^2\ D^5\ k_e^4\ (1-\omega)^5\ \rho_a^2\ gH_c^2} \right)^{1/5} \qquad \text{(II-21)}$$

where k_e = entrainment coefficient

Q = heat liberation due to combustion, Btu/hr

ω = inverse coefficient of volumetric expansion due to combustion

The inverse volumetric expansion coefficient, ω, can be obtained from

$$\omega = \frac{1}{1 + [H_c/rC_{pg}T_{ar}]} \qquad \text{(II-22)}$$

where T_{ar} = air temperature, ^{o}R

Steward states that Equation II-21 should not be taken too seriously for specific details in view of the assumptions involved. However, it can be expected to hold for any flame that is turbulent throughout a major portion of its length and one that entrains air entirely from its sides.

One problem in applying Equation II-21 is obtaining a value of the entrainment coefficient. Steward gives no information on evaluating this coefficient.

Akita and Yumoto (3) measured the burning rate of liquid methanol in open water-cooled circular vessels from 1 to 60 cm diameter, and in concentric vessels having three compartments of the same area and diameters from 10 to 30 cm. The liquid surface was always kept at a constant level near the vessel rim by means of an overflow type refueling device. The experimental results showed that the burning rate in a concentric vessel is the largest at the vessel rim next to the flame base and decreases quickly with the distance from the rim. This tendency is most marked in a small vessel with laminar burning, and is gradually lost in large vessels which correspond to the turbulent flow region. This difference in burning rates causes a radial flow at the liquid surface in small vessels. The total burning rate of a concentric vessel is equal to that in a single vessel of the same size, and the burning rate in an outside compartment is not in the least affected by replacing the fuel in the inside compartments with water. These results indicate that the burning in the inside regions of a pool and inner rims of a concentric vessel do not play an important role in heat transfer from the flame to the liquid surface. The authors state that for vessel diameters of about 3 to 20 cm, the exponent on the right-most term of Equation II-3 was found to be about 0.2, instead of 0.25, so they conclude that Spalding's theory does not explain their results satisfactorily. A value of 0.55

for the exponent for a vessel diameter range of 3 to 20 cm, and an exponent of 0.15 for diameters less than 3 cm is obtained from their data.

Akita and Yumoto further state that the theory based on Equation II-4 is rather semi-quantitative and, hence, it is impossible to apply it directly to their experimental data. Accordingly, they introduced the following empirical local conductive and convective coefficients

$$K = Kr, \quad \text{at } R = R_r$$
$$K = 0 \quad \text{at } R \neq R_r \qquad \text{(II-23)}$$

$$U = U_r \exp\left[-\alpha_r R_r (1-R/R_r)\right] \qquad \text{(II-24)}$$

where K_r = conductive coefficient at the vessel rim supporting the flame, Btu-ft/hr-ft^2-^{o}F

R = radius-ft

R_r = radius of vessel-ft

U_r = convective coefficient at the vessel rim supporting the flame, Btu/hr-ft^2-^{o}F

α_r = absorption coefficient-ft^{-1}

Equation II-23 was derived from the observation that the inside rims in a concentric vessel have no effect upon the burning rate. Equation II-24 was selected as a general form corresponding to the fact that the radial burning rate profile decreases exponentially from the outermost vessel rim toward the center. Neglecting the radiation term and substituting

Equations II-23 and II-24 into Equation II-4 the following equation results

$$v = \frac{2(T_f - T_b)}{\rho_l H_V} \left\{ \frac{K_r}{R_r} + \frac{U_r}{\alpha_r} \left[1 - \frac{(1-e^{-\alpha_r})}{\alpha_r} \right] \right\} \qquad \text{(II-25)}$$

In this equation the values of T_f m K_r, and U_r and α_r are unknown so an absolute value of the linear burning rate cannot be obtained. However, if (K_r/U_r) and α_r are given in anyway, at least the ratio of burning rate alone can be calculated. Using their data for the burning rate of methanol at various single vessel diameters, the authors obtained a value of $K_r/U_r = .7$ and a curve showing that α_r decreases rapidly with diameter. The authors then used these values to obtain a good prediction of the ratios of burning rates of methanol given by Burgess, Strasser and Grumer (15).

Atallah (5) measured flame heights visually and photographically for eleven pure organic liquids burning in insulated pans whose diameter ranged from 0.8 to 36.9 cm. The liquids were: n-hexane, cyclohexane, i-pentane, heptane, benzene, xylene, methanol, i-propanol, n-butanol, acetone, and methylethyl ketone. A plot of the flame height, H_m, versus $\left[\frac{M_m T_m}{M D_{-m}} \left(\frac{1}{C_{fs}} - \frac{1}{2} \right) \right]$ produced the following dimensional equations

$$H_m = (1.0 \pm 0.2) \left[\frac{M_m T_m}{M D_{-m}} \left(\frac{1}{C_{fs}} - \frac{1}{2} \right) \right]$$

$$\text{for } [\ ] < 10 \qquad \text{(II-26)}$$

$$H_m = (7.5 \pm 1.5) \left[\frac{M_m T_m}{M \underline{D}_m} \left(\frac{1}{C_{fs}} - \frac{1}{2} \right) \right]^{.358}$$

for [ ] > 20 (II-27)

where $\underline{D}_m$ = diffusion coefficient, cm^2/sec

H_m = flame height, cm

M = molecular weight of fuel, g/g-mole

M_m = mass burning rate of fuel, gm/cm

T_m = fuel boiling point temperature, ^oK

The large scatter in the data was attributed to the difficulties in obtaining proper flame heights visually and photographically. The author also states that most of the liquid fuel vapor is generated at the walls of the small pans. Air diffuses into the thin shell of vapor produced at the wall quite easily, thus completing the combustion process at a relatively shorter flame height.

Welker (20) extrapolated his acetone, benzene, cyclohexane and n-hexane burning rate data for wind-blown pool fires to calm conditions. Two major differences appear when the results are compared with the data of Burgess, Strasser, and Grumer (15). The first is that the burning rates for large liquid fires obtained by extrapolating his data are more than twice those found previously. The second is that the burning rate apparently increases until the pan diameter is larger than previously expected. Indeed, an estimate shows that the pan diameter must be about 15 feet for the maximum burning rate to be reached.

Corlett and Fu (21) measured the steady burning rates of methanol, ethanol and acetone in thin-walled stainless steel burners of 0.6 to 30 cm diameter. Normally the burners were flush full and fully exposed to ambient air. The authors conclude that the energy loss from an open-tube burner by convection in the ambient atmosphere is not an important factor in determining the pool-burning rates. Furthermore, burning rates measured with the burner sidewall noninsulated are in no case exceeded by those of Atallah (5), whose vessel sidewalls were insulated with asbestos tape. The effects of the pan wall conductance (thickness times thermal conductivity) were investigated and, in general, increased wall conductance results in decreased burning rate. The effect of wall conductance variation, although appreciable, is not decisive even for the relatively small burner diameter used. In practice, the wall conductance should be kept as low as possible. Another conclusion is that radiation and convection heat transfer are each significant in both luminous and nonluminous fires in the diameter range studied. The radiative fraction increases gradually with increasing pool diameters.

A series of steady experiments was also carried out with burners filled to various liquid levels. Small liquid decreases from flush full (1 to 5 mm) were found to cause gentle decreases in burning rate for pools of diameter 1 cm. This characteristic tends in principle to stabilize the liquid

level while destabilizing fuel consumption rates, however, the effect is very mild. In general, results become increasingly complicated with decreasing liquid level, where wall conductance plays an increasingly significant role in determination of burning rates. When wall conduction becomes a dominant mode of heat transfer, there appears to be a tendency toward unstable, limit cycle operation; heat stored in the wall causes rapid vaporization, blowing the flames temporarily from the tube; the wall then cools, the flames drop back into the tube, and the walls heat again. Increasingly severe instability is observed at smaller diameters, and is observed in the smallest burners studied (<1 cm diameter) for attempted operation at any liquid level.

Blackshear and Murty (11) employed vertical and horizontal fuel-soaked wicks to determine the influence of size (d), orientation, and fuel molecular weight (M), on the burning rate. The fuel-consumption rates in wick burning are found to be nearly the same as in comparable burning experiments in which liquid fuels burn in horizontal pans. The burning rate, expressed as a product of mass-transfer coefficient in the limit of no mass transfer times a driving force, yields a mass transfer coefficient that varies as $d^n M^m$. For vertical wicks $n = -1/4$ when $d < 10$ cm, $n = 0$ when $d > 10$ cm, and $m = -2/3$ for $d = 10$ cm. For horizontal wicks (flame on top) $n = -1/2$ for $d < 10$ cm, $n \simeq 0$ for $d > 10$ cm; $m = -1$ for $d = 10$ cm. For horizontal wicks (flame on bottom) n is

estimated as -1/4 for the entire size range, and m = -1/3 for d = 10 cm.

The authors concluded that over the range of sizes studied the vertical and horizontal (flame on bottom) fuel-surface burning rates are controlled primarily by convection. The horizontal fuel-surface (flame on top) burning rates are controlled by convection and rim conduction for d < 1 cm, convection for 1 < d < 20 cm, and by convection and radiation for d > 20 cm. The influence of radiation appears to behave as though the gas between the radiating flame and the fuel surface is nonabsorbing for 20 < d < 200 cm. For big fires (d > 1000 cm), it is suggested that fire becomes optically thick, and the dominant mode of heat transfer is convection. As a first approximation the heat transfer coefficient for this condition is

$$h \simeq 0.04\ \rho\ \mu\ C_p\ [1 + \frac{16}{3}\ \sigma\ T_f^3/K\kappa]^{2/3} \qquad \text{(II-28)}$$

Deshpande (24) measured the flame height for acetone, benzene, cyclohexane, n-hexane, and methanol flames. A plot of H/D versus $M_1/\rho\sqrt{gD}$ shows considerable scatter so a correlation was not obtained. The data appear to be grouped according to each fuel and indicate additional parameters are needed for a correlation. The author doesn't indicate what density, ρ, was used but calculations from listed data shows that it was the value of air at room temperature.

The author also plotted v_∞ against the ratio of the heat of combustion to the sum of the heat of vaporization and sensible heat of the fuel. Methanol, cyclohexane, and n-hexane seem to lie on a straight line but acetone is far below and benzene is above the line. The data of Burgess, Grumer, and Wolfard (14) are consistently lower than those obtained in this study. The author obtains v_∞ by extrapolating a plot of v versus $(1-e^{-\kappa D})$ to the point where $e^{-\kappa D}$ is zero. The author doesn't give the values of κ, which would have a definite effect on the values of v_∞ obtained.

Masliyah and Steward (45) mathematically simulated a flame by two zones. The first zone is the combustion region and extends from the fuel source up to the point at which enough air has been entrained to provide a stoichiometric mixture of fuel and air. The second zone is the hot gas plume starting at the end of the combustion zone and extending to infinity. The pertinent differential equations for these zones were derived based on the assumptions of Steward (68), which were listed earlier. The radiative interchange between flame and a plume surrounding its base was determined with the following assumptions:

1. The flame is a gray gas.
2. The scattering of radiation is negligible.
3. The emission of radiation at any point in the flame is proportional to the concentration of the original source fluid at that point.

4. The receiving surface is a black body.

After considerable mathematical manipulations, the following equation for the height of the combustion zone, H_z, was obtained

$$H_z = 1.43 \left[1 - \frac{1}{(r+1)^{2/5}}\right]\left(\frac{M_1^2 (r+1)^2 \rho_g}{(k_e)^4 \pi^2 (\rho_a)^3 g(1-\rho_g/\rho_a)}\right)^{1/5} \quad \text{(II-29)}$$

The authors also assumed that the heat flux required to vaporize the fuel is due entirely to radiation. With this assumption and Equation II-29, a graphical solution is presented for the fuel burning rate as a function of the pan diameter, the enthalpy required to raise the fuel to its boiling point, and "the degree of darkness" of the flame. The "degree of darkness" is the product of the flame height of the combustion zone and a proportionality constant defining an absorption coefficient. A combustion zone temperature of 2300°R and a stoichiometric mass air to fuel ratio of 15 were assumed. The burning rate data of Blinov and Khudyokov (12) for gasoline and crude petroleum shows that the "degree of darkness" lies between 1 and 10. The authors conclude that for small pan diameters of an inch or less the major heat transfer mechanism is conduction down the side of the pan. For pan diameters of one foot or more, radiation appears to be the major mechanism of heat transfer.

After all the assumptions made in this study, one still has to estimate values of "the degree of darkness",

which are a strong function of the soot formation in the flame. A value of the entrainment coefficient, k_e, is also required. The authors give a value of $k_e = .05625$ without any justification. The premultiplier 1.43 in Equation II-29 should be 1.49.

Using the same assumptions presented in reference 68, Steward (69) presents the following equation for the flame height at which stoichiometric mixing occurs

$$\frac{H_z}{R_r} = 1.49\left(\frac{N_{co}}{\pi^2 (k_e)^4}\right)^{1/5} \qquad \text{(II-30)}$$

where N_{co} is a dimensionless group called the combustion number defined as

$$N_{co} = \frac{Q^2 (r+\omega\rho_a/\rho_g)^2 \omega}{\rho_a^2 H_c^2 g R_r^5 (1-\omega)^5} \qquad \text{(II-31)}$$

The author forgot to include the inverse volumetric expansion ratio, ω, in the numerator of Equation II-31. If one compares Equation II-30 with II-21, it can be seen that they are identical except for the ω^3 instead of ω term in the numerator. The derivation of Equation II-21 was not given, so it may contain an error.

Steward considers the hot gas plume above the burning zone as a buoyant jet which cools upon mixing with the entrained air. Solving the equations for these conditions leads to the following equation for the additional height of

the jet required to entrain a certain fraction of excess air,

$$\frac{H_E}{R_r} = 0.196 \left(\frac{Q^2 (r+\omega\rho_a/\rho_g)^2 \omega}{\pi^2 k_e^4 H_c^2 \rho_a^2 g R_r^5 (1-\omega)} \right)^{1/5} \qquad \text{(II-32)}$$

$$[(1+E_x)^{3/5} - 1]$$

The total height at which a given percent excess air has been entrained is obtained from the sum of the stoichiometric mixing height, H_z, plus the height to obtain the required excess air, H_E. Therefore, the sum of Equations II-30 and II-32 is

$$\frac{H}{R_r} = \left[1.49 + 0.916 (1-\omega)^{4/5} \left| (1+E_x)^{3/5} - 1 \right| \right] \times \left[\frac{N_{co}}{\pi^2 k_e^4} \right]^{1/5} \qquad \text{(II-33)}$$

The author considers that for some particular quantity of excess air the visible flame height should correspond to the height predicted by Equation II-33. This assumption ignores any difference in the visible radiative properties of the combustion products of the various fuels. When the visible flame height to source radius ratio for a number of fuels was plotted against the combustion number, the following relationship, which lies very close to the 400% excess air line, was obtained

$$\log_{10} \left(\frac{H}{R_r}\right) = 0.2 \log_{10} N_{co} + 1.21 \qquad \text{(II-34)}$$

This equation can be expressed in a more usable form as

$$\frac{H}{R_r} = 16.22\ (N_{co})^{0.2} \qquad \text{(II-35)}$$

This equation predicts that the flame height is independent of the burner diameter which is contrary to observed values.

Atallah and Allan (6) recommended Equation II-19 given by Thomas (72), but state that its applicability to all liquid fuels is questioned. The authors also recommend that the linear burning rate can be estimated from the following correlation found by Burgess, Strasser, and Grumer (15)

$$v_l = 0.211\ (10^{-6})\left(\frac{H_c}{H_v}\right)\left(1-e^{-\kappa D}\right) \qquad \text{(II-36)}$$

Wood, Blackshear, and Eckert (83) measured the flame height for acetone and methanol burning in a 152 cm diameter sand-wick burner. The following correlations for flame height were given

Acetone for $0.5 < H/D < 2$

$$\frac{H}{D} = 23\left[\frac{M_s}{\rho_g\sqrt{gD}}\right]^{0.54} \qquad \text{(II-37)}$$

Acetone for $0.02 < H/D < 0.5$

$$\frac{H}{D} = 4.6\ (10^{11})\left[\frac{M_s}{\rho_g\sqrt{gD}}\right]^{3.9} \qquad \text{(II-38)}$$

Methanol for $0.02 < H/D < 0.5$

$$\frac{H}{D} = 2.7 \times 10^{6}\left[\frac{M_s}{\rho_g\sqrt{gD}}\right]^{2.6} \qquad \text{(II-39)}$$

No attempt was made to account for the different character of the fuels and ρ_g is assumed to be 1.3 (10^{-3}) gm/cm^3 or the density of air. The authors recorrelated the data of Atallah and arrived at the following equation for the flame height for liquid fuels

$$\frac{H}{D} = 44 \left[\frac{M_s}{\rho_g \sqrt{gD}}\right]^{0.51} \qquad 1.5 < \frac{H}{D} < 13 \qquad \text{(II-40)}$$

Nakakuki (49) assumed that the flame shape was conical and that the fuel surface receives radiant heat from an annulus in the combustion zone. He also assumes that all the radiant heat to the vessel is transferred to the fuel over a length that is not clearly defined, but must be the fuel depth. With these assumptions, an equation is developed for the linear burning rate which contains several unknown terms lumped into one premultiplier. Using glass vessels of 1.08 and 2.04 cm diameter and n-hexane fuel, values from 0.7 to 2 cm^2/min were obtained for the premultiplier. The premultiplier was found to increase gradually with atmospheric pressure but rapidly with oxygen concentration. The freeboard height also appears to have some effect on this value.

The equation for the linear burning rate is useless since it contains the flame height and this value along with the premultiplier cannot be obtained a priori.

Orloff and DeRis (51) proposed that turbulent convection-dominated pool fires can be correlated by their turbulent ceiling fire theory (Reference 52). The model

presented is based on the observations:

1. That the turbulent burning rate, in the absence of radiation, is independent of pool diameter and essentially independent of radial position.
2. That fully developed turbulent burning rates are insensitive to the rim height.

These two observations suggested that one might predict pool burning rates with a one-dimensional vertical mixing model. Therefore, by using Spalding's mass transfer concepts, the pool burning rate can be predicted by

$$M_s = \left[\frac{K}{C_p}\right]_{1/4} \zeta^{-1} B_s \left[\frac{\ln(1+B_s)}{B_s}\right]^{n_1} \qquad \text{(II-41)}$$

where ζ = stagnant film thickness, ft.

The term $[\ln (1+B_s)/B_s]$ corrects for the heat blockage (i.e., insulating) effect associated with blowing of fluid away from the vaporizing surface. The subscript 1/4 on the first term of Equation II-41 indicates that the thermal conductivity and specific heat are evaluated at the temperature and composition one-quarter of the way between the fuel surface and flame corresponding to the release of 1/4 of the fuel's chemical energy.

From turbulent free convection between two horizontal surfaces, it is known that the entire temperature drop occurs across thin layers adjacent to the surface. Such resistance layers can be regarded as stagnant films with perfect mixing taking place in the outer bulk flow. Orloff and DeRis applied

this stagnant film concept to pool burning to obtain the following equation for the layer thickness,

$$\frac{1}{\zeta} = 0.15 \left(\frac{g(\rho_a - \rho_f)}{(\mu\alpha)_{1/2}} \right)^{1/3} \qquad \text{(II-42)}$$

The subscript "1/2" indicates that the viscosity and thermal diffusivity are evaluated at a temperature and composition midway between the fuel surface and flame corresponding to the release of half the fuel's chemical energy. Combining Equations II-41 and II-42, and taking n_1 to be 2/3, the equation for the fuel burning rate becomes

$$M_s = 0.15 \left(\frac{K}{C_p} \right)_{1/4} \left(\frac{g(\rho_a - \rho_f)}{(\mu\alpha)_{1/2}} \right)^{1/3} B_s \left(\frac{\ln(1+B_s)}{B_s} \right)^{2/3} \qquad \text{(II-43)}$$

The choice of 1/4 and 1/2 position for evaluating the physical properties are intuitive and were found to best represent the data in the authors' ceiling fire study. The choice of $n_1 = 2/3$ represents the best empirical fit of Corlett's data (Reference 19, 20). Since the Prandtl number $P_r = C_p \mu/K$ is essentially independent of temperature and composition for typical combustion gases, the authors define a dimensionless mass transfer number, M_n, as

$$M_n = \frac{M_s}{\mu_{1/4}} \left(\frac{(\mu^2)_{1/2} (P_r)^2}{\rho_{1/2} (\rho_a - \rho_f) g} \right)^{1/3} \qquad \text{(II-44)}$$

Equation II-43 can now be written as

$$M_n = 0.15 \, B_s \left(\frac{\ln (1+B_s)}{B_s} \right)^{2/3} \qquad \text{(II-45)}$$

Using Equation II-45, M_n was plotted against B_s and compared with the data of Cortlett (19, 20). The results show that the correlation holds for a wide variety of fuels provided they are not highly radiative. There is a sudden drop in the burning rate as B_s decreases, which indicates that there is a minimum value for B_s below which the fuel mixture cannot burn, and above which the fuel mixture burns according to the pool burning correlation. This minimum value of B_s is quite sensitive to both fuel chemistry and percentage of supplied inert. The authors suggest that the breakdown in their correlation at low values of B_s may be caused by

1. Chemical kinetic effects.
2. Transition to laminar flow.
3. The influence of stoichiometry on the fluid flow.

All three of these effects were neglected in their model.

Summary of Flame Height and Fuel Burning Rate

From this survey on fuel burning rates and flame height predictions, one can conclude that there is a universal agreement that the fuel burning rate is controlled by the heat feedback to the fuel and not by chemical kinetics. There is agreement that conduction is the dominant mode of heat transfer at pan diameters less than 2 cm (0.8 in); convection is dominant for pan diameters from 2 to 20 cm (8 in) and that radiation is the dominant mode for pan diameters from 20 to 200 cm (80 in). There is speculation that convection again

becomes the dominant mode of heat transfer for pan diameters larger than 200 cm. Most of the experimental work has been with pan diameters less than 20 cm, which is too small for practical interest. There is a careless use of terms such as convection coefficient, conduction coefficient, gas properties, etc. without being specific about their evaluation. In many cases air properties at room temperature are used for the pertinent physical properties. The effects of pan rim and freeboard height are still not clearly defined and the importance of these parameters is conflicting.

The prediction of flame height is by no means exact. Most correlations involve a modified Froude number, but a number of dimensional correlations also exist. There is even disagreement on what is the height of a flame. The effect of pan diameter on the flame height is not exactly known.

In addition, one can conclude that

1. No correlation exists for the convective coefficient between flame and fuel.
2. Absorption coefficients for fuels are scarce and of questionable accuracy.
3. The characteristic dimension used in radiative heat transfer is generally taken as the pan diameter, but this is valid only for a hemispherical flame.

Flame Temperature

Can a flame temperature be defined? In a classical thermodynamic sense, temperature is defined only for a

system in thermal equilibrium. There is some doubt that thermal equilibrium exists in a flame. In flame fronts reaction rates may be comparable with the molecular relaxation times and particle may have as few as 10,000 collisions so equilibrium may not be reached. In this event, it is necessary to specify several temperatures, translational, rotational, vibrational, and electronic or in an extreme case to specify a set of population distributions for all molecular energy levels of each species.

A theoretical or adiabatic flame temperature can be calculated from thermochemical data. This result is accomplished by using energy conservation and by assuming no heat losses, complete combustion of the fuel and no dissociation. Details of this procedure can be found in Gaydon and Wolfhard (30) or Siegel and Howell (63). The theoretical flame temperature is only reached in the center of rather large premixed flames in the region just above the inner cone. Diffusion flames, small premixed flames and turbulent flames of all kinds will normally fail to reach the full adiabatic temperature due to appreciable heat loss or incomplete combustion.

Shimy (61) gives the following formula for obtaining the average value of the flame temperature of any group of hydrocarbons and alcohols:

$$T_{fc} = 10\ \Delta H_c/[0.5(nC) + 0.1(nH)] \qquad \text{(II-46)}$$

where T_{fc} = flame temperature, ^{o}C

ΔH_c = molar heat of combustion at 25^{o}C, K-cal/mole

nC = number of carbon atoms

nH = number of hydrogen atoms

The author states that temperature is a measure of molecular translational speed. The lighter a molecule of a given molecular structure, the higher its translational speed and consequently the higher its flame temperature. In alcohols, the reverse is true because the presence of a single oxygen atom in the alcohol compounds necessitates the deduction of the heat of formation of water, 68.387 K cal/mole, from the heat of combustion of the alcohol compound. This has a substantial effect on the heat of combustion of the lighter molecular structures, but only a slight effect on the heavier structures. Table II-3 compares the flame temperatures calculated by this method with the theoretical adiabatic flame temperatures given in Siegel and Howell (63) and Gaydon and Wolfhard (30). Flame temperatures calculated by Equation II-46 are in good agreement with the theoretical values. This equation is much simplier to use and could provide a starting temperature for the more tedious trial and error theoretical flame temperature calculations.

There is no perfect way of measuring flame temperatures. All methods are subject to both practical and theoretical limitations. The most common methods of flame temperature measurement are optical, the use of thermocouples

TABLE II-3

Comparison of Flame Temperatures Calculated by Shimy's (61) Equation with Theoretical Adiabatic Flame Temperature

Fuel	Flame Temperature, °C	
	Shimy	Theoretical
Methane, CH_4	2362	2012, 2222
Octane, C_8H_{18}	2253	--
Acetylene, C_2H_2	2600	2586, 2523
Ethylene, C_2H_4	2409	2250
Benzene, C_6H_6	2177	2211
Methyl Alcohol, CH_3OH	1800	--

or resistance thermometers, and the sodium-line reversal technique. Optical measurements have the advantage of not disturbing the flame, but do not allow a point-by-point study of the temperature distribution of the flame. One of the most frequently used methods of measuring flame temperature is the sodium-line reversal method. Gaydon and Wolfhard (30) state that it is not always realized that the result of this measurement is the effective electronic excitation temperature for the particular element used, and it is not necessarily more likely to give a true estimate of the temperature of the flame gases than other methods such as those for effective rotational temperature or effective vibrational temperature, which are often frowned on as meaningless. Details of

these and other methods can be found in Gaydon and Wolfhard (30).

Whether a flame is in thermal equilibrium or not, investigators will report values of flame temperature. It is difficult to determine if the variation in these temperatures are due to the flame or to inherent errors in the measurement techniques. No further consideration will be given to these topics, but a presentation of existing flame temperatures for the fuels used in this study follows.

Rasbash, Rogowski, and Stark (57) used the Schmidt method and an optical pyrometer to measure the temperature of four flames. These values are shown in Table II-4.

TABLE II-4

Flame Temperatures from Rasbash, Rogowski and Stark (57)

Fuel	Flame Temperature ^{o}K			
	Optical Red	Optical Green	Hottel & Broughton	Schmidt Method
Ethanol	1025	1080	1290	1218
Benzole	1050	1089	1190	921
Petrol	1089	1132	1250	1026
Kerosene	1083	1120	1210	990

The filament of the optical pyrometer was assumed to radiate as a blackbody, therefore, the optical temperatures are those at which a blackbody would give the same intensity of red

and green radiation in the flames. The authors state that it is difficult to calculate the true flame temperature from these readings since this would require an accurate knowledge of emissivity and wavelength for the different flames. However, approximate estimations of the true temperature were made, using graphs given by Hottel and Broughton, and the results are also shown in Table II-4. In every case the estimated true temperature was greater than the temperature evaluated by the Schmidt method. This result is probably due to the fact that the pyrometer was sighted on the incandescent edge of the flame, whereas the Schmidt temperature was a mean temperature throughout the flame.

Gordon, Smith and McNesby (32) used a 1 mil platinim-platinum-rhodium thermocouple to measure the temperature of a 1 inch diameter methanol flame. Temperatures of 350 and 375°C were obtained near the wick of the flame, while temperatures of 980, 1150, and 1300°C were obtained along the central axis going towards the tip of the flame.

Bader (7) used chrome-alumel thermocouples peened into 1 inch square, 1/16 inch thick mild steel plates to measure the flame temperature of JP-4 jet fuel fires. This method was used to give a more stable temperature reading compared to a bare junction thermocouple. The thermocouples were arranged in a circular pattern so that three thermocouples, 120 degrees apart, were at each of 6 different levels above the fuel surface. The results of these measurements are

shown in Figure II-5. Bader states that an exact prediction of temperatures expected in a particular fire cannot be made. Figure II-5 shows the wide range of fire temperatures measured in "similar" fires and indicates the difficulty in predicting the temperature of a given fire. Over a large number of tests an average fire temperature will result and this value is approximately 1850^{o}F.

Gordon and McMillan (31) used thermocouples with the spacing shown in Figure II-6 to measure the temperature of flames from JP-4 fuel, burning in a 12 ft x 24 ft pan. Table II-5 shows the variation in flame temperature with height above the fuel. "Outer" refers to the mean of the thermocouples located near the pan edge and "inner" refers to the mean values of the remaining thermocouples. These temperatures are considerably lower than those obtained by Bader (7), but the variation between tests is smaller.

Welker used an optical pyrometer to measure the temperature of acetone, benzene, cyclohexane, and n-hexane wind-blown flames. The optical temperature was invarient with changes in wind velocity and these results are summarized in Table II-6.

Neill (50) also used an optical pyrometer to obtain the temperature of acetone, cyclohexane, n-hexane and JP-4 flames. These results are given in Table II-7.

Deshpande (24) used two chromel-alumel thermocouples to measure the temperatures of acetone, benzene, cyclohexane,

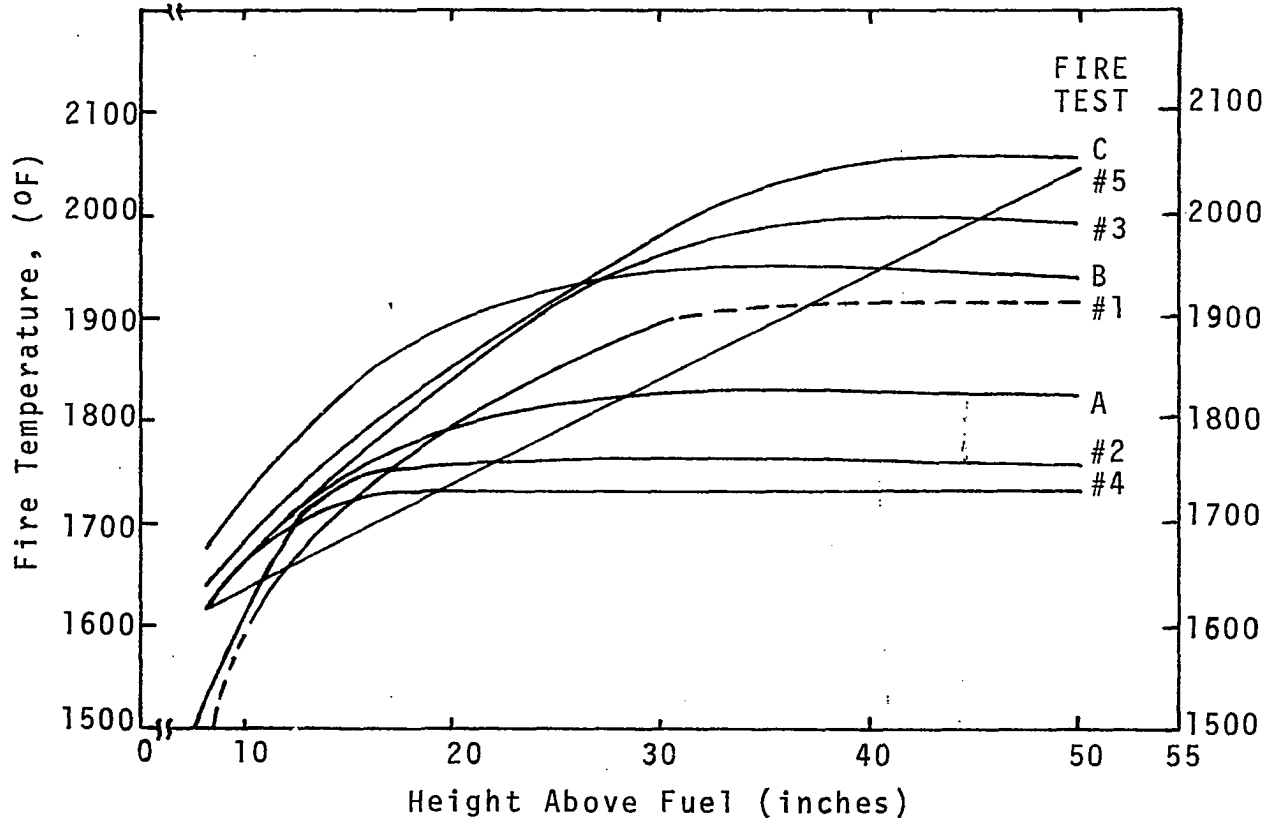


Figure II-5. Bader's Data for the Temperature Distribution in JP-4 Fuel Fires 5 Minutes After Ignition.

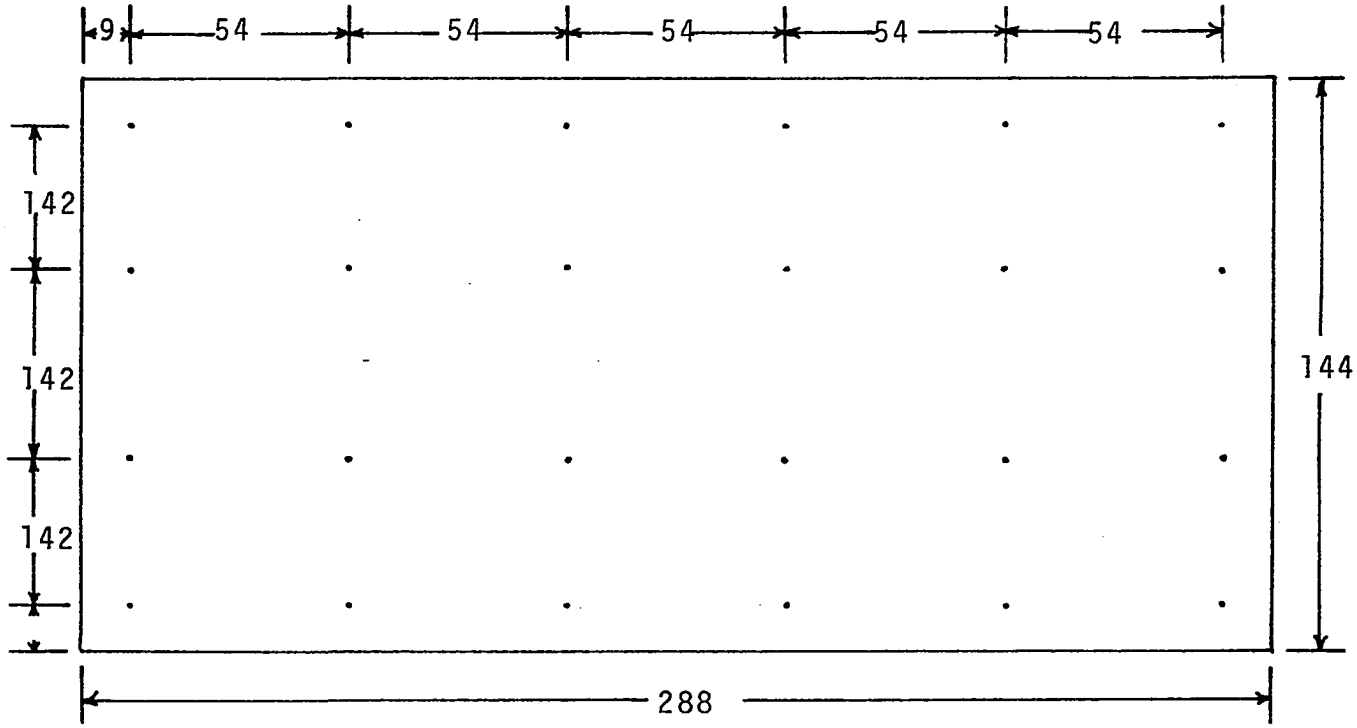


Figure II-6. Thermocouple Spacing used by Gordon and McMillan (31).

TABLE II-5

JP-4 Fuel Flame Temperatures from Gordon and McMillan (31)

Height Above Fuel Inches	Temperature, °F					
	Inner			Outer		
	Test 3	Test 4	Test 5	Test 3	Test 4	Test 5
6	1017	908	1094	1114	1115	1146
18	1343	1405	1455	1117	1171	1207
30	1598	1697	1594	1200	1269	1447
42	1490	1607	1697	1124	1198	1368
66	1409	1587	1573	1034	1064	1124

TABLE II-6

Optical Flame Temperatures from Welker (80)

Nominal Burner Dia., in	Optical Flame Temperature, °F			
	Acetone	Benzene	Cyclohexane	n-Hexane
6	2180	2080	2190	2240
8	2170	2040	2200	2240
12	2180	2020	2160	2200
18	2260	--	2200	2220
24	2300	--	--	--

TABLE II-7

Optical Flame Temperatures from Neill (50)

Burner Dia., in	Optical Flame Temperature, °F			
	Acetone	Cyclohexane	n-Hexane	JP-4
6	2182	--	2150	--
12	--	2035	2115	1980
18	2030	--	2015	--
24	2100	--	--	--

n-hexane and methanol flames. The tip of one couple was bare while the other was embedded in a copper rod of unspecified size, and shape. The location of the thermocouples in the flames was not given, but the author states that the temperature measured by the thermocouples was found to be a function of location in the fire. The mean temperatures obtained in this study are listed in Table II-8. Temperature variations between similar runs were several hundred degrees. In some runs the rod thermocouple gave readings higher than the bare couple, which should not have occurred if both thermocouples were at the same location.

Summary of Flame Temperature

From this survey, one can conclude that

1. Temperatures vary with position in flame.
2. Thermocouples appear to give lower flame temperatures

TABLE II-8

Flame Temperatures from Deshpande (24)

Nominal Burner Dia., in	Flame Temperatures, °F									
	Acetone		Benzene		Cyclohexane		n-hexane		Methanol	
	Bare	Rod	Bare	Rod	Bare	Rod	Bare	Rod	Bare	Rod
2	1290	--	1290	--	1250	--	1330	--	1550	--
4	1395	--	1257	--	1160	--	1245	680	1538	--
6	1325	--	1370	--	1200	--	1270	--	1240	--
8	1240	1010	1370	1380	1140	1100	1120	1090	1240	1170
12	1322	1375	--	--	1395	1440	1351	1317	1370	1350
18	1470	1500	--	--	1240	1300	--	--	1370	1260
24	1410	1350	--	--	--	--	1290	1400	1460	1310

than optical methods.

3. Considerable variation in flame temperature exists between similar flames.
4. The adiabatic flame temperature is not reached.
5. The burner size has no appreciable effect on the optical flame temperature.

Soot Formation

The published literature contains numerous articles on carbon or soot formation in flames. A detailed review of the literature is beyond the scope of this dissertation, but a brief discussion on soot formation is appropriate.

The process of soot formation is far from understood. The mechanism may depend on the temperature in the region of the flame in which the formation of free carbon occurs, on whether or not oxygen is present, and on the nature of the fuel. Porter (55) states that for all hydrocarbons at pressures near atmospheric, decomposition is the only reaction of importance above 1000°C with the single exception that the carbon polymer graphite is formed. The formation of carbon is, however, associated with the simultaneous or preliminary decomposition of the hydrocarbon to simpler molecules and not with polymerization to higher hydrocarbons. In spite of the diversity of method and the often conflicting results, the primary reactions occurring in homogeneous systems at high temperatures, mostly between 700°C and 1100°C, are fairly well represented by the following scheme:

Methane ⟶ Ethane, hydrogen

Ethane ⟶ Ethylene, hydrogen

Ethylene ⟶ Acetylene, hydrogen

Higher Paraffins ⟶ Lower paraffins, olefins

Higher Olefins ⟶ Lower olefins, paraffins, acetylene

Acetylene ⟶ Carbon, hydrogen

Aromatics ⟶ Carbon, hydrogen, acetylene, methane

Except in the case of aromatics the course of the reactions suggests that acetylene is the last product to appear before carbon formation. It is not surprising that only small amounts of acetylene are isolated in some cases as it decomposed very readily to carbon and hydrogen. This behavior partly explains the difficulty in interpreting the reactions of aromatics where a high temperature is required for decomposition, resulting in an apparent direct dissociation to carbon and hydrogen. There seems to be no doubt, however, that the condensation of aromatics occurs to a decreasing extent at temperatures above 750°C. Unless polymers of very high molecular weight are formed in the preheating zone, before temperatures of about 1000°C are reached, complete thermal decomposition will occur.

If oxygen is present, oxidation reactions will compete at every step with the thermal decomposition mechanism, and oxygen will also facilitate chain initiation. Even in

the low temperature oxidation of hydrocarbons, however, decomposition predominates over polymerization, unless high pressures and very low temperatures are used and the primary products isolated are lower hydrocarbons, aldehydes, alcohols, esters, peroxides, etc. Formaldehyde and methyl alcohol decompose mainly to CO and H_2 and consequently no carbon is observed either in thermal decomposition or their flames. All other compounds decompose thermally to hydrocarbons and CO and, therefore, no difference in the mechanism of the subsequent carbon formation is to be expected.

The formation of carbon from acetylene involves neither the formation of higher hydrocarbons nor a dissociation to C_2 and only one alternative remains-a simultaneous polymerization and dehydrogenation.

Behrens (9) states that soot formation occurs by a break-down of hydrocarbons and uniting C-atoms. The soot particles have colloidal dimensions and undergo considerable thermal diffusion in the high temperature gradient region of the burning zone, provided they are formed in the middle region of the reaction zone. The soot particles then migrate to the colder unburned mixture and to the interior of the flame cone over the burner; there they ascend along the inner conical surface of the flame till they reach the vertex and emerge, as in the benzol flame. When soot particles form at the downstream part of the burning zone, where the temperature gradient is again small, thermal diffusion no longer

plays a role, and the soot leaves uniformly overall sides of of the conical surface with the products of combustion. This is the acetylene type of soot distribution. In higher hydrocarbon flames (e.g. benzene, octane), soot formation occurs at the beginning of the combustion zone.

From their studies on methane, propane, ethylene and benzene flames, Arthur and Napier (4) concluded that there is no evidence that fuel type has any influence on the nature of the carbonaceous deposits obtained. Oxygen is present in the carbonaceous deposits in the form of associated hydroxyl and carbonyl groups. Diphenyl is not a main step in the formation of carbon in flames, but can be a by-product with some fuels. The material formed in flames and referred to a soot, lamp black and carbon black is composed mainly of carbon, hydrogen and oxygen. Although this material can be regarded as amorphous carbon with a graphite type of crystal lattice, the presence of covalently bound hydrogen and oxygen is an important feature of its structure and must not be ignored. Carbon cannot form by the polymerization of C_2. Carbon can be formed in flames by the pyrolysis of the fuel, but it is felt that pyrolysis alone is at most a minor part of the process of carbon formation. A probable initial state in carbon formation is decomposition to acetylene.

Fenimore, Jones and Moore (28) suggested that soot grows by deposition of carbon from simple hydrocarbons and that the growth is opposed by oxidation, by hydroxyl radicals

or perhaps that growth is by some reaction product of hydrocarbon with hydrogen atoms, and oxidation is by water. If oxidation is by hydroxyl radicals, one can rationalize the existance of a dead space between the blue-green reaction zone and the zone of carbon formation. It is reasonable to postulate that a large (perhaps nonequilibrium) concentration of hydroxyl exists in the reaction zone, and that this must decay somewhat before soot growth can occur. Soot formation occurs via acetylene since no burned gas was found to be free of acetylene. Benzene cannot give soot via acetylene, however because it is 17 times as effective a soot producer as acetylene, even when allowance is made for its greater carbon content, therefore, carbon may be formed from benzene in diffusion flames as well as from acetylene.

Gordon, Smith and McNesby (34) state that in many of the flames studied the acetylene concentration increases with the ability of the flame to form soot, in conformity with the mechanism postulated by Porter (55). However, there are some exceptions, the most glaring of which is the benzene diffusion flame. This flame is a most efficient soot former, yet is has an acetylene concentration about the same magnitude as that found in a methane diffusion flame, and the temperature distribution inside the flame is, if anything, somewhat lower than for the methane flame. Therefore, there must be materials other than acetylene which can form carbon particles. Unsaturated species must be present for carbon formation. In

a methanol flame where there is only a small percentage of any unsaturated hydrocarbon no soot is formed. The most likely way that carbon particles can be formed is via free radical addition to unsaturates, ultimately forming a polymer which does not depolymerize but rather dehydrogenates at higher temperatures. Ethylene found in the flame will certainly add radicals but at flame temperatures these radicals should be very unstable, and break down to ethylene and a small free radical. Acetylene offers a better path since the larger radical formed by the reaction of acetylene and the radical is probably more stable to the inverse reaction. Also by addition of two more acetylene molecules, benzene can be formed and the original radical regenerated. The benzene so formed is readily converted to a phenyl radical. Phenyl radicals can also be formed when the acetylene free radicals add two acetylene molecules and form a ring. These phenyl radicals add to benzene and produce large condensed rings with concurrent loss of H_2. The polynuclear aromatics can carbonize further by loss of hydrogen in the hotter regions of the flame. Indeed in a study of the pyrolysis of methane, one of the authors was able to detect evidence for the existence of many polynuclear aromatic hydrocarbons in the products. This mechanism would also account for the excellent ability of benzene to carbonize since the phenyl radical would be able to add to the benzene parent forming a large free radical which in turn would add more benzene, and rapidly form a large polynuclear configuration with concurrent loss of H_2.

Acetylene can take the place of a benzene molecule in these reactions, and an acetylenyl free radical can replace a phenyl radical. Thus the carbonaceous particle is probably a copolymer of benzene and acetylene. Large free radicals can combine. In a highly condensed ring system, the free electron is mobile so that the steric factor for the re-combination reaction between two large radicals should not be much smaller than for methyl radical re-combination. This reaction must be important in forming soot particles, since the maximum size of soot particle occurs in the part of the flame where all the small precursor molecules have almost entirely disappeared.

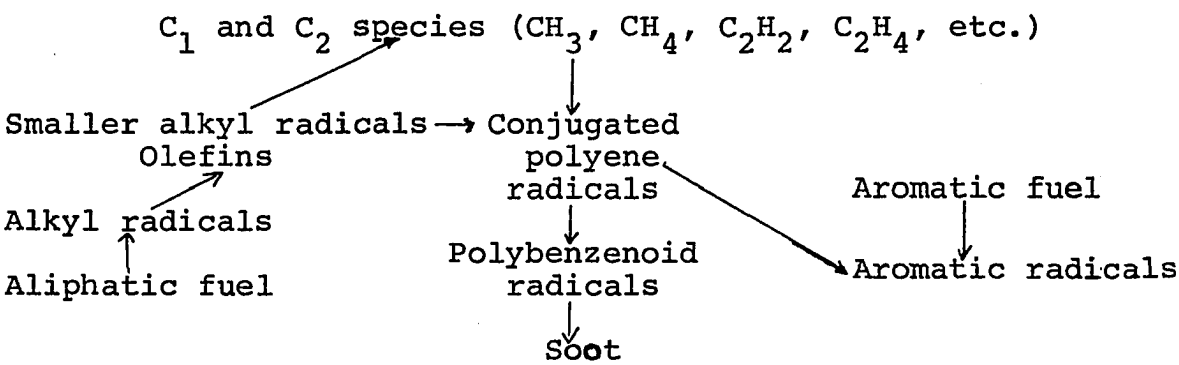
Tesner (70) implies that the formation of carbon black by thermal decomposition of hydrocarbons is a process of formation of a dispersed phase and takes place in two stages: nucleus formation and particle growth. These stages have different mechanisms. The temperature required to form carbon black nuclei is much higher than that necessary for particle growth or for decomposition of the hydrocarbon on the walls to form a layer of solid carbon. For the decomposition of benzene, the carbon layer begins to form at a measurable rate of 750°C, while carbon black particles appear only at 950°C. Thus to form carbon black nuclei by the decomposition of a hydrocarbon, the latter must be "superheated" at 150 to 200°C. The rate of nucleus formation and of particle growth depend essentially on the temperature, and,

therefore, the rate of heating of the hydrocarbon is the most important factor, determining the overall rate of the decomposition and the degree of the resulting carbon black.

Stehling, Frazee and Anderson (67) found that there is no sharp dividing line between carbon-with hydrogen, hydrocarbon groups or even free electrons on edge atoms and corners and condensed aromatic structures. Even graphite fits as the end-product in a gradual change starting from benzene. Once the earlier stages of dehydrogenation are accomplished, it is apparent that there are two basic types of compounds which may serve as starting points for building up such structures: acetylenic and aromatic compounds. Both represent structures which have been sufficiently stripped of hydrogen so that unusually strong carbon-to-carbon bonding is possible. The low reactivity of benzene, napthalene, etc., as contrasted to acetylene and vinylacetylene shows that carbon formation cannot, in general, result from polymerization of compounds such as acetylene to polycyclic aromatics which then undergo condensation and dehydrogenation to f m carbon. With all of the acetylenic compounds-acetylene itself, vinylacetylene and octatriyne there is a concentration effect, with decomposition and carbon formation occurring more readily at higher total or partial pressures. This behavior indicates that early stages of reaction involve energy build-up by combination reactions, probably involving a diradical or similar excited state. With sufficient diluent present, simple

polymerization would occur, but if the energy is cumulative, ordinary free radicals can be formed in later steps.

Thomas (71) states that soot is not carbon, but an aggregate of large polybenzenoid hydrocarbon radicals. Another conclusion is that compounds isolated from flames are not necessarily intermediates in the process of soot formation, but are species that have fallen by the wayside. They are products of premature chain termination. The very fact that they have been isolated means that they were not reactive enough to go on to form soot. Based on simple considerations of time and temperature, Thomas proposes that the growing intermediates in the soot formation process are highly conjugated free radicals and presents the following proposed scheme of reactions.



(Very large polybenzenoid radicals)

Based on their study of carbon formation from aromatic hydrocarbons, Davis and Scully (23) concluded the following:

1. Benzene rings favor soot formation.
2. Attached methyl groups promote soot formation even further.
3. Hydrogen acts as an inhibitor.
4. Hetero-atoms contained in aromatic rings lead to ring rupture and to inhibition of soot formation.
5. Hetero-atoms attached to rings in general inhibit soot formation due to ring rupture (dominated by the stability at high temperatures of such species as CO and CN), but NO_2 groups attached to aromatic rings detach themselves as such.
6. Polycondensed aromatics favor soot formation.
7. Five-membered rings are unstable unless they are attached to an aromatic ring as with idene.
8. Chlorobenzene produced the highest soot yield of any compound studied. This is due to the ready formation of hydrogen chloride and the polymerization of phenyl radicals.
9. There is evidence of ring-fission followed by ring-closure mechanims operating as with o-toluidine.
10. Any excess oxygen and possible other oxygen-containing compounds can strip off methyl groups from aromatic side chains, resulting in a decreased yield of soot.

This survey on soot formation is necesarily brief and Gaydon and Wolfhard (30) aptly summarizes the presentation by stating that in spite of all the published information, it cannot be said quantitatively for a particular flame how much carbon is formed by a particular process.

CHAPTER III

FLAME HEAT TRANSFER

Energy Transfer Mechanism in a Flame

The mechanism whereby energy is transferred from a flame to a solid is not clearly understood. Kilham (39) lists the following possible processes:

1. Convection from the hot flame gases to the solid.
2. Radiation from hot flame gases.
3. Catalytic combination of free radicals or atoms in the flame gases, on the surface of the solid, with liberation of energy. It has been demonstrated from spectroscopic data that free radicals and atoms such as CH, OH, C_2O and H have a transient existence in combustion processes, and it is, therefore, conceivable that these unstable species may undergo recombination on the surface of a solid.
4. Catalytic combustion on the surface of the solid. Flameless incandescent surface combustion by burning gas-air mixtures in contact with surfaces of refractory materials at red heat have been obtained. The Bone-M'Court radiophragm process was developed along these lines.

5. Transference of excess energy by collision of high-energy gas molecules with the solid. During combustion processes, the energy which is liberated does not always appear immediately as an increase in the kinetic energy of the molecules of the system. Part of the energy may be used up in raising the potential energy of some particular species and a finite time may elapse before this energy either appears as radiation or is degraded to normal thermal energy of the molecules.
6. Exothermic displacement of equilibria, e.g., the water gas equilibrium. The temperature of a solid immersed in a flame will always be less than the temperature of the flame gases, consequently its presence will lead to a modification of the water gas equilibrium in the gases in its vicinity. Lowering the temperature of the gases will result in increased formation of carbon dioxide and hydrogen, with consequent emission of heat.

Method for Obtaining Heat Flux from Flames

In general the majority of heat transfer to a body inside a flame is by convection and radiation; the other processes, if taking place at all, would only be expected with certain combinations of gases and solids. For this study it is assumed that the convective and radiative transfer are independent of one another. This somewhat simplifies the problem solution since the coupled radiative transport and momentum transport equations are harder to solve.

Referring to Figure III-1, and writing a heat balance around the probe,

$$q_r + q_c = q_e + q_w + \rho_p\, q_r \qquad \text{(III-1)}$$

where q_c = net convective flux from flame to probe, Btu/hr-ft^2

q_e = radiative flux emitted by probe, Btu/hr-ft^2

q_f = radiative flux leaving flame, Btu/hr-ft^2

q_m = radiative flux measured by radiometer, Btu/hr-ft^2

q_r = radiative flux from flame to probe, Btu/hr-ft^2

q_w = flux removed by water, Btu/hr-ft^2

ρ_p = reflectivity of probe

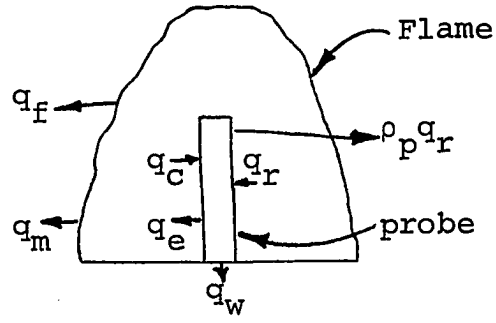


Figure III-1. Probe Heat Fluxes.

The flux removed by the water q_w is calculated from

$$q_w = W\, C_w\, (T_{wo} - T_{wi})/A_p \qquad \text{(III-2)}$$

where W = mass flow rate of water in probe, lbm/hr

C_w = specific heat of water, Btu/lbm-°F

T_{wo} = temperature of water leaving probe, °F

T_{wi} = temperature of water entering probe, °F

The radiative flux emitted by the probe q_e is obtained from

$$q_e = \varepsilon_p \sigma T_p^4 \qquad \text{(III-3)}$$

where ε_p = emittance of probe surface

T_p = temperature of probe surface, °R

σ = $0.1714(10^{-8})$, Btu/hr-ft^2-°R

For fuels that burn with a luminous flame, a layer of soot is deposited on the probe shortly after ignition, therefore, an emittance of 1.0 is assumed. Without soot an emittance of 0.8 is obtained for oxidized stainless steel. The radiative flux leaving the flame will be obtained from the radiative flux measured by the radiometer, q_m. The radiative flux from the flame to the probe, q_r, will be obtained from the solution of the radiative transport equation. This solution will be discussed in more detail later in this chapter. The convective flux from flame to probe, q_c, will then be calculated from Equation III-1. This flux can also be obtained from

$$q_c = h\ (T_f - T_p) \qquad \text{(III-4)}$$

where h = convective heat transfer coefficient, Btu/hr-ft^2-°F

T_f = flame temperature, °R

Unfortunately the heat transfer coefficient, h, is unknown, but estimates can be obtained from

$$Nu = C_1 (Re)^m (Pr)^{n1} \qquad \text{(III-5)}$$

where Nu = Nusselt number = hX/K

C_1 = constant

Re = Reynolds number = $XV\rho/\mu$

Pr = Prandtl number = $C_p\mu/K$

m = constant

n_1 = constant

X = characteristic dimension of surface, ft

K = thermal conductivity of fluid, Btu/hr-ft^2-°F/ft

V = velocity of fluid, ft/hr

μ = absolute viscosity of fluid, lbm/ft-hr

C_p = specific heat of fluid, Btu/lbm-°F

ρ = density of fluid, lbm/ft^3

The prediction of convective heat transfer coefficients will be discussed in greater detail later in this chapter.

Review of Flame Total Heat Flux Data

Experimental data on total heat transfer rates from natural flames are scarce. Bader (7) constructed three heat flux meters and inserted them at different locations in fires from JP-4 fuel burning above 18 ft square pans (324 ft^2 area). The highest incident heat flux measured in each test varied from 25,960 to 47,540 Btu/hr-ft^2. Bader neglected the heat input due to convection and considered the fire to be a black-body source. The heat flux meter was essentially a thin

steel plate with one face exposed to the fire and the other face exposed to a copper slug. For accurate data, the steel must achieve a steady-state temperature and the copper temperature should be less than 300°F. A small part of Bader's data is given in Table III-1. From these data, it is doubtful that fluxes in excess of 36,000 Btu/hr-ft^2 were obtained.

Copley (18) presents an analytical expression for the temperature-time history for an infinite hollow cylinder enveloped by a luminous flame. The flame and the outer surface of the cylinder were assumed to be graybodies. A large cylinder (11.61 in O.D. x 40 in long) and a small cylinder (3.92 in O.D. x 13.5 in long) were suspended horizontally in the center of an 18 ft long by 10 ft wide by 1 ft deep fuel pan. The center line of each cylinder was approximately 36 in above the fuel surface. One hundred and ten gallons (approximately 1 in depth) of military grade JP-4 jet fuel were used in each test which lasted approximately 5 minutes. The slope of the temperature-time curves is approximately constant up to 150 seconds, after which the flames began to subside. These values were used in the analytical equation to calculate a surface heat flux of 30,400 Btu/hr-ft^2 for the large cylinder and 30,800 Btu/hr-ft^2 for the small cylinder. The Stefan-Boltzmann equation and flame temperature data were used to calculate the radiant heat flux to the small cylinder. These values were plotted against time and graphically integrated between 20 and 150 sec to give an average heat flux of 31,400 Btu/hr-ft^2.

TABLE III-1

Bader's Heat Flux Meter Data

Meter No.	Height Above Fuel, in	Test Time min	Steel Temperature °F	Copper Temperature °F	Flux Based on Steel Temperature Btu/hr-ft^2	Flux Based on Steel and Copper Temperature Btu/hr-ft^2
1	29	3	1270	200	30706	30381
		5	1200	320	26030	25396
		8	1270	510	30706	29189
2	21	3	1230	190	27964	27658
		5	1200	300	26030	25458
		8	1230	465	27964	26709
3	34	3	1330	210	35192	4847
		5	1350	400	792	35854
		7	1370	810	38444	33985

The flame temperature was obtained from time-averaged measurements of several shielded iron-constantan thermocouples placed in the fire. The measured flame temperatures varied between 1500°F and 1700°F; the mean value was 1610°F.

Law (40) states that fires in organic liquids have similar temperatures and a value of 1100°C (2012°F) is suggested based on the results of Rasbash, et al. (57). The flame emittance depends on the thickness but over about 1.5 meters (59.06 in), their emittance can be taken as unity, giving a radiation intensity of about 17 W/cm^2 (53,890 $Btu/hr-ft^2$). A flame temperature of 2012°F gives a heat flux of 64,000 $Btu/hr-ft^2$; therefore, Law made an error in the flux calculation. She also states that for a tank surrounded by petrol flames in a dike, fluxes of 6.3 to 8.8 W/cm^2 (19,971 to 27,896 $Btu/hr-ft^2$) for uncooled tanks were obtained. In this case the flames are thin and not highly emissive; therefore, the fluxes are consistent with a flame temperature of the order 1100°C.

Neill (50) obtained total heat transfer rates by inserting a water filled boiler type heat transfer probe (4.475 inch diameter) into flames from 7 fuels using 3 burner sizes and a cluster of nine 6-inch burners. The soot accumulation on the probe resulted in an exponential decrease in heat tranfer with time. Initial total heat transfer rates are given in Table III-2.

TABLE III-2

NEILL'S INITIAL TOTAL HEAT TRANSFER RATES
(Btu/hr-ft^2)

Fuel	Burner Size			
	Single 12-inch	Single 18-inch	Single 24-inch	Cluster of 9[a] 6-inch
Methanol	5,500	7,250	9,000	--
Acetone	9.100	12,000	14,500	12,500[b]
Hexane	15,000	20,500	--	30,000
Cyclohexane	16,000	15,000[c]	--	26,000
JP-4	9,600	19,500	--	31,000
Napalm Test Solvent	13,000	--	--	--
Benzol	11,500[d]	--	--	--

[a]Eight 6-inch diameter burners clustered around a single center burner, all spaced 12 inches apart.

[b]Flames probably not completely merged.

[c]Data obtained from unstable fire.

[d]Data questionable, unable to confirm fire coverage.

Deshpande (24) used a three-turn coil of 1/4-inch copper tubing as a heat flux meter to measure the total heat transfer from flames of four fuels in circular burners. The length of the tubing inside the fire was about 2 feet and the coil was mounted 8 inches above the liquid fuel surface. The results of this study are given in Table III-3. These results are the maximum values obtained and decrease with time due to soot formation on the coil.

TABLE III-3

DESHPANDE'S TOTAL HEAT TRANSFER RATES, BTU/HR-FT^2

Fuel	Burner Diameter, in			
	8	12	18	24
Acetone	16,100	22,100	29,600	19,500
Cyclohexane	14,500	30,900	32,900	--
n-Hexane	16,200	21,800	--	--
Methanol	14,550	18,900	16,050	22,400

Thomas, et al. (73) used a heat flux meter mounted 1-2 cm (0.39-0.79 in) above the fuel surface of a 91 cm (35.83 in) diameter ethyl alcohol flame to measure the total heat transfer back towards the fuel surface. Total heat transfer rates of 0.95, 1.04 and 0.86 cal/cm^2-sec (12,608, 13,803 and 11,414 Btu/hr-ft^2) were obtained at a radius of 0, 19, and 38 cm (0, 7.48, 14.96 in).

Wood, et al. (83) measured the heat flux from methanol and acetone flames back to the fuel surface. A 5-foot diameter aluminum pan was filled with sand, which was then saturated with fuel. Acetone burned at a steady rate almost immediately after ignition for about one minute, and methanol provided a steady burning rate for approximately 3 minutes. Radiometers were constructed and located at a radius of 0, 8.23, 15.12, and 22.64 inches in the burner. These radiometers did not have windows and the flux measured should be a total flux, even though the authors claimed it to be a radiant flux.

These values are plotted against time after ignition and the methanol data shows a constant flux for a short time period, while the acetone data does not. Estimated mean fluxes are 863, 557, 425, and 319 Btu/hr-ft^2 for the methanol flame and 1221, 1221, 1035, and 571 Btu/hr-ft^2 for the acetone flame for a radius of 0, 8.23, 15.12, and 22.64 inches respectively. These values are very low and there appears to be an error either in the scale of the figure or in designating that the values are fluxes. In an appendix Wood, et al., treat these measured values as intensities, yet the type of radiometers used normally measures the heat flux. In another figure values of total radiant heat flux to the surface of the burner are plotted against time. For the steady burning rate period, the methanol flame flux is 2124 Btu/hr-ft^2 and the acetone flame flux is 4247 Btu/hr-ft^2. These values are approximately equal to the sum of the fluxes measured at the 4 positions. One should use these data with caution.

Radiative Heat Transfer Theory

Since a flame is a burning gas that can emit, absorb, and scatter radiation, the mechanism and solution of radiative transfer is applicable. Radiative properties of gases exhibit very irregular wavelength dependencies. As a result the absorption or emission by gases is significant only in certain wavelength regions, especially at temperature levels below a few thousand degrees Kelvin. A brief description of radiation

in gases will be given. For additional details, one should consult Penner (53), Tien (77), or Siegel and Howell (63).

A radiating gas is composed of molecules, atoms, ions, and free electrons. These particles have various energy levels associated with them. The photon is the basic unit of radiative energy. Radiative emission will consist of the release of photons of energy, and absorption will be the capture of photons by a particle. When a photon is emitted or absorbed, the energy of the particle will be correspondingly decreased or increased. The absorption or emission of thermal radiation is associated with transitions between energy levels of the atoms or molecules that constitute the gas. These transitions are classified as bound-bound, bound-free, and free-free.

A bound-bound transition occurs when a photon is absorbed or emitted by an atom or molecule and there is no ionization or recombination of ions and electrons. The atom or molecule moves from one quantized bound energy state to another. These states can be rotational, vibrational, or electronic in molecules, and electronic in atoms. Since the bound-bound energy changes are associated with specific energy levels, the absorption and emission coefficients will be sharply peaked functions of frequency in the form of a series of spectral lines. These lines do not have a finite width due to various broadening effects, such as, natural broadening,

Doppler broadening, collision broadening, and stark broadening. Natural broadening results from the uncertainty in the exact levels of the transition energy states, which is related to the Heisenberg uncertainty principle. Doppler broadening is important at high temperature and occurs because the atoms or molecules of the gas are not stationary, but have a distribution of velocities associated with their thermal energy. If an atom or molecule is moving with a certain velocity and is emitting at a certain frequency then the frequency of the waves reaching an observer will be longer if the emitter is moving towards the observer and shorter if the emitter is moving away from the observer. Collision broadening results when the collision rate experienced by any given atom or molecule of the gas is increased due to an increase in the gas pressure. Collision broadening is important at high pressures and low temperatures and is often the chief contributor to line broadening for engineering infrared conditions. Stark broadening occurs when strong electrical fields are present. It often occurs in ionized gases due to radiating particle interactions with the electrons and protons. Stark and collision broadening are often lumped under the general heading "pressure broadening." Both effects depend on the pressure of the broadening component of the gas. Broadening has been discussed here under the assumption that only one atomic or molecular species is present in the gas. If the gas consists of more than one component, then collision broadening in the gas

is caused by both collisions with like molecules (self-broadening) and by collisions with other species.

Vibrational energy modes are always coupled with rotational modes. The rotational spectral lines superimposed on the vibrational line give a band of closely spaced spectral lines. If these are averaged together into one continuous region, it becomes a "vibration-rotation" band. Rotational transitions within a given vibrational state are associated with energies at long wavelengths, $\sim$ 8 to 1000 microns. Vibration-rotation transitions are at infrared wavelengths of about 1.5 to 20 microns. Electronic transitions are at short-wavelengths in the visible region, 0.4 to 0.7 microns, and at portions of the ultraviolet and infrared near the visible region. At industrial temperatures the radiation is principally from vibrational and rotational transitions; at high temperatures (above several thousand °R), it is the electronic transitions that are important.

A bound-free absorption (photoionization) occurs when an atom absorbed a photon with sufficient energy to cause ionization. The resulting ion and electron are free to take on any kinetic energy; hence the bound-free absorption coefficient is a continuous function of the photon energy frequency as long as the photon energy is sufficiently large to cause ionization. The reverse process is a free-bound emission (photorecombination). Here, an ion and free electron combine, a photon of energy is released, and the energy of the resulting

atom drops to that of a discrete bound state. The free-bound emission produces a continuous spectrum as the combining particles can have any initial kinetic energy. Since bound-free transitions occur only when the gas is ionized, radiation absorption and emission stemming from these processes are generally important only in high-temperature applications.

A free-free transition results when a free electron passes near an ion and interacts with its electric field. The electron can absorb a photon thereby going to a higher kinetic energy, or it can emit a photon and drop to a lower free energy. Since the initial and final free energies can have any values, a continuous absorption or emission spectrum is produced. A free-free transition can also be produced if an electron passes very close to a neutral atom, since very close to an atom an electric field may exist. This process is much less probable than electron-positive ion interactions. In general, the absorption and the emission of radiation by free-free transitions are less important than by bound-free transitions.

In addition to absorption, a medium may also scatter photons, Scattering is defined as any change in the direction of propagation of the photons. This process is due to local nonhomogeneities within the medium, resulting from suspended solid particles or liquid droplets. Scattering can also be produced by the gas molecules. When radiant energy is scattered with no change in frequency, the scattering is referred to as coherent scattering.

If the scattering of radiation in a gas is strictly molecular scattering (i.e., there are no foreign particles present), it is designated as Rayleigh scattering. The Rayleigh theory predicts that the spectral intensity of the scattered radiation will vary as the fourth power of the frequency; that is, the scattering is predominantly at the shorter wavelengths. Rayleigh scattering is important in atmospheric phenomena, but it is usually unimportant in engineering applications. Mie scattering is concerned with electromagnetic scattering from spherical particles. This theory is applied to situations where foreign particles are present in the gas. Additional information can be obtained from Love (42), and Siegel and Howell (63).

Problems involving radiative heat transfer in absorbing, emitting and scattering media can be solved by two methods. Method 1 makes no assumption about thermal equilibrium whereas method 2 requires thermal equilibrium or local thermal equilibrium. Both methods are based on the solution of the transport equation (A-14) developed in Appendix A. This equation is

$$\frac{1}{C}\frac{\partial I_\lambda}{\partial t} + \vec{s}\cdot\nabla I_\lambda = J_\lambda - \beta_\lambda I_\lambda \qquad \text{(III-6)}$$

where I_λ = monochromatic intensity, Btu/hr-ft^2 - micron-steradian

C = speed of light, ft/hr

t = time, hr

β_λ = monochromatic extinction coefficient, ft^{-1}

J_λ = effective monochromatic volume emission coefficient, Btu/ft^3-hr - micron-steradian

$\hat{s}$ = unit vector in the direction of motion

In the derivation of the equation of transfer, frequency was chosen to designate the monochromatic field properties because the energy of a photon is proportional to the frequency and is conserved as the photon traverses different media. The speed of light in a given medium is related to that in a vacuum by

$$C = C_o/n \qquad \text{(III-7)}$$

where C_o = speed of light in a vacuum, ft/hr

n = index of refraction of media

Now the wavelength λ, is given by

$$\lambda = C/\nu \qquad \text{(III-8)}$$

where ν = frequency, hr^{-1}

Thus, the wavelength corresponding to a fixed frequency will vary with the media through which the energy propagates. For gases $n \simeq 1$; therefore, the use of λ or ν as subscripts for monochromatic properties is interchangeable. Throughout the remainder of this dissertation, λ will be used as a subscript for monochromatic properties since reported data are in terms of wavelength.

For steady state conditions Equation III-6 reduces to

$$\vec{s}\cdot\nabla I_\lambda = J_\lambda - \beta_\lambda I_\lambda \qquad \text{(III-9)}$$

If the coordinate s is laid off in the direction of the unit vector $\vec{s}$, the directional derivative $\vec{s}\cdot\nabla I_\lambda$ becomes dI_λ/ds and Equation III-9 becomes

$$\frac{dI_\lambda}{ds} = J_\lambda - \beta_\lambda I_\lambda \qquad \text{(III-10)}$$

This equation is a nonhomogeneous, linear, first order differential equation that can be solved with the integrating factor $e^{\int \beta_\lambda ds}$ to give

$$I_\lambda = I_\lambda(o)\ e^{-\beta_\lambda s} + (J_\lambda/\beta_\lambda)(1 - e^{-\beta_\lambda s}) \qquad \text{(III-11)}$$

where $I_\lambda(o)$ is the intensity at s = o. If Equation III-10 is divided through by β_λ, and the term $\beta_\lambda ds$ is replaced by $d\tau$, the following equation is obtained

$$\frac{dI_\lambda}{d\tau} = \frac{J_\lambda}{\beta_\lambda} - I_\lambda \qquad \text{(III-12)}$$

Now τ is called the "optical thickness" of the medium and is defined as

$$\tau = \int_0^s \beta_\lambda\ ds \qquad \text{(III-13)}$$

Method 1 uses experimental values of J_λ and β_λ in Equation III-11 to obtain the intensity variation in a flame.

Method 2 assumes no scattering, therefore, $J_\lambda = j_\lambda$ and $\beta_\lambda = \kappa_\lambda$ where j_λ is the monochromatic v lume emission

coefficient Btu/ft^3-hr - micron-steradian, and κ_λ is the monochromatic absorption coefficient, ft^{-1}. Since local thermodynamic equilibrium exists then j_λ can be expressed as

$$j_\lambda = n^2 \kappa_\lambda I_{b,\lambda}(T) \qquad \text{(III-14)}$$

where $I_{b,\lambda}(T) = 2h_p C_o^2/[n^2\lambda^5(e^{h_p C_o/n\lambda kT} - 1)]$ = monochromatic intensity of a blackbody, Btu/hr-ft^2 - micron-steradian

h_p = Planck's constant

k = Boltzmann's constant

T = temperature of medium, °R

Equation III-12 can now be written as

$$\frac{dI_\lambda}{d\tau} = n^2 I_{b,\lambda}(T) - I_\lambda \qquad \text{(III-15)}$$

This equation has been solved numerous times for a medium between infinite parallel plates. Solutions also exist for a medium between concentric spheres and infinitely long concentric cylinders. Most of these solutions are exercises in mathematics or comparisons of approximate solutions to the equation of transfer, and are not very useful in a practical sense.

For heat transfer purposes, the heat flux is the quantity of interest and it can be obtained by

$$q_\lambda = \int_\Omega I_\lambda \cos\theta \, d\Omega \qquad \text{(III-16)}$$

where q_λ = monochromatic heat flux, Btu/hr-ft^2-micron

θ = angle between surface normal and the direction of the intensity vecter, degrees

Ω = solid angle between gas volume and target, steradian

For the total heat flux Equation III-14 must be integrated over the entire frequency range as follows:

$$q = \int_0^\infty q_\lambda \, d\lambda \qquad \text{(III-17)}$$

where q = total heat flux, Btu/hr-ft^2

Methods for Obtaining Absorption and Emission Coefficients

In order to solve the radiative transport equation values of J_λ and β_λ are needed. For thermodynamic equilibrium, expressions for the monochromatic absorption coefficient can, in principal, be derived through the application of quantum mechanics. However, with the exception of monatomic and diatomic gases, the complexity of the calculations has made this approach generally impractical. Absorption coefficients can also be obtained from spectral data, and this technique will be briefly discussed.

Earlier it was mentioned that bound-bound transitions of an atom or molecule result in numerous spectral lines with a very small frequency spread, often called discrete spectra, while bound-free and free-free transitions yield continuous spectra. The spectral lines for bound-bound transitions are

generally broadened due to four effects, and the resulting line-overlapping produces a band spectra. Isolated spectral lines are usually observed in the atomic spectra due to electronic transitions. The shape of this line depends on the type of broadening. The profile of spectral lines is important because it determines how the emission or absorption varies with pressure, temperature, optical path length and the intrinsic properties of the radiating gas. The width of a line can be arbitrary, and it is conventional to use the half-intensity width, sometimes called the line half-width, that is, the width at the half of the maximum intensity level. Correlations exist for the absorption coefficient in terms of line half-width and frequency for the different broadening mechanisms.

In most cases of practical interest, spectral lines overlap. When this occurs, each line cannot absorb as great a fraction of the radiation as when it is isolated, therefore, a band of overlapped lines always absorbes less than a band of isolated lines. The radiation from a band of overlapping lines depends on the spacing between spectral lines, their intensity, and half-width variations. The many rapid variations of the absorption coefficient in a band with respect to frequency make it extremely difficult to calculate the band emittance or absorptance even with a large computer.

Within a small frequency range in a band, the mean spectral emittance over this range can be represented with reasonable accuracy by theoretical models, called band models or narrow-band models. They are useful not only for calculating the mean spectral emittance in a band, but also for correlating experimental data obtained from low-resolution spectra meters. To calculate band emittances or absorptances, further approximations are needed to indicate the frequency dependence of the mean spectral emittance through the variations of mean line intensity, half-width and line spacing in the band. These approximations are often called the wide-band models.

There exist several theoretical band models depending on regular spacing between the spectral lines. For most practical situations, it is sufficient to consider only the two models representing two extreme arrangements of the spectral lines. These are the Elasser model and the statistical model. The Elasser model assumes that the spectral lines are equally spaced and all have the same intensity and half-width. This rejoin presentation is good for the spectrum of most diatomic gases such as CO, NO, etc., and other triatomic gases under certain conditions such as CO_2 and N_2O at small path lengths so that only the stronger, regularly spaced lines appear. The statistical model of a band, sometimes called the Mayer-Goody model, assumes that the location of the spectral lines is randomly distributed. This case often results for the spectra of relatively complex molecules such as H_2O, CO_2, and other

polyatomic molecules. The derivation of the mean spectral emittance involves the probability distributions of line intensities and positions. The Elasser model always predicts a greater absorption than the statistical model since regular spaced spectral lines have less overlapping. The deviation in general is small, and in no case exceeds 20 percent. The two models coincide in both the weak and strong absorption limits.

Since exact numerical calculation of band radiation is difficult, a number of approximate methods have been developed. The box model, the exponential wide-band model, and a single continuous correlation are three of these methods. They do not yield any indication of the frequency dependence of the mean spectral emittance, but are very simple and convenient in predicting band emittances.

The box model approximates a band by a rectangular box of calculable width (effective band width) with a suitably determined average absorption coefficient. Penner (53) has successfully applied this method to the evaluation of band emittance of diatomic gases. It may also be employed for polyatomic gases as a first approximation. This method is restricted to moderately high pressures and small or medium path lengths because the line structure of the band is not accounted for. The effective band width is determined from the relative intensities of the rotational lines in a

vibrational-rotational band. The average absorption coefficient is obtained from the integrated intensity of the band.

Edwards and Menard (26) considered various models for the band absorption of vibrational-rotational bands. Based on the consideration of different molecular models of the vibrating rotator and of different narrow band models, they concluded that three parameters are necessary for a complete description of band absorption. These are the mean line intensity to spacing ratio, the mean line-width to spacing ratio at 1 atm, and the effective broadening pressure. They suggested empirical functions for the first two parameters. The parameter for the mean intensity to line spacing is an exponential function and this function led to the name exponential wide-band model. Edwards and Menard obtained a number of approximate expressions for the band absorption by substituting the first two parameters into the general statistical model.

A single continuous correlation is desirable for the total band absorptance or the band emittance over the whole path-length range. Tien and Louder (78) arrived at such an expression by considering a set of common mathematical properties of the total band absorptance, i.e., total band absorptance must be a positive, monotonically increasing function of mass path length, it must have its maximum slope at the optically thin limit, and in dimensionless form, the function for total band absorptance must posses two asymptotes.

The preceding discussion on line and band radiation is limited to homogeneous gas bodies. In general, the nonhomogeneity in the gas body is characterized by the local temperature, pressure, and concentration. No exact solution exists for the general problem of radiation from nonhomogeneous paths. The Curtis-Godson approximation is the most useful and convenient solution to the problem. This method assigns to a nonhomogeneous path an equivalent homogeneous path with suitably defined spectroscopic parameters. The radiation from such an equivalent path can then be calculated as in the case of homogeneous paths. The Curtis-Godson approximation is exact in the weak- and strong-line limits, with and without overlapping of lines. For the intermediate range, it also provides a good representation.

The discussion on line and band radiation was only concerned with radiation resulting from bound-bound transitions. The results are important and useful in most engineering systems, where the temperature of the gas is usually 100°-1000°K. At temperatures above 1000°K, bound-free and free-free transitions become important radiation mechanisms as a consequence of ionization or dissociation of the atom or molecule. These mechanisms result in continuous absorption or emission. Their coefficients are related to the Einstein coefficient for induced absorption. Calculation of the Einstein coefficient is extremely involved and has been done only for atoms of relatively simple structure. Utilizing the

simple correspondence principle in earlier quantum theory, Kramers first obtained the theoretical result of the absorption coefficient for bound-free transitions (or photoionization) of the hydrogen atom. Subsequent quantum-mechanical calculations indicate that this result can be used for other free-bound and free-free transitions when corrected by use of the Gaunt factor.

The discussion on calculating absorption coefficients from spectral data is brief and additional details can be found in Tien (77). Due to the complexity of calculations and the lack of spectral data, it is believed that absorption coefficients can be obtained easier from experimental data. The above techniques were based on the assumption of thermodynamic equilibrium with no scattering. Flames are not in thermodynamic equilibrium and may not even be in local thermodynamic equilibrium, so these methods may not be useful at all.

Hood (33) used the boundary condition that $I_\lambda(0) = 0$ at $s = 0$ in Equation III-11 to obtain the following equation for the intensity from a flame

$$I_\lambda = \frac{J_\lambda}{\beta_\lambda} (1 - e^{-\beta_\lambda s}) \qquad \text{(III-18)}$$

This boundary condition assumes no external radiation source and can be visualized by referring to Figure III-2. Hood obtained average values of J_λ and β_λ from 1/2 inch to 3/4 inch laminar diffusion flames for acetone, benzene, cyclohexane, n-hexane, and methanol. Measurements were made of the

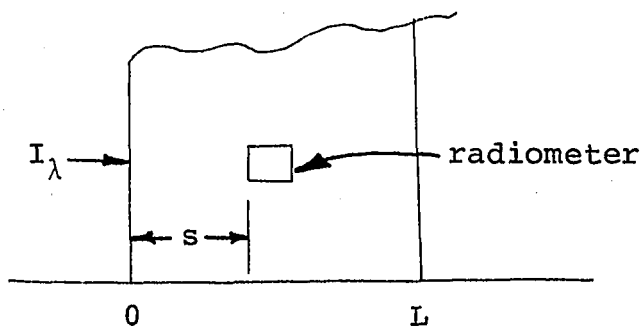


Figure III-2. Geometry for Intensity Variation Through a Flame.

intensity of the flame, intensity of a globar source, intensity of the globar source focused through the flame, and the path length through the flame. Using these measurements the average value of β_λ was obtained from

$$e^{-\beta_\lambda s} = \frac{I_\lambda \text{ (attenuated source + flame)} - I_\lambda \text{ (flame)}}{I_\lambda \text{ (source)}} \qquad \text{(III-19)}$$

Using this value of β_λ, an average value of J_λ was calculated from Equation III-18.

Because of the difficulties Hood encountered in maintaining sufficient accuracy in his measurements, Tsai (79) used two different size laminar diffusion flames to obtain different path lengths. By measuring the intensity of each of these flames and then solving Equation III-18 by an iterative technique, average values of J_λ and β_λ were obtained for acetone, benzene, cyclohexane, natural gas, n-hexane, and methanol. The extinction coefficients obtained correspond to

the section of the flame that gave the maximum emission. Tsai's values of the extinction coefficient are significantly higher than those obtained by Hood for the same fuels. In this comparison the differences in the results cannot be attributed to differences in instrument resolution since the same instrument and instrument settings were used in both experiments. Tsai states that the values of J_λ and β_λ were scattered throughout the entire emission region for every fuel and that the scatter is due to the small flicker of the flames.

Pfenning (54) used a laminar diffusion flame that had an elliptical cross section in the horizontal plane. Emission data were taken for the paths along the major and minor axes of the cross section of acetone and natural gas flames. These data were used in Equation III-18 to calculate emission and extinction coefficients. Pfenning felt that the use of a single flame for two paths would be a significant improvement over the use of two different sized flames, since this procedure would guarantee that the same flame regime was being considered in the two paths. Profiles of the average intensity for the principal emission bands of these flames have shown the following:

1. Radiation fields extend outside the visible flame cone as much as the visible flame diameter horizontally and twice the height of the visible cone vertically.
2. The size of the emission envelope varies with wavelength. The maximum size occurs at 4.3 microns (peak of the CO_2

emission band). Another extension about half the size of the 4.3 micron envelope occurs at 2.7 microns (peak of the combined CO_2 and H_2O emission band). All other emission from the flame is confined to the luminous flame cone.

3. Maximum intensity was emitted from the CO_2 emission band at 4.3 microns and the next strongest emission band, which is about half the strength, occurred from the combined CO_2 and H_2O emission at 2.7 microns.
4. Two positions of maximum intensity occurred: along the path through the center of the flame at the height just above the inner reaction zone (at approximately 0.6 of visible flame height) and along a path through the edge of the visible cone and adjacent to the inner reaction zone at a height of approximately 0.4 of the visible flame height.

Intensity profile data revealed the path lengths used to calculate values of maximum emission and extinction coefficients were incorrect in the primary emission bands. However, the visible path lengths were used to calculate the coefficients after attempts to adjust the path lengths were unsuccessful. When emission extended beyond the visible flame cone and the extension distance was added to the visible flame paths, solutions for the extinction coefficient from the transport equation were negative. Negative extinction coefficients are meaningless. The extension of the emission region

beyond the luminous cone should decrease the values of maximum emission and extinction coefficients. As seen from the transport equation, the decrease in the extinction coefficient implies that a greater flame thickness is required to obtain maximum emission. While the increased path lengths are important in the calculation of the radiative flux from small flames (1.0 to 10.0 centimeters visible thickness), the additional path length has very little effect on prediction calculations for medium flames (10.0 to 100.0 centimeters visible thickness) and large flames (over 100 centimeter visible thickness). Probably for the medium flames and certainly for the large flames the additional emission path is well within the errors involved in measuring the visible path length. Average maximum emission and extinction coefficients obtained by the single flame two-path technique have shown:

1. Reproducibility of the coefficients requires accurate measurements of intensity and path length, plus excellent stability of the flame and monochromator detection and recording system.
2. For the primary emission bands, path lengths greater than the visible paths need to be considered in coefficient calculation from small flames. Paths through the inner reaction zone have order of magnitude lower emission and thereby cause large variations of the coefficients along vertical extent of the flame.

3. Calculations with the set of coefficients for the section of the flame just above the inner reaction zone (0.6 of the visible flame height) yield the maximum total intensity for both fuels. The thickness of the flame required to obtain the maximum emission was calculated to be approximately 100 centimeters for a natural gas flame and 50 centimeters for an acetone flame. The values represent the limits for "optically-thick" flames.

The methods of Hood, Tsai, and Pfenning show that the emission and extinction coefficients for flames are strong and irregular functions of frequency. To simplify calculations, it would be desirable to have mean values of these coefficients. For gases a Planck mean and a Rosseland mean absorption coefficient can be defined. If the gas is transparent for all frequencies, the Planck mean absorption coefficient κ_p is appropriate and is defined as

$$\kappa_p = \frac{\int_0^\infty \kappa_\lambda \, I_{b,\lambda}(T) \, d\lambda}{\int_0^\infty I_{b,\lambda}(T) \, d\lambda} \qquad \text{(III-20)}$$

The Rosseland mean absorption coefficient κ_R should be used when the gas is opaque for all frequencies and is defined as

$$\kappa_R = \frac{\int_0^\infty \frac{dI_{b,\lambda}(T)}{dT}\, d\lambda}{\int_0^\infty \frac{1}{K_\lambda} \frac{dI_{b,\lambda}(T)}{dT}\, d\lambda} \qquad \text{(III-21)}$$

Both of these coefficients are based on thermal equilibrium. Since the absorption coefficient for flames is an irregular function over a narrow wavelength, a mean absorption coefficient could be defined as

$$\kappa = \frac{\int_{\lambda_1}^{\lambda_2} \kappa_\lambda\, d\lambda}{\int_{\lambda_1}^{\lambda_2} d\lambda} \qquad \text{(III-22)}$$

Several techniques have been used to obtain a mean absorption coefficient for flames. Rasbash, et al. (57), assumed that flames radiate as gray bodies whose emittance is defined by

$$\varepsilon_f = 1 - e^{(-\kappa L)} \qquad \text{(III-23)}$$

The Schmidt method was used to obtain the flame emittance. For a known flame thickness Equation III-23 was used to calculate the absorption coefficient. The results obtained are given in Table III-4.

Burgess, et al. (14), obtained mean absorption coefficients from plots of steady fuel burning rates as a function

TABLE III-4

ABSORPTION COEFFICIENT AND EMITTANCE OF FLAMES FROM RASBASH, ET AL. (57)

Fuel	Emittance	Flame Width, L		Absorption Coefficient	
		cm	in	cm^{-1}	in^{-1}
Alcohol	0.066	18	7.08	0.0037	0.0094
Petrol	0.36	22	8.66	0.020	0.0508
Kerosene	0.37	18	7.08	0.026	0.066
Benzol	0.59	22	8.66	0.039	0.099
Benzol	0.70	29	11.42	0.041	0.104
Benzol	0.72	30	11.81	0.042	0.107

of the pool diameter. The curves represent the empirical expression

$$v = v_\infty \ (1 - e^{-\kappa D}) \qquad \text{(III-24)}$$

where v = linear burning rate, ft/min

v_∞ = linear burning rate at $D = \infty$, ft/min

D = pool diameter, ft

Two points for each fuel were taken from these plots and used to obtain values of v_∞ and κ, and these values are given in Table III-5.

Neill (50) assumed that the total heat flux from a flame can be expressed by

$$q_f = q_\infty \ (1 - e^{-\beta L}) \qquad \text{(III-25)}$$

TABLE III-5

ABSORPTION COEFFICIENTS AND MAXIMUM LINEAR BURNING RATES OF LIQUID FUELS FROM BURGESS, ET AL. (14)

Liquid Fuel	Absorption Coefficient		V_∞	
	cm^{-1}	in^{-1}	cm/min	ft/min
Hexane	0.019	0.0483	0.73	0.02390
Butane	0.027	0.0686	0.79	0.02590
Benzene	0.026	0.0660	0.60	0.01967
Xylene	0.012	0.0305	0.58	0.01902
Methanol	0.046	0.1168	0.17	0.00558
Unsymmetrical Dimethyl Hydrazine	0.025	0.0635	0.38	0.01247
Hydrogen	0.07	0.1778	1.40	0.04600
LNG	0.030	0.0762	0.66	0.02160

where q_f = total heat flux from flame, $Btu/hr\text{-}ft^2$

L = total path length through flame, in

β = mean extinction coefficient for flame, in^{-1}

q_∞ = heat flux from flame for $L = \infty$, $Btu/hr\text{-}ft^2$

Values of q_∞ and β were obtained by simultaneous solution of Equation III-25 for two different lengths of flames from a 2-inch wide channel burner. These results are given in Table III-6.

Welker and Sliepcevich (81) used a narrow angle radiometer to measure the total heat flux q_f from JP-4 flames from a 2-inch wide burner for path lengths of 4, 6, 12, and 16 inches. Equation III-25 was used to obtain a value of 31,000 for q_∞ and a value of 0.156 for β. The authors state that the

TABLE III-6

NEILL'S DATA FOR THE EXTINCTION COEFFICIENTS AND MAXIMUM HEAT FLUX FOR FLAMES FROM A 2-INCH WIDE CHANNEL BURNER (50)

Fuel	L in	q_f* Btu/hr-ft^2	q_∞ Btu/hr-ft^2	β in^{-1}
Methanol	6.5	2673	5080	0.112
	24	4717		
Acetone	7	6395	10000	0.158
	11	8072		
Hexane	9	8806	22600	0.055
	13	11531		
Cyclohexane	10	10483	30700	0.045
	16	14886		
JP-4	10	10273	23700	0.060
	13	14676		
Benzol	10	11531	38500	0.036
	16	16773		

*Radiometer located about 30 inches from flames. Atmospheric transmissivity is approximately 0.95.

value of β is high, since an optically thick fire, i.e., a fire which would emit 99 percent of the maximum radiant flux, would be only about 30 inches thick, a value significantly lower than that accepted by most investigators. The reason for this abnormally high value of β is the small scale of turbulence in the test fires. With a burner only 2 inches wide, the size of individual flame zones is also small, but the number of flame interfaces is realtively large. Since

emission and extinction occur primarily at the flame interfaces (where fuel and air are in the proper proportions for combustion), the extinction coefficient becomes larger as the scale of turbulence becomes smaller.

The only difference between Neill's data and that of Welker and Sliepcevich is a different type of radiometer was used to measure the heat flux from the flame. Some possible explanations for the difference in values of q_∞ and β are the calibration of the radiometer, the alignment of the radiometer, or the sensitivity of Equation III-25. Values of q_f and L were taken from Figure 2 of Welker and Sliepcevich and used in a non-linear estimation program to obtain values of q_∞ and β. The values obtained were 27,730 for q_∞ and 0.245 for β. This calculation shows that Equation III-25 is extremely sensitive to data variations.

Neill's values of β agree with the κ values of Burgess, et al. for hexane and methanol but their values of benzene differ widely. Neill's coefficient for benzene is approximately one-third the value given by Rasbash, et al.

Calculation Methods for Radiative Heat Transfer

As mentioned earlier there are two methods available for calculating the radiative heat transfer in absorbing, emitting and scattering media. These methods will now be adapted to radiative transfer from flames. Method 1 involves the substitution of Equation III-18 into Equation III-16 to obtain

$$q_f = \int_{\Omega} \frac{J_\lambda}{\beta_\lambda} (1 - e^{-\beta_\lambda S}) \cos\theta \, d\Omega \qquad \text{(III-26)}$$

To obtain the total heat flux from flames, q_f, Equation III-26 has to be integrated over all wavelengths.

If one assumes that a mean value for the emission and extinction coefficient exists, and then integrates Equation III-26 over a hemispherical solid angle the following equation is obtained

$$q_f = \frac{\pi J}{\beta} (1 - e^{-\beta S}) \qquad \text{(III-27)}$$

comparing this equation with Equation III-25 shows that $q_\infty = \pi J/\beta$, and $S = L$.

Generally, the heat transfer between a radiating source and a target is desired, so a geometrical relationship between the source and target must be considered. For diffuse surfaces this relationship is accomplished by using a geometrical configuration factor F. It can be shown that the heat flux received by a target from a flame can be expressed by

$$q_t = F_{t \to f} \, q_f \qquad \text{(III-28)}$$

where q_t = heat flux received by target from flame, Btu/hr-ft^2

$F_{t \to f}$ = geometrical configuration factor between target and flame

Now Equation III-27 can be written as

$$q_t = q_\infty F_{t\to f} (1 - e^{-\beta L}) \qquad \text{(III-29)}$$

Method 1 will refer to the use of this equation.

Method 2 assumes thermodynamic equilibrium and requires the solution of Equation III-15 with the boundary condition $I_\lambda(0) = 0$ at $\tau = 0$. The results is the following equation:

$$I_\lambda = n^2 I_{b,\lambda}(T)(1 - e^{-\tau_\lambda}) \qquad \text{(III-29A)}$$

Replacing τ_λ with $\kappa_\lambda S$, assuming $n = 1$, and substituting Equation III-29A into III-16, the following results

$$q_{f,\lambda} = I_{b,\lambda}(T) \int_\Omega (1 - e^{-\kappa_\lambda S}) \cos\theta \, d\Omega \qquad \text{(III-29B)}$$

Once again this equation has to be integrated over wavelength to obtain the total heat flux.

If Equation III-29B is integrated over a hemispherical solid angle the following is obtained

$$q_{f,\lambda} = \pi I_{b,\lambda}(T)(1 - e^{-\kappa_\lambda S}) = \alpha_{f,\lambda} \pi I_{b,\lambda}(T) \qquad \text{(III-30)}$$

where $\alpha_{f,\lambda} = (1 - e^{-\kappa_\lambda S})$ = monochromatic flame absorptance
Since thermal equilibrium is assumed, then by Kirchoff's law the emittance of the flame is equal to its absorptance. Therefore, Equation III-30 becomes

$$q_{f,\lambda} = \varepsilon_{f,\lambda} \pi I_{b,\lambda}(T) \qquad \text{(III-31)}$$

where $\varepsilon_{f,\lambda}$ = monochromatic emittance of flame

The emittance of a non-luminous flame can be predicted in the same manner as the emittance of a real gas. A total non-luminous flame emittance ε_g is defined as

$$\varepsilon_g = \frac{\int_0^\infty I_{b,\lambda}(T_f)\left[1 - e^{(-\kappa_{g,\lambda}L)}\right] d\lambda}{\sigma T_f^4} \qquad \text{(III-32)}$$

where $\kappa_{g,\lambda}$ = monochromatic absorption coefficient of non-luminous flame

T_f = flame temperature, °R

If the non-luminous flame is assumed to consist only of carbon dioxide and water vapor, then the emittance can be determined by a method developed by Hottel (34) which expresses the emissivity as

$$\varepsilon_g = C_{CO_2} \varepsilon_{CO_2} + C_{H_2O} \varepsilon_{H_2O} - \Delta\varepsilon \qquad \text{(III-33)}$$

where ε_{CO_2} = emittance due to carbon dioxide

ε_{H_2O} = emittance due to water vapor

$\Delta\varepsilon$ = correction factor to account for the spectral overlap of the carbon dioxide and water absorption bands

C_{CO_2} = pressure correction for carbon dioxide

C_{H_2O} = pressure correction for water vapor

Hottel gives charts for the determination of ε_{CO_2}, ε_{H_2O} and $\Delta\varepsilon$ based on the flame temperature with the partial pressure-path length as a parameter. Charts are also presented for the pressure correction terms. If Equation III-30 is integrated over wavelength and Equation III-32 is utilized, the following equation results

$$q_f = \varepsilon_g \sigma T_f^4 \qquad \text{(III-34)}$$

Hottel (34) states that the monochromatic emittance of a luminous flame can be expressed as

$$\varepsilon_{\ell,\lambda} = 1 - e^{-C_s L f(\lambda)} \qquad \text{(III-35)}$$

where $\varepsilon_{\ell,\lambda}$ = monochromatic emittance of luminous flames

C_s = soot volume concentration (average volume of particles per unit volume of flame)

$f(\lambda)$ = function representing the absorption coefficient, the soot concentration, and possibly the particle size and size distribution function of the flame

Hottel suggests that $f(\lambda)$ can be represented by

$$f(\lambda) = k_1/\lambda^a \qquad \text{(III-36)}$$

where k_1 and a are constants and

a = 0.95 for the infrared region down to λ = 0.8 microns

a = 1.39 in the visible spectrum near λ = 0.6 microns

(say $\lambda \simeq$ 0.3 to 0.8 microns)

Siddall and McGrath (62) also found that Equation III-36 is applicable and for the range of λ = 1 to 7 microns, mean values of "a" are given in Table III-7.

TABLE III-7

MEAN VALUES OF "a" FOR SEVERAL SOOTS AS GIVEN BY SIDDALL AND McGRATH (62)

Source of Soot	a
Amylacetate	0.89, 1.04
Avtur Kerosene	0.77
Benzene	0.94, 0.95
Candle	0.0.93
Furnace Samples	0.96, 1.14, 1.25
Petrotherm	1.06
Propane	1.00

Siddall and McGrath also conclude that:

1. It appears impossible to specify a general but simple form for the variation of "a" with λ which will be true for all materials. In some cases the variation of "a" with λ may be approximated by an equation of the form $a = a_1 + a_2 b\lambda$ in some cases, where a_1 and a_2 are constants. In other cases, "a" can be represented by a general polynomial in λ (a quadratic may be satisfactory).
2. Mean values of "a" appear to be independent of the particle size but appear to show a definite correlation with the carbon-hydrogen ratio of the soot.

Siddall and McGrath state that the total emittance of a flame ε_f can be expressed as

$$\varepsilon_f = \varepsilon_s + \varepsilon_g (1 - \varepsilon_s) \qquad \text{(III-37)}$$

where ε_s = total emittance of soot particles

Sato and Matsumoto (59) define the monochromatic emittance of a luminous flame as

$$\varepsilon_{f,\lambda} = 1 - e^{-([k_1/\lambda^a]\ L_e + K_{g,\lambda})L} \qquad \text{(III-38)}$$

where L_e = effective thickness of a cloud of particles, ft/ft (sum of the particle thickness per unit thickness of flame)

Equation III-38 was substituted into Equation III-31 and integrated over wavelength to obtain

$$q_f = \sigma T_f^4 \left[1 - \frac{15}{\pi^4} (1 - \varepsilon_g) \frac{d^4}{dX^4} \ln \Gamma(X + 1)\right] \qquad \text{(III-39)}$$

where $\Gamma(X+1)$ = the gamma function

$X = k_1 L_e L T_f / C_2 = k_1 V_p L T_f / C_2$

C_2 = second Planck constant

V_p = volume fraction of particles in flame

$k_1 = 0.57$

It can be seen from Equation III-39, that the total emittance of a luminous flame ε_f is given by

$$\varepsilon_f = 1 - (1 - \varepsilon_g)\left(\frac{15}{\pi^4}\right) \frac{d^4}{dX^4} \ln \Gamma(X + 1) \qquad \text{(III-40)}$$

Comparing this equation with Equation III-37, it can be seen that

$$\varepsilon_s = 1 - \frac{15}{\pi^4} \frac{d^4}{dX^4} \ln \Gamma(X + 1) \qquad \text{(III-41)}$$

Thring, et al. (75) give the following formula for the prediction of the emittance from practical luminous flames

$$\varepsilon_f = 1 - (1 - \varepsilon_g)\, e^{(-k_2 \lambda^{-a} \overline{C}_s L)} \qquad \text{(III-42)}$$

where k_2 = constant

$\overline{C}_s$ = mean concentration of soot at the flame temperature, mg/liter

They state that the value of "a" is close to 1. Values of $k_1\lambda^{-a}$ were calculated from Mie theory using the real refractive index and the absorption index of baked electrode carbon at 2250°K. Values of $k_2\lambda^{-a}$ were obtained from the monochromatic emittance, measured by the Krulbaum method, of a laboratory diffusion flame, and for the monochromatic emittance, measured by the Schmidt method, for the Sheffield furnace and the Ijmuiden furnace flames. These results are summarized in Table III-8. Considering the methods of measuring the flame emittance, the values of $k_2\lambda^{-a}$ for the lab flame and the Ijmuiden furnace flame are in reasonable agreement. The wide discrepancy in the Sheffield furnace values may be due to a cold core of fuel along the axis of the flame. A comparison of Equations III-37 and III-42 hows that

TABLE III-8

COMPARISON OF EXPERIMENTAL AND THEORETICAL VALUES OF $k_2\lambda^{-a}$

Weighted Mean Wavelength, Microns	$k_2\lambda^{-a}$, liters/mg-cm			
	Theoretical	Lab Flame	Sheffield Furnace	Ijmuiden Furnace
0.65	0.043	0.040		
2.60	0.0089		0.0295	
2.30	0.0107			0.0135

$$\varepsilon_s = 1 - e^{-k_2\lambda^{-a}\bar{C}_s L} \qquad \text{(III-43)}$$

Yagi and Iino (84) applied Mie theory with the assumption that the soot has a real refraction index of 2 and an absorption index of 0.7, to derive the following expression for the total emittance soot

$$\varepsilon_s = 1 - \frac{\zeta(4,\ 1 + 2.877\ C_s L T_f)}{\zeta(4)} \qquad \text{(III-44)}$$

where $\zeta(i) = \sum_{n=1}^{\infty} 1/n^i$, $\zeta(i,b) = \sum_{n=0}^{\infty} \frac{1}{(n+b)^i}$

are the Riemann's zeta function.

Hottell and Sarofim (36) calculated a total emittance from soot based on Equation III-35 and with the spectral distribution of blackbody radiation expressed by Wien's equation rather than Planck's because of the low λT range of interest. This total emittance is expressed as

$$\varepsilon_s = 1 - [1 + k_1 C_s L T_f / C_2]^{-4} \qquad \text{(III-45)}$$

the authors recommend a value of k_1/C_2 of 5 cm^{-1}-°K^{-1} (85 ft^{-1}-°R^{-1}).

In the previous developments scattering by the soot particles was neglected. Thring, et al. (76) states that when the ratio of the particle circumference to wavelength, $\pi d_p/\lambda$, is less than 0.25, scattering is negligible relative to extinction. This is true for many flames where the soot particle diameter is 0.06 microns or less. When larger particles are present they scatter unpolarized thermal radiation in all directions with a bias towards the forward direction as $\pi d_p/\lambda$ increases. For this case the monochromatic emittance is given by

$$\varepsilon_{s,\lambda} = [1 - e^{-k_1 \lambda^{-a} \bar{C}_s L}] \frac{(\beta_s - \sigma_s)}{\beta_s} \qquad \text{(III-46)}$$

where ε_s = extinction coefficient for soot particles, in^{-1}

σ_s = scattering coefficient for soot particles, in^{-1}

To determine the effect of temperature on the extinction of radiation by a soot particle, Howarth, et al. (37) curve-fit the dispersion equations, derived from classical electron theory, to measured values of the refractive and absorption indices of pyrographite at 300°K. The resulting equation was used to obtain values of the refractive and absorption indices at other temperatures. The Mie theory was then

used to calculate the attenuation coefficient. It was concluded that the variation of the mean attenuation coefficient with flame temperature is less than 1 percent per 100°K, and can be regarded as independent of temperature for large turbulent flames. Reported variations in the mean attenuation coefficient between flames cannot be accounted for by a difference in soot temperature between different flames. Since soots form part of a large spectrum of mesomorphous carbons whose refractive indices vary with carbon-hydrogen ratio, then differences in the mean attenuation coefficient suggests that there are variations in the carbon-hydrogen ratio of soots between different flames.

Lowes and Newall (43) used the Mie theory and existing data for the absorption and refractive index of a number of soots from oil, propane and acetylene flames to calculate the extinction and scattering coefficients of a soot particle. Using these coefficients and assuming values of flame soot concentration, density, temperature, width and soot particle size, Equation III-46 was integrated over wavelength to obtain the total emittance of soot dispersions in luminous flames. A comparison of these values shows that the emittance of a soot dispersion is strongly dependent on the refractive index of the soot, which is itself a function of its origin and chemical composition. An average emittance variation of 37 percent between gas and oil soots and 22 percent between soots from oil flames can be expected. The predicted temperature

dependence of the optical properties of soot has been found to increase the flame emittance by as much as 25 percent.

This survey of the techniques for predicting the emittance from flames reveals the following:

1. The emittance of a non-luminous flame can be calculated from Equation III-33, derived for the emittance of a gas composed of CO_2, H_2O, and other non-radiating elements. For natural flames, one can assume that only the stoichiometric amount of air is available.
2. For luminous flames, the total emittance is composed of the emittance of a non-luminous flame and the emittance of a cloud of soot particles and can be predicted by Equation III-37.
3. The emittance of the soot particles depends on the size of the particles. For particle diameters larger than 0.08λ, scattering becomes important and Equation III-46 must be used. For smaller particle diameters Equations III-41, III-43, III-44, and III-45 are available. These equations were all based on Mie theory and the differences in the calculated emittance has not been determined.
4. The equations for the emittance of soot particles have the unknowns k_1, k_2, a, $\overline{C}_s$.
5. Values of "a" are reported for various types of soot, but no general equation exists for its prediction.
6. The value of 0.57 for k_1 is the only one given, and a tentative value of k_1/C_2 is given as 5 cm^{-1}-$°K^{-1}$. This would

give a calculated value of $k_1 = 7.19$. Thus the value of k_1 needs to be determined.

7. Values of $k_2\lambda^{-a}$ can be calculated from Mie theory and a few experimental values are available. Comparisons between theory vary from good to poor. Additional experimental values are required.
8. The soot concentration is a definite unknown. Since the process of soot formation in hydrocarbon flames is not yet fully understood, there is no quantitative theoretical relationship for even an approximate calculation of the soot concentration in flames.
9. All experimental measurements on soot emittance are from small laboratory flames or furnace jet flames. No references were found for natural flames.
10. For natural flames, the amount of air that diffuses into the flame in unknown so the luminous emittance cannot be calculated without some assumptions.

From the preceding discussion, it can be concluded that the emittance of a luminous flame cannot be accurately calculated, and one has to rely on experimental values. To the author's knowledge no experimental values for the emittance of medium to large size natural luminous flames of liquid fuels are available. In spite of these shortcomings, if it is assumed that a total emittance of a luminous flame can be obtained, then the radiant heat flux from the flame to a target can be calculated by

$$q_t = \varepsilon_f F_{t \rightarrow f} \sigma T_f^4 \qquad \text{(III-47)}$$

The use of this equation will be referred to as Method 2A.

All the methods for calculating the radiant heat flux from flames requires a value for the path length L, through the flames. In Methods 1 and 2, the path length is taken into account by the integration over solid angle. For Methods 1A and 2A a single value of L is required. What value of L is to be used for a particular flame shape when L varies with the path through the flame? The concept of a mean beam length L_b can be used for certain cases. The mean beam length is defined as the required radius of a gas hemisphere such that it radiates a flux to the center of its base equal to the average flux radiated to the area of interest by the actual volume of gas. The mean beam length for an optically thin gas radiating to its entire boundary is given by

$$L_{b,o} = 4V_g/A_g \qquad \text{(III-48)}$$

where $L_{b,o}$ = mean beam length for optically thin gas, ft.

V_g = volume of gas, ft^3

A_g = total surface area of gas volume, ft^2

For gases of other optical thickness, a simple correction factor applied to Equation III-48 will result in an average mean beam length L_a. Hottel and Sarofim (36) state that this correction factor varies between 0.8 and 0.95 suggest using a value of 0.88. Consequently, when interest is in the flux

to the entire bounding area of a gas mass of any shape, the average mean beam length is approximately

$$L_a = 3.5\ V_g/A_g \qquad \text{(III-49)}$$

Additional details on this method and values of the mean beam length for various geometric shapes can be found in Hottel and Sarofim (36).

Review of Previous Work on Radiative Heat Flux from Flames

Shahrokhi (60) used Methods 1 and 2 to calculate the monochromatic heat flux from methanol and acetone sheet, tilted sheet, cylindrical and conical flames to a differential element of area external to the flame and in a plane parallel to the base of the flame. In this analysis the flame was divided into N x M zones and the integral in Equations III-26 and III-29 was evaluated by summations over the N x M zones in the flames. The resulting monochromatic flux was then integrated over wavelength by the Gauss quadrature method to obtain the total heat flux. Values of J_λ and B_λ were obtained from Hood (33). Radiative heat flux measurements were made on a 12.5 x 2.5 x 10 cm sheet of flame and a 2.5 cm dia x 10 cm high cylindrical flame for methanol and acetone fuels. The radiometer was mounted in a vertical plane at the same elevation as the burner. Shahrokhi (60) claims good agreement between measured fluxes and those calculated by Method I. In all cases, measured values were less than those calculated by

Method 1, except as the radiometer was moved closer to the flame, interaction effects between the flame and radiometer resulted in higher measured values. Method 2 yielded consistently higher total fluxes than Method 1, since $I_{b,\lambda}(T)$ is expected to be larger than J_λ/B_λ. In the numerical prediction methods, the target (radiometer face) was in the horizontal plane, while in the experimental work the target was in the vertical plane. The magnitude of this difference needs investigation.

Tsai (79) used his measured values of J_λ and B_λ and Shahrokhi's calculation procedure for Method 1 to predict the heat flux from cylindrical flames of acetone, n-hexane, and cyclohexane. He then compared his results with Huffman's (38) heat flux data from merging flames. It was found that in most cases, the predicted values are higher, because the volume occupied by the inner core region is not excluded from the flame size determination and because of the air entrained into the turbulent flames during combustion. The regions occupied by the inner cone and the entrained air do not radiate as effectively as the outer cone.

Neill (50) used Method 1 to calculate the radiative flux from acetone, cyclohexane, n-hexane, and methanol cylindrical flames to a cylinder inside the flames. Values of J_λ and B_λ were taken from Tsai (79). Neill found that these data predicted an unrealistically small optical thickness for all fuels except methanol. Neill then applied Method 1A based on

values of q_∞ and κ that he obtained from flames in 2-inch wide channels. Method 2A was used for a hypothetical flame composition corresponding to the equilibrium reaction of normal hexane with 48 mole percent of the stoichiometric air required for burning all the carbon to CO_2. The equilibrium concentrations were obtained from Mody and Lott (47) based on the minimum free energy technique. A flame temperature of 1960°F, a soot concentration of 0.225 mg/liter of flame volume and an absorption coefficient of 0.005 $(\text{cm-mg/liter})^{-1}$ was used in the calculation of the radiant flux from a hemispherical flame. When these fluxes were plotted against flame thickness on log-log paper a straight line resulted. The equation of this line is

$$q_f = 2450\ (L)^{0.565} \qquad \text{(III-50)}$$

Neill then used this equation to make the radiation calculations for all the luminous flames. The calculated radiant flux incident on the test cylinder is presented in Table III-9 for the methanol flames and Table III-10 for the luminous flames. The methanol flame sizes changed so much due to large pulsations of the flame, that two flame sizes were used with each calculation method. One flame size was considered to be a cone shaped flame which tapered from the burner rim to a thickness of 1 to 2 inches around the test cylinder. The cone shaped flame remained fixed and was about the minimum flame

TABLE III-9

NEILL'S RADIANT FLUX DATA FOR METHANOL FLAMES (50)

Burner Diameter in	Radiative Heat Flux, Btu/hr-ft^2			
	Method 1		Method 1A	
	Cone	0.67 Factor	Cone	0.67 Factor
12	5161	4270	1073	1205
18	5162	6535	1249	1800
24	6630	8173	1571	2340

TABLE III-10

NEILL'S CALCULATED RADIANT FLUX FOR LUMINOUS FLAMES (50)

Fuel	Burner Diameter inches	Radiative Heat Flux, Btu/hr-ft^2		
		Method 1	Method 1A	Method 2A
Acetone	Cluster*	8245	7900	9316
	12	7610	4013	4906
	18	7941	5241	6083
	24	8239	7840	9295
Hexane	Cluster	10560	11480	10410
	12	10550	8728	8394
	18	10560	12083	10866
Cyclohexane	Cluster	21186	12820	9966
	12	20886	8519	8619
	18	21180	11080	8946
JP-4	Cluster	--	12010	9842
	12	--	8610	7598
	18	--	9700	8312
Benzol	12	--	9200	7601
Napalm	12	--	--	7200

*Nine 6-inch diameter burners in a cluster.

size. The other flame size calculations were made by applying a factor of 0.67 to the radiant heating from the maximum flame diameter, i.e., the diameter of the flame pulses.

Neill concluded that none of the radiation calculation methods and data provide much more than a rough estimate of the radiant heat transfer from flames.

Deshpande (24) assumed that the flame was a blackbody and used the Stefan-Boltzman law with measured flame temperatures to obtain the radiative heat flux from flames. These values are given in Table III-11.

TABLE III-11

DESHPANDE'S CALCULATED RADIATIVE HEAT FLUX VALUES FOR FLAMES

Fuel	Burner Diameter inches	Radiative Flux Btu/hr-ft^2
Acetone	8	7990
	12	16600
	18	25300
	24	18400
Cyclohexane	8	10200
	12	22450
	18	16450
n-Hexane	8	9940
	12	20500
Methanol	8	12150
	12	18400
	18	15020
	24	16900

Deshpande also presents figures of measured values of radiant heating external to flames, as a function of the distance from the flame. He compares the data to values calculated by Canfield (16) who used Tsai's data for J_λ and β_λ. No details of the calculation procedure are given. The figures show that predicted heat fluxes are lower for methanol, but much higher for cyclohexane than experimental values. Acetone has higher predicted fluxes for smaller burners but smaller predicted fluxes for larger burners than experimental values.

Thomas, et al. (73) list values of 10,485, 10,883, and 7,565 Btu/hr-ft^2 for the mean downward radiative flux from an ethyl alcohol flame to its fuel surface at a radius of 0, 7,48, and 14.96 inches respectively.

Remarks

Method 1 is the best technique for calculating the radiative flux from flames. This method requires good data for J_λ and β_λ to justify the added complexity of the triple integration. Values of J_λ and β_λ are available for several fuels but their accuracy is questionable. Some doubt exists whether these values for small laminar flames are applicable to large turbulent flames. Method 2 is the next best technique but it also requires accurate values of the absorption coefficient κ_λ. This method also requires the assumption of thermodynamic equilibrium, which may or may not exist even on a local scale. Method 1A rates as the next best calculation

technique. By using a narrow angle radiometer external to a flame, values of q_∞ and β can be obtained. The disadvantage of this method is the sensitivity of these values to measured data. Another disadvantage is the selection of the appropriate path length through the flame. Method 2A is the least attractive technique as it requires a flame temperature and a flame emittance. The existence of a flame temperature is inseparably bound up with the definition of thermodynamic equilibrium. In spite of this, measured values of flame temperature are obtained by various techniques. To calculate the total emittance of a luminous flame, the composition of the flame gas and the soot concentration is required. Unfortunately the chemistry of fuel combustion is not developed well enough to permit the calculation of the total flame emittance. The flame emittance also requires the specification of a single path length through the flame.

Convective Heat Transfer

The second important mode of heat transfer by flames is convection, which can be classified as either "forced" or "free" or "natural." The flow pattern under forced or free convection can be either laminar or turbulent, depending upon the velocity of flow and the fluid physical properties. Free convection occurs when the fluid motion is caused by a density difference resulting from a temperature difference between the fluid and a surface. Forced convection occurs when the

relative velocity between the fluid and surface is caused by a mechanical means.

As stated earlier, the heat transfer coefficient is obtained from the Nusselt number, which can be predicted by EquationIII-5, which is

$$Nu = C_1 (Re)^m (Pr)^{n_1}$$

For free convection, the Reynolds number is difficult to evaluate so the following equation is used to predict the Nusselt number

$$Nu = C_1 (Ra)^{n_1} \qquad \text{(III-51)}$$

where Ra = Rayleigh Number = Gr Pr

The Grashof number Gr is defined as

$$Gr = \frac{X^3 \rho^2 g B \Delta T}{\mu^2} \qquad \text{(III-52)}$$

where g = acceleration of gravity, ft/hr^2

B = fluid volumetric coefficient of expansion, $°F^{-1}$

ΔT = temperature difference between fluid and surface, °F

The Prandtl number Pr is defined as

$$Pr = C_p \mu / k \qquad \text{(III-53)}$$

The values of C_1 and n_1 in Equation III-51 depend on the Rayleigh number and on the surface configuration and

orientation. Since this study uses a vertical cylinder as the heat transfer surface, only values of C_1 and n_1 for vertical planes and cylinders will be presented. The physical properties are evaluated at the film temperature, which is the arithmetic mean temperature of fluid and surface. The local heat transfer coefficient for vertical surfaces varies with distance along the surface, because as the fluid flows along the surface, the flow pattern changes from laminar at the lower end to turbulent at the upper end. If this local coefficient is integrated over the height of the surface, then an average heat transfer coefficient results. This is the value of interest and the characteristic dimension in the Grashof number will be the height of the surface.

For short vertical planes and cylinders, McAdams (46) recommends that for $10^9 < Ra < 10^{12}$, C_1 is 0.13 and n_1 is 1/3; for $10^4 < Ra < 10^9$, C_1 is 0.59 and n_1 is 1/4. Eckert and Jackson (25) recommend that for $10^5 < Ra < 10^8$, C_1 is 0.555 and n_1 is 1/4; for $10^{10} < Ra < 10^{12}$, C_1 is 0.0210 and n_1 is 2/5. No recommendations are given for the transition region for $10^8 < Ra < 10^{10}$. A plot of the recommended equations shows that the laminar and turbulent region curves intersect at a Rayleigh number of approximately 2×10^9. Bayley (8) recommends that $C_1 = 0.1$ and $n_1 = 1/3$ for the turbulent region. Cheesewright (17) recommends the following equation for $10^4 < Gr < 2(10^9)$.

$$Nu = (0.472)(Gr)^{0.25} \qquad \text{(III-54)}$$

For $Ra > 10^{10}$, a curve is given for the Nusselt number. If a straight line is drawn through this data, the following equation results

$$Nu = (0.203)(Gr)^{0.34} \qquad \text{(III-55)}$$

Nagendra (48), et al., recommend the following equations for the Nusselt number of short cylinders, long cylinders and wires:

$$\text{Short cylinders:} \quad \frac{(Ra)_D D_c}{L_c} > 10^4 \quad (Nu)_D = 0.60\left[\frac{(Ra)_D D_c}{L_c}\right]^{0.25} \qquad \text{(III-56)}$$

$$\text{Long cylinders:} \quad 0.05 < \left[\frac{(Ra)_D D_c}{L_c}\right] < 10^4$$

$$(Nu)_D = 1.37\left[\frac{(Ra)_D D_c}{L_c}\right]^{0.16} \qquad \text{(III-57)}$$

$$\text{Wires:} \quad \frac{(Ra)_D D_c}{L_c} < 0.05 \quad (Nu)_D = 0.93\left[\frac{(Ra)_D D_c}{L_c}\right]^{0.05} \qquad \text{(III-58)}$$

where D_c = cylinder diameter, ft

L_c = cylinder height, ft

$(Nu)_D$ = Nusselt number based on cylinder diameter

$(Ra)_D$ = Rayleigh number based on cylinder diameter

Free convection correlations were presented for both vertical plates and cylinders. The question arises as to whether the correlation for flat plates is applicable to a cylinder. Sparrow and Greg (66) made an analytical comparison between a vertical flat plate and a vertical cylinder. The

ratio of the Nusselt number for cylinders to that for plates is plotted against the factor $[2^{5/2}(X/D_c)/(Gr)_x^{1/4}]$ with the Prandtl number as a parameter. The resulting curves show that the Nusselt number for a cylinder is always higher than that for a plate. The difference is small for low values of x but increases as x increases.

Since natural flames are buoyant, one may assume that free convection rather than forced convection is the dominant heat transfer mode. For large fuel burning rates, forced convection heat transfer may prevail over free convection. Therefore, the constants C_1, m and n_1 for Equation III-5 will be given for laminar region. No known correlation exists for the Nusselt number of a fluid flowing along the outside of a tube. For forced convection laminar flow over a flat plate, McAdams gives a value of $C_1 = 0.644$, $m = 0.5$, and $n_1 = 1/3$.

The use of these correlations for a flame requires that the composition of the flame be known, so that physical properties can be evalauted. Since an accurate knowledge of a diffusion flame composition is unknown, it is assumed that the physical properties of air are applicable. This is a common assumption. When one obtains measured convective heat fluxes from a flame, the assumption is made that other forms of energy transfer due to chemical reactions are not present. If these mechanisms are present then measured

convective heat transfer coefficient will be higher than those predicted by the correlations presented.

A comparison of these correlations is given in Table III-12. These calculations are based on a 1.875-inch diameter cylinder, 15.75 inches long. The flame temperature is assumed to be 2200°F, and the surface temperature is taken as 200°, 800" and 1400°F. For these conditions the Rayleigh number is $4.876(10^7)$, $1.607(10^7)$, $1.141(10^7)$ for film temperatures of 1200°, 1500° and 1800°F. Those values of the Rayleigh number indicates that laminar free convection occurs. For forced convection, the flame velocity is assumed to be 3 ft/sec.

TABLE III-12

COMPARISON OF CONVECTION CORRELATIONS

Correlation	Surface Temperature, °F					
	200		800		1400	
	Nu	h	Nu	h	Nu	h
$Nu = 0.13\ (Ra)^{1/3}$	47.4	1.33*	32.8	1.12*	29.3	1.11*
$Nu = 0.555(Ra)^{1/4}$	46.4	1.30	35.1	1.20	32.3	1.22
$Nu = 0.472(Gr)^{1/4}$	43.1	1.21	33.1	1.13	30.4	1.15
$Nu = 1.37[\frac{(Ra)_D D_c}{L_c}]^{0.16}$	5.95	1.40	4.98	1.42	4.71	1.50
$Nu = 0.664(Re)^{1/2} \times (Pr)^{1/3}$	41.0	1.15	30.0	1.02	25.0	0.94

*Units of h are Btu/hr-ft^2-°F.

It can be seen from Table III-12 that the correlations are in reasonable agreement and that the convective heat transfer coefficient should be in the range of 1-2 Btu/hr-ft^2-°F.

Neill (50) obtained convective heat fluxes by subtracting the calculated radiant flux from the total heat flux. These values are given in Table III-13 for the methanol flame and Table III-14 for the luminous flames.

Neill prefers Method 1A for calculating the radiant heat flux. For methanol Neill prefers the 0.67 factor data and believes that the flames from the 12-inch burner did not give complete cylinder coverage, therefore, the convective fluxes are low. Assuming that a flux of 7,000 Btu/hr-ft^2 represents the average convective heat transfer rate for methanol flames, Neill calculates a heat transfer coefficient of 3.5 Btu/hr-ft^2-°F. For luminous flames the convective heat transfer rates obtained by Method 1A and 2A agree reasonably well. An average convective flux of 7000 Btu/hr-ft^2 can be used for single burners. Of course the variation is $\pm$ 50 to $\pm$ 100 percent. A heat transfer coefficient of 4 Btu/hr-ft^2 can be calculated from this flux value. These calculated coefficients are about twice as high as values predicted from empirical correlations used. No explanation is given for the high convective fluxes obtained for the cluster burner. After considering the approximations Neill made and the questionable emission and extinction coefficient data,

TABLE III-13

CONVECTIVE HEAT FLUX FOR METHANOL FLAMES FROM NEILL'S DATA

Burner Diameter inches	Convective Heat Flux, Btu/hr-ft^2			
	Method 1		Method 1A	
	Cone	0.67 Factor	Cone	0.67 Factor
12	339	1230	4427	4295
18	2088	715	6001	5450
24	2370	827	7429	6660

TABLE III-14

NEILL'S CONVECTIVE HEAT FLUX FOR LUMINOUS FLAMES

Fuel	Burner Diameter inches	Convective Heat Flux, Btu/hr-ft^2		
		Method 1	Method 1A	Method 2A
Acetone	Cluster*	4255	4600	3184
	12	1490	5087	4194
	18	4059	6759	5917
	24	6261	6600	5205
Hexane	Cluster	19440	18520	19590
	12	4450	6272	6606
	18	9940	8417	9643
Cyclohexane	Cluster	4814	13180	16043
	12	-4886	7481	7381
	18	-5680	4420	6554
JP-4	Cluster	--	18990	21158
	12	--	990	2002
	18	--	9800	11188
Benzol	12	--	1800	3399
Napalm	12	--	--	5800

*Nine 6-inch diameter burners in a cluster.

it is difficult to say whether or not existing empirical correlations for convective heat transfer can be applied to flames.

Despande (24) also obtained convective heat fluxes from flames by subtracting a calculated radiant flux from a measured total heat flux. These results are presented in Table III-15.

TABLE III-15

CONVECTIVE FLUX FOR FLAMES FROM DESHPANDE

Fuel	Burner Diameter inches	Convective Heat Flux Btu/hr-ft^2-°F	Convective Heat Transfer Coefficient Btu/hr-ft^2-°F
Acetone	8	8100	5.42
	12	5500	3.45
	18	4300	2.53
	24	1100	0.64
Cyclohexane	8	4300	3.15
	12	8450	4.42
	18	16450	12.20
n-Hexane	8	6260	4.74
	12	1300	0.87
Methanol	8	2400	1.62
	12	500	0.29
	18	1030	0.62
	24	5500	3.26

The high values of the heat transfer coefficient are due to the low flame temperatures used to calculate the radiative heat flux.

Thomas, et al. (73) give values of 2124, 2920 and 3849 for the convective heat flux from an ethanol flame to its fuel surface at a radius of 0, 7.48 and 14.96 inches, respectively.

Remarks on Flame Heat Transfer

After reviewing the experimental results on the radiative and convective heat fluxes from flames, it can be concluded that data are not sufficient or accurate enough to allow more than an estimate of flame heat transfer. For these reasons, this study was undertaken.

CHAPTER IV

FACILITIES AND EQUIPMENT

Building

All experimental work was conducted in the static-test chamber of the low velocity wind tunnel building located on the North Campus of the University of Oklahoma. Figure IV-1 shows the arrangement and principal dimensions of the building. The burn table, burner, and probe assembly were located in the center of the static test room and Figure IV-2 shows this equipment. The fuel tank and instruments were located in the observation room and Figure IV-3 shows their arrangement.

The 12 ft x 12 ft hood in the static test room extended from the ceiling down to a level about 8 feet from the floor. This hood collected smoke and soot from the flames for removal by the two 48-inch exhaust fans located in the louvered section above the test room. One fan was located in the northeast corner of the louvered section and the other in the southwest corner. These fans had no effect on the flames and were successful in removing the smoke from the room except for benzene flames.

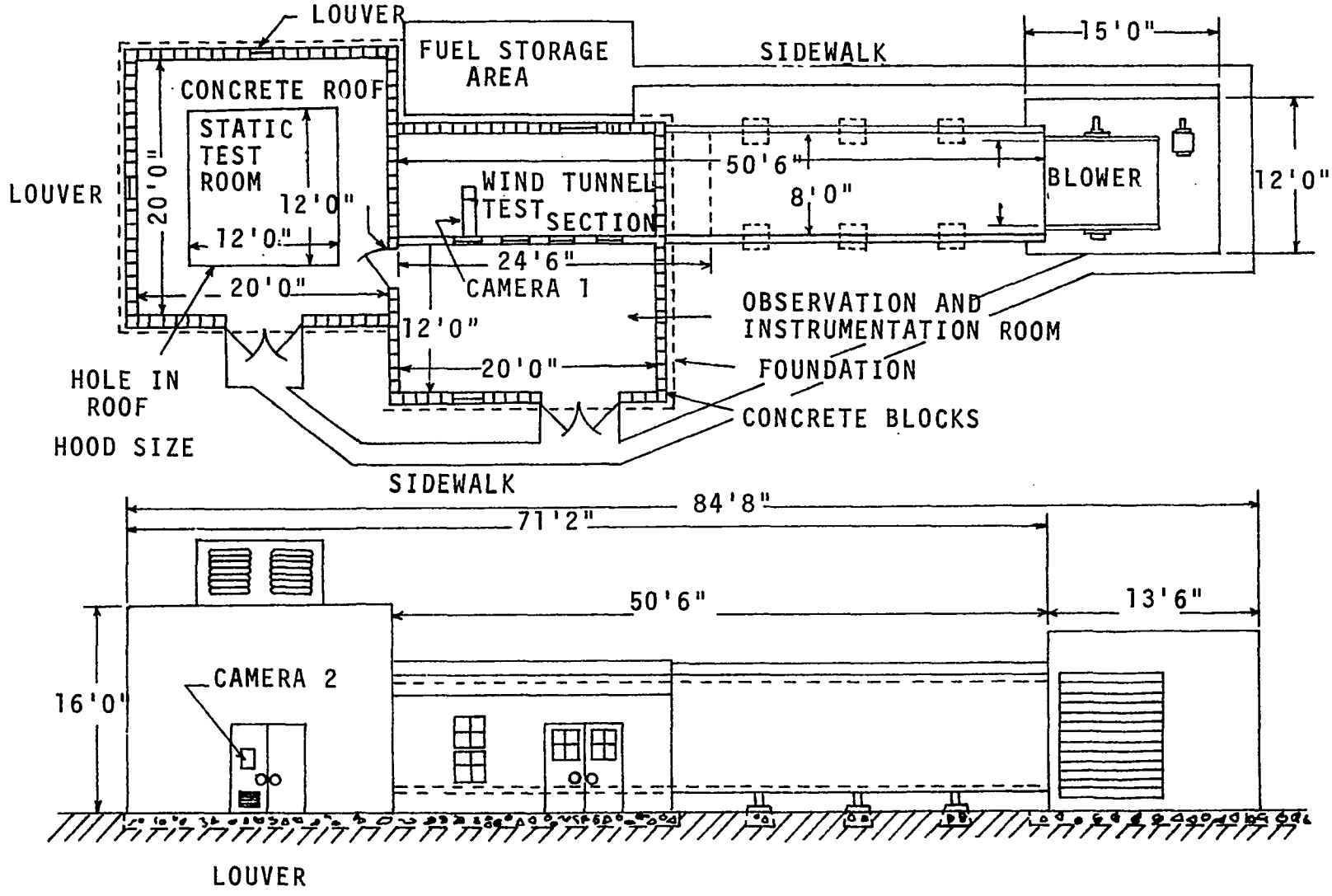


Figure IV-1. Low Velocity Wind Tunnel.

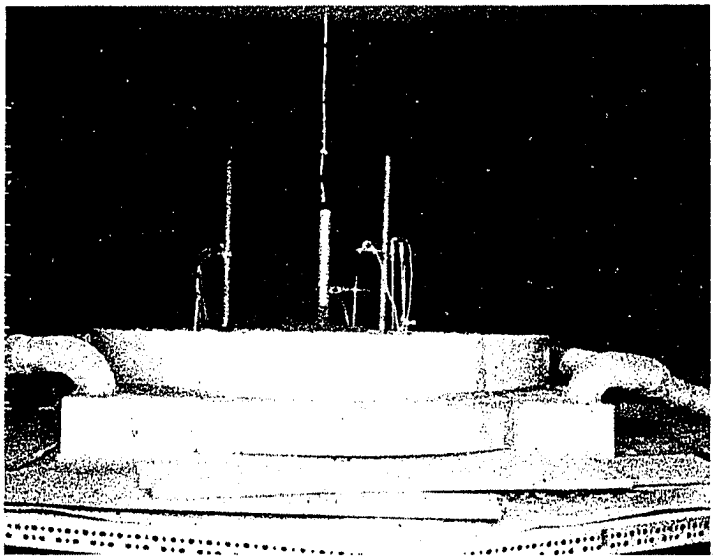


Figure IV-2. Burn Table and Associated Equipment Located in Static Test Room.

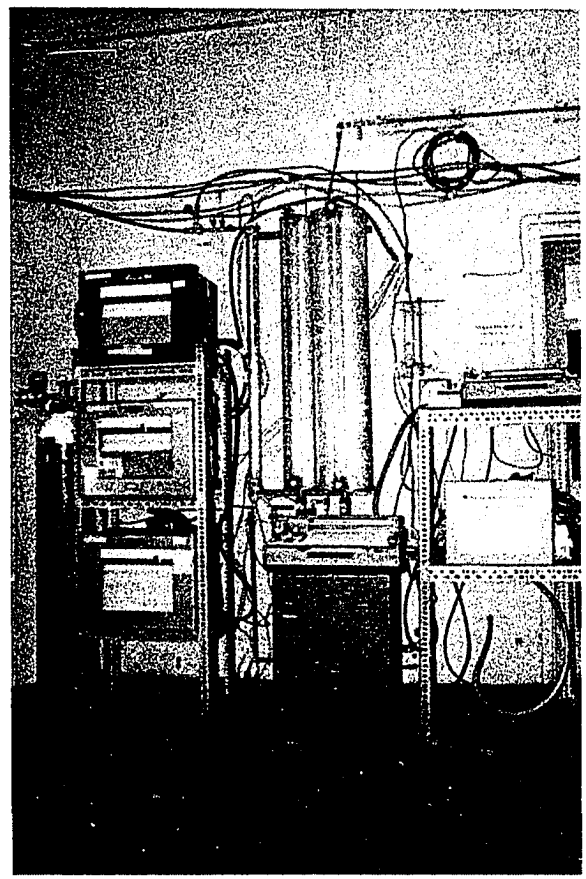


Figure IV-3. Instruments and Equipment Located in Observation Room.

Air entered the test room through three 18-inch square louvers located on the north, east and south walls of the room. The south and east louvers were at floor level and the north louver was in the bottom section of one of the double doors. These louvers were manually adjusted to control the air flow into the room as described in Chapter V.

Probe

The probe is immersed in the center of the flames and serves as a heat transfer measuring device. The probe assembly and parts are shown in Figures IV-4 through IV-12. Figure IV-13 is a photograph of the assembled unit and radiometer supports and shows the location of the water inlet and outlet thermocouples. This design was chosen for the following reasons:

1. It simplifies construction and assembly.
2. The design is symmetrical with circular fuel pans.
3. The small vertical cylinder disrupts the flame shape less than other geometrical shapes.
4. The size of the probe ensures it complete coverage by the flame.
5. Mounting the fuel pan around the probe was much simpler than supporting the probe above the fuel pan.
6. The main reason for this design was to obtain a high surface temperature which would eliminate or reduce the effect of soot accumulation on the probe.

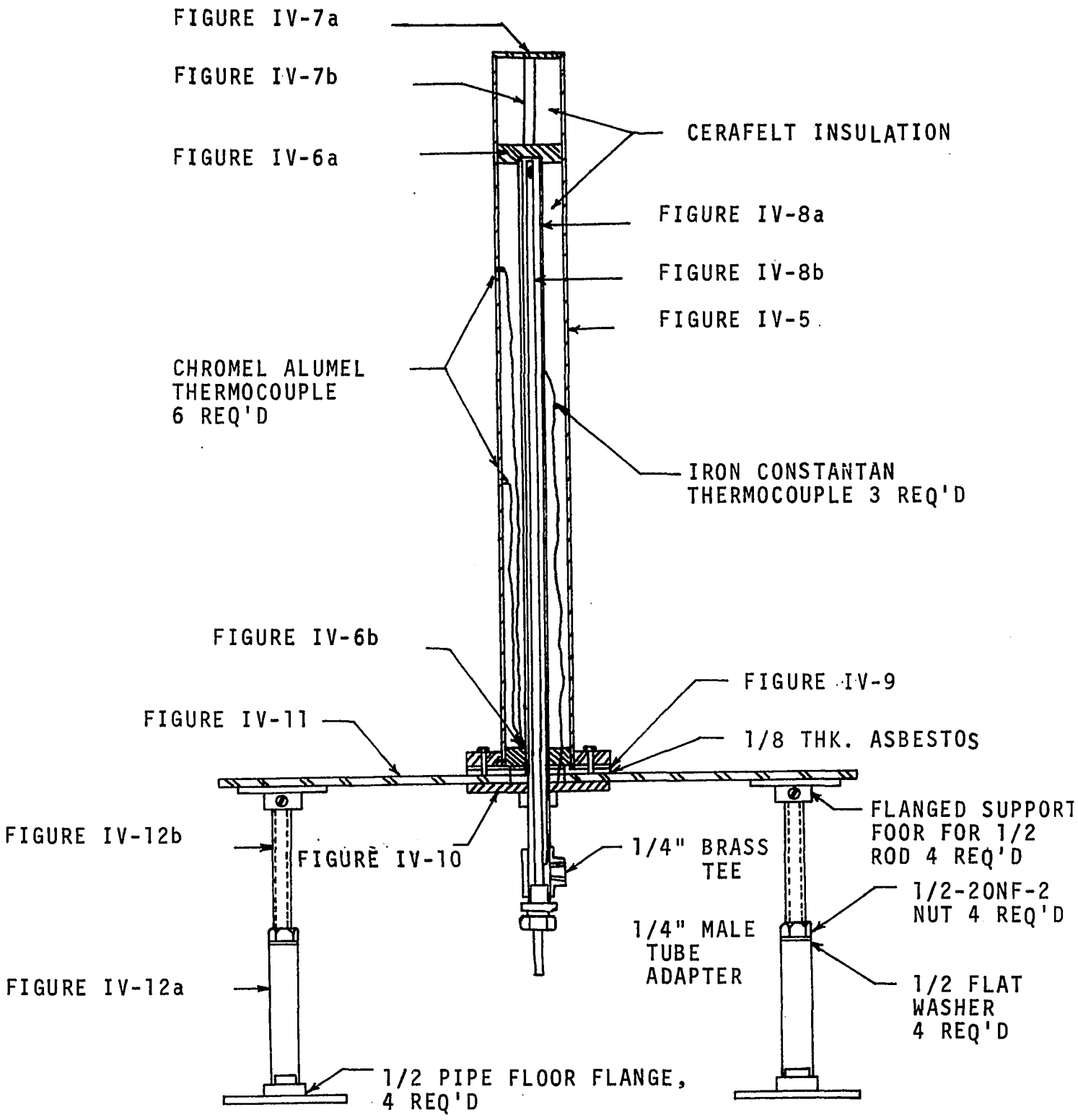


Figure IV-4. Probe Assembly.

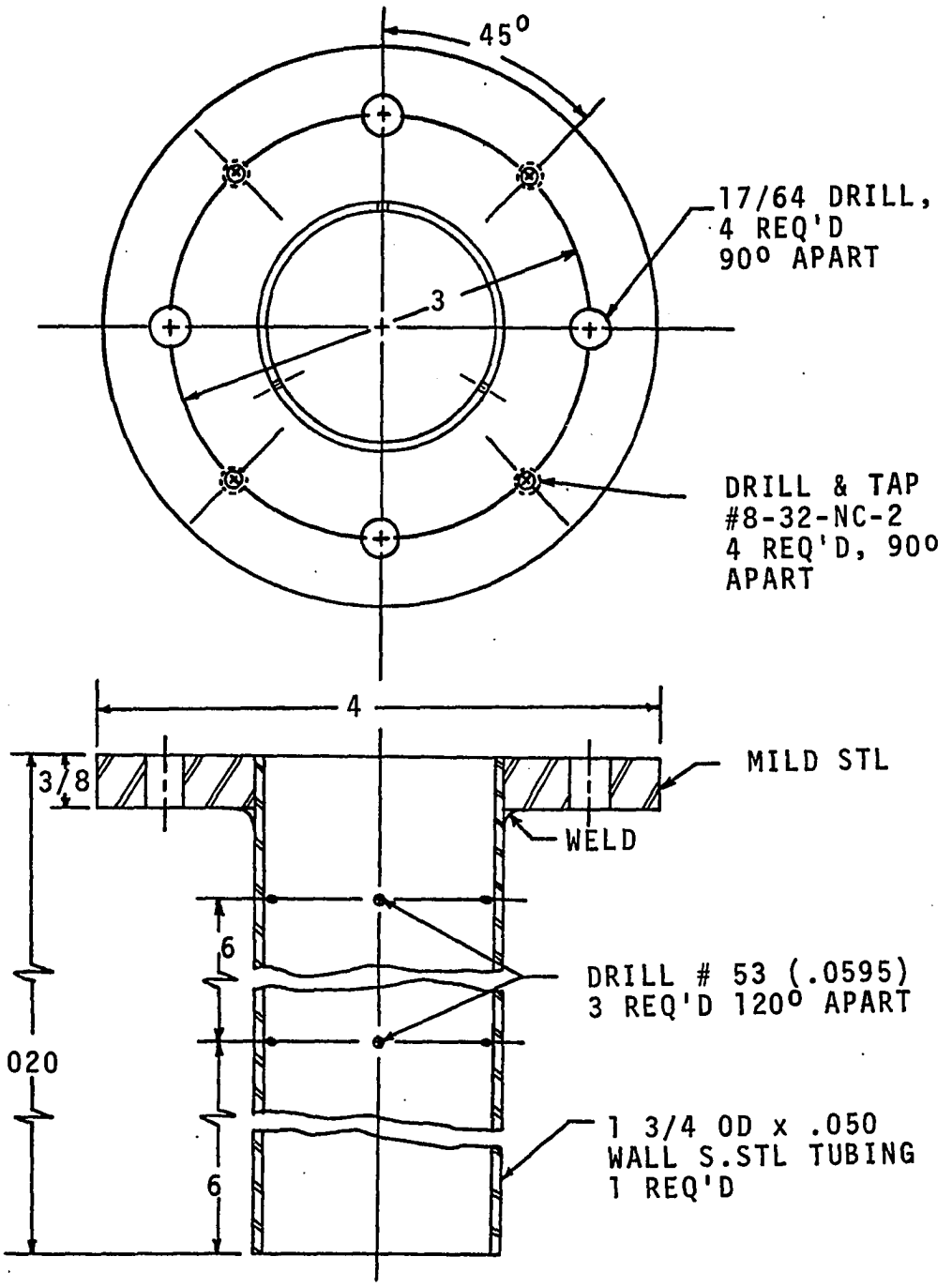


Figure IV-5. Probe Outer Shell.

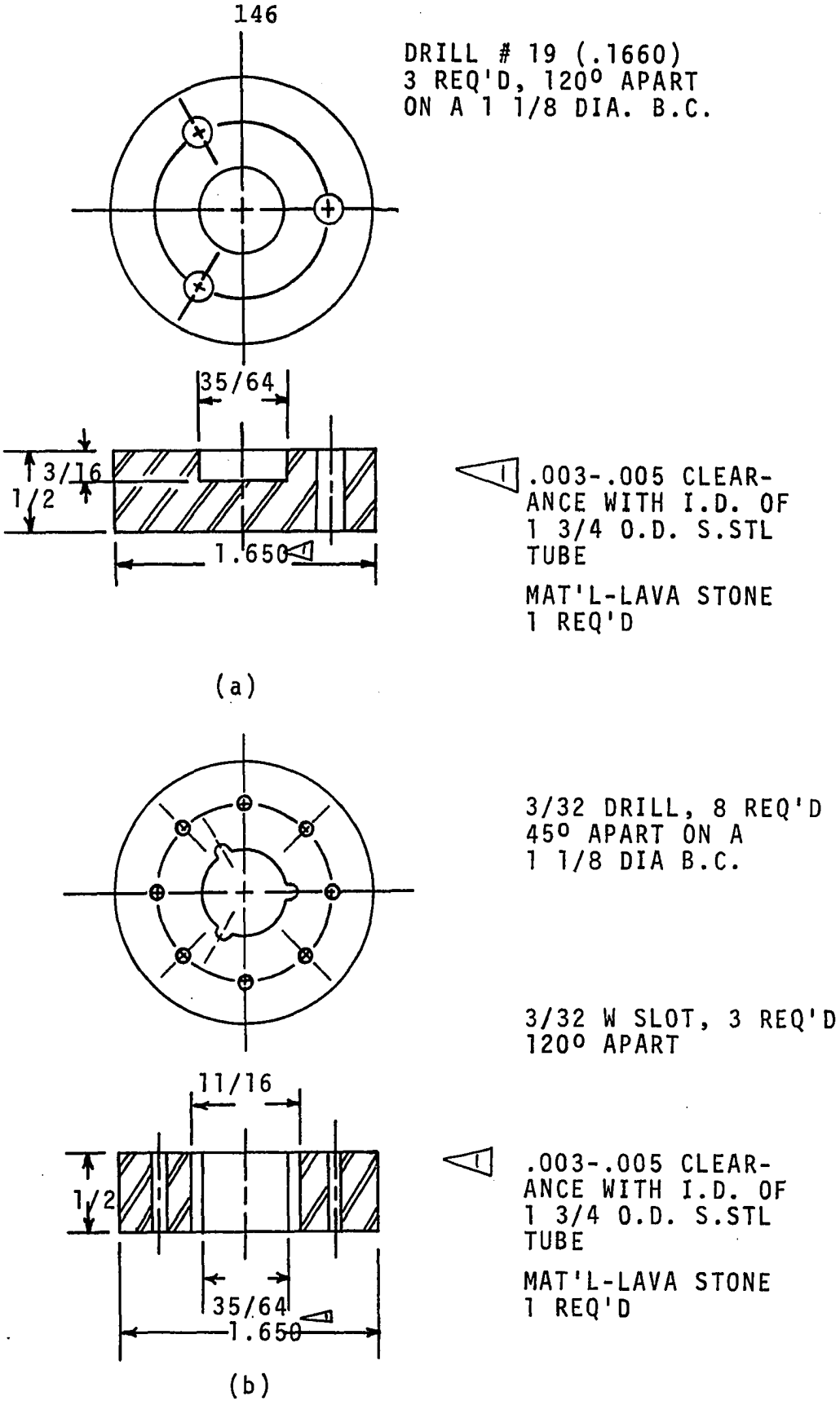
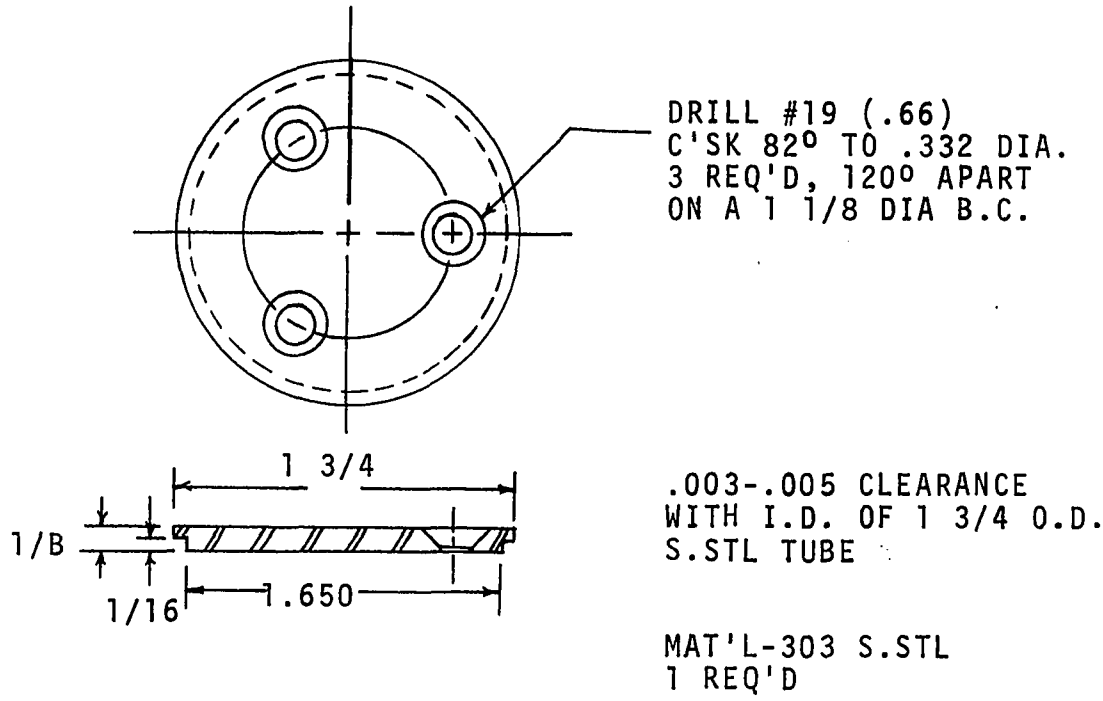
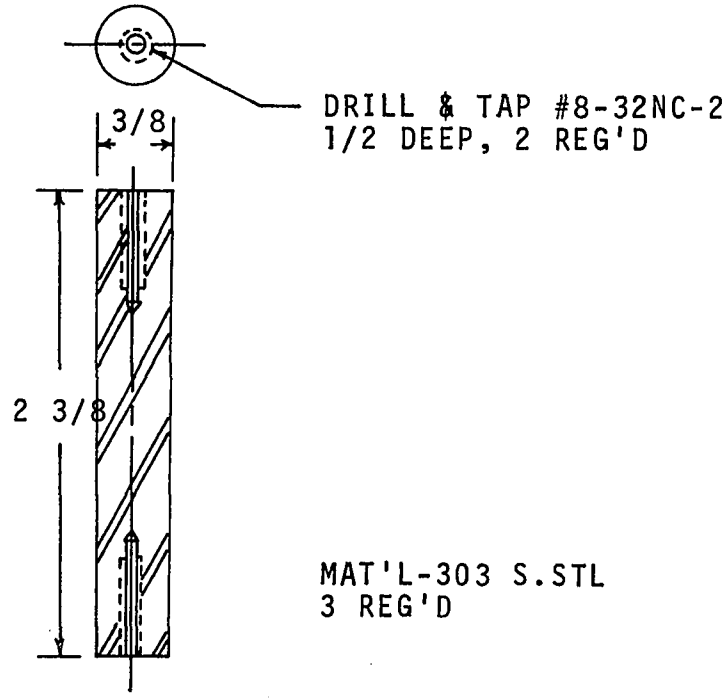


Figure IV-6. (a) Top Insulating Spacer.
(b) Bottom Insulating Spacer.



(a)



(b)

Figure IV-7. (a) Top Cap.
(b) Spacer Rod.

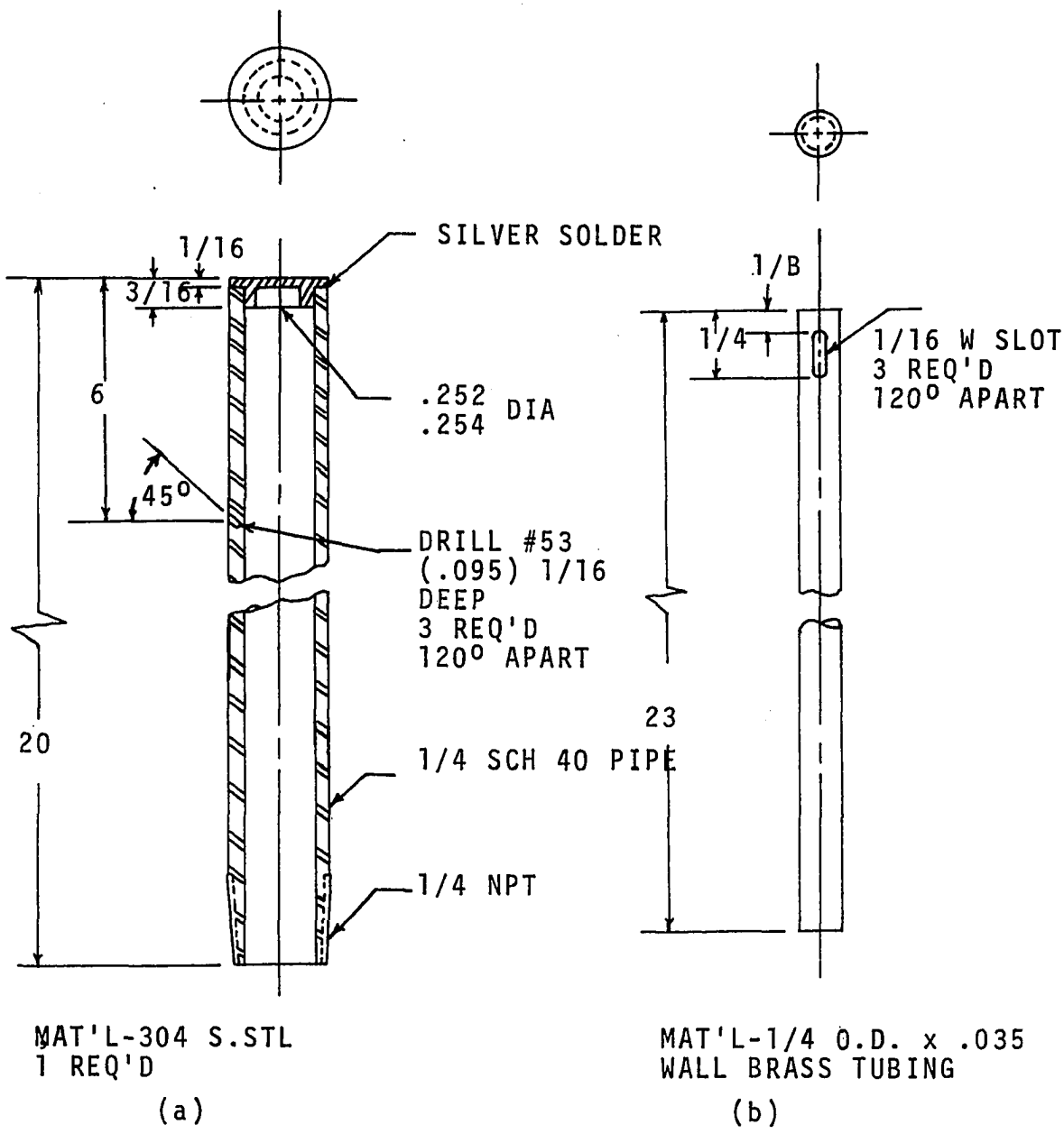


Figure IV-8. (a) Outer Pipe of Bayonet Exchanger.
(b) Inner Pipe of Bayonet Exchanger.

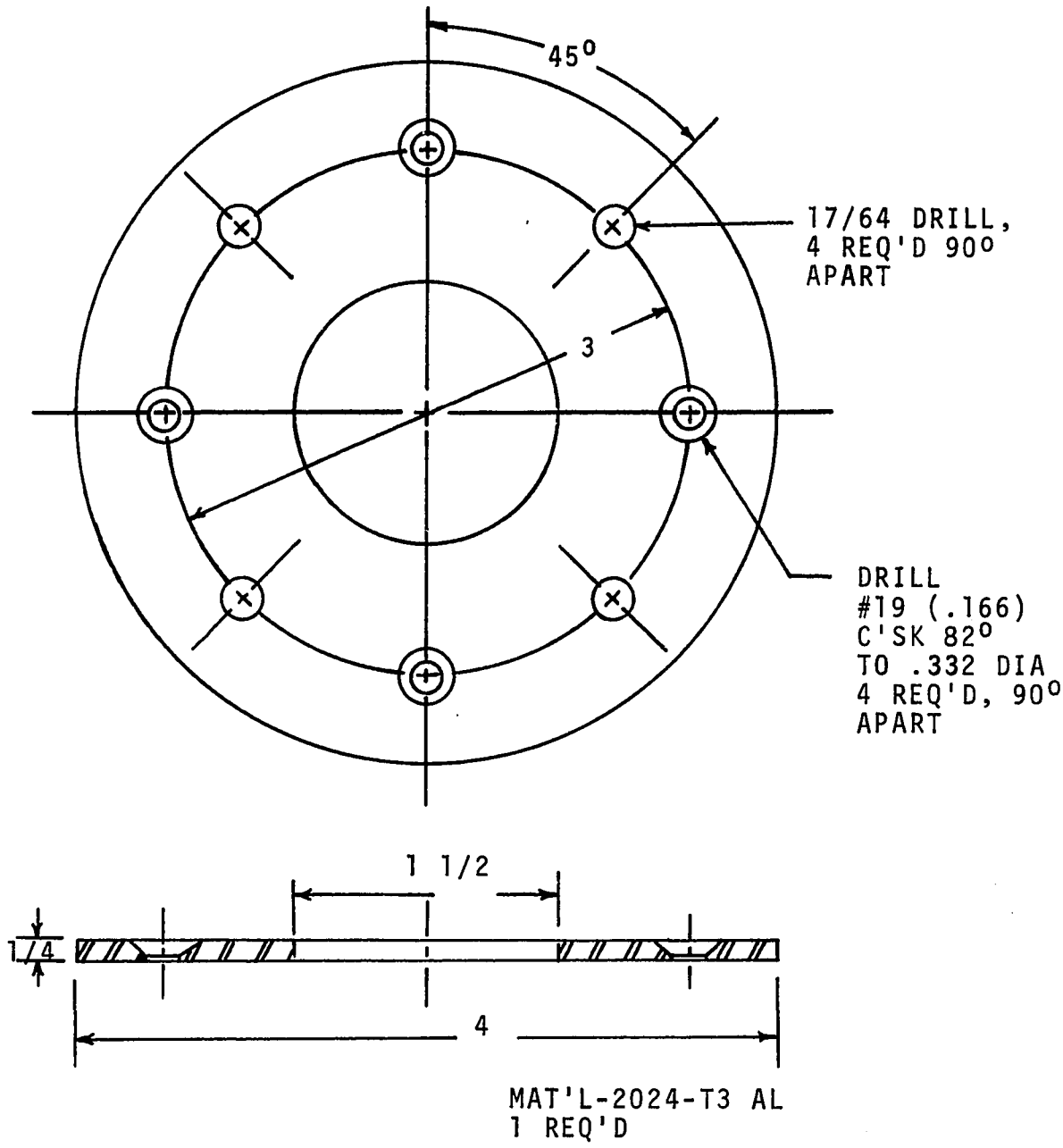


Figure IV-9. Lower Insulating Spacer Retainer.

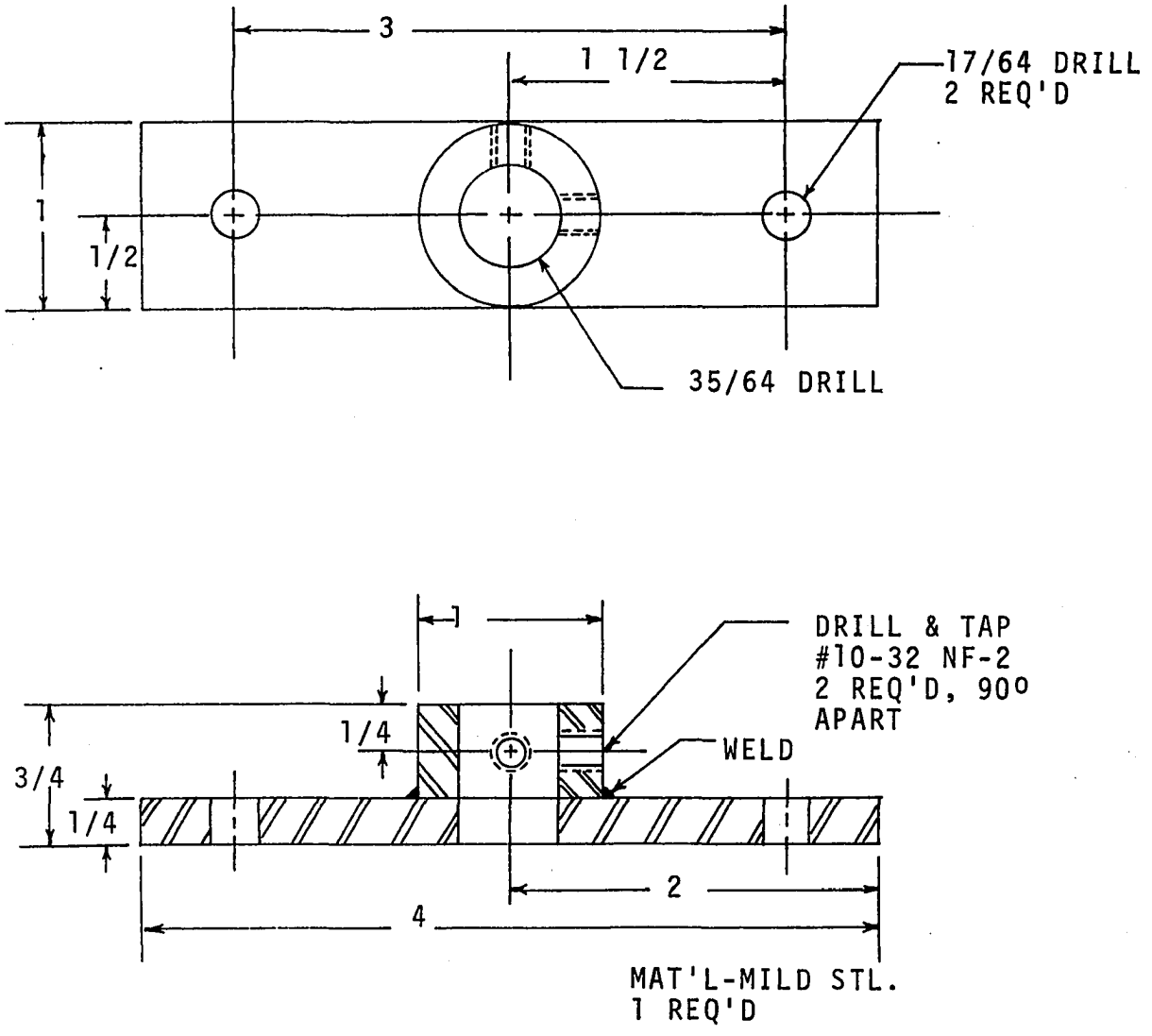


Figure IV-10. Bayonet Exchanger Support Bar.

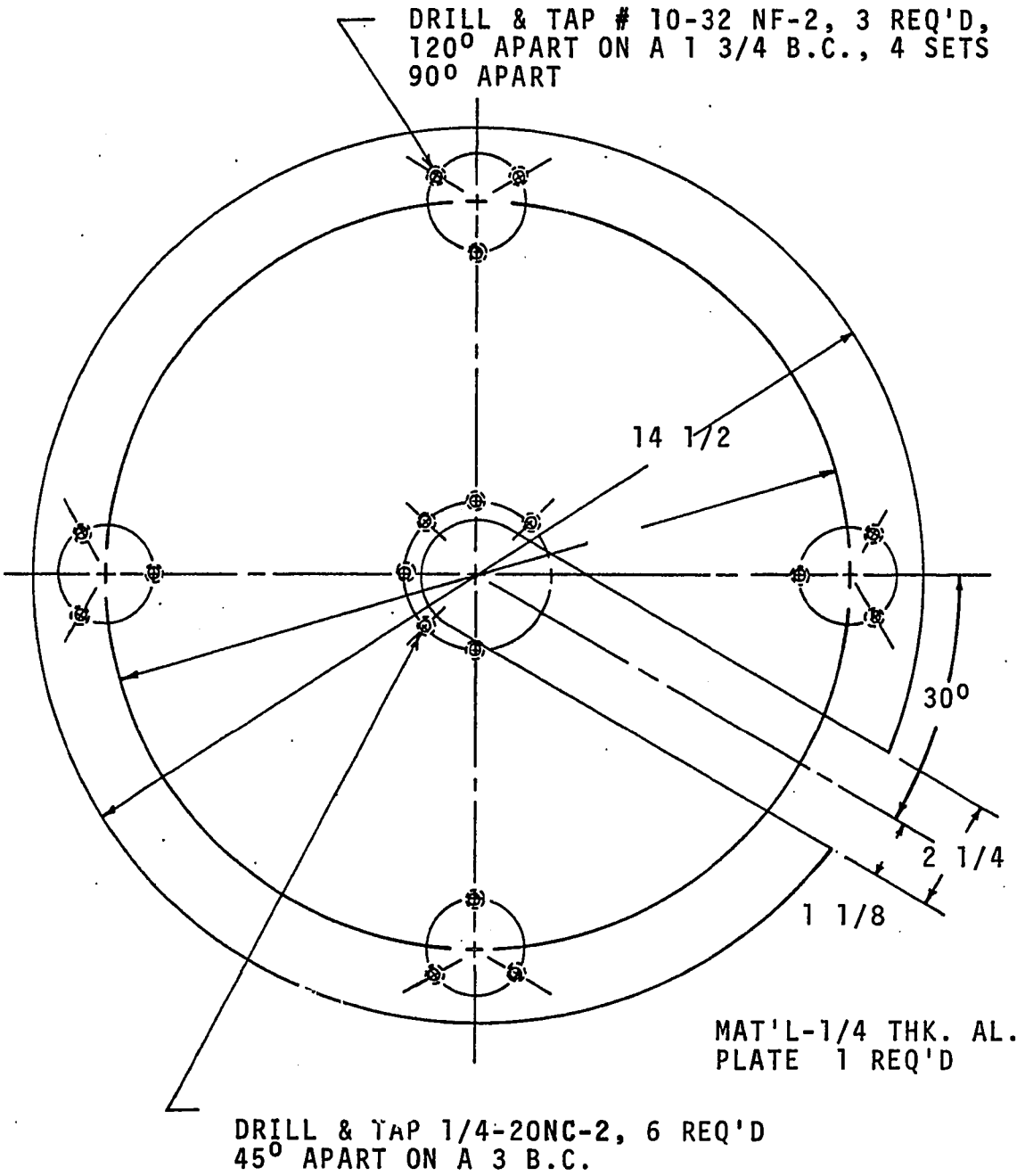


Figure IV-11. Probe Support Plate.

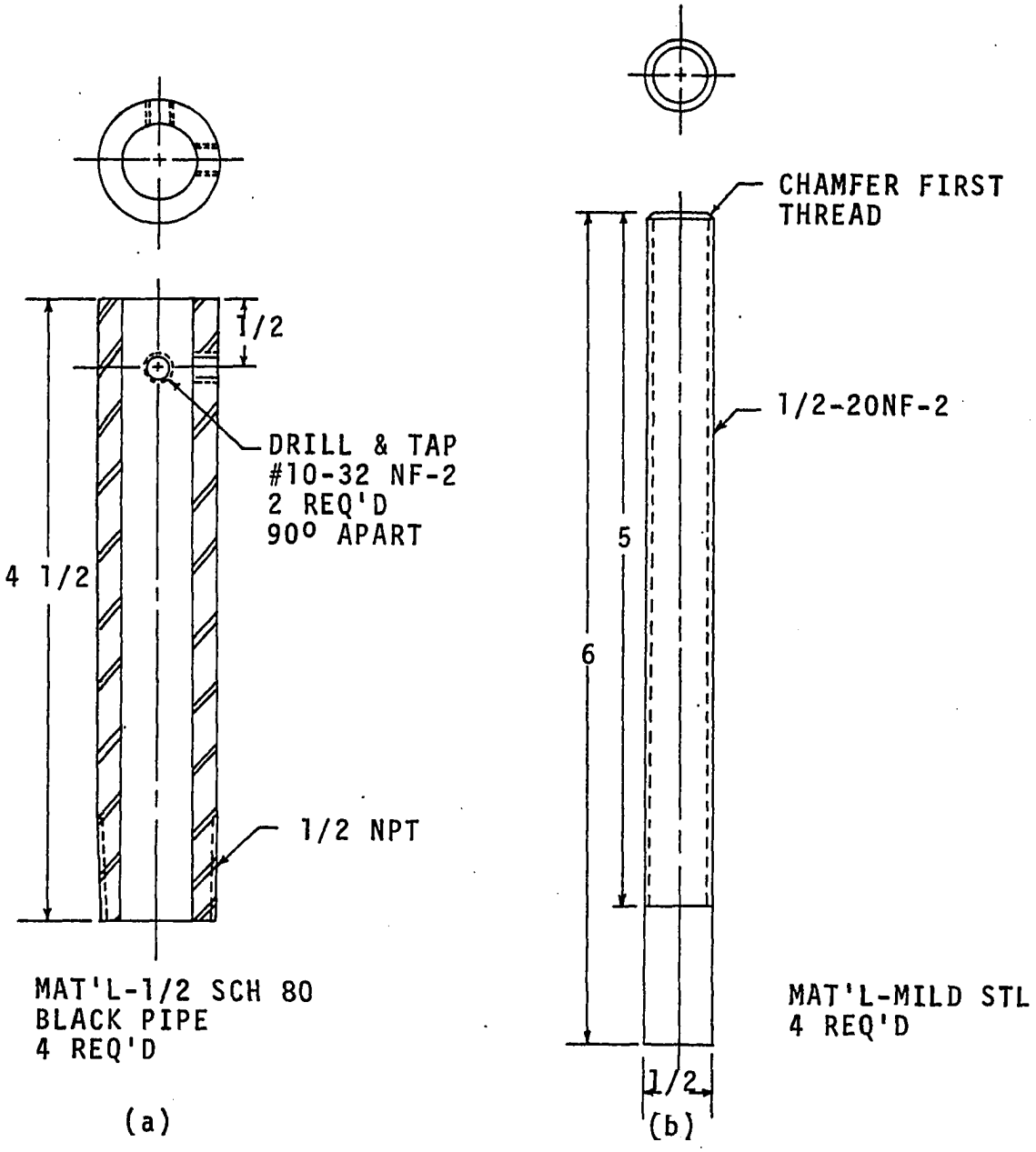


Figure IV-12. (a) Lower Support Leg.
(b) Upper Support Leg.

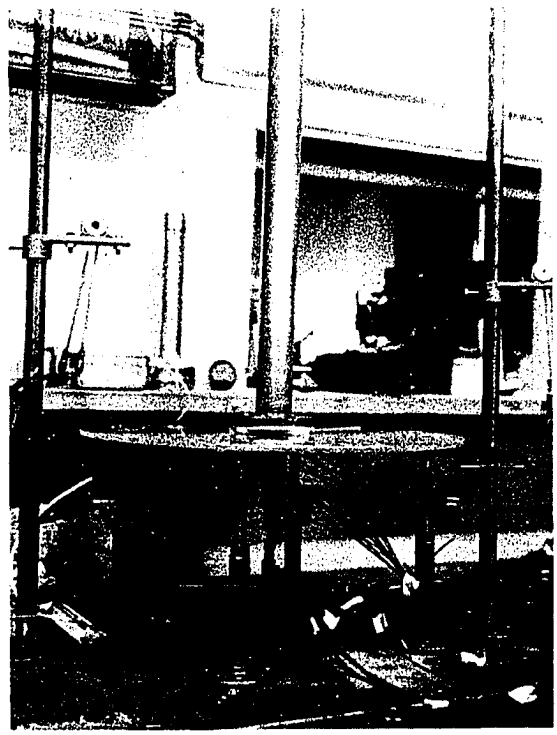


Figure IV-13. Photograph of Probe Assembly and Radiometer Supports.

Neill (50) experienced decreasing heat transfer rates due to soot accumulation on his constant temperature water boiler probe. Deshpande (24) also had decreasing heat transfer rates due to soot accumulation on his water cooled probe. Additional unreported studies at the Flame Dynamics Laboratory showed soot accumulation on a hot oil cooled probe with an 800°F surface temperature.

The probe is essentially an insulated bayonet heat exchanger. Water enters the center tube of the heat exchanger and flows down the annulus. Iron-constantan thermocouples are located at the inlet and outlet of the heat exchanger. Three 24 ga iron-constantan thermocouples were installed in the outer pipe of the heat exchanger with Sauereisen No. 1 Paste Insalute Adhesive Cement. Two of these couples were torn loose from the wall at a later date when the heat exchanger top cap had to be resoldered. Six 24 ga chromel-alumel thermocouples were inserted in the outer shell of the probe. These couples were made by inserting a ceramic insulator over the wires and then twisting the exposed wires. The twisted wires were inserted through the wall of the outer shell until the insulator touched the inside diameter of the tube. The couples were brazed to the tube and the excess wire and brazing material was filed off.

Burners and Fuel Supply System

Three cylindrical carbon steel pans were used during these tests. The dimensions of these burners are given in Figure IV-14. Each burner was supported by asbestos columns resting on the probe support plate. The burners were insulated from the probe by 1/8 inch thick asbestos. After the fuel line was connected, the burner was leveled.

Fuel was stored outside the building in 55 gallon drums. A 1/2-inch copper line was installed between this area and the fuel tank located inside the observation room. Fuel was transferred from the drums to the tank by a Tuthill Fill-Rite Piston Type "Double-Acting" Hand Pump Model F-152. Several thin-wall aluminum fuel tanks were available but only the 10-inch I.D. by 48-inch deep tank was used. A scale was attached to the sight glass on the tank to permit flow measurements to be made. The fuel tank was volumetrically calibrated with water and held 1245 ml of fuel per inch of depth.

The fuel level in the burner was controlled by a constant head siphon system developed by Welker (80) and shown schematically in Figure IV-15. Additional details on the operation of this system can be obtained in Appendix D.

Burn Table

The burn table served as a support for the probe assembly and burners and principal dimensions are shown in

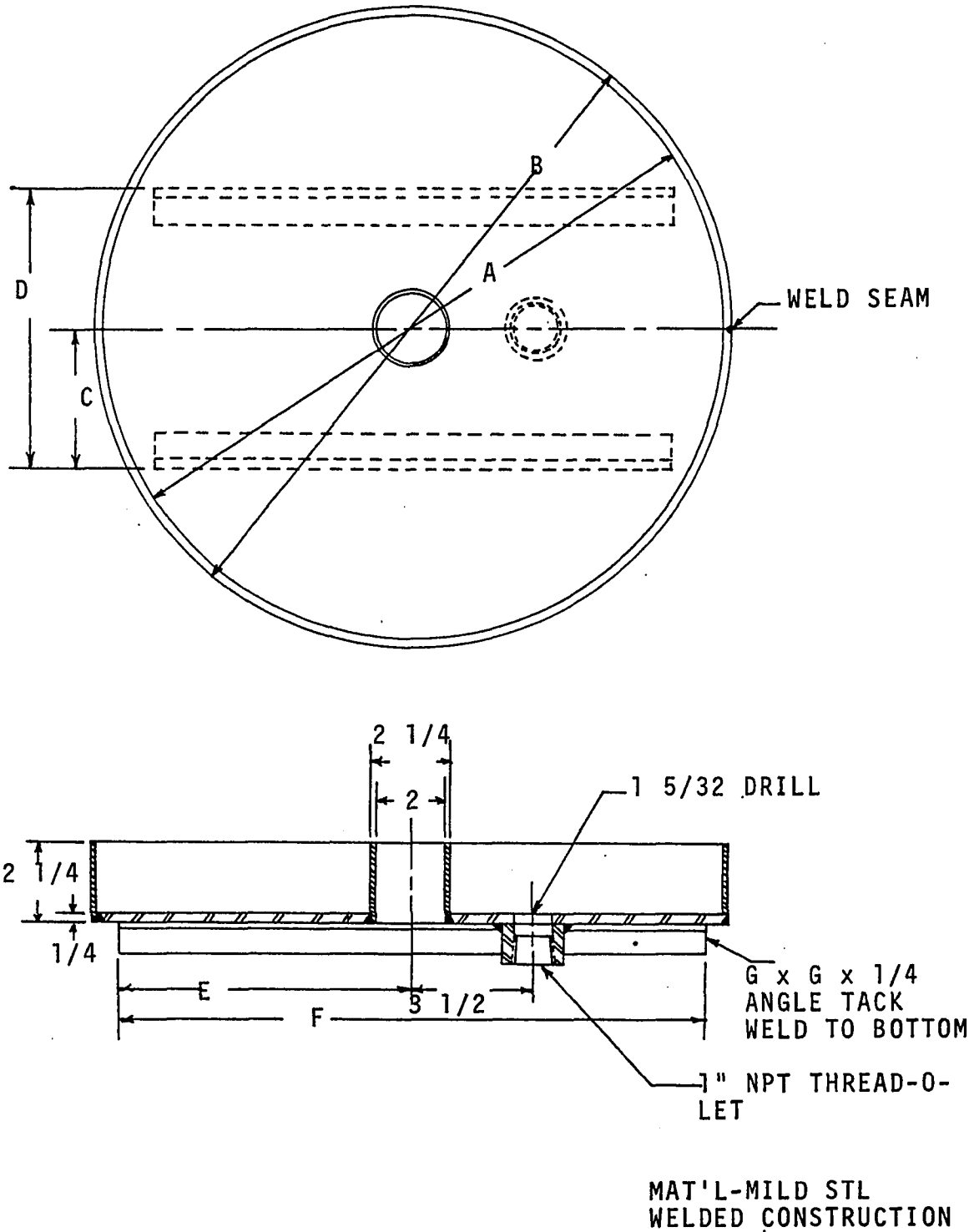


Figure IV-14. Burner.

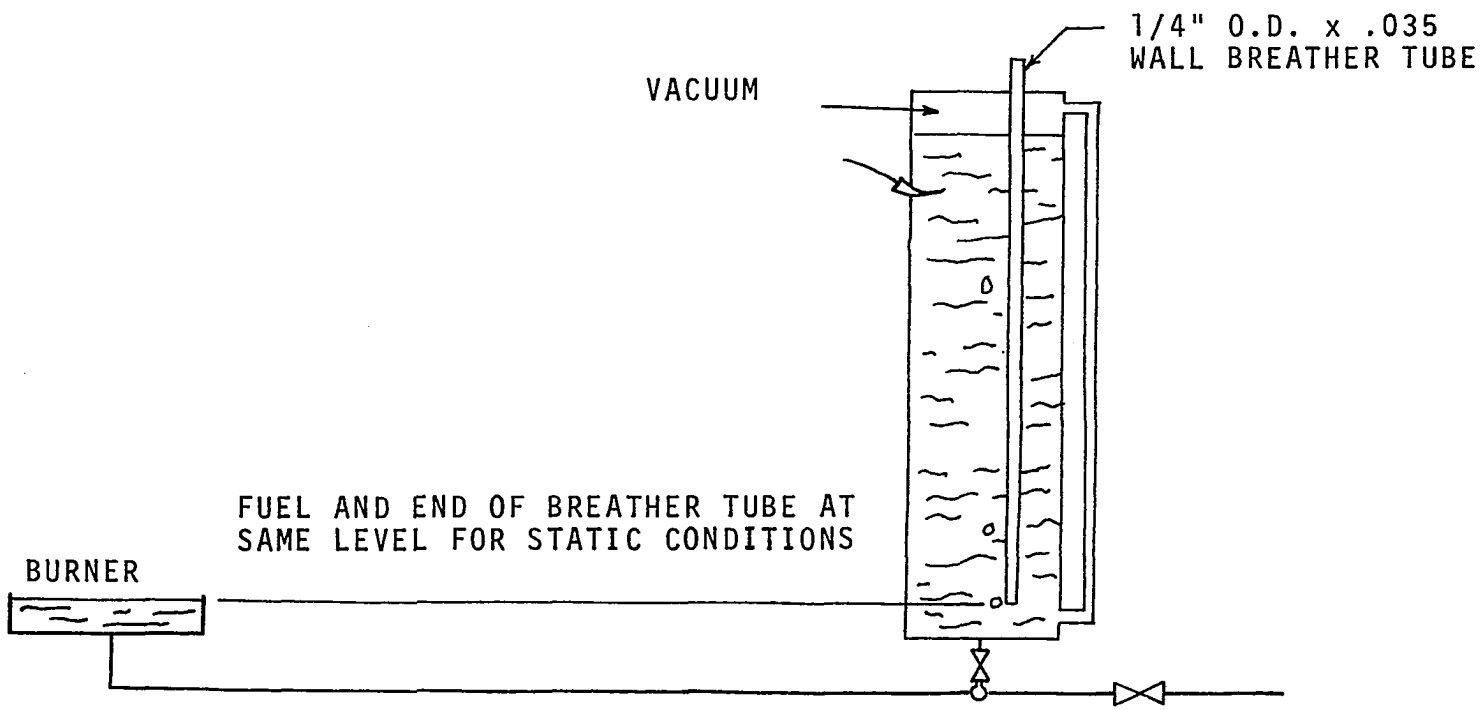


Figure IV-15. Schematic Diagram of Fuel Level Control System.

Figures IV-16 and IV-17. This table was constructed for flame studies but had not been extensively used. Four inch sections of stove pipe surrounded the burner and acted as flow straighteners for the air supply. The double row of 7/8-inch tubes were connected to three centrifugal blowers, each capable of delivering 2000 cfm of air. This air supply acted as a shield against stray air currents that might cause the flame to tilt.

Camera and Film

The cameras were used to photograph the flames and their locations are shown in Figure IV-1. Cameras 1 and 2 were pinhole cameras whose details are given in Figures IV-18 through IV-22. Figure IV-23 is a photograph of a pinhole camera and the Polaroid film holder. Camera 3 was either a Polaroid Model 108 or Model 101 camera.

The shape of a flame is constantly changing, and a mean shape is necessary for determining the flame size and radiative heat transfer. For this reason, the pinhole camera was built. These cameras are easy to use and are resistant to dirt, dust, and soot. Camera No. 1 was bolted to a shelf on the inside of the wind tunnel and could be operated through a window in the observation room. Camera No. 2 was bolted to the bottom of a box mounted on the outside of the north door of the test room. This camera was approximately 90° from Camera No. 1.

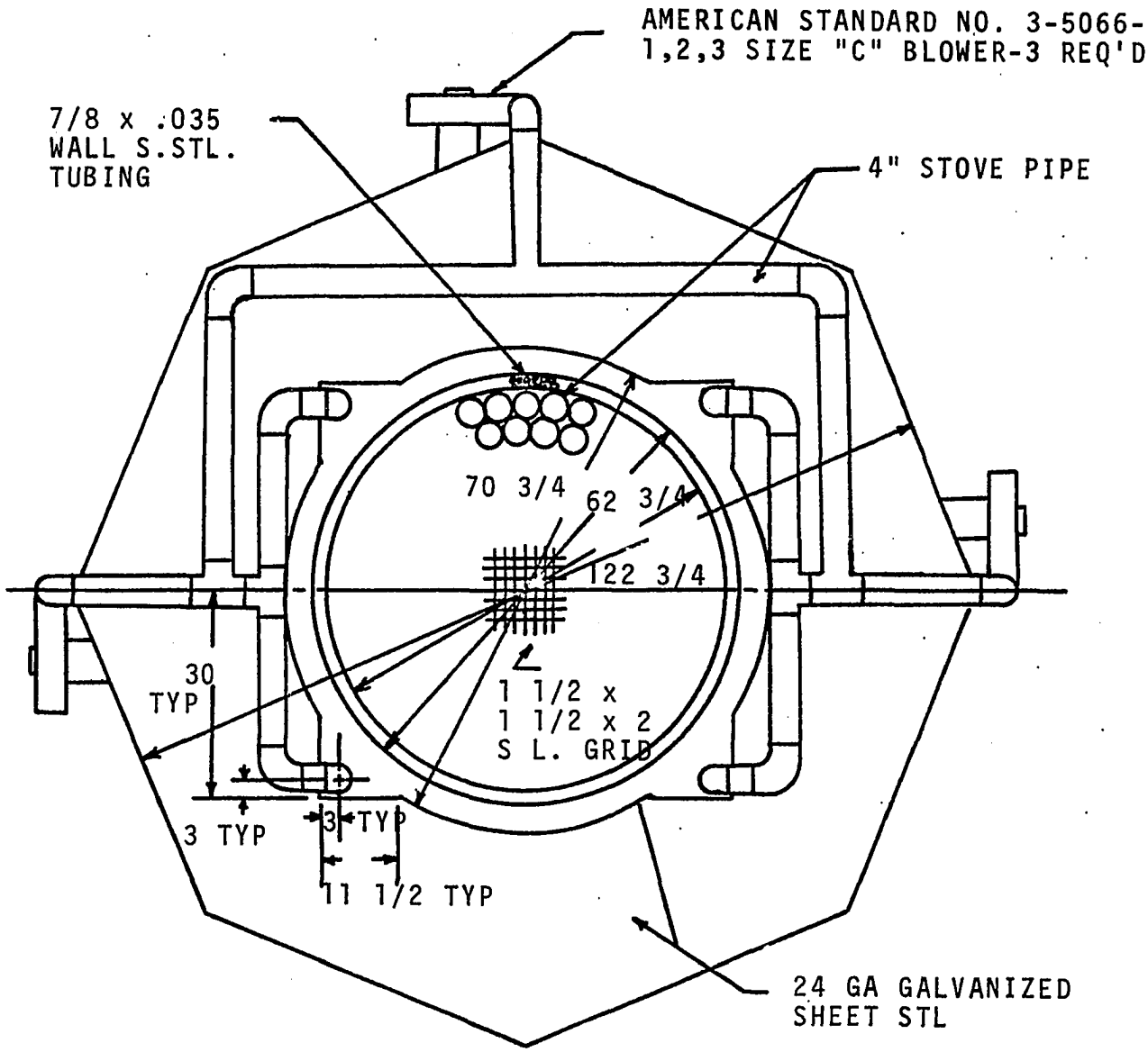


Figure IV-16. Plan View of Burn Table.

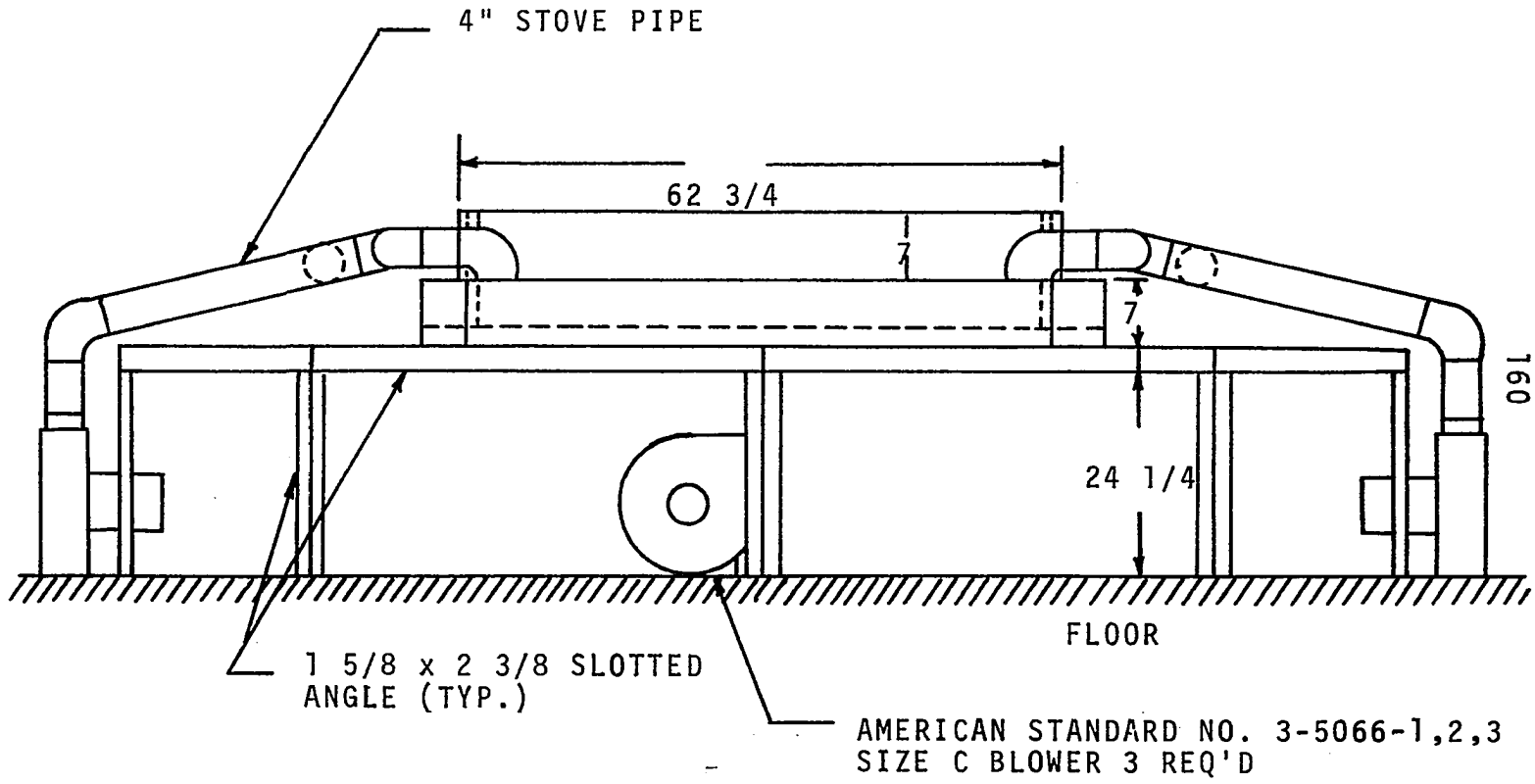


Figure IV-17. Elevation View of Burn Table.

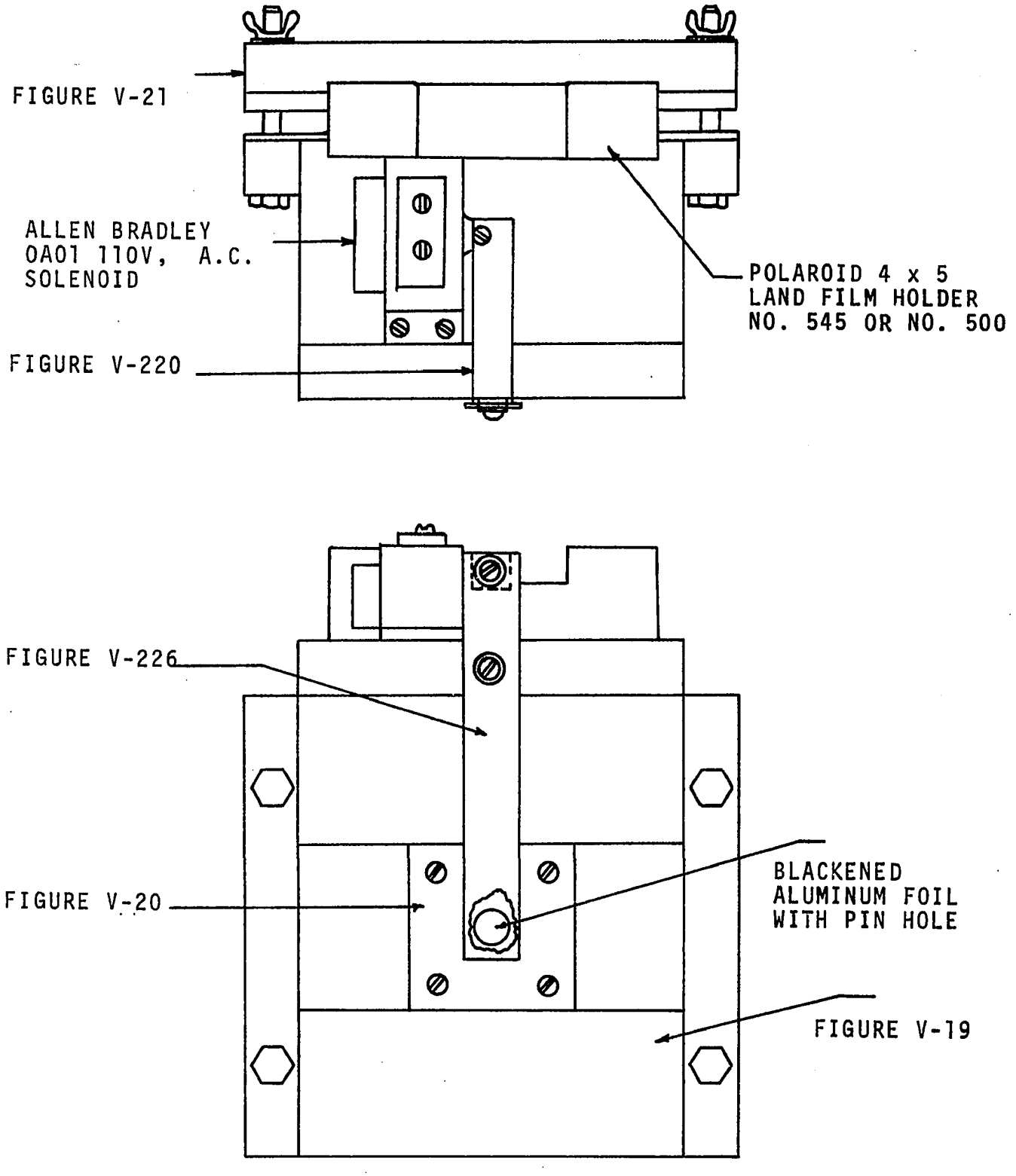
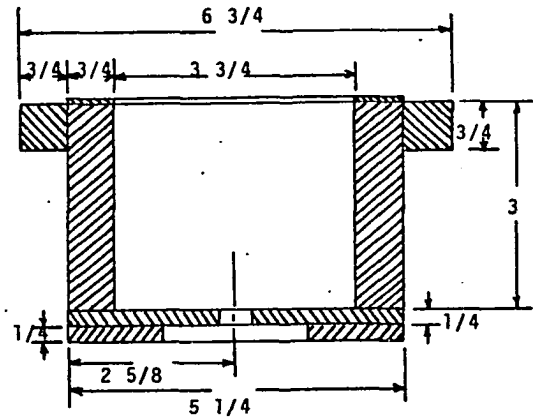
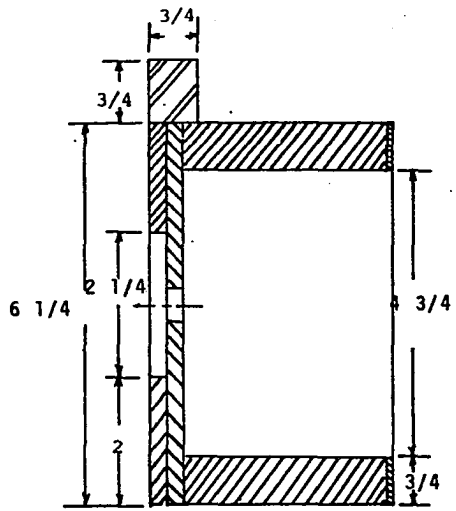


Figure IV-18. Assembly of Pinhole Camera.



NOTE: PAINT FLAT BLACK SPRAY INSIDE
W/ NEXTEL VELVET COATING #101-C10
BLACK
GLUE AND NAIL ALL JOINTS.



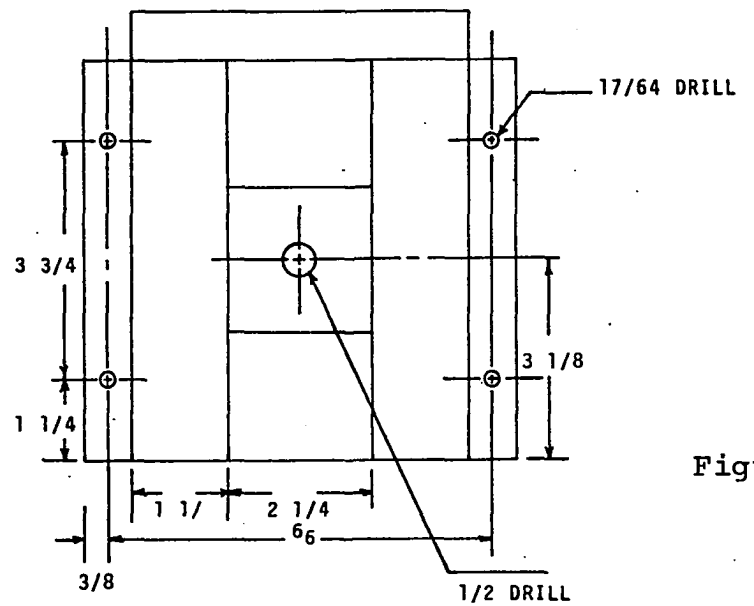


Figure IV-19. Body of Pinhole Camera.

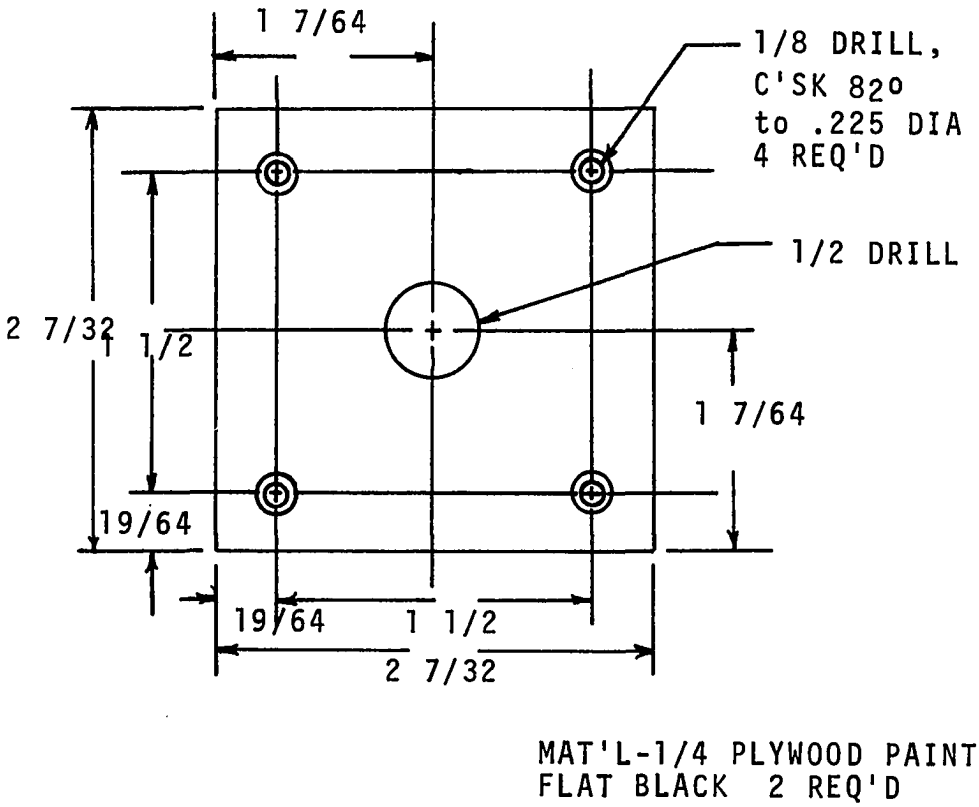


Figure IV-20. Foil Holder for Pinhole Camera.

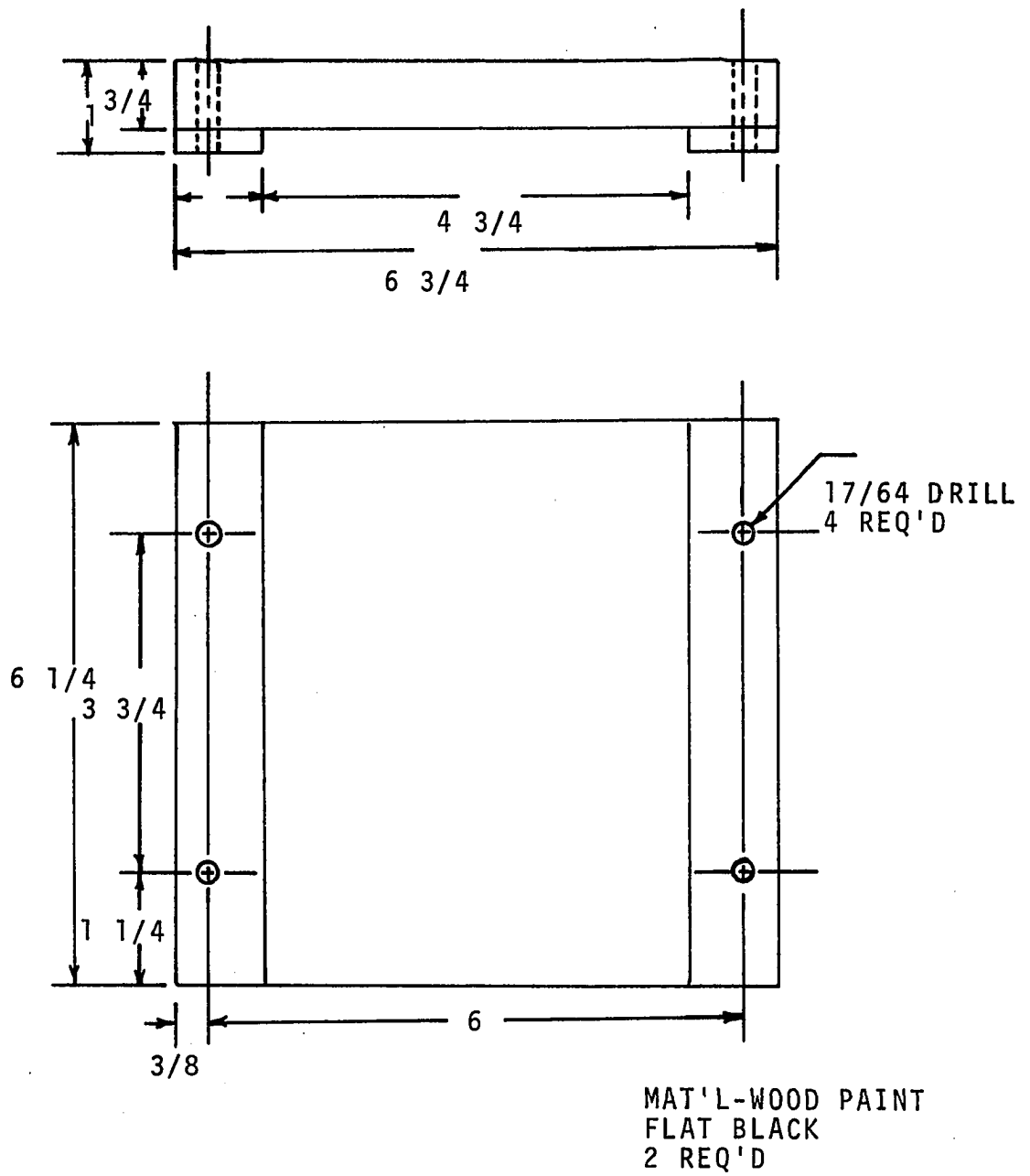
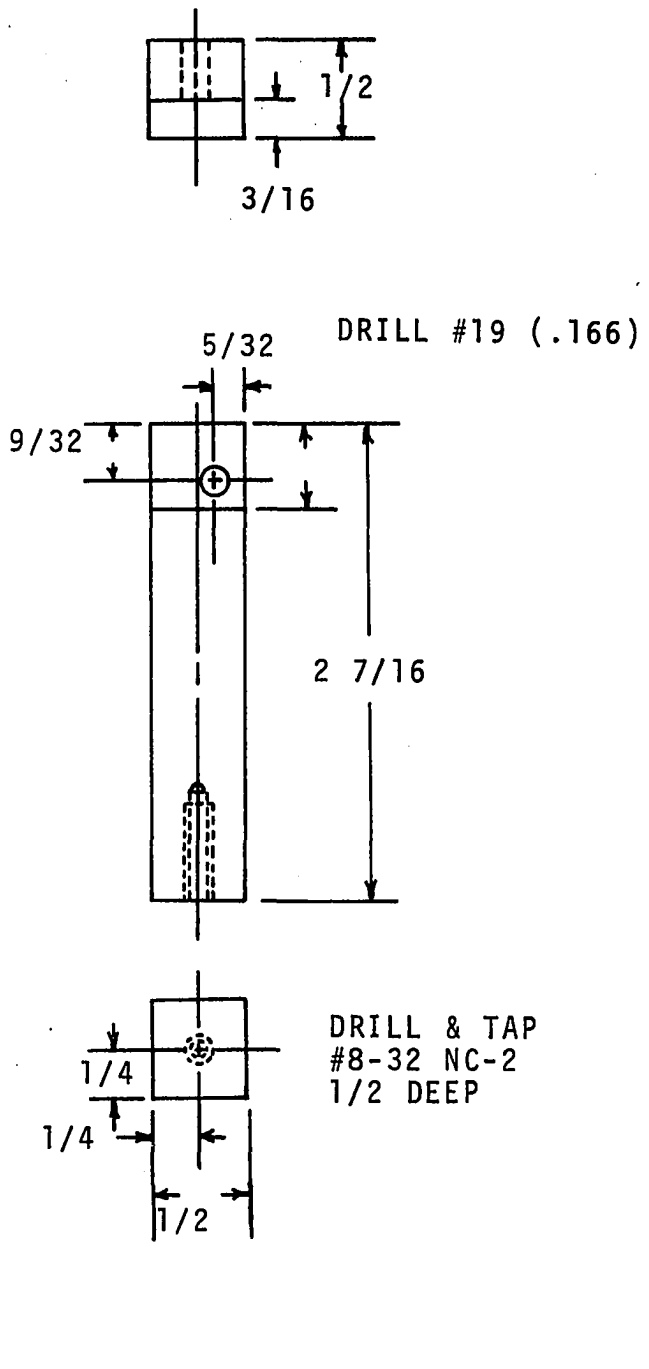


Figure IV-21. Back for Pinhole Camera.



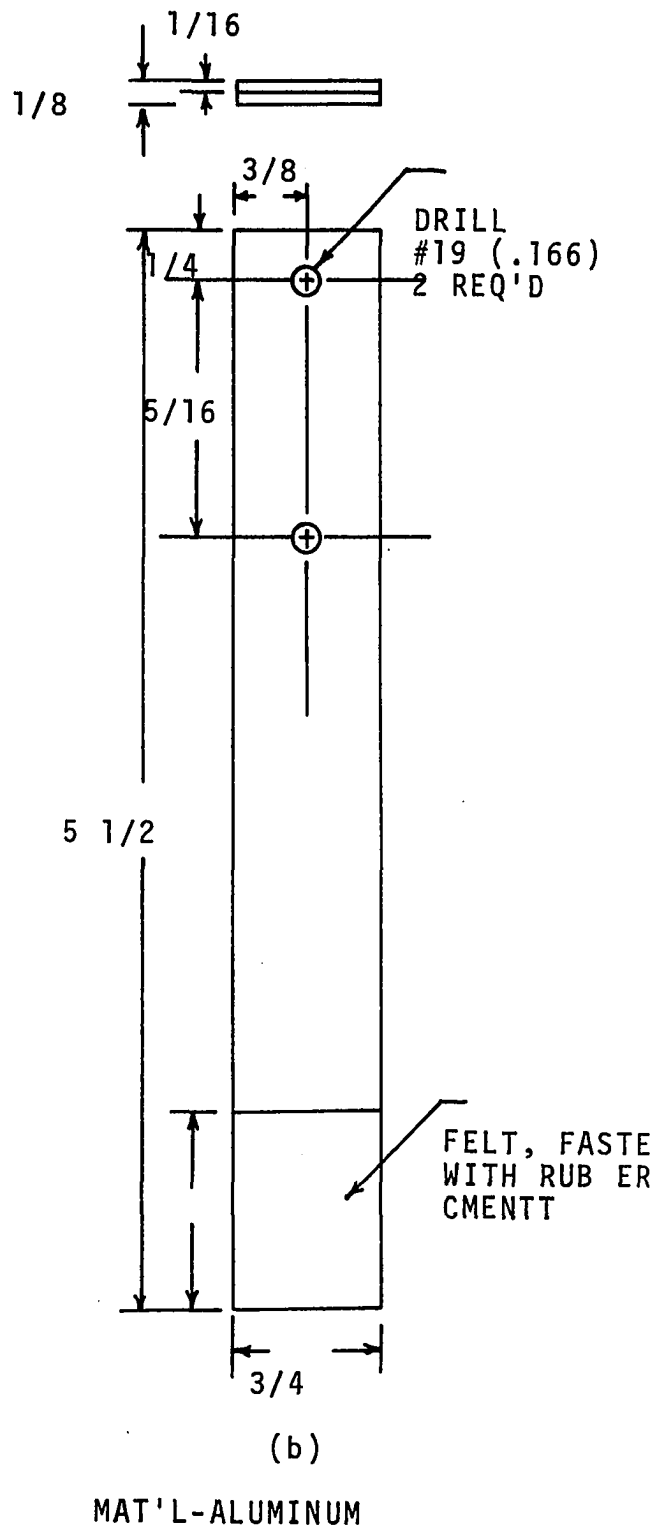


Figure IV-22. (a) Shutter Connecting Bar for Pinhole Camera.
(b) Shutter for Pinhole Camera.

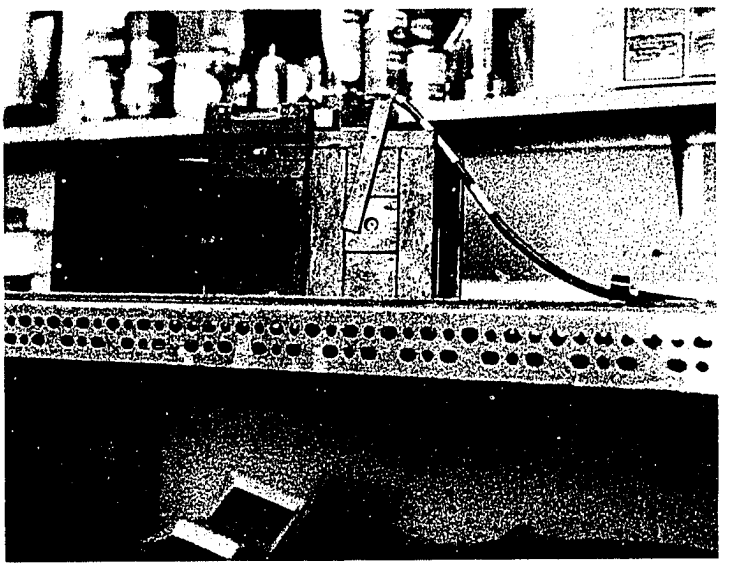


Figure IV-23. Photograph of Pinhole Camera and Polaroid Film Holder.

Camera No. 3 was used to photograph the instantaneous shape of the flame. Immediately before a photograph was desired, this camera was placed in a fixed position on a shelf, located on the test room wall adjacent to the door from the observation room. The camera was removed from the shelf immediately after the picture was taken.

Black and white film with a 3000 ASA speed rating was used in all the flame photography. Cameras 1 and 2 utilized a Polaroid 4 x 5 Land Film Type 57. Polaroid Type 47 Land roll film was used with the Model 108 camera and Polaroid Type 107 Land film pack was used with Model 101 camera.

Radiometers and Flame Temperature Sensors

Radiometers

The two radiometers were Gardon type heat flux meters manufactured by Medtherm Corp. Both radiometers were water cooled, had sapphire windows, and were nitrogen purged to prevent soot accumulation on the window. Radiometer 81510 has a 150° view angle, a sensitivity of 20 Btu/ft^2 sec at 12.08 mv and its calibration curve is shown in Figure IV-24. This curve can be represented by the equation

$$qm = 5960 \text{ (mv) Btu/hr-ft}^2 \qquad \text{(IV-1)}$$

Radiometer 72804 was equipped with a water cooled view restrictor that reduced the view angle to 7 degrees. Its calibration curve is shown in Figure IV-25, and the equation

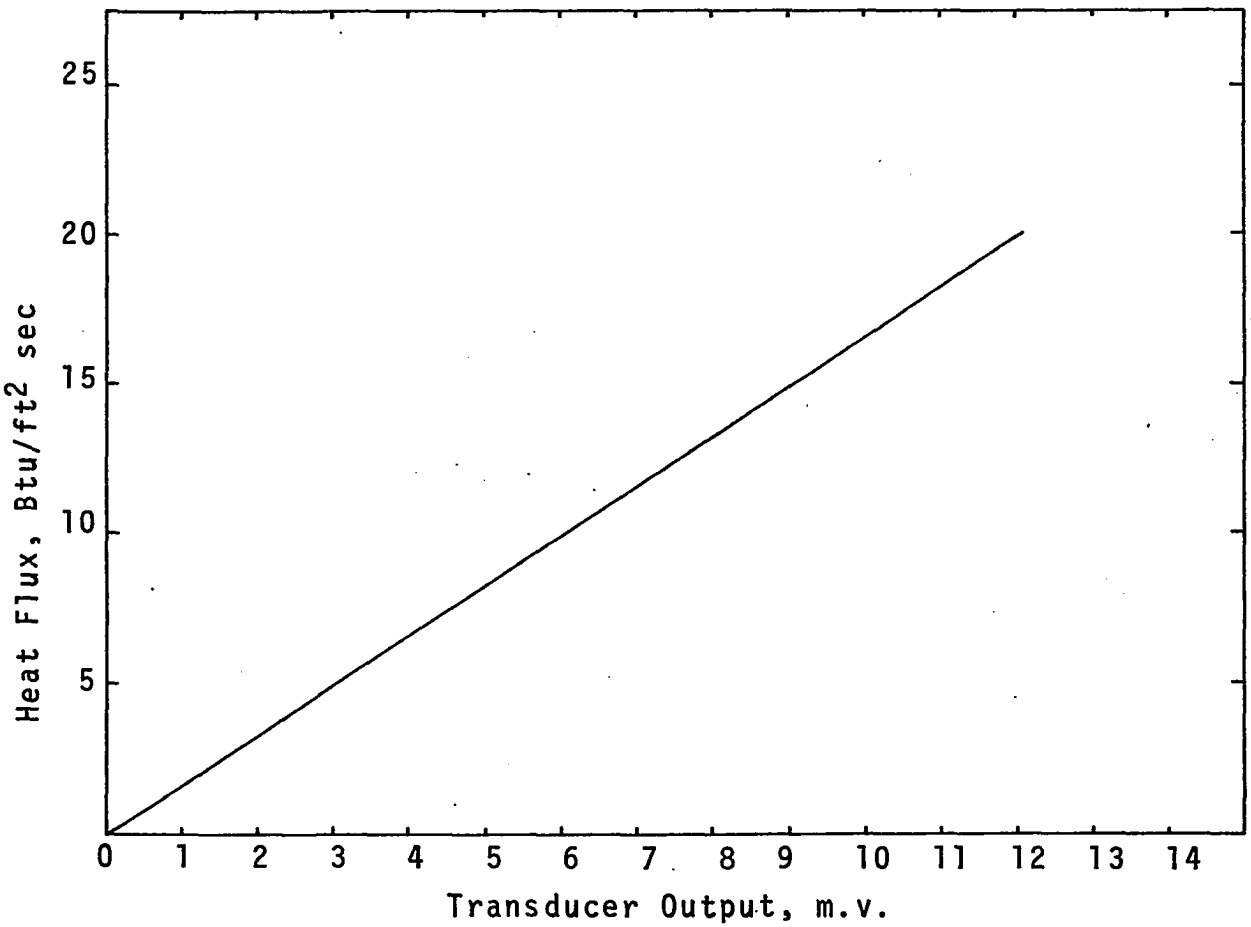


Figure IV-24. Calibration Curve for Radiometer 81510.

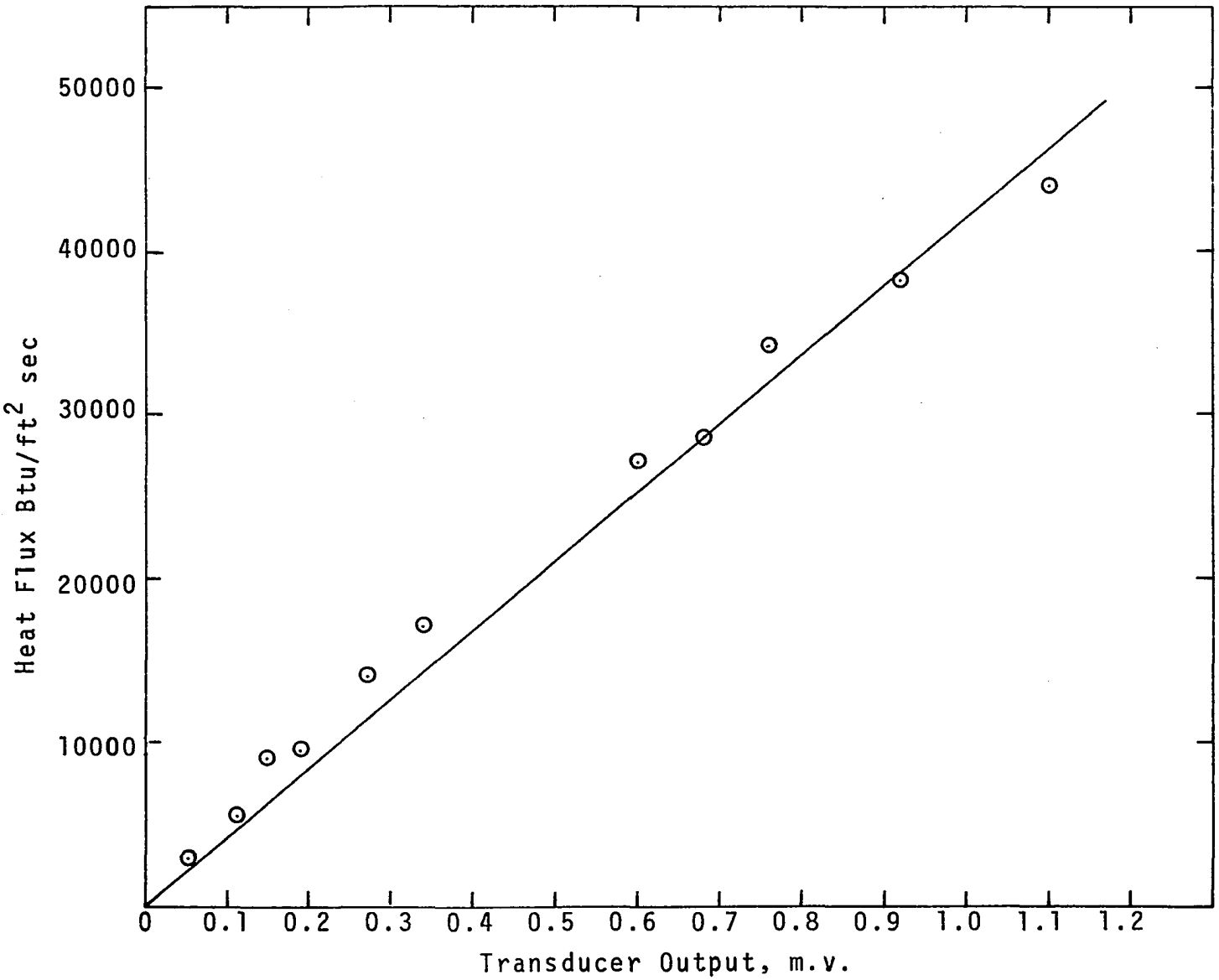


Figure IV-25. Calibration Curve for Radiometer 72804 with a 7° View Restrictor.

of this curve is

$$qm = 42000 \text{ (mv) Btu/hr-ft}^2 \qquad \text{(IV-2)}$$

The radiometers were wrapped with asbestos tape and clamped to the mounting bracket shown in Figure IV-26. This bracket was slipped over a 1/2-inch pipe, fastened to the burn table, and held in position by two 1/4-inch set screws. The location of the radiometers is shown in Figure IV-27.

Flame Temperature Sensors

The flame temperature for all fuels except methanol was measured with a Leeds & Northrup 8623-C double adjustment potentiometer type optical pyrometer. This instrument is a disappearing type brightness pyrometer, with null-balance, lamp current measuring circuit with ranges of 775-1225°C and 1075-1750°C.

A small cylinder, whose dimensions are shown in Figure IV-28 was suspended above the flames by a cable. A chromel-alumel thermocouple was inserted in the center of the cylinder. The temperature obtained by this method needs to be corrected to give flame temperatures.

Instrumentation

Table IV-1 contains the additional instrumentation used for this study.

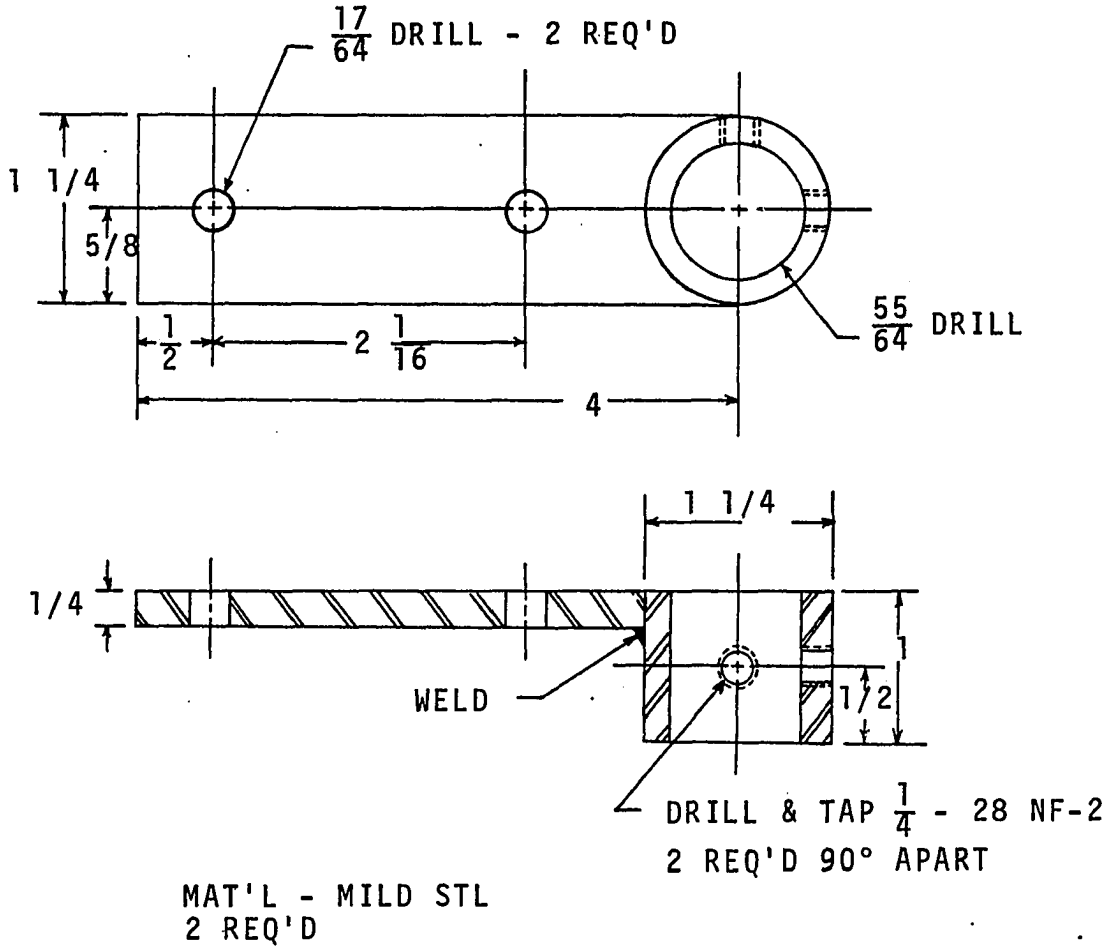


Figure IV-26. Radiometer Mounting Bracket.

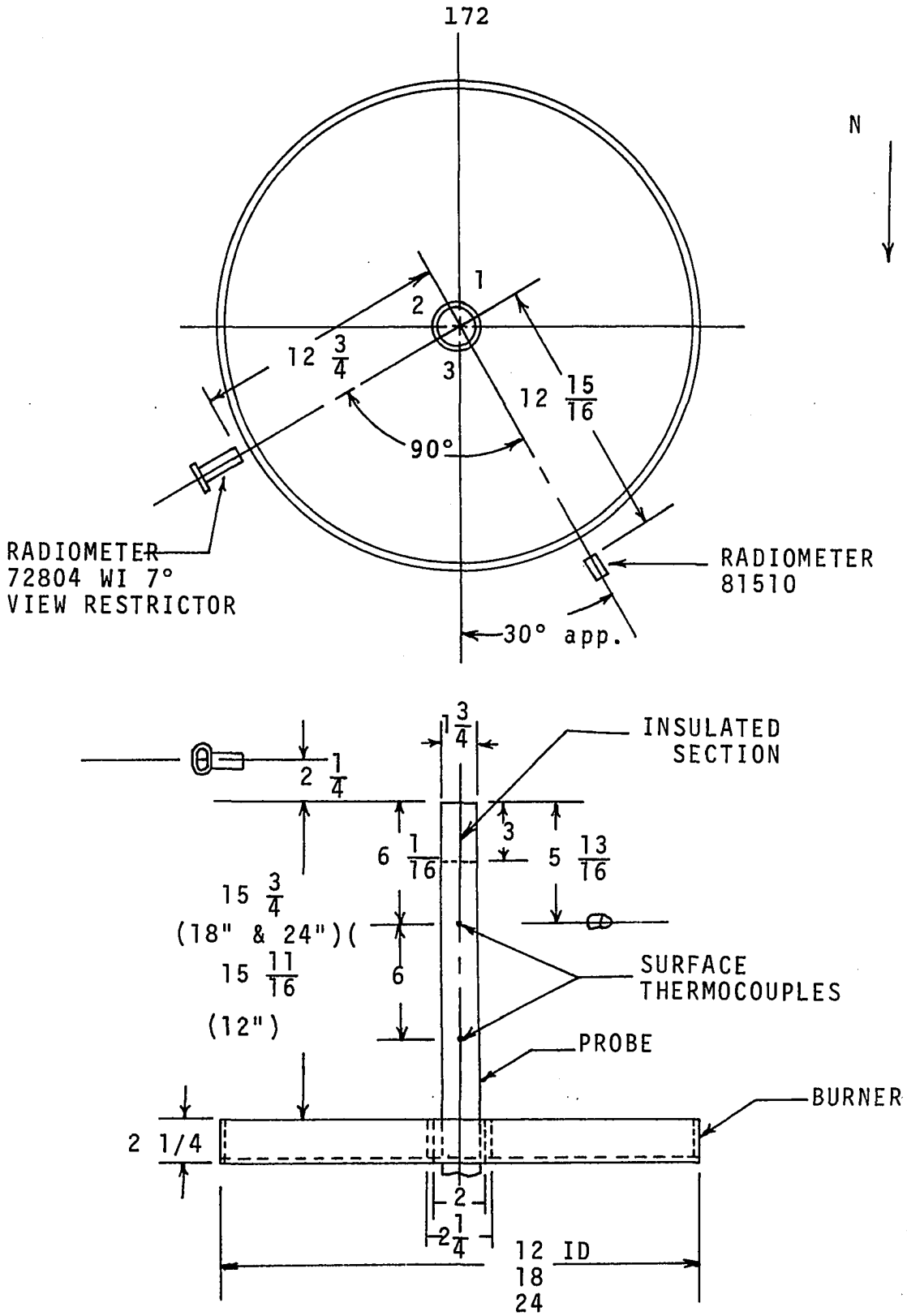


Figure IV-27. Radiometer and Thermocouple Locations.

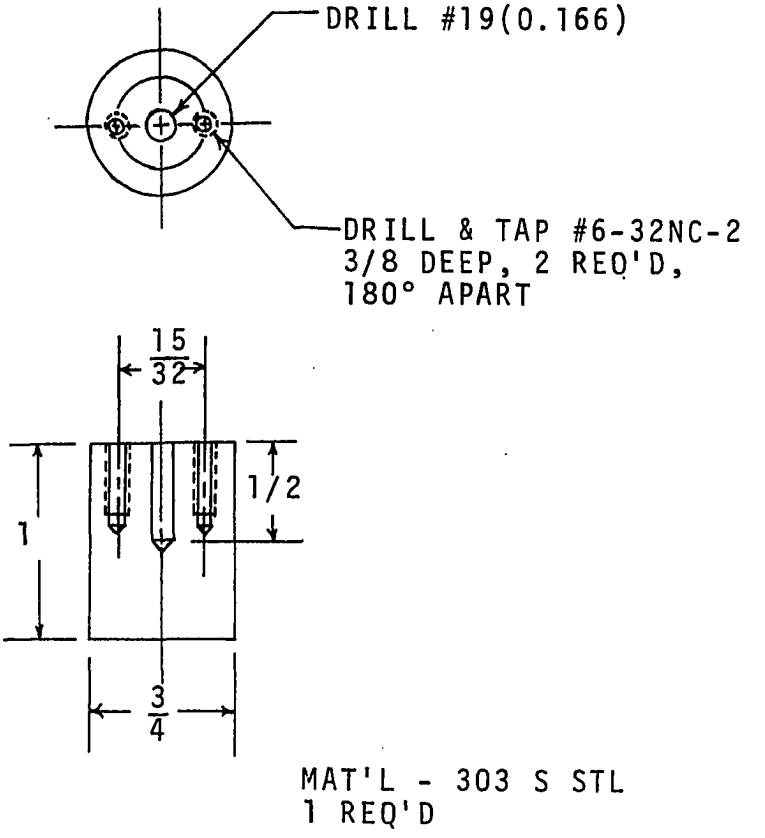


Figure IV-28. Temperature Sensing Cylinder.

TABLE IV-1

ADDITIONAL INSTRUMENTATION

Quantity	Instrument	Use
1	Roger Gilmont Instruments, Inc. flowmeter No. F1500 Serial No. E928, range 0-0.5 gpm	Measure water flow in probe heat exchanger
1	Leeds & Northrup Co. Speedomax W, 12 point recorder, chart speed 4 & 30 in/hr, time/point 6 sec, response time 1 sec full travel, Type K thermocouple range card	Measure probe surface temperature
2	Leeds & Northrup Co. Speedomax X/L 680 millivolt recorder, range 1, 2, 5, 10, 50, 100 mv, chart speed 30, 300, 600, 1200, 2250 cm/hr, span step 0.5 sec min, response time 1.5 sec max	Measure output from radiometers
1	Honeywell Brown Electronik Model Y153X18-P-II-III-(66) -L Single Pen Recorder,0-2000°F Type K thermocouple	Cylinder flame temperature measurement
1	Honeywell Brown Electronik Model SY153X18(PH)-II- -III-66(L) Single Pen Recorder, 0-2000°F Type K thermocouple	Cylinder flame temperature measurement
1	Honeywell Brown Electronik Model 153X64P12-X-141, twelve point recorder 0-100°F Type J thermocouple	Measure probe heat exchanger water inlet and outlet temperature
1	Honeywell Brown Electronik Model 153X64P12-X-141, twelve point recorder 0-100°F Type J thermocouple	Measure temperature of fuel, test room air, probe water inlet and outlet, probe heat exchanger surface

TABLE IV-1--Continued

Quantity	Instrument	Use
1	The Standard Electric Time Co. Type S-60 Reset Timer Minutes and Seconds	Short term fuel consumption time
1	Precision Scientific Co., reset timer, minutes and hundreds	Total test time

CHAPTER V

EXPERIMENTAL PROCEDURE

Numerous experiments were conducted prior to the planned series of tests in order to evaluate the performance of the equipment, to obtain operating ranges for the variables and to learn how to stabilize the flame. To obtain a stable free-burning flame was more of an art than a science with these experiments. It was determined that the exhaust fan had no significant effect on the flame; the air cushion around the burn table helped to stabilize the flame from stray air currents in the test room; if the wind velocity outside the building was excessive, a stable fire could not be obtained; and the small louvers at the base of the test room had to be adjusted to obtain a symmetrical flame. The louver facing the wind was normally closed and sealed. This was generally the north or south louver as the prevailing winds were in these directions. The east louver did not have a significant effect on the flame. If the wind was from the east the flame could not be stabilized because there was no louver on the west side. The air flow into the test room from a louver would hit the opposite wall and reverse itself.

Air flow from the east would travel up the wind tunnel. A small louver in the wind tunnel had no effect on the flame. One of the original aims of these tests was to eliminate the effects of the soot deposits on the probe. It was discovered that when the fuel was allowed to burn completely out of the pan, that just before extinguishment the flame column decreased in height and all the soot was burned off the probe. When this occurred, the surface temperature of the probe was completely uniform and was slightly higher than obtained during the test. To obtain a small height flame, the burner was filled with sand and the fuel was allowed to diffuse through the sand bed. A small bright flame was obtained, but the flame was not uniform due to the uneven diffusion of the fuel through the sand. The sand was replaced by expanded perlite and some improvement in the fuel diffusion resulted. Once again it was difficult to control the amount and diffusion of the fuel. If too much fuel were present, a tall flame resulted and the perlite bed expanded and expulsion of the bed occurred. Another disadvantage of the sand or perlite bed is the longer time periods required for all the fuel to burn out of the bed after fuel flow is ceased.

During these tests it was noticed that the soot formation occurred in the first few minutes of the test and did not have a significant effect on the heat removed from the probe. Therefore, it was decided to conduct the tests

with plain fuel pans and to keep the fuel level near the bottom of the pan.

In all tests the following experimental procedure was followed:

1. The exhaust fans in the test room were started.
2. The Brown recorders were left on constantly and the L & N recorders were switched on and allowed a minimum of 30 minutes to warm-up.
3. Water was circulated through the probe at a pre-set rate.
4. The probe surface and radiometers were cleaned with methanol.
5. Pinhole Camera No. 2 was mounted in position.
6. Fuel was transferred from the 55 gal drum to the tank in the control room with a drum pump.
7. The constant head syphon rod was set to the desired level.
8. The valve on the bottom of the fuel tank was opened until the fuel filled the line to the burner.
9. Nitrogen flow was started to the radiometers.
10. All instruments were checked to insure proper operation.
11. Initial values of fuel level and water rate were recorded.
12. The valve on the fuel tank was opened and the fuel level was allowed to reach a quasi-stable position. Complete stability was not obtained in the 24-inch diameter pan because the time required caused too much fuel vapors to collect around the table.

13. The fuel was then ignited. All fuels except Jet A were ignited by a lighted match thrown into the fuel. Jet A required a burning wad of paper to ignite.
14. The test timer was started immediately after ignition and all recorder charts were marked, and the fuel level was recorded.
15. The air blowers were switched on.
16. Periodically during the test instantaneous burning rate data were obtained.
17. Flame temperatures were measured with the optical pyrometer.
18. About 10 minutes were required before the probe surface temperature reached steady state. When this occurred these values and visual observation of the flame from two locations determined if the flame was concentric with the probe. If not, the small louvers on the door and walls of the test room were adjusted to obtain stability.
19. Water flow remained steady throughout the test and was constantly monitered.
20. Pictures of the flame were taken after the flame was judged to be stable.
21. Tests times of approximately 30 to 60 minutes were normal.
22. To conclude a test, the valve on the fuel tank was closed and the test timer stopped. Fuel was then drained from the pan to extinguish the flame.

23. The water flow to the probe was increased to its maximum to cool the probe.
24. The air blowers were turned off and the valve on the nitrogen cylinder was closed.
25. The test time and final fuel level were recorded.
26. After the probe had cooled sufficiently, the soot thickness was measured with a small scale.
27. Soot was then brushed and vacuumed from the probe, fuel pan, and surrounding area.
28. Charts were removed from the recorders.
29. If additional tests were to be run, the test procedure was started at step 3. If no more tests were to be run, the fuel was drained from the tank, water flow was stopped, the exhaust fans were turned off, and the L & N recorders were also turned off.

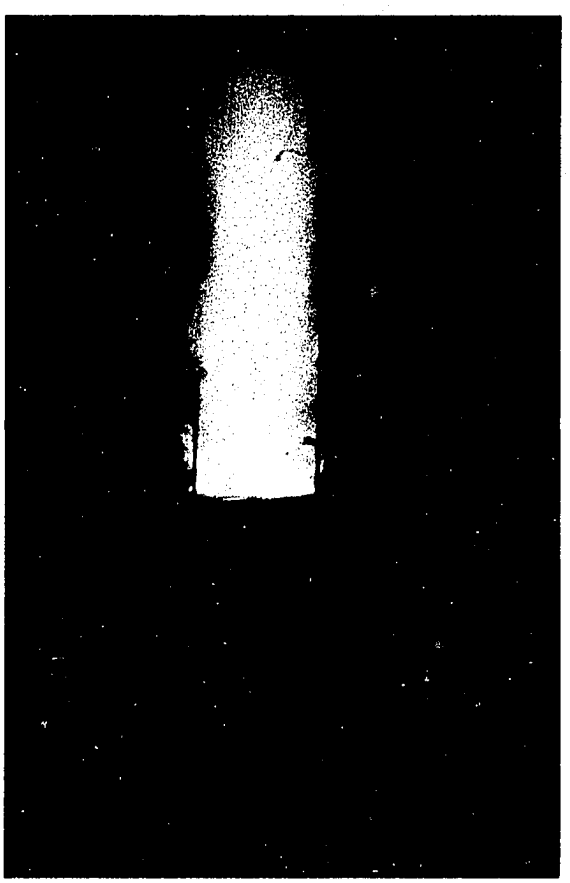
CHAPTER VI

RESULTS FOR FLAME SHAPE, SIZE, SOOT ACCUMULATION, TEMPERATURE AND FUEL BURNING RATE

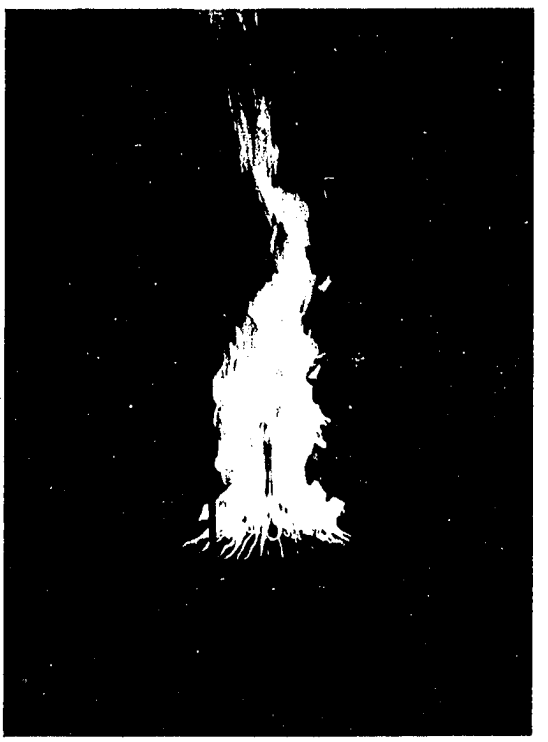
Flame Shape and Size

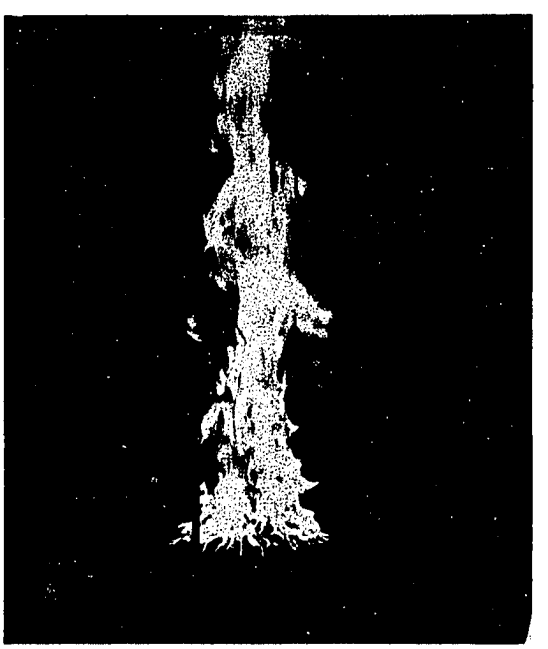
In order to evaluate the flame radiant heat flux, the size and shape of the flame is necessary. To obtain these data, photographs were taken of the flame during the test with two pinhole cameras, Numbers 1 and 2, and a Polaroid camera, Number 3. The location of these cameras is shown in Figure IV-1. The pinhole cameras produced time-average photographs and the Polaroid provided an instantaneous picture. Figures VI-1 through VI-21 contain a photograph from cameras 2 and 3 for each fuel and burner size. Since camera 1 was located further from the flame than camera 2, its photographs were primarily used for checking the flame concentricity.

All flames pulsate in the form of a series of necks and bulges. Except for methanol, fuel vapors expand outwards from the rim of the burner and then as air mixes with these vapors the flame moved inwards towards the probe where a bulge is formed. These flame bulges can be larger than the



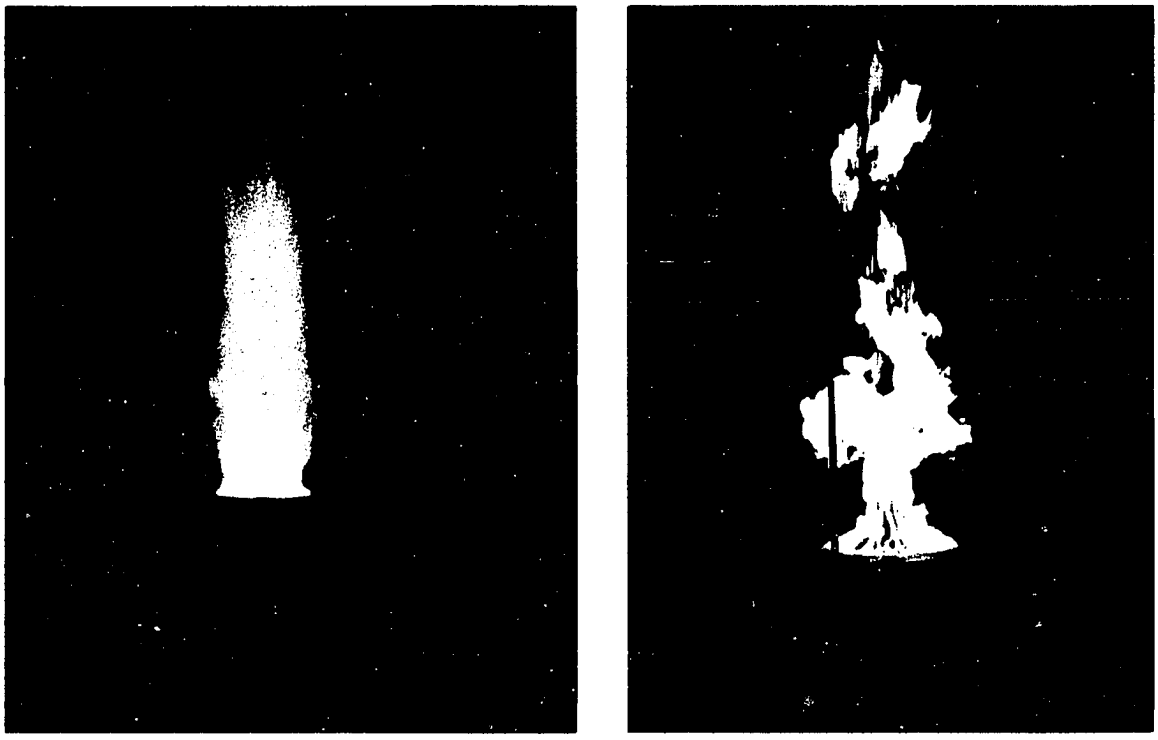
a. Time Averaged.





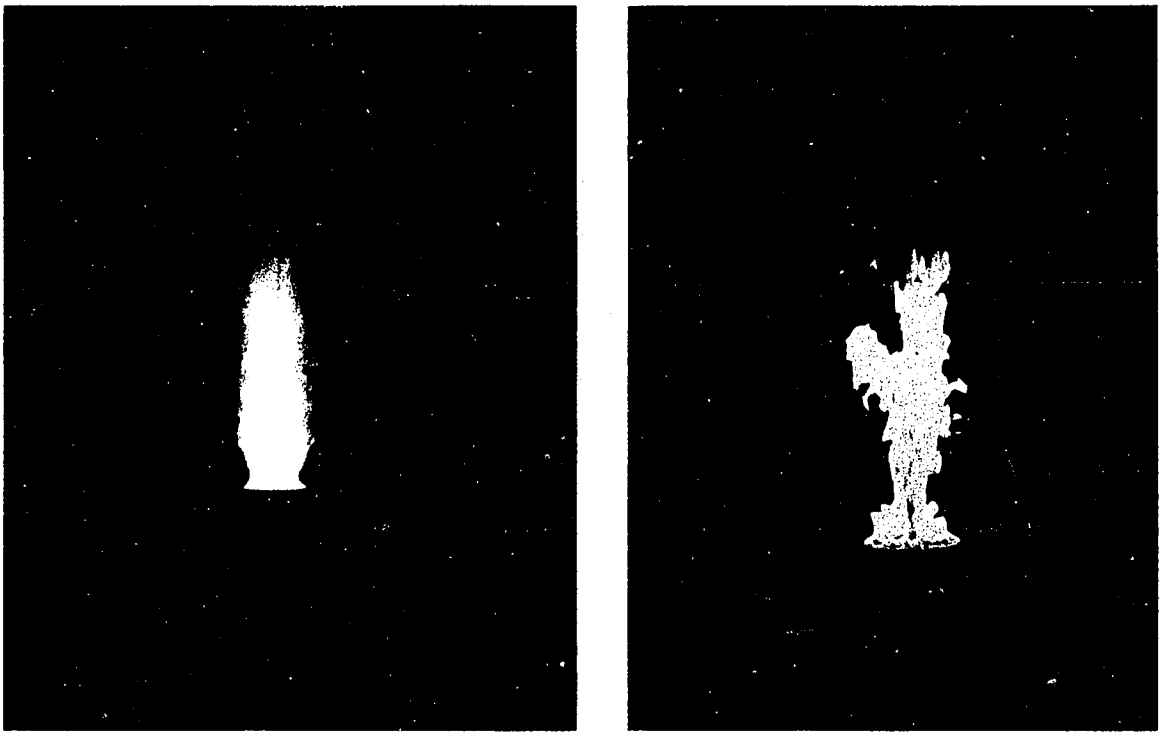
b. Instantaneous.

Figure VI-1. 24 Inch Diameter Acetone Flame.



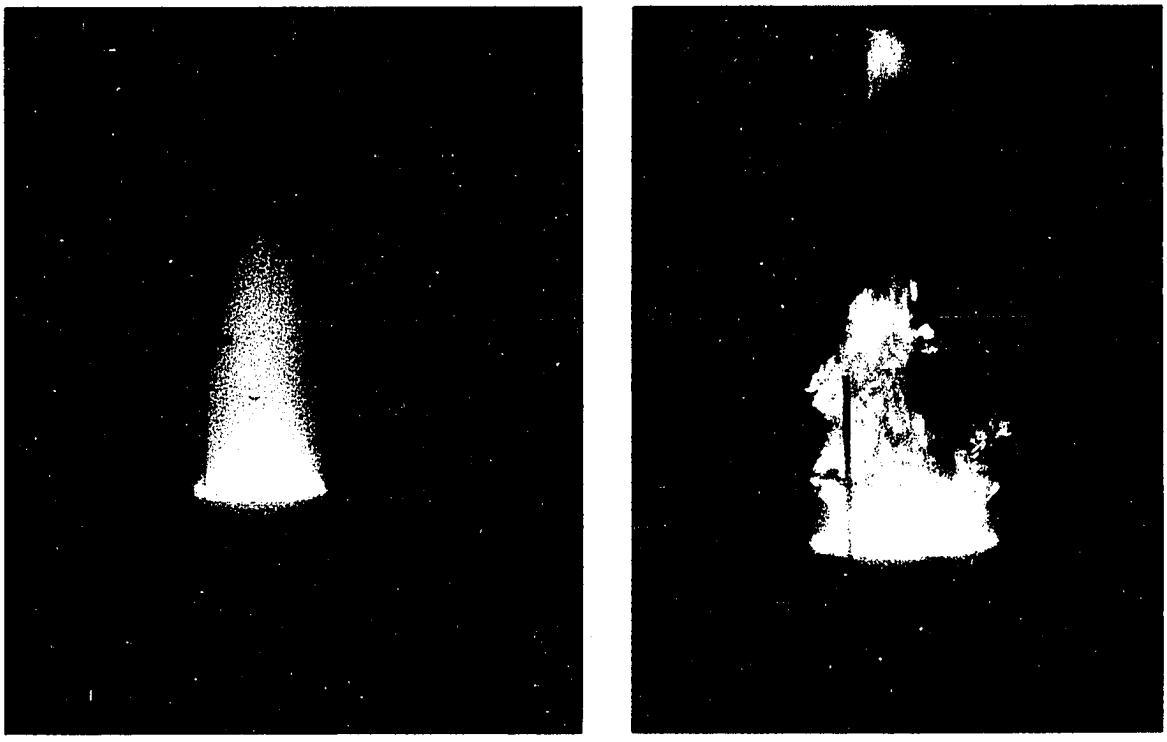
b. Instantaneous. a. Time Averaged.

Figure VI-2. 18 Inch Diameter Acetone Flame.



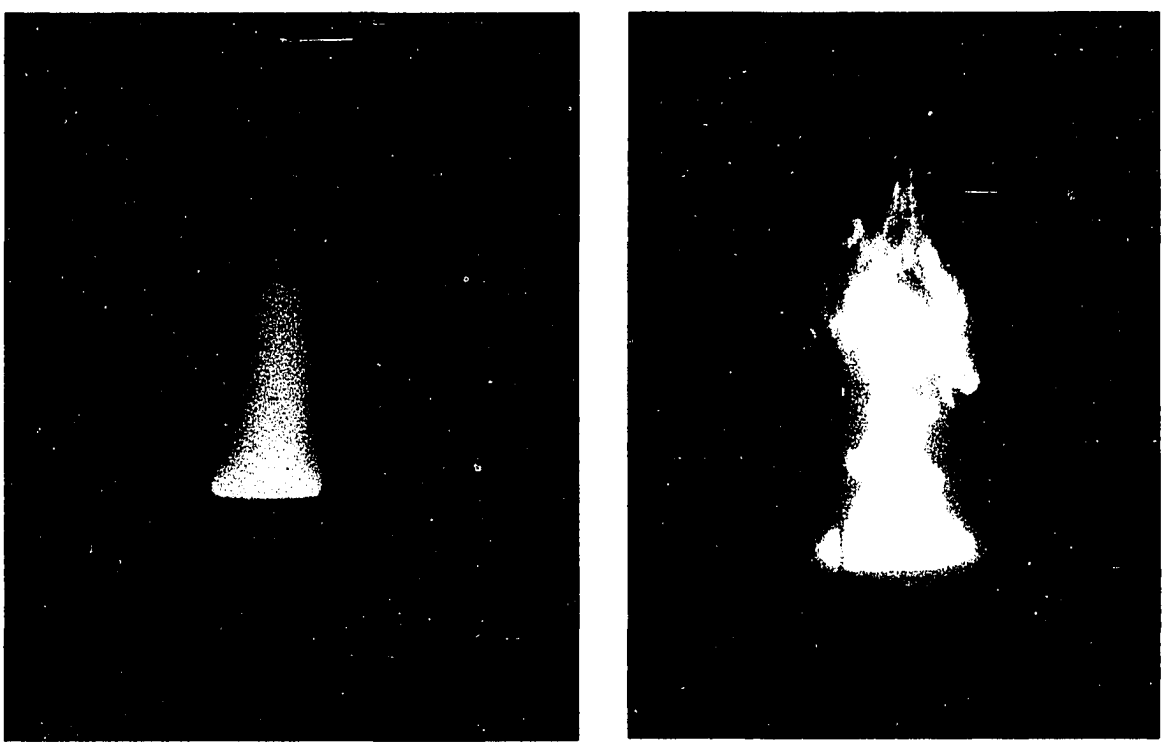
a. Time Averaged. b. Instantaneous

Figure VI-3. 12 Inch Diameter Acetone Flame.



a. Time Averaged. b. Instantaneous

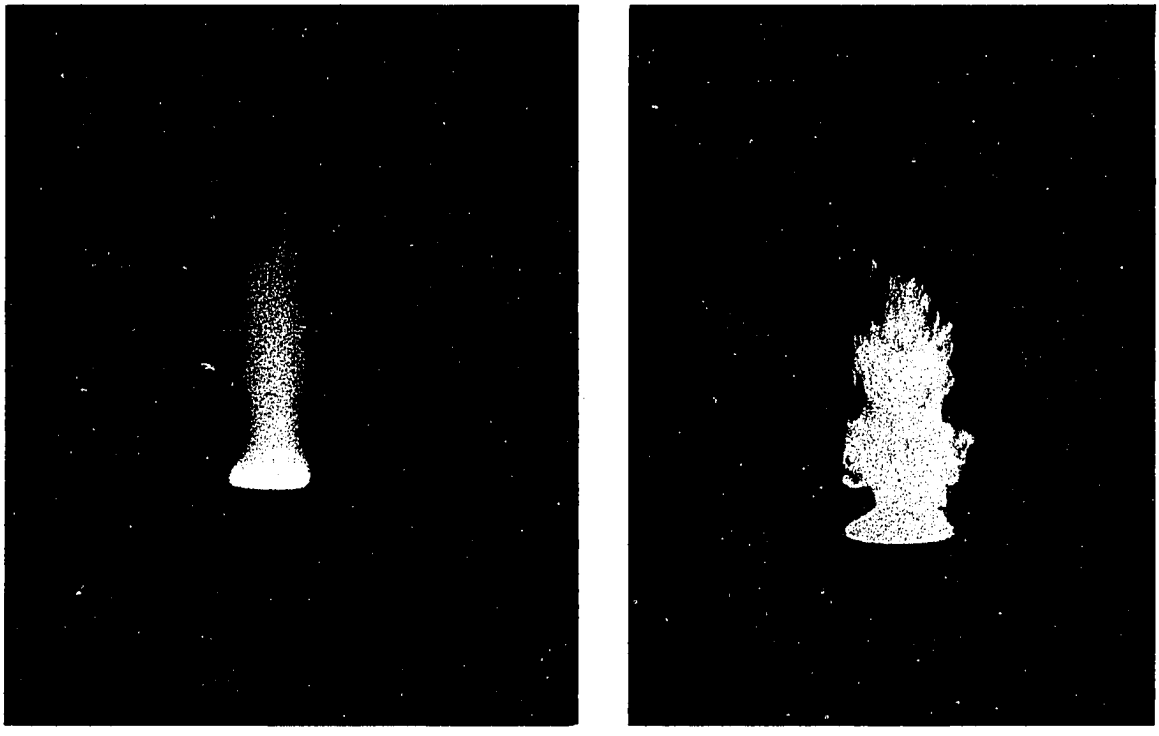
Figure VI-4. 24 Inch Diameter Benzene Flame.



a. Time Averaged

b. Instantaneous.

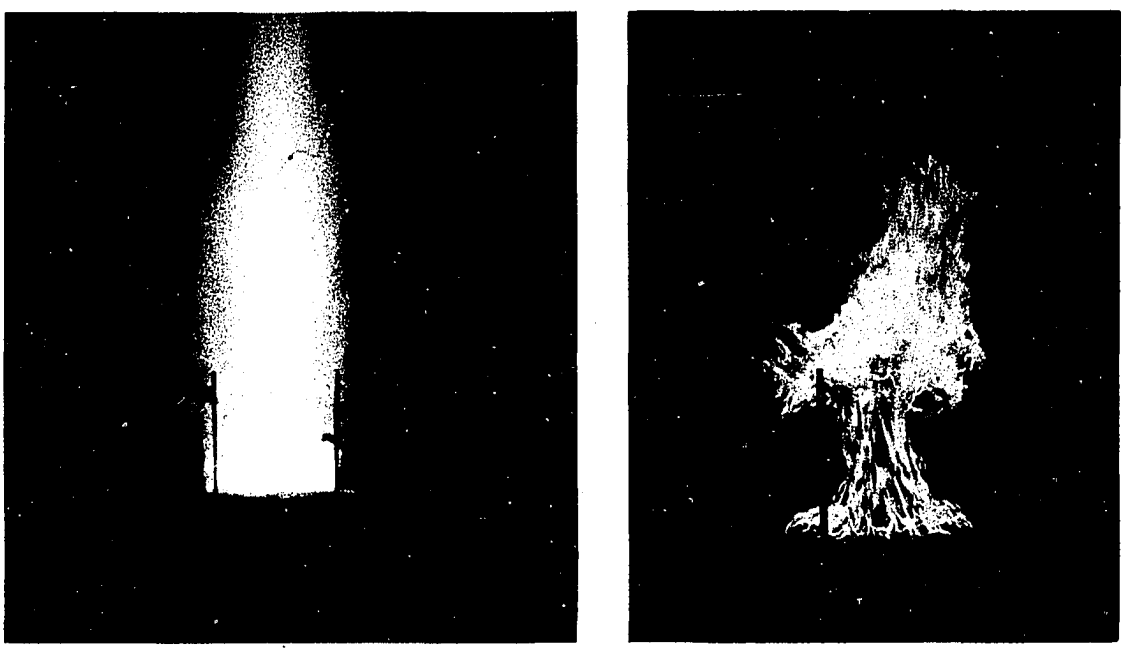
Figure VI-5. 18 Inch Diameter Benzene Flame.



a. Time Averaged.

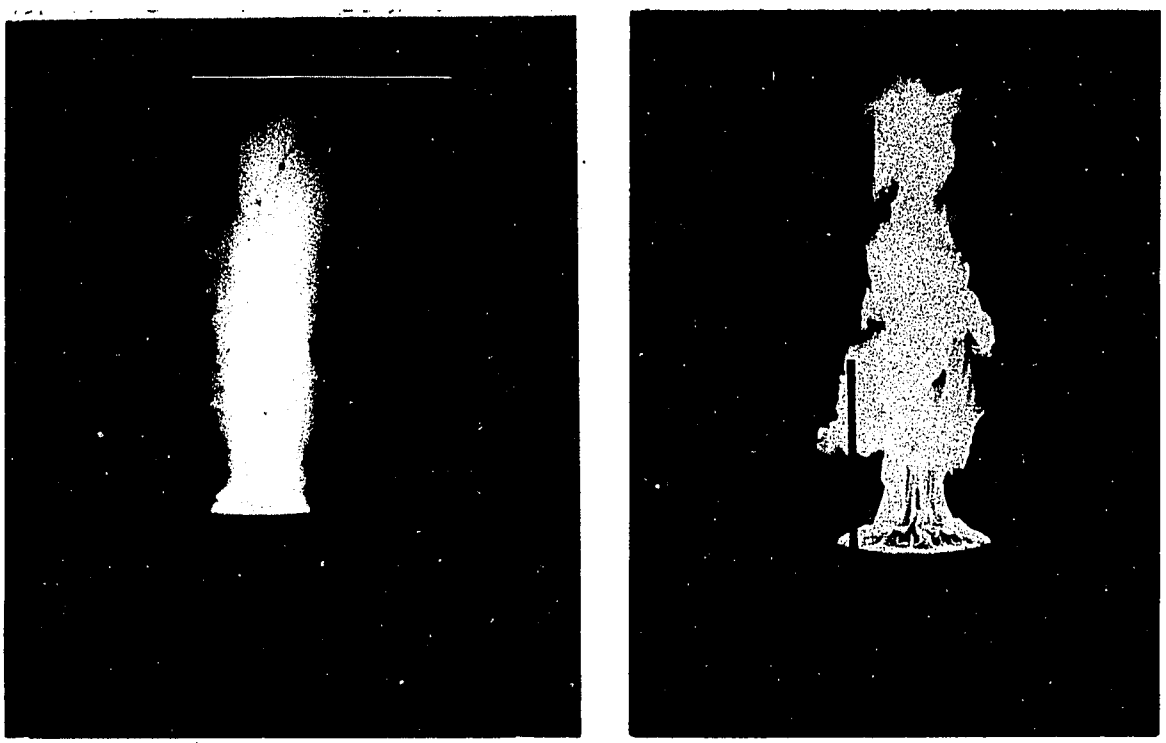
b. Instantaneous

Figure VI-6. 12 Inch Diameter Benzene Flame.



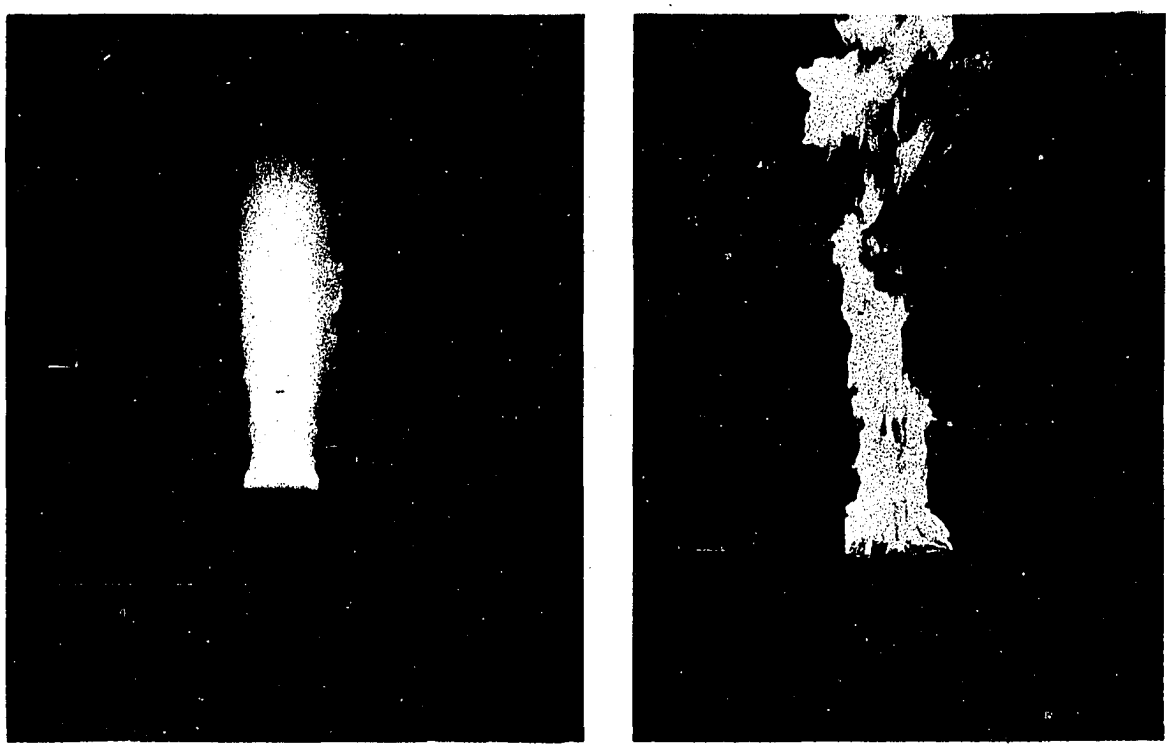
a. Time Averaged. b. Instantaneous.

Figure VI-7. 24 Inch Diameter Cyclohexane Flame.



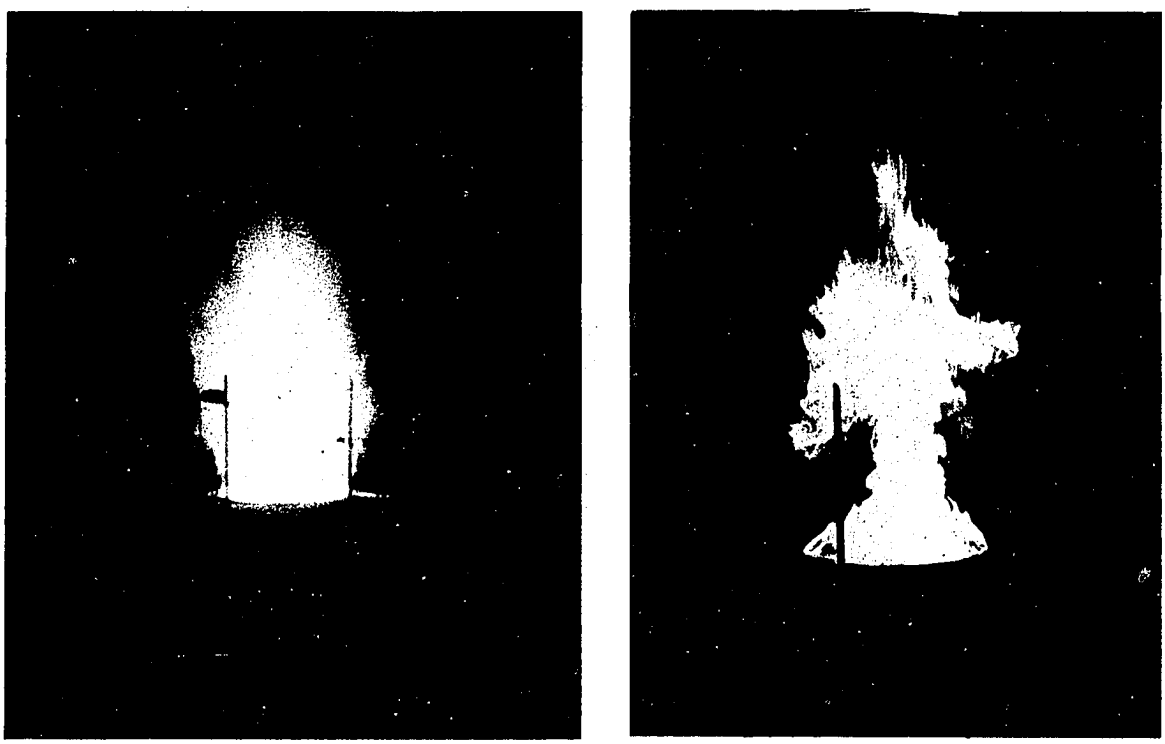
a. Time Averaged. b. Instantaneous.

Figure VI-8. 18 Inch Diameter Cyclohexane Flame.



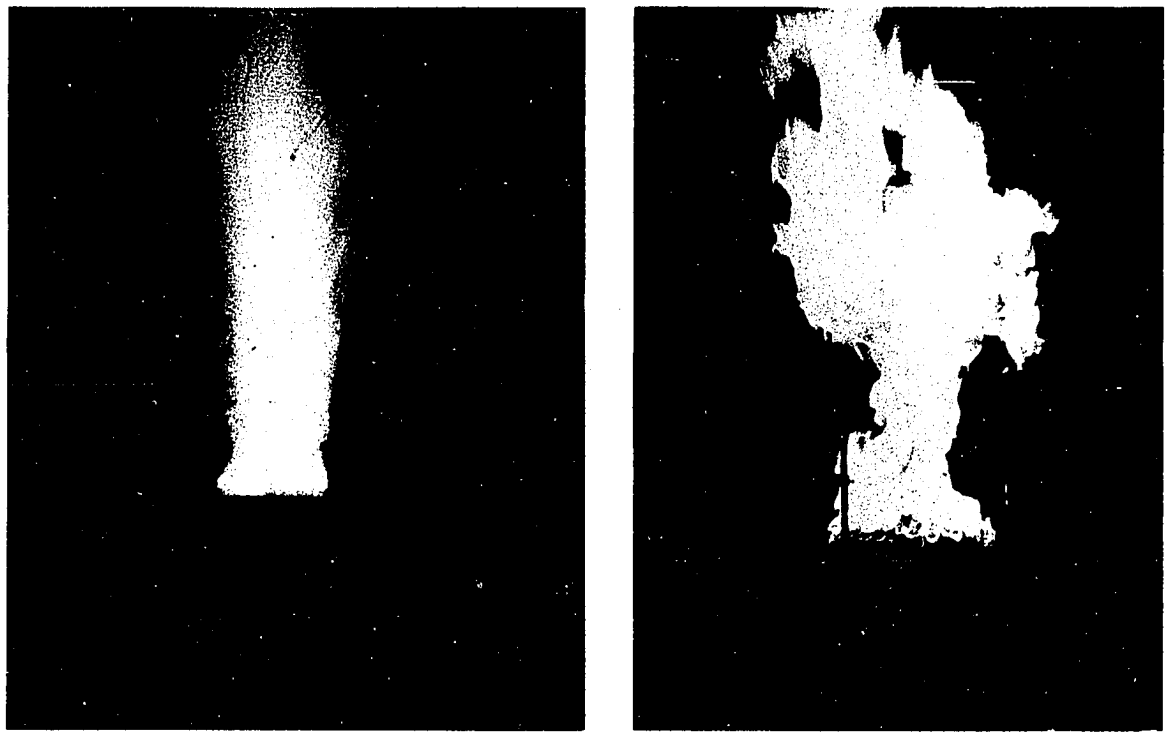
a. Time Averaged. b. Instantaneous.

Figure VI-9. 12 Inch Diameter Cyclohexane Flame.



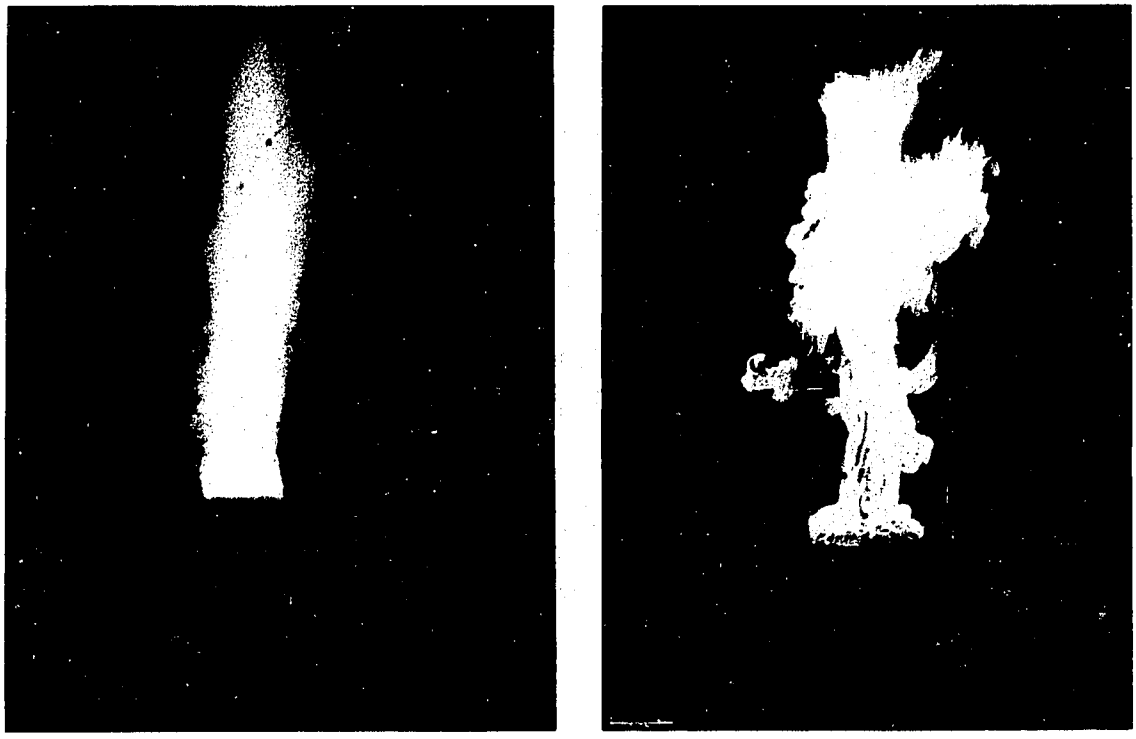
a. Time Averaged. b. Instantaneous.

Figure VI-10. 24 Inch Diameter n-Hexane Flame.



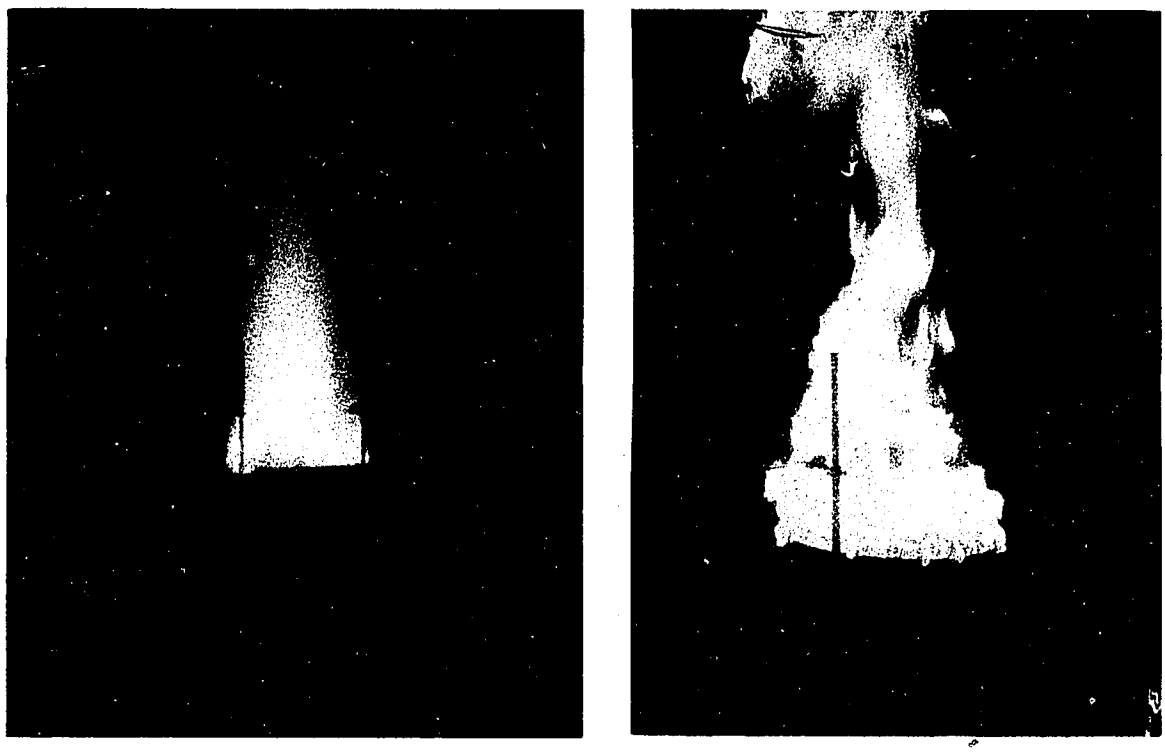
a. Time Averaged. b. Instantaneous.

Figure VI-11. 18 Inch Diameter n-Hexane Flame.



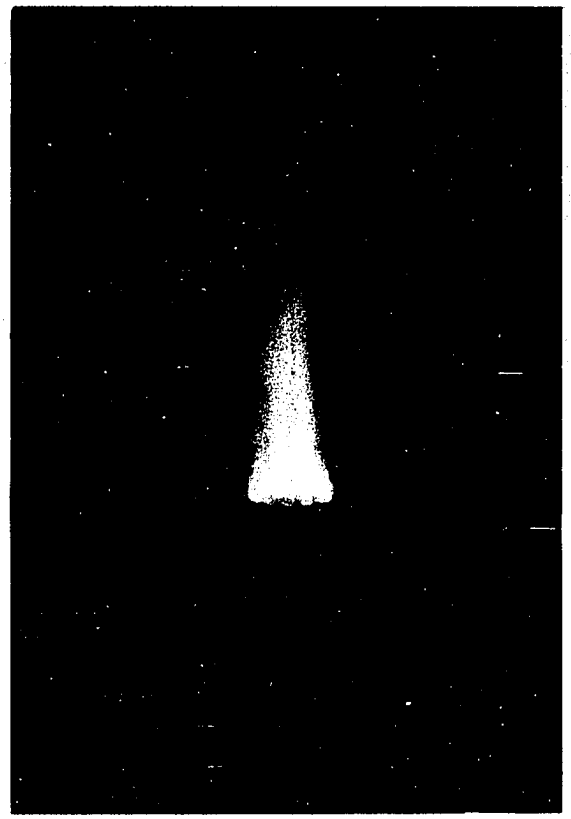
a. Time Averaged. b. Instantaneous

Figure VI-12. 12 Inch Diameter n-Hexane Flame.

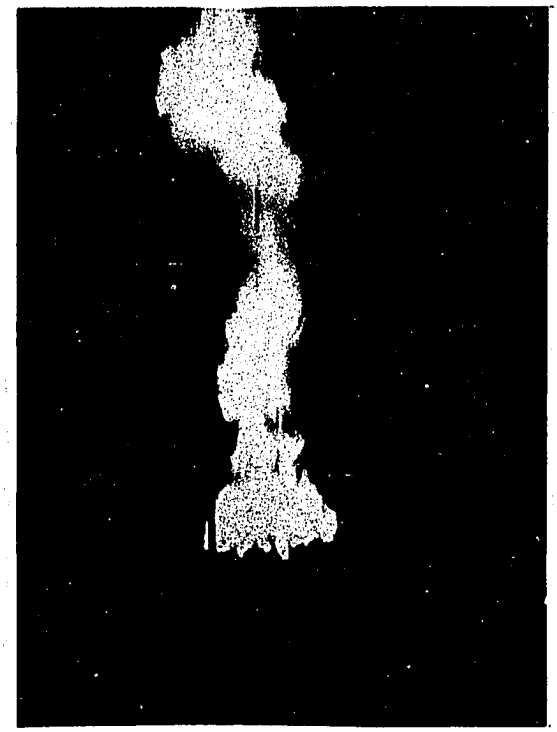


a. Time Averaged. b. Instantaneous.

Figure VI-13. 24 Inch Diameter Jet-A Flame.



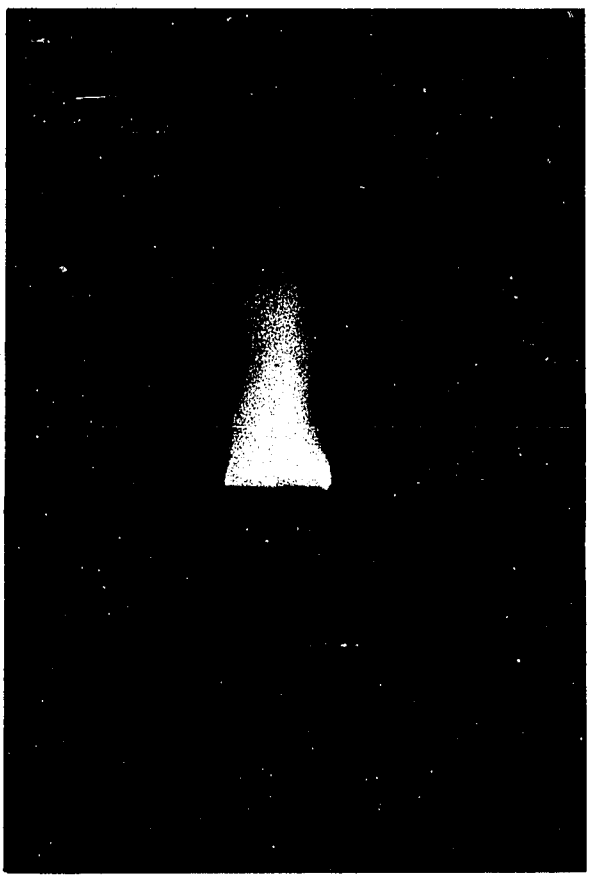
a. Time Averaged.



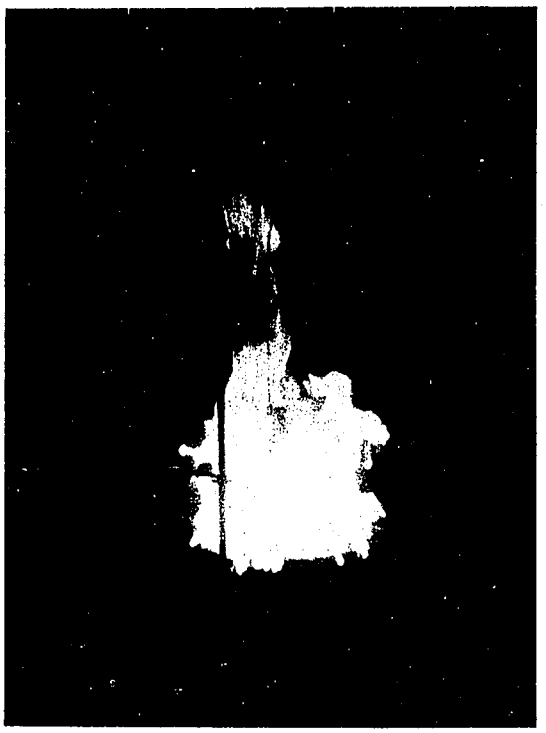


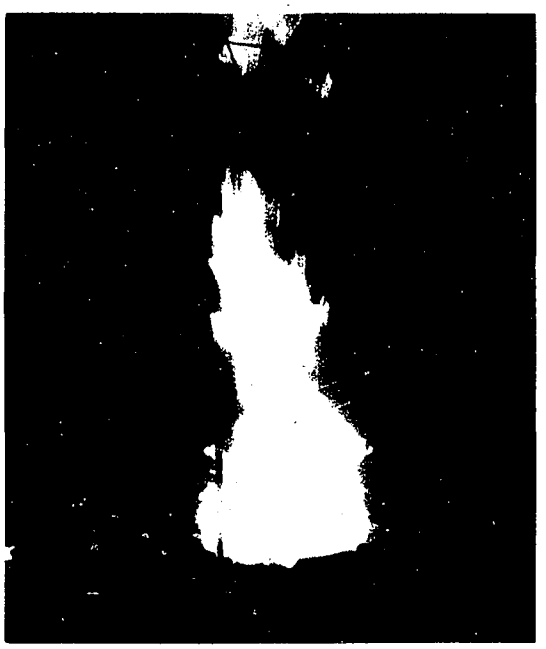
b. Instantaneous.

Figure VI-14. 18 Inch Diameter Jet-A Flame.



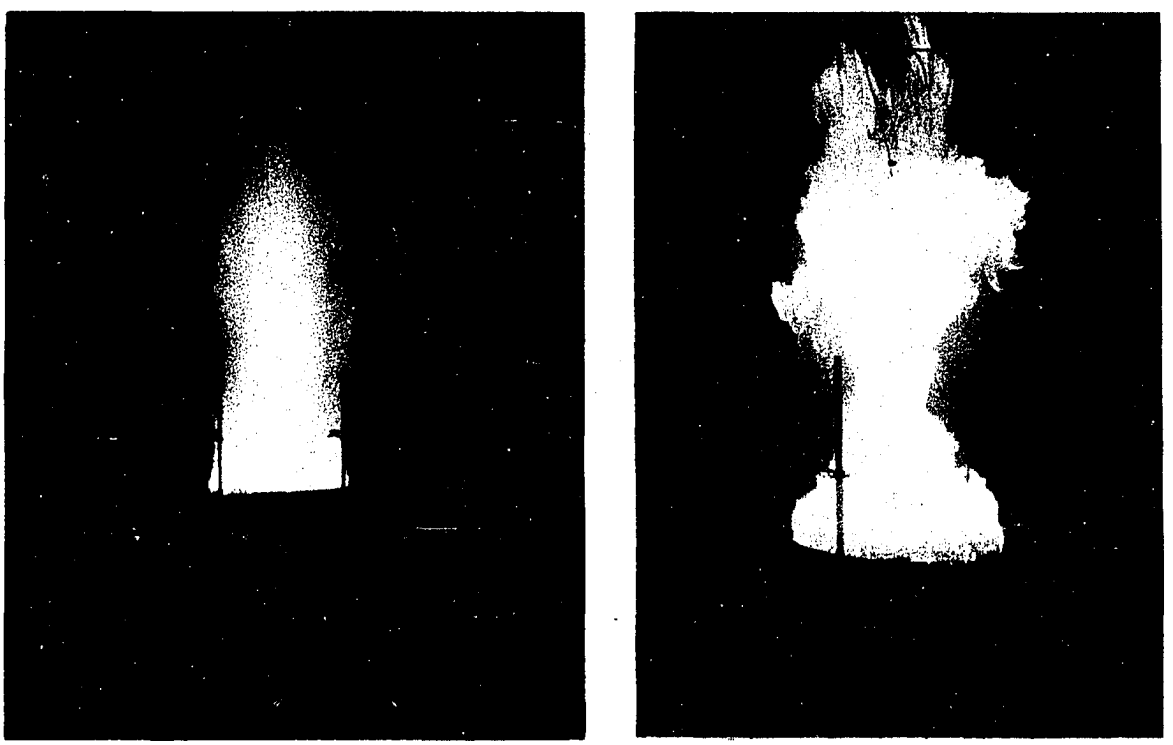
a. Time Averaged.





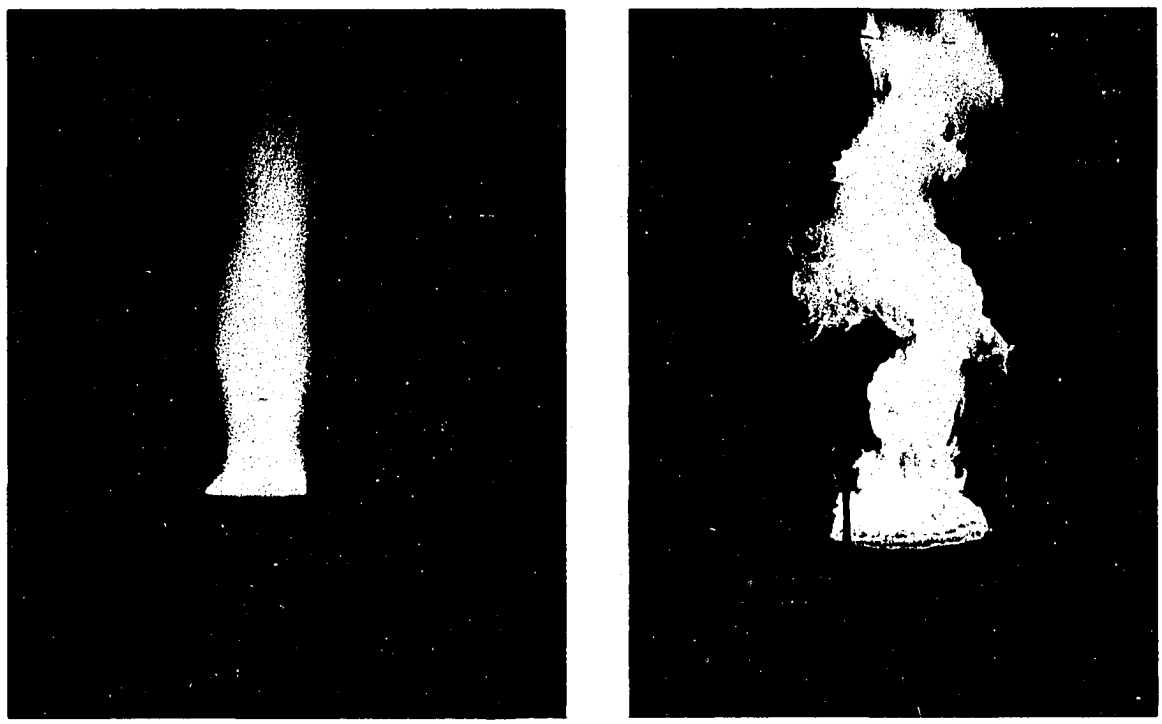
b. Instantaneous.

Figure VI-15. 12 Inch Diameter Jet-A Flame.



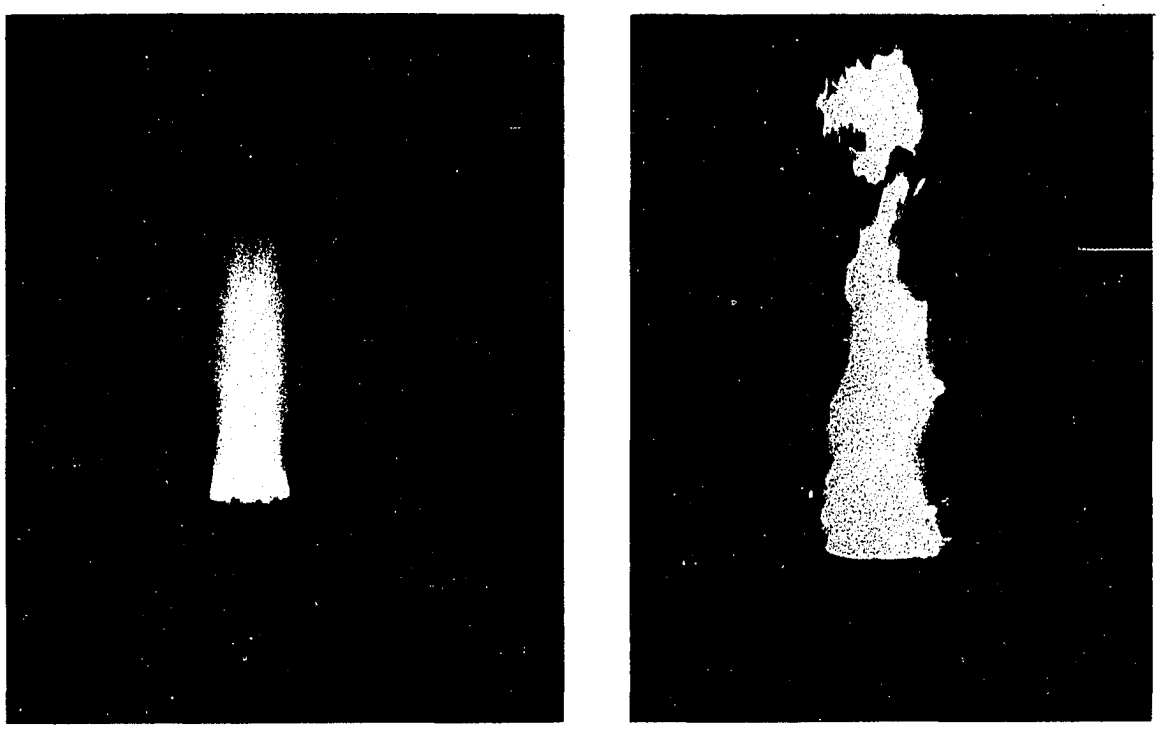
a. Time Averaged. b. Instantaneous.

Figure VI-16. 24 Inch Diameter JP-4 Flame.



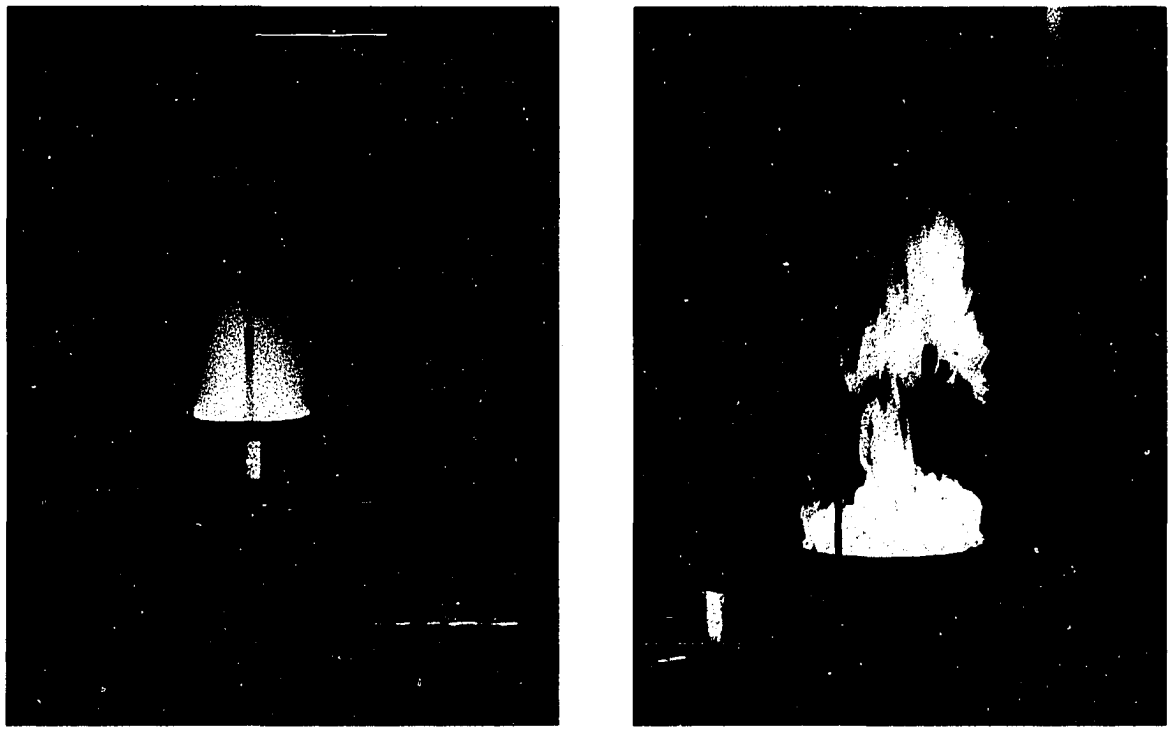
a. Time Averaged. b. Instantaneous.

Figure VI-17. 18 Inch Diameter JP-4 Flame.



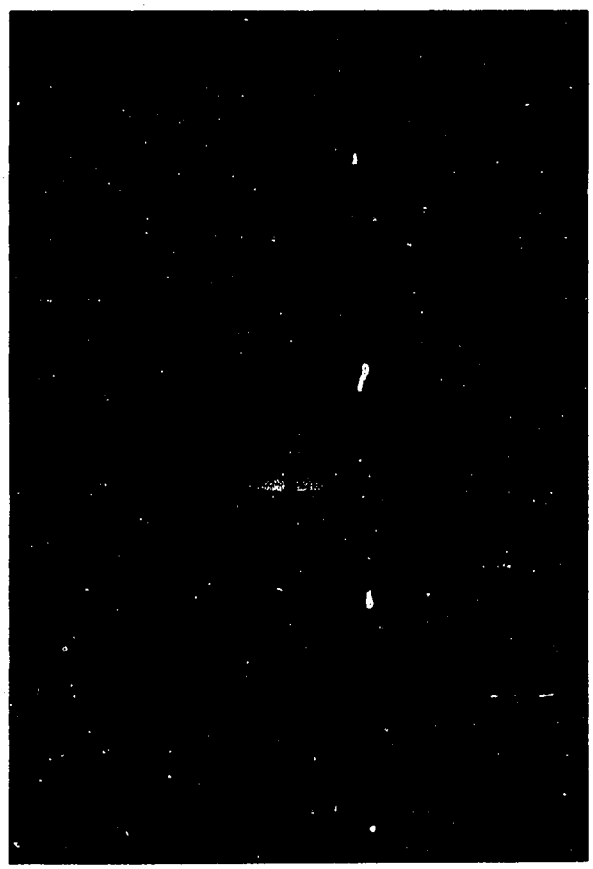
a. Time Averaged. b. Instantaneous.

Figure VI-18. 12 Inch Diameter JP-4 Flame.

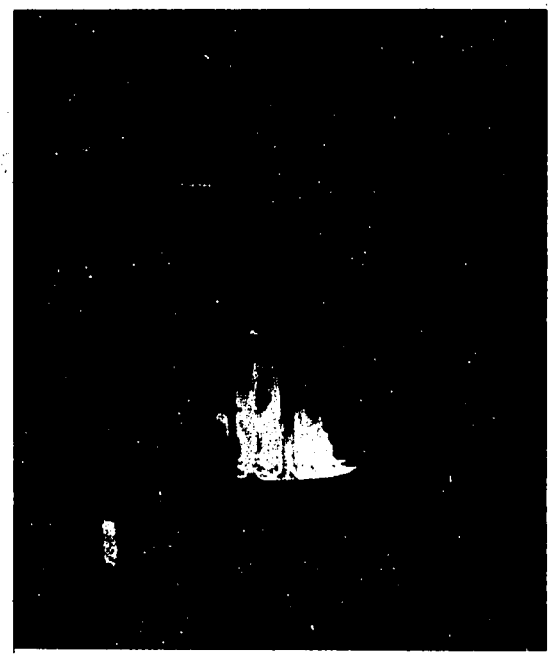


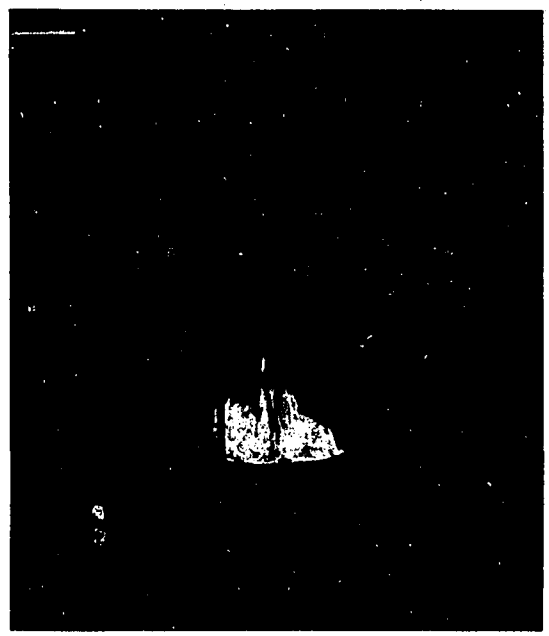
a. Time Averaged. b. Instantaneous.

Figure VI-19. 24 Inch Diameter Methanol Flame.



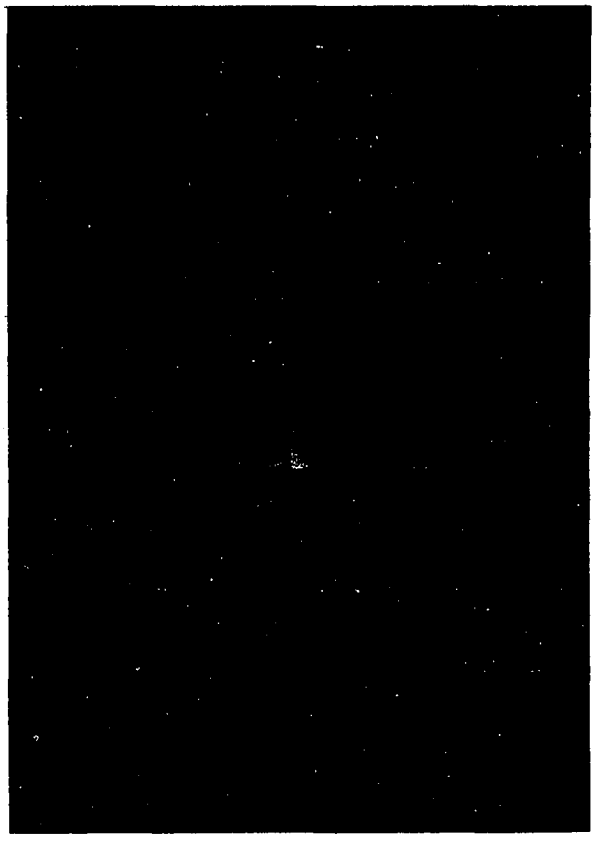
a. Time Averaged.



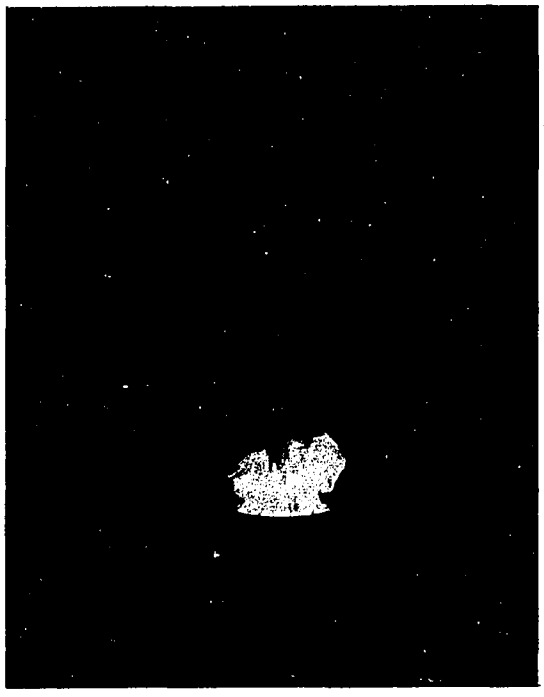


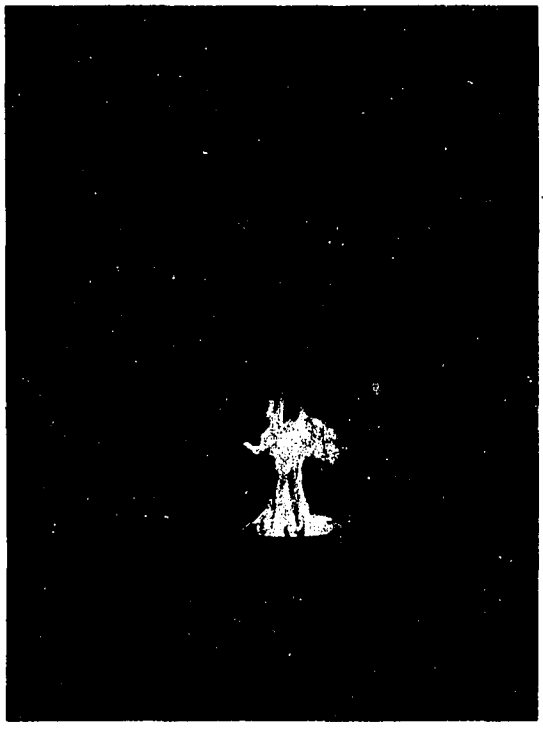
b. Instantaneous.

Figure VI-20. 18 Inch Diameter Methanol Flame.



a. Time Averaged.





b. Instantaneous.

Figure VI-21. 12 Inch Diameter Methanol Flame.

burner diameter and move vertically where they decrease in size or even separate into isolated flame zones. Acetone, cyclohexane, n-hexane and JP-4 flames have a clear layer of fuel vapors above the pan rim. Jet A fuel vapors tend to spill over the side of the fuel pan and burn below the rim. Benzene flames produce large amounts of smoke which precludes close observance of the flame and makes photographs difficult to obtain. Methanol flames tend to move inward from the burner walls just above the liquid surface. These flames are dim and are difficult to photograph.

From the instantaneous photographs shown in Figures VI-1, VI-14, VI-15, VI-20 and VI-21, it can be seen that the flame size and shape are constantly changing. This change necessitates the use of the time-averaged photogrpahs. Even these photographs have varying shapes. Tables VI-1 through VI-7 contain the diameter, height and surface area for the flames used in this study. For comparison purposes the surface area of a cone, paraboloid, semi-ellipsoid, and cylinder are included. The flame diameter was measured just above the burner rim and the flame height was taken as the maximum visible height obtained, even if flame separation occurred. The flame surface areas were measured by a planimeter. From these tables, it can be seen that no one shape is characteristic of free burning flames.

TABLE VI-1

FLAME SIZE AND PROJECTED AREA FOR ACETONE

Run Number	Camera Number	Test Time min	Flame Diameter in	Flame Height in	Projected Area, in^2				
					Flame	Cylinder	Semi-Ellipsoid	Para-boloid	Conical
090171-24-1-1	1	18.4	24.5	97.0	1809	2377	1867	1584	1188
	2	23.0	24.0	87.7	1772	2149	1688	1433	1074
	3	27.0	24.0	69.0	828	1653	1298	1102	827
090171-24-1-2	1	25.0	25.0	63.3	1326	1582	1243	1055	791
	2	30.0	24.5	64.7	1521	1585	1245	1057	793
	3	33.8	24.0	31.5	457	756	594	504	378
090171-24-1-3	1	22.3	24.5	87.8	1856	2151	1689	1434	1076
	2	27.1	24.5	87.0	1890	2132	1674	1421	1066
	3	31.3	24.0	69.0	852	1656	1301	867	828
	3	31.9	24.0	69.0	659	1656	1301	867	828
081271-18-1-1	1	17.0	18.4	63.6	1092	1170	919	780	585
	2	22.4	18.7	65.1	1098	1217	956	811	609
	3	28.3	18.0	40.5	422	729	573	486	365
081271-18-1-2	1	17.0	18.4	67.0	1076	1244	977	829	622
	2	21.7	18.7	65.8	1051	1231	967	821	615
	3	25.9	18.0	40.5	450	729	573	486	365
				65.5	576	1179	926	786	590
081271-18-1-3	1	16.1	18.4	66.6	1107	1225	962	817	613
	2	31.9	18.7	65.1	1035	1217	956	811	609
	3	33.4	18.5	48.5	532	897	705	598	449

TABLE VI-1--Continued

Run Number	Camera Number	Test Time min	Flame Diameter in	Flame Height in	Projected Area, in^2				
					Flame	Cylinder	Semi-Ellipsoid	Para-boloid	Conical
070771-12-1-1	1	36.2	11.7	46.5	343	544	427	363	272
	2	42.5	11.9	47.1	486	561	441	374	280
	3	44.5	12.0	35.5	259	426	335	284	213
070771-12-1-2	1	29.7	12.2	45.4	421	531	417	354	266
	2	32.2	12.2	45.6	523	543	426	362	271
	3	35.7	12.2	38.3	278	467	367	311	234
070871-12-1-1	1	40.5	12.2	47.5	484	556	437	371	278
	2	43.3	1 .2	46.0	565	547	430	365	274
	3	45.3	12.5	52.6	259	658	517	439	329

TABLE VI-2

FLAME SIZE AND PROJECTED AREA FOR BENZENE

Run Number	Camera Number	Test Time min	Flame Diameter in	Flame Height in	Projected Area, in^2				
					Flame	Cylinder	Semi-Ellipsoid	Para-boloid	Conical
090171-24-2-1	1	18.0	26.0	--	--	--	--	--	--
	2	25.0	26.6	59.6	972	1585	1245	1057	793
	3	27.9	25.8	50.0	824	1290	1013	860	645
090171-24-2-2	1	12.0	24.5	36.8	452	902	708	601	451
	2	22.0	24.8	67.6	1121	1677	1317	1118	838
	3	25.5	24.3	36.0	564	875	687	583	437
				68.5	686	1664	1308	1110	832
090171-24-2-3	1	21.0	24.5	49.0	640	1201	943	801	600
	2	25.8	24.8	67.6	1270	1677	1317	1118	838
	3	30.1	24.0	49.5	556	1188	933	792	594
081171-18-2-1	1	16.3	19.4	49.3	406	956	751	637	478
	2	21.0	19.4	65.1	737	1263	992	842	632
	3	26.0	20.0	43.0	568	860	675	573	430
081171-18-2-2	1	22.7	18.9	51.3	390	970	762	647	485
	2	26.0	20.9	70.8	902	1480	1162	987	740
	3	30.2	20.0	54.5	663	1090	856	727	545
081171-18-2-3	1	21.7	19.4	--	--	--	--	--	--
	2	24.9	22.3	54.3	557	1211	951	807	605
	3	29.9	20.0	65.0	765	1300	1021	867	650

TABLE VI-2--Continued

Run Number	Camera Number	Test Time min	Flame Diameter in	Flame Height in	Projected Area, in^2				
					Flame	Cylinder	Semi-Ellipsoid	Para-boloid	Conical
070671-12-2-1	1	28.5	15.3	30.1	187	461	362	307	230
	1	36.0	16.3	30.1	281	491	386	327	245
	2	33.2	16.5	46.0	502	759	596	506	380
	3	40.8	15.2	59.1	727	898	705	599	449
070671-12-2-2	1	24.3	15.8	46.5	343	735	577	490	367
	2	30.0	15.8	67.0	643	1059	832	706	529
	3	35.5	15.2	33.2	363	505	397	337	252
070671-12-2-3	1	33.0	13.8	39.3	187	542	426	361	271
	1	43.6	13.8	41.3	312	570	448	380	285
	2	38.0	13.7	48.1	416	659	518	439	330
	2	47.6	13.7	47.1	423	645	507	430	328
	3	33.8	13.2	35.5	291	469	368	313	234

TABLE VI-3

FLAME SIZE AND PROJECTED AREA FOR CYCLOHEXANE

Run Number	Camera Number	Test Time min	Flame Diameter in	Flame Height in	Projected Area, in^2				
					Flame	Cylinder	Semi-Ellipsoid	Para-boloid	Conical
083071-24-3-1	1	18.3	27.6	100.1	2465	2763	2170	1842	1381
	2	22.2	25.9	89.9	2392	2328	1828	1552	1164
	3	25.5	24.5	68.5	903	1678	1318	1119	839
083071-24-3-2	1	23.5	25.5	44.9	952	1145	899	763	573
	2	28.4	24.8	49.6	1208	1230	966	820	615
	3	33.3	24.0	23.0	442	552	433	368	276
083071-24-3-3	1	21.0	26.0	94.9	2215	2467	1938	1645	1234
	2	24.6	25.2	89.9	2353	2266	1780	1511	1133
	3	27.7	24.8	56.0	915	1389	1091	926	694
081071-18-3-1	1	17.8	18.9	85.0	1388	1607	1262	1071	803
	2	21.7	19.1	84.5	1553	1614	1268	1076	807
	3	26.1	18.9	56.8	733	1074	844	716	537
081071-18-3-2	1	16.6	21.4	89.1	2121	1907	1498	1271	953
	2	21.7	20.1	91.7	2055	1843	1447	1229	922
	3	22.7	19.8	63.7	1122	1261	990	841	631
081071-18-3-3	1	24.6	18.9	48.2	718	911	715	607	456
	2	30.7	18.7	54.3	941	1015	797	677	508
	3	32.2	18.9	32.8	606	620	487	413	310

TABLE VI-3--Continued

Run Number	Camera Number	Test Time min	Flame Diameter in	Flame Height in	Projected Area, in^2				
					Flame	Cylinder	Semi-Ellipsoid	Para-boloid	Conical
070171-12-3-1	1	30.2	14.8	79.1	1092	1171	920	781	585
	2	36.0	14.7	73.3	1153	1078	847	719	539
	3	42.1	13.4	59.1	583	792	622	528	396
070171-12-3-2	1	26.4	14.8	78.1	1185	1156	908	771	578
	2	28.0	14.7	87.3	1357	1283	1008	855	642
	3	27.0	12.5	41.1	350	514	404	343	257
070171-12-3-3	1	33.1	14.3	72.0	920	1030	809	687	515
	2	40.1	14.7	69.8	1176	1026	806	684	513
	3	44.8	12.9	64.2	694	828	650	552	414

TABLE VI-4

FLAME SIZE AND PROJECTED AREA FOR N-HEXANE

Run Number	Camera Number	Test Time min	Flame Diameter in	Flame Height in	Projected Area, in^2				
					Flame	Cylinder	Semi-Ellipsoid	Para-boloid	Conical
083171-24-4-1	1	22.7	25.5	62.3	1435	1589	1248	1059	794
	2	27.0	24.5	58.2	1623	1426	1120	951	713
	3	28.6	24.3	60.0	759	1458	1145	972	729
083171-24-4-2	1	20.0	25.5	65.3	1497	1665	1308	1110	833
	2	24.0	24.8	74.8	2109	1855	1457	1237	927
	3	27.4	24.0	58.5	609	1404	1103	936	702
				66.5	645	1596	1253	835	798
083171-24-4-3	1	16.8	26.5	115.4	3416	3058	2402	2039	1529
	2	20.1	25.8	89.9	2454	2328	1828	1552	1294
	3	22.5	24.5	68.0	939	1666	1308	1111	888
081071-18-4-1	1	14.8	21.4	106.4	2652	2277	1788	1518	1139
	2	19.2	20.9	91.7	2384	1917	1506	1278	958
	3	23.5	19.8	64.2	1621	1271	998	847	636
081071-18-4-2	1	13.4	21.4	106.4	2480	2277	1788	1518	1139
	2	17.8	20.1	91.0	2149	1829	1436	1219	915
	3	--	--	--	--	--	--	--	--
081171-18-4-1	1	17.0	20.9	106.4	2480	2277	1788	1518	1139
	2	20.3	20.9	91.0	2337	1902	1494	1268	951
	3	24.7	18.8	50.0	494	940	738	627	470

TABLE VI-4--Continued

Run Number	Camera Number	Test Time min	Flame Diameter in	Flame Height in	Projected Area, in^2				
					Flame	Cylinder	Semi-Ellipsoid	Para-boloid	Conical
070271-12-4-1	1	24.0	14.8	81.9	1404	1212	952	808	599
	2	30.0	15.1	91.7	1443	1385	1088	923	692
	3	38.7	13.8	56.3	1006	777	610	518	389
070271-12-4-2	1	25.2	14.8	81.2	1544	1202	944	801	601
	2	31.0	14.4	75.5	1114	1087	854	725	544
	3	35.7	13.8	58.2	950	803	631	535	402
070271-12-4-3	1	27.9	15.5	85.2	1513	1346	1057	897	673
	2	33.0	15.8	84.1	1372	1329	1044	886	663
	3	37.3	12.9	38.3	434	494	388	329	247

TABLE VI-5

FLAME SIZE AND PROJECTED AREA FOR JET A

Run Number	Camera Number	Test Time min	Flame Diameter in	Flame Height in	Flame	Cylinder	Semi-Ellipsoid	Para-boloid	Conical
083171-24-5-1	1	23.4	26.0	42.9	390	1115	876	743	558
	2	26.5	25.9	79.4	1364	2056	1615	1371	1028
	3	29.9	25.0	42.0	599	1050	825	700	525
041671-24-5-1	1	21.3	24.5	46.0	374	1127	885	751	564
	2	17.0	24.5	56.0	878	1372	1078	915	686
	3	19.5	24.9	60.5	1028	1507	1184	1005	753
041671-24-5-2	1	19.0	25.5	42.9	406	1094	859	729	547
	2	23.0	28.8	59.6	1388	1717	1349	1145	858
	3	25.2	27.7	63.2	1152	1751	1375	1167	875
041671-24-5-3	1	35.0	25.5	35.7	562	910	715	607	455
	2	27.5	26.3	56.0	1067	1473	1157	982	736
	3	30.5	25.4	63.7	1136	1618	1271	1079	809
080971-18-5-1	1	23.4	19.4	58.4	796	1133	890	755	567
	2	28.7	19.4	58.0	918	1125	884	750	563
	3	32.5	19.4	55.8	681	1083	851	722	541
042171-18-5-1	1	25.4	18.9	48.3	530	1002	787	668	456
	2	27.1	19.8	64.3	878	1273	1000	849	637
	3	32.2	19.2	36.5	537	701	551	467	350
	3			58.6	625	1125	884	750	563

TABLE VI-5--Continued

Run Number	Camera Number	Test Time min	Flame Diameter in	Flame Height in	Projected Area, in^2				
					Flame	Cylinder	Semi-Ellipsoid	Para-boloid	Conical
042171-18-5-2	1	21.3	18.4	50.3	468	926	727	617	463
	2	28.0	20.1	60.0	753	1206	947	804	603
	3	33.6	21.7	45.2	534	981	770	654	490
	3	37.2	19.8	47.5	579	941	739	627	470
042171-18-5-3	1	33.8	18.9	49.3	468	932	732	621	466
	1	64.6	18.9	53.3	546	1007	791	671	504
	2	37.4	19.8	58.6	580	1160	911	773	580
	3	62.3	18.9	31.8	465	601	472	401	301
070971-12-5-1	1	40.1	12.8	46.5	343	595	467	397	298
	2	41.6	12.9	44.6	269	575	452	383	288
	3	46.0	12.9	45.2	360	583	458	389	292
042771-12-5-1	1	39.1	15.3	52.6	390	805	632	537	402
	2	43.8	15.5	54.6	486	846	664	564	423
	3	45.3	13.4	48.5	419	650	511	433	325
042771-12-5-2	1	23.9	15.3	45.4	250	695	546	463	347
	2	34.4	13.7	45.3	361	621	488	414	310
	3	40.2	12.7	53.5	429	679	533	453	340
042771-12-5-3	1	26.2	16.3	37.3	250	608	478	405	304
	2	28.9	15.8	48.2	596	762	598	508	381
	3	32.4	12.9	37.8	412	488	383	325	244

TABLE VI-5--Continued

Run Number	Camera Number	Test Time min	Flame Diameter in	Flame Height in	Projected Area, in^2				
					Flame	Cylinder	Semi-Ellipsoid	Para-boloid	Conical
042871-12-5-1	1	26.6	16.3	44.4	296	724	569	483	362
	2	28.3	16.5	59.0	612	974	765	649	487
	3	32.5	15.7	63.7	697	1000	785	667	500
	3	38.7	15.2	45.2	439	687	540	458	344
042871-12-5-2	1	26.9	16.8	48.5	468	8 5	650	543	407
	2	28.5	15.8	58.2	651	920	723	613	460
	3	34.5	17.1	40.6	393	694	545	463	347

TABLE VI-6

FLAME SIZE AND PROJECTED AREA FOR JP-4

Run Number	Camera Number	Test Time min	Flame Diameter in	Flame Height in	Projected Area, in^2				
					Flame	Cylinder	Semi-Ellipsoid	Para-boloid	Conical
042971-12-6-1	1	27.4	15.8	53.6	499	847	665	565	423
	2	29.0	14.7	54.6	565	803	630	535	401
	3	30.5	13.8	48.0	442	662	520	441	331
042971-12-6-2	1	25.2	15.8	53.6	530	847	665	565	423
	2	26.9	15.5	55.3	776	857	673	571	429
	3	28.2	13.8	60.5	553	835	656	557	417
042971-12-6-3	1	36.7	14.8	46.5	421	688	540	459	344
	1	23.6	15.8	62.8	577	992	779	661	496
	2	30.0	15.5	67.6	729	1048	823	699	524
	3	31.8	13.2	55.4	452	731	574	487	366
062271-12-6-1	2	18.7	13.3	48.9	423	905	710	603	452
	2	38.6	13.3	49.6	416	918	721	612	459
	2	43.7	13.3	48.2	471	892	700	595	446
042171-18-6-1	1	24.9	19.4	74.8	1107	1451	1139	967	726
	2	29.6	20.5	75.1	1216	1540	1209	1027	770
	3	31.0	18.9	62.8	834	1187	932	791	593
042717-18-6-2	1	19.5	20.4	64.6	842	1318	1035	879	659
	2	24.3	21.6	84.5	1223	1825	1433	1217	913
	3	29.5	21.2	64.6	1113	1370	1076	913	685

TABLE VI-6--Continued

Run Number	Camera Number	Test Time min	Flame Diameter in	Flame Height in	Projected Area, in^2				
					Flame	Cylinder	Semi-Ellipsoid	Para-boloid	Conical
042171-18-6-3	1	40.0	20.4	70.7	936	1442	1132	961	721
	2	24.5	20.5	67.9	1067	1392	1093	928	696
	1	26.2	18.9	62.5	702	1181	927	787	591
	1	31.6	18.9	62.5	624	1181	927	787	591
	3	41.1	19.2	67.9	556	816	641	544	404
081071-18-6-1	1	12.5	18.9	71.6	1014	1276	1002	851	638
	2	19.0	19.4	83.7	1310	1540	1209	1027	770
	3	21.8	21.1	72.0	975	1519	1192	1013	760
041771-24-6-1	1	25.3	25.0	57.1	624	1428	1121	952	714
	2	29.2	24.5	61.8	886	1514	1189	1009	757
	3	31.6	24.9	57.2	907	1424	1118	949	712
041771-24-6-2	1	16.8	25.0	64.3	827	1608	1262	1072	804
	2	20.8	26.6	795	1694	2115	1660	1410	1057
	3	26.7	25.4	63.7	1178	1618	1270	1079	809
041771-24-6-3	1	23.3	25.0	55.1	702	1378	1082	919	689
	2	27.3	24.5	70.4	1051	1725	1354	1150	862
	3	31.7	25.4	64.1	1159	1628	1278	1085	814
083171-24-6-1	1	14.5	26.5	72.5	1030	1921	1508	1281	921
	2	18.4	25.9	91.3	1968	2365	1857	1577	1182
	3	21.0	24.5	64.0	907	1568	1231	1045	784

TABLE VI-7

FLAME SIZE AND PROJECTED AREA FOR METHANOL

Run Number	Camera Number	Test Time min	Flame Diameter in	Flame Height in	Projected Area, in^2				
					Flame	Cylinder	Semi-Ellipsoid	Para-boloid	Conical
082771-24-7-1	1	23.0	24.5	25.5	265	625	491	417	312
	2	27.0	23.7	29.4	549	697	547	465	348
	3	30.5	23.8	44.0	568	1047	822	698	524
083071-24-7-1	1	23.7	24.5	21.5	203	527	414	351	263
	2	32.0	23.4	22.6	392	529	415	353	264
	3	25.2	24.0	20.5	296	492	386	328	246
083081-24-7-2	1	17.5	24.5	21.5	250	527	414	351	263
	2	24.0	23.5	20.8	392	487	382	325	243
	3	25.0	24.0	24.5	379	588	462	392	294
083071-24-7	1	25.0	24.5	22.5	265	551	433	367	276
	2	32.0	23.4	19.0	361	445	350	297	222
	3	33.5	23.8	21.5	351	512	402	341	256
081271-18-7-1	1	21.4	15.3	16.6	78	254	199	169	127
	1	36.0	17.9	21.7	140	388	305	259	194
	2	30.5	17.3	21.9	133	379	298	253	181
	3	33.6	17.5	19.0	158	333	262	222	166
	3	37.8	18.0	17.0	181	306	240	204	153
081271-18-7-2	1	28.2	18.0	22.7	218	409	321	273	204
	2	--	--	--	--	--	--	--	--
	3	40.5	18.0	23.0	233	414	325	276	207

TABLE VI-7--Continued

Run Number	Camera Number	Test Time min	Flame Diameter in	Flame Height in	Projected Area, in^2				
					Flame	Cylinder	Semi-Ellipsoid	para-boloid	Conical
081271-18-7-3	1	20.0	18.0	20.7	109	373	293	249	186
	2	32.4	18.0	21.2	126	382	300	255	191
	3	35.6	18.0	19.0	209	342	276	228	171
070871-12-7-1	1	30.1	11.2	16.0	62	179	141	119	90
	2	40.5	11.5	16.0	55	184	145	213	92
	2	49.0	11.5	16.0	63	184	145	123	92
	3	46.2	12.0	16.2	124	194	152	129	97
070871-12-7-2	1	25.5	11.2	19.9	31	223	175	149	111
	2	31.0	11.5	19.0	47	219	172	146	109
	3	36.1	11.5	18.9	131	127	170	145	109
070871-12-7-3	1	44.5	11.7	17.9	94	209	164	139	105
	2	48.0	11.5	20.8	94	239	188	159	120
	3	54.2	12.0	8.8	95	106	83	71	53
	3	55.8	12.0	16.2	118	194	152	129	97

Soot Accumulation

As mentioned earlier, if the flame height was lowered, a point was reached where the soot was burned off the probe. This condition is obtained with a low fuel level, but is difficult to obtain and control. This condition appears to have been reached for runs 090171-24-1-2, 038071-24-3-2, and 083171-24-4-1, 2. An examination of the heat transfer data shows that the soot accumulation on the probe has no significant effect on the time rate of heat removed by the water. In fact the soot layer increases the emittance of the probe to that of a blackbody and eliminates the problem of specifying an emittance for the stainless steel.

The soot accumulated on the probe generally in an even layer, whose mean thickness is given in Table VI-8. The soot was light and powdery and could easily be brushed or peeled from the probe. In numerous instances when the flame was being extinguished, the soot was blown from the probe surface. Table VI-8 shows that the soot thickness increased as the burner size decreased. The probe surface temperature was cooler for these cases and this resulted in the increased thickness. Benzene produced the worse sooting conditions and heavier deposits near the probe top occurred in the form of finger-like sections.

Flame Temperature

Flame temperatures were measured with an optical pyrometer for all fuels except methanol whose flames were too dim

TABLE VI-8

MEAN THICKNESS OF SOOT ACCUMULATION ON PROBE

Fuel	Mean Soot Thickness, Inches		
	24" Burner	18" Burner	12" Burner
Acetone	0-0.015	0.010-0.015	0.015
Benzene	0.062	0.094	0.125-0.187
Cyclohexane	0.015	0.015	0.032
n-Hexane	0-0.015	0.010-0.015	0.032
Jet A	0.015	0.032	0.050-0.062
JP-4	0.010-0.015	0.025	0.032-0.047

to obtain a reading. No significant difference in flame temperature resulted among burner sizes. Mean flame temperatures obtained are: 1992°F for acetone, 1922°F for benzene, 1953°F for cyclohexane, 2056°F for n-hexane, 1850°F for Jet A, and 1935°F for JP-4. The temperatures for the single component fuels are about 100°-200°F lower than the values obtained by Welker (80) and about 100°F lower than the values obtained by Neill (50). The temperature for JP-4 is about 50°F lower than Neill's value but about 100°F higher than the mean value given by Bader (7). For benzene, flame temperature measurements must be made shortly after ignition because the smoke produced will result in lower optical readings.

Fuel Burning Rate

The fuel burning rate was obtained by observing the fuel tank level at various times throughout a test run.

these results are presented in Figures VI-22 through VI-28, which show that the volume regression rate is a linear function of time.

Flame Height Correlation

From the slopes of Figures VI-22 through VI-28, the fuel burning rate for each run was obtained. These data are given in Tables VI-9 through VI-15 along with values of dimensionless flame height and Froude Number. The cross-sectional area of the burners is 3.11398, 1.73953 and 0.75779 ft^2 for the 24, 18 and 12 inch diameter burners respectively. These values were used to compute the mass velocity and mass burning rate per unit area from the measured volumetric data. For the computation of the dimensionless flame height and Froude Number, an equivalent diameter of 1.8125, 1.3125, and 0.8125 ft was used for the 24, 18 and 12 inch burners respectively. The use of an equivalent diameter instead of the burner inside diameter is an arbitrary choice and additional studies would have to be conducted to determine the most appropriate value to use.

In previous studies the density of room temperature air was used in the computation of the Froude Number. This value arose from the studies of burning wood where the density of the fuel vapor was unknown. For liquid fuels the vapor density of the fuel at its boiling point is known and is the appropriate value to be used. For Jet A and JP-4 the densities

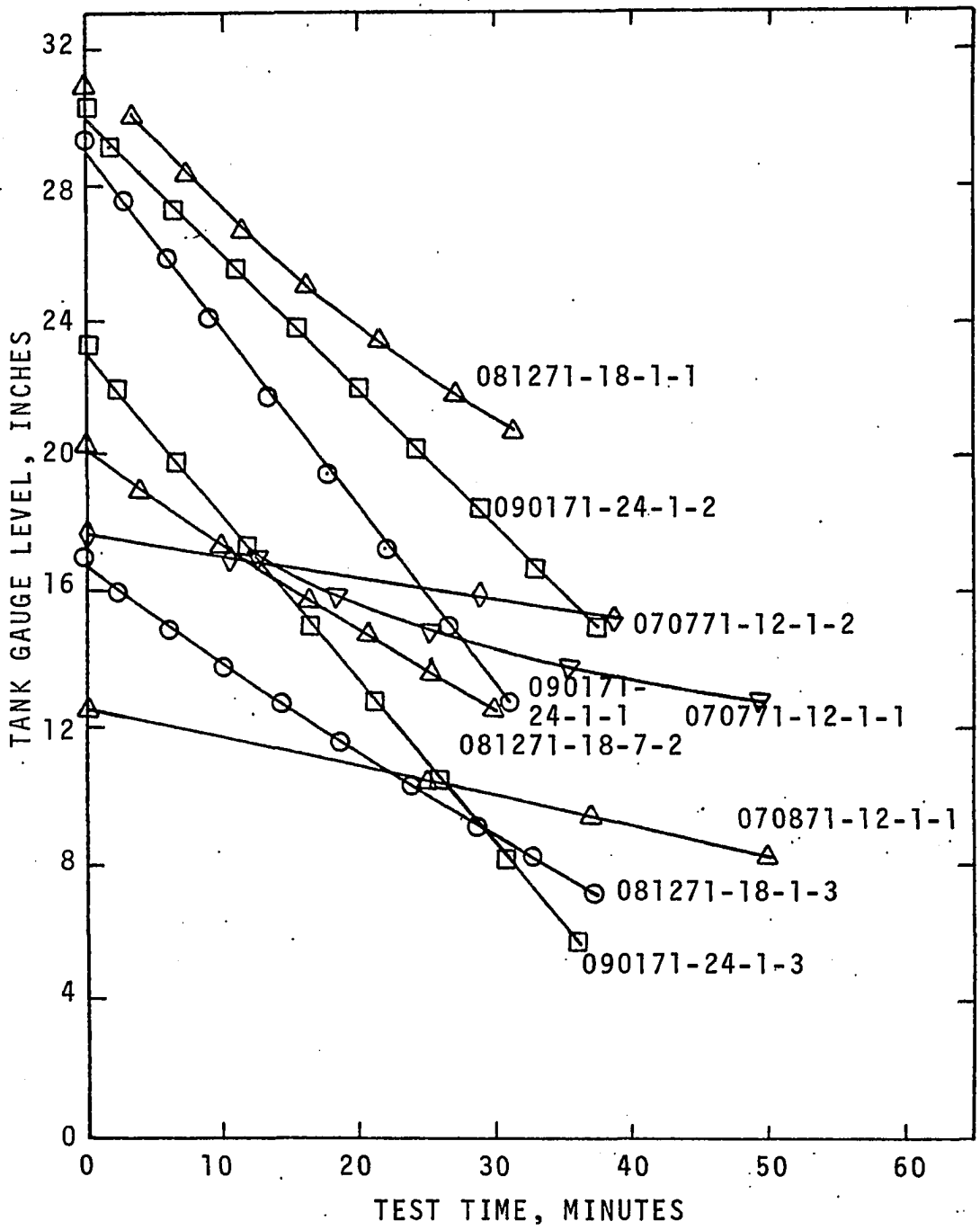


Figure VI-22. Tank Gauge Level as a Function of Time for Acetone.

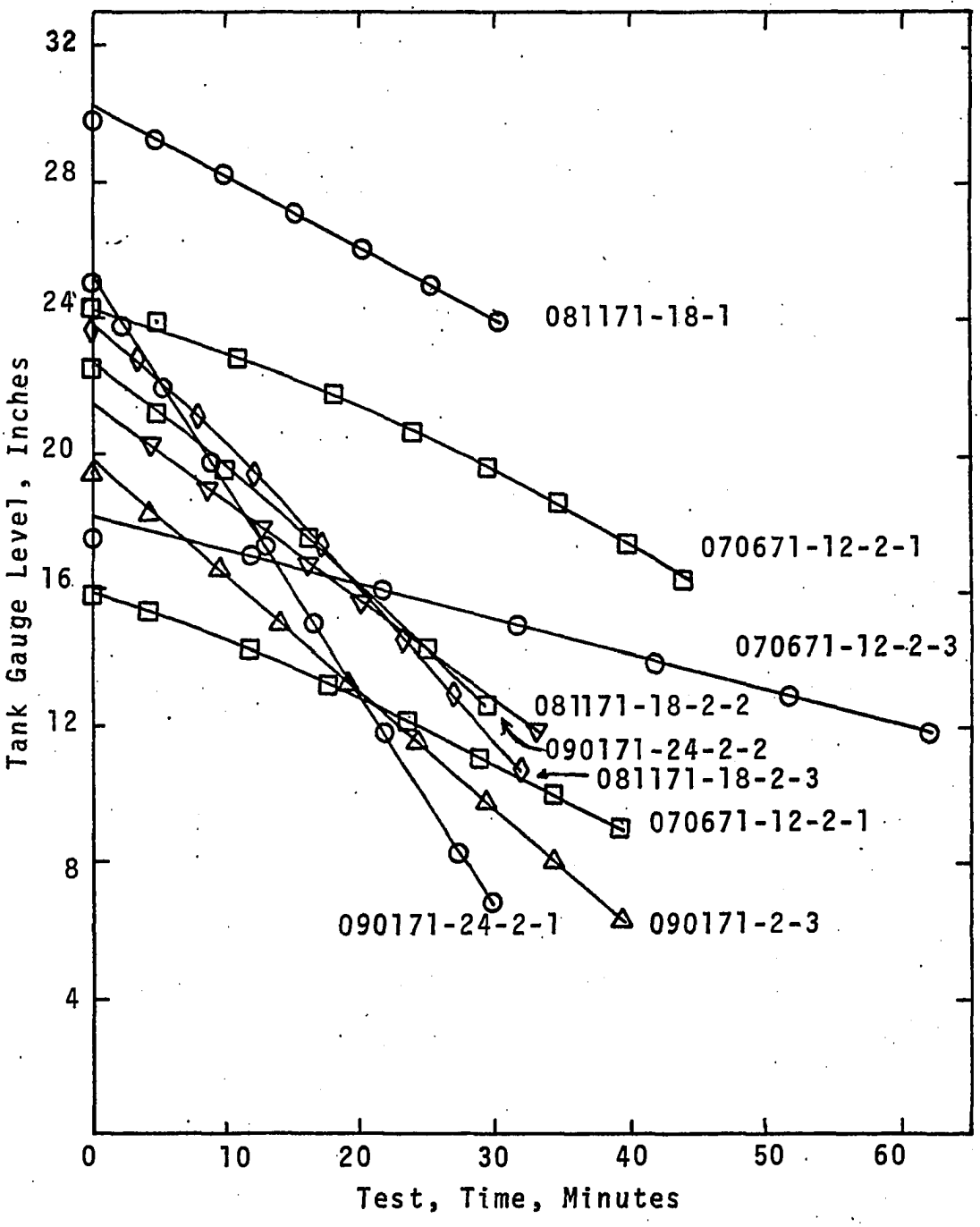


Figure VI-23. Tank Gauge Level as a Function of Time for Benzene.

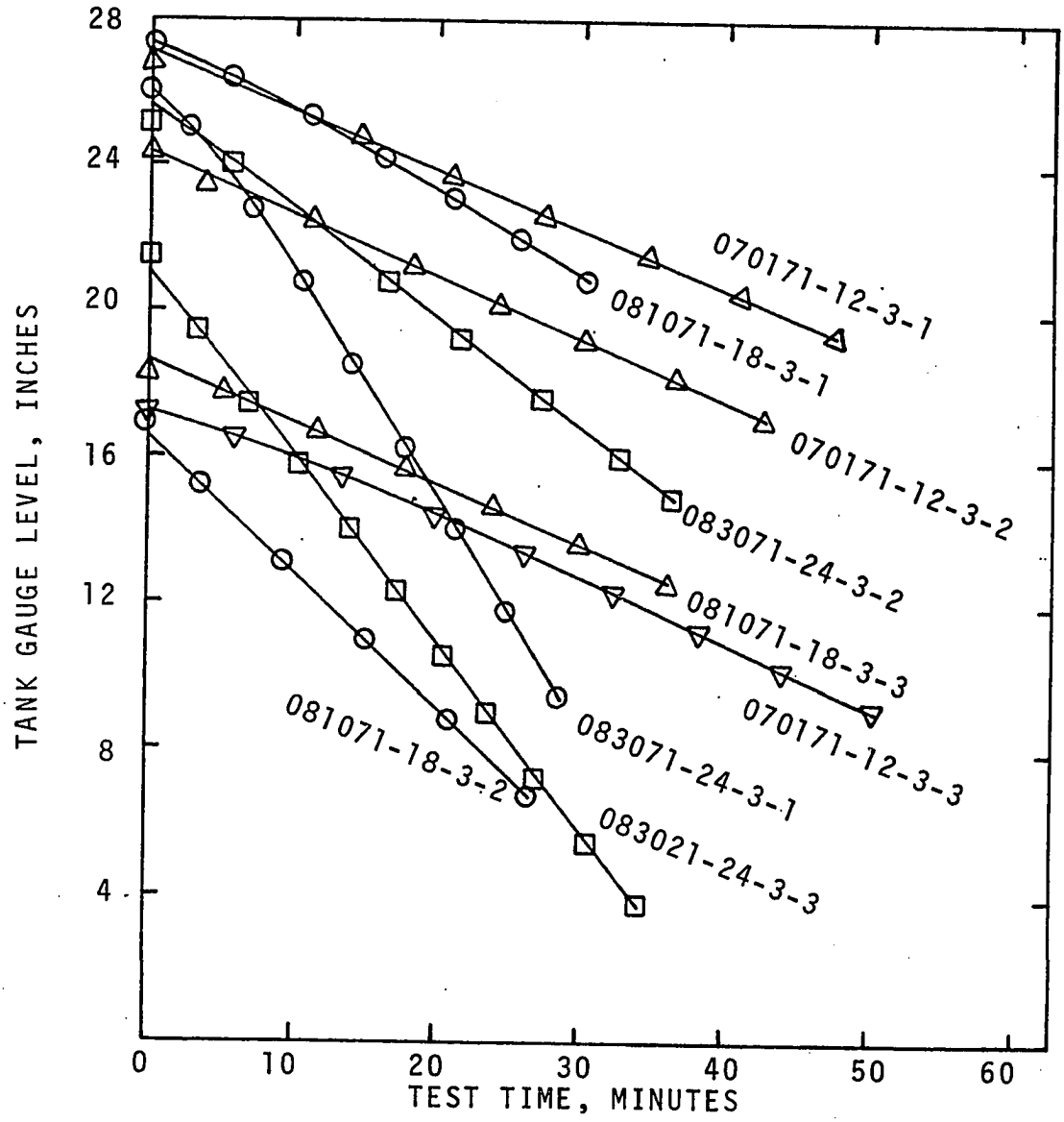


Figure VI-24. Tank Gauge Level as a Function of Time for Cyclohexane.

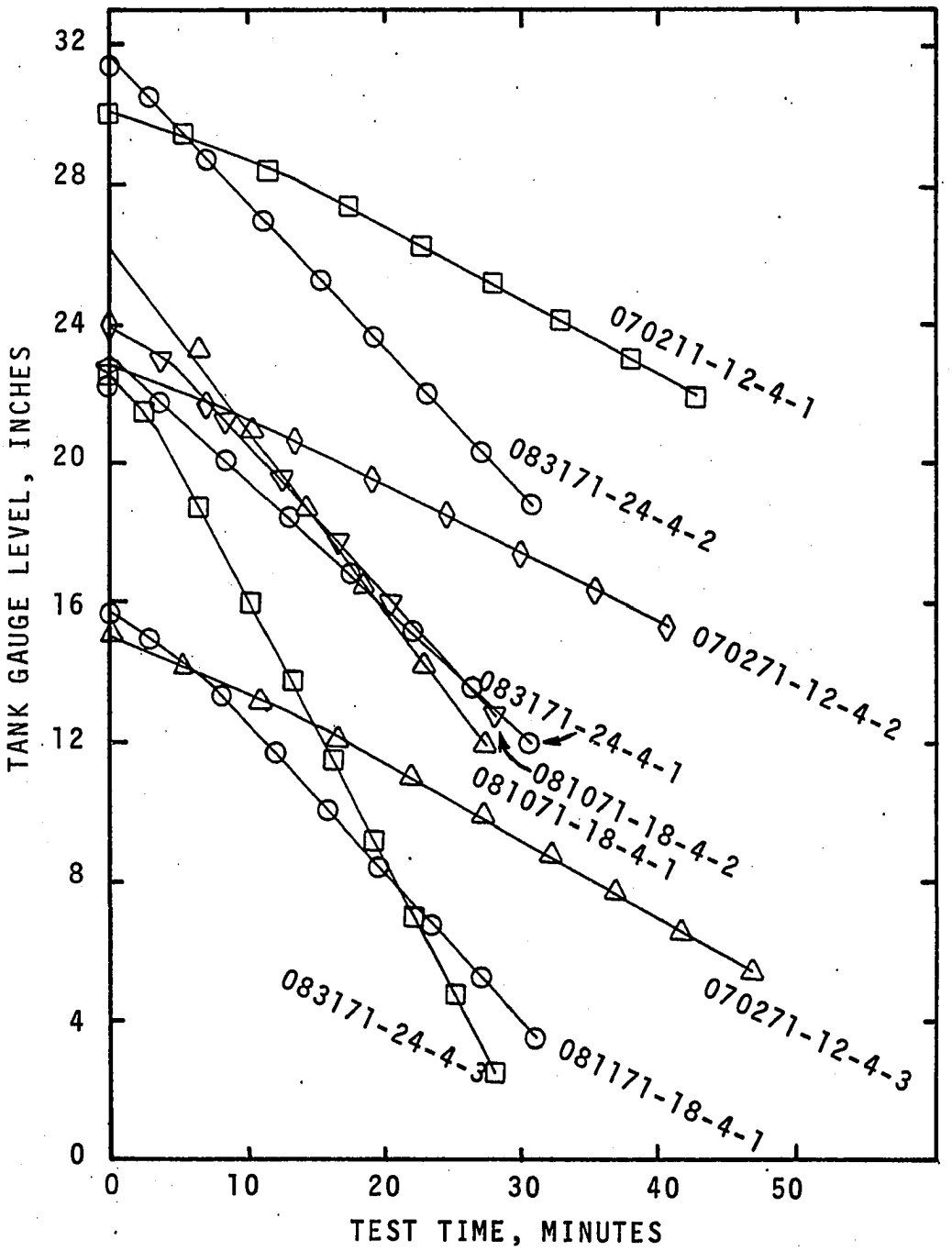


Figure VI-25. Tank Gauge Level as a Function of Time for n-Hexane.

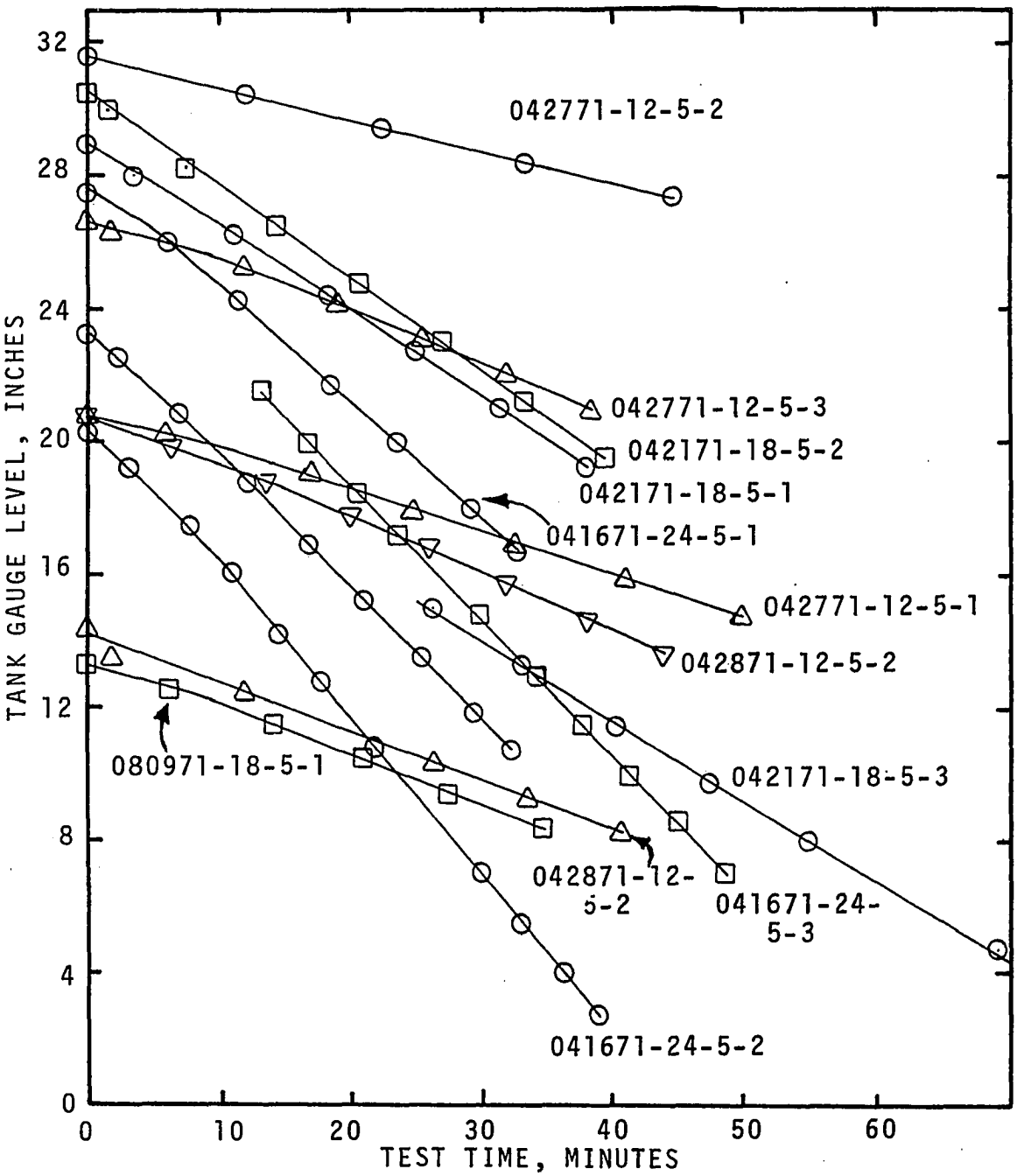


Figure VI-26. Tank Gauge Level as a Function of Time for Jet A.

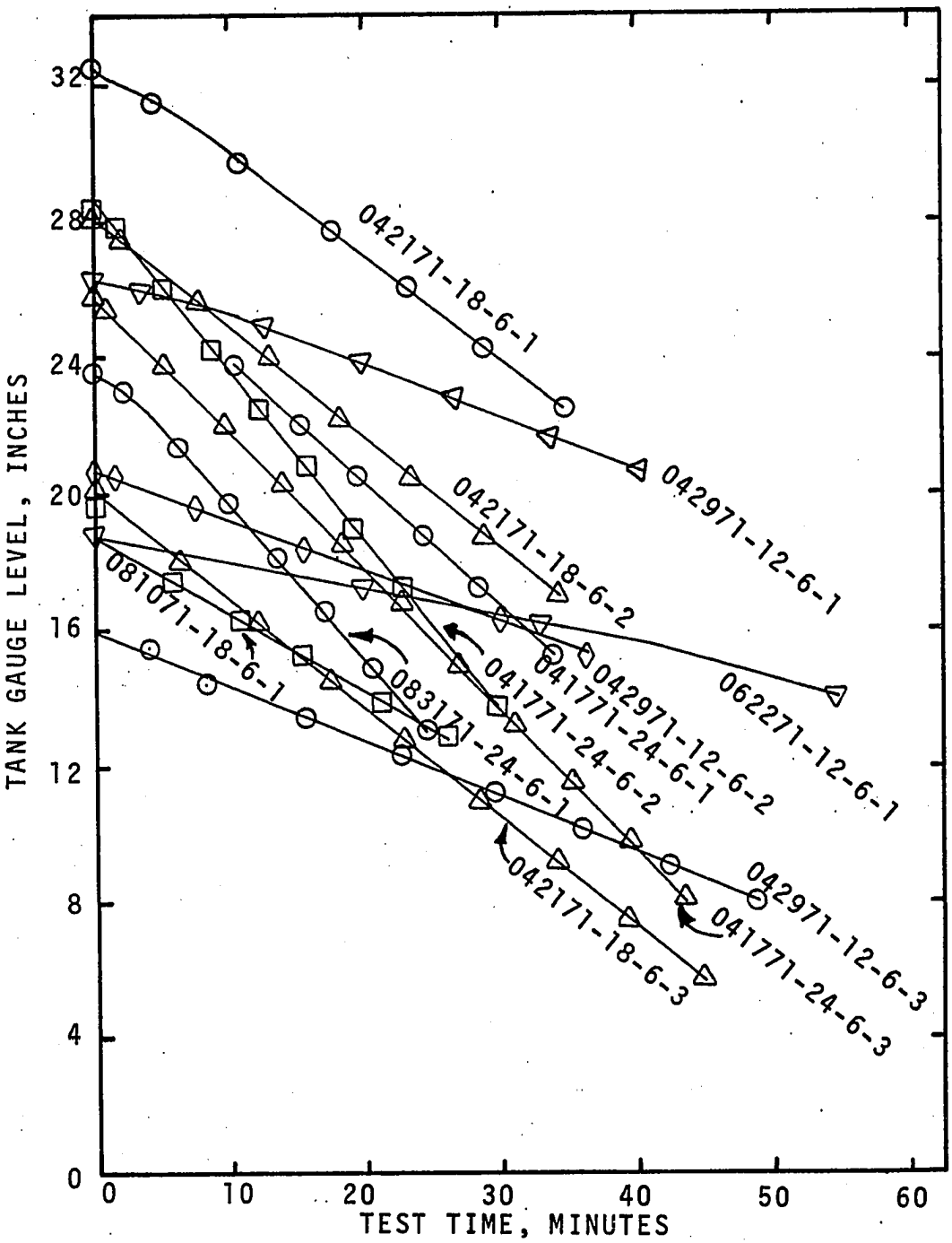


Figure VI-27. Tank Gauge Level as a Function of Time for JP-4.

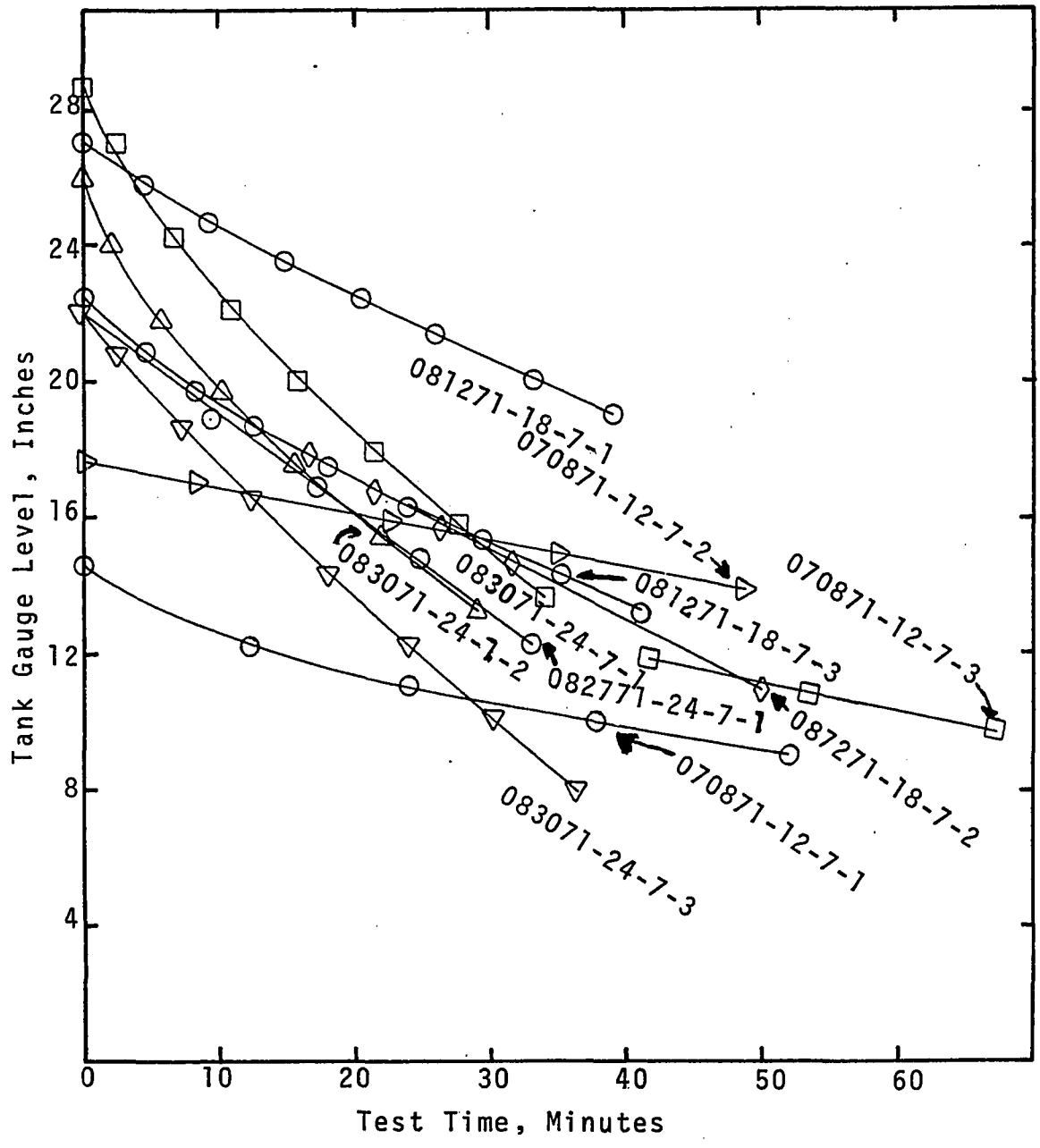


Figure VI-28. Tank Gauge Level as a Function of Time for Methanol.

TABLE VI-9

ACETONE BURNING RATE, H/D_e, AND FROUDE NUMBER

Run Number	Fuel Temp °F	Fuel Spec. Grav.	Fuel Burning Rate				Flame Size		$\frac{H}{D}_e$	Froude Number $M_s/\rho_v\sqrt{gD_e}$
			cc/min	cm/min	lbm/hr	$\frac{lbm}{hr\text{-}ft^2}$	Diameter inches	Height inches		
090171-24-1-1	74.8	0.790	643.54	0.222	67.25	21.60	24.5	97	4.46	0.00585
090171-24-1-2	76.0	0.789	492.37	0.170	51.39	16.50	24.5	65	2.97	0.00447
090171-24-1-3	75.9	0.789	591.29	0.204	61.71	19.82	24.5	87	4.00	0.00537
081271-18-1-1	76.0	0.789	329.93	0.204	34.43	19.80	18.7	65	4.14	0.00630
081271-18-1-2	76.7	0.789	294.38	0.182	30.72	17.66	18.7	66	4.18	0.00562
081271-18-1-3	78.8	0.788	303.99	0.188	31.69	18.22	18.7	65	4.14	0.00580
070771-12-1-1	88.0	0.785	89.31	0.127	9.27	12.24	11.9	47	4.83	0.00495
070771-12-1-2	87.0	0.785	79.89	0.113	8.30	10.95	12.2	46	4.68	0.00443
070871-12-1-1	85.0	0.786	107.98	0.153	11.23	14.82	12.2	46	4.71	0.00599

TABLE VI-10

BENZENE BURNING RATE, H/D_e, AND FROUDE NUMBER

Run Number	Fuel Temp °F	Fuel Spec. Grav.	Fuel Burning Rate				Flame Size		$\frac{H}{D_e}$	Froude Number $M_s/\rho_v\sqrt{gD_e}$
			cc/min	$\frac{cm}{min}$	$\frac{lbm}{hr}$	$\frac{lbm}{hr\text{-}ft^2}$	Diameter inches	Height inches		
090171-24-2-1	81.3	0.871	774.00	0.268	89.18	28.64	26.6	59.6	2.74	0.00619
090171-24-2-2	83.0	0.871	494.94	0.156	51.84	16.65	24.8	67.6	3.11	0.00360
090171-24-2-3	82.4	0.871	429.10	0.148	49.44	15.87	24.8	49.0	2.25	0.00343
081171-18-2-1	83.0	0.871	266.96	0.165	30.76	17.68	19.4	65.0	4.14	0.00449
081171-18-2-2	81.7	0.871	361.46	0.224	41.65	23.94	20.9	70.8	4.50	0.00608
081171-18-2-3	84.3	0.870	539.27	0.334	62.06	35.68	22.3	54.3	3.45	0.00906
070671-12-2-1	71.0	0.877	271.70	0.386	31.52	41.59	16.5	46.0	4.71	0.01343
070671-12-2-2	79.0	0.873	264.89	0.376	30.59	40.37	15.8	67.0	6.87	0.01303
070671-12-2-3	82.0	0.873	127.04	0.180	14.67	19.36	13.7	48.0	4.89	0.00625

TABLE VI-11

CYCLOHEXANE BURNING RATE, H/D_e, AND FROUDE NUMBER

Run Number	Fuel Temp °F	Fuel Spec. Grav.	Fuel Burning Rate				Flame Size		$\frac{H}{D_e}$	Froude Number $\frac{M_s}{\rho_v\sqrt{gD_e}}$
			cc/min	$\frac{cm}{min}$	$\frac{lbm}{hr}$	$\frac{lbm}{hr\text{-}ft^2}$	Diameter inches	Height inches		
083071-24-3-1	75.7	0.775	769.80	0.266	78.92	25.34	25.9	100.1	4.60	0.00509
083071-24-3-2	78.0	0.774	366.65	0.127	37.54	12.06	24.8	49.6	2.28	0.00242
083071-24-3-3	79.5	0.773	630.62	0.218	64.48	20.71	25.2	94.9	4.36	0.00416
081071-18-3-1	77.6	0.774	280,83	0.174	28.75	16.53	19.1	84.5	5.36	0.00390
081071-18-3-2	76.7	0.774	464.14	0.287	47.52	27.32	20.1	92.0	5.82	0.00645
081071-18-3-3	79.4	0.773	208.84	0.129	21.35	12.28	18.7	54.3	3.45	0.00290
070171-12-3-1	79.5	0.773	203.05	0.288	20.76	27.40	14.7	73.3	7.52	0.00822
070171-12-3-2	81.0	0.772	213.29	0.303	21.78	28.74	14.7	87.3	8.96	0.00863
070171-12-3-3	81.0	0.772	211.87	0.301	21.64	28.55	14.7	69.8	7.16	0.00857

TABLE VI-12

n-HEXANE BURNING RATE, H/D_e, AND FROUDE NUMBER

Run Number	Fuel Temp °F	Fuel Spec. Grav.	Fuel Burning Rate				Flame Size		$\frac{H}{D_e}$	Froude Number $M_s/\rho_v\sqrt{gD_e}$
			cc/min	$\frac{cm}{min}$	$\frac{lbm}{hr}$	$\frac{lbm}{hr\text{-}ft^2}$	Diameter inches	Height inches		
083171-24-4-1	74.7	0.657	450.58	0.156	39.16	12.58	24.5	58.2	2.68	0.00238
083171-24-4-2	75.6	0.656	522.67	0.181	45.36	14.57	24.8	74.8	3.44	0.00276
083171-24-4-3	76.8	0.656	948.50	0.328	82.31	26.43	25.9	116.0	5.31	0.00501
081071-18-4-1	82.9	0.653	638.58	0.395	55.16	31.71	20.9	106.0	6.76	0.00707
081071-18-4-2	84.0	0.653	555.22	0.344	47.96	27.57	20.1	106.0	6.76	0.00614
081171-18-4-1	80.2	0.654	536.45	0.332	46.41	26.68	20.9	106.0	6.76	0.00594
070271-12-4-1	75.0	0.657	261.25	0.371	22.71	29.96	15.1	91.7	9.40	0.00848
070271-12-4-2	76.0	0.656	245.69	0.349	21.32	28.14	14.4	75.5	7.74	0.00797
070271-12-4-3	77.0	0.656	272.81	0.388	23.67	31.24	15.8	84.1	8.63	0.00884

TABLE VI-13

JET A BURNING RATE, H/D_e, AND FROUDE NUMBER

Run Number	Fuel Temp °F	Fuel Spec. Grav.	Fuel Burning Rate				Flame Size		$\frac{H}{D_e}$	Froude Number $M_s/\rho_v\sqrt{gD_e}$
			cc/min	$\frac{cm}{min}$	$\frac{lbm}{hr}$	$\frac{lbm}{hr\text{-}ft^2}$	Diameter inches	Height inches		
083171-24-5-1	83.5	0.793	506.10	0.175	53.09	17.05	25.9	79.4	3.65	0.00761
041671-24-5-1	71.0	0.798	437.56	0.151	46.19	14.83	24.5	56.0	2.57	0.00662
041671-24-5-2	73.0	0.797	590.00	0.204	62.20	19.98	28.8	59.6	2.74	0.00891
041671-24-5-3	77.0	0.795	507.52	0.175	53.37	17.14	26.3	56.0	2.57	0.00765
080971-18-5-1	83.0	0.793	193.30	0.120	20.28	11.66	19.4	58.0	3.68	0.00341
042171-18-5-1	81.0	0.794	327.96	0.203	34.45	19.80	19.8	64.3	4.08	0.00580
042171-18-5-2	81.0	0.794	297.73	0.184	31.27	17.98	20.1	60.0	3.81	0.00527
042171-18-5-3	81.5	0.793	300.66	0.186	31.54	18.13	18.9	53.3	3.38	0.00531
070971-12-5-1	83.0	0.793	73.15	0.104	7.67	10.13	12.9	44.6	4.57	0.00164
042771-12-5-1	75.0	0.796	158.47	0.225	16.69	22.02	15.5	54.6	5.60	0.00357
042771-12-5-2	75.5	0.796	117.51	0.167	12.37	16.33	13.7	45.3	4.65	0.00265
042771-12-5-3	75.0	0.796	207.28	0.294	21.83	28.80	15.8	48.2	4.94	0.00467
042871-12-5-1	76.5	0.795	217.88	0.309	22.91	30.24	16.5	45.2	4.64	0.00490
042871-12-5-2	78.5	0.795	181.06	0.257	19.04	25.12	15.8	58.2	5.97	0.00408

TABLE VI-14

JP-4 BURNING RATE, H/D_e, AND FROUDE NUMBER

Run Number	Fuel Temp °F	Fuel Spec. Grav.	Fuel Burning Rate				Flame Size		$\frac{H}{D_e}$	Froude Number $M_s/\rho_v\sqrt{gD_e}$
			cc/min	$\frac{cm}{min}$	$\frac{lbm}{hr}$	$\frac{lbm}{hr\text{-}ft^2}$	Diameter inches	Height inches		
083171-24-6-1	83.0	0.766	582.78	0.201	59.05	18.96	25.9	91.3	4.20	0.00985
041771-24-6-1	67.0	0.772	454.50	0.157	46.41	14.90	24.5	61.8	2.84	0.00774
041771-24-6-2	67.0	0.772	621.83	0.215	63.50	20.39	26.6	79.5	3.66	0.01059
041771-24-6-3	68.0	0.772	516.70	0.179	52.77	16.94	24.5	70.4	3.24	0.00880
081071-18-6-1	76.5	0.768	286.73	0.177	29.13	16.75	19.4	83.7	5.31	0.00571
042171-18-6-1	67.0	0.772	381.33	0.236	38.94	22.39	20.5	75.1	4.77	0.00763
042171-18-6-2	65.5	0.773	409.85	0.254	41.91	24.09	21.6	84.5	5.36	0.00821
042171-18-6-3	68.5	0.772	396.34	0.245	40.47	23.27	20.5	67.9	4.31	0.00793
062271-12-6-1	74.0	0.769	139.57	0.198	14.20	18.73	13.3	49.6	5.09	0.00354
042971-12-6-1	63.0	0.774	191.57	0.272	19.61	25.88	14.7	54.6	5.60	0.00484
042971-12-6-2	65.0	0.773	181.06	0.257	18.51	24.43	15.5	55.3	5.67	0.00461
042971-12-6-3	66.0	0.773	202.85	0.288	20.74	27.37	15.8	62.8	6.44	0.00517

TABLE VI-15

METHANOL BURNING RATE, H/D_e, AND FROUDE NUMBER

Run Number	Fuel Temp °F	Fuel Spec. Grav.	Fuel Burning Rate				Flame Size		$\frac{H}{D}_e$	Froude Number $M_s/\rho_v\sqrt{gD_e}$
			cc/min	$\frac{cm}{min}$	$\frac{lbm}{hr}$	$\frac{lbm}{hr\text{-}ft^2}$	Diameter inches	Height inches		
082771-24-7-1	87.1	0.786	363.16	0.126	37.76	12.13	23.7	44.0	2.02	0.00611
083071-24-7-1	75.7	0.790	412.06	0.142	43.06	13.82	23.4	22.6	1.04	0.00696
083071-24-7-2	79.1	0.789	402.36	0.139	41.99	13.49	23.4	24.5	1.13	0.00679
083071-24-7-3	83.6	0.787	430.49	0.149	44.82	14.39	23.4	21.5	0.99	0.00724
081271-18-7-1	80.3	0.788	231.89	0.143	24.17	13.90	17.3	21.9	1.39	0.00822
081271-18-7-2	81.3	0.788	259.19	0.160	27.02	15.53	18.0	23.0	1.46	0.00919
081271-18-7-3	82.7	0.787	229.56	0.142	23.90	13.74	18.0	21.2	1.35	0.00813
070871-12-7-1	85.0	0.787	92.81	0.132	9.66	12.75	11.5	16.0	1.64	0.00959
070871-12-7-2	87.5	0.786	97.48	0.138	10.14	13.37	11.5	19.0	1.95	0.01005
070871-12-7-3	86.5	0.786	102.25	0.145	10.63	14.03	11.5	20.8	2.13	0.01055

of n-undecane and n-octane were used but may not be appropriate since the composition of the vapor leaving these mixtures is unknown. Figure IV-29 shows H/D_e as a function of the Froude Number. It can be seen that an additional correlating parameter is required. It can be argued that the quantity of combustion air is important, so if the H/D_e values of the single component fuels are multiplied by the ratio of $7.15/r_v$, the data variation are improved as can be seen in Figure VI-30. Stoichiometric values of r_v were assumed in these calculations. The jet fuels were not included because their value of r_v is unknown and the use of r_v values for n-octane and u-undecane results in excessive H/D_e predictions. A least squares analysis of the data in Figure VI-30 produces the following correlation.

$$(H/D_e)(7.15/r_v) = 23.4\ (M_s/\ _v\ g\ D_e)^{.6} \qquad \text{(VI-1)}$$

The 0.6 exponent on the Froude Number agrees well with the .61 value of Equation II-18 and the 0.51 value of Equation II-39. One cannot explicitly compare the premultiplier value due to the use of different densities and the $7.15/r_v$ value, but for methanol the premultiplier in these equations is approximately double that obtained in Equation VI-1.

Burning Rate Correlation

If the fuel burning rate is assumed to be heat transfer controlled, the Figure VI-31 shows the heat rates associated with the fuel and burner.

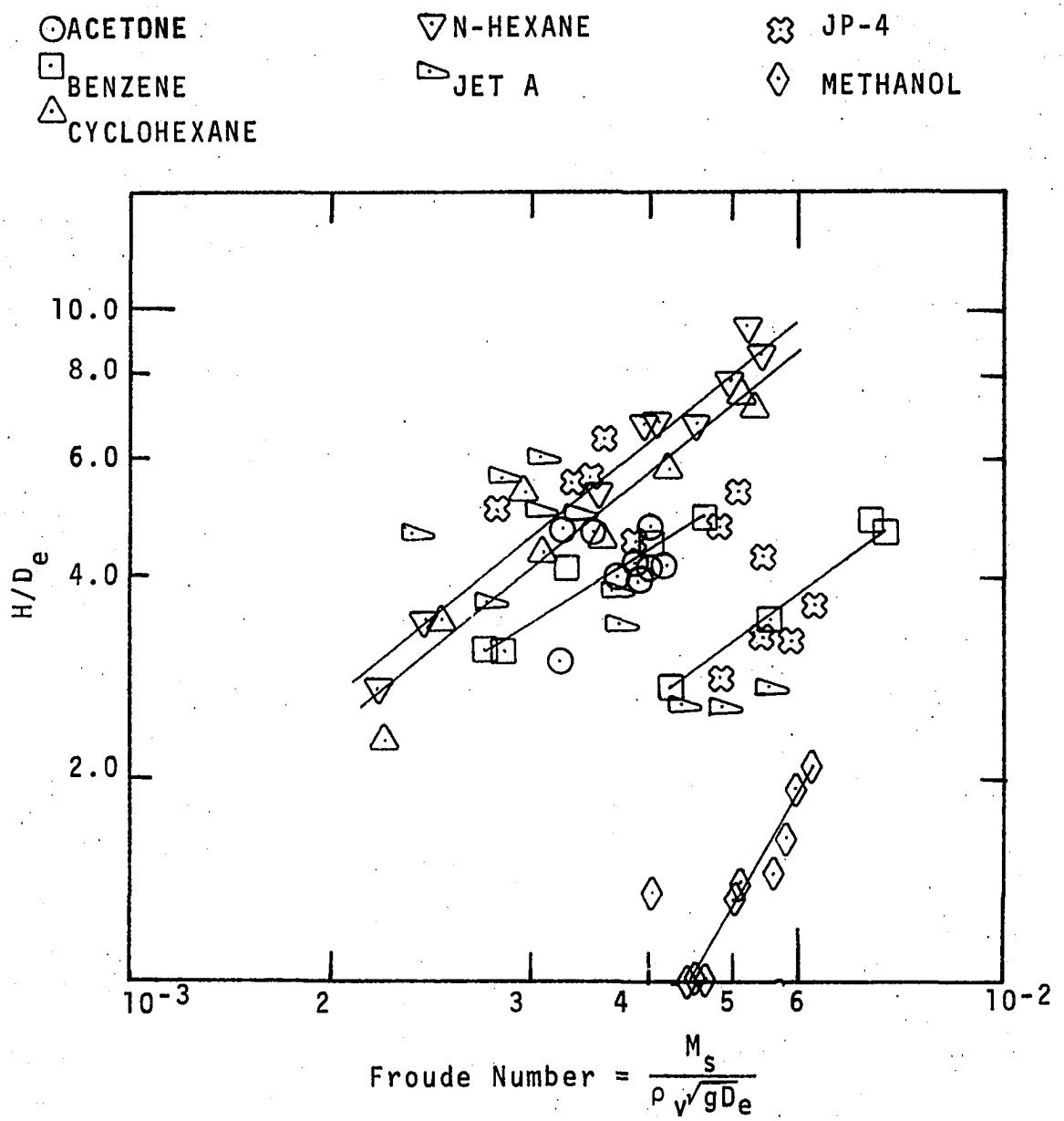


Figure VI-29. H/D_e as a Function of Froude Number.

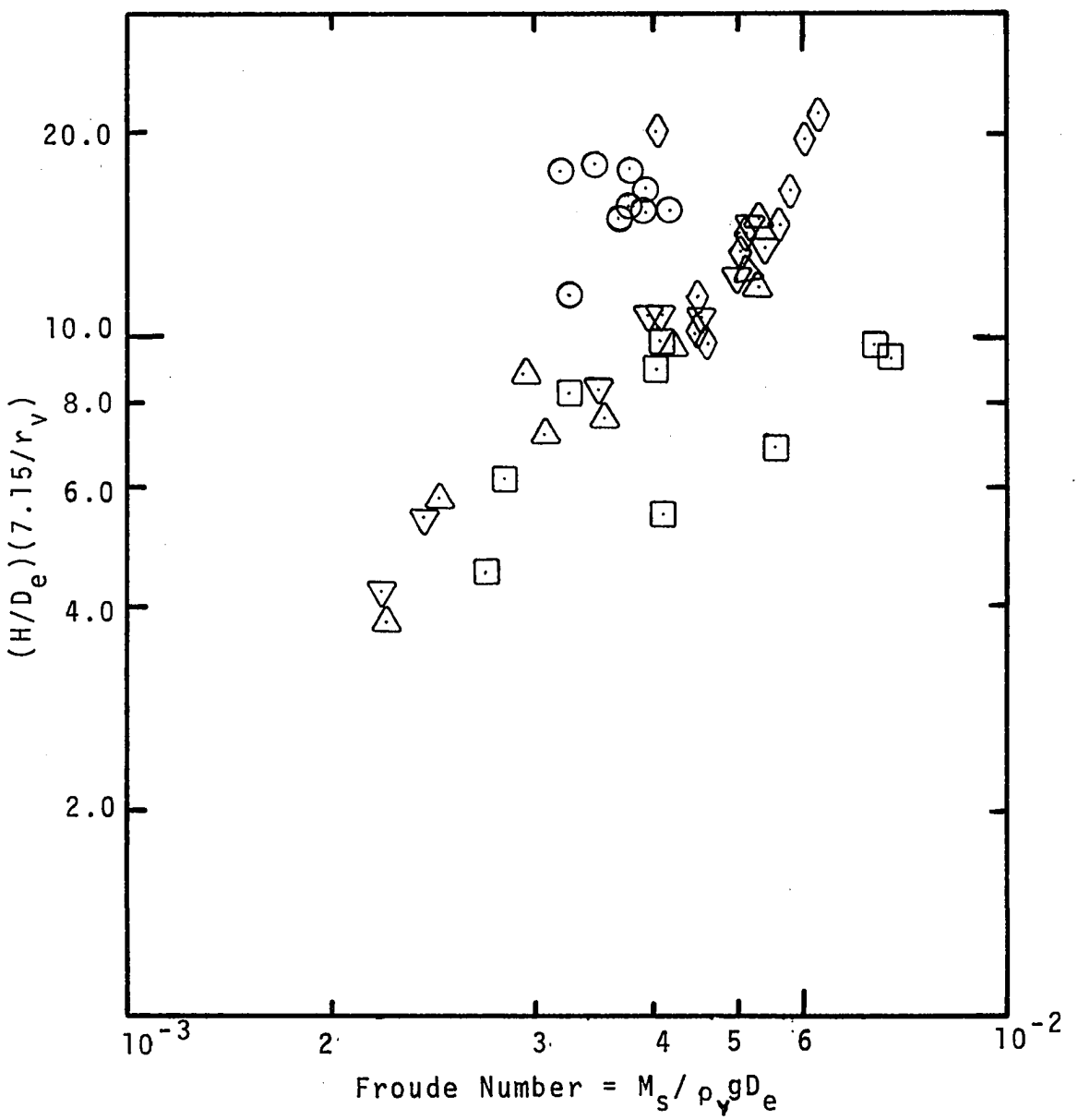


Figure VI-30. Modified Dimensionless Flame Height as a Function of Froude Number.

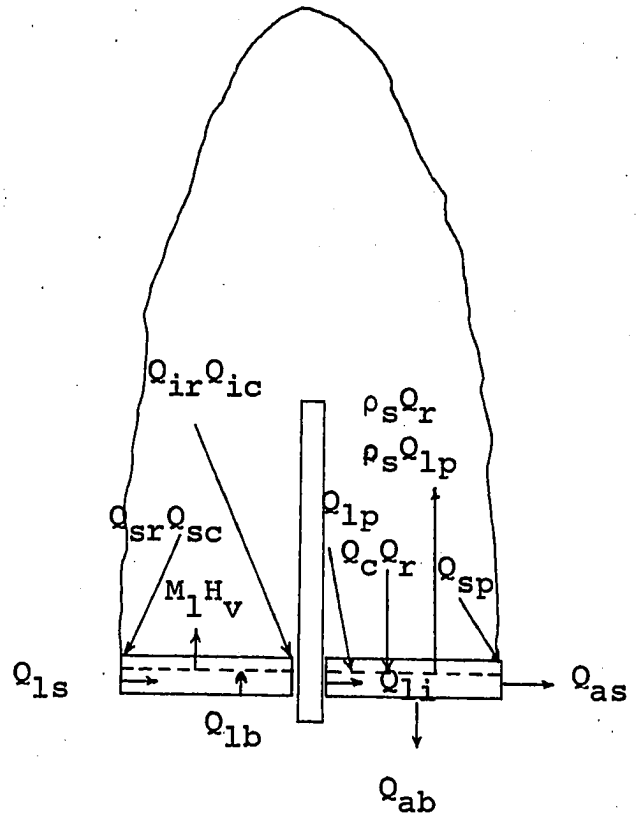


Figure VI-31. Burner and Fuel Heat Rates.

Assuming that the probe and fuel pan are black bodies, a heat balance on the fuel leads to the following equation:

$$Q_{ls} + Q_c + Q_{lb} + Q_r + Q_{lp} + Q_{li} = \rho_s(Q_{lp} + Q_r) + M_l H_v \quad \text{(VI-2)}$$

where Q_c = convective heat transfer from flame to fuel, Btu/hr

Q_{lb} = convective heat transfer from pan bottom to fuel, Btu/hr

Q_{li} = convective heat transfer from pan center to fuel, Btu/hr

Q_{lp} = radiative heat transfer from probe to fuel, Btu/hr

Q_{ls} = convective heat transfer from pan side to fuel, Btu/hr

Q_r = radiative heat transfer from flame to fuel, Btu/hr

$_s$ = reflectivity of fuel surface

Assuming that the fuel pan is hotter than the fuel, a heat balance around the burner produces the following equation

$$Q_{ls} + Q_{as} + Q_{ab} + Q_{lb} + Q_{li} = Q_{sr} + Q_{sp} + Q_{sc} + Q_{ic} + Q_{ir} \quad \text{(VI-3)}$$

where Q_{ab} = convective heat transfer from pan bottom to air, Btu/hr

Q_{as} = convective heat transfer from pan sides to air, Btu/hr

Q_{ic} = convective heat transfer from flame to pan center, Btu/hr

Q_{ir} = radiative heat transfer from flame to pan center, Btu/hr

Q_{sc} = convective heat transfer from flame to pan side, Btu/hr

Q_{sp} = radiative heat transfer from probe to pan side, Btu/hr

Q_{sr} = radiative heat transfer from flame to pan side, Btu/hr

Now prediction of the individual heat rates for the solution of Equation VI-2 and 3 is a formidable task. Since the surface area of the burner center section is small, one may neglect the terms Q_{ic}, Q_{ir} and Q_{li}, even though fuel boiling was observed around this surface. If the fuel pan temperature is assumed to be equal to the boiling point of the fuel, then the term, Q_{sc}, can be neglected as the temperature difference between the rising fuel vapor and the pan is nearly zero. The heat loss from the pan side to the air, Q_{as} and Q_{ab}, can be predicted from free convection theory. Similarly the heat transfer from the pan to the fuel Q_{ls} and Q_{lb} can be predicted. The heat transfer coefficients used to predict these values were computed from equations given in McAdams (46). Values of Q_{as}, Q_{ab}, Q_{lb} and Q_{ls} for a ½" fuel depth are shown in Table VI-16. The value of Q_{ls} varies as the 1.75 power of the fuel depth, but due to other uncertainties only the one value was given for comparative results.

The values of Q_{lp} and Q_{sp} will not be computed as as the view factor from the probe to the liquid surface and the burner are not readily available. Considering the absorptance of the flame, these values would be further reduced and can be considered negligible. No known correlation exists for obtaining Q_c, which could be obtained from Equation VI-2 provided the remaining terms in the equation could be accurately evaluated.

The use of a mean beam length allows the radiative flux to be computed to any boundary of the flame. Therefore, the values of Q_{sr} and Q_r can be obtained. Using the radiant fluxes, q_m/F_{tf}, given in Tables VIII-22 through VIII-28, these values were computed and are shown in Table VI-17. Values of $M_l H_v$ were computed from the measured burning rates and are also included in the above table. Now reflectivity data for liquids are scarce and not available for these liquids, so the reflected energy could not be computed.

Several things become obvious when the results in Table VI-16 and 17 are examined. It can be seen that the values of Q_r alone exceed the computed values of $M_l H_v$ and points out the need for liquid reflectivities. The existence of a few inches of fuel vapors above the liquid surface could also result in an appreciable absorption of radiant energy and thereby reduce the amount of heat transferred by radiation. The assumption that the pan temperature reaches the boiling point of the fuel is based on Emmons (27) measurement of a pan bottom temperature in excess of the boiling point of its acetone fuel. Pan temperatures were not measured in this study but for times in excess of 5 minutes after flame extinguishment, the fuel pan was still too hot to touch. The use of these high pan temperatures results in computed heat transfer rates to the fuel from the pan bottom in excess of the measured rates. The pan is primarily heated by the radiant flux from the flame, but the resulting values of Q_{sr} are not high enough

TABLE VI-16

HEAT TRANSFER RATES FROM FUEL PAN BOTTOM AND SIDE

Fuel	Burner Diameter in	Q_{as} Btu/hr	Q_{ab} Btu/hr	Q_{lb} Btu/hr 1/2"	Q_{ls} Fuel Depth Btu/hr
Acetone	24	93	53	16752	646
	18	70	30	9358	484
	12	46	13	4077	323
Benzene	24	178	101	26217	977
	18	133	59	14645	732
	12	89	24	6380	488
Cyclohexane	24	181	102	19754	784
	18	134	60	11035	588
	12	90	24	4807	392
n-Hexene	24	137	80	20519	719
	18	103	45	11462	539
	12	69	19	4993	360
Jet A	24	882	500	144943	3849
	18	659	292	80968	2887
	12	441	121	35372	1925
JP-4	24	654	377	121461	4625
	18	488	216	67850	3469
	12	327	90	29558	2313
Methanol	24	122	70	21853	814
	18	91	40	12207	610
	12	61	16	5318	407

TABLE VI-17

HEAT TRANSFER RATES FROM RADIATION AND BY FUEL

Run Number	M_ℓ lbm/hr	$M_\ell H_v$ Btu/hr	Q_r Btu/hr	Q_{sr} 1.5" Freeboard Btu/hr
090171-24-1-1	67.25	16755	21539	5433
090171-24-1-2	51.39	12804	32669	8240
090171-24-1-3	61.71	15375	18485	4662
081271-18-1-1	34.43	8578	9145	3097
081271-18-1-2	30.72	7654	8675	2938
081271-18-1-3	31.69	7896	9158	3101
070771-12-1-1	9.27	2310	3490	1808
070771-12-1-2	8.30	2068	4133	2142
070771-12-1-3	11.23	2798	4843	2512
090171-24-2-1	89.18	18908	46623	11759
090171-24-2-2	51.84	10991	44222	11153
090171-24-2-3	49.44	10482	43188	10893
081171-18-2-1	30.76	6522	20219	6846
081171-18-2-2	41.65	8831	23818	8065
081171-18-2-3	62.06	13158	25378	8594
070671-12-2-1	31.52	6683	8460	4384
070671-12-2-2	30.59	6486	9214	4774
070671-12-2-3	14.67	3110	7517	3896
083071-24-3-1	78.92	15342	32887	8295
083071-24-3-2	37.54	7298	41416	10446
083071-24-3-3	64.48	12535	35446	8940
081071-18-3-1	28.75	5589	14563	4932
081071-18-3-2	47.52	9238	17303	5859
081071-18-3-3	21.35	4150	21339	7226
070171-12-3-1	20.76	4036	5383	2790
070171-12-3-2	21.78	4234	5533	2867
070171-12-3-3	21.64	4207	5774	2992
083171-24-4-1	39.16	7327	45417	11455
083171-24-4-2	45.36	8468	41808	10545
083171-24-4-3	82.31	15400	33220	8379
081071-18-4-1	55.16	10320	15384	5210
081071-18-4-2	47.96	8973	17195	5823
081171-18-4-1	46.41	8683	15151	5131
070271-12-4-1	22.71	4249	5403	2800
070271-12-4-2	21.32	3989	6010	3114
070271-12-4-3	23.67	4428	5554	2878

TABLE VI-17--Continued

Run Number	M_ℓ lbm/hr	$M_\ell H_v$ Btu/hr	Q_r Btu/hr	Q_{sr} 1.5" Freeboard Btu/hr
083171-24-5-1	53.09	18450	48313	12185
041671-24-5-1	46.19	16052	46897	11828
041671-24-5-2	62.20	21616	50297	12686
041671-24-5-3	53.37	18548	42727	10776
080971-18-5-1	20.28	7048	15630	5293
042171-18-5-1	34.45	11972	23482	7952
042171-18-5-2	31.27	10867	21342	7227
042171-18-5-3	31.54	10961	20427	6917
070971-12-5-1	7.67	2666	3570	1850
042771-12-5-1	16.69	5800	7994	4143
042771-12-5-2	12.37	4299	8015	4153
042771-12-5-3	21.83	7587	8528	4419
042871-12-5-1	22.91	7962	8142	4220
042871-12-5-2	19.04	6617	5889	3052
083171-24-6-1	59.05	18073	42478	10714
041771-24-6-1	46.41	14205	40018	10093
041771-24-6-2	63.50	19435	42226	10650
041771-24-6-3	52.77	16151	42366	10685
081071-18-6-1	29.13	8916	14586	4939
042171-18-6-1	38.94	11918	19234	6513
042171-18-6-2	41.91	12827	19509	6606
042171-18-6-3	40.47	12387	18943	6414
062271-18-6-1	14.20	4346	5403	2800
042971-12-6-1	19.61	6002	7883	4085
042971-12-6-2	18.51	5665	7522	3898
042971-12-6-3	20.74	6348	7701	3991
082771-24-7-1	37.76	19452	15371	3876
083071-24-7-1	43.06	22183	14343	3618
083071-24-7-2	41.99	21632	14259	3596
083071-24-7-3	44.82	23089	15072	3801
081271-18-7-1	24.17	12451	7631	2584
081271-18-7-2	27.02	13920	7962	2696
081271-18-7-3	23.90	12312	6668	2258
070871-12-7-1	9.66	4976	2555	1324
070871-17-7-2	10.14	5224	2430	1259
070871-12-7-3	10.63	5476	2405	1246

to account for the large values of Q_{ls} and Q_{lb}. One can only conclude that the pan temperature does not reach the temperature of the fuel boiling point, the free convection equations for the heat transfer coefficient are in error, or the temperature of the fuel in the pan is higher than the values used.

In view of the preceding results, no correlation of the fuel burning rate will be attempted. If one examines the data given in Tables VI-9 through VI-15, it can be seen that the fuel burning rate is not just a function of the pan diameter and fuel physical properties. The fuel pan temperature and freeboard height are undoubtedly important parameters that must be considered. Convective heat losses to the ambient air are negligible and this confirms the conclusion of Corlett and Fu (21). This study had a few cases of very low fuel level and even a partially dry fuel pan. For these cases one would have to consider the transmissivity of the fuels and the changed heat transfer mechanism due to the liquid free surface.

CHAPTER VII

GEOMETRY OF RADIATIVE TRANSFER BETWEEN FLAME AND OBJECT

In Chapter III, four methods for predicting the radiant heat transfer from flames were presented. Two of these methods, Method 1 and Method 2, require integration over the flame geometry and wavelength to obtain the radiant flux from a flame to a target. The geometrical relationships for a target surrounded by a flame and for a target external to a flame will be developed.

The radiant flux from a flame incident on a target is obtained from

$$q_r = \int_{\lambda_1}^{\lambda_2} \int_{\Omega} I_\lambda \cos\theta \, d\Omega \, d\lambda \qquad \text{(VII-1)}$$

By substituting the appropriate expression for I_λ and Ω, this equation is applicable for a target located inside or outside a flame.

Target Surrounded by a Flame

The intensity variation in a flame is expressed by Equation III-18 which is

$$I_\lambda = \frac{J_\lambda}{\beta_\lambda} (1 - e^{-\beta_\lambda L}) \qquad \text{(VII-2)}$$

The total path length L and the solid angle Ω depend on the flame geometry. Figure VII-1 shows the details of the system geometry, in which the angle ϕ lines in the horizontal plane and the angle γ lies in the vertical plane. The differential solid angle $d\Omega$ is expressed as

$$d\Omega = \frac{dA_f}{L^2} = \frac{[L \sin (\pi/2-\gamma)\ d\phi][Ld (\pi/2-\gamma)]}{L^2}$$

which reduces to

$$d\Omega = - \cos \gamma\ d\phi\ d\gamma \qquad \text{(VII-3)}$$

From Figure III-1, it can be shown that

$$\cos \theta = - \cos \phi \cos \gamma \qquad \text{(VII-4)}$$

Substituting Equations VII-2, VII-3, and VII-4 into Equation VII-1, the following is obtained

$$q_r = \int_{\lambda_1}^{\lambda_2} \int_{\gamma_a}^{\gamma_b} \int_{-\pi/2}^{\pi/2} \frac{J_\lambda}{\beta_\lambda} (1 - e^{-\beta_\lambda L}) \cos^2\gamma \cos \phi\ d\phi\ d\gamma\ d\lambda \qquad \text{(VII-5)}$$

Before an expression for the path length L through the flame can be developed, the flame shape must be known. It was shown in Chapter VI that a single geometric shape for a flame does not exist. The visible flame shape is representable by a geometric shape varying from a cone to a cylinder. Since one cannot accurately predict the exact flame shape,

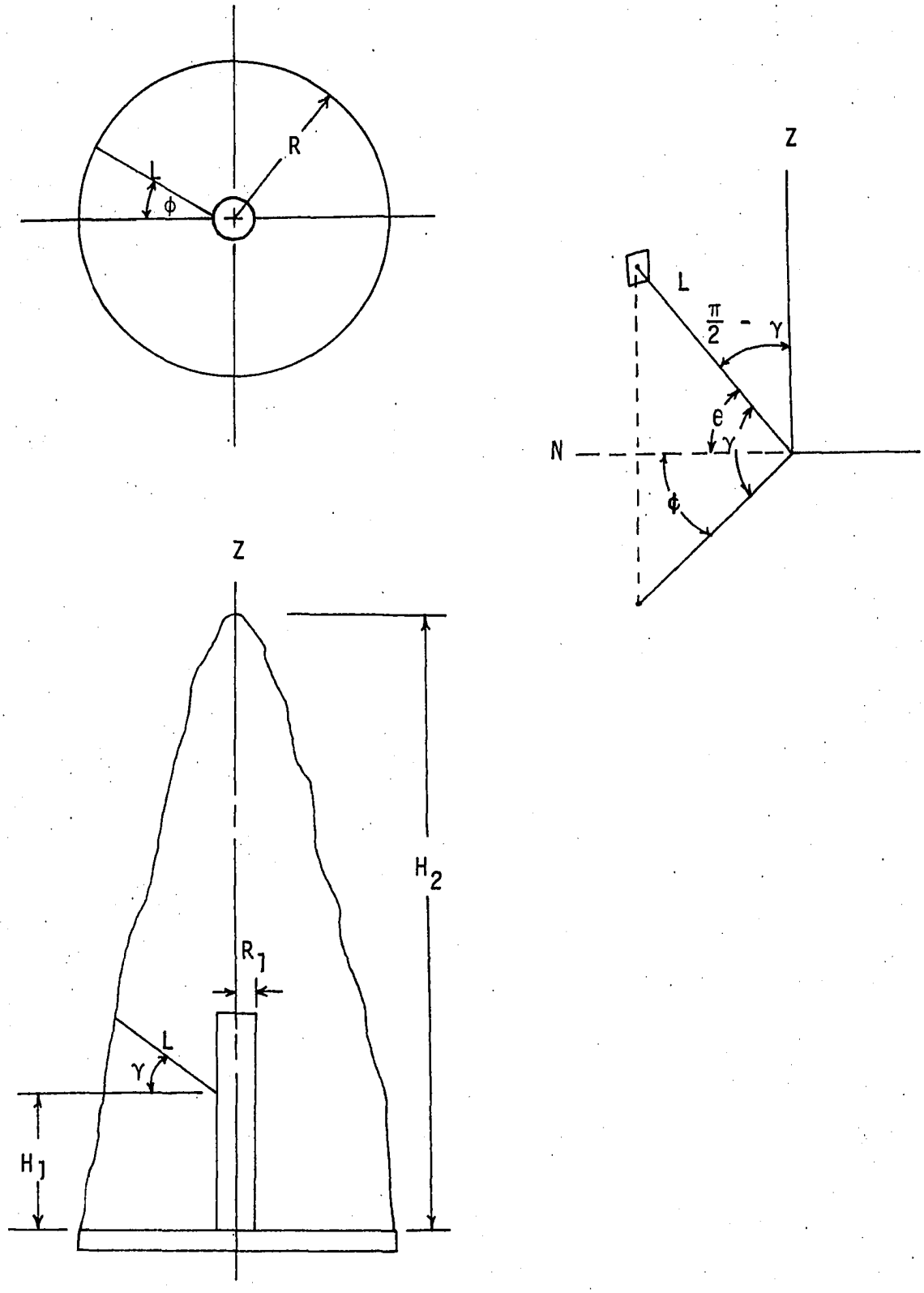


Figure VII-1. System Geometry for Cylindrical Target Surrounded by a Flame of Circular Cross-Section.

the path length expression will be developed for a cone and a cylinder.

Cylindrical Shaped Flame

For a flame with a circular cross section, the path length L to the vertical sides of the flame is given by

$$L = \left(-R_1 \cos\phi + \sqrt{R_2^2 - R_1^2 \sin^2\phi}\right)/\cos\gamma \qquad \text{(VII-6)}$$

where R_1 = radius of probe, in

R_2 = radius of flame at burner, in

ϕ = horizontal direction angle, radians

γ = vertical direction angle, radians

Substituting this expression into Equation VII-5 results in the the heat flux from the sides $(q_r)_s$ which is

$$(q_r)_s = 2 \int_{\lambda_1}^{\lambda_2} \int_{\gamma_a}^{\gamma_b} \int_0^{\pi/2} \frac{J_\lambda}{\beta_\lambda} \cdot \left[1 - e^{-\beta_\lambda \left(-R_1 \cos\phi + \sqrt{R_2^2 - R_1^2 \sin^2\phi}\right)/\cos\gamma}\right] \cdot \cos^2\gamma \cos\phi \, d\phi \, d\gamma \, d\lambda \qquad \text{(VII-7)}$$

For this case the limits on the angle are

$$\gamma_a = -\tan^{-1}\left(\frac{H_1}{R_2 - R_1}\right); \quad \gamma_b = \tan^{-1}\left(\frac{H_2 - H_1}{R_2 - R_1}\right) \qquad \text{(VII-8)}$$

where H_2 = height of flame above burner, in

H_1 = height of target above burner, in

A closed form solution of Equation III-7 is not apparent for the integrations over the flame geometry, and no functional relationship exists for the terms involving wavelength. Therefore, one must turn to numerical techniques obtain a solution. For the geometrical integrations, Simpson's rule could be applied, but Neill (50) found that a four-point Gauss Quadrature gave sufficient accuracy with the minimum amount of computation. Existing emission and extinction coefficient data are available only at randomly spaced wavelengths, so a trapezoidal rule will be used for the integration over wavelength. The accuracy of this technique is more than offset by the inaccuracy of the data.

The Gaussian integration of moments formula is

$$\int_0^1 f(x)\,dx = \sum_{i=0}^{i=n_2} w_i f(X_i) \qquad \text{(VII-9)}$$

where $f(x)$ = function to be integrated

w_i = weight factor for Gaussian integration of moments

x_i = abscissa for Gaussian integration of moments

$f(x_i)$ = function $f(x)$ evaluated as x_i

When the limits of integration are different from these specified in Equation VII-9, then the formula for the Gaussian integration of moments becomes

$$\int_a^b f(x)\,dx = (b-a)\sum_{i=0}^{i=n_2} w_i\, f(u_i) \qquad \text{(VII-10)}$$

where $f(u_i)$ = function $f(x)$ evaluated at u_i, given by

$$u_i = (b-a)\,x_i + a \qquad \text{(VII-11)}$$

Values of x_i and w_i can be found in Abramowitz and Stegun (1).

Applying a closed form integration and these numerical techniques to Equation VII-7, results in the following

$$(q_r)_s = \pi \sum_{j=1}^{m-1} \left[\left(\frac{J}{\beta}\right)_{j+1} + \left(\frac{J}{\beta}\right)_j\right]\left[\frac{\lambda_{j+1} - \lambda_j}{2}\right]$$

$$\cdot\Bigg[1/2 \sum_{i=1}^{4} w_i \left(\gamma_b - \gamma_a + \frac{\sin 2\gamma_b}{2} - \frac{\sin 2\gamma_a}{2}\right)\cos\phi_i$$

$$- \sum_{i=1}^{4} (\gamma_b - \gamma_a)\, w_i \cos\phi_i \sum_{k=1}^{4} w_k \cos^2\gamma_b$$

$$\cdot\, e^{-\beta_j(-R_1\cos\phi_i + \sqrt{R_2^2 - R_1^2\sin^2\phi_i})/\cos\gamma_k}\Bigg] \qquad \text{(VII-12)}$$

where $\phi_i = \frac{\pi}{2}(x_i)$ (VII-13)

$$\gamma_k = (\gamma_b - \gamma_a)\,x_k + \gamma_a \qquad \text{(VII-14)}$$

The path length from the target to any point along the bottom of a cylindrical flame is given by

$$L = H_i/\sin\gamma \qquad \text{(VII-15)}$$

Substituting this expression into Equation VII-7, the following equation is obtained

$$(q_r)_b = 2 \int_{\lambda_1}^{\lambda_2} \int_{0}^{\pi/2} \int_{-\pi/2}^{\gamma_a} \frac{J_\lambda}{\beta_\lambda} (1 - e^{-\beta_\lambda H_1/\sin \gamma}) \cdot \cos^2\gamma \cos \phi \, d\gamma \, d\phi \, d\lambda \qquad \text{(VII-16)}$$

Using closed form and numerical integration, this equation becomes

$$(q_r)_b = \pi \sum_{j=1}^{m-1} \left[\left(\frac{J}{\beta}\right)_{j+1} + \left(\frac{J}{\beta}\right)_j \right] \frac{(\lambda_{j+1} - \lambda_j)}{2} \cdot \left[1/2 \sum_{i=1}^{4} w_i \left(\gamma_a + \frac{\sin 2\gamma_a}{2} + \frac{\pi}{2}\right) \cos \phi_i - \sum_{i=1}^{4} w_i \cos \phi_i \left(\gamma_a + \frac{\pi}{2}\right) - \sum_{k=1}^{4} w_k \cos^2\gamma_k e^{-\beta_j H_1/\sin \gamma_k} \right] \qquad \text{(VII-17)}$$

where $\phi_i = \frac{\pi}{2} (x_i)$ (VII-18)

$$\gamma_k = (\gamma_a + \pi/2) \, x_k - \pi/2 \qquad \text{(VII-19)}$$

The path length from the target to any point along the top of a cylindrical flame is given by

$$L = (H_2 - H_1)/\sin \gamma \qquad \text{(VII-20)}$$

Substituting this expression into Equation VII-7, the following equation is obtained:

$$(q_r)_t = 2 \int_{\lambda_1}^{\lambda_2} \int_{0}^{\pi/2} \int_{\gamma_b}^{\pi/2} \frac{J_\lambda}{\beta_\lambda} \left[1 - e^{-\beta_\lambda (H_2 - H_i)/\sin \gamma}\right] \cdot \cos^2\gamma \cos \phi \, d\gamma \, d\phi \, d\lambda \qquad \text{(VII-21)}$$

Using the closed form and numerical integration, this equation becomes

$$(q_r)_t = \pi \sum_{j=1}^{m-1} \left[\left(\frac{J}{\beta}\right)_{j+1} + \left(\frac{J}{\beta}\right)_j\right] \frac{(\lambda_{j+1} + \lambda_j)}{2} \cdot \left\{1/2 \sum_{i=1}^{4} w_1 \left(\pi/2 - \gamma_b - \frac{\sin 2\gamma_b}{2} \cos \phi_i\right) - \sum_{i=1}^{4} w_i \cos \phi_i \left(\pi/2 - \gamma_b\right) - \sum_{k=1}^{4} w_k \cos^2\gamma_k \, e^{-\beta_j (H_2 - H_1)/\sin \gamma_b}\right\} \qquad \text{(VII-22)}$$

where $\phi_i = \pi/2 \ (x_i)$ (VII-23)

$$\gamma_k = (\pi/2 - \gamma_b) \, x_k + \gamma_b \qquad \text{(VII-24)}$$

The total heat flux from a cylindrical flame to a target is given by

$$q_r = (q_r)_s + (q_r)_b + (q_r)_t \qquad \text{(VII-25)}$$

Conical Shaped Flame

For a conical shaped flame, the path length L to the sides of the flame is given by

$$L = \frac{[-R_1 \cos\phi + \sqrt{R_2^2(1 - H_1/H_2)^2 - R_1^2 \sin^2\phi}]\ \sin[\tan^{-1}(H_2/R_2)]}{\sin\ [\pi - \gamma - \tan^{-1}(H_2/R_2)]} \qquad \text{(VII-26)}$$

Substituting this expression into Equation VII-5, the following equation for the heat flux from the side of the flame is

$$(q_r)_s = 2 \int_{\lambda_1}^{\lambda_2} \int_{\gamma_a}^{\gamma_b} \int_{0}^{\pi/2} \frac{J_\lambda}{\beta_\lambda}$$

$$\cdot \left\{1 - e^{-\beta_\lambda \left[\frac{-R_1\cos\phi + \sqrt{R_2^2(1-H_1/H_2)^2 - R_1^2\sin^2\phi} \cdot \sin\ [\tan^{-1}(H_2/R_2)]}{\sin\ [\pi - \gamma - \tan^{-1}(H_2/R_2)]}\right]}\right\}$$

$$\cdot\ \cos^2\gamma \cos\phi\ d\phi\ d\gamma\ d\lambda \qquad \text{(VII-27)}$$

For this case γ_a is given by Equation VII-8.

Applying a closed form and numerical integration to Equation VII-27 results in

$$(q_r)_s = \pi \sum_{j=1}^{n-1} \left[\left(\frac{J}{\beta}\right)_{j+1} + \left(\frac{J}{\beta}\right)_j\right] \frac{(\lambda_{j+1} - \lambda_j)}{2}$$

$$\cdot \left\{1/2 \sum_{i=1}^{4} w_i (\gamma_b - \gamma_a + \frac{\sin 2\gamma_b}{2} - \frac{\sin 2\gamma_a}{2}) \cos\phi_i \right.$$

$$\left. - \sum_{i=1}^{4} (\gamma_b - \gamma_a)\ w_i \cos\phi_i \sum_{k=1}^{4} w_k \cos^2\gamma_k \right.$$

$$\left. \cdot\ e^{\left\{-\beta_j \left[\frac{-R_1\cos\phi_i + \sqrt{R_2^2(1-H_1/H_2)^2 - R_1^2\sin^2\phi_i}}{\sin[\pi - \gamma_k - \tan^{-1}(H_2/R_2)]}\right] \sin[\tan^{-1}(\frac{H_2}{r_2})]\right\}} \right\} \qquad \text{(VII-28)}$$

where $\phi_i = \pi/2 \ (x_i)$ (VII-29)

$$\gamma_k = (\pi/2 - \gamma_a) \ x_k + \gamma_a \quad \text{(VII-30)}$$

The heat flux from the bottom of the flame to the target is given by Equation VII-17. The total heat flux from a conical flame to a target inside the flame is given by

$$q_r = (q_r)_s + (q_r)_b \quad \text{(VII-31)}$$

Target External to a Flame

The geometry for the radiant heat transfer from a flame to an external target is shown in Figure VII-2.

The differential solid angle between the flame and target is expressed as

$$d\Omega = \frac{dA_f}{s^2} = \frac{s \ [\sin \ (\pi/2 - \gamma) \ d\phi] [sd \ (\pi/2 - \gamma)]}{s^2} \quad \text{(VII-32)}$$

which reduces to

$$d\Omega = - \cos \gamma \ d\phi \ d\gamma \quad \text{(VII-33)}$$

From Figure VII-2, it can be shown that

$$\cos \theta = - \cos \phi \ \cos \gamma \quad \text{(VII-34)}$$

Substituting Equations VII-33 and VII-34 into Equation VII-1, the following is obtained

$$q_r = 2 \int_{\lambda_1}^{\lambda_2} \int_{\gamma_a}^{\gamma_b} \int_{0}^{\phi_2} I_\lambda \cos^2 \gamma \cos \phi \ d\phi \ d\gamma \ d\lambda \quad \text{(VII-35)}$$

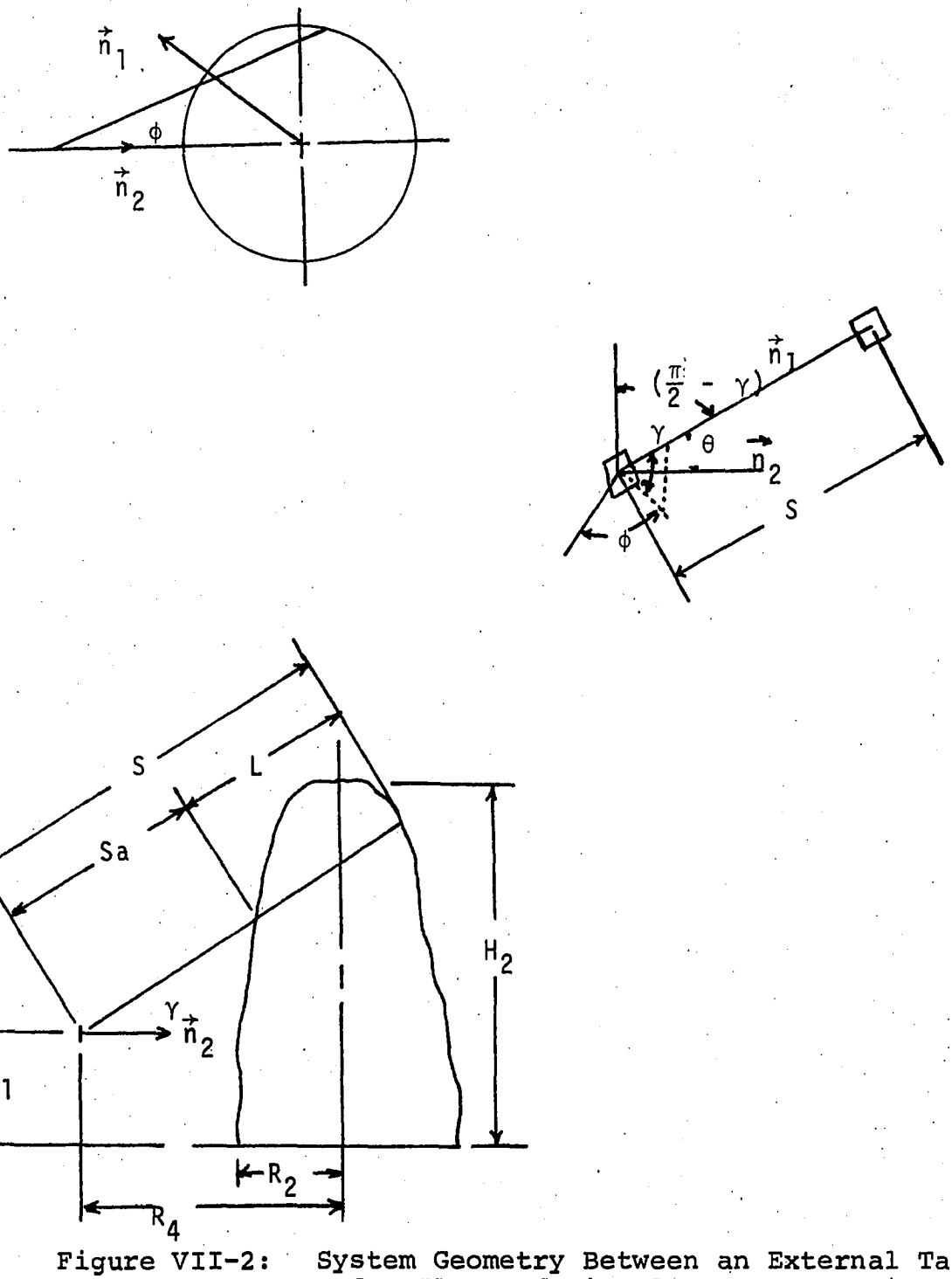


Figure VII-2: System Geometry Between an External Target and a Flame of Circular Cross-Section.

the intensity of the flame is given by Equation VII-2. This value must be reduced by the transmittance of the atmosphere which is

$$\tau_{a\lambda} = e^{-\kappa_{a\lambda} s_a} \qquad \text{(VII-36)}$$

where $\tau_{a\lambda}$ = atmospheric monochromatic transmittance

$\kappa_{a\lambda}$ = atmospheric monochromatic absorption coefficient, in^{-1}

s_a = path length through the atmosphere, in

Combining Equations VII-2, VII-35, and VII-36, results in the following

$$q_r = 2 \int_{\lambda_1}^{\lambda_2} \int_{\gamma_a}^{\gamma_b} \int_{0}^{\phi_2} \frac{J_\lambda}{\beta_\lambda} e^{-\kappa_{a\lambda} s_a (1-e^{-\beta\lambda L})} \cos^2\gamma \cos\phi \, d\phi \, d\gamma \, d\lambda \qquad \text{(VII-37)}$$

The path lengths s_a, and L depend on the flame shape and expressions for these lengths will be developed for circular and conical shaped flames.

Cylindrical Shaped Flame

The path length L between the vertical sides of a cylindrical flame is given by

$$L = [2 \sqrt{R_2^2 - R_4^2 \sin^2\phi}]/\cos\gamma \qquad \text{(VII-38)}$$

The path length s_a from the target to the near vertical side of the flame is

$$s_a = [R_4 \cos\phi - \sqrt{R_2^2 - R_4^2 \sin^2\phi}]/\cos\gamma \qquad \text{(VII-39)}$$

Substituting Equation VII-38 and VII-39 into Equation VII-37 results in

$$(q_r)_s = 2 \int_{\lambda_1}^{\lambda_2} \int_{\gamma_a}^{\gamma_b} \int_{0}^{\phi_2} \frac{J_\lambda}{\beta_\lambda} e^{-\kappa_a \lambda \left\{\frac{R_4\cos\phi - \sqrt{R_2^2 - R_4^2\sin^2\phi}}{\cos\gamma}\right\}} \cdot \left(1 - e^{-\beta_\lambda \left\{\frac{2\sqrt{R_2^2 - R_4^2 \sin^2\phi}}{\cos\gamma}\right\}}\right) \cos^2\gamma \cos\phi \, d\phi \, d\gamma \, d\lambda \qquad \text{(VII-40)}$$

where $$\phi_2 = \sin^{-1}(R_2/R_4) \qquad \text{(VII-41)}$$

$$\gamma_a = -\tan^{-1}[H_1/(R_4 + R_2)] \qquad \text{(VII-42)}$$

$$\gamma_b = \tan^{-1}[(H_2 - H_1)/(R_4 + R_2)] \qquad \text{(VII-42A)}$$

Numerically integrating Equation VII-40 results in

$$(q_r)_s = 2 \sum_{j=1}^{n-1} \left[\left(\frac{J}{\beta}\right)_{j+1} + \left(\frac{J}{\beta}\right)_j\right] \left\{\frac{\lambda_{j+1} - \lambda_j}{2}\right\} \cdot \left\{\phi_2 \sum_{i=1}^{4} (\gamma_b - \gamma_a) \, w_i \cos\phi_i \sum_{k=1}^{4} w_k \cos^2(\gamma_k) \cdot \left(e^{-(\kappa_a)_j [R_4 \cos\phi_i - \sqrt{R_2^2 - R_4^2 \sin^2\phi_i}]/\cos\gamma_k} \cdot \left(1 - e^{-\beta_j (2\sqrt{R_2^2 - R_4^2 \sin^2\phi_i})/\cos\gamma_k}\right)\right)\right\} \qquad \text{(VII-43)}$$

where $$\phi_i = \phi_2 \, x_i \qquad \text{(VII-44)}$$

$$\gamma_k = (\gamma_b - \gamma_a) \, x_k + \gamma_a \qquad \text{(VII-45)}$$

The path length L along the bottom of the flame is given by

$$L = \frac{-H_1}{\sin\gamma} - \left[\frac{R_4\cos\phi - \sqrt{R_2^2 - R_4^2\sin^2\phi}}{\cos\gamma}\right] \qquad \text{(VII-46)}$$

The path length from the target to the flame is expressed by Equation VII-39. Substituting Equation VII-39 and VII-46 into Equation VII-37 gives the following equation for the heat flux from the bottom of the flame to the target.

$$(q_r)_b = 2\int_{\lambda_1}^{\lambda_2}\int_{\gamma_c}^{\gamma_a}\int_0^{\phi_3}\left(\frac{J_\lambda}{\beta_\lambda}\right) e^{-\kappa_{a,\lambda}\left(\frac{R_a\cos\phi - \sqrt{R_2^2 - R_4^2\sin^2\phi}}{\cos\gamma}\right)} \cdot \left[1 - e^{-\beta_\lambda\left(\frac{H_1}{\sin\gamma} - \frac{R_4\cos\phi - \sqrt{R_2^2 - R_4^2\sin^2\phi}}{\cos\gamma}\right)}\right] \cdot \cos^2\gamma\cos\phi\, d\phi\, d\gamma\, d\lambda \qquad \text{(VII-47)}$$

where $\gamma_c = -\tan^{-1}[H_1/(R_4 - R_2)]$ (VII-48)

Numerical integration of Equation VII-47 results in

$$(q_r)_b = 2\sum_{j=1}^{n-1}\left[\left(\frac{J}{\beta}\right)_{j+1} + \left(\frac{J}{\beta}\right)_j\right]\frac{(\lambda_{j+1} - \lambda_j)}{2} \cdot \left\{\sum_{i=1}^{4}(\gamma_a - \gamma_c)\, w_i\cos\phi_i \sum_{k=1}^{4}\phi_3 w_k\cos^2\gamma_k \left[e^{-(\kappa_a)_j(R_4\cos\phi_i - \sqrt{R_2^2 - R_4^2\sin^2\phi_i})/\cos\gamma_k} \left(1 - e^{-\beta_j\left(\frac{H_1}{\sin\gamma_k} - \frac{R_4\cos\phi_i - \sqrt{R_2^2 - R_4^2\sin^2\phi_i}}{\cos\gamma_k}\right)}\right)\right]\right\} \qquad \text{(VII-49)}$$

$$\phi_3 = \tan^{-1}\sqrt{\left[\frac{2\,R_4\,(-H_1/\tan\gamma)}{(-H_1/\tan\gamma)^2 + R_4^2 - R_2^2}\right] - 1} \qquad \text{(VII-50)}$$

where $\phi_i = \phi_3\, x_i$

$$\gamma_k = (\gamma_a - \gamma_c)\, x_k + \gamma_c \qquad \text{(VII-51)}$$

The path length along the top of the flame cylinder is given by

$$L = \frac{(H_2 - H_1)}{\sin\gamma} - \frac{(R_4\cos\phi - \sqrt{R_2^2 - R_4^2\sin^2\phi})}{\cos\gamma} \qquad \text{(VII-52)}$$

The path length from the target to the flame is again given by Equation VII-39. The heat flux from the top of the flame to the target is obtained by substituting Equations VII-39 and VII-52 into Equation VII-37 and is

$$(q_r)_t = 2\int_{\lambda_1}^{\lambda_2}\int_{\gamma_b}^{\gamma_d}\int_{0}^{\phi_4}\left(\frac{J_\lambda}{\beta_\lambda}\right)\left[e^{-\kappa_{a,\lambda}(R_4\cos\phi - \sqrt{R_2^2 - R_4^2\sin^2\phi})/\cos\gamma}\right]$$

$$\cdot\left[1 - e^{-\beta_\lambda\left(\frac{H_2-H_1}{\sin} - \frac{R_4\cos\phi - \sqrt{R_2^2 - R_4^2\sin^2\phi}}{\cos\gamma}\right)}\right]$$

$$\cdot\cos^2\gamma\cos\phi\, d\phi\, d\gamma\, d\lambda \qquad \text{(VII-53)}$$

where $\gamma_d = \tan^{-1}\left[(H_2 - H_1)/(R_4 - R_2)\right]$ (VII-54)

Numerical integration of Equation VII-53 results in

$$(q_r)_t = 2\sum_{j=1}^{n-1}\left[\left(\frac{J}{\beta}\right)_{j+1} + \left(\frac{J}{\beta}\right)_j\right]\frac{(\lambda_{j+1} - \lambda_j)}{2}$$

$$\cdot\left\{\sum_{i=1}^{4}(\gamma_d - \gamma_b)\, w_i \cos\phi_i \sum_{k=1}^{4}\phi_4 w_k \cos^2\gamma_k\right.$$

$$\left[e^{-(\kappa_a)_j(R_4\cos\phi_i - \sqrt{R_2^2 - R_4^2\sin^2\phi_i})/\cos\gamma_k}\right.$$

$$\left.\left.\left(1 - e^{-\beta_j\left(\frac{H_2-H_1}{\sin\gamma} - \frac{R_4\cos\phi_i - R_2^2 - R_4^2\sin^2\phi_i}{\cos\gamma_k}\right)}\right)\right]\right\} \qquad \text{(VII-54A)}$$

$$\phi_4 = \tan^{-1}\sqrt{\left\{\frac{2R_4(H_2 - H_1)/\tan\gamma}{\left(\frac{H_2 - H_1}{\tan\gamma}\right)^2 + R_4^2 - R_2^2}\right\}^2 - 1} \qquad \text{(VII-55)}$$

where $\phi_i = \phi_4 x_i$ (VII-56)

$$\gamma_i = (\gamma_d - \gamma_b)\, x_k + \gamma_b \qquad \text{(VII-57)}$$

Conical Flame

The path length L between the sides of a conical flame is given by

$$L = \frac{\sin[\tan^{-1}(H_2/R_2)]\left[\sqrt{R_3^2 - R_4^2\sin^2\phi} + \sqrt{R_o^2 - R_4^2\sin^2\phi}\right]}{\sin\left[\pi - \gamma - \tan^{-1}(H_2/R_2)\right]} \qquad \text{(VII-58)}$$

where

$$R_3 = \frac{\left(\frac{H_2}{R_2}\right)(-H_2 + H_1 + R_4\tan\gamma\cos\phi) \pm \tan\gamma\sqrt{(-H_2 + H_1 + R_4\tan\gamma\cos\phi)^2 - R_4^2\sin^2\phi\left[\left(\frac{H_2}{R_2}\right)^2 - \tan^2\gamma\right]}}{(H_2/R_2)^2 - \tan^2\gamma} \qquad \text{(VII-59)}$$

and

$$R_0 = \frac{\frac{-H_2}{R_2}(-H_2+H_1+R_4 \tan\gamma \cos\phi) \pm \tan\gamma \sqrt{(-H_2+H_1+R_4\tan\gamma\cos\phi)^2 - R_4^2\sin^2\phi[(\frac{H_2}{R_2})^2-\tan^2\gamma]}}{(H_2/R_2)^2 - \tan^2\gamma} \quad \text{(VII-60)}$$

The plus (+) sign is used when γ is positive and the minus (-) sign is used when γ is negative.

The path length s_a from the target to the near side of the flame is

$$s_a = \frac{R_4 \cos\phi}{\cos\gamma} - \sqrt{\frac{R_3^2 - R_4^2 \sin^2\phi}{\cos\gamma}} \quad \text{(VII-61)}$$

Substituting Equations VII-58 and VII-61 into Equation VII-37, the heat flux from the side of a conical flame to an external target is expressed by the following equation

$$(q_r)_s = 2 \int_{\lambda_1}^{\lambda_2} \int_0^{\phi_5} \int_{\gamma_a}^{\gamma_b} \frac{J_\lambda}{\beta_\lambda} [e^{-\kappa_{a,\lambda}(R_4 \cos\phi - \sqrt{R_3^2-R_4^2\sin^2\phi})/\cos\gamma}] \cdot \left\{1 - e^{-\beta_\lambda \left[\frac{\sin[\tan^{-1} H_2/R_2]\sqrt{R_3^2-R_4^2\sin^2\phi+R_0^2-R_4^2\sin^2\phi}}{\sin[\pi - \gamma - \tan^{-1}(H_2/R_2)]}\right]}\right\} \cdot \cos^2\gamma \cos\phi \, d\phi \, d\gamma \, d\lambda \quad \text{(VII-62)}$$

where $\phi_5 = \sin^{-1} [R_2(H_2 - H_1 - R_4 \tan\gamma)/R_4]$ (VII-63)

$\gamma_a = - \tan^{-1} [H_1/(R_4 + R_2)]$ (VII-64)

$\gamma_b = \tan^{-1} [(H_2 - H_1)/(R_4 + R_2)]$ (VII-65)

Numerical integration of Equation VII-62 provides the following equation:

$$(q_r)_s = 2(\gamma_b - \gamma_a) \sum_{j=1}^{m-1} \left[\left(\frac{J}{\beta}\right)_{j+1} + \left(\frac{J}{\beta}\right)_j\right] \frac{(\lambda_{j+1} - \lambda_j)}{2}$$

$$\cdot \Bigg(\sum_{k=1}^{4} w_k \, (\cos^2 \gamma_k) \, \phi_5 \sum_{i=1}^{4} (w_i \cos \phi_i)$$

$$\cdot \left\{ e^{-(\kappa_a)_j (R_4 \cos \phi_i - \sqrt{R_3^2 - R_4^2 \sin^2 \phi_i})/\cos \gamma_k} \right\}$$

$$\cdot \left\{ 1 - e^{-\beta_j \left\{ \frac{\sin(\tan^{-1}[H_2/R_2]) \, (\sqrt{R_3^2 - R_4^2 \sin^2 \phi_i} + \sqrt{R_0^2 - R_4^2 \sin^2 \phi_i}}{\sin\{\pi - \gamma - \tan^{-1}(H_2/R_2)\}} \right\}} \right\} \Bigg) \quad \text{(VII-66)}$$

where $\phi_i = \phi_5 \, x_i$

$$\gamma_k = (\gamma_b - \gamma_a) \, x_i + \gamma_a \quad \text{(VII-67)}$$

The path length from the side nearest the target to the bottom of the flame is given by

$$L = \frac{H_1}{\sin \gamma} - \frac{R_4 \cos \phi + \sqrt{R_3^2 - R_4^2 \sin^2 \phi}}{\cos \gamma} \quad \text{(VII-68)}$$

The path length s_a from the target to the near side of the flame can be obtained from Equation VII-61. Substituting Equations VII-68 and VII-61 into Equation VII-37, the following equation for the heat flux from the bottom of the flame to an external target is obtained.

$$(q_r)_b = 2 \int_{\lambda_1}^{\lambda_2} \int_{0}^{\phi_3} \int_{\gamma_c}^{\gamma_a} \frac{J_\lambda}{\beta_\lambda} \left[e^{-\kappa_{a,\lambda} (R_4 \cos\phi - \sqrt{R_3^2 R_4^2 \sin^2\phi})/\cos\gamma} \right]$$

$$\cdot \left[1 - e^{-\beta_\lambda \left(\frac{H_1}{\sin\gamma} - \frac{R_4 \cos\phi + \sqrt{R_3^2 - R_4^2 \sin^2\phi}}{\cos\gamma} \right)} \right]$$

$$\cdot \cos^2\gamma \cos\phi \, d\gamma \, d\phi \, d\lambda \qquad \text{(VII-69)}$$

where $\gamma_c = - \tan^{-1} [H_1/(R_4 - R_2)]$ (VII-70)

Numerically integrating Equation VII-69, the following equation is obtained:

$$(q_r)_b = 2(\gamma_a - \gamma_c) \sum_{j=1}^{m-1} \left[\left(\frac{J}{\beta}\right)_{j+1} + \left(\frac{J}{\beta}\right)_j \right] \frac{(\lambda_{j+1} - \lambda_j)}{2}$$

$$\cdot \left\{ \sum_{k=1}^{4} (w_k \cos^2\gamma_k) \; \phi_3 \sum_{i=1}^{4} (w_i \cos\phi_i) \right.$$

$$\cdot \left[e^{-(\kappa_a)_j [R_4 \cos\phi_i - \sqrt{R_3^2 - R_4^2 \sin^2\phi_i}]/\cos\gamma_k} \right]$$

$$\left. \cdot \left(1 - e^{-\beta_\lambda \left(\frac{H_1}{\sin\gamma_k} - \frac{R_4 \cos\phi_i + \sqrt{R_3^2 - R_4^2 \sin^2\phi_i}}{\cos\gamma_k} \right)} \right) \right\} \qquad \text{(VII-71)}$$

where $\phi_i = \phi_3 \, x_i$ (VII-72)

$\gamma_k = (\gamma_a - \gamma_c) \, x_k + \gamma_c$ (VII-73)

CHAPTER VIII

HEAT TRANSFER RESULTS

Determination of Flame Emission and Extinction Coefficients from Narrow Angle Radiometer Data

The mean and maximum radiant fluxes as measured by the narrow angle radiometer are shown as a function of path length through the flame in Figures VIII-1 through VIII-6. The path length is the visible flame width at the centerline of the radiometer obtained from the time-averaged flame photographs taken by Camera No. 2. The path length for the methanol flame is hard to define due to its faint glow, therefore, the data were not usable.

A nonlinear curve-fit program was used with this data to obtain values of q_∞ and β from Equation III-25. From q_∞, the value of J was calculated. These results are given in Table VIII-1.

This technique is very sensitive to the input data supplied, so a large number of data points should be used. There is no assurance that the values of J and β obtained by this method are true values. They may be the best coefficient to represent the data over the range of input values. Comparing these values of q_∞ and β with those given by Neill (50)

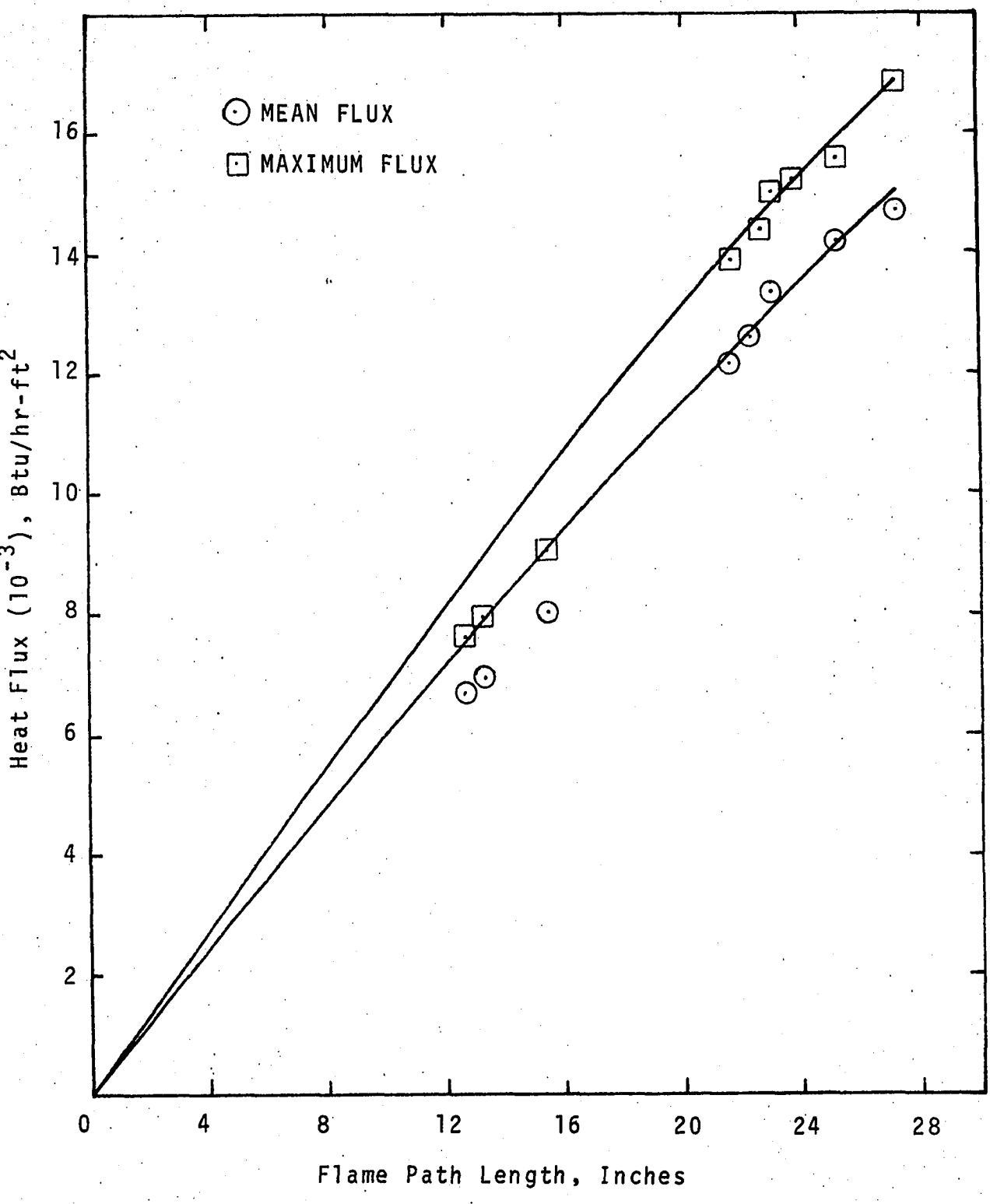


Figure VIII-1. Radiometer 72804 Heat Flux versus Flame Flame Path Length for Acetone.

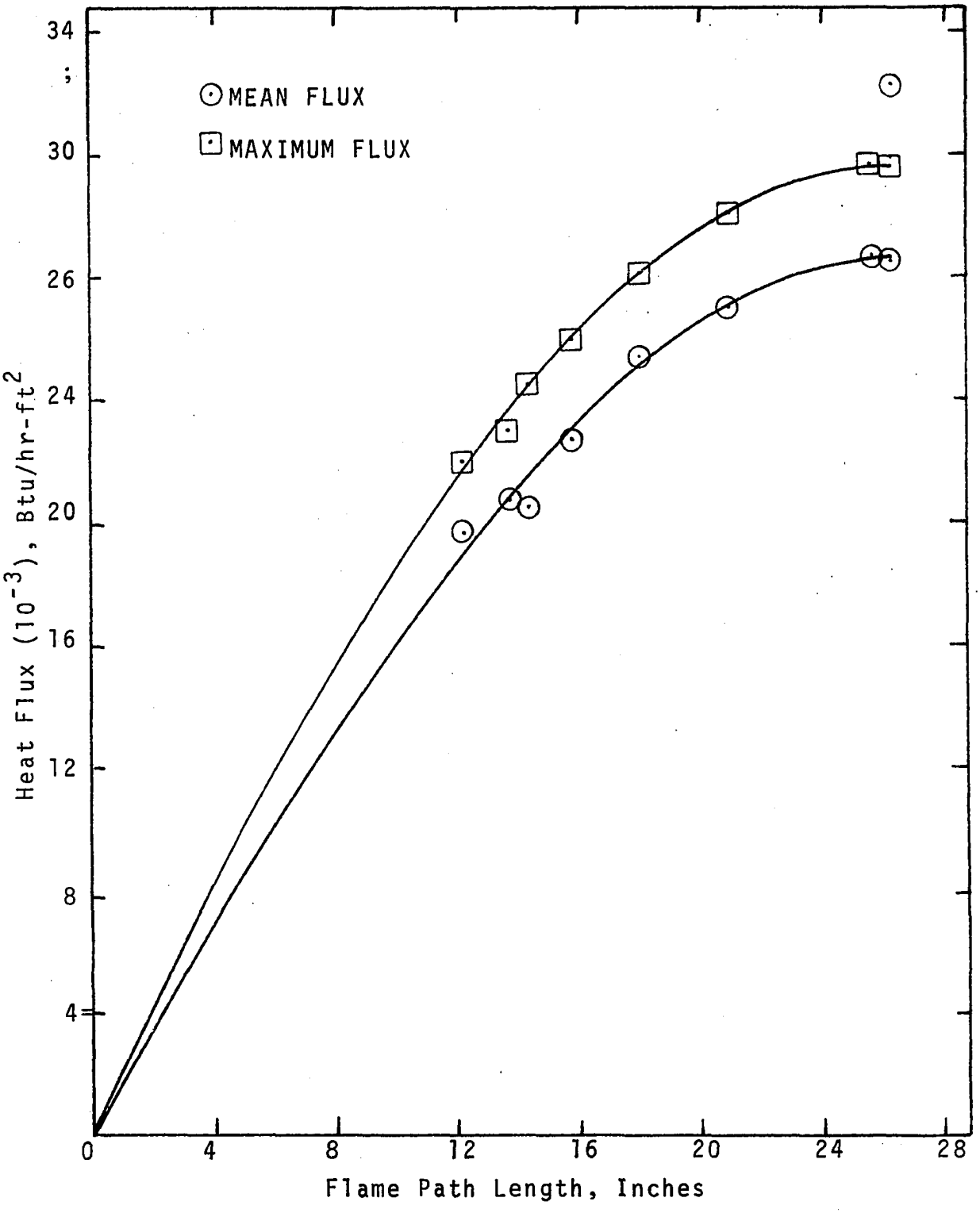


Figure VIII-2. Radiometer 72804 Heat Flux versus Flame Path Length for Benzene.

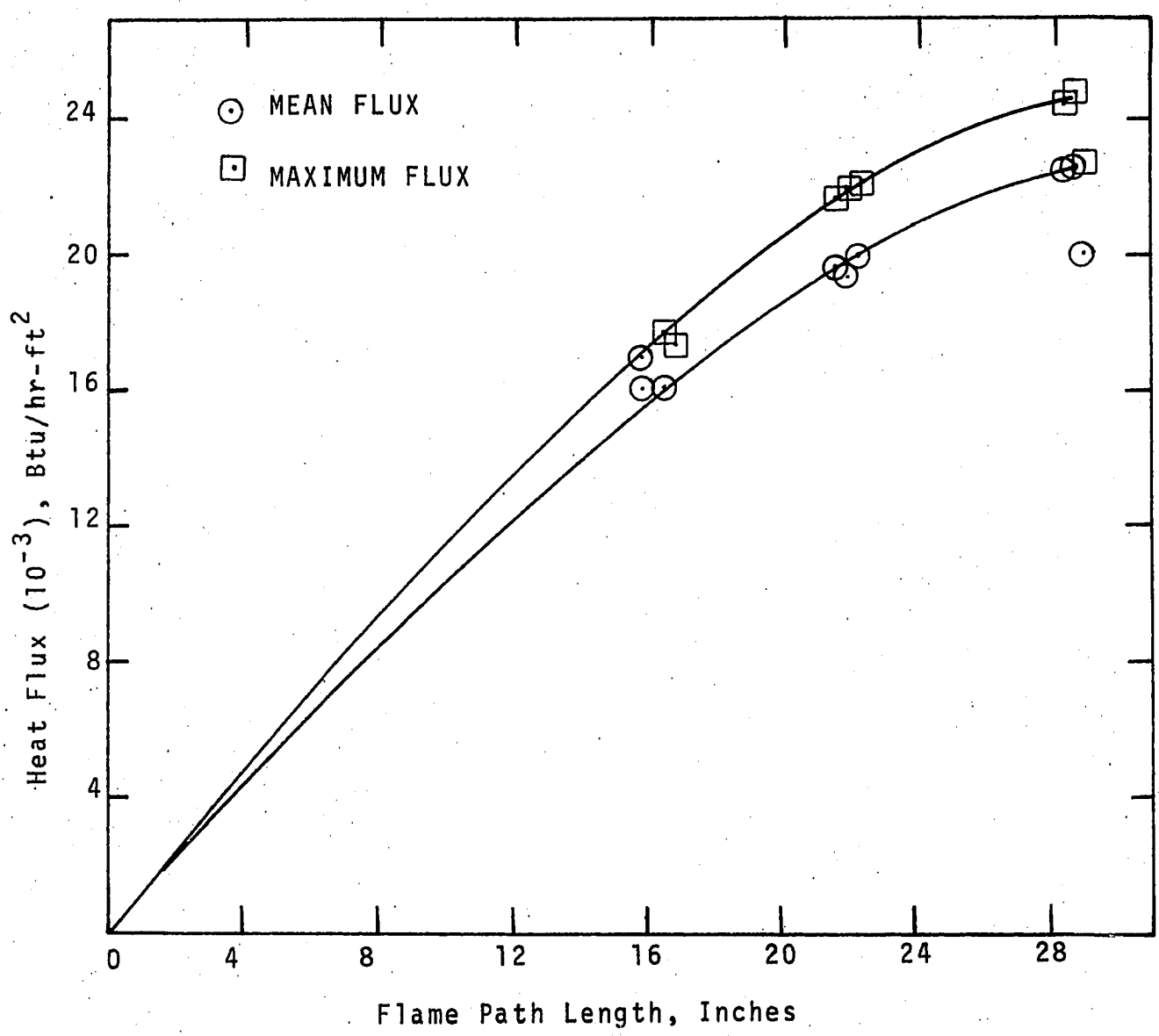


Figure VIII-3. Radiometer 72804 Heat Flux versus Flame Path Length for Cyclohexane.

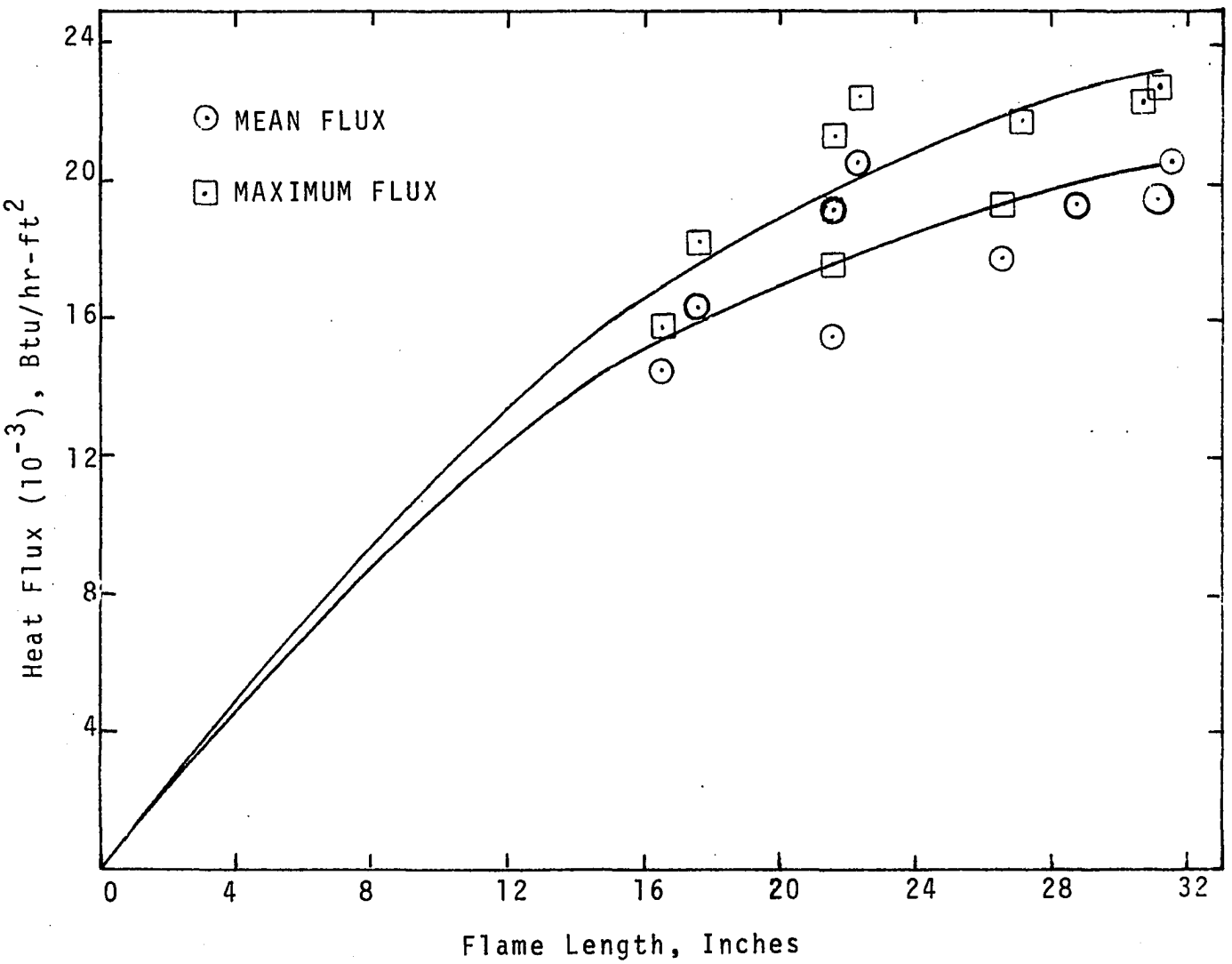


Figure VIII-4. Radiometer 72804 Heat Flux versus Flame Path Length for n-Hexane.

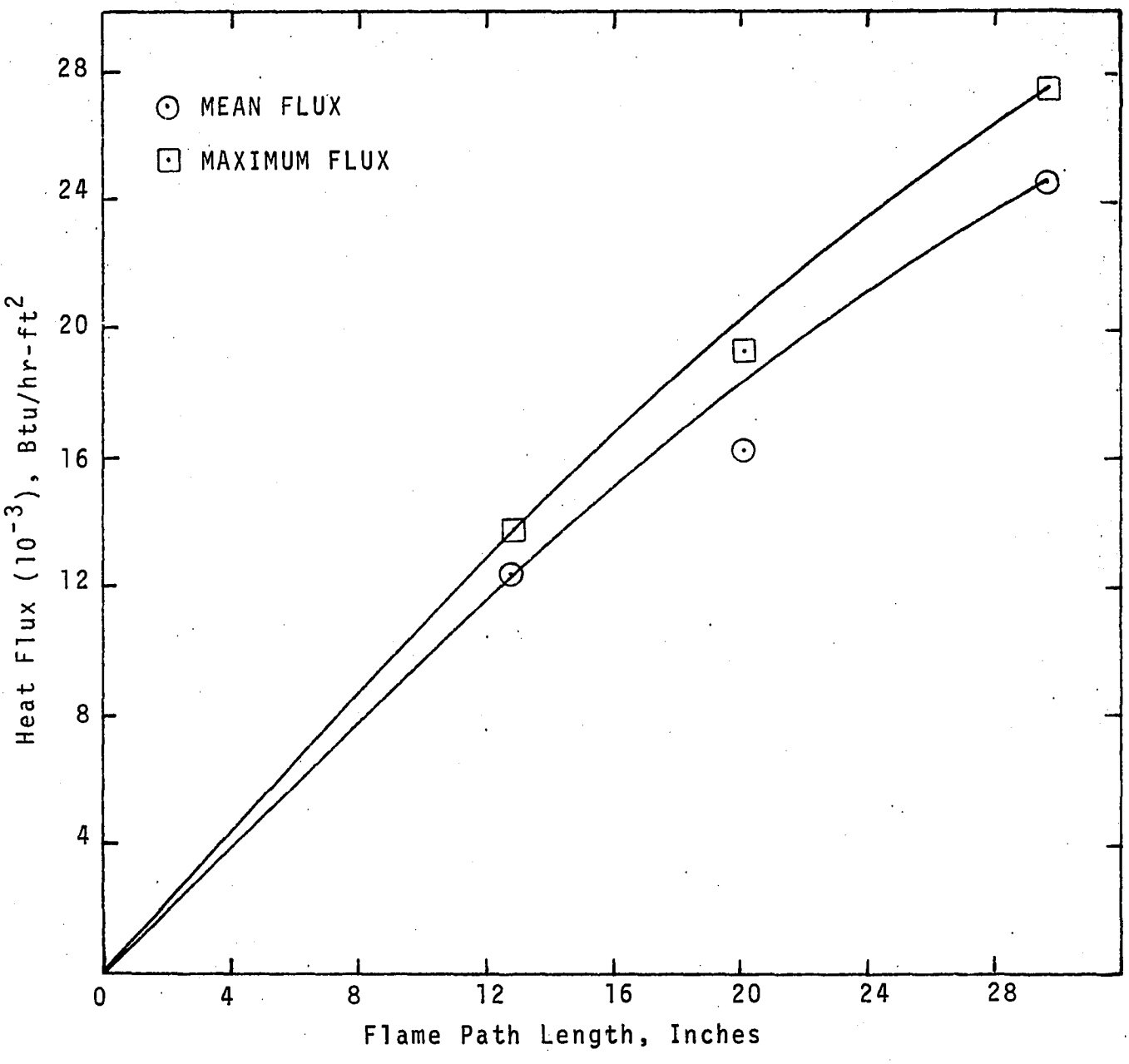


Figure VIII-5. Radiometer 72804 Heat Flux versus Flame Path Length for Jet-A.

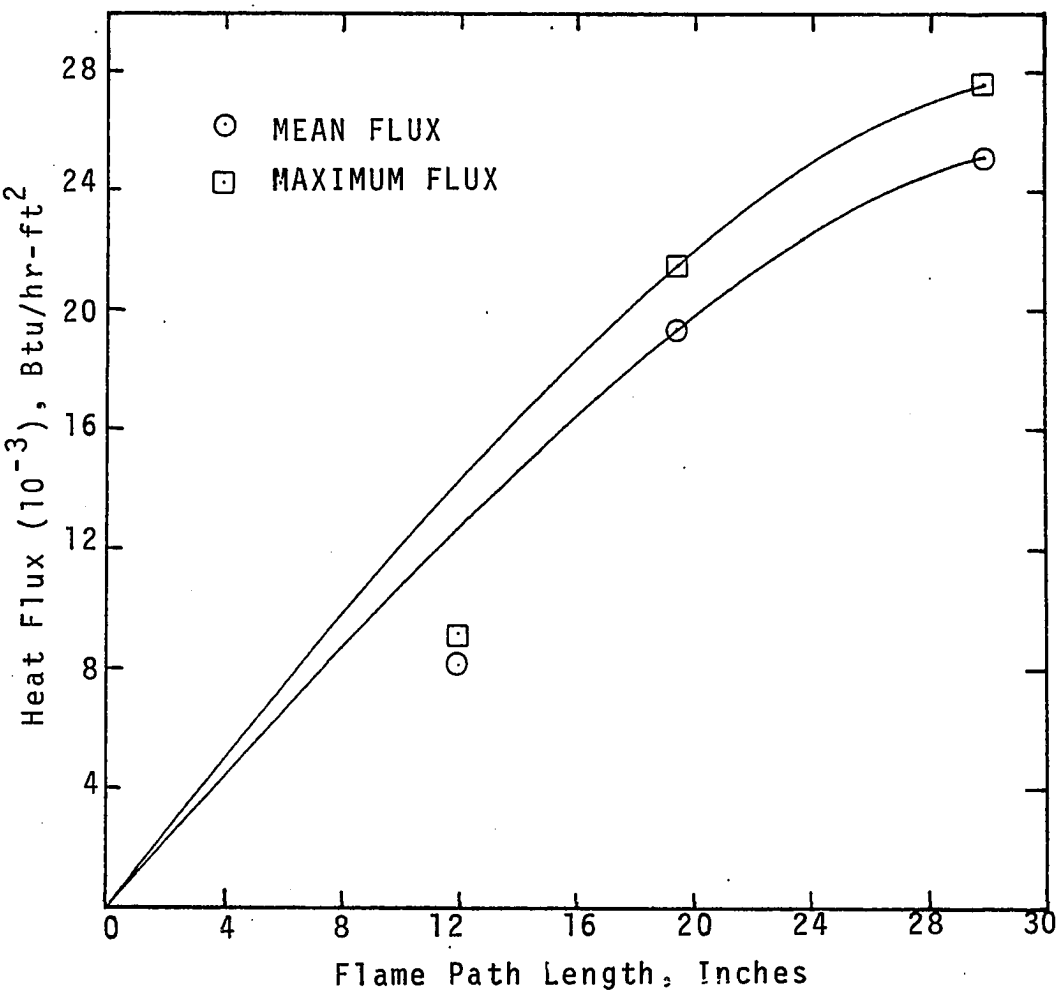


Figure VIII-6. Radiometer 72804 Heat Flux versus Flame Path Length for JP-4.

TABLE VIII-1

EMISSION AND EXTINCTION COEFFICIENTS OBTAINED FROM RADIOMETER 72804 DATA

Fuel	Maximum Flux Data			Mean Flux Data		
	q_∞ $\frac{Btu}{hr\text{-}ft^2}$	J $\frac{Btu}{hr\text{-}ft^3}$	β in^{-1}	q_∞ $\frac{Btu}{hr\text{-}ft^2}$	J $\frac{Btu}{hr\text{-}ft^3}$	β in^{-1}
Acetone	48172	2926.	0.0159	39141	2646.	0.0177
Benzene	38049	10392.	0.0715	34750	9106.	0.0686
Cyclohexane	37917	5504.	0.0380	31902	5313.	0.0436
n-Hexane	28042	6159.	0.0575	23562	5985.	0.0665
JP-4	39154	6132.	0.0410	36827	5416.	0.0385
Jet-A	66125	4509.	0.01785	57051	4162.	0.0191

shows that the cyclohexane and n-hexane coefficients are in reasonable agreement, but the values for acetone and JP-4 are not. For benzene, the q_∞ values are almost identical, but the values of β differ by a factor of 1.8. These differences may be due to the differences in the type of flames or to the sensitivity of the calculation procedure.

Radiant Flux Calculations Using Radiometer 72804 Data

The emission and extinction coefficients listed in Table VIII-1 along with Neill's (50) methanol values were used in the calculation of the radiant heat flux to a target inside and outside of a flame. In Chapter VIII, equations were developed for the radiative flux inside and outside both cylindrical and conical shaped flames. Four computer programs were developed in basic language to handle the computations. These programs are listed in Appendix E. Program CYLIF solves Equation VII-12, 17 and 22 for the radiative flux to a target

inside a cylindrical flame. Program CONIF solves Equations VII-17 and VII-28 for the radiative flux to a target inside a conical shaped flame. Program CYLOF solves Equations VIII-43, 49 and 55 for the radiative flux to a target external to a cylindrically shaped flame. Program CONOF solves Equations VIII-66 and 71 for the radiative flux to a target external to a conical shaped flame. Tables VIII-2 to VIII-8 show the results obtained from these calculations for the 7 fuels used in this study. Since the pulsating flames produced a pulsating radiative flux measurement, these tables include calculations for both maximum and mean fluxes. One should use the mean values for further computations.

The radiative heat flux to the target located inside the flame varies little with the flame shape. From Tables VIII-2 through VIII-8, it can be seen that the calculated radiative flux increases approximately 10 percent from a conical-shaped flame to a cylindrical shaped flame for all fuels and burners. The calculated radiative flux to a radiometer external to the flame varies considerably with flame shape, and also with flame size. For all flames except those of Jet-A and methanol the calculated radiative flux for a cylindrically shaped flame is approximately 25-35, 35-50, 50-90 percent higher than a conical shaped flame for burner sizes of 24, 18 and 12 inch respectively. The calculated radiative flux from a cylindrical shaped Jet-A flame is approximately 65 percent higher than that of a conical shaped flame for all burner sizes. The calculated radiative flux from a cylindrical shaped methanol flames varies from 120 to 180

TABLE VIII-2

RADIANT HEAT FLUXES FOR ACETONE CALCULATED WITH RADIOMETER 72804

EMISSION AND EXTINCTION COEFFICIENTS

Run Number	Height Above Pan in	Conical Shaped - Flame				Cylindrical Shaped - Flame				Radiometer 81510	
		q_r, Btu/hr-ft^2		q_m, Btu/hr-ft^2		q_r, Btu/hr-ft^2		q_m, Btu/hr-ft^2		q_m, Btu/hr-ft^2	
		Maximum	Mean	Maximum	Mean	Maximum	Mean	Maximum	Mean	Maximum	Mean
090171-24-1-1	3.6875	7462	6683			8028	7178				
	9.6875	8265	7399	8798	7836	9259	8273	11132	10409	8344	6515
090171-24-1-2	3.6875	7223	6472			8022	7174				
	9.6875	7817	7003	7560	6743	9252	8268	11611	10304	13023	9882
090171-24-1-3	3.6875	7404	6632			8026	7177				
	9.6875	8158	7305	8492	7566	9258	8273	11706	10386	7105	5591
081271-18-1-1	3.6875	5911	5307			6492	5821				
	9.6875	6179	5547	4537	4059	7316	6555	7000	6237	4637	3719
081271-18-1-2	3.6875	5919	5315			6492	5821				
	9.6875	6196	5562	4568	4086	7316	6557	7003	6240	4411	3528
081271-18-1-3	3.6875	5911	5307			6492	5821				
	9.6875	6179	5547	4537	4059	7316	6555	7000	6237	4697	3725
070771-12-1-1	3.6875	3919	3530			4379	3940				
	9.6875	3676	3310	1603	1440	4721	4245	2924	2620	2611	1979
070771-12-1-2	3.6875	4001	3602			4482	4031				
	9.6875	3754	3379	1660	1492	4844	4354	3062	2742	3195	2408
070871-12-1-1	3.6875	4001	3602			4482	4031				
	9.6875	3754	3379	1660	1492	4844	4354	3062	2742	3206	2825

TABLE VIII-3

RADIANT HEAT FLUXES FOR BENZENE CALCULATED WITH RADIOMETER 72804

EMISSION AND EXTINCTION COEFFICIENTS

Run Number	Height Above Pan in	Conical Shaped - Flame				Cylindrical Shaped - Flame				Radiometer 81510	
		q_r, Btu/hr-ft^2		q_m, Btu/hr-ft^2		q_r, Btu/hr-ft^2		q_m, Btu/hr-ft^2		q_m, Btu/hr-ft^2	
		Maximum	Mean	Maximum	Mean	Maximum	Mean	Maximum	Mean	Maximum	Mean
090171-24-2-1	3.6875	20265	17813			21389	19052				
	9.6875	21852	19181	18891	16879	24215	21597	26681	23947	18919	14972
090171-24-2-2	3.6875	19695	17360			20702	18424				
	9.6875	21224	18694	18532	16555	23334	20793	25103	22516	16700	13542
090171-24-2-3	3.6875	19695	17360			20702	18424				
	9.6875	21224	18694	16119	14382	23334	20793	24841	22278	16570	13226
081171-18-2-1	3.6875	17223	15174			18194	16149				
	9.6875	17987	15837	12373	11018	20145	17900	17302	15466	10299	8559
081171-18-2-2	3.6875	18039	15912			18967	16848				
	9.6875	19114	16851	14397	12835	21121	18783	19442	17396	13184	10925
081171-18-2-3	3.6875	18451	16198			19631	17450				
	9.6875	19361	16970	14362	12802	21966	19549	21326	19097	15300	12469
070671-12-2-1	3.6875	15272	13385			16499	14622				
	9.6875	15088	13619	8027	7128	18028	15991	13281	11844	8940	6878
070671-12-2-2	3.6875	15178	13375			16044	14213				
	9.6875	15462	13619	8890	7899	17466	15486	12509	11153	9262	7146
070671-12-2-3	3.6875	13463	11818			14556	12879				
	9.6875	12968	11370	5950	5274	15656	13862	9850	8765	6109	4977

TABLE VIII-4

RADIANT HEAT FLUXES FOR CYCLOHEXANE CALCULATED WITH RADIOMETER 72804

EMISSION AND EXTINCTION COEFFICIENTS

Run Number	Height Above Pan in	Conical Shaped - Flame				Cylindrical Shaped - Flame				Radiometer 81510	
		q_r, Btu/hr-ft^2		q_m, Btu/hr-ft^2		q_r, Btu/hr-ft^2		q_m, Btu/hr-ft^2		q_m, Btu/hr-ft^2	
		Maximum	Mean	Maximum	Mean	Maximum	Mean	Maximum	Mean	Maximum	Mean
083071-24-3-1	3.6875	12944	12051			13619	12699				
	9.6875	14364	13346	15235	14036	15627	14535	19300	17631	13172	10520
083071-24-3-2	3.6875	12115	11166			13247	12370				
	9.6875	12833	11793	10730	9967	15149	14112	17617	16138	16480	12683
083071-24-3-3	3.6875	12696	11827			13389	12494				
	9.6875	14023	13036	14342	13232	15333	14274	18437	16863	13721	11032
081071-18-3-1	3.6875	10515	9869			11131	10462				
	9.6875	11195	10490	8531	7948	12465	11691	11470	10599	7421	6062
081071-18-3-2	3.6875	10939	10258			11535	10829				
	9.6875	11770	11019	9589	8916	12975	12154	12549	11575	8899	7611
081071-18-3-3	3.6875	10086	9429			10964	10311				
	9.6875	10358	9666	6856	6412	12253	11500	10947	10129	10377	8678
070171-12-3-1	3.6875	8590	8109			9149	8649				
	9.6875	8754	8255	5057	4748	10001	9436	7222	6729	4589	3856
070171-12-3-2	3.6875	8670	8191			9149	8648				
	9.6875	8947	8442	5374	5041	10001	9436	7242	6746	4780	3964
070171-12-3-3	3.6875	8565	8083			9150	8649				
	9.6875	8694	8196	4962	4660	10001	9436	7216	6724	5025	4136

TABLE VIII-5

RADIANT HEAT FLUXES FOR n-HEXANE CALCULATED WITH RADIOMETER 72804

EMISSION AND EXTINCTION COEFFICIENTS

Run Number	Height Above Pan in	Conical Shaped - Flame				Cylindrical Shaped - Flame				Radiometer 81510	
		q_r, Btu/hr-ft^2		q_m, Btu/hr-ft^2		q_r, Btu/hr-ft^2		q_m, Btu/hr-ft^2		q_m, Btu/hr-ft^2	
		Maximum	Mean	Maximum	Mean	Maximum	Mean	Maximum	Mean	Maximum	Mean
083171-24-4-1	3.6875	12326	11345			13157	12175				
	9.6875	13176	12089	11146	10206	14908	13741	16334	14730	17565	13738
083171-24-4-2	3.6875	12563	11596			13244	12250				
	9.6875	13647	12559	12525	11428	15021	13837	16746	15088	16260	12803
083171-24-4-3	3.6875	13079	12082			13552	12514				
	9.6875	14503	13356	15030	13624	15415	14176	17977	16155	13172	10627
081071-18-4-1	3.6875	11556	10760			12018	11185				
	9.6875	12510	11619	10437	9563	13457	12480	12844	11666	8338	7057
081071-18-4-2	3.6875	11286	10523			11737	10939				
	9.6875	12166	11316	9780	8976	13102	12168	12059	10972	8869	7564
081171-18-4-1	3.6875	11556	10760			12018	11185				
	9.6875	12510	11619	10437	9563	13457	12480	12844	11666	8142	6950
070271-12-4-1	3.6875	9279	8730			9710	9131				
	9.6875	9609	9025	5790	5379	10574	9916	7514	6920	4983	3987
070271-12-4-2	3.6875	8884	8364			9382	8834				
	9.6875	9031	8492	5016	4674	10174	9555	6923	6388	5388	4208
070271-12-4-3	3.6875	9546	8966			10026	9416				
	9.6875	9891	9275	6107	5668	10963	10267	8101	7447	5525	4308

TABLE VIII-6

RADIANT HEAT FLUXES FOR JET A CALCULATED WITH RADIOMETER 72804

EMISSION AND EXTINCTION COEFFICIENTS

Run Number	Height Above Pan in	Conical Shaped - Flame				Cylindrical Shaped - Flame				Radiometer 81510	
		q_r, Btu/hr-ft^2		q_m, Btu/hr-ft^2		q_r, Btu/hr-ft^2		q_m, Btu/hr-ft^2		q_m, Btu/hr-ft^2	
		Maximum	Mean	Maximum	Mean	Maximum	Mean	Maximum	Mean	Maximum	Mean
083171-24-5-1	3.6875	11795	10686			12762	11656				
	9.6875	13017	11779	13834	12603	14768	13479	19557	17763		15455
041671-24-5-1	3.6875	11062	9956			12237	11180				
	9.6875	11849	10643	10692	9753	14098	12874	17454	15867		14185
041671-24-5-2	3.6875	12462	11172			13766	12562				
	9.6875	13669	12229	12255	11172	16040	14629	19430	17650		16152
041671-24-5-3	3.6875	11639	10448			12892	11772				
	9.6875	12576	11266	11868	10820	14929	13626	19368	17595		13721
080971-18-5-1	3.6875	9316	8447			10230	9360				
	9.6875	9698	8781	7036	6428	11558	10571	11352	10343		6616
042171-18-5-1	3.6875	953	8659			10399	9514				
	9.6875	10046	9110	7682	7017	11772	10765	11836	10781		10162
042171-18-5-2	3.6875	9598	8701			10521	9625				
	9.6875	10073	9119	7651	6988	11926	10905	12144	11061		9387
042171-18-5-3	3.6875	9069	8214			10017	9167				
	9.6875	9325	8432	6407	5856	11289	10327	10770	9816		8404
070971-12-5-1	3.6875	6494	5910			7241	6640				
	9.6875	6488	5567	2781	2548	7863	7207	5190	4744		2211
042771-12-5-1	3.6875	7744	7046			8507	7794				
	9.6875	7745	7040	4448	4070	9407	8615	7434	6786		6068
042771-12-5-2	3.6875	6858	6237			7641	7005				
	9.6875	6551	5950	3153	2887	8346	7647	5824	5322		5305
042771-12-5-3	3.6875	7787	7067			8644	7919				
	9.6875	7689	6969	4302	3937	9525	8768	7655	6987		6610
042871-12-5-1	3.6875	8149	7405			8967	8212				
	9.6875	8222	7463	4993	4567	9976	9132	8359	7627		6622
042871-12-5-2	3.6875	7908	7200			8647	7921				
	9.6825	7989	7266	4768	4362	9581	8772	7727	7052		4566

TABLE VIII-7

RADIANT HEAT FLUXES FOR JP-4 CALCULATED WITH RADIOMETER 72804

EMISSION AND EXTINCTION COEFFICIENTS

Run Number	Height Above Pan in	Conical Shaped - Flame				Cylindrical Shaped - Flame				Radiometer 81510	
		q_r, Btu/hr-ft^2		q_m, Btu/hr-ft^2		q_r, Btu/hr-ft^2		q_m, Btu/hr-ft^2		q_m, Btu/hr-ft^2	
		Maximum	Mean	Maximum	Mean	Maximum	Mean	Maximum	Mean	Maximum	Mean
083171-24-6-1	3.6875	14123	12574			14894	13361				
	6.6875	15606	13893	16144	14555	17068	15327	20844	18870		13589
041771-24-6-1	3.6875	13377	11827			14396	12904				
	6.6875	14393	12710	12791	11504	16430	14743	18881	17072		12105
041771-24-6-2	3.6875	14255	12664			15134	13580				
	6.6875	15700	13942	15514	13980	17374	15608	20857	18882		13560
041771-24-6-3	3.6875	13476	11949			14397	12905				
	6.6875	14619	12953	13494	12143	16432	14745	18949	17135		12815
081071-18-6-1	3.6875	11684	10387			12358	11048				
	6.6875	12451	11067	9558	8578	13842	12387	12820	11549		6175
042171-18-6-1	3.6875	12060	10709			12832	11478				
	6.6875	12858	11412	10154	9116	14441	12930	14065	12681		8642
042171-18-6-2	3.6875	12560	11169			13285	11891				
	6.6875	13563	12059	11577	10405	15016	13454	15402	13898		9268
042171-18-6-3	3.6875	11992	10633			12832	11478				
	6.6875	12702	11255	9774	8772	14441	12930	14038	12656		8511
062271-12-6-1	3.6875	8521	7533			9305	8291				
	6.6875	8209	7251	3862	3447	10067	8974	6551	5870		3463
042971-12-6-1	3.6875	9297	8227			10080	8988				
	6.6875	9210	8143	4879	4360	11007	9822	7847	7040		5644
042971-12-6-2	3.6875	9694	8577			10501	9367				
	6.6875	9695	8571	5407	4834	11523	10288	8615	7735		5710
042971-12-6-3	3.6875	9920	8792			10655	9506				
	6.6875	10076	8925	5941	5314	11714	10460	8938	8027		5972

TABLE VIII-8

RADIANT HEAT FLUXES FOR METHANOL CALCULATED WITH EMISSION

AND EXTINCTION COEFFICIENTS FROM NEILL (50)

Run Number	Height Above Pan in	Conical Shaped - Flame		Cylindrical Shaped - Flame		Radiometer 81510	
		q_r, Btu/hr-ft^2	q_m, Btu/hr-ft^2	q_r, Btu/hr-ft^2	q_m, Btu/hr-ft^2	q_m, Btu/hr-ft^2 Maximim	Mean
082771-24-7-1	3.6875	3310		3479			
	9.6875	3430	2372	3844	3645	5775	4494
083071-24-7-1	3.6875	3192		3455			
	9.6875	2966	1430	3791	3385	5448	4136
083071-24-7-2	3.6875	3205		3458			
	9.6875	3042	1535	3803	3423	5382	4113
083071-24-7-3	3.6875	3184		3453			
	9.6875	2914	1368	3780	3358	5621	4345
081271-18-7-1	3.6875	2723		3038			
	9.6875	2310	867	3274	2151	3534	2807
081271-18-7-2	3.6875	2797		3098			
	9.6875	2444	968	3351	2316	3821	3075
081271-18-7-3	3.6875	2778		3096			
	9.6875	2352	896	3341	2264	3183	2563
070871-12-7-1	3.6875	1969		2384			
	9.6875	1096	316	2468	934	1520	1192
070871-12-7-2	3.6875	2026		2387			
	9.6875	1370	380	2497	1052	1591	1228
070871-12-7-3	3.6875	2053		2388			
	9.6875	1486	418	2503	1103	1639	1246

percent of that of a conical shaped flame. These large differences in the methanol flames are probably due to the difficulty in measuring the flame size.

If one compares the calculated radiative flux to a radiometer external to the flame with the measured value, considerable variation occurs that cannot be attributed to flame shape and size alone. For acetone and JP-4 flames about half the measured values fall between the values calculated for a cylindrical and conical shaped flame while the other half have values less than those for a conical shaped flame. For benzene and Jet-A, the measured values are less than those calculated for a conical shaped flame. For cyclohexane, and n-hexane, the measured values are principally less than those calculated for a conical shaped flame. For methanol the measured values are greater than those calculated for a cylindrical shaped flame. These discrepancies can be attributed to using the emission and extinction coefficients from one region of the flame to represent the entire flame.

Heat Transfer Results Using Data from Radiometer 72804

Assuming that the calculated external radiative flux nearest the measured value is the most representative of the flame, then the corresponding internal radiative fluxes will be the values used for the probe heat balance. Equation III-2 was used to determine the heat flux removed by the water. Equation III-3 was used to determine the radiative flux emitted by the probe. Equation III-1 was used to calculate the

convective heat flux from flame to probe and Equation III-4 was applied to obtain the convective heat transfer coefficient. These results are presented in Table VIII-9-15. From these tables it can be seen that considerable variation exists in the convective heat flux. In fact, there are a number of runs for Benzene, Cyclohexane, and n-Hexane where the convective flux would be negative. This is due to the emission and extinction coefficients used for these flames. Remember that these values produced calculated external radiant fluxes for a conical shaped flame that were higher than measured values. The convective heat fluxes are in the same range as those obtained by Neill (50) and Deshpande (24). The convective heat transfer coefficient decreases with increasing temperature difference between the flame and probe surface, which is contrary to heat transfer principles. This is due to inaccurate flame temperature measurements. Undoubtedly there are considerable temperature gradients in a flame as indicated by Bader (7) and Gordan and McMillan (31), so the use of a mean optical pyrometer value will cause such discrepancies. The flame convective coefficients are several orders of magnitude larger than would be predicted by convective heat transfer theory and this difference cannot be attributed to the temperature difference alone.

TABLE VIII-9

HEAT TRANSFER RESULTS FOR ACETONE USING FLAME RADIANT FLUX CALCULATED WITH RADIOMETER 72804 DATA

Run Number	Flame Size Inches		Height Above Pan Inches	Probe Temp °F	q_e Btu/hr-ft^2	q_w Btu/hr-ft^2	q_t Btu/hr-ft^2	q_r Btu/hr-ft^2	q_c Btu/hr-ft^2	T_f °F	h_c *
	Dia	Ht									
090171-24-1-1	24.5	97	3.6875	946	6698	654	7352	6683	669	2015	0.626
			9.6875	1106	10308		10962	7399	3563		3.920
090171-24-1-2	24.5	65	3.6875	1246	14519	1060	15579	7174	8405	2027	10.762
			9.6875	1250	14655		15715	8268	7447		9.584
090171-24-1-3	24.5	87	3.6875	933	6454	651	7105	6632	473	2010	0.439
			9.6875	1137	11149		11800	7305	4495		5.149
081271-18-1-1	18.7	65	3.6875	922	6252	600	6852	5307	1545	1983	1.456
			9.6875	1058	9101		9701	5547	4154		4.491
081271-18-1-2	18.7	66	3.6875	922	6252	595	6847	5315	1532	1980	1.448
			9.6875	1050	8911		9506	5562	3944		4.241
081271-18-1-3	18.7	65	3.6875	943	6641	627	7268	5307	1961	1976	1.898
			9.6875	1066	9295		9922	5547	4375		4.808
070771-12-1-1	11.9	47	3.6875	854	5110	522	5632	3940	1692	1980	1.503
			9.6875	966	7087		7609	4245	3364		3.318
070771-12-1-2	12.2	46	3.6875	917	6162	571	6733	4031	2702	1980	2.542
			9.6875	1008	7960		8531	4354	4177		4.297
070871-12-1-1	12.2	46	3.6875	893	5744	523	6267	4031	2236	1980	2.057
			9.6875	951	6794		7317	4354	2963		2.879

*Units: Btu/hr-ft^2-°F.

TABLE VIII-10

HEAT TRANSFER RESULTS FOR BENZENE USING FLAME RADIANT FLUX CALCULATED WITH RADIOMETER 72804 DATA

Run Number	Flame Size Inches		Height Above Pan Inches	Probe Temp °F	q_e Btu/hr-ft^2	q_w Btu/hr-ft^2	q_t Btu/hr-ft^2	q_r Btu/hr-ft^2	q_c Btu/hr-ft^2	T_f °F	h_c *
	Dia	Ht									
090171-24-2-1	26.6	59.6	3.6875	1421	21457	1211	22668	17813	4855	1922	9.691
			9.6875	1526	26664		27875	19181	8694		21.955
090171-24-2-2	24.8	67.6	3.6875	1497	25141	1676	26817	17360	9457	1935	21.591
			9.6875	1468	23683		25359	18694	6665		14.272
090171-24-2-3	24.8	49.0	3.6875	1534	27096	1742	28838	17360	11478	1922	29.582
			9.6875	1470	23782		25524	18694	6830		15.111
081171-18-2-1	19.4	65.0	3.6875	1209	13300	929	14229	15174	--	1922	--
			9.6875	1230	31982		14911	15837	--		--
081171-18-2-2	20.9	70.8	3.6875	1241	14349	956	15305	15912	--	1922	--
			9.6875	1305	16634		17590	16851	739		1.198
081171-18-2-3	22.3	54.3	3.6875	1299	16409	1018	17427	16198	1229	1922	1.973
			9.6875	1402	20603		21621	16970	4651		8.944
070671-12-2-1	16.5	46.0	3.6875	1095	10022	737	10759	13385	--	1922	--
			9.6875	1124	10790		11527	13619	--		--
070671-12-2-2	15.8	67.0	3.6875	1114	10520	764	11284	13375	--	1922	--
			9.6875	1153	11602		12366	13619	--		--
070671-12-2-3	13.7	48.0	3.6875	1062	9197	731	9928	11818	--	1922	--
			9.6875	1023	8290		9021	11370	--		--

*Units: Btu/hr-ft^2-°F.

TABLE VIII-11

HEAT TRANSFER RESULTS FOR CYCLOHEXANE USING FLAME RADIANT FLUX CALCULATED WITH RADIOMETER 72804 DATA

Run Number	Flame Size Inches		Height Above Pan Inches	Probe Temp °F	q_e Btu/hr-ft^2	q_w Btu/hr-ft^2	q_t Btu/hr-ft^2	q_r Btu/hr-ft^2	q_c Btu/hr-ft^2	T_f °F	h_c *
	Dia	Ht									
083071-24-3-1	25.9	100.1	3.6875	1059	9125	780	9905	12051	--	1955	--
			9.6875	1214	13460		14240	13346	894		1.206
083071-24-3-2	24.8	49.6	3.6875	1382	19732	1371	21103	11886	9217	1935	16.667
			9.6875	1340	17993		19364	13180	6184		10.393
083071-24-3-3	25.2	94.9	3.6875	1091	9919	826	10745	11827	--	1928	--
			9.6875	1215	13492		14318	13036	1282		1.798
081071-18-3-1	19.1	84.5	3.6875	1006	7917	726	8637	9869	--	1976	--
			9.6875	1106	10308		11034	10490	544		0.625
081071-18-3-2	20.1	92.0	3.6875	999	7767	680	8447	10258	--	1986	--
			9.6875	1134	11065		11745	11019	726		0.852
081071-18-3-3	18.7	54.3	3.6875	1219	13621	1122	14743	10044	4699	1989	6.103
			9.6875	1192	12766		13888	10944	2944		3.694
070171-12-3-1	14.7	73.3	3.6875	944	6660	618	7278	8109	--	1935	--
			9.6875	1035	8562		9180	8255	925		1.028
070171-12-3-2	14.7	87.3	3.6875	947	6717	616	7333	8191	--	1935	--
			9.6875	1038	8631		9247	8442	805		0.897
070171-12-3-3	14.7	69.8	3.6875	973	7228	629	7857	8083	--	1935	--
			9.6875	1031	8470		9099	8196	903		0.999

*Units: Btu/hr-ft^2-°F.

TABLE VIII-12

HEAT TRANSFER RESULTS FOR N-HEXANE USING FLAME RADIANT FLUX CALCULATED WITH RADIOMETER 72804 DATA

Run Number	Flame Size Inches		Height Above Pan Inches	Probe Temp °F	q_e Btu/hr-ft^2	q_w Btu/hr-ft^2	q_t Btu/hr-ft^2	q_r Btu/hr-ft^2	q_c Btu/hr-ft^2	T_f °F	h_c *
	Dia	Ht									
083171-24-4-1	24.5	58.2	3.6875	1340	17993	1394	19387	12175	7212	2008	11.75
			9.6875	1332	17675		19069	13741	5328		7.88
083171-24-4-2	24.8	74.8	3.6875	1258	14932	1106	16038	11596	3336	2005	4.47
			9.6875	1297	16334		17440	12559	4881		6.89
083171-24-4-3	25.9	116.0	3.6875	1018	8179	762	8941	12082	--	2006	--
			9.6875	1179	12369		13131	13356	--		--
081071-18-4-1	20.9	106.0	3.6875	983	7431	680	8111	10760	--	2075	--
			9.6875	1116	10574		11254	11619	--		--
081071-18-4-2	20.1	106.0	3.6875	998	7745	671	8416	10523	--	2123	--
			9.6875	1124	10790		11461	11316	145		0.15
081171-18-4-1	20.9	106.0	3.6875	966	7087	676	7763	10760	--	2121	--
			9.6875	1111	10440		11116	11619	--		--
070271-12-4-1	15.1	91.7	3.6875	986	7493	626	8119	8730	--	2056	--
			9.6875	1026	8358		8984	9025	--		--
070271-12-4-2	14.4	75.5	3.6875	957	6910	626	7536	8364	--	2056	--
			9.6875	1024	8313		8939	8492	447		0.43
070271-12-4-3	15.8	84.1	3.6875	984	7452	658	8110	8966	--	2056	--
			9.6875	1048	8864		9522	9275	247		0.25

*Units: Btu/hr-ft^2-°F.

TABLE VIII-13

HEAT TRANSFER RESULTS FOR JET A USING FLAME RADIANT FLUX CALCULATED WITH RADIOMETER 72804 DATA

Run Number	Flame Size Inches Dia	Flame Size Inches Ht	Height Above Pan Inches	Probe Temp °F	q_e Btu/hr-ft^2	q_w Btu/hr-ft^2	q_t Btu/hr-ft^2	q_c Btu/hr-ft^2	q_r Btu/hr-ft^2	T_f °F	h_c *
083171-24-5-1	25.9	79.4	3.6875	1310	16823	1068	17891	6235	11656	1866	11.21
			9.6875	1309	16785		17853	4374	13479		7.85
041671-24-5-1	24.5	56	3.6875	1328	17518	1222	18740	7560	11180	1866	14.05
			9.6875	1366	19055		20277	7403	12824		14.81
041671-24-5-2	28.8	59.6	3.6875	1324	17362	1257	18619	6057	12562	1866	11.18
			9.6875	1409	20915		19658	5029	14629		11.00
041671-24-5-3	26.3	56	3.6875	1330	17596	1433	19029	8581	10448	1866	16.01
			9.6875	1417	21275		22708	11442	11266		25.48
080971-18-5-1	19.4	58	3.6875	1205	13173	878	14051	5604	8447	1850	8.69
			9.6875	1184	12520		13398	4617	8781		6.93
042171-18-5-1	19.8	64.3	3.6875	1237	14215	1000	15215	5701	9514	1850	9.30
			9.6875	1279	15675		16675	5910	10765		10.35
042171-18-5-2	20.1	60	3.6875	1213	13427	964	14391	4766	9625	1850	7.48
			9.6875	1280	15711		16675	5770	10905		10.12
042171-18-5-3	18.9	53.3	3.6875	1204	13141	960	14101	4934	9167	1850	7.64
			9.6875	1230	13982		14942	4615	10327		7.44
070971-12-5-1	12.9	44.6	3.6875	1022	8269	646	8915	3005	5910	1850	3.63
			9.6875	976	7288		7934	2367	5567		2.71
042771-12-5-1	15.5	54.6	3.6875	1196	12890	854	13744	5950	7794	1850	9.10
			9.6875	1071	9417		10271	1656	8615		2.13
042771-12-5-2	13.7	45.3	3.6875	1156	11689	839	12528	5523	7005	1850	7.96
			9.6875	1091	9919		10758	3111	7647		4.10
042771-12-5-3	15.8	48.2	3.6875	1194	12828	929	13757	5838	7919	1850	8.90
			9.6875	1233	14080		15009	6241	8768		10.12
042871-12-5-1	16.5	54.2	3.6875	1184	12520	929	13449	5237	8212	1850	7.86
			9.6875	1227	13883		14812	5680	9132		9.12
042871-12-5-2	15.8	58.2	3.6875	1208	13268	1563	14831	6910	7921	1850	10.76
			9.6875	1143	11317		12880	4108	8772		5.81

*Units: Btu/hr-ft^2-°F.

TABLE VIII-14

HEAT TRANSFER RESULTS FOR JP-4 USING FLAME RADIANT FLUX CALCULATED WITH RADIOMETER 72804 DATA

Run Number	Flame Size Inches		Height Above Pan Inches	Probe Temp °F	q_e Btu/hr-ft^2	q_w Btu/hr-ft^2	q_t Btu/hr-ft^2	q_r Btu/hr-ft^2	q_c Btu/hr-ft^2	T_f °F	h_c *
	Dia	Ht									
083171-24-6-1	25.9	91.3	3.6875	1220	13654	966	14620	12574	2046	1920	2.92
			9.6875	1291	16112		17078	13893	3185		5.06
041771-24-6-1	24.5	61.8	3.6875	1343	18113	1482	19595	11827	7768	1920	13.46
			9.6875	1365	19014		20496	12710	7786		14.03
041771-24-6-2	26.6	79.5	3.6875	1266	15212	1106	16318	12644	3674	1920	5.61
			9.6875	1345	18194		19300	13942	5358		9.32
041771-24-6-3	24.5	70.4	3.6875	1288	16002	1316	17318	11949	5369	1920	8.50
			9.6875	1364	18972		20288	12953	7335		13.19
081071-18-6-1	19.4	83.7	3.6875	1078	9590	724	10314	10387	--	1935	--
			9.6875	1134	11065		11789	11067	722		0.90
042171-18-6-1	20.5	75.1	3.6875	1141	11261	897	12158	10709	1449	1935	1.82
			9.6875	1215	13492		14389	11412	2977		4.13
042171-18-6-2	21.6	84.5	3.6875	1144	11346	1637	12983	11169	1814	1935	2.29
			9.6875	1201	13046		14683	12059	2624		3.57
042171-18-6-3	20.5	67.9	3.6875	1150	11516	930	12446	10633	1813	1935	2.31
			9.6875	1194	12828		13758	11255	2503		3.38
062271-12-6-1	13.3	49.6	3.6875	1013	8069	695	8764	7533	1231	1935	1.34
			9.6875	1016	8135		8830	7251	1555		1.69
042971-12-6-1	14.7	54.6	3.6875	1170	12099	862	12961	8227	4734	1935	6.19
			9.6875	1136	11121		11983	8143	3840		4.81
042971-12-6-2	15.5	55.3	3.6875	1120	10682	785	11467	8577	2890	1935	3.55
			9.6875	1175	12248		13033	8521	4512		5.94
042971-12-6-3	15.8	62.8	3.6875	1143	11317	876	12193	8792	3401	1935	4.29
			9.6875	1163	11893		12769	8925	3844		4.98

*Units: Btu/hr-ft^2-°F.

TABLE VIII-15

HEAT TRANSFER RESULTS FOR METHANOL USING FLAME RADIANT FLUX CALCULATED WITH DATA FROM NEILL (50)

Run Number	Flame Size Inches Dia	Flame Size Inches Ht	Height Above Pan Inches	Probe Temp °F	q_e Btu/hr-ft^2	q_w Btu/hr-ft^2	q_t Btu/hr-ft^2	q_r Btu/hr-ft^2	q_c Btu/hr-ft^2	T_f °F	h_c *
082771-24-7-1	23.7	44	3.6875	1109	8310	719	9029	3479	5550	2140	5.38
			9.6875	1050	7129		7848	3844	4004		3.67
083071-24-7-1	23.4	22.6	3.6875	1111	8352	694	9046	3455	5591	2140	5.43
			9.6875	1048	7091		7785	3791	3944		3.66
083071-24-7-2	23.4	24.5	3.6875	1115	8437	716	9153	3458	5695	2140	5.57
			9.6875	1056	7243		7959	3803	4156		3.83
083071-24-7-3	23.4	21.5	3.6875	1112	8374	706	9080	3453	5627	2140	5.47
			9.6875	1049	7110		7816	3780	4036		3.70
081271-18-7-1	17.3	21.9	3.6875	1068	7475	654	8129	3038	5091	2140	4.75
			9.6875	986	5995		6649	3274	3375		2.92
081271-18-7-2	18.0	23.0	3.6875	1063	7377	663	8040	3098	4942	2140	4.59
			9.6875	965	5654		6317	3351	2966		2.52
081271-18-7-3	18.0	21.2	3.6875	1066	7436	620	8056	3096	4960	2140	4.62
			9.6875	970	5734		6354	3341	3013		2.58
070871-12-7-1	11.5	16.0	3.6875	1022	6614	525	7139	2384	4755	2140	4.25
			9.6875	841	3928		4453	2387	2066		1.59
070871-12-7-2	11.5	19.0	3.6875	1025	6668	553	7221	2387	4834	2140	4.34
			9.6875	873	4329		4882	2497	2385		1.88
070871-12-7-3	11.5	20.8	3.6875	1017	6526	557	7083	2388	4695	2140	4.18
			9.6875	842	3940		4497	2503	1994		1.54

*Units: Btu/hr-ft^2-°F

Radiant Heat Flux for Cylindrical Shaped Flames Using the Data of Neill, Pfenning and Tsai

In order to assess the effect of other values of emission and extinction coefficients, the data of Neill (50), Pfenning (54) and Tsai (79) were used with programs CYCLIF and CYCLOF to calculate the radiant flux inside and exterior to flames. These results are presented in Tables VIII-16 to VIII-21. From these tables, it can be seen that the spectral data of Pfenning and Tsai from small laminar flames indicates that the flames used in this study are optically thick. For acetone, Tsai's data gives results that are 43 percent lower than those of Pfenning. Tsai's calculated external radiant flux values are in close agreement with the measured values. Neill's data produces calculated external radiative flux values that are approximately 15 to 50 percent higher than the measured values.

For cyclohexane, Tsai's values of the calculated external radiative flux are in good agreement with Neill's values for the 24" diameter burner, but are 10-20 percent higher for the 18" burner and 35-55 percent higher for the 12" burner. Neill's values range from 25 percent to 70 percent higher than the measured fluxes.

For n-hexane, Neill's values of the external radiative flux are 14-18 percent higher than Tsai's for the 24" burner, and 1-3 percent higher for the 18" burner, but are 12-17 percent lower for the 12" burner. Neill's values are

TABLE VIII-16

RADIANT HEAT FLUX FOR A CYLINDRICAL-SHAPED ACETONE FLAME USING EXTINCTION AND EMISSION COEFFICIENTS FROM TSAI (79), PFENNING (54), AND NEILL (50)

Run Number	Flame Size in Diameter	Flame Size in Height	Radiometer 81510 q_m Btu/hr-ft^2	Height Above Pan in	Tsai's Data q_m Btu/hr-ft^2	Tsai's Data q_r Btu/hr-ft^2	Ffenning's Data q_m Btu/hr-ft^2	Ffenning's Data q_r Btu/hr-ft^2	Neill's Data q_m Btu/hr-ft^2	Neill's Data q_r Btu/hr-ft^2
090171-24-1-1	24.5	97	6515	3.6875 9.6875	5154	5723 5725	12014	13324 13476	8229	8001 8699
090171-24-1-2	24.5	65	9882	3.6875 9.6875	5124	5723 5725	11951	13324 13476	8182	8001 8698
090171-24-1-3	24.5	87	5591	3.6875 9.6875	5146	5723 5725	12001	13324 13476	8219	8001 8698
081271-18-1-1	18.7	65	3719	3.6875 9.6875	3910	5723 5725	9038	13267 13407	5830	7398 7939
081271-18-1-2	18.7	66	3528	3.6875 9.6875	3911	5723 5725	9039	13267 13407	5831	7398 7939
081271-18-1-3	18.7	65	3725	3.6875 9.6875	3910	5723 5725	9038	13267 13407	5830	7398 7939
070771-12-1-1	11.9	47	1979	3.6250 9.6250	2403	5720 5721	5465	12907 13008	3126	6003 6281
070771-12-1-2	12.2	46	2408	3.6250 9.6250	2467	5720 5721	5616	12907 13008	3237	6089 6380
070871-12-1-1	12.2	46	2825	3.6250 9.6250	2467	5720 5721	5616	12907 13008	3237	6089 6380

TABLE VIII-17

RADIANT HEAT FLUX FOR A CYLINDRICAL-SHAPED BENZENE FLAME USING EXTINCTION AND EMISSION COEFFICIENTS FROM TSAI (79) AND NEILL (50)

Run Number	Flame Size in Diameter	Flame Size in Height	Radiometer 81510 q_m Btu/hr-ft^2	Height Above Pan in	Tsai's Data q_r Btu/hr-ft^2	Tsai's Data q_m Btu/hr-ft^2	Neill's Data q_r Btu/hr-ft^2	Neill's Data q_m Btu/hr-ft^2
090171-24-2-1	26.6	59.6	14972	3.6875 9.6875	19865 19872	18528	13294 15269	18822
090171-24-2-2	24.8	67.6	13542	3.6875 9.6875	19865 19872	17844	12907 14776	17493
090171-24-2-3	24.8	49	13226	3.6875 9.6825	19865 19872	17689	12899 14763	17263
081171-18-2-1	19.4	65	8559	3.6875 9.6875	19865 19872	13980	10934 12270	11466
081171-18-2-2	20.9	70.8	10925	3.6875 9.6875	19865 19872	15116	11519 13010	13075
081171-18-2-3	22.3	54.3	12469	3.6875 9.6875	19865 19872	16055	12036 13665	14504
070671-12-2-1	16.5	46	6878	3.6250 9.6250	19864 19871	11708	9679 10724	8505
070671-12-2-2	15.8	67	7146	3.6250 9.6250	19863 19870	11240	9365 10335	7981
070671-12-2-3	13.7	48	4977	3.6250 9.6250	19860 19867	9603	8359 9098	6119

TABLE VIII-18

RADIANT HEAT FLUX FOR A CYLINDRICAL-SHAPED CYCLOHEXANE FLAME USING EXTINCTION AND EMISSION COEFFICIENTS FROM TSAI (79) AND NEILL (50)

Run Number	Flame Size in Diameter	Flame Size in Height	Radiometer 81510 q_m Btu/hr-ft^2	Height Above Pan in	Tsai's Data q_r Btu/hr-ft^2	Tsai's Data q_m Btu/hr-ft^2	Neill's Data q_r Btu/hr-ft^2	Neill's Data q_m Btu/hr-ft^2
083071-24-3-1	25.9	100.1	10520	3.6875 9.6875	18464 18515	17370	12506 14305	17276
083071-24-3-2	24.8	49.6	12683	3.6875 9.6875	18463 18514	16484	12186 13894	15823
083071-24-3-3	25.2	94.9	11032	3.6875 9.6875	18464 18515	16942	12307 14050	16528
081071-18-3-1	19.1	84.5	6062	3.6875 9.6875	18449 18500	12818	10323 11529	10415
081071-18-3-2	20.1	92	7611	3.6875 9.6875	18453 18502	13538	10682 11982	11369
081071-18-3-3	18.7	54.3	8678	3.6875 9.6875	18447 18495	12463	10175 11342	9955
070171-12-3-1	14.7	73.3	3856	3.6250 9.6250	18407 18450	9650	8524 9317	6616
070171-12-3-2	14.7	87.3	3964	3.6250 9.6250	18407 18450	9663	8524 9316	6633
070171-12-3-3	14.7	69.8	4136	3.6250 9.6250	18407 18450	9646	8525 9317	6611

TABLE VIII-19

RADIANT HEAT FLUX FOR A CYLINDRICAL-SHAPED n-HEXANE FLAME USING EXTINCTION AND COEFFICIENTS FROM TSAI (79) AND NEILL (50)

Run Number	Flame Size in Diameter	Flame Size in Height	Radiometer 81510 q_m Btu/hr-ft^2	Height Above Pan	Tsai's Data q_r Btu/hr-ft^2	Tsai's Data q_m Btu/hr-ft^2	Neill's Data q_r Btu/hr-ft^2	Neill's Data q_m Btu/hr-ft^2
083171-24-4-1	24.5	58.2	13738	3.6875 9.6875	12752 12762	11295	10287 11669	12868
083171-24-4-2	24.8	74.8	12803	3.6875 9.6875	12752 12762	11478	10357 11759	13196
083171-24-4-3	25.9	116	10627	3.6875 9.6875	12752 12762	11984	10603 12073	14176
081071-18-4-1	20.9	106	7057	3.6875 9.6875	12751 12761	9737	9381 10514	10097
081071-18-4-2	20.1	106	7564	3.6875 9.6875	12751 12761	9351	9158 10233	9474
081071-18-4-3	20.9	106	6950	3.6875 9.6875	12751 12761	9737	9381 10514	10097
070271-12-4-1	15.1	91.7	3987	3.6250 9.6250	12746 12755	6887	7539 8234	5875
070271-12-4-2	14.4	75.5	4208	3.6250 9.6250	12744 12753	6535	7282 7920	5410
070271-12-4-3	15.8	84.1	4308	3.6250 9.6250	12747 12757	7229	7787 8540	6338

TABLE VIII-20

RADIANT HEAT FLUX FOR A CYLINDRICAL-SHAPED JP-4 FLAME USING EXTINCTION AND EMISSION COEFFICIENTS FROM NEILL (50)

Run Number	Flame Size Inches		Radiometer 81510 q_m	Height Above Pan Inches	q_r Neill's Data	q_m
	Diameter	Height	Btu/hr-ft^2		Btu/hr-ft^2	Btu/hr-ft^2
083171-24-6-1	25.9	91.3	13589	3.6875 9.6875	11781 13385	15472
041771-24-6-1	24.5	61.8	12105	3.6875 9.6875	11444 12954	14129
041771-24-6-2	26.6	79.5	13560	3.6875 9.6875	11802 13412	15518
041771-24-6-3	24.5	70.4	12815	3.6875 9.6875	11445 12955	14174
081071-18-6-1	19.4	83.7	6175	3.6875 9.6875	10013 11134	9840
042171-18-6-1	20.5	75.1	8642	3.6875 9.6875	10352 11563	10735
042171-18-6-2	21.6	84.5	9268	3.6875 9.6875	10674 11971	11686
042171-18-6-3	20.5	67.9	8511	3.6875 9.6875	10353 11563	10717
062271-12-6-1	13.3	49.6	3463	3.6250 9.6250	7716 8319	5213
042971-12-6-1	14.7	54.6	5644	3.6250 9.6250	8306 9036	6187
042971-12-6-2	15.4	55.3	5710	3.6250 9.6250	8623 9425	6759
042971-12-6-3	15.8	62.8	5972	3.6250 9.6250	8738 9567	6996

TABLE VIII-21

RADIANT HEAT FLUX FOR A CYLINDRICAL-SHAPED METHANOL FLAME USING EXTINCTION AND EMISSION COEFFICIENTS FROM TSAI (79)

Run Number	Flame Size Inches		Radiometer 81510 q_m Btu/hr-ft^2	Height Above Pan Inches	q_r Tsai's Data	q_m
	Diameter	Height			Btu/hr-ft^2 q_r	Btu/hr-ft^2 q_m
082771-24-7-1	23.7	44.0	4494	3.6875 9.6875	1894 1895	1611
083071-24-7-1	23.4	22.6	4136	3.6875 9.6875	1894 1895	1542
083071-24-7-2	23.4	24.5	4113	3.6875 9.6875	1894 1895	1546
083071-24-7-3	23.4	21.5	4345	3.6875 9.6875	1894 1895	1541
081271-18-7-1	17.3	21.9	2807	3.6875 9.6875	1893 1894	1133
081271-18-7-2	18.0	23.0	3075	3.6875 9.6875	1893 1894	1188
081271-18-7-3	18.0	21.2	2563	3.6875 9.6875	1893 1894	1180
070871-12-7-1	11.5	16.0	1192	3.6250 9.6250	1890 1891	631
070871-12-7-2	11.5	19.0	1228	3.6250 9.6250	1890 1891	687
070871-12-7-3	11.5	20.8	1246	3.6250 9.6250	1890 1891	707

are from 3 to 45 percent higher than the measured fluxes except for one case where the measured value is about 7 percent higher.

For JP-4 Neill's values of the calculated external radiative flux are generally 10-25 percent higher than the measured values.

For methanol Tsai's calculated external radiative flux values are generally 45-65 percent lower than the measured values. From Table VIII-8, Neill's values for the calculated radiative flux external to a cylindrical shape flame are 11 to 23 percent lower than the measured values.

These results enhance the fact that numerous sets of emission and extinction coefficients can be obtained and are dependent on the measuring technique and flame structure. In order to further assess the effects of the emission and extinction coefficients, the radiative fluxes calculated with Neill's data will be compared with that obtained with the data from Radiometer 72804 for a cylindrical shaped flame.

For acetone, Neill's results for the external flux are approximately 21 and 65 percent lower for the 24" and 18" burner, but are 19 percent higher for the 12" burner, than the values obtained in the study. The internal flux values reveal that Neill's results are 5-11, 21-27 and 46-52 percent higher for the 24, 18 and 12 inch diameter burners respectively.

For cyclohexane, Neill's results for the external flux are approximately 2 percent lower for all burner sizes than

the values obtained in this study. Accordingly, Neill's calculated internal fluxes are about 1.5 percent lower than those obtained in this study.

For n-hexane, Neill's results for the external flux are approximately 14 percent lower than the values used in this study. Consequently, Neill's value for the internal radiative flux is approximately 16 percent lower than that obtained in this study.

For JP-4, Neill's results for the external flux are 17, 15 and 12 percent lower than the values used in this study for the 24, 18 and 12" burners respectively. This results in Neill's calculated internal fluxes being 12, 10 and 8 percent lower than the values obtained in this study.

Application of Configuration Factor and Mean Path Length to Obtain Emission and Extinction Coefficients from Radiometer 81510 Data

Since the application of the emission and extinction coefficient data obtained from radiometer 72804 measurements resulted in calculated radiative fluxes external to flames that were in poor agreement with values measured by radiometer 81510, these measured data will be used to obtain additional sets of emission and extinction coefficients. Radiometer 81510 has a 150° view angle, therefore, the path length through the flame is variable. If one assumes that an appropriate value for the path length can be defined, then

Equation III-29 can be solved to obtain the emission and extinction coefficients. Note that this equation contains the configuration factor $F_{t\to f}$ from the radiometer to the flame, whereas the use of Equation III-25 with radiometer 72804 readings did not. Considering the various flame shapes shown in Chapter VI and the lack of existing configuration factors for such shapes, there is required an additional assumption before the coefficients can be obtained. If the radiometer is assumed to be a differential element of area and the flame shape to be a cylinder, then $F_{t\to f}$ can be calculated by using configuration factor algebra and the equation given by Love (42) for the configuration factor for a differential area whose normal passes through the center of one end of a finite-length right-circular cylinder and is perpendicular to the axis of the cylinder. These values of $F_{t\to f}$ are given in Tables VIII-22 through VIII-28. Now these values along with the computed values of q_m for a cylindrical shaped flame from Tables VIII-2 through VIII-8 and the values q_∞ from Table VIII-1 were used with Equation III-29 to compute the mean path length L_a, through the flame. The mean beam length for an optically thin gas radiating to its entire boundary is given by Equation III-48 which becomes for a cylindrical shaped flame

$$L_{b,o} = \frac{2D_f H_2}{2H_2+D_f} \qquad \text{(VIII-1)}$$

TABLE VIII-22

CONFIGURATION FACTOR AND MEAN PATH LENGTH DATA FOR A CYLINDRICAL-SHAPED ACETONE FLAME

Run Number	Flame Size Inches		$F_{t \to f}$	$q_m/F_{t \to f}$ Btu/hr-ft^2		L_a in	L_{bo} in	L_a/L_{bo}
	Diameter	Height		Calculated	Measured			
090171-24-1-1	24.5	97	.94193	11051	6917	18.743	21.753	.862
090171-24-1-2	24.5	65	.94193	10939	10491	18.519	20.615	.898
090171-24-1-3	24.5	87	.94193	11026	5936	18.694	21.476	.870
081271-18-1-1	18.7	65	.70749	8816	5257	14.417	16.348	.882
081271-18-1-2	18.7	66	.70749	8820	4987	14.425	16.380	.881
081271-18-1-3	18.7	65	.70749	8816	5265	14.417	16.348	.882
070771-12-1-1	11.9	47	.42972	6097	4605	9.567	10.563	.906
070771-12-1-2	12.2	46	.44152	6210	5454	9.761	10.772	.906
070771-12-1-3	12.2	46	.44153	6210	6398	9.761	10.772	.906

TABLE VIII-23

CONFIGURATION FACTOR AND MEAN PATH LENGTH DATA FOR A CYLINDRICAL-SHAPED BENZENE FLAME

Run Number	Flame Size Inches		$F_{t \to f}$	$q_m/F_{t \to f}$ Btu/hr-ft^2		L_a in	$L_{b,o}$ in	$L_a/L_{b,o}$
	Diameter	Height		Calculated	Measured			
090171-24-2-1	26.6	59.6	1.00000	23947	14972	17.044	21.747	.784
090171-24-2-2	24.8	67.6	.95362	23611	14201	16.585	20.956	.791
090171-24-2-3	24.8	49.0	.95362	23362	13869	16.262	19.792	.822
081171-18-2-1	19.4	65.0	.73636	21003	11623	13.519	16.884	.801
081171-18-2-2	20.9	70.8	.79791	21802	13692	14.391	18.212	.790
081171-18-2-3	22.3	54.3	.85467	22344	14589	15.015	18.501	.816
070671-12-2-1	16.5	46.0	.61608	19225	11164	11.745	13.991	.839
070671-12-2-2	15.8	67.0	.58769	18978	12159	11.515	14.134	.815
070671-12-2-3	13.7	48.0	.50171	17470	9920	10.184	11.976	.850

TABLE VIII-24

CONFIGURATION FACTOR AND MEAN PATH LENGTH DATA FOR A CYLINDRICAL-SHAPED CYCLOHEXANE FLAME

Run Number	Flame Size Inches		$F_{t \to f}$	$q_m/F_{t \to f}$ Btu/hr-ft^2		L_a in	L_{bo} in	L_a/L_{bo}
	Diameter	Height		Calculated	Measured			
083071-24-3-1	25.9	100.1	.99616	17699	10561	18.560	22.933	.809
083071-24-3-2	24.8	49.6	.95362	16923	13300	17.340	19.840	.874
083071-24-3-3	25.2	94.9	.96915	17400	11383	18.082	22.246	.813
081071-18-3-1	19.1	84.5	.72404	14639	8372	14.084	17.161	.821
081071-18-3-2	20.1	92.0	.76519	15127	9947	14.743	18.121	.814
081071-18-3-3	18.7	54.3	.70741	14318	12267	13.663	15.953	.856
070171-12-3-1	14.7	73.3	.54278	12397	7104	11.285	13.360	.845
070171-12-3-2	14.7	87.3	.54278	12427	7302	11.320	13.558	.835
070171-12-3-3	14.7	69.8	.54278	12389	7620	11.275	13.300	.848

TABLE VIII-25

CONFIGURATION FACTOR AND MEAN PATH LENGTH DATA FOR A CYLINDRICAL-SHAPED N-HEXANE FLAME

Run Number	Flame Size Inches		$F_{t \to f}$	$q_m/F_{t \to f_2}$ Btu/hr-ft^2		L_a in	L_{bo} in	L_a/L_{bo}
	Diameter	Height		Calculated	Measured			
083171-24-4-1	24.5	58.2	.94192	15638	14585	16.388	20.240	.810
083171-24-4-2	24.8	74.8	.95362	15822	13426	16.740	21.273	.787
083171-24-4-3	25.9	116.0	.99616	16217	10668	17.529	23.137	.758
081071-18-4-1	20.9	106.0	.79793	14620	8844	14.570	18.751	.777
081071-18-4-2	20.1	106.0	.76519	14339	9885	14.104	18.359	.768
081071-18-4-3	20.9	106.0	.79793	14620	8710	14.570	18.751	.777
070271-12-4-1	15.1	91.7	.55915	12376	7130	11.202	13.951	.803
070271-12-4-2	14.4	75.5	.53060	12039	7931	10.757	13.146	.818
070271-12-4-3	15.8	84.1	.58778	12670	7329	11.603	14.443	.803

TABLE VIII-26

CONFIGURATION FACTOR AND MEAN PATH LENGTH DATA FOR A CYLINDRICAL-SHAPED JET A FLAME

Run Number	Flame Size Inches		$F_{t \to f}$	$q_m/F_{t \to f}$ Btu/hr-ft^2		L_a in	L_{bo} in	L_a/L_{bo}
	Diameter	Height		Calculated	Measured			
083171-24-5-1	25.9	79.4	.99616	17831	15515	19.622	22.268	.881
041671-24-5-1	24.5	56.0	.94192	16845	15060	18.321	20.103	.911
041671-24-5-2	28.8	59.6	1.00000	17650	16152	19.380	23.196	.836
041671-24-5-3	26.3	56.0	1.00000	17595	13721	19.307	21.299	.906
080971-18-5-1	19.4	58.0	.73632	14047	8985	14.798	16.620	.890
042171-18-5-1	19.8	64.3	.75282	14321	13499	15.133	17.158	.882
042171-18-5-2	20.1	60.0	.76513	14456	12269	15.299	18.540	.826
042171-18-5-3	18.9	53.3	.71565	13716	11743	14.397	16.054	.897
070971-12-5-1	12.9	44.6	.46933	10108	4711	10.210	11.270	.906
042771-12-5-1	15.5	54.6	.57522	11797	10549	12.129	13.573	.894
042771-12-5-2	13.7	45.3	.50156	10611	10577	10.774	11.900	.905
042771-12-5-3	15.8	48.2	.58734	11896	11254	12.243	13.575	.902
042871-12-5-1	16.5	54.2	.61631	12375	10745	12.802	14.320	.894
042871-12-5-2	15.8	58.2	.58759	12002	7771	12.366	13.912	.889

TABLE VIII-27

CONFIGURATION FACTOR AND MEAN PATH LENGTH DATA FOR A CYLINDRICAL-SHAPED JP-4 FLAME

Run Number	Flame Size Inches		$F_{t \to f}$	$q_m/F_{t \to f}$ Btu/hr-ft^2		L_a in	L_{bo} in	L_a/L_{bo}
	Diameter	Height		Calculated	Measured			
083171-24-6-1	25.9	91.3	.99616	18943	13641	18.761	22.683	.827
041771-24-6-1	24.5	61.8	.94193	18124	12851	17.599	20.447	.861
041771-24-6-2	26.6	79.5	1.00000	18882	13560	18.673	22.788	.819
041771-24-6-3	24.5	70.4	.94193	18191	13605	17.692	20.869	.848
081071-18-6-1	19.4	83.7	.73640	15683	8385	14.412	17.385	.829
042171-18-6-1	20.5	75.1	.78157	16225	11057	15.087	18.038	.836
042171-18-6-2	21.6	84.5	.82640	16818	11215	15.845	19.152	.827
042171-18-6-3	20.5	67.9	.78155	16193	10890	15.047	17.811	.845
062271-12-6-1	13.3	49.6	.48569	12086	7130	10.332	11.728	.881
042971-12-6-1	14.7	54.6	.54253	12976	10403	11.284	12.956	.871
042971-12-6-2	15.5	55.3	.57523	13447	9926	11.801	13.595	.868
042971-12-6-3	15.8	62.8	.58765	13659	10163	12.038	14.034	.858

TABLE VIII-28

CONFIGURATION FACTOR AND MEAN PATH LENGTH DATA FOR A CYLINDRICAL-SHAPED METHANOL FLAME

Run Number	Flame Size Inches		$F_{t \to f}$	$q_m/F_{t \to f}$ Btu/hr-ft^2		L_a in	$L_{b,o}$ in	$L_a/L_{b,o}$
	Diameter	Height		Calculated	Measured			
082771-24-7-1	23.7	44.0	.91048	4253	4936	16.204	18.671	.868
083071-24-7-1	23.4	22.6	.89794	4117	4606	14.850	15.418	.963
083071-24-7-2	23.4	24.5	.89817	4154	4579	15.198	15.837	.960
083071-24-7-3	23.4	21.5	.89774	4088	4840	14.584	15.154	.962
081271-18-7-1	17.3	21.9	.63987	3577	4387	10.875	12.402	.877
081271-18-7-2	18.0	23.0	.67191	3675	4577	11.473	12.938	.887
081271-18-7-3	18.0	21.2	.66862	3613	3833	11.093	12.636	.878
070871-12-7-1	11.5	16.0	.35348	2761	3372	7.002	8.460	.828
070871-12-7-2	11.5	19.0	.38292	2870	3207	7.432	8.828	.842
070871-12-7-3	11.5	20.8	.39259	2929	3174	7.674	9.009	.852

The values of L_a were divided by $L_{b,o}$ to obtain the correction factor for non-optically thick flames. All of these calculations are listed in Tables VIII-22 through VIII-28. The mean values of the correction factor for non-optical thickness are 0.888 for acetone, 0.812 for benzene, 0.835 for cyclohexane, 0.789 for n-hexane, 0.887 for Jet-A, 0.848 for JP-4, and 0.892 for methanol. The mean of these values is 0.85 which is in good agreement with the value of 0.88 recommended by Hottel and Sarofim (36).

The measured values of q_m were divided by the appropriate values of $F_{t\to f}$ and these results are plotted against L_a in Figures VIII-7 through VIII-9. From these figures, it can be seen that for most of the fuels several curves result. A non-linear curve-fit program was used with Equation III-29 to obtain the sets of extinction and emission coefficients corresponding to the curves for each fuel. These values are given in Table VIII-29.

The appropriate value of J and β was used in Programs CYLIF and CYLOF to calculate the radiant heat flux internal and external to a cylindrically shaped flame. The convective heat fluxes and heat transfer coefficients were obtained in the same manner as described earlier. These results are presented in Tables VIII-30 through VIII-36. The small difference between the calculated and measured external radiant heat flux is due to either the numerical integration or to the approximation of the radiometer with a differential area for computation of the configuration factor, $F_{t\to f}$.

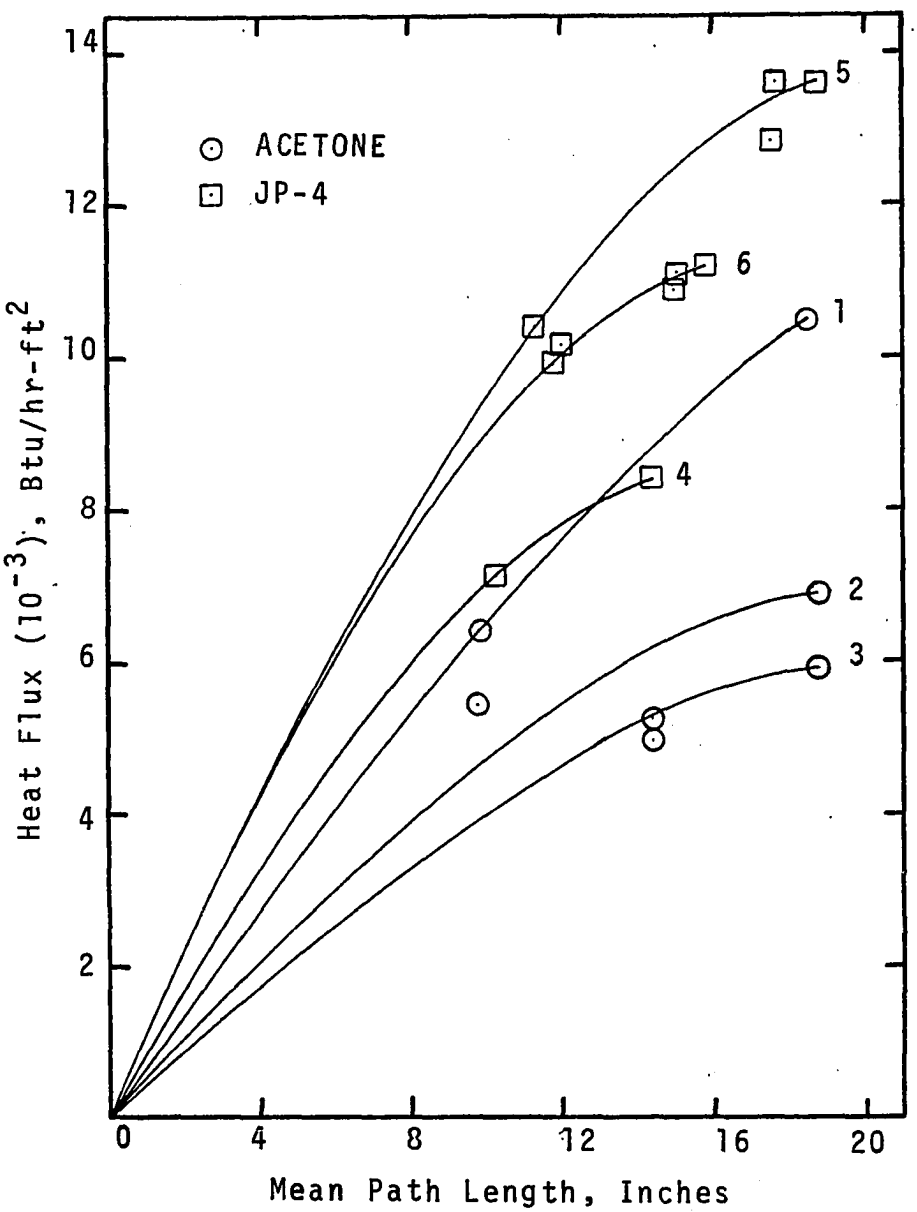


Figure VIII-7. Heat Flux versus Mean Path Length for Acetone and JP-4.

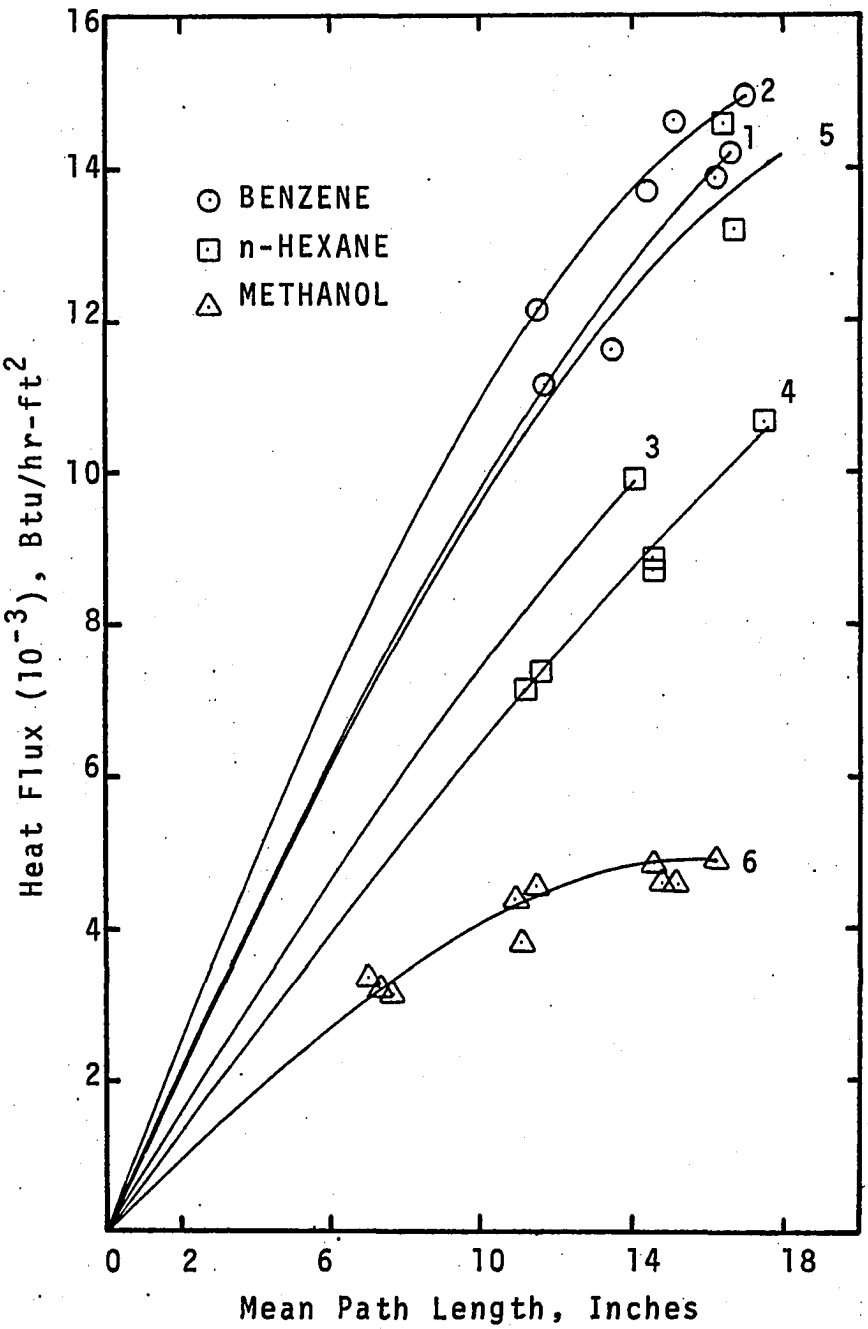


Figure VIII-8. Heat Flux versus Mean Path Length for Benzene, n-Hexane and Methanol.

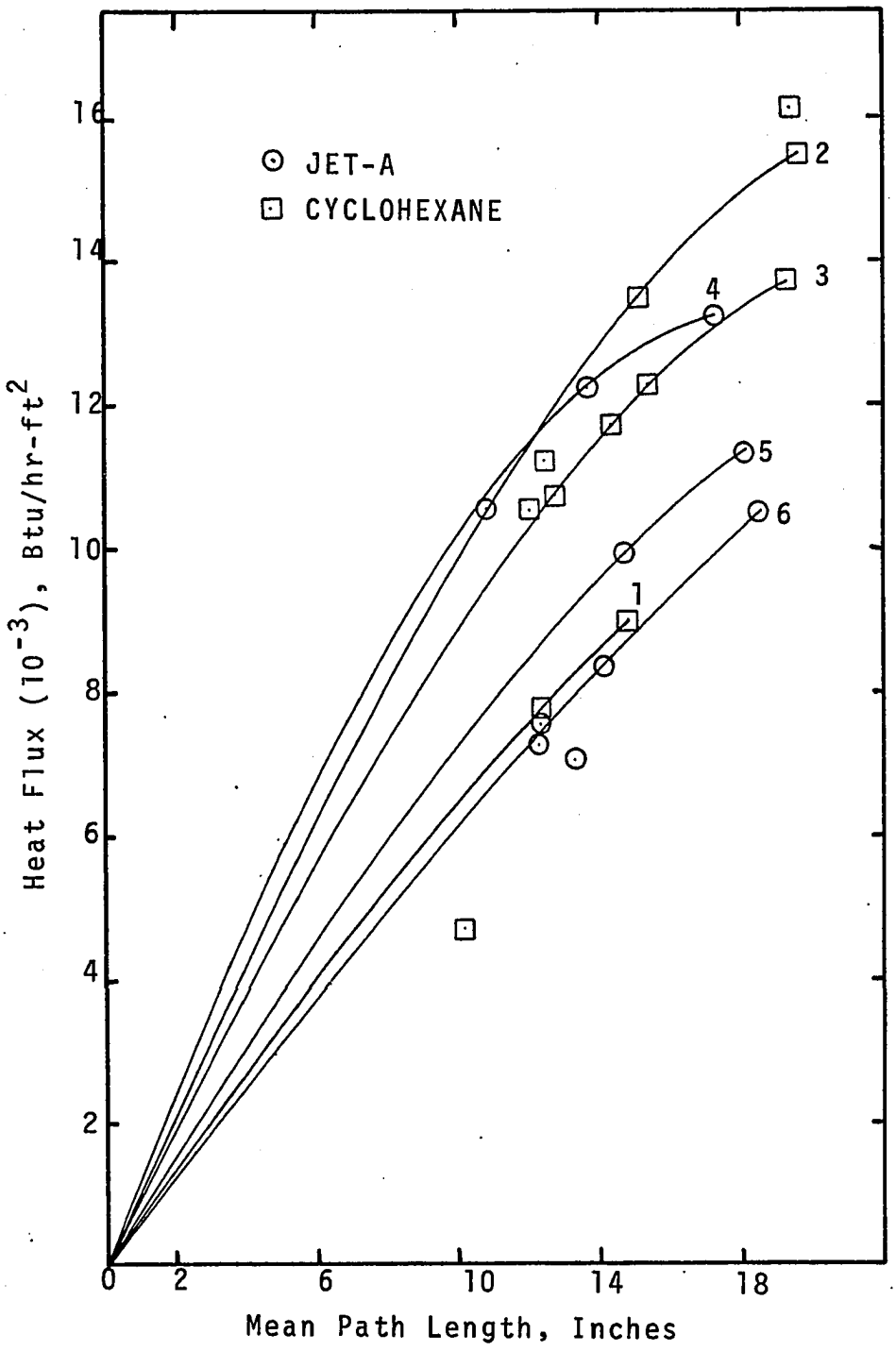


Figure VIII-9. Heat Flux versus Mean Path Length for Cyclohexane and Jet-A.

TABLE VIII-29

EMISSION AND EXTINCTION COEFFICIENTS OBTAINED FROM RADIOMETER 81510 DATA

Fuel	Figure Number	Curve Number	q_∞ Btu/hr-ft^2	J Btu/hr-ft^3	β in^{-1}
Acetone	VIII-1	1	21380	2973	0.0364
		2	9538	2510	0.0689
		3	8182	2163	0.0692
Benzene	VIII-2	1	25580	4656	0.04765
		2	20510	4729	0.07838
Cyclohexane	VIII-3	4	15170	7017	0.1211
		5	19710	3588	0.04766
		6	22130	2925	0.0346
n-Hexane	VIII-2	3	15720	3999	0.0666
		4	21910	2938	0.0351
		5	22600	4748	0.055
Jet A	VIII-3	1	24833	2884	0.0304
		2	26350	4710	0.0468
		3	25610	4441	0.0454
JP-4	VIII-1	4	10700	4345	0.1063
		5	22850	4242	0.0486
		6	19520	4486	0.06017
Methanol	VIII-2	6	5822	2488	0.1119

TABLE VIII-30

HEAT TRANSFER RESULTS FOR ACETONE USING FLAME RADIANT FLUX
CALCULATED WITH RADIOMETER 81510 DATA

Run Number	q_m Btu/hr-ft^2 Meas	q_m Btu/hr-ft^2 Calc	J Btu/hr-ft^2	β in^{-1}	Height Above Pan inches	q_t Btu/hr-ft^2	q_r Btu/hr-ft^2	q_c Btu/hr-ft^2	T_f-T_p °F	h_c *
090171-24-1-1	6515	6119	2510	0.0689	3.6875	7352	5041	2311	1069	2.16
					9.6875	10962	5684	5278	909	5.81
090171-24-1-2	9882	9575	2973	0.0364	3.6875	15579	7172	8407	781	10.76
					9.6875	15715	8202	7513	777	9.67
090171-24-1-3	5591	5250	2163	0.0692	9.6875	7105	4335	2770	1077	2.57
					9.6875	11800	4887	6913	873	7.92
081271-18-1-1	3719	3452	2163	0.0692	3.6875	6852	3743	3109	1061	2.93
					9.6875	9701	4136	5565	925	6.02
081271-18-1-2	3528	3453	2163	0.0692	3.6875	6847	3743	3104	1058	2.93
					9.6875	9506	4136	5370	930	5.77
081271-18-1-3	3725	3452	2163	0.0692	3.6875	7268	3743	3525	1033	3.41
					9.6875	9922	4136	5786	910	6.36
070771-12-1-1	1979	1905	2510	0.0689	3.6250	5632	3185	2447	1126	2.17
					9.6250	7609	3394	4215	1014	4.16
070771-12-1-2	2408	2775	2973	0.0364	3.6250	6733	4251	2482	1063	2.33
					9.6250	8531	4577	3954	972	4.07
070871-12-1-1	2825	2775	2973	0.0364	3.6250	6267	4251	2016	1087	1.85
					9.6250	7317	4577	2740	1029	2.66

*Units: Btu/hr-ft^2-°F.

TABLE VIII-31

HEAT TRANSFER RESULTS FOR BENZENE USING FLAME RADIANT FLUX CALCULATED WITH RADIOMETER 81510 DATA

Run Number	q_m Btu/hr-ft^2 Meas	q_m Btu/hr-ft^2 Calc	J Btu/hr-ft^2	β in^{-1}	Height Above Pan inches	q_t Btu/hr-ft^2	q_r Btu/hr-ft^2	q_c Btu/hr-ft^2	T_f-T_p °F	h_c *
090171-24-2-1	14972	14941	6140	0.0784	3.6875	22668	12043	10625	501	21.21
					9.6875	27875	13572	14303	396	36.12
090171-24-2-2	13542	13779	4656	0.0477	3.6875	26817	10588	16229	438	37.05
					9.6875	25359	12060	13299	467	28.48
090171-24-2-3	13226	13615	4656	0.0477	3.6875	28838	10585	18253	388	47.04
					9.6875	25524	12054	13470	452	29.80
081171-18-2-1	8559	9202	4656	0.0477	3.6875	14229	9088	5141	713	7.21
					9.6875	14911	10153	4758	692	6.88
081171-18-2-2	10925	10942	6140	0.0784	3.6875	15305	10854	4451	681	6.54
					9.6875	17590	12054	5536	617	8.97
081171-18-2-3	12469	11980	6140	0.0784	3.6875	17427	11216	6211	623	9.97
					9.6875	21621	12515	9106	520	17.51
070671-12-2-1	6878	6910	4656	0.0477	3.6250	10759	8107	2652	827	3.21
					9.6250	11527	8947	2580	798	3.23
070671-12-2-2	7146	7089	6140	0.0784	3.6250	11284	9219	2065	808	2.56
					9.6250	12366	10036	2330	769	3.03
070671-12-2-3	4977	5026	4656	0.0477	3.6250	9928	7054	2874	860	3.34
					9.6250	9021	7652	1369	899	1.52

*Units: Btu/hr-ft^2-°F.

TABLE VIII-32

HEAT TRANSFER RESULTS FOR CYCLOHEXANE USING FLAME RADIANT FLUX CALCULATED WITH RADIOMETER 81510 DATA

Run Number	q_m Btu/hr-ft^2 Meas	q_m Btu/hr-ft^2 Calc	J Btu/hr-ft^2	β in^{-1}	Height Above Pan inches	q_t Btu/hr-ft^2	q_r Btu/hr-ft^2	q_c Btu/hr-ft^2	T_f-T_p °F	h_c *
083071-24-3-1	10520	10615	2925	0.0346	3.6875	9905	7394	2511	896	2.80
					9.6875	14240	8497	5743	741	4.73
083071-24-3-2	12683	11833	7017	0.1211	3.6875	21103	10947	10156	553	18.37
					9.6875	19364	12077	7287	595	12.25
083071-24-3-3	11032	10960	3588	0.0477	3.6875	10745	8236	2509	837	3.00
					9.6875	14318	9392	4926	713	6.91
081071-18-3-1	6062	6262	2925	0.0346	3.6875	8637	6013	2624	970	2.71
					9.6875	11034	6743	4291	870	4.93
081071-18-3-2	7611	7568	3588	0.0477	3.6875	8447	7168	1279	987	1.30
					9.6875	11745	8032	3713	852	4.36
081071-18-3-3	8678	8152	7017	0.1211	3.6875	14743	9845	4898	770	6.36
					9.6875	13888	10685	3203	797	4.02
070171-12-3-1	3856	3917	2925	0.0346	3.6250	7278	4914	2364	991	2.39
					9.6250	9180	5389	3791	900	4.21
070171-12-3-2	3964	3928	2925	0.0346	3.6250	7333	4914	2419	988	2.45
					9.6250	9247	5389	3858	897	4.30
070171-12-3-3	4136	3914	2925	0.0346	3.6250	7857	4914	2943	962	3.06
					9.6250	9099	5389	3710	904	4.10

*Units: Btu/hr-ft^2-°F.

TABLE VIII-33

HEAT TRANSFER RESULTS FOR n-HEXANE USING FLAME RADIANT FLUX CALCULATED WITH RADIOMETER 81510 DATA

Run Number	q_m Btu/hr-ft^2 Meas	q_m Btu/hr-ft^2 Calc	J Btu/hr-ft^2	β in^{-1}	Height Above Pan inches	q_t Btu/hr-ft^2	q_r Btu/hr-ft^2	q_c Btu/hr-ft^2	T_f-T_p °F	h_c *
083171-24-4-1	13738	12868	4748	0.055	3.6875	19387	10287	9100	668	13.62
					9.6875	19069	11669	7400	676	10.95
083171-24-4-2	12803	13196	4748	0.055	3.6875	16038	10357	5681	747	7.61
					9.6875	17440	11759	5681	708	8.02
083171-24-4-3	10627	10621	3999	0.0351	3.6875	8941	7404	1537	988	1.56
					9.6875	13131	8506	4625	827	5.59
081071-18-4-1	7057	7353	2938	0.0351	3.6875	8111	6422	1689	1092	1.55
					9.6875	11254	7255	3999	959	4.17
081071-18-4-2	7564	7325	3999	0.0666	3.6875	8416	7305	1111	1125	0.99
					9.6875	11461	8126	3335	999	3.34
081171-18-4-1	6950	7353	2938	0.0351	3.6875	7763	6422	1341	1155	1.16
					9.6875	11116	7255	3861	1010	3.82
070271-12-4-1	3987	4128	2938	0.0351	3.6250	8119	5033	3086	1070	2.88
					9.6250	8984	5532	3452	1030	3.35
070271-12-4-2	4208	4260	3999	0.0666	3.6250	7536	5887	1649	1099	1.50
					9.6250	8939	6380	2559	1032	2.48
070271-12-4-3	4308	4473	2938	0.0351	3.6250	8110	5215	2895	1072	2.70
					9.6250	9522	5757	3765	1008	3.74

*Units: Btu/hr-ft^2-°F.

TABLE VIII-34

HEAT TRANSFER RESULTS FOR JET A USING FLAME RADIANT FLUX CALCULATED WITH RADIOMETER 81510 DATA

Run Number	q_m Btu/hr ft^2 Meas	q_m Btu/hr ft^2 Calc	J Btu/hr-ft^2	β in^{-1}	Height Above Pan inches	q_t Btu/hr-ft^2	q_c Btu/hr-ft^2	q_r Btu/hr-ft^2	T_f-T_p °F	h_c *
083171-24-5-1	15455	15102	4710	0.0468	3.6875	17891	6849	11042	556	12.32
					9.6875	17853	5232	12621	557	9.39
041671-24-5-1	14185	13703	4710	0.0468	3.6875	18740	8050	10690	538	14.97
					9.6875	20277	8108	12169	500	16.22
041671-24-5-2	16152	15071	4710	0.0468	3.6875	18619	7556	11063	542	13.94
					9.6875	19658	7011	12647	457	15.34
041671-24-5-3	13721	14366	4441	0.0454	3.6875	19029	8509	10520	536	15.88
					9.6875	22708	10675	12033	449	23.78
080971-18-5-1	6616	6514	2884	0.0304	3.6875	14051	7929	6122	645	12.29
					9.6875	13398	6514	6884	666	9.78
042171-18-5-1	10162	9698	4710	0.0468	3.6875	15215	5856	9359	613	9.55
					9.6875	16675	6197	10478	571	10.85
042171-18-5-2	9387	9465	4441	0.0454	3.6875	14391	5417	8974	637	8.50
					9.6875	16675	6611	10064	570	11.60
042171-18-5-3	8404	8501	4441	0.0454	3.6875	14101	5490	8611	646	8.50
					9.6875	14942	5336	9606	620	8.60
070971-12-5-1	2211	3074	2884	0.0304	3.6250	8915	4502	4413	828	5.44
					9.6250	7934	3150	4784	874	3.60
042771-12-5-1	6068	6054	4441	0.0454	3.6250	13744	6287	7457	654	9.61
					9.6250	10271	2082	8189	779	2.67
042771-12-5-2	5305	5097	4710	0.0468	3.6250	12528	4761	7767	694	6.86
					9.6250	10758	2781	7977	759	3.66
042771-12-5-3	6610	6545	4710	0.0468	3.6250	13757	4986	8771	656	7.60
					9.6250	15009	6777	8232	617	10.98
042871-12-5-1	6622	6741	4441	0.0454	3.6250	13449	5642	7807	666	8.47
					9.6250	14812	6188	8624	623	9.93
042871-12-5-2	4566	4503	2884	0.0304	3.6250	14831	9612	5219	642	14.97
					9.6250	12880	7110	5770	707	10.06

*Units: Btu/hr-ft^2-°F.

TABLE VIII-35

HEAT TRANSFER RESULTS FOR JP-4 USING FLAME RADIANT FLUX CALCULATED WITH RADIOMETER 81510 DATA

Run Number	q_m Btu/hr-ft^2 Meas	q_m Btu/hr-ft^2 Calc	J Btu/hr-ft^2	β in^{-1}	Height Above Pan inches	q_t Btu/hr-ft^2	q_r Btu/hr-ft^2	q_c Btu/hr-ft^2	T_f-T_p °F	h_c *
083171-24-6-1	13589	13404	4242	0.0486	3.6875	14620	9838	4782	700	6.83
					9.6875	17078	11235	5843	629	9.29
041771-24-6-1	12105	12184	4242	0.0486	3.6875	19595	9529	10066	577	17.45
					9.6875	20496	10840	9656	555	17.40
041771-24-6-2	13560	13445	4242	0.0486	3.6875	16318	9857	6461	654	9.88
					9.6875	19300	11260	8694	575	15.12
041771-24-6-3	12815	12226	4242	0.0486	3.6875	17318	9529	7789	632	12.32
					9.6875	20288	10841	9447	556	16.99
081071-18-6-1	6175	5818	4354	0.1063	3.6875	10314	6566	3748	857	4.37
					9.6875	11789	7179	4610	801	5.76
042171-18-6-1	8642	8855	4486	0.0602	3.6875	12158	8544	3614	794	4.55
					9.6875	14389	9543	4846	720	6.73
042171-18-6-2	9268	9639	4486	0.0602	3.6875	12983	8809	4174	791	5.28
					9.6875	14683	9879	4804	734	6.54
042171-18-6-3	8511	8840	4486	0.0602	3.6875	12446	8544	3902	785	4.97
					9.6875	13758	9543	4215	741	5.69
062271-12-6-1	3463	3302	4354	0.1063	3.6250	8764	5333	3431	922	3.72
					9.6250	8830	5682	3148	919	3.43
042971-12-6-1	5644	5173	4242	0.0486	3.6250	12961	6763	6198	765	8.10
					9.6250	11983	7383	4600	799	5.76
042971-12-6-2	5710	5667	4242	0.0486	3.6250	11467	7035	4432	815	5.44
					9.6250	13033	7717	5316	760	6.99
042971-12-6-3	5972	5874	4242	0.0486	3.6250	12193	7134	5059	792	6.39
					9.6250	12769	7840	4929	772	6.38

*Units: Btu/hr-ft^2-°F.

TABLE VIII-36

HEAT TRANSFER RESULTS FOR METHANOL USING FLAME RADIANT FLUX
CALCULATED WITH RADIOMETER 81510 DATA

Run Number	q_m Btu/hr-ft^2 Meas	q_m Btu/hr-ft^2 Calc	J Btu/hr-ft^2	β in^{-1}	Height Above Pan inches	q_t Btu/hr-ft^2	q_r Btu/hr-ft^2	q_c Btu/hr-ft^2	T_f-T_p °F	h_c *
082771-24-7-1	4494	4176	2488	0.1119	3.6875	9029	3986	5043	1031	4.89
					9.6875	7848	4404	3444	1090	3.16
083071-24-7-1	4136	3879	2488	0.1119	3.6875	9046	3958	5088	1029	4.94
					9.6875	7785	4343	3442	1092	3.15
083071-24-7-2	4113	3921	2488	0.1119	3.6875	9153	3961	5192	1025	5.07
					9.6875	7959	4357	3602	1084	3.32
083071-24-7-3	4345	3848	2488	0.1119	3.6875	9080	3956	5124	1028	4.98
					9.6875	7816	4330	3486	1091	3.20
081271-18-7-1	2807	2463	2488	0.1119	3.6875	8129	3472	4657	1072	4.34
					9.6875	6649	3750	2899	1154	2.51
081271-18-7-2	3075	2654	2488	0.1119	3.6875	8040	3548	4492	1077	4.17
					9.6875	6317	3839	2478	1175	2.11
081271-18-7-3	2563	2593	2488	0.1119	3.6875	8056	3546	4510	1074	4.20
					9.6875	6354	3828	2526	1170	2.16
070871-12-7-1	1192	1071	2488	0.1119	3.6250	7139	2726	4413	1118	3.95
					9.6250	4453	2828	1625	1299	1.25
070871-12-7-2	1228	1206	2488	0.1119	3.6250	7221	2729	4492	1115	4.03
					9.6250	4882	2860	2022	1267	1.60
070871-12-7-3	1246	1264	2488	0.1119	3.6250	7083	2730	4353	1123	3.88
					9.6250	4497	2867	1670	1298	1.29

*Units: Btu/hr-ft^2-°F

The convective heat fluxes obtained in this manner are higher than those obtained in Tables VIII-9 through VIII-15 except for methanol whose values are 7 to 10 percent lower. In most cases the convective heat flux decreases as the burner size decreases. Correspondingly, there is an increase in the temperature difference between flame and probe. One cannot entirely attribute these effects to the decrease in the mass burning rate per unit area, since an examination of these data in Chapter VI indicates that the convective heat flux is not a strong function of this variable. If one assumes that free convection is the dominant mode of heat transfer, there is sufficient evidence to support this claim. As noted earlier in this chapter, the decrease in heat transfer coefficient with an increase in temperature difference is due to the lack of accurate flame temperature measurements at the point of interest. There are several runs where exceedingly high heat transfer coefficients resulted. For run numbers 090171-24-1-2, 083071-24-3-2, and 083171-24-4-1, the probe possibly was free of soot which changes the emittance of the probe surface, so the calculated convective flux and heat transfer coefficients would be too high. For benzene runs 090171-24-2-1, 2 and 3, the most probable cause of the high heat transfer coefficients is the low flame temperature, but no explanation can be given for the high convective flux. The high convective heat transfer coefficients for Jet A and JP-4 are probably due to the flame temperature measurements.

Local Nusselt and Rayleigh numbers were computed for the data in Tables VIII-30 through VIII-36, using the distance along the probe as the characteristic dimension. These results are presented in Figure VIII-10. It can be seen that considerable scatter in the data occurs and that to attempt a general correlation would be futile, but still useful information can be obtained. According to Equation III-51, the free convection Nusselt number is expressed as

$$Nu = C_1 (Ra)^{n_1} \qquad \text{(VIII-2)}$$

If one applies this equation to each fuel the values of C_1 and n_1 obtained are shown in Table VIII-37. Now divide the data of Figure VIII-10 into two parts, one having Nusselt numbers 10 to 35 for the lower Rayleigh numbers and 50 to 130 for the higher Rayleigh numbers, and two corresponding to Nusselt numbers from 35 to 90 and 130 to 420 for the low and high Rayleigh numbers, respectively. This division roughly corresponds to separating the higher heat transfer coefficient data from the lower values. These data were fitted to Equation VIII-2 and the resulting values of C_1 and n_1 are shown in Table VIII-37.

The Rayleigh numbers obtained were less than $1.4(10^6)$ which is the laminar region for free convection. If one compares the coefficients of Table VIII-37 with the values given in Chapter III, it can be seen that the methanol value for C_1 is about three times larger than the value of 0.56 to

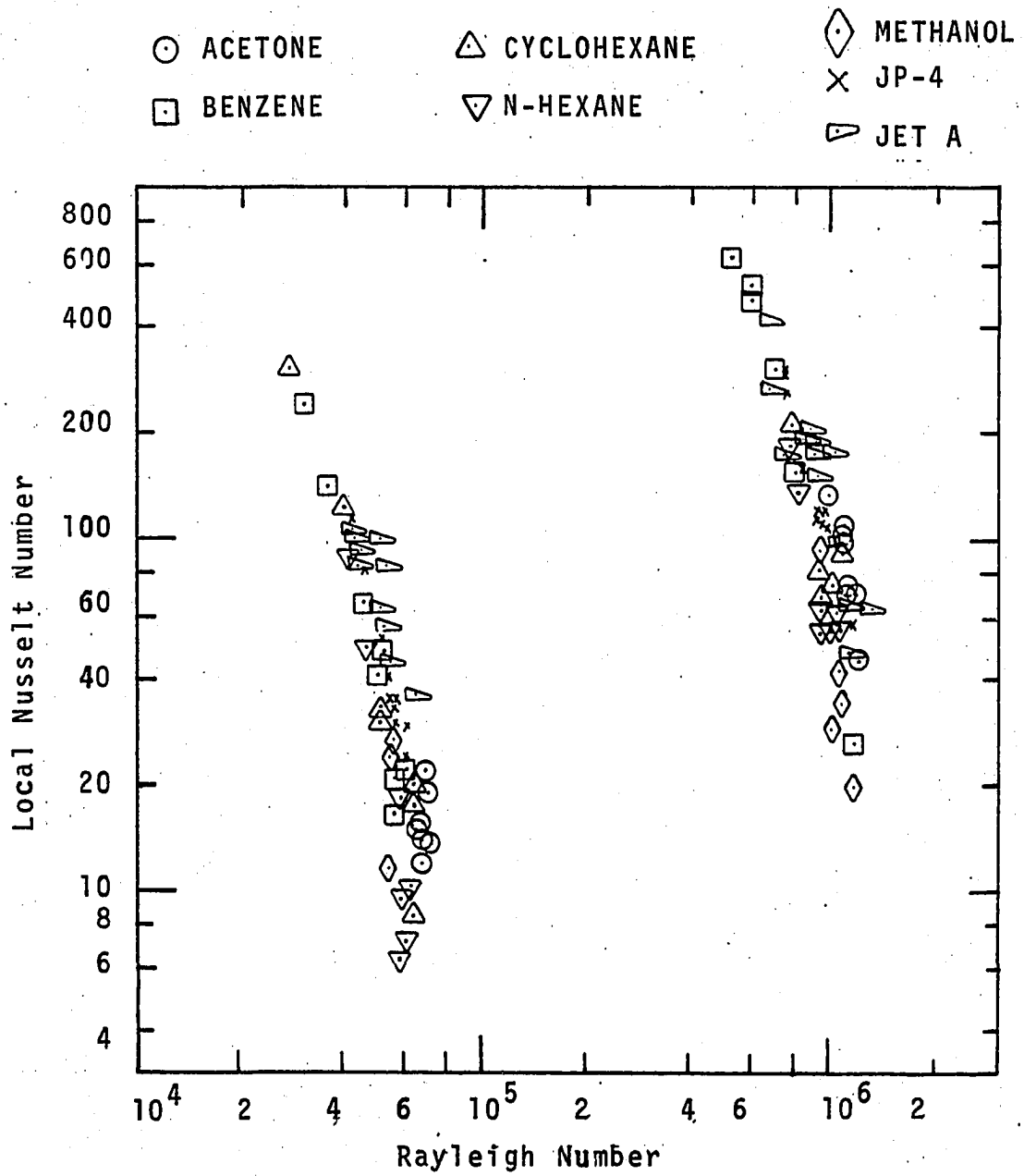


Figure VIII-10. Local Nusselt Number for Probe as a Function of Rayleigh Number.

TABLE VIII-37

COEFFICIENTS FOR FREE CONVECTION CORRELATION FOR FLAMES

Fuel	C_1	n_1
Acetone	0.026	0.576
Benzene	0.147	0.447
Cyclohexane	0.042	0.545
n-Hexane	0.041	0.534
Jet A	2.499	0.310
JP-4	0.327	0.414
Methanol	1.742	0.246
Mixed (Low Nu Number)	0.130	0.460
Mixed (High Nu Number)	0.738	0.403

0.59 while n_1 is essentially identical to 1/4. The coefficients for the remaining fuels are similar to the turbulent free convection values of C_1 = 0.02 to 0.13 and n_1 = 1/3 to 0.4, except for Jet A whose value of C_1 is much larger. Therefore for prediction purposes, one should use the turbulent free-convection coefficients for all fuels except those resembling alcohols, whose free-convection coefficients are for the laminar region.

Heat Transfer Results Using Temperature Data from Small Cylinder

The 3/4 inch diameter by 1 inch long stainless steel cylinder inserted in the flames near the probe top was intended to be a flame temperature sensing device. It is

obvious that to obtain the flame temperature from this data, the convective heat transfer coefficient is required. Considering the variation in these values, it was decided to compute the convective flux and heat transfer coefficient from the small cylinder temperature data for additional comparison purposes.

Using the values of q_∞ and β from Table VIII-1, and the equations from Chapter III, the heat fluxes for the side of the small cylinder were calculated and the results are given in Tables VIII-38 through VIII-44. The convective heat transfer coefficients are generally higher than those listed in Tables VIII-30 through VIII-36, especially for Jet A and JP-4. Nusselt and Rayleigh numbers were calculated for these data based on a 1 inch characteristic dimension and these values are plotted in Figure VIII-11. This figure shows the same type of scatter obtained in Figure VIII-10. This type of scatter cannot be entirely attributed to the flame temperatures and emission and extinction coefficient data, as radiometer 72804 was located in this region and the flame temperature should be representative of the optically measured values.

Earlier it was deduced that the Nusselt number was not a strong function of the mass burning rate per unit area. There is a tendency for the convective flux to be somewhat dependent on the mass burning rate alone. This result suggests that a mixed convection phenomena might occur, but until considerably more accurate flame temperature and radiation coefficient data are obtained, this occurrence cannot be predicted.

TABLE VIII-38

HEAT TRANSFER RESULTS FOR ACETONE USING TEMPERATURE DATA FROM SMALL CYLINDER

Run Number	T_c °F	q_e Btu/hr-ft^2	L in	q_r Btu/hr-ft^2	q_c Btu/hr-ft^2	T_f °F	T_f-T_c °F	h_c *
090171-24-1-1	1245	14485	12.22	7613	6872	2015	770	8.92
090171-24-1-2	1311	16861	13.22	8166	8695	2027	716	12.14
090171-24-1-3	1316	17052	11.48	7197	9855	2010	694	14.20
081271-18-1-1	1188	12643	11.12	6993	5650	1983	795	7.11
081271-18-1-2	1158	11747	10.42	6592	5155	1980	822	6.27
081271-18-1-3	1140	11233	10.78	6799	4434	1976	836	5.30
070771-12-1-1	1098	10099	7.38	4793	5306	1980	882	6.02
070771-12-1-2	1055	9029	6.28	4118	4911	1980	925	5.31
070771-12-1-3	985	7473	5.92	3894	3579	1980	995	3.60

*Units: Btu/hr-ft^2-°F.

TABLE VIII-39

HEAT TRANSFER RESULTS FOR BENZENE USING TEMPERATURE DATA FROM SMALL CYLINDER

Run Number	T_c °F	q_e Btu/hr-ft^2	L in	q_r Btu/hr-ft^2	q_c Btu/hr-ft^2	T_f °F	$T_f - T_c$ °F	h_c *
090171-24-2-1	1585	29977	15.00	22332	7645	1922	337	22.69
090171-24-2-2	1551	28032	13.28	20776	7256	1935	384	18.90
090171-24-2-3	1555	28256	13.28	20776	7480	1922	367	20.38
081171-18-2-1	1355	18600	8.62	15513	3087	1922	567	5.44
081171-18-2-2	1456	23099	10.08	17346	5753	1922	466	12.35
081171-18-2-3	1437	22196	10.78	18162	4034	1922	485	8.32
070671-12-2-1	1131	10982	7.52	14005	--	1922	791	--
070671-12-2-2	1291	16112	6.48	12471	3641	1922	631	5.77
070671-12-2-3	1079	9615	5.72	11278	--	1922	843	--

*Units: Btu/hr-ft^2-°F.

TABLE VIII-40

HEAT TRANSFER RESULTS FOR CYCLOHEXANE USING TEMPERATURE DATA FROM SMALL CYLINDER

Run Number	T_c °F	q_e Btu/hr-ft^2	L in	q_r Btu/hr-ft^2	q_c Btu/hr-ft^2	T_f °F	T_f-T_c °F	h_c *
083071-24-3-1	1320	17206	14.62	15037	2169	1955	635	3.42
083071-24-3-2	1348	18315	16.18	16146	2169	1935	587	3.70
083071-24-3-3	1375	19434	15.27	15508	3926	1928	553	7.10
081071-18-3-1	1275	15531	10.42	11648	3883	1976	701	5.53
081071-18-3-2	1286	15929	10.78	11963	3966	1986	700	5.67
081071-18-3-3	1375	19434	10.58	11789	7645	1989	614	12.45
070171-12-3-1	1245	14485	8.02	9414	5071	1935	690	7.35
070171-12-3-2	1224	13784	7.88	9276	4508	1935	711	6.34
070171-12-3-3	1256	14862	7.52	8918	5944	1935	679	8.75

*Units: Btu/hr-ft^2-°F.

TABLE VIII-41

HEAT TRANSFER RESULTS FOR N-HEXANE USING TEMPERATURE DATA FROM SMALL CYLINDER

Run Number	T_c °F	q_e Btu/hr-ft^2	L in	q_r Btu/hr-ft^2	q_c Btu/hr-ft^2	T_f °F	T_f-T_c °F	h_c *
083171-24-4-1	1331	17636	14.63	14656	2980	2008	677	4.40
083171-24-4-2	1330	17596	14.63	14656	2940	2005	675	4.36
083171-24-4-3	1334	17754	14.63	14656	3098	2006	672	4.61
081071-18-4-1	1263	15106	10.78	12057	3049	2075	812	3.75
081071-18-4-2	1295	16260	14.02	14287	1973	2123	828	2.38
081171-18-4-1	1270	15353	10.42	11778	3575	2121	851	4.20
070271-12-4-1	1111	10440	7.88	9610	830	2056	945	0.87
070271-12-4-2	1261	15036	10.12	11541	3495	2056	795	4.40
070271-12-4-3	1240	14315	9.62	11135	3180	2056	816	3.90

*Units: Btu/hr-ft^2-°F.

TABLE VIII-42

HEAT TRANSFER RESULTS FOR JET-A USING TEMPERATURE DATA FROM SMALL CYLINDER

Run Number	T_c °F	q_e Btu/hr-ft^2	L in	q_r Btu/hr-ft^2	q_c Btu/hr-ft^2	T_f °F	T_f-T_c °F	h_c *
083171-24-5-1	1504	25502	14.48	13785	11717	1866	362	32.37
041671-24-5-1	1513	25973	11.88	11581	14392	1866	353	40.77
041671-24-5-2	1578	29568	14.02	13403	16165	1866	288	56.13
041671-24-5-3	1472	23880	12.78	12357	11523	1866	394	29.24
080971-18-5-1	1140	11233	9.32	9303	1930	1850	710	2.72
042171-18-5-1	1403	20647	9.52	9485	11162	1850	447	24.97
042171-18-5-2	1376	19476	9.68	9630	9846	1850	474	20.77
042171-18-5-3	1346	18234	9.08	9084	9150	1850	504	18.15
070971-12-5-1	1234	14114	6.08	6255	7859	1850	616	12.76
042771-12-5-1	1287	15965	7.38	7501	8464	1850	563	15.03
042771-12-5-2	1272	15424	6.48	6642	8782	1850	578	15.19
042771-12-5-3	1343	18113	7.52	7633	10480	1850	507	20.67
042871-12-5-1	1353	18518	7.88	7972	10546	1850	497	21.22
042871-12-5-2	1152	11574	7.52	7633	3941	1850	698	5.65

*Units: Btu/hr-ft^2-°F.

TABLE VIII-43

HEAT TRANSFER RESULTS FOR JP-4 USING TEMPERATURE DATA FROM SMALL CYLINDER

Run Number	T_c °F	q_e Btu/hr-ft^2	L in	q_r Btu/hr-ft^2	q_c Btu/hr-ft^2	T_f °F	T_f-T_c °F	h_c *
083171-24-6-1	1440	22337	14.48	15738	6599	1920	480	13.75
041771-24-6-1	1440	22337	11.88	13518	8819	1920	480	18.37
041771-24-6-2	1465	23536	12.92	14433	9103	1920	455	20.01
041771-24-6-3	1436	22150	11.88	13518	8632	1920	484	17.83
081071-18-6-1	1281	15747	9.32	11103	4644	1935	654	7.10
042171-18-6-1	1348	18315	9.88	11652	6663	1935	587	11.35
042171-18-6-2	1378	19561	10.42	12170	7391	1935	557	13.27
042171-18-6-3	1359	18765	9.88	11652	7113	1935	576	12.35
062271-12-6-1	1337	17873	5.58	7119	10754	1935	598	17.98
042971-12-6-1	1317	17091	6.98	8678	8413	1935	618	13.61
042971-12-6-2	1313	16937	7.38	9108	7829	1935	622	12.59
042971-12-6-3	1301	16483	7.52	9257	7226	1935	634	11.40

*Units: Btu/hr-ft^2-°F.

TABLE VIII-44

HEAT TRANSFER RESULTS FOR METHANOL USING TEMPERATURE DATA FROM SMALL CYLINDER

Run Number	T_c °F	q_e Btu/hr-ft^2	L in	q_r Btu/hr-ft^2	q_c Btu/hr-ft^2	T_f °F	T_f-T_c °F	h_c *
082771-24-7-1	973	7228	11.48	3676	3552	2140	1167	3.04
083071-24-7-1	950	6775	11.32	3650	3125	2140	1190	2.62
083071-24-7-2	948	6736	11.32	3650	3086	2140	1192	2.59
0830 1-24-7-3	959	6949	11.32	3650	3299	2140	1181	2.79
081271-18-7-1	961	6989	8.28	3070	3919	2140	1179	3.32
081271-18-7-2	933	6454	8.62	3145	3309	2140	1207	2.74
081271-18-7-3	958	6930	8.62	3145	3785	2140	1182	3.20
070871-12-7-1	593	2107	5.38	2299	--	2140	--	--
070871-12-7-2	717	3289	5.38	2299	990	2140	1423	0.70
070871-12-7-3	655	2649	5.38	2299	350	2140	1485	0.24

*Units: Btu/hr-ft^2-°F.

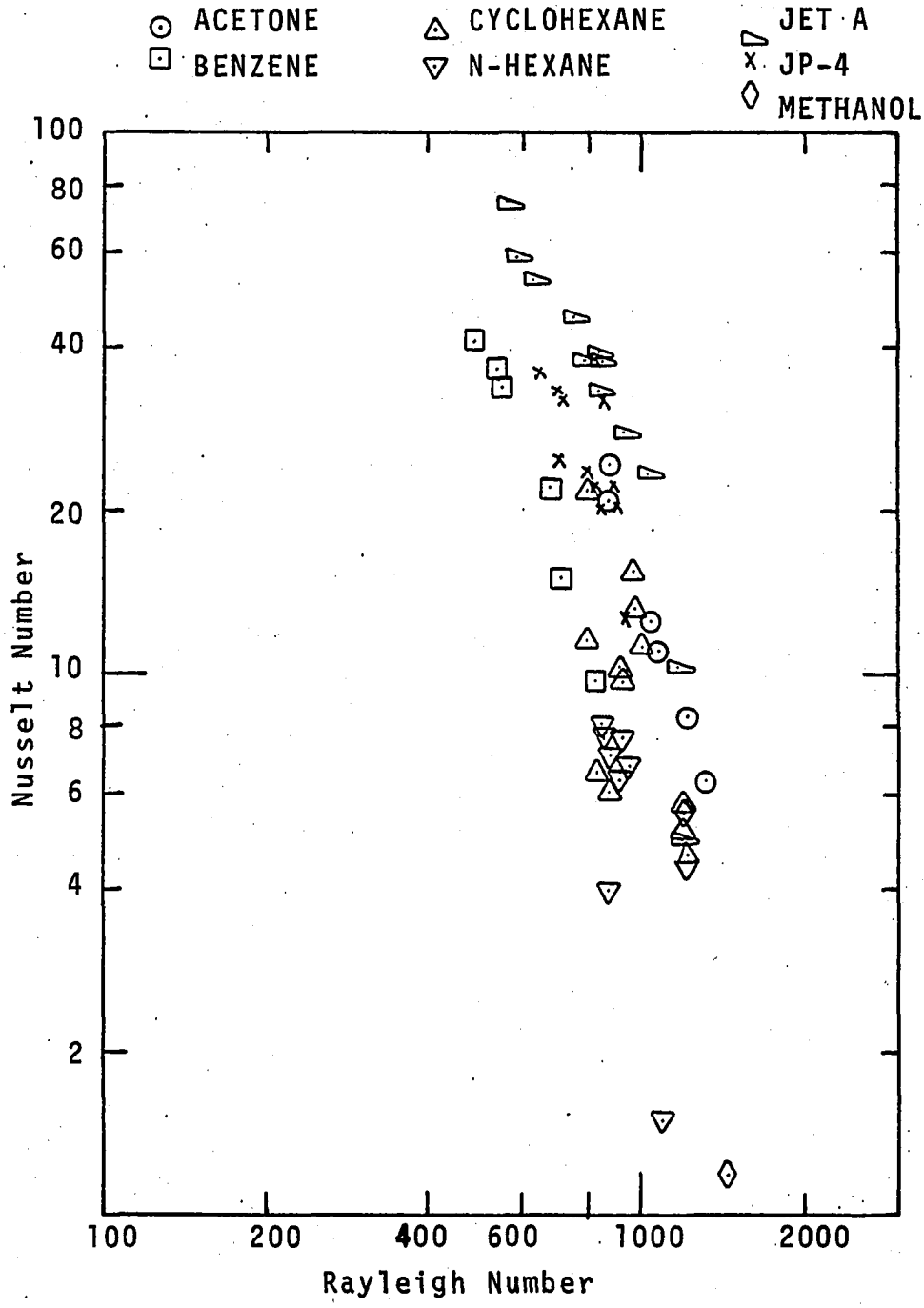


Figure VIII-11. Nusselt Number for Small Cylinder as a Function of Rayleigh Number.

CHAPTER IX

CONCLUSIONS AND RECOMMENDATIONS

Conclusions

In this study it was seen that natural flames from liquid fuels consist of a pulsating series of necks and bulges that constantly changes size and shape. Time averaged-photographs revealed shapes varying from conical to cylindrical. The flame height was taken as the maximum visible height on the time-averaged photographs. For single component fuels this height was found to be a function of .6 power of the Froude number, based on the equivalent diameter of the burner and the fuel vapor density. A simple multiplying factor that accounts for the volumetric combustion air allows the data to be correlated with a single equation. The lack of appropriate vapor density and volumetric combustion air for mixed fuels prevented the data on Jet A and JP-4 from being included. It appears that the air requirements are similar to n-Hexane and Cyclohexane.

One purpose of this study was to obtain measurements uneffected by soot deposits. It was found that soot will accumulate on surfaces with temperatures as high as 1500°F.

This soot was light and powdery and could easily be removed from the probe. It was observed that as a flame was being extinguished a condition was reached where all the soot was burned off the probe. This condition could be duplicated with flames from a sand-filled burner pan or with a very low fuel level in the pan.

The fuel burning rates could not be used to predict unknown convective heat transfer from the flame to the fuel, because it was shown that the heat supplied to the fuel is a function of many individual terms. Calculated values of the radiant heat from the flame to the fuel and the heat supplied from the bottom of the hot fuel pan each exceed the measured amount of heat required to vaporize the fuel. A zone of fuel vapors was noticed above the burner, and this zone could absorb a considerable amount of the radiant energy from the flame. Part of the radiative flux could also be reflected from the fuel surface. The high heat transfer from the bottom of the fuel pan indicates that the assumption of a fuel pan temperature equivalent to the fuel boiling point is erroneous. The fuel pan was still too hot to touch several minutes after the flame was extinguished, so the heat transfer coefficient correlation is another possible error source. These calculations have shown that the fuel pan temperature and the freeboard height are important variables for determining the fuel burning rate. Heat losses from the pan to the air were shown to be small in comparison to the other heat transfer rates and can be neglected.

Flame temperatures obtained with an optical pyrometer are in reasonable agreement with existing data. No appreciable variation in temperature was noted with the different burner sizes.

Flame emission and extinction coefficient data were obtained from narrow-angle radiometer measurements. These coefficients resulted in excessive calculated radiative fluxes, for both cylindrical and conical shaped flames. The emission and extinction coefficient data of Tsai, Neill, and Pfenning were also used. Tsai and Pfenning's coefficients resulted in optically thick flames. Neill's values resulted in high calculated radiative flux values.

The flames were now assumed to be cylindrical and mean beam lengths were computed from the calculated external radiative flux. These lengths agreed well with existing prediction methods. The mean beam lengths were used with the measured radiative flux data from a wide angle radiometer to compute new values for the emission and extinction coefficients. These calculations revealed that emission and extinctions coefficients need to be treated as sets instead of unique values and that two to three sets of coefficients can be obtained for flames from the same fuel. Convective heat fluxes obtained with these data are in reasonable agreement with existing data. Convective coefficients calculated with these data show considerable scatter and even decrease with increasing temperature difference. This observation can be attributed to the temperature

variations inside the flame that cannot be determined from external optical temperature measurements. The convective heat transfer coefficients obtained are several orders of magnitude higher than values predicted from existing correlations for gases. It was not possible to obtain a general correlation for the heat transfer coefficient, and considering the accuracy of the flame temperature measurements, one should use the convective fluxes for heat transfer calculations.

Temperature data from a small cylinder suspended in the flame was also used to obtain convective heat fluxes and heat transfer coefficients. These data also show the same type of scatter obtained with the probe data. Temperature inaccuracies alone cannot explain the results obtained and mixed convection, instead of free convection, may be the heat transfer mechanism. Extremely accurate data would be needed to verify this effect.

From the results of this study, one can conclude that more research needs to be conducted, as will be discussed in the next section. For present heat transfer predictions the mean beam length approach gives results whose accuracy compares favorably with the more detailed integrations methods. The heat transfer to small targets inside large flames was found to be somewhat insensitive to the flame shape, but targets external to the flame are more dependent on the size and shape of the flame.

Recommendations

Additional research on natural flames should include the following:

1. Optical properties of the fuel and its vapor should be determined.
2. Temperatures of the fuel and burner should be measured for different fuel levels.
3. The air flow into the flame should be measured at a number of locations around the flame perimeter.
4. The temperature distribution inside the flame, especially near the fuel pan, should be determined.
5. The composition of the flame should be measured at several locations, which will require development of sampling techniques.
6. Flame size measurement techniques should be studied.
7. The radiative heat flux back to the fuel should be thoroughly measured and compared with existing computations methods.
8. The variation of emission and extinction coefficients within a flame should be determined.
9. Criteria should be developed for describing the turbulence of a flame.
10. The variation of flame properties with burner shape should be investigated.

It is imperative that larger size flames be studied. The sizes used in this study appear to be in a transitional region.

Cylindrical burners are ideal for a number of these studies, but channel burners are better suited for heat transfer studies due to the simplified geometry. A vertical heat transfer surface containing numerous radiometers and temperature sensors could be placed adjacent to the burner. The surface should be cooled to eliminate emittance problems. A data acquisition system is necessary to handle the larger amount of data. Extra care should be taken to obtain the most accurate data as small errors in measurement can lead to large errors in results especially in determining emission and extinction coefficients.

NOMENCLATURE

a	constant or integration limit
a_1	constant
a_2	constant
a_3	constant
a_4	constant
A	area of volume element, ft^2
A_g	surface area of gas, ft^2
A_p	probe surface area, ft^2
A_s	fuel pan cross-sectional area, in^2
A_T	fuel tank cross-sectional area, in^2
b	integration limit
B	fluid volumetric coefficient of expansion, $°F^{-1}$
B_a	air volumetric coefficient of expansion, $°F^{-1}$
B_E	Emmons' heat ratio
B_s	Spalding's transfer number
C	speed of light, ft/hr
C_{CO_2}	pressure correction for carbon dioxide
C_f	mole fraction of fuel
C_{fs}	stoichiometric mole fraction of fuel
C_{H_2O}	pressure correction for water vapor

C_p specific heat of fluid, Btu/lbm-°F

C_{pa} specific heat of air, Btu/lbm-°F

C_{pg} specific heat of fuel gas, Btu/lbm-°F

C_{pl} liquid fuel specific heat, Btu/lbm-°F

C_{po} specific heat of fuel pan, Btu/lbm-°F

C_s soot volume concentration

$\overline{C_s}$ mean concentration of soot at flame temperature, mg/l

C_w specific heat of water, Btu/lbm-°F

C_0 speed of light in a vacuum, ft/hr

C_1 constant

C_2 second Planck constant

d burner diameter, mm

d_p particle diameter, ft

D burner diameter, ft

D_c cylinder diameter, ft

D_e burner equivalent diameter, ft

D_f flame diameter, in

D_l fuel line diameter, in

D_T fuel tank diameter

$\overline{D}$ diffusivity, ft^2/hr

$\overline{D}_m$ diffusion coefficient cm^2/sec

E_a radiant energy change within a volume element, Btu

E_c radiant energy leaving a volume element, Btu

E_e radiant energy emitted in a volume element, Btu

E_i radiant energy entering a volume element, Btu

E_s radiant energy scattered into a volume element, Btu

E_x fraction of excess air

$f(u_i)$ function f(x) evaluated at x_i

f(x) arbitrary function

$f(x_i)$ function f(x) evaluated at x_i

$f(\lambda)$ function representing the absorption coefficient, soot concentration, and possibly the particle size distribution function of a flame

F configuration factor

$F_{t \to f}$ configuration factor between target and flame

g acceleration of gravity, ft/hr^2

Gr Grashof Number

$(Gr)_x$ local Grashof number based on a distance x

h convective heat transfer coefficient, $Btu/hr\text{-}ft^2\text{-}°F$

h_a air enthalpy, Btu/lbm

h_{ab} air enthalpy at temperature of fuel boiling point, Btu/lbm

h_l liquid fuel enthalpy, Btu/lbm

h_{lb} liquid fuel enthalpy at its boiling point, Btu/lbm

h_p Planck's constant

H height of flame, ft

H_b height of fuel rod above elevation of pan bottom, in

H_c net heating value of fuel, Btu/lbm

ΔH_c molar heat of combustion at 25°C, kcal/mole

H_E height of flame required to entrain a certain fraction of excess air, ft

H_m height of flame, cm

H_p depth of fuel in pan, in

H_R height of fuel rod above top of fuel tank, in

H_T height of fuel in tank above elevation of pan bottom at any time t_m, in

H_v fuel heat of vaporization, Btu/lbm

H_{ve} effective fuel heat of vaporization, Btu/lbm

H_z height of combustion zone, ft

H_1 height of target above burner, in

H_2 height of flame, in

i index

$I_{b,\lambda}(T)$ monochromatic intensity of a blackbody, Btu/hr-ft^2-micron-steradian

I_λ monochromatic intensity, Btu/hr-ft^2-micron-steradian

j index when used as a subscript

j_λ, j_γ monochromatic volume emission coefficient, Btu/ft^3-hr-micron-steradian

J mean effective volume emission coefficient, Btu/ft^3-hr-steradian

J_λ, J_γ effective monochromatic volume emission coefficient, Btu/ft^3-hr-micron-steradian

k Boltzman's constant

k index when used as a subscript

k_e entrainment coefficient, dimensionless

k_1 constant

k_2 constant

K	fluid thermal conductivity, Btu/hr-ft^2-°F
K_a	air thermal conductivity, Btu-ft/hr-ft^2-°F
K_r	conduction coefficient at rim of vessel supporting the flame, Btu-ft/hr-ft^2-°F
L	total path length through flame, inches
L_a	average mean beam length, ft, in
L_b	mean beam length, ft
$L_{b,o}$	mean beam length for an optically thin gas, ft, in
L_c	length of a cylinder, ft
L_e	effective thickness of a cloud of particles, ft/ft (sum of the particle thickness per unit thickness)
L_l	length of fuel line, ft
m	constant
m_{O_2a}	mass concentration of oxygen in air
m_l	number of absorption and emission data points
M	fuel molecular wt
M_l	fuel burning rate, lbm/hr
M_m	fuel burning rate, gm/sec
M_n	mass transfer number
M_s	fuel burning rate per unit surface area, lbm/ft^2-hr
n	refractive index of medium
nC	number of carbon atoms
nH	number of hydrogen atoms
n_1	constant
n_2	number of points in Gauss quadrature
n_3	constant

N_{co} Steward's combustion number

Nu Nesselt number

$(Nu)_D$ Nusselt number based on cylinder diameter

P exponent

$p_\nu(\vec{s}', \vec{s})$ scattering or phase function

Pr Prandtl number

q_c convective heat flux from flame to probe, Btu/hr-ft^2

q_e radiative flux emitted by probe, Btu/hr-ft^2

q_f radiative flux leaving flame, Btu/hr-ft^2

$q_{f,\lambda}$ monochromatic radiant flux from flame, Btu/hr-ft^2-micron

q_m radiative flux measured by radiometer, Btu/hr-ft^2

q_r radiative flux from flame to probe, Btu/hr-ft^2

q_t radiant heat flux received by target from flame, Btu/hr-ft^2

q_w flux removed by water, Btu/hr-ft^2

q_λ, q_ν monochromatic radiant heat flux, Btu/hr-ft^2-micron

q_∞ radiant heat flux from an infinite size flame, Btu/hr-ft^2

Q heat liberation due to combustion, Btu/hr

Q_{ab} convective heat transferred from pan bottom to air, Btu/hr

Q_{as} convective heat transferred from pan side to air, Btu/hr

Q_b heat transferred to fuel, Btu/hr

Q_c convective heat transferred from flame to fuel, Btu/hr

Q_{cD} convective heat transferred from air to pan, Btu/hr

Q_g volume flow rate of fuel gas, ft^3/hr

Q_{ic} convective heat transferred from flame to pan center, Btu/hr

Q_{ir} radiant heat transferred from flame to pan center, Btu/hr

Q_l sensible heat gain by fuel, Btu/hr

Q_{lb} convective heat transferred from pan bottom to fuel, Btu/hr

Q_{li} convective heat transferred from pan center to fuel, Btu/hr

Q_{lp} radiant heat transferred from probe to fuel, Btu/hr

Q_{ls} convective heat transferred from pan side to fuel, Btu/hr

Q_o heat loss from fuel to pan bottom, Btu/hr

Q_r radiant heat transferred from flame to fuel, Btu/hr

Q_{sc} convective heat transferred from flame to pan side, Btu/hr

Q_{sr} radiant heat transferred from flame to pan side, Btu/hr

Q_{sp} radiant heat transferred from probe to pan side, Btu/hr

r mass of oxygen required for combustion of a unit mass of fuel, lbm/lbm

r_v	volume of air required for combustion of a unit volume of fuel, ft^3/ft^3
R	radius, ft
Ra	Rayleigh number
$(Ra)_D$	Rayleigh number based on the diameter of a cylinder
Re	Reynolds number
R_r	radius of burner, ft
R_1	radius of probe, in
R_2	radius of flame at burner, in
R_3	radius of conical flame at H_1, in
R_4	horizontal distances from flame center to a target, in
s	path length, inches
$\vec{s}$	unit vector in the direction of motion
s_a	path length from external target to flame, in
t	time, hr
t_m	time, minutes
T	temperature of medium, °F
ΔT	temperature difference between fluid and surface, °F
T_a	air temperature, °F
T_{ak}	air temperature, °K
T_{aR}	air temperature, °R
T_b	fuel surface temperature, °R
T_c	cylinder flame temperature, °F
T_f	flame temperature, °F, °R

T_{fc} flame temperature, °C

T_l fuel temperature, °F

T_m fuel boiling point temperature, °F

ΔT_o fuel pan temperature rise, °F

T_p probe surface temperature, °F, °R

T_s fuel surface temperature, °F

T_{wi} water temperature entering probe, °F

T_{wo} water temperature leaving probe, °F

u_i variable defined by Equation VII-10

U overall coefficient of heat transfer, Btu/hr-ft^2-°F

U_R convection coefficient at rim of vessel supporting combustion, Btu/hr-ft^2-°F

v linear fuel burning rate, ft/min

$\vec{v}$ velocity vector, ft/hr

v_c linear fuel burning rate corrected for pan heating, ft/hr

v_l linear fuel burning rate, mm/min

v_x local component of velocity in x direction, ft/hr

v_y local component of velocity in y direction, ft/hr

v_z local component of velocity in z direction, ft/hr

v_∞ linear burning rate for an infinite flame size, ft/min, cm/min

V velocity of fluid, ft/hr

V_g gas volume, ft^3

V_p volume fraction of particles in a flame

w_i weight factor for Gaussian integration of moments

w_l mass of fuel, lbm

w_o mass of fuel pan, lbm

W mass flow rate of water through probe, lbm/hr

x characteristic surface dimension, ft

x_i abscissa for Gaussian integration of moments

X $k_1 V_p L T_f/C_2$

Δz fuel pan level change, ft

z_g height of fuel in tank above floor, in

z_p height of fuel in pan above floor, in

GREEK

α thermal diffusivity, ft^2/hr

α_a thermal diffusivity of air, ft^2/hr

$\alpha_{f,\lambda}$ monochromatic flame absorptance

α_r absorption coefficient, ft^{-1}

β mean extinction coefficient, in^{-1}

β_s extinction coefficient for soot particles, in^{-1}

$\beta_{\lambda,\nu}$ monochromatic extinction coefficient, in^{-1}

ν vertical direction angle, radians

γ_a vertical direction angle from target to lower edge of flame side, radians

γ_b vertical direction angle from target to upper edge of flame side, radians

δ stagnant film thickness, ft

$\Delta\varepsilon$ correction factor to account for the spectral overlap of the carbon dioxide water absorption bands

ε_{CO_2} emittance due to carbon dioxide

ε_f total emittance of a luminous flame

$\varepsilon_{f,\lambda}$ monochromatic emittance of a flame

ε_g total non-luminous flame emittance

ε_{H_2O} emittance due to water vapor

$\varepsilon_{l,\lambda}$ monochromatic emittance of a luminous flame

ε_p emittance of probe surface

ε_s total emittance of soot particles

$\varepsilon_{s,\lambda}$ monochromatic emittance of a cloud of soot particles

θ angle between surface normal and direction of intensity vector, radians

κ mean absorption coefficient, in^{-1}

$\kappa_{a,\lambda}$ monochromatic absorption coefficient of atmosphere, in^{-1}

$\kappa_{g,\lambda}$ monochromatic absorption coefficient of non-luminous flames, in^{-1}

κ_p Planck mean absorption coefficient, in^{-1}

κ_R Rosseland mean absorption coefficient, in^{-1}

$\kappa_\lambda, \kappa_\nu$ monochromatic absorption coefficient, in^{-1}

λ wavelength, ft^{-1}

μ absolute viscosity of fluid, lbm/ft-hr

μ_a absolute viscosity of air, lbm/ft-hr

ν frequency, hr^{-1}

ρ density of fluid, lbm/ft^3

ρ_a density of air, lbm/ft^3

ρ_g density of cold fuel gas, lbm/ft^3

ρ_l density of liquid fuel, lbm/ft^3

ρ_p reflectance of probe surface

ρ_s reflectivity of fuel surface

ρ_v density of fuel vapor at boiling point, lbm/ft^3

σ Stefan-Boltzman constant, $\dot{1}1714(10^{-8})$ $Btu/hr\text{-}ft^2\text{-}°R^4$

σ_s scattering coefficient for soot particles, in^{-1}

$\sigma_\lambda, \sigma_\nu$ monochromatic scattering coefficient

$\tau_{a,\lambda}$ monochromatic absorption coefficient of atmosphere

τ_λ monochromatic optical thickness

ϕ horizontal direction angle, radians

ϕ_2 maximum horizontal direction angle between a flame and external target, radians

ω inverse coefficient of volumetric expansion due to combustion

Ω, Ω' solid angle, steradians

REFERENCES

1. Abramowitz, M., and Stegun, I. A. (Editors). Handbook of Mathemathematical Functions, National Bureau of Standards, Applied Mathematics Series No. 55, Washington (June, 1964).

2. Agoston, G. A. "Controlling Mechanisms in the Burning of Pools of Liquid Fueld," Combustion and Flame 6 212-214 (Sept. 1962)

3. Akita, K., and Yumoto, T. "Heat Transfer in Small Pools and Rates of Burning of Liquid Methanol." Tenth Symposium (International) on Combustion, 943-948, The Combustion Institute, Pittsburgh (1965).

4. Arthur, J. R., and Napier, D. H. "Formation of Carbon and Related Materials in Diffusion Flames." Fifth Symposium (International) on Combustion, 303-315, Reinhold Publishing Corp., New York (1955).

5. Atallah, S. "Flame Heights and Burning Rates of Liquid Fuels in Open Trays," Combustion and Flame 9, 203-205 (June, 1965).

6. Atallah, S., and Allan, D. S. "Safe Separation Distances from Liquid Fuel Fires," Fire Technology 1, 47-56 (1971).

7. Bader, B. E. "Heat Transfer in Liquid Hydrocarbon Fuel Fires." Proceedings, International Symposium for Packaging and Transportation of Radioactive Materials, sponsored by Sandia Corp. and U.S. Atomic Energy Commission, SC-R-R-P. 79-106 , 65-98, Albuquerque, New Mexico (Jan. 12-15, 1965):79-106.

8. Bayley, F. J. "An Analysis of Turbulent Free-Convection Heat Transfer." Proceedings of the Institution of Mechanical Engineers, 169, No. 20, 361 (1955).

9. Behrene, H. "Flame Instabilities and Combustion Mechanism." Fourth Symposium on Combustion, 538-545, The Williams and Wilkins Co., Baltimore (1953).

10. Bird., R. B., Stewart, W. E., and Lightfoot, E. L. Transport Phenomena, John Wiley & Sons, Inc., New York (1960).

11. Blackshear, Jr., P. L., and Murty, K. A. "Some Effects of Size, Orientation and Fuel Molecular Weight on the Burning of Fuel-Soaked Wicks." Eleventh Symposium (International) on Combustion, p. 545-552, The Combustion Institute, Pittsburgh (1967).

12. Blinov, V. I. and Khudyakov, G. N. "Certain Laws Governing Diffusion Burning of Liquids." Dokl. Akad. Nauk. SSSR. 113, 1094-1098 (1957). English Translation--Proceedings of the Academy of Sciences of the U.S.S.R. Physical Chemistry Section 113, 241 (1957).

13. Burgess, D., and Grumer, J. "Comments on The Burning Rate of Liquid Fuels from Open Trays by Natural Convection, by D. B. Spalding," Fire Research Abstracts and Reviews 4, 236-238 (1962).

14. Burgess, D. S., Grumer, J., and Wolfhard, H. G. "Burning of Liquid Fuels in Large and Small Open Trays." International Symposium on the Use of Models in Fire Research, W. G. Berl, (editor), pp. 68-75, National Academy of Science-National Research Council, Publication 786, Washington (1961).

15. Burgess, D. S., Strasser, A., and Grumer, J. "Diffusive Burning of Liquids in Open Trays." Fire Research Abstracts and Reviews, 3, No. 3, 177-192 (1961).

16. Canfield, J. "Radiative Heat Flux from Flames: A Comparison of Predicted and Experimental Values." Unpublished special problem submitted to the Department of Engineering Physics, University of Oklahoma (1968).

17. Cheesewright, R. "Turbulent Natural Convection from a Vertical Plane Surface." Trans. ASME Ser. C., J. Heat Transfer 90, No. 1, 1-8 (Feb., 1968).

18. Copley, J. A. "An Analytical Method for Predicting the Temperature-Time History of a Hollow Cylinder Enveloped in Flames." Technical Report No. 2073, U.S. Naval Weapons Laboratory, Dahlgren, Virginia (Dec. 9, 1966) AD 804 084.

19. Corlett, R. C. "Gas Fires with Pool-Like Boundary Conditions." Combustion and Flame 12, 19-32 (1968).

20. Corlett, R. C. "Gas Fires with Pool-Like Boundary Conditions: Further Results and Interpretation." Combustion and Flame 14, 351-360 (1970).

21. Corlett, R. C., and Fu, T. M. "Some Recent Experiments with Pool Fires." Pyrodynamics 4, 253-269, (1966).

22. Crane Co. Engineering Division. "Flow of Fluids Through Valves, Fittings and Pipe." Technical Paper No. 410, Crane Co., Chicago (1957).

23. Davies, R. A., and Scully, D. B. "Carbon Formation from Aromatic Hydrocarbons II." Combustion and Flame 10, 165-170, (June, 1966).

24. Deshpande, V.A. "Heat Transfer and Burning Rates of Liquid Fueled Fires." Master's Thesis, University of Oklahoma (1968).

25. Eckert, E. R. G., and Jackson, T. W. "Analysis of Turbulent Free-Convection Boundary Layer on Flat Plate." NACA TN 2207 (1950).

26. Edwards, D. K., and Menard, W. A. "Comparison of Models for Correlations of Total Band Absprption." Applied Optics 3, 621-625 (1964).

27. Emmons, H. W. "Some Observations on Pool Burning." International Symposium on the Use of Models in Fire Research, W. G. Berl, (editor), p. 50-67, National Academy of Sciences-National Research Council, Publication 786, Washington (1961).

28. Fenimore, C. P., Jones, G. W., and Moore, G. E. "Carbon Formation in Quenched Flat Flames at 1600°F." Sixth International Symposium on Combustion, 242-246, Reinhold Publishing Corp., New York (1957).

29. Fons, W. L. "Rate of Combustion from Free Surfaces of Liquid Hydrocarbons." Combustion and Flame 5, 283-287 (Sept., 1961).

30. Gaydon, A. G., and Wolfard, H. G. Flames, Their Structure, Radiation and Temperature, 3rd Ed. Revised, Chapman and Hall Ltd., London (1970).

31. Gordon, W., and McMillan, R. D. "Temperature Distribution Within Aircraft-Fuel Fires." Fire Technology, 1, No. 1, 52-61, Feb., 1965.

32. Gordon, A. S., Smith, S. R., and McNesby, J. R. "Study of the Chemistry of Diffusion Flames." Seventh Symposium (International) on Combustion, 317-324, Butterworths Scientific Publications, London (1959).

33. Hood, J. D. "A Method for the Determination of the Radiative Properties of Flames." Ph.D. Thesis, University of Oklahoma (1966).

34. Hottel, H. C. "Radiant-Heat Transmission" in McAdams, W. H., Heat Transmission, 3rd Ed., McGraw-Hill, New York, p. 55-125, (1954).

35. Hottel, H. C. "Review of Certain Laws Governing Diffusive Burning of Liquids by V. I. Blinov and G. N. Khudyakov." Fire Research Abstracts and Reviews 1, 41-44, (Sept., 1958).

36. Hottel, H. C., and Sarofim, A. F. Radiative Transfer, McGraw-Hill, New York, (1967).

37. Howarth, C. R., Foster, P. J., and Thring, M. W. "The Effect of Temperature on the Extinction of Radiation by Soot Particles." Proceedings of the Third International Heat Transfer Conference, Vol. V, The American Institute of Chemical Engineers, New York (1966), p. 122-128.

38. Huffman, K. G. "The Interaction and Merging of Flames from Burning Liquids." Ph.D. Dissertation, The University of Oklahoma (1967).

39. Kilham, J. K. "Energy Transfer from Flame Gases." Third Symposium on Combustion Flame and Explosion Phenomena, p. 733-740, The Williams and Wilkins Co., Baltimore (1949).

40. Law, M. "Structural Fire Protection in the Process Industry." Building, 86-90 (July 18, 1969).

41. Lewis, B., and Von Elbe, G. Combustion, Flames and Explosions of Gases, New York, Academic Press (1961).

42. Love, T. J. Radiative Heat Transfer, Charles E. Merrill Publishing Co., Columbus, Ohio (1968).

43. Lowes, T. M., and Newall, A. J. "The Emissivities of Flame Soot Dispersions." Combustion and Flame 16, 191-194 (1971).

44. Magnus, G. "Tests on Combustion Velocity of Liquid Fuels and Temperature Distribution in Flames and Beneath Surface of the Burning Liquid." International Symposium on the Use of Models in Fire Research, W. G. Berl (editor), p. 76-92, National Academy of Sciences-National Research Council, Publication 786, Washington (1961).

45. Masliyah, J. H., and Steward, F. R. "Radiative Heat Transfer from a Turbulent Diffusion Buoyant Flame with Mixing Controlled Combustion." Combustion and Flame 13, 613-625 (Dec., 1969).

46. McAdams, W. H. Heat Transmission, McGraw-Hill, New York (1954).

47. Mody, P. J. and Lott, J. L. "Flame Temperatures and Equilibrium Compositions for Six Fuel-Air Systems." Internal Memorandum, Project 1454, University of Oklahoma Research Institute, (Dec., 1965).

48. Nagendra, H. R., Tirunaraganan, M. A., and Ramachandran, A., Trans. ASME Ser. C. J. Heat Transfer 92, No. 1, 191-194 (Feb., 1970).

49. Nakakuki, A. "Liquid Burning Rate in the Laminar Flame Region." Combustion and Flame 17, 449-451 (1971).

50. Neill, D. T. "Heat Transfer from Uncontrolled Buoyant Diffusion Flames." Ph.D. Dissertation, University of Oklahoma (1966).

51. Orloff, L., and DeRis, J. "A Dimensionless Correlation of Pool Burning Data." Combustion and Flame 18, 381-388 (1972).

52. Orloff, L., and DeRis, J. "Cellular and Turbulent Ceiling Fires." Combustion and Flame 18, 389-401 (1972).

53. Penner, S. S. Quantitative Molecular Spectroscopy and Gas Emissivities, Addison-Wesley Publishing Co., New York (1959).

54. Pfenning, D. B. "Radiative Transfer from Laminar Diffusion Flames." Ph.D. Dissertation, University of Oklahoma (1970).

55. Porter, G. "Carbon Formation in the Combustion Wave." Fourth Symposium on Combustion, 248-252, The Williams & Wilkins Co., Baltimore (1953).

56. Putnam, A. A., and Speich, C. F. "A Model Study of the Interaction of Multiple Turbulent Diffusion Flames." Ninth Symposium (International) on Combustion, 867-875, Academic Press, New York (1963).

57. Rasbash, D. J., Rogowski, Z. W. and Stark, W. V. "Properties of Fires of Liquids." Fuel 35, 94-107 (1956).

58. Sampson, D. H. Radiative Contributions to Energy and Momentum Transport in a Gas, New York, Interscience Publishers (1965).

59. Sato, T., and Matsumoto, R. "Radiant Heat Transfer from Luminous Flame." International Developments in Heat Transfer, Part IV, The American Society of Mechanical Engineers, New York (1961), p. 804-811.

60. Shahroki, F. "Numerical Technique for Calculation of Radiant Energy Flux to Targets from Flames." Ph.D. Dissertation, University of Oklahoma (1965).

61. Shimy, A. A. "Calculating Flammability Characteristics of Hydrocarbons and Alcohols." Fire Technology 6, 135-139 (1970).

62. Siddall, R. G., and McGrath, I. A. "The Emissivity of Luminous Flames." Ninth Symposium (International) on Combustion, W.G. Berl, e.d., Academic Press (1963) p. 102-110.

63. Siegel, R., and Howell, J. R. Thermal Radiation Heat Transfer, Vol. III, Radiation Transfer with Absorbing, Emitting and Scattering Media, NASA SP-164, Washington (1971).

64. Spalding, D. B. "The Combustion of Liquid Fuel." Fourth Symposium (International) on Combustion, 847-864, The Williams & Wilkins Co., Baltimore (1953).

65. Spalding, D. B. "The Burning Rate of Liquid Fuels from Open Trays by Natural Convection." Fire Research Abstracts and Reviews, 4, 234-236 (1962).

66. Sparrow, E. M., and Gregg, J. L. "Laminar-Free Convection Heat Transfer from the Outer Surface of a Vertical Circular Cylinder." Trans. ASME, 78, 1823-1829 (Nov., 1956).

67. Stehling, F. C., Frazee, J. D., and Anderson, R. C. "Mechanisms of Nucleation in Carbon Formation." Eighth Symposium (International) on Combustion, 774-784, The Williams and Wilkins Co., Baltimore (1962).

68. Steward, F. R. "Linear Flame Heights for Various Fuels." Combustion and Flame 8, 171-178, (Sept., 1964).

69. Steward, F. R. "Prediction of the Height of Turbulent Diffusion Buoyant Flames." Combustion Science and Technology 2, 203-212 (1970).

70. Tesner, P. A. "Formations of Dispersed Carbon by Thermal Decomposition of Hydrocarbons." Seventh Symposium (International) on Combustion, 546-553, Butterworths Scientific Publications, London (1959).

71. Thomas, A. "Carbon Formation in Flames." Combustion and Flame 6, 46-50, (March, 1962).

72. Thomas, P. H. "The Size of Flames from Natural Fires." Ninth Symposium (International) on Combustion, 844-859, Academic Press, New York (1963).

73. Thomas, P. H., Baldwin, R., and Heselden, A. J. M. "Buoyant Diffusion Flames: Some Measurements of Air Entrainment, Heat Transfer and Flame Merging." Tenth Symposium (International) on Combustion, p. I-5-1-I-5-13, The Combustion Institute, Pittsburgh (1965).

74. Thomas, P. H., Webster, C. T., and Raftery, M. M. "Some Experiments on Buoyant Diffusion Flames." Combustion and Flame 5, 359-367 (1961).

75. Thring, M. W., Foster, P. J., McGrath, I. A., and Ashton, J. S. "Prediction of the Emissivity of Hydrocarbon Flames." International Developments in Heat Transfer, Part IV, The American Society of Mechanical Engineers, New York, (1961), p. 796-803.

76. Thring, M. W., Beer, J. M., and Foster, P. J. "The Radiative Properties of Luminous Flames." Proceedings of the Third International Heat Transfer Conference, Vol. V. The American Institute of Chemical Engineers, New York (1966), p. 101-111.

77. Tien, C. L. "Thermal Radiation Properties of Gases." Advances in Heat Transfer, V5, 253-324, Academic Press, New York (1966) edited by T. F. Irvine, Jr., and J. P. Hartnett.

78. Tien, C. L., and Lowder, J. E. "A Correlation for Total Band Absorptance of Radiating Gases," International J. Heat and Mass Transfer 9, 698-701 (1966).

79. Tsai, W. "Radiative Transport Properties of Flames." Ph.D. Dissertation, University of Oklahoma (1968).

80. Welker, J. R. "The Effect of Wind on Uncontrolled Buoyant Diffusion Flames from Burning Liquids." Ph.D. Dissertation, University of Oklahoma (1965).

81. Welker, J. R., and Sliepcevich, C. M. "Heat Transfer by Direct Flame Contact Fire Tests--Phase I." Report No. UE-122-FR, Subcontract No. HM48-71-01, University Engineers, Inc., Norman, Oklahoma, (July, 1971).

82. Wohl, K., Gazley, D., and Kapp, N. "Diffusion Flames." Third Symposium on Combustion, Flames and Explosion Phenomena, 288-300, The Williams & Wilkins Co., Baltimore (1949).

83. Wood, B. D., Blackshear, P. L., and Eckert, E. R. G. "Mass Fire Model: An Experimental Study of the Heat Transfer to Liquid Fuel Burning from a Sand-Filled Pan Burner." Combustion Science and Technology, 4, 113-129 (1971).

84. Yagi, S., and Iino, H. "Radiation from Soot Particles in Luminous Flames." Eighth Symposium (International) on Combustion, The Williams and Wilkins Co., Baltimore, (1962), p. 288-293.

APPENDICES

APPENDIX A

DEVELOPMENT OF EQUATION OF TRANSFER

The principal quantity that describes a radiation field is the intensity. For an absorbing, emitting, and scattering medium, the intensity varies from point to point and also with direction through every point. Thus for a general radiation field,

$$I_\nu = I_\nu(\vec{r}, \vec{s}, t)$$

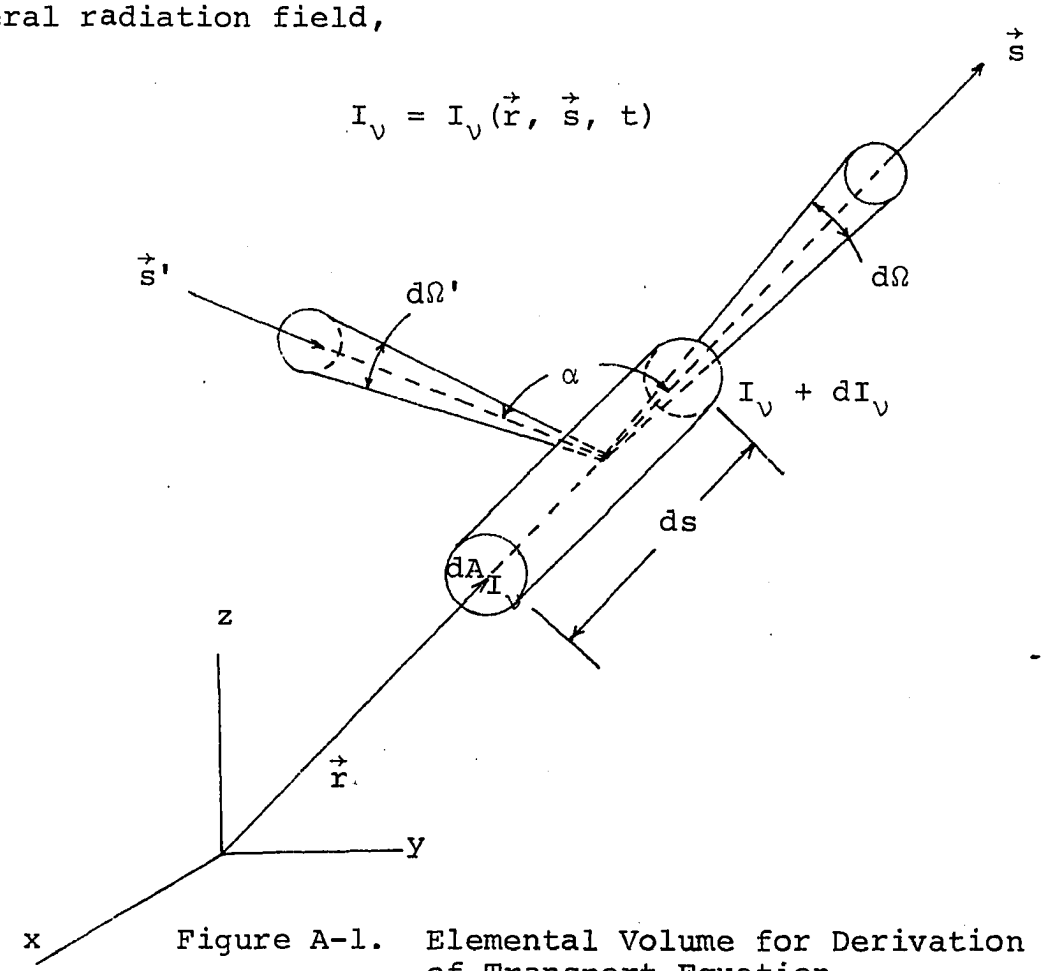


Figure A-1. Elemental Volume for Derivation of Transport Equation.

In deriving the equation of transfer, the Eulerian point of view is adopted. This approach involves writing a radiant energy balance about an elemental volume taken along a pencil of rays contained in a differential solid angle.

Consider a cylindrical volume element, Figure 1, with a cross sectional area dA and length ds in an absorbing, emitting, and scattering medium having an absorption coefficient κ_ν, a scattering coefficient σ_ν, and an emission coefficient j_ν. The axis of the cylinder coincides with the direction of a unit vector $\vec{s}$. I_ν is the spectral intensity in the $\vec{s}$ direction entering the cylinder and $I_\nu + dI_\nu$ is the spectral intensity leaving the cylinder.

From the definition of intensity, the energy entering the volume element across dA in the frequency interval $(\nu, \nu + d\nu)$, during a time dt, and contained within the solid angle $d\Omega$ is given by

$$E_i = I_\nu \, dA \, d\Omega \, d\nu \, dt \qquad \text{(A-1)}$$

The energy leaving the volume element is

$$E_o = (I_\nu + dI_\nu) \, dA \, d\Omega \, d\nu \, dt \qquad \text{(A-2)}$$

Part of this energy will be absorbed and scattered by the matter within the volume element and this loss of energy is

$$E_a = (\kappa_\nu + \sigma_\nu) \, I_\nu \, ds \, dA \, d\Omega \, d\nu \, dt \qquad \text{(A-3)}$$

During the time interval dt and frequency interval $(\nu, \nu + d\nu)$, the matter inside the volume elements emits energy into the solid angle $d\Omega$, and this emission is

$$E_e = j_\nu \, dA \, ds \, d\Omega \, d\nu \, dt \qquad \text{(A-4)}$$

The energy entering the volume element from the scattering of radiation from all other directions into the $\vec{s}$ direction is

$$E_s = \left(\frac{\sigma_\nu}{4\pi} \int_{\Omega'=4} p_\nu(\vec{s}',\vec{s}) \, I_\nu(\vec{s}') \, d\Omega' \right) dA \, ds \, d\Omega \, d\nu \, dt \qquad \text{(A-5)}$$

Here the function $p_\nu(\vec{s}',\vec{s})$ is called the scattering or phase function, and $I_\nu(\vec{s}')$ is the incident intensity contained within the solid angle $d\Omega'$ in the direction of a unit vector $\vec{s}'$. The scattering function, $p_\nu(\vec{s}',\vec{s})$ is defined so that $p_\nu(\vec{s}',\vec{s}) \, d\Omega'/4\pi$ represents the probability that an incoming pencil of rays $(s',d\Omega')$ will be scattered into direction $(s,d\Omega)$. Since the sum of the probability over all directions must be equal to unity, then

$$(1/4\pi) \int_{\Omega'=4\pi} p_\nu(\vec{s}',\vec{s}) \, d\Omega' = 1$$

This implies that the scattering function is normalized to unity.

An energy balance on the element of volume gives

$$E_i + E_e + E_s - E_o - E_a = 0$$

or

$$I_\nu \, dA \, d\Omega \, d\nu \, dt + j_\nu \, dA \, ds \, d\Omega \, d\nu \, dt$$

$$+ \left[\frac{\sigma_\nu}{4\pi} \int_{\Omega'=4\pi} p_\nu(\vec{s}', \vec{s}) \, I_\nu(\vec{s}') \, d\Omega' \right] dA \, ds \, d\Omega \, d\nu \, dt$$

$$- [I_\nu + dI_\nu] \, dA \, d\Omega \, d\nu \, dt - (\kappa_\nu + \sigma_\nu) \, ds$$

$$\cdot \, I_\nu \, dA \, d\Omega \, d\nu \, dt = 0 \qquad \text{(A-6)}$$

Divide by $dA \, d\Omega \, d\nu$ to obtain

$$I_\nu + j_\nu \, ds + \left(\frac{\sigma_\nu}{4\pi} \int_{\Omega'=4\pi} p_\nu(\vec{s}', \vec{s}) \, I_\nu(\vec{s}') \, d\Omega' \, ds \right) - I_\nu - dI_\nu$$

$$- (\kappa_\nu + \sigma_\nu) \, I_\nu(\vec{s}) \, ds = 0$$

or

$$\frac{dI_\nu}{ds} = j_\nu - (\kappa_\nu + \sigma_\nu) \, I_\nu + \frac{\sigma_\nu}{4\pi} \int_{\Omega'=4\pi} p_\nu(\vec{s}', \vec{s}) \, I_\nu(\vec{s}') \, d\Omega' \qquad \text{(A-7)}$$

Now the distance ds traversed by the pencil of rays is C dt, where C is the velocity of light, and dI_ν can be represented by

$$dI_\nu = \frac{\partial I_\nu}{\partial x} \, dx + \frac{\partial I_\nu}{\partial y} \, dy + \frac{\partial I_\nu}{\partial z} \, dz + \frac{\partial I_\nu}{\partial t} \, dt \qquad \text{(A-8)}$$

Now the term on the left side of Equation A-7 becomes

$$\frac{dI_\nu}{ds} = \frac{dI_\nu}{C \, dt} = \frac{1}{C} \left[\frac{\partial I_\nu}{\partial x} \frac{dx}{dt} + \frac{\partial I_\nu}{\partial y} \frac{dy}{dt} + \frac{\partial I_\nu}{\partial z} \frac{dz}{dt} + \frac{\partial I_\nu}{\partial t} \right] \qquad \text{(A-9)}$$

which reduces to

$$\frac{dI_\nu}{Cdt} = \frac{1}{C}\left[\frac{\partial I_\nu}{\partial x} v_x + \frac{\partial I_\nu}{\partial y} v_y + \frac{\partial I_\nu}{\partial z} v_z + \frac{\partial I_\nu}{\partial t}\right] = \frac{\partial I_\nu}{\partial t} + \vec{v}\cdot\nabla I_\nu \tag{A-10}$$

where v_x, v_y, v_z are the local components of velocity vector $\vec{v}$. Since $\vec{v} = C\,\vec{s}$, Equation A-10 becomes

$$\frac{dI_\nu}{Cdt} = \frac{1}{C}\left[\frac{\partial I_\nu}{\partial t} + C\,\vec{s}\cdot\nabla I_\nu\right] = \frac{1}{C}\frac{DI_\nu}{Dt}$$

where D/Dt is the substantial derivative. Substituting Equation A-11 into Equation A-7, we obtain

$$\frac{1}{C}\frac{\partial I_\nu}{\partial t} + \vec{s}\cdot\nabla I_\nu = j_\nu - (\kappa_\nu + \sigma_\nu)\, I_\nu + \frac{\sigma_\nu}{4\pi}\int_{\Omega'=4\pi} p_\nu(\vec{s}',\vec{s})\, I_\nu(\vec{s}')\, d\Omega' \tag{A-12}$$

This integro differential equation is called the equation of transfer.

Define an effective emission coefficient J_ν, as

$$J_\nu = j_\nu + \frac{\sigma_\nu}{4\pi}\int_{\Omega'=4\pi} p_\nu(\vec{s}',\vec{s})\, I_\nu(\vec{s}')\, d\Omega' \tag{A-13}$$

This coefficient represents the radiant energy leaving an element of volume of matter in the direction ($\vec{s}$, $d\Omega$) per unit volume, per unit solid angle, per unit frequency, and per unit time. The extinction coefficient, β_ν, is defined by

$$\beta_\nu = (\kappa_\nu + \sigma_\nu) \tag{A-14}$$

Using Equations A-13 and A-14, Equation A-12 can be written as

$$\frac{1}{C}\frac{\partial I_\nu}{\partial t} + \vec{s} \cdot \nabla I_\nu = J_\nu - \beta_\nu I_\nu \tag{A-15}$$

In most engineering problems, the term $\frac{1}{C}\,(\partial I_\nu/\partial t)$ is approximately zero, due to the magnitude of C, and the radiative transfer can be considered as quasi-stationary.

Sampson (58) used the Boltzman equation for photons to arrive at the radiative transport equation (Equation 2.39), which is identical to Equation A-12 without the scattering term.

For heat transfer purposes, the spectral heat flux is defined as

$$\vec{q}_\nu = \int_\Omega I_\nu \, \vec{s} \, d\Omega \tag{A-16}$$

For steady state conditions the heat flux can be obtained by integrating Equation A-15 to obtain

$$\int_\Omega \vec{s}\cdot\nabla I_\nu \, d\Omega = \int_\Omega (J_\nu - \beta_\nu I_\nu) \, d\Omega \tag{A-17}$$

The term on the left side of Equation A-16 can be expressed as

$$\vec{s}\cdot\nabla I_\nu = \nabla\cdot(\vec{s}\, I_\nu) = \nabla I_\nu \cdot \vec{s} + I_\nu \nabla\cdot\vec{s} \tag{A-18}$$

Since $\vec{s}$ is a unit vector, then $\nabla \cdot \vec{s} = 0$, and $\nabla I_\nu \cdot \vec{s} = \vec{s} \cdot \nabla I_\nu$, therefore the left side of Equation A-18 becomes

$$\int_\Omega \nabla \cdot (\vec{s}\ I_\nu)\ d\Omega = \nabla \cdot \int_\Omega \vec{s}\ I_\nu\ d\Omega = \nabla \cdot \vec{q}_\nu \qquad \text{(A-19)}$$

Substituting Equation A-19 into Equation A-17 gives the following

$$\nabla \cdot \vec{q}_\nu = \int_\Omega (J_\nu - \beta_\nu I_\nu)\ d\Omega \qquad \text{(A-20)}$$

This equation is identical to Equation 3.1 in Sampson (58) and Equation 14.6-3 in Bird, et al. (10) for the steady state condition.

APPENDIX B

FUEL PROPERTIES

Five out of the seven fuels used in this study are single component liquids. The remaining two liquids are jet fuels. Jet-A is a high-flash point kerosene type fuel with an initial boiling point of 355°F and an end point of 490°F. JP-4 is a relatively wide-boiling range distillate, produced by blending gasoline and light petroleum distillates and has an average initial boiling point of 140°F and an end point of 470°F. Table B-1 contains physical constants of these fuels along with data for n-undecane and n-octane whose properties will be used for Jet-A and JP-4 respectively. Table B-2 contains transport properties of the fuels at the mean temperature between 80°F and the fuel boiling point.

TABLE B-1

PHYSICAL CONSTANTS OF FUELS

Fuel Type:	Acetone Ketone	Benzene Aromatic	Cyclohexane Cyclo-Paraffin	n-Hexane Normal Paraffin	Jet-A Aviation Kerosene	JP-4 Wide Range Distillate	Methanol Alcohol	n-Octane Normal Paraffin	n-Undecane
Formula	CH_3COCH_3	C_6H_6	C_6H_{12}	C_6H_{14}	--	--	CH_3OH	C_8H_{18}	$C_{11}H_{24}$
Molecular Weight	58.1	78.108	84.156	86.172	--	--	32.042	114.224	156.32
Boiling Point at 14.7 psia, °F	133.0	176.18	177.33	155.73	355-490	140-470	148.1	258.2	384.6
Specific Gravity 60°F/60°F	0.795	0.8845	0.7834	0.6640	0.802	0.775	0.796	0.7068	0.74017
Temperature Coef. of Density $lbm/ft^3/°F$	0.00047	0.00066	0.00068	0.00075	--	--	--	0.00063	--
Degree API	--	28.6	49.0	81.6	39-51	45-57	--	68.7	--
Net Heat of Combustion Btu/lbm	12280.	17270.	18680.	19240	18400	18400	8580	--	--
Heat of Vaporization, Btu/lbm	220.	169.3	153.7	144.0	--	--	473.	131.9	129.6
Combustion Air ft^3/ft^3	19.05	35.80	42.96	45.35	--	--	7.15	59.55	80.95
Combustion Air lbm/lbm	9.47	13.32	14.83	15.29	--	--	6.43	15.10	15.05

TABLE B-2

TRANSPORT PROPERTIES OF FUELS

Fuel	T °F	C_p Btu/lb-°F	μ $\frac{lbm}{ft\text{-}hr}$	ρ $\frac{lbm}{ft^3}$	K $\frac{Btu\text{-}ft}{hr\text{-}ft^2\text{-}°F}$	B $°F^{-1}$
Acetone	105	0.550	0.6534	48.0	0.103	0.000837
Benzene	128	0.445	1.0164	52.3	0.084	0.000718
Cyclo-hexane	127	0.420	1.4762	46.0	0.084	0.000593
n-Hexane	118	0.567	0.605	38.7	0.079	0.000854
n-Octane	225	0.573	0.726	43.6	0.082	0.000726
n-Undecane	265	0.585	1.0648	44.9	0.079	0.000679
Methanol	114	0.620	0.9922	47.6	0.120	0.000692

It is assumed that the transport properties of a flame are approximated by air properties. The air properties were computed from the following equations:

$$\rho_a = 39.71729/T_{aR} \tag{B-1}$$

$$\mu_a = 241.92(10^7)\ 145.9(T_{aK})^{1.5}/(T_{aK} + 110.4) \tag{B-2}$$

$$C_{pa} = \left[6.713 + 0.0004697(T_{aK}) + 0.1147(10^{-5})(T_{aK})^2 - 0.4696(10^{-9})(T_{aK})^3\right]/28.97 \tag{B-3}$$

$$B_a = 1/T_{aR} \tag{B-4}$$

$$K_a = \frac{241.9(0.6325)(10^{-5})(T_{aK})^{1/2}\left[1+\left(254.4/T_{aK}\right)(10)^{-12/T_{aK}}\right]}{1 + \frac{254.4(10)^{-12/T_{ak}}}{T_{am}}} \tag{B-5}$$

where T_{aK} = air temperature, °K

T_{aR} = air temperature, °R

Table B-3 gives the results of these calculations for temperatures from 100°-3000°F.

TABLE B-3

PHYSICAL PROPERTIES OF AIR

T_a °F	B_a $°F^{-1}$	e_a $\frac{lbm}{ft^3}$	μ_a $\frac{lbm}{ft\text{-}hr}$	C_{pa} $\frac{Btu}{lbm\text{-}°F}$	K_a $\frac{Btu}{ft\text{-}hr\text{-}°F}$
100.00	0.00179	0.07092	0.04592	0.24011	0.01425
200.00	0.00152	0.06018	0.05191	0.24219	0.01676
300.00	0.00132	0.05226	0.05745	0.24441	0.01913
400.00	0.00116	0.04618	0.06263	0.24674	0.02138
500.00	0.00104	0.04137	0.06749	0.24917	0.02352
600.00	0.00094	0.03747	0.07208	0.25169	0.02556
700.00	0.00086	0.03424	0.07645	0.25428	0.02751
800.00	0.00079	0.03152	0.08061	0.25691	0.02937
900.00	0.00074	0.02920	0.08459	0.25958	0.03117
1000.00	0.00068	0.02720	0.08842	0.26227	0.03290
1100.00	0.00064	0.02546	0.09210	0.26496	0.03457
1200.00	0.00060	0.02393	0.09566	0.26763	0.03618
1300.00	0.00057	0.02257	0.09910	0.27027	0.03774
1400.00	0.00054	0.02135	0.10244	0.27287	0.03926
1500.00	0.00051	0.02026	0.10568	0.27539	0.04073
1600.00	0.00049	0.01928	0.10883	0.27784	0.04216
1700.00	0.00046	0.01839	0.11189	0.28018	0.04355
1800.00	0.00044	0.01757	0.11488	0.28241	0.04491
1900.00	0.00042	0.01683	0.11780	0.28451	0.04624
2000.00	0.00041	0.01615	0.12065	0.28645	0.04753
2100.00	0.00039	0.01551	0.12344	0.28823	0.04880
2200.00	0.00038	0.01493	0.12617	0.28983	0.05004
2300.00	0.00036	0.01439	0.12884	0.29123	0.05125
2400.00	0.00035	0.01389	0.13146	0.29242	0.05244
2500.00	0.00034	0.01342	0.13404	0.29337	0.05361
2600.00	0.00033	0.01298	0.13656	0.29407	0.05476
2700.00	0.00032	0.01257	0.13904	0.29450	0.05588
2800.00	0.00031	0.01218	0.14148	0.29466	0.05699
2900.00	0.00030	0.01182	0.14388	0.29451	0.05807
3000000	0.00029	0.01148	0.14624	0.29405	0.05914

APPENDIX C

TABULAR SUMMARY OF DATA

TABLE C-1

EXPERIMENTAL DATA FOR ACETONE FLAMES

Run No: 090171-24-1-1 Fuel: Acetone Burner Dia, In: 24 Test Time, Min: 31.15 Water Flow, lb/hr: 52

Test Time Interval Minutes	Probe Surface Temperature, °F									Cylinder Flame Temp, °F	Air Temp °F	Fuel Temp °F
	1T	2T	3T	Mean T	1B	2B	3B	Mean B	Probe Mean			
11.1-16.2	1107	1083	1123	1104	965	931	967	954	1029	1253	85.3	74.8
16.2-21.2	1110	1081	1132	1108	960	923	960	948	1028	1245	86.3	74.8
21.2-26.2	1107	1076	1126	1103	957	920	958	945	1024	1245	86.8	74.8
26.2-31.2	1109	1077	1131	1106	956	917	958	944	1025	1237	87.5	75.0

Test Time Interval Minutes	Probe Water Temp, °F			q_w*	Radiometer 81510				Radiometer 72804 with 7° View			
	In	Out	Diff		Min mv	Max mv	Mean mv	Mean Flux*	Min mv	Max mv	Mean mv	Mean Flux*
11.2-16.2	84.10	90.25	6.15	653.8	.790	1.470	1.130	6735.1	.302	.376	.339	14238
16.2-21.2	84.64	90.80	6.16	654.8	.785	1.475	1.130	6735.1	.300	.368	.334	14028
21.2-26.2	84.83	90.98	6.15	653.8	.785	1.400	1.093	6514.6	.305	.371	.338	14196
26.2-31.2	84.66	90.87	6.21	660.1	.785	1.395	1.090	6496.7	.307	.375	.341	14322

*Units: Btu/hr-ft^2.

TABLE C-1--Continued

Run No: 0.090171-24-1-2 Fuel: Acetone Burner Dia, In: 24 Test Time, Min: 38.51 Water Flow, lb/hr: 46.8

Test Time Interval Minutes	Probe Surface Temperature, °F									Cylinder Flame Temp, °F	Air Temp °F	Fuel Temp °F
	1T	2T	3T	Mean T	1B	2B	3B	Mean B	Probe Mean			
13.5-18.5	1212	1289	1266	1256	1246	1254	1274	1258	1257	1320	89.9	76.0
18.5-23.5	1198	1284	1266	1249	1241	1256	1277	1258	1254	1318	90.5	76.0
23.5-28.5	1204	1278	1263	1248	1242	1245	1265	1251	1250	1323	91.5	76.0
28.5-33.5	1225	1272	1256	1251	1250	1230	1252	1244	1248	1311	92.2	75.9
33.5-38.5	1234	1266	1253	1251	1257	1221	1252	1243	1247	1308	92.7	75.8

Test Time Interval Minutes	Probe Water Temp, °F			q_w*	Radiometer 81510				Radiometer 72804 with 7° View			
	In	Out	Diff		Min mv	Max mv	Mean mv	Mean Flux*	Min mv	Max mv	Mean mv	Mean Flux*
13.5-18.5	83.78	93.83	10.05	961.5	1.160	2.160	1.660	9894.0	.294	.402	.348	14616
18.5-23.5	83.98	94.55	10.57	1011.3	1.130	2.190	1.660	9894.0	.303	.400	.356	14952
23.5-28.5	84.30	95.18	10.88	1040.9	1.130	2.235	1.683	10031.1	.299	.404	.351	14742
28.5-33.5	84.57	95.65	11.08	1060.0	1.130	2.185	1.658	9882.1	.302	.401	.351	14742
33.5-38.5	84.69	95.97	11.28	1079.2	1.120	2.190	1.655	9864.2	.299	.397	.348	14616

TABLE C-1--Continued

Run No: 090171-24-1-3 Fuel: Acetone Burner Dia, In: 24 Test Time, Min: 36.21 Water Flow, lb/hr: 46.8

Test Time Interval Minutes	Probe Surface Temperature, °F									Cylinder Flame Temp, °F	Air Temp °F	Fuel Temp °F
	1T	2T	3T	Mean T	1B	2B	3B	Mean B	Probe Mean			
11.2-16.2	1092	1093	1132	1106	939	927	964	943	1025	1322	90.3	75.9
16.2-21.2	1089	1097	1134	1107	928	926	958	937	1022	1322	92.8	75.9
21.2-26.2	1079	1092	1132	1101	921	923	951	932	1016	1320	93.5	75.9
26.2-31.2	1088	1096	1138	1107	926	923	954	934	1021	1316	94.0	75.9
31.2-36.2	1089	1100	1140	1110	921	924	950	932	1021	1320	94.1	75.8

Test Time Interval Minutes	Probe Water Temp, °F			q_w*	Radiometer 81510				Radiometer 72804 with 7° View			
	In	Out	Diff		Min mv	Max mv	Mean mv	Mean Flux*	Min mv	Max mv	Mean mv	Mean Flux*
11.2-16.2	83.87	90.61	6.74	644.8	.695	1.215	.955	5692.1	.292	.367	.329	13818
16.2-21.2	84.07	90.87	6.80	650.6	.685	1.195	.940	5602.7	.291	.361	.326	13692
21.2-26.2	84.32	91.13	6.81	651.5	.690	1.160	.925	5513.2	.295	.361	.328	13776
26.2-31.2	84.42	91.18	6.76	646.7	.680	1.220	.950	5662.3	.292	.358	.325	13650
31.2-36.2	84.52	91.37	6.85	655.4	.680	1.195	.938	5590.7	.293	.367	.330	13860

TABLE C-1--Continued

Run No: 081271-18-1-1 Fuel: Acetone Burner Dia, In: 18 Test Time, Min: 31.56 Water Flow, lb/hr: 44.2

Test Time Interval Minutes	Probe Surface Temperature, °F									Cylinder Flame Temp, °F	Air Temp °F	Fuel Temp °F
	1T	2T	3T	Mean T	1B	2B	3B	Mean B	Probe Mean			
11.6-16.6	1040	1066	1047	1051	916	963	943	941	996	1178	84.3	75.8
16.6-21.6	1030	1064	1045	1046	902	955	933	930	988	1179	85.1	76.0
21.6-26.6	1025	1057	1042	1041	893	942	924	920	981	1188	85.2	76.0
26.6-31.6	1021	1054	1040	1038	890	938	920	916	977	1189	86.2	76.0

Test Time Interval Minutes	Probe Water Temp, °F			q_w*	Radiometer 81510				Radiometer 72804 with 7° View			
	In	Out	Diff		Min mv	Max mv	Mean mv	Mean Flux*	Min mv	Max mv	Mean mv	Mean Flux*
11.6-16.6	82.56	89.30	6.74	612.0	.484	.792	.638	3802.7	.281	.356	.319	13398
16.6-21.6	82.60	89.27	6.67	605.6	.484	.816	.650	3874.2	.282	.356	.319	13398
21.6-26.6	82.62	89.25	6.63	602.0	.470	.778	.624	3719.2	.278	.357	.318	13356
26.6-31.6	82.81	89.35	6.54	593.8	.464	.774	.619	3689.4	.275	.358	.317	13314

TABLE C-1--Continued

Run No: 081271-18-1-2 Fuel: Acetone Burner Dia, In: 18 Test Time, Min: 29.95 Water Flow, lb/hr: 39.

Test Time Interval Minutes	Probe Surface Temperature, °F									Cylinder Flame Temp, °F	Air Temp °F	Fuel Temp °F
	1T	2T	3T	Mean T	1B	2B	3B	Mean B	Probe Mean			
10-15	1044	1070	1054	1056	915	947	941	934	995	1128	84.5	76.9
15-20	1033	1070	1048	1050	902	947	928	926	988	1148	87.5	76.8
20-25	1029	1071	1050	1050	898	944	924	922	986	1158	87.5	76.7
25-30	1026	1066	1046	1046	892	937	922	917	982	1158	86.8	76.6

Test Time Interval Minutes	Probe Water Temp, °F			q_w*	Radiometer 81510				Radiometer 72804 with 7° View			
	In	Out	Diff		Min mv	Max mv	Mean mv	Mean Flux*	Min mv	Max mv	Mean mv	Mean Flux*
10-15	82.86	90.25	7.39	592.1	.446	.756	.601	3582.1	.232	.322	.277	11634
15-20	83.19	90.61	7.42	594.5	.446	.742	.594	3540.4	.250	.323	.286	12012
20-25	83.27	90.69	7.42	594.5	.444	.740	.592	3528.5	.248	.330	.289	12138
25-30	83.38	90.81	7.43	595.3	.436	.720	.578	3445.0	.251	.331	.291	12222

TABLE C-1--Continued

Run No: 081271-18-1-3 Fuel: Acetone Burner Dia, In: 18 Test Time, Min: 37.6 Water Flow, lb/hr: 39

Test Time Interval Minutes	Probe Surface Temperature, °F									Cylinder Flame Temp, °F	Air Temp °F	Fuel Temp °F
	1T	2T	3T	Mean T	1B	2B	3B	Mean B	Probe Mean			
12.6-17.6	1037	1091	1071	1066	906	968	950	941	1004	1162	89.0	79.2
17.6-22.6	1035	1094	1073	1067	901	974	952	942	1005	1147	90.3	79.1
22.6-27.6	1035	1097	1074	1069	901	980	952	944	1006	1148	91.2	79.0
27.6-32.6	1030	1096	1073	1066	895	979	956	943	1005	1140	91.4	78.8
32.6-37.6	1027	1098	1073	1066	890	978	951	940	1006	1136	91.0	78.7

Test Time Interval Minutes	Probe Water Temp, °F			q_w*	Radiometer 81510				Radiometer 72804 with 7° View			
	In	Out	Diff		Min mv	Max mv	Mean mv	Mean Flux*	Min mv	Max mv	Mean mv	Mean Flux*
12.6-17.6	83.34	91.10	7.76	621.7	.468	.822	.645	3844.4	.251	.344	.298	12516
17.6-22.6	83.51	91.27	7.76	621.7	.460	.792	.626	3731.1	.252	.343	.298	12516
22.6-27.6	83.71	91.53	7.82	626.5	.472	.796	.634	3778.8	.255	.350	.302	12684
27.6-32.6	83.75	91.58	7.83	627.3	.462	.788	.625	3725.2	.257	.342	.300	12600
32.6-37.6	83.88	91.68	7.80	624.9	.464	.776	.620	3695.4	.255	.342	.298	12516

TABLE C-1--Continued

Run No: 070771-12-1-1 Fuel: Acetone Burner Dia, In: 12 Test Time, Min: 49.53 Water Flow, lb/hr: 36.4

Test Time Interval Minutes	Probe Surface Temperature, °F									Cylinder Flame Temp, °F	Air Temp °F	Fuel Temp °F
	1T	2T	3T	Mean T	1B	2B	3B	Mean B	Probe Mean			
14.5-19.5	984	991	1001	992	893	884	894	890	941	1114	92.0	88.0
19.5-24.5	975	981	989	982	880	875	880	878	930	1093	92.5	88.0
24.5-29.5	967	975	980	974	871	865	871	869	922	1112	92.0	88.0
29.5-34.5	961	964	974	966	860	855	864	860	913	1105	92.5	88.0
34.5-39.5	959	962	970	964	852	852	861	855	909	1098	92.0	88.0
39.5-44.5	961	963	974	966	849	853	861	854	910	1091	91.5	87.5
44.5-49.5	961	963	971	965	854	850	859	854	910	1098	92.0	87.0

Test Time Interval Minutes	Probe Water Temp, °F			q_w*	Radiometer 81510				Radiometer 72804 with 7° View			
	In	Out	Diff		Min mv	Max mv	Mean mv	Mean Flux*	Min mv	Max mv	Mean mv	Mean Flux*
14.5-19.5	85.97	93.14	7.17	538.8	.254	.496	.375	2235.1	.169	.217	.193	8106
19.5-24.5	86.16	93.27	7.13	534.3	.242	.470	.356	2121.9	.166	.210	.188	7896
24.5-29.5	86.39	93.45	7.06	530.5	.232	.452	.342	2038.4	.167	.215	.191	8022
29.5-34.5	86.56	93.51	6.99	525.3	.222	.424	.323	1925.2	.170	.212	.191	8022
34.5-39.5	86.75	93.66	6.91	519.2	.230	.428	.329	1960.9	.169	.215	.192	8064
39.5-44.5	86.94	93.88	6.94	521.5	.226	.438	.332	1978.8	.171	.215	.193	8106
44.5-49.5	87.14	94.01	6.84	516.2	.234	.444	.339	2020.5	.170	.212	.191	8022

TABLE C-1--Continued

Run No: 070871-12-1-1 Fuel: Acetone Burner Dia, In: 12 Test Time, Min: 50.03 Water Flow, lb/hr: 39.0

Test Time Interval Minutes	Probe Surface Temperature, °F									Cylinder Flame Temp, °F	Air Temp °F	Fuel Temp °F
	1T	2T	3T	Mean T	1B	2B	3B	Mean B	Probe Mean			
25-30	944	945	959	949	898	853	892	881	915	995	90.5	85.0
30-35	948	952	962	954	905	862	903	890	922	986	90.5	85.0
35-40	937	968	961	955	932	881	925	913	934	976	90.5	85.0
40-45	935	955	961	950	925	864	913	901	926	985	91.0	85.0
45-50	941	944	962	949	897	852	897	882	916	1007	91.0	85.0

Test Time Interval Minutes	Probe Water Temp, °F			q_w*	Radiometer 81510				Radiometer 72804 with 7° View			
	In	Out	Diff		Min mv	Max mv	Mean mv	Mean Flux*	Min mv	Max mv	Mean mv	Mean Flux*
25-30	85.86	92.29	6.43	517.7	.400	.540	.470	2801.3	.144	.187	.165	6930
30-35	85.84	92.27	6.43	517.7	.404	.540	.472	2813.2	.141	.182	.161	6762
35-40	85.85	92.42	6.57	529.0	.412	.536	.474	2825.2	.136	.181	.158	6636
40-45	85.99	92.58	6.59	530.6	.416	.536	.476	2837.1	.144	.183	.163	6846
45-50	86.01	92.49	6.48	521.7	.412	.536	.474	2825.2	.131	.171	.151	6342

TABLE C-1--Continued

Run No: 070771-12-1-2 Fuel: Acetone Burner Dia, In: 12 Test Time, Min: 38.71 Water Flow, lb/hr: 37.7

Test Time Interval Minutes	Probe Surface Temperature, °F									Cylinder Flame Temp, °F	Air Temp °F	Fuel Temp °F
	1T	2T	3T	Mean T	1B	2B	3B	Mean B	Probe Mean			
13.7-18.7	974	986	999	986	890	889	895	891	939	1059	91.0	87.0
18.7-23.7	976	986	1001	988	889	897	901	896	942	1060	91.0	87.0
23.7-28.7	978	991	1004	991	895	901	903	900	945	1065	91.0	87.0
28.7-33.7	982	998	1008	963	905	921	924	917	956	1055	91.5	87.0
33.7-38.7	987	1011	1005	1001	999	1007	1023	1010	1005	955	92.0	87.0

Test Time Interval Minutes	Probe Water Temp, °F			q_w*	Radiometer 81510				Radiometer 72804 with 7° View			
	In	Out	Diff		Min mv	Max mv	Mean mv	Mean Flux*	Min mv	Max mv	Mean mv	Mean Flux*
13.7-18.7	85.79	92.77	6.98	543.2	.256	.510	.383	2282.8	.162	.210	.186	7812
18.7-23.7	85.95	93.00	7.05	548.7	.262	.536	.399	2378.1	.156	.202	.119	7518
23.7-28.7	85.98	93.16	7.18	558.8	.262	.552	.407	2425.8	.156	.200	.178	7476
28.7-33.7	86.07	93.37	7.30	568.1	.272	.550	.411	2449.7	.144	.188	.166	6972
33.7-38.7	86.15	93.95	7.80	607.1	.306	.534	.420	2503.3	.088	.134	.111	4662

TABLE C-2

EXPERIMENTAL DATA FOR BENZENE FLAMES

Run No: 090171-24-2-1 Fuel: Benzene Burner Dia, In: 24 Test Time, Min: 29.7 Water Flow, lb/hr: 52

Test Time Interval Minutes	Probe Surface Temperature, °F									Cylinder Flame Temp, °F	Air Temp °F	Fuel Temp °F
	1T	2T	3T	Mean T	1B	2B	3B	Mean B	Probe Mean			
9.7-14.7	1471	1446	1474	1464	1268	1321	1318	1302	1383	1539	99.5	81.4
14.7-19.7	1487	1507	1493	1496	1298	1335	1351	1328	1412	1554	99.5	81.3
19.7-24.7	1481	1543	1531	1518	1310	1319	1328	1319	1419	1585	99.5	81.25
24.7-29.7	1481	1578	1546	1535	1342	1344	1348	1311	1423	1610	99.5	81.1

Test Time Interval Minutes	Probe Water Temp, °F			q_w*	Radiometer 81510				Radiometer 72804 with 7° View			
	In	Out	Diff		Min mv	Max mv	Mean mv	Mean Flux*	Min mv	Max mv	Mean mv	Mean Flux*
9.7-14.7	86.53	96.29	9.76	1037.5	1.845	2.960	2.403	14322.5	.624	.807	.716	30072
14.7-19.7	86.96	97.58	10.62	1128.9	1.710	3.100	2.405	14334.4	.639	.842	.741	31122
19.7-24.7	87.34	98.42	11.08	1177.8	1.910	3.375	2.643	15753.0	.791	.961	.876	36792
24.7-29.7	87.68	99.39	11.71	1244.8	1.930	3.260	2.595	15466.9	.830	1.027	.929	39018

*Units: Btu/hr-ft^2.

TABLE C-2--Continued

Run No: 090171-24-22 Fuel: Benzene Burner Dia, In: 24 Test Time, Min: 29.33 Water Flow, lb/hr: 78.0

Test Time Interval Minutes	Probe Surface Temperature, °F									Cylinder Flame Temp, °F	Air Temp °F	Fuel Temp °F
	1T	2T	3T	Mean T	1B	2B	3B	Mean B	Probe Mean			
9.3-14.3	1336	1530	1502	1456	1474	1567	1547	1529	1493	1509	99.7+	83.2
14.3-19.3	1412	1506	1500	1473	1473	1524	1506	1501	1487	1535	99.7+	83.0
19.3-24.3	1405	1507	1496	1469	1472	1504	1486	1487	1478	1551	99.7+	83.0
24.3-29.3	1377	1515	1493	1465	1485	1519	1501	1502	1482	1566	99.7+	82.9

Test Time Interval Minutes	Probe Water Temp, °F			q_w*	Radiometer 81510				Radiometer 72804 with 7° View			
	In	Out	Diff		Min mv	Max mv	Mean mv	Mean Flux*	Min mv	Max mv	Mean mv	Mean Flux*
9.3-14.3	85.11	94.84	9.73	1551.5	1.730	2.830	2.280	13589.4	.554	.706	.630	26460
14.3-19.3	85.57	95.91	10.34	1648.8	1.735	2.735	2.235	13321.2	.610	.740	.675	28350
19.3-24.3	85.77	96.27	10.50	1674.3	1.720	2.740	2.230	13291.4	.612	.742	.677	28434
24.3-29.3	86.14	96.84	10.70	1706.2	1.765	2.930	2.350	14066.6	.612	.780	.696	29232

TABLE C-2--Continued

Run No: 090171-24-2-3 Fuel: Benzene Burner Dia, In: 24 Test Time, Min: 39.24 Water Flow, lb/hr: 78.0

Test Time Interval Minutes	Probe Surface Temperature, °F									Cylinder Flame Temp, °F	Air Temp °F	Fuel Temp °F
	1T	2T	3T	Mean T	1B	2B	3B	Mean B	Probe Mean			
14.2-19.2	1467	1477	1477	1474	1495	1546	1541	1527	1501	1479	99.7+	82.5
19.2-24.2	1405	1512	1509	1475	1401	1557	1544	1534	1505	1535	99.7+	82.4
24.2-29.2	1395	1505	1506	1469	1491	1535	1536	1521	1495	1555	99.7+	82.4
27.2-34.2	1365	1519	1515	1466	1501	1573	1563	1546	1506	1569	99.7+	82.3
34.2-39.2	1383	1482	1530	1465	1517	1548	1576	1547	1506	1551	99.7+	82.2

Test Time Interval Minutes	Probe Water Temp, °F			q_w*	Radiometer 81510				Radiometer 72804 with 7° View			
	In	Out	Diff		Min mv	Max mv	Mean mv	Mean Flux*	Min mv	Max mv	Mean mv	Mean Flux*
14.2-19.2	85.95	96.27	10.32	1645.6	1.700	2.830	2.265	13500.0	.594	.692	.643	27006
19.2-24.2	86.10	96.90	10.80	1722.1	1.655	2.710	2.182	13005.3	.590	.730	.660	27720
24.2-29.2	86.33	97.19	10.86	1731.7	1.645	2.685	2.165	12904.0	.610	.746	.648	28496
29.2-34.2	86.66	97.78	11.12	1733.1	1.675	2.945	2.310	13768.2	.598	.792	.695	29190
34.2-39.2	87.09	98.39	11.30	1801.8	1.775	3.205	2.490	14841.0	.508	.778	.645	27006

TABLE C-2--Continued

Run No: 081171-18-2-1 Fuel: Benzene Burner Dia, In: 18 Test Time, Min: 30.25 Water Flow, lb/hr: 41.6

Test Time Interval Minutes	Probe Surface Temperature, °F									Cylinder Flame Temp, °F	Air Temp °F	Fuel Temp °F
	1T	2T	3T	Mean T	1B	2B	3B	Mean B	Probe Mean			
10.3-15.3	1247	1216	1251	1238	1200	1223	1202	1208	1223	1307	100+	83.0
15.3-20.3	1245	1235	1240	1240	1201	1218	1194	1204	1222	1351	100+	83.0
20.3-25.3	1237	1227	1234	1233	1204	1220	1204	1209	1221	1355	100+	82.9
25.3-30.3	1220	1217	1218	1218	1217	1218	1205	1213	1216	1387	100+	82.8

Test Time Interval Minutes	Probe Water Temp, °F			q_w*	Radiometer 81510				Radiometer 72804 with 7° View			
	In	Out	Diff		Min mv	Max mv	Mean mv	Mean Flux*	Min mv	Max mv	Mean mv	Mean Flux*
10.3-15.3	84.50	94.67	10.17	869.1	1.100	1.655	1.377	8207.3	585	.611	.598	25116
15.3-20.3	84.91	95.36	10.45	893.1	1.150	1.690	1.420	8463.6	548	.652	.600	25200
20.3-25.3	85.22	96.11	10.89	930.6	1.175	1.720	1.447	8624.5	550	.665	.607	25494
25.3-30.3	85.56	96.84	11.28	964.0	1.110	1.775	1.442	8594.7	512	.698	.605	25410

TABLE C-2--Continued

Run No: 081171-18-2-2 Fuel: Benzene Burner Dia, In: 18 Test Time, Min: 33.09 Water Flow, lb/hr: 44.2

Test Time Interval Minutes	Probe Surface Temperature, °F									Cylinder Flame Temp, °F	Air Temp °F	Fuel Temp °F
	1T	2T	3T	Mean T	1B	2B	3B	Mean B	Probe Mean			
8.1-13.1	1330	1197	1284	1270	1212	1273	1262	1249	1260	1318	100+	81.8
13.1-18.1	1294	1204	1299	1266	1235	1244	1226	1235	1250	1330	100+	81.8
18.1-23.1	1301	1247	1315	1288	1238	1233	1218	1230	1259	1423	100+	81.7
23.1-28.1	1315	1283	1323	1307	1248	1241	1226	1238	1273	1456	100+	81.5
28.1-33.1	1329	1310	1325	1321	1258	1253	1251	1254	1288	1494	100+	81.5

Test Time Interval Minutes	Probe Water Temp, °F			q_w*	Radiometer 81510				Radiometer 72804 with 7° View			
	In	Out	Diff		Min mv	Max mv	Mean mv	Mean Flux*	Min mv	Max mv	Mean mv	Mean Flux*
8.1-13.1	86.02	95.86	9.84	893.5	1.320	1.865	1.592	9488.7	.568	.708	.638	26796
13.1-18.1	86.28	96.17	9.89	898.0	1.400	2.045	1.722	10263.6	.517	.648	.582	24444
18.1-23.1	86.70	96.82	10.12	918.9	1.405	2.060	1.732	10323.2	.542	.678	.610	25620
23.1-28.1	86.99	97.50	10.51	954.3	1.445	2.235	1.840	10966.9	.559	.715	.637	26754
28.1-33.1	87.28	98.23	10.95	994.3	1.515	2.340	1.927	11485.4	.610	.752	.681	28602

TABLE C-2--Continued

Run No: 081171-18-2-3 Fuel: Benzene Burner Dia, In: 18 Test Time, Min: 32.05 Water Flow, lb/hr: 46.8

Test Time Interval Minutes	Probe Surface Temperature, °F									Cylinder Flame Temp, °F	Air Temp °F	Fuel Temp °F
	1T	2T	3T	Mean T	1B	2B	3B	Mean B	Probe Mean			
12.1-17.1	1419	1169	1192	1260	1274	1310	1307	1297	1279	1250	99.7+	84.5
17.1-22.1	1391	1321	1313	1342	1263	1306	1280	1289	1315	1303	99.7+	84.4
22.1-27.1	1406	1424	1392	1407	1264	1314	1289	1289	1348	1437	99.7+	84.3
27.1-32.1	1446	1482	1441	1456	1295	1338	1320	1318	1387	1475	99.7+	84.3

Test Time Interval Minutes	Probe Water Temp, °F			q_w*	Radiometer 81510				Radiometer 72804 with 7° View			
	In	Out	Diff		Min mv	Max mv	Mean mv	Mean Flux*	Min mv	Max mv	Mean mv	Mean Flux*
12.1-17.1	87.95	97.82	9.87	948.9	1.490	2.225	1.858	11074.2	.431	.598	.515	21630
17.1-22.1	88.00	97.95	9.95	956.6	1.540	2.380	1.960	11682.1	.357	.557	.457	19194
22.1-27.1	88.09	98.67	10.58	1017.2	1.560	2.595	2.078	12385.4	.373	.582	.478	20076
27.1-32.1	88.33	99.57	11.24	1080.6	1.750	2.729	2.238	13339.1	.434	.621	.528	22176

TABLE C-2--Continued

Run No: 070671-12-2-1 Fuel: Benzene Burner Dia, In: 12 Test Time, Min: 43.7 Water Flow, lb/hr: 39

Test Time Interval Minutes	Probe Surface Temperature, °F									Cylinder Flame Temp, °F	Air Temp °F	Fuel Temp °F
	1T	2T	3T	Mean T	1B	2B	3B	Mean B	Probe Mean			
8.7-13.7	1138	1156	1149	1148	1142	1140	1147	1143	1145	1202	93.5	71.0
13.7-18.7	1117	1157	1108	1127	1129	1112	1127	1123	1125	1138	93.5	71.0
18.7-23.7	1111	1142	1102	1118	1102	1094	1102	1099	1109	1148	94.5	71.0
23.7-28.7	1088	1120	1106	1105	1078	1070	1067	1072	1088	1230	95.5	71.0
28.7-33.7	1116	1114	1059	1096	1072	1095	1078	1082	1089	1131	94.5	71.0
33.7-38.7	1181	1171	1160	1171	1111	1160	1122	1131	1151	1305	97.0	70.5
38.7-43.7	1254	1246	1239	1246	1166	1214	1162	1181	1241	1416	100.0	70.5

Test Time Interval Minutes	Probe Water Temp, °F			q_w*	Radiometer 81510				Radiometer 72804 with 7° View			
	In	Out	Diff		Min mv	Max mv	Mean mv	Mean Flux*	Min mv	Max mv	Mean mv	Mean Flux*
8.7-13.7	85.14	94.34	9.20	740.7	.738	1.046	.892	5316.6	.467	.576	.521	21882
13.7-18.7	85.03	94.23	9.20	740.7	.600	.844	.722	4303.3	.336	.470	.403	16926
18.7-23.7	84.98	94.11	9.13	735.1	.614	.968	.791	4714.6	.370	.529	.449	18858
23.7-28.7	84.95	93.88	8.93	719.0	.682	1.108	.895	5334.4	.463	.604	.533	22386
28.7-33.1	84.92	93.86	8.94	719.8	.610	1.068	.839	5000.7	.297	.463	.380	15960
33.7-38.7	85.20	94.79	9.59	772.1	.934	1.892+	1.413+	8421.9	.468	.631	.549	23058
38.7-43.7	85.60	96.18	10.58	851.8	1.100	2.545	1.772	10561.6	.500	.672	.586	24612

TABLE C-2--Continued

Run No: 070671-12-2-2 Fuel: Benzene Burner Dia, In: 12 Test Time, Min: 39.49 Water Flow, lb/hr: 39

Test Time Interval Minutes	Probe Surface Temperature, °F									Cylinder Flame Temp, °F	Air Temp °F	Fuel Temp °F
	1T	2T	3T	Mean T	1B	2B	3B	Mean B	Probe Mean			
14.5-19.5	1065	1172	1120	1119	1144	1125	1127	1132	1126	1185	97.5	79.0
19.5-24.5	1075	1171	1052	1099	1139	1130	1125	1131	1115	1102	97.0	79.0
24.5-29.5	1129	1147	1152	1143	1123	1132	1100	1118	1131	1291	98.0	79.0
29.5-34.5	1159	1139	1160	1153	1117	1126	1099	1114	1133	1309	96.5	79.0
34.5-39.5	1166	1119	1121	1135	1091	1115	1102	1103	1119	1231	96.0	79.0

Test Time Interval Minutes	Probe Water Temp, °F			q_w*	Radiometer 81510				Radiometer 72804 with 7° View			
	In	Out	Diff		Min mv	Max mv	Mean mv	Mean Flux*	Min mv	Max mv	Mean mv	Mean Flux*
14.5-19.5	84.37	93.49	9.12	734.3	.634	.912	.773	4607.3	.393	.519	.456	19152
19.5-24.5	84.74	93.73	8.99	723.8	.672	1.160	.916	5459.6	.344	.497	.420	17640
24.5-29.5	84.93	94.20	9.27	746.3	.880	1.632	1.256	7486.1	.442	.571	.506	21252
29.5-34.5	85.10	94.67	9.49	746.1	.844	1.554	1.199	7146.4	.427	.566	.496	20832
34.5-39.5	85.45	94.82	9.37	754.4	.816	1.530	1.173	6991.4	.378	.512	.445	18690

TABLE C-2--Continued

Run No: 070671-12-2-3 Fuel: Benzene Burner Dia, In: 12 Test Time, Min: 62.09 Water Flow, lb/hr: 37.7

Test Time Interval Minutes	Probe Surface Temperature, °F									Cylinder Flame Temp, °F	Air Temp °F	Fuel Temp °F
	1T	2T	3T	Mean T	1B	2B	3B	Mean B	Probe Mean			
27.1-32.1	1033	1097	1000	1043	1074	1106	1083	1088	1066	1032	101.5	82.5
32.1-37.1	989	1074	975	1013	1056	1082	1060	1066	1039	1036	102.0	82.0
37.1-42.1	976	1055	937	989	1036	1066	1039	1047	1018	904	101.0	82.0
42.1-47.1	994	1036	971	1000	1032	1075	1024	1044	1022	1079	102.5	82.0
47.1-52.1	1003	1021	1051	1035	1059	1107	1040	1069	1047	1222	102.5	82.0
52.1-57.1	1021	1033	1050	1035	1064	1107	1046	1072	1054	1235	100.0	82.0
57.1-62.1	1050	1054	1045	1050	1048	1085	1037	1057	1053	1225	101.5	82.0

Test Time Interval Minutes	Probe Water Temp, °F			q_w*	Radiometer 81510				Radiometer 72804 with 7° View			
	In	Out	Diff		Min mv	Max mv	Mean mv	Mean Flux*	Min mv	Max mv	Mean mv	Mean Flux*
27.1-32.1	86.15	95.62	9.47	734.0	.406	.654	.530	3158.9	.240	.373	.306	12852
32.1-37.1	86.38	95.57	9.19	715.2	.402	.678	.540	3218.5	.288	.469	.378	15876
37.1-42.1	86.48	95.42	8.98	698.9	.346	.630	.488	2908.6	.187	.358	.272	11424
42.1-47.1	86.57	95.52	8.95	696.6	.564	.914	.739	4404.6	.419	.526	.472	19824
47.1-52.1	86.65	96.14	9.49	738.6	.646	1.042	.844	5030.5	.397	.514	.455	19110
52.1-57.1	86.77	96.50	9.73	757.3	.648	1.010	.829	4941.1	.433	.535	.484	20328
57.1-62.1	86.94	96.78	9.84	765.8	.644	1.022	.833	4964.9	.412	.510	.461	19362

TABLE C-3

EXPERIMENTAL DATA FOR CYCLOHEXANE FLAMES

Run No: 083071-24-3-1 Fuel: Cyclohexane Burner Dia, In: 24 Test Time, Min: 28.68 Water Flow, lb/hr: 45.5

Test Time Interval Minutes	Probe Surface Temperature, °F									Cylinder Flame Temp, °F	Air Temp °F	Fuel Temp °F
	1T	2T	3T	Mean T	1B	2B	3B	Mean B	Probe Mean			
8.7-13.7	1214	1236	1223	1236	1019	1076	1052	1049	1137	1297	95.8	75.7
13.7-18.7	1224	1237	1234	1232	1036	1094	1080	1070	1151	1320	96.2	75.7
18.7-23.7	1211	1210	1221	1214	1055	1044	1078	1059	1137	1320	96.6	75.7
23.7-28.7	1203	1212	1281	1211	1038	1048	1071	1052	1132	1317	97.0	75.7

Test Time Interval Minutes	Probe Water Temp, °F			q_w*	Radiometer 81510				Radiometer 72804 with 7° View			
	In	Out	Diff		Min mv	Max mv	Mean mv	Mean Flux*	Min mv	Max mv	Mean mv	Mean Flux*
8.7-13.7	85.39	93.33	7.94	738.5	1.360	2.160	1.780	10609.3	.529	.623	.576	24192
13.7-18.7	85.64	93.94	8.30	772.0	1.350	2.250	1.800	10728.5	.503	.604	.554	23268
18.7-23.7	85.83	94.22	8.39	780.4	1.320	2.210	1.765	10519.0	.489	.590	.540	22680
23.7-28.7	86.10	95.10	9.00	837.1	1.320	2.165	1.743	10388.7	.483	.587	.535	22470

*Units: Btu/hr-ft^2.

TABLE C-3--Continued

Run No: 083071-24-3-2 Fuel: Cyclohexane Burner Dia, In: 24 Test Time, Min: 36.46 Water Flow, lb/hr: 46.8

Test Time Interval Minutes	Probe Surface Temperature, °F									Cylinder Flame Temp, °F	Air Temp °F	Fuel Temp °F
	1T	2T	3T	Mean T	1B	2B	3B	Mean B	Probe Mean			
11.5-16.5	1300	1346	1297	1314	1332	1382	1372	1362	1338	1298	95.4	78.0
16.5-21.5	1313	1356	1310	1326	1344	1397	1390	1377	1352	1317	96.2	78.0
21.5-26.5	1325	1361	1326	1337	1353	1399	1396	1383	1360	1335	96.7	78.0
26.5-31.5	1325	1363	1331	1340	1354	1397	1395	1382	1361	1348	96.9	77.9
31.5-36.5	1344	1356	1327	1342	1356	1391	1388	1378	1360	1343	97.7	77.8

Test Time Interval Minutes	Probe Water Temp, °F			q_w*	Radiometer 81510				Radiometer 72804 with 7° View			
	In	Out	Diff		Min mv	Max mv	Mean mv	Mean Flux*	Min mv	Max mv	Mean mv	Mean Flux*
11.5-16.5	85.22	97.92	12.70	1281.3	1.460	2.735	2.098	12504.6	.364	.517	.441	18522
16.5-21.5	85.51	98.72	13.21	1404.3	1.495	2.805	2.150	12814.6	.383	.529	.456	19152
21.5-26.5	85.50	97.48	11.98	1341.2	1.510	2.780	2.145	12784.8	.402	.537	.470	19740
26.5-31.5	85.51	97.08	11.57	1371.4	1.490	2.765	2.128	12683.5	.412	.543	.478	20076
31.5-36.5	85.71	97.43	11.72	1389.1	1.510	2.720	2.115	12606.0	.412	.553	.483	20286

TABLE C-3--Continued

Run No: 083071-24-3-3 Fuel: Cyclohexane Burner Dia, In: 24 Test Time, Min: 34.16 Water Flow, lb/hr: 65.0

Test Time Interval Minutes	Probe Surface Temperature, °F									Cylinder Flame Temp, °F	Air Temp °F	Fuel Temp °F
	1T	2T	3T	Mean T	1B	2B	3B	Mean B	Probe Mean			
9.2-14.2	1187	1221	1215	1208	1054	1094	1092	1080	1144	1345	97.3	79.8
14.2-19.2	1188	1236	1227	1217	1054	1119	1105	1093	1155	1364	97.8	79.7
19.2-24.2	1185	1237	1227	1216	1048	1121	1098	1089	1153	1373	97.9	79.5
24.2-29.2	1181	1237	1228	1215	1052	1124	1102	1093	1154	1375	98.9	79.4
29.2-34.2	1189	1243	1232	1221	1052	1134	1108	1098	1160	1373	99.8	79.3

Test Time Interval Minutes	Probe Water Temp, °F			q_w*	Radiometer 81510				Radiometer 72804 with 7° View			
	In	Out	Diff		Min mv	Max mv	Mean mv	Mean Flux*	Min mv	Max mv	Mean mv	Mean Flux*
9.2-14.2	85.54	91.47	5.93	788.0	1.365	2.230	1.798	10716.6	.484	.570	.527	22134
14.2-19.2	85.81	91.97	6.16	818.5	1.385	2.295	1.840	10966.9	.495	.585	.540	22680
19.2-24.2	86.03	92.27	6.24	829.2	1.425	2.370	1.898	11312.6	.500	.597	.549	23058
24.2-29.2	86.20	92.54	6.34	842.4	1.415	2.310	1.863	11104.0	.488	.583	.536	22512
29.2-34.2	86.36	92.78	6.42	853.1	1.405	2.305	1.855	11056.3	.497	.589	.543	22806

TABLE C-3--Continued

Run No: 081071-18-3-1 Fuel: Cyclohexane Burner Dia, In: 18 Test Time, Min: 30.35 Water Flow, lb/hr: 39

Test Time Interval Minutes	Probe Surface Temperature, °F									Cylinder Flame Temp, °F	Air Temp °F	Fuel Temp °F
	1T	2T	3T	Mean T	1B	2B	3B	Mean B	Probe Mean			
10.3-15.3	1115	1102	1115	1111	1022	1001	1013	1012	1061	1246	87.7	77.8
15.3-20.3	1104	1101	1104	1103	995	1016	1001	1004	1054	1270	89.0	77.7
20.3-25.3	1096	1102	1099	1099	980	1031	999	1003	1051	1275	89.0	77.6
25.3-30.3	1098	1106	1100	1101	985	1046	998	1010	1056	1285	90.3	77.5

Test Time Interval Minutes	Probe Water Temp, °F			q_w*	Radiometer 81510				Radiometer 72804 with 7° View			
	In	Out	Diff		Min mv	Max mv	Mean mv	Mean Flux*	Min mv	Max mv	Mean mv	Mean Flux*
10.3-15.3	82.96	91.82	8.86	709.8	.725	1.165	.945	5632.5	.397	.512	.450	18900
15.3-20.3	83.24	92.16	8.92	714.7	.765	1.195	.980	5841.1	.413	.514	.464	19488
20.3-25.3	83.48	92.53	9.05	725.1	.785	1.255	1.020	6079.5	.426	.519	.473	19866
25.3-30.3	83.74	92.96	9.22	738.7	.815	1.285	1.050	6258.3	.423	.514	.469	19698

TABLE C-3--Continued

Run No: 08171-18-3-2 Fuel: Cyclohexane Burner Dia, In: 18 Test Time, Min: 26.47 Water Flow, lb/hr: 39

Test Time Interval Minutes	Probe Surface Temperature, °F									Cylinder Flame Temp, °F	Air Temp °F	Fuel Temp °F
	1T	2T	3T	Mean T	1B	2B	3B	Mean B	Probe Mean			
7.3-12.3	1138	1139	1124	1134	996	1020	990	1002	1068	1236	100	76.8
12.3-17.3	1128	1136	1126	1130	973	1019	999	997	1064	1265	100	76.75
17.3-22.3	1145	1145	1132	1141	1025	1026	964	1005	1073	1286	100	76.7
22.3-27.3	1137	1132	1127	1132	986	1018	977	994	1063	1291	100	76.6

Test Time Interval Minutes	Probe Water Temp, °F			q_w*	Radiometer 81510				Radiometer 72804 with 7° View			
	In	Out	Diff		Min mv	Max mv	Mean mv	Mean Flux*	Min mv	Max mv	Mean mv	Mean Flux*
7.3-12.3	84.05	92.38	8.33	667.4	.980	1.474	1.227	7313.2	.415	.519	.467	19614
12.3-17.3	84.45	92.89	8.44	676.2	1.020	1.442	1.231	7337.0	.420	.522	.471	19782
17.3-22.3	84.63	93.17	8.54	684.2	1.086	1.510	1.298	7736.4	.422	.533	.477	20034
22.3-27.3	84.93	93.43	8.50	681.0	1.078	1.526	1.302	7760.3	.428	.529	.478	20076

TABLE C-3--Continued

Run No: 081071-18-3-3 Fuel: Cyclohexane Burner Dia, In: 18 Test Time, Min: 36.23 Water Flow, lb/hr: 39.0

Test Time Interval Minutes	Probe Surface Temperature, °F									Cylinder Flame Temp, °F	Air Temp °F	Fuel Temp °F
	1T	2T	3T	Mean T	1B	2B	3B	Mean B	Probe Mean			
11.2-16.7	1113	1176	1228	1172	1182	1212	1221	1205	1187	1306	93.1	79.7
16.2-21.2	1082	1224	1226	1177	1167	1229	1238	1211	1194	1309	93.0	79.5
21.2-26.2	1111	1208	1246	1188	1191	1225	1239	1218	1203	1356	93.8	79.4
26.2-31.2	1126	1195	1255	1192	1198	1225	1236	1220	1206	1375	94.4	79.3
31.2-36.2	1152	1178	1256	1195	1210	1216	1227	1218	1207	1384	95.2	79.2

Test Time Interval Minutes	Probe Water Temp, °F			q_w*	Radiometer 81510				Radiometer 72804 with 7° View			
	In	Out	Diff		Min mv	Max mv	Mean mv	Mean Flux*	Min mv	Max mv	Mean mv	Mean Flux*
11.2-16.2	83.96	94.91	10.95	877.3	1.048	1.604	1.326	7903.3	.358	.477	.418	17556
16.2-21.2	84.34	96.53	12.19	976.6	1.084	1.602	1.343	8004.6	.407	.522	.465	19530
21.2-26.2	84.50	97.65	13.15	1053.6	1.064	1.694	1.378	8213.2	.418	.534	.476	19992
26.2-31.2	84.76	98.48	14.72	1179.3	1.210	1.750	1.480	8821.2	.404	.527	.466	19572
31.2-36.2	85.00	99.15	14.15	1133.7	1.240	1.778	1.509	8994.0	.396	.513	.450	18900

TABLE C-3--Continued

Run No: 070171-12-3-1 Fuel: Cyclohexane Burner Dia, In: 12 Test Time, Min: 47.67 Water Flow, lb/hr: 50.7

Test Time Interval Minutes	Probe Surface Temperature, °F									Cylinder Flame Temp, °F	Air Temp °F	Fuel Temp °F
	1T	2T	3T	Mean T	1B	2B	3B	Mean B	Probe Mean			
17.7-22.7	1053	1061	1041	1052	971	979	997	982	1017	1136	90.0	79.5
22.7-27.7	1050	1048	1038	1045	964	947	967	959	1002	1151	90.5	79.5
27.7-32.7	1041	1043	1035	1040	969	935	951	952	996	1204	92.0	79.5
32.7-37.7	1040	1037	1029	1035	968	926	937	944	990	1245	92.0	79.5
37.7-42.7	1038	1032	1023	1031	963	933	922	939	985	1271	92.0	79.0
42.7-47.7	1033	1029	1021	1028	946	935	930	937	982	1257	92.0	79.0

Test Time Interval Minutes	Probe Water Temp, °F			q_w*	Radiometer 81510				Radiometer 72804 with 7° View			
	In	Out	Diff		Min mv	Max mv	Mean mv	Mean Flux*	Min mv	Max mv	Mean mv	Mean Flux*
17.7-22.7	82.68	88.58	5.90	617.53	.502	.726	.614	3659.6	.286	.382	.334	14028
22.7-27.7	82.77	88.70	5.93	620.66	.500	.726	.628	3743.0	.306	.390	.348	14616
27.7-32.7	82.91	88.82	5.91	618.58	.506	.726	.631	3760.9	.332	.420	.376	15792
32.7-37.7	83.07	88.97	5.90	617.53	.524	.770	.647	3856.3	.342	.414	.378	15876
37.7-42.7	83.10	89.04	5.94	621.72	.540	.778	.659	3927.8	.360	.422	.391	16422
42.7-47.7	83.25	89.14	5.93	620.66	.538	.806	.672	4005.3	.354	.422	.388	16296

TABLE C-3--Continued

Run No: 070171-12-3-2 Fuel: Cyclohexane Burner Dia, In: 12 Test Time, Min: 42.76 Water Flow, lb/hr: 46.80

Test Time Interval Minutes	Probe Surface Temperature, °F									Cylinder Flame Temp, °F	Air Temp °F	Fuel Temp °F
	1T	2T	3T	Mean T	1B	2B	3B	Mean B	Probe Mean			
12.8-17.8	1036	1045	1047	1043	976	951	966	964	1004	1234	92.0	81.0
17.8-22.8	1039	1044	1041	1041	944	957	971	957	999	1205	92.0	81.0
22.8-27.8	1040	1044	1040	1041	946	054	968	956	999	1188	93.5	81.0
27.8-32.8	1041	1036	1036	1038	963	930	948	947	992	1224	94.0	80.5
32.8-37.8	1037	1038	1035	1037	973	935	941	950	993	1245	94.0	80.0
37.8-42.8	1035	1035	1029	1033	945	942	945	944	989	1235	94.0	80.0

Test Time Interval Minutes	Probe Water Temp, °F			q_w*	Radiometer 81510				Radiometer 72804 with 7° View			
	In	Out	Diff		Min mv	Max mv	Mean mv	Mean Flux*	Min mv	Max mv	Mean mv	Mean Flux*
12.8-17.8	83.01	89.39	6.38	616.39	.530	.810	.670	3993.4	.351	.421	.386	16212
17.8-22.8	83.32	89.72	6.40	618.33	.540	.804	.672	4005.3	.337	.409	.373	15666
22.8-27.8	83.53	90.03	6.50	627.99	.542	.790	.666	3969.5	.338	.414	.376	15792
27.8-32.8	83.78	90.15	6.38	616.39	.528	.802	.665	3963.6	.345	.420	.383	16086
32.8-37.8	83.87	90.31	6.44	622.19	.538	.796	.667	3975.5	.368	.427	.398	16716
37.8-42.8	84.11	90.54	6.43	621.22	.550	.818	.684	4076.8	.359	.426	.393	16506

TABLE C-3--Continued

Run No: 070171-12-3-3 Fuel: Cyclohexane Burner Dia, In: 12 Test Time, Min: 50.5 Water Flow, lb/hr: 39.0

Test Time Interval Minutes	Probe Surface Temperature, °F									Cylinder Flame Temp, °F	Air Temp °F	Fuel Temp °F
	1T	2T	3T	Mean T	1B	2B	3B	Mean B	Probe Mean			
15.5-20.5	1030	1050	1041	1042	982	974	975	977	1009	1179	95.0	81.0
20.5-25.5	1016	1043	1039	1033	999	958	966	974	1004	1232	94.5	81.0
25.5-30.5	1020	1043	1034	1032	988	967	973	976	1004	1214	95.8	81.0
30.5-35.5	1036	1030	1022	1029	965	975	967	969	999	1183	96.0	81.0
35.5-40.5	1034	1039	1027	1033	985	1010	976	990	1012	1159	95.7	81.0
40.5-45.5	1019	1038	1034	1030	983	957	937	959	995	1253	95.3	81.0
45.5-50.5	1018	1037	1030	1028	983	955	937	958	993	1276	96.0	80.5

Test Time Interval Minutes	Probe Water Temp, °F			q_w*	Radiometer 81510				Radiometer 72804 with 7° View			
	In	Out	Diff		Min mv	Max mv	Mean mv	Mean Flux*	Min mv	Max mv	Mean mv	Mean Flux*
15.5-20.5	83.89	91.66	7.77	625.5	.532	.788	.660	3933.8	.345	.413	.378	15876
20.5-25.5	84.02	91.71	7.69	619.1	.500	.750	.625	3725.2	.361	.412	.387	16254
25.5-30.5	84.25	91.95	7.70	619.9	.516	.784	.650	3874.2	.354	.405	.380	15960
30.5-35.5	84.55	92.28	7.73	622.4	.548	.860	.704	4196.0	.362	.410	.386	16212
35.5-40.5	84.64	92.55	7.91	636.8	.560	.864	.712	4243.7	.349	.396	.373	15666
40.5-45.5	84.63	92.42	7.79	627.2	.530	.864	.667	3975.5	.370	.409	.390	16380
45.5-50.5	84.85	92.53	7.68	618.3	.542	.800	.671	3999.3	.378	.420	.399	16758

TABLE C-4

EXPERIMENTAL DATA FOR n-HEXANE FLAMES

Run No: 083171-24-4-1 Fuel: n-Hexane Burner Dia, In: 24 Test Time, Min: 31.11 Water Flow, lb/hr: 50.70

Test Time Interval Minutes	Probe Surface Temperature, °F									Cylinder Flame Temp, °F	Air Temp °F	Fuel Temp °F
	1T	2T	3T	Mean T	1B	2B	3B	Mean B	Probe Mean			
11.1-16.1	1271	1356	1317	1315	1304	1359	1357	1340	1327	1332	85.6	74.7
16.1-21.1	1310	1352	1317	1326	1308	1358	1355	1344	1335	1340	87.0	74.7
21.1-26.1	1323	1356	1315	1331	1322	1356	1353	1344	1338	1340	88.7	74.8
26.1-31.1	1333	1353	1313	1333	1317	1347	1344	1336	1335	1331	89.2	74.9

Test Time Interval Minutes	Probe Water Temp, °F			q_w*	Radiometer 81510				Radiometer 72804 with 7° View			
	In	Out	Diff		Min mv	Max mv	Mean mv	Mean Flux*	Min mv	Max mv	Mean mv	Mean Flux*
11.1-16.1	83.38	95.19	11.81	1224.1	1.595	2.880	2.238	13339.1	.360	.477	.419	17598
16.1-21.1	83.76	96.42	12.66	1312.1	1.660	2.960	2.310	13768.2	.388	.501	.445	18690
21.1-26.1	86.96	97.27	13.31	1379.5	1.655	2.965	2.310	13768.2	.405	.518	.467	19614
26.1-31.1	84.25	97.84	13.59	1408.5	1.670	2.930	2.300	13708.6	.477	.535	.476	19992

*Units: Btu/hr-ft^2.

TABLE C-4--Continued

Run No: 083171-24-42 Fuel: n-Hexane Burner Dia, In: 24 Test Time, Min: 30.91 Water Flow, lb/hr: 63.70

Test Time Interval Minutes	Probe Surface Temperature, °F									Cylinder Flame Temp, °F	Air Temp °F	Fuel Temp °F
	1T	2T	3T	Mean T	1B	2B	3B	Mean B	Probe Mean			
10.9-15.9	1232	1259	1252	1248	1147	1214	1194	1185	1216	1350	88.8	75.6
15.9-20.9	1275	1302	1292	1290	1222	1255	1256	1244	1267	1347	90.7	75.7
20.9-25.9	1289	1301	1293	1297	1236	1270	1277	1261	1269	1330	91.5	75.6
25.9-30.9	1299	1313	1296	1303	1247	1275	1286	1269	1286	1326	92.5	75.5

Test Time Interval Minutes	Probe Water Temp, °F			q_w*	Radiometer 81510				Radiometer 72804 with 7° View			
	In	Out	Diff		Min mv	Max mv	Mean mv	Mean Flux*	Min mv	Max mv	Mean mv	Mean Flux*
10.9-15.9	83.27	90.14	6.87	894.6	1.455	2.495	1.975	11771.5	.437	.527	.482	20244
15.9-20.9	83.60	91.50	7.90	1028.7	1.575	2.695	2.135	12725.2	.436	.536	.486	20412
20.9-25.9	83.98	92.57	8.59	1118.6	1.550	2.740	2.145	12784.8	.432	.545	.489	20538
25.9-30.9	84.27	93.26	8.99	1170.7	1.575	2.750	2.163	12893.1	.442	.542	.492	20664

TABLE C-4--Continued

Run No: 083171-24-43 Fuel: n-Hexane Burner Dia, In: 24 Test Time, Min: 27.96 Water Flow, lb/hr: 63.7

Test Time Interval Minutes	Probe Surface Temperature, °F									Cylinder Flame Temp, °F	Air Temp °F	Fuel Temp °F
	1T	2T	3T	Mean T	1B	2B	3B	Mean B	Probe Mean			
8-13	1168	1187	1164	1173	1024	1034	1004	1021	1097	1289	94.3	77.0
13-18	1156	1190	1162	1169	1002	1036	1004	1014	1092	1328	94.8	76.9
18-23	1155	1197	1176	1176	992	1043	1004	1013	1095	1334	96.0	76.8
23-28	1173	1211	1193	1192	1000	1058	1024	1027	1110	1340	96.4	76.5

Test Time Interval Minutes	Probe Water Temp, °F			q_w*	Radiometer 81510				Radiometer 72804 with 7° View			
	In	Out	Diff		Min mv	Max mv	Mean mv	Mean Flux*	Min mv	Max mv	Mean mv	Mean Flux*
8-13	84.16	89.98	5.82	757.9	1.335	2.220	1.778	10597.4	.386	.458	.422	17724
13-18	84.58	90.38	5.80	755.3	1.335	2.230	1.783	10627.2	.385	.458	.422	17724
18-23	84.84	90.65	5.81	756.6	1.335	2.200	1.778	10597.4	.386	.457	.422	17724
23-28	85.04	90.99	5.95	774.8	1.355	2.220	1.788	10657.0	.391	.466	.429	18438

TABLE C-4--Continued

Run No: 081071-18-4-1 Fuel: n-Hexane Burner Dia, In: 18 Test Time, Min: 27.46 Water Flow, lb/hr: 46.8

Test Time Interval Minutes	Probe Surface Temperature, °F									Cylinder Flame Temp, °F	Air Temp °F	Fuel Temp °F
	1T	2T	3T	Mean T	1B	2B	3B	Mean B	Probe Mean			
12.5-17.5	1116	1116	1111	1114	951	1023	990	988	1051	1243	97.0	83.0
17.5-22.5	1121	1119	1115	1118	963	1021	969	981	1050	1263	97.0	82.9
22.5-27.5	1119	1120	1114	1118	968	1006	962	979	1048	1278	98.8	82.7

Test Time Interval Minutes	Probe Water Temp, °F			q_w*	Radiometer 81510				Radiometer 72804 with 7° View			
	In	Out	Diff		Min mv	Max mv	Mean mv	Mean Flux*	Min mv	Max mv	Mean mv	Mean Flux*
12.5-17.5	84.86	91.85	6.99	672.0	.946	1.348	1.147	6836.4	.427	.528	.478	20076
17.5-22.5	85.09	92.20	7.11	683.6	.972	1.400	1.186	7068.9	.438	.533	.486	20412
22.5-27.5	85.54	92.65	7.11	683.6	.992	1.448	1.220	7271.5	.438	.544	.491	20622

TABLE C-4--Continued

Run No: 081071-18-4-2 Fuel: n-Hexane Burner Dia, In: 18 Test Time, Min: 27.57 Water Flow, lb/hr: 41.6

Test Time Interval Minutes	Probe Surface Temperature, °F									Cylinder Flame Temp, °F	Air Temp °F	Fuel Temp °F
	1T	2T	3T	Mean T	1B	2B	3B	Mean B	Probe Mean			
7.6-12.6	1131	1126	1124	1127	994	1015	956	988	1058	1259	97.6	84.4
12.6-17.6	1123	1117	1122	1121	974	1014	968	985	1053	1270	98.6	84.2
17.6-22.6	1123	1118	1130	1124	1014	1021	960	998	1061	1295	99.5	84.0
22.6-27.6	1128	1122	1128	1126	1014	1023	959	999	1062	1306	99.5	83.9

Test Time Interval Minutes	Probe Water Temp, °F			q_w*	Radiometer 81510				Radiometer 72804 with 7° View			
	In	Out	Diff		Min mv	Max mv	Mean mv	Mean Flux*	Min mv	Max mv	Mean mv	Mean Flux*
7.6-12.6	85.78	93.40	7.62	651.2	1.002	1.456	1.229	7325.2	.430	.525	.478	20026
12.6-17.6	86.17	93.95	7.78	664.9	1.006	1.434	1.220	7271.5	.435	.517	.476	19992
17.6-22.6	86.45	94.30	7.85	670.9	1.050	1.488	1.269	7564.6	.405	.520	.463	19446
22.6-27.6	86.72	94.64	7.92	676.8	1.072	1.488	1.280	7629.1	.415	.516	.466	19572

TABLE C-4--Continued

Run No: 081171-18-4-1 Fuel: n-Hexane Burner Dia, In: 18 Test Time, Min: 31.00 Water Flow, lb/hr: 41.6

Test Time Interval Minutes	Probe Surface Temperature, °F									Cylinder Flame Temp, °F	Air Temp °F	Fuel Temp °F
	1T	2T	3T	Mean T	1B	2B	3B	Mean B	Probe Mean			
11-16	1132	1122	1113	1122	1015	1006	938	986	1054	1265	94.4	80.5
16-21	1126	1116	1103	1115	1000	987	930	972	1044	1270	95.9	80.4
21-26	1117	1114	1102	1111	978	981	932	964	1037	1273	97.5	80.2
26-31	1103	1109	1107	1106	945	987	956	963	1035	1276	97.4	80.0

Test Time Interval Minutes	Probe Water Temp, °F			q_w*	Radiometer 81510				Radiometer 72804 with 7° View			
	In	Out	Diff		Min mv	Max mv	Mean mv	Mean Flux*	Min mv	Max mv	Mean mv	Mean Flux*
11-16	84.12	92.06	7.94	678.5	.974	1.376	1.175	7003.3	.406	.505	.456	19152
16-21	84.55	92.54	7.99	682.9	.972	1.370	1.171	6979.5	.406	.506	.456	19152
21-26	84.90	92.81	7.91	676.1	.952	1.352	1.152	6866.2	.409	.513	.461	19362
26-31	85.15	93.08	7.83	669.1	.936	1.305	1.119	6669.5	.417	.509	.463	19446

TABLE C-4--Continued

Run No: 070271-12-4-1 Fuel: n-Hexane Burner Dia, In: 12 Test Time, Min: 42.66 Water Flow, lb/hr: 39.0

Test Time Interval Minutes	Probe Surface Temperature, °F									Cylinder Flame Temp, °F	Air Temp °F	Fuel Temp °F
	1T	2T	3T	Mean T	1B	2B	3B	Mean B	Probe Mean			
12.7-17.7	1014	1025	1020	1020	959	934	919	937	979	1227	89.	75.
17.7-22.7	1016	1022	1014	1017	944	932	911	929	973	1233	89.	75.
22.7-27.7	1019	1031	1019	1023	919	995	997	970	997	1167	90.7	75.
27.7-32.7	1025	1027	1023	1025	924	1012	1011	982	1004	1111	91.5	75.
32.7-37.7	1043	1028	1020	1030	946	1037	1034	1006	1018	1098	92.0	75.
37.7-42.7	1034	1042	1035	1037	938	1022	1024	995	1016	1123	92.5	75.

Test Time Interval Minutes	Probe Water Temp, °F			q_w*	Radiometer 81510				Radiometer 72804 with 7° View			
	In	Out	Diff		Min mv	Max mv	Mean mv	Mean Flux*	Min mv	Max mv	Mean mv	Mean Flux*
12.7-17.7	81.25	88.61	7.36	592.6	.482	.714	.598	3564.2	.344	.396	.370	15540
17.7-22.7	81.46	88.77	7.31	588.5	.492	.760	.626	3731.1	.344	.393	.368	15456
22.7-27.7	81.85	89.42	7.57	609.4	.496	.834	.665	3963.6	.315	.375	.345	14490
27.7-32.7	82.09	89.88	7.79	627.2	.502	.836	.669	3987.4	.315	.375	.345	14490
32.7-37.2	82.31	90.29	7.98	642-5	.524	.910	.717	4273.5	.320	.376	.348	14616
37.7-42.7	82.52	90.59	8.07	649.7	.514	.821	.693	4130.5	.313	.373	.343	14406

TABLE C-4--Continued

Run No: 070271-12-4-2 Fuel: n-Hexane Burner Dia, In: 12 Test Time, Min: 40.51 Water Flow, lb/hr: 36

Test Time Interval Minutes	Probe Surface Temperature, °F									Cylinder Flame Temp, °F	Air Temp °F	Fuel Temp °F
	1T	2T	3T	Mean T	1B	2B	3B	Mean B	Probe Mean			
10.5-15.5	1011	1037	1027	1025	972	981	972	975	1000	1207	92	76
15.5-20.5	991	1031	1025	1016	970	940	958	956	986	1223	93.5	76
20.5-25.5	998	1036	1014	1016	981	961	981	974	995	1189	92	76
25.5-30.5	1009	1036	1032	1026	970	974	952	965	996	1259	93.3	76
30.5-35.5	1014	1026	1024	1021	946	966	945	952	987	1261	92.5	76
35.5-40.5	1015	1030	1026	1024	948	975	940	954	989	1266	92.5	76

Test Time Interval Minutes	Probe Water Temp, °F			q_w*	Radiometer 81510				Radiometer 72804 with 7° View			
	In	Out	Diff		Min mv	Max mv	Mean mv	Mean Flux*	Min mv	Max mv	Mean mv	Mean Flux*
10.5-15.5	82.59	90.07	7.48	602.2	.474	.806	.640	3814.6	.321	.406	.364	15288
15.5-20.5	82.93	90.44	7.51	604.6	.438	.710	.574	3421.2	.329	.411	.370	15540
20.5-25.5	83.18	90.84	7.66	616.7	.454	.754	.604	3600.0	.322	.409	.366	15372
25.5-30.5	83.37	91.09	7.72	621.6	.498	.908	.703	4190.0	.350	.434	.392	16464
30.5-35.5	83.71	91.46	7.75	624.6	.514	.908	.711	4237.8	.344	.431	.388	16296
35.5-40.5	83.90	91.73	7.83	630.4	.514	.896	.705	4202.0	.347	.434	.391	16422

TABLE C-4--Continued

Run No: 070271-12-4-3 Fuel: n-Hexane Burner Dia, In: 12 Test Time, Min: 46.67 Water Flow, lb/hr: 39.0

Test Time Interval Minutes	Probe Surface Temperature, °F									Cylinder Flame Temp, °F	Air Temp °F	Fuel Temp °F
	1T	2T	3T	Mean T	1B	2B	3B	Mean B	Probe Mean			
11.7-16.7	980	1057	1048	1028	1004	993	978	992	1010	1259	94.2	77
16.7-21.7	994	1045	1039	1026	984	968	979	977	1002	1267	95.2	77
21.7-26.7	1039	1062	1039	1047	973	991	1000	988	1017	1203	96.0	77
26.7-31.7	1042	1065	1038	1048	983	990	1002	992	1020	1193	96.5	77
31.7-36.7	1043	1062	1043	1049	972	985	994	984	1017	1240	97.0	77
36.7-41.7	1038	1057	1045	1047	977	981	974	977	1012	1266	98.0	77
41.7-46.7	1036	1048	1039	1041	975	970	957	967	1004	1298	98.3	77

Test Time Interval Minutes	Probe Water Temp, °F			q_w*	Radiometer 81510				Radiometer 72804 with 7° View			
	In	Out	Diff		Min mv	Max mv	Mean mv	Mean Flux*	Min mv	Max mv	Mean mv	Mean Flux*
11.7-16.7	82.98	90.79	7.81	628.8	.476	.820	.648	3862.2	.351	.434	.393	16506
16.7-21.7	83.31	91.09	7.72	621.6	.474	.798	.636	3790.7	.328	.415	.372	15624
21.7-26.7	83.81	91.72	7.91	636.8	.508	.900	.704	4196.0	.302	.403	.353	14826
26.7-31.7	84.06	92.23	8.17	657.8	.494	.884	.689	4106.6	.305	.407	.356	14952
31.7-36.7	84.30	92.44	8.14	655.4	.522	.932	.727	4333.1	.313	.416	.365	15330
36.7-41.7	84.54	92.73	8.19	659.4	.534	.964	.749	4464.2	.338	.434	.386	16212
41.7-46.7	84.74	92.80	8.06	648.9	.536	.960	.748	4458.3	.347	.442	.395	16590

TABLE C-5

EXPERIMENTAL DATA FOR JET A FLAMES

Run No: 083171-24-5-1 Fuel: Jet A Burner Dia, In: 24 Test Time, Min: 32.29 Water Flow, lb/hr: 52

Test Time Interval Minutes	Probe Surface Temperature, °F									Cylinder Flame Temp, °F	Air Temp °F	Fuel Temp °F
	1T	2T	3T	Mean T	1B	2B	3B	Mean B	Probe Mean			
12.3-17.3	1317	1274	1394	1328	1323	1339	1288	1317	1323	1487	98.9	83.6
17.3-22.3	1335	1241	1393	1323	1313	1346	1286	1315	1319	1502	99.8	83.5
22.3-27.3	1321	1209	1394	1308	1313	1335	1288	1312	1310	1504	99.8	83.4
27.3-32.3	1297	1202	1389	1296	1307	1325	1282	1305	1300	1504	99.8	83.1

Test Time Interval Minutes	Probe Water Temp, °F			q_w*	Radiometer 81510				Radiometer 72804 with 7° View			
	In	Out	Diff		Min mv	Max mv	Mean mv	Mean Flux*	Min mv	Max mv	Mean mv	Mean Flux*
12.3-17.3	85.94	95.57	9.63	1023.7	1.955	3.125	2.540	15139.1	.532	.680	.606	25452
17.3-22.3	84.34	96.40	10.06	1069.4	1.980	3.260	2.620	15615.9	.537	.674	.606	25452
22.3-27.3	86.56	96.58	10.02	1065.2	1.985	3.245	2.615	15586.1	.509	.655	.582	24444
27.3-32.3	86.80	96.85	10.05	1068.3	1.920	3.170	2.545	15168.9	.504	.639	.572	24024

*Units: Btu/hr-ft^2.

TABLE C-5--Continued

Run No: 041671-24-5-1 Fuel: Jet A Burner Dia, In: 24 Test Time, Min: 32.74 Water Flow, lb/hr: 32.5

Test Time Interval Minutes	Probe Surface Temperature, °F									Cylinder Flame Temp, °F	Air Temp °F	Fuel Temp °F
	1T	2T	3T	Mean T	1B	2B	3B	Mean B	Probe Mean			
12.7-17.7	1361	1357	1384	1367	1338	1341	1302	1327	1347	1534	82	71.0
17.7-22.7	1362	1338	1394	1365	1339	1344	1300	1328	1346	1513	83	71.0
22.7-27.7	1328	1325	1395	1349	1344	1342	1293	1326	1338	1504	84.5	71.0
27.7-32.7	1341	1328	1392	1354	1346	1343	1290	1326	1340	1485	85.0	71.0

Test Time Interval Minutes	Probe Water Temp, °F			q_w*	Radiometer 81510				Radiometer 72804 with 7° View			
	In	Out	Diff		Min mv	Max mv	Mean mv	Mean Flux*	Min mv	Max mv	Mean mv	Mean Flux*
12.7-17.7	74.84	92.12	17.28	1153.7			2.360	14066				
17.7-22.7	76.05	94.26	18.21	1215.7			2.400	14305				
22.7-27.7	76.59	95.24	18.65	1245.1			2.410	14364				
27.7-32.7	76.73	95.81	19.08	1273.9			2.380	14185				

TABLE C-5--Continued

Run No: 041671-24-5-2 Fuel: Jet A Burner Dia, In: 24 Test Time, Min: 38.96 Water Flow, lb/hr: 338

Test Time Interval Minutes	Probe Surface Temperature, °F									Cylinder Flame Temp, °F	Air Temp °F	Fuel Temp °F
	1T	2T	3T	Mean T	1B	2B	3B	Mean B	Probe Mean			
9-14	1290	1210	1461	1320	1322	1308	1312	1314	1317	1616	86.5	73
14-19	1255	1193	1448	1299	1320	1314	1311	1315	1307	1594	87.0	73
19-24	1252	1182	1435	1290	1329	1317	1318	1321	1306	1578	87.5	73
24-29	1421	1414	1421	1419	1316	1325	1328	1323	1371	1509	86	73
29-34	1438	1404	1391	1411	1311	1339	1321	1324	1367	1456	87	73
34-39	1438	1330	1421	1396	1320	1350	1301	1324	1360	1554	88	73

Test Time Interval Minutes	Probe Water Temp, °F			q_w*	Radiometer 81510				Radiometer 72804 with 7° View			
	In	Out	Diff		Min mv	Max mv	Mean mv	Mean Flux*	Min mv	Max mv	Mean mv	Mean Flux*
9-14	73.96	90.43	16.47	1143.6			3,028	18048				
14-19	74.33	90.89	16.56	1149.9			2.920	17404				
19-24	74.62	91.14	16.52	1147.1			2.897	17267				
24-29	75.12	93.00	17.88	1241.5			2.315	13798				
29-34	75.41	93.78	18.37	1275.5			2.301	13715				
34-39	75.59	93.67	18.08	1255.4			2.489	14835				

TABLE C-5--Continued

Run No: 041671-24-5-3 Fuel: Jet A Burner Dia, In: 24 Test Time, Min: 48.81 Water Flow, lb/hr: 33.8

Test Time Interval Minutes	Probe Surface Temperature, °F									Cylinder Flame Temp, °F	Air Temp °F	Fuel Temp °F
	1T	2T	3T	Mean T	1B	2B	3B	Mean B	Probe Mean			
13.8-18.8	1297	1323	1415	1345	1343	1355	1315	1338	1341	1516	84	77
18.8-23.8	1434	1418	1404	1419	1343	1348	1319	1337	1378	1502	83	77
23.8-28.8	1438	1421	1393	1417	1338	1333	1324	1332	1375	1472	83	77
28.8-33.8	1439	1417	1390	1415	1328	1327	1307	1321	1368	1481	84	77
33.8-38.8	1435	1403	1398	1412	1325	1329	1306	1320	1366	1502	83.5	77
38.8-43.8	1433	1404	1390	1409	1314	1324	1296	1311	1360	1495	83.5	77
43.8-48.8	1436	1410	1397	1414	1317	1326	1293	1312	1363	1502	84.5	77

Test Time Interval Minutes	Probe Water Temp, °F			q_w*	Radiometer 81510				Radiometer 72804 with 7° View			
	In	Out	Diff		Min mv	Max mv	Mean mv	Mean Flux*	Min mv	Max mv	Mean mv	Mean Flux*
13.8-18.8	74.27	93.28	19.62	1362.3			2.535	15109				
18.8-23.8	74.70	95.13	20.43	1418.6			2.330	13887				
23.8-28.8	74.92	95.73	20.81	1445.00			2.290	13649				
28.8-33.8	75.08	95.74	20.66	1434.6			2.285	13619				
33.8-38.8	75.22	95.85	20.63	1432.5			2.315	13798				
38.8-43.8	75.42	95.91	20.49	1422.7			2.290	13649				
43.8-48.8	75.64	96.10	20.46	1420.7			2.305	13738				

TABLE C-5--Continued

Run No: 080971-18-5-1 Fuel: Jet A Burner Dia, In: 18 Test Time, Min: 34.8 Water Flow, lb/hr: 39

Test Time Interval Minutes	Probe Surface Temperature, °F									Cylinder Flame Temp, °F	Air Temp °F	Fuel Temp °F
	1T	2T	3T	Mean T	1B	2B	3B	Mean B	Probe Mean			
9.8-14.8	1214	1176	1124	1171	1170	1199	1189	1186	1179			
14.8-19.8	1226	1141	1194	1187	1192	1215	1206	1204	1196			
19.8-24.8	1202	1215	1125	1181	1205	1202	1212	1206	1194			
24.8-29.8	1138	1234	1190	1187	1222	1191	1199	1204	1196			
29.8-34.8	1086	1251	1118	1152	1235	1193	1226	1218	1185			

Test Time Interval Minutes	Probe Water Temp, °F			q_w*	Radiometer 81510				Radiometer 72804 with 7° View			
	In	Out	Diff		Min mv	Max mv	Mean mv	Mean Flux*	Min mv	Max mv	Mean mv	Mean Flux*
9.8-14.8	81.42	91.66	10.24	820.4	.850	1.255	1.053	6276.2	.290	.438	.364	15288
14.8-19.8	81.72	92.45	10.73	859.7	1.055	1.715	1.385	8255.0	.350	.480	.415	17430
19.8-24.8	81.70	92.57	10.87	870.9	.885	1.305	1.095	6526.5	.276	.426	.351	14742
24.8-29.8	81.95	92.92	10.97	878.9	.875	1.345	1.110	6615.9	.310	.462	.386	16212
29.8-34.8	82.08	93.12	11.04	884.5	.750	1.090	.880	5245.0	.236	.386	.311	13062

TABLE C-5--Continued

Run No: 042171-18-5-1 Fuel: Jet A Burner Dia, In: 18 Test Time, Min: 38.13 Water Flow, lb/hr: 31.2

Test Time Interval Minutes	Probe Surface Temperature, °F									Cylinder Flame Temp, °F	Air Temp °F	Fuel Temp °F
	1T	2T	3T	Mean T	1B	2B	3B	Mean B	Probe Mean			
13.18.1	1274	1287	1297	1286	1238	1254	1247	1246	1266	1359	81.0	81.0
18.1-23.1	1263	1279	1302	1281	1235	1254	1234	1241	1261	1380	82.0	81.0
23.1-28.1	1256	1270	1303	1276	1235	1249	1227	1237	1257	1403	82.0	81.0
28.1-33.1	1264	1274	1300	1279	1232	1248	1222	1234	1257	1400	82.5	81.0
33.1-38.1	1278	1272	1297	1282	1219	1248	1224	1230	1256	1390	83.0	81.0

Test Time Interval Minutes	Probe Water Temp, °F			q_w*	Radiometer 81510				Radiometer 72804 with 7° View			
	In	Out	Diff		Min mv	Max mv	Mean mv	Mean Flux*	Min mv	Max mv	Mean mv	Mean Flux*
13.1-18.1	74.22	89.65	15.43	989.0			1.650	9834				
18.1-23.1	74.18	89.68	15.50	993.5			1.710	10192				
23.1-28.1	74.16	89.80	15.64	1002.4			1.705	10162				
28.1-33.1	74.23	89.95	15.62	1001.2			1.740	10371				
33.1-38.1	74.35	90.00	15.63	1003.1			1.695	10103				

TABLE C-5--Continued

Run No: 042171-18-5-2 Fuel: Jet A Burner Dia, In: 18 Test Time, Min: 39:43 Water Flow, lb/hr: 28.6

Test Time Interval Minutes	Probe Surface Temperature, °F									Cylinder Flame Temp, °F	Air Temp °F	Fuel Temp °F
	1T	2T	3T	Mean T	1B	2B	3B	Mean B	Probe Mean			
9.4-14.4	1267	1291	1293	1284	1232	1251	1245	1243	1263	1376	82.0	81.0
14.4-19.4	1251	1281	1293	1275	1225	1243	1224	1231	1253	1398	82.5	81.0
19.4-24.4	1269	1299	1275	1281	1203	1227	1216	1215	1248	1376	85.0	81.0
24.4-29.4	1272	1303	1279	1285	1206	1230	1219	1218	1252	1376	85.5	81.0
29.4-34.4	1268	1287	1271	1275	1197	1220	1201	1206	1241	1327	86.5	81.0
34.4-39.4	1275	1295	1276	1282	1195	1222	1201	1209	1244	1376	86.5	81.0

Test Time Interval Minutes	Probe Water Temp, °F			q_w*	Radiometer 81510				Radiometer 72804 with 7° View			
	In	Out	Diff		Min mv	Max mv	Mean mv	Mean Flux*	Min mv	Max mv	Mean mv	Mean Flux*
9.4-14.4	73.43	89.57	16.14	948.3			1.635	9745				
14.4-19.4	73.86	90.04	16.18	950.6			1.660	9894				
19.4-24.4	74.38	90.65	16.27	955.9			1.560	9298				
24.4-29.4	74.58	91.05	16.47	967.7			1.575	9387				
29.4-34.4	74.85	91.35	16.49	968.8			1.575	9687				
34.4-39.4	75.04	91.51	16.47	967.7			1.615	9626				

TABLE C-5--Continued

Run No: 042171-18-5-3 Fuel: Jet A Burner Dia, In: 18 Test Time, Min: 68.95 Water Flow, lb/hr: 26.6

Test Time Interval Minutes	Probe Surface Temperature, °F									Cylinder Flame Temp, °F	Air Temp °F	Fuel Temp °F
	1T	2T	3T	Mean T	1B	2B	3B	Mean B	Probe Mean			
29-34	1208	1263	1247	1239	1197	1201	1212	1203	1221	1319	82.5	82.0
34-39	1165	1244	1252	1220	1210	1204	1198	1204	1212	1946	83.5	82.0
39-44	1107	1201	1262	1190	1226	1228	1191	1215	1203	1389	84.5	81.5
44-49	1160	1244	1271	1225	1226	1225	1198	1215	1220	1395	85.5	81.5
59-59	1172	1302	1261	1245	1233	1214	1219	1222	1234	1335	85.5	81.0
59-64	1226	1255	1230	1237	1180	1178	1189	1182	1210	1312	86.0	81.0
64-69	1107	1234	1229	1190	1211	1187	1194	1197	1194	1320	86.5	81.0

Test Time Interval Minutes	Probe Water Temp, °F			q_w*	Radiometer 81510				Radiometer 72804 with 7° View			
	In	Out	Diff		Min mv	Max mv	Mean mv	Mean Flux*	Min mv	Max mv	Mean mv	Mean Flux*
29-34	74.13	90.66	16.53	971.2			1.320	7868				
34-39	74.32	90.72	16.40	963.6			1.410	8404				
39-44	74.54	90.83	16.29	957.1			1.510	9000				
44-49	74.63	90.94	16.31	958.3			1.505	8970				
54-59	74.56	91.24	16.68	980.0			1.355	8076				
59-64	74.87	91.16	16.29	957.1			1.325	7897				
64-69	74.81	90.87	16.06	943.6			1.250	7450				

TABLE C-5--Continued

Run No: 070971-12-5-1 Fuel: Jet A Burner Dia, In: 12 Test Time, Min: 49.91 Water Flow, lb/hr: 39.0

Test Time Interval Minutes	Probe Surface Temperature, °F									Cylinder Flame Temp, °F	Air Temp °F	Fuel Temp °F
	1T	2T	3T	Mean T	1B	2B	3B	Mean B	Probe Mean			
24.9-29.9	888	1000	968	952	1053	1044	1068	1055	1004	881	90	83
29.9-34.9	874	972	911	919	1037	1027	1055	1040	979	843	90	83
34.9-39.9	972	1017	924	971	1056	1069	1062	1062	1017	814	90	83
39.9-44.9	917	1002	964	961	1027	1010	1026	1021	991	923	90	83
44.9-49.9	962	1026	982	990	1026	1919	1022	1022	1006	997	90	83

Test Time Interval Minutes	Probe Water Temp, °F			q_w*	Radiometer 81510				Radiometer 72804 with 7° View			
	In	Out	Diff		Min mv	Max mv	Mean mv	Mean Flux*	Min mv	Max mv	Mean mv	Mean Flux*
24.9-29.9	83.97	92.16	8.19	659.4	.282	.388	.335	1996.7	.215	.268	.242	10164
29.9-34.9	84.03	91.91	7.88	634.4	.264	.354	.309	1841.7	.159	.251	.205	8610
34.9-39.9	84.14	92.06	7.92	637.7	.340	.516	.428	2551.0	.193	.297	.245	10290
39.9-44.9	84.16	92.19	8.03	646.5	.320	.422	.371	2211.3	.262	.329	.296	12432
44.9-49.9	84.39	92.50	8.11	653.0	.362	.520	.441	2628.5	.265	.348	.307	12894

TABLE C-5--Continued

Run No: 042771-12-5-1 Fuel: Jet A Burner Dia, In: 12 Test Time, Min: 49.99 Water Flow, lb/hr: 31.2

Test Time Interval Minutes	Probe Surface Temperature, °F									Cylinder Flame Temp, °F	Air Temp °F	Fuel Temp °F
	1T	2T	3T	Mean T	1B	2B	3B	Mean B	Probe Mean			
15-20	1202	980	1159	1114	1247	1212	1249	1236	1175	1231	78.5	75.5
20-25	1183	1099	1195	1159	1223	1236	1226	1228	1194	1225	76.5	75.0
25-30	1159	1044	1187	1130	1216	1223	1223	1221	1176	1263	77.0	75.0
30-35	1047	1043	1232	1107	1209	1221	1210	1213	1160	1281	76.5	75.0
35-40	983	991	1216	1063	1192	1201	1203	1199	1131	1285	75.0	75.0
40-45	971	1020	1209	1067	1183	1208	1196	1196	1131	1287	75.5	75.0
45-50	984	1059	1203	1082	1181	1208	1187	1192	1137	1290	75.5	75.0

Test Time Interval Minutes	Probe Water Temp, °F			q_w*	Radiometer 81510				Radiometer 72804 with 7° View			
	In	Out	Diff		Min mv	Max mv	Mean mv	Mean Flux*	Min mv	Max mv	Mean mv	Mean Flux*
15-20	73.58	86.41	12.83	826.4			1.208	7200				
20-25	73.62	86.92	13.30	856.6			1.124	6699				
25-30	73.40	86.84	13.44	865.7			1.074	6401				
30-35	72.95	86.41	13.46	866.9			1.086	6473				
35-40	72.50	85.70	13.20	850.2			1.046	6234				
40-45	72.06	85.17	13.11	844.4			1.018	6068				
45-50	71.78	85.02	13.24	852.8			1.018	6068				

TABLE C-5--Continued

Run No: 042771-12-5-2 Fuel: Jet A Burner Dia, In: 12 Test Time, Min: 44.75 Water Flow, lb/hr: 31.2

Test Time Interval Minutes	Probe Surface Temperature, °F									Cylinder Flame Temp, °F	Air Temp °F	Fuel Temp °F
	1T	2T	3T	Mean T	1B	2B	3B	Mean B	Probe Mean			
19.8-24.8	1202	1165	1209	1192	1210	1231	1213	1218	1205	1236	79.0	75.5
24.8-29.8	1187	1018	1140	1115	1197	1214	1219	1210	1163	1168	79.0	75.5
29.8-34.8	1082	1037	1161	1093	1138	1173	1146	1152	1123	1240	76.5	75.5
34.8-39.8	1083	1024	1159	1089	1147	1180	1154	1160	1125	1272	77.0	75.5
39.8-44.8	1096	1029	1164	1096	1169	1203	1164	1179	1138	1271	77.0	75.5

Test Time Interval Minutes	Probe Water Temp, °F			q_w*	Radiometer 81510				Radiometer 72804 with 7° View			
	In	Out	Diff		Min mv	Max mv	Mean mv	Mean Flux*	Min mv	Max mv	Mean mv	Mean Flux*
19.8-24.8	74.10	87.78	13.68	881.1			.980	5841				
24.8-29.8	73.67	87.17	13.50	869.5			.914	8448				
29.8-34.8	72.89	85.74	12.85	827.7			.786	4685				
34.8-39.8	72.60	85.34	12.74	820.6			.866	5162				
39.8-44.8	72.35	85.28	12.93	832.8			.904	5388				

TABLE C-5--Continued

Run No: 042771-12-5-3 Fuel: Jet A Burner Dia, In: 12 Test Time, Min: 38.41 Water Flow, lb/hr: 31.2

Test Time Interval Minutes	Probe Surface Temperature, °F									Cylinder Flame Temp, °F	Air Temp °F	Fuel Temp °F
	1T	2T	3T	Mean T	1B	2B	3B	Mean B	Probe Mean			
13.4-18.4	1218	1249	1240	1236	1209	1222	1202	1211	1223	1336	76.5	75
18.4-23.4	1221	1247	1239	1236	1207	1219	1190	1205	1221	1351	78.0	75
23.4-28.4	1225	1243	1231	1233	1201	1217	1177	1198	1216	1350	78.0	75
28.4-33.4	1227	1242	1229	1233	1189	1212	1170	1190	1212	1343	79.0	75
33.4-38.4	1224	1240	1221	1228	1180	1196	1161	1179	1204	1332	79.0	75

Test Time Interval Minutes	Probe Water Temp, °F			q_w*	Radiometer 81510				Radiometer 72804 with 7° View			
	In	Out	Diff		Min mv	Max mv	Mean mv	Mean Flux*	Min mv	Max mv	Mean mv	Mean Flux*
13.4-18.4	71.05	85.02	13.97	899.8			1.062	6330				
18.4-23.4	71.29	85.57	14.28	919.8			1.076	6413				
23.4-28.4	71.61	85.98	14.37	925.6			1.112	6628				
28.4-33.4	71.83	86.32	14.49	933.3			1.108	6604				
33.4-38.4	71.88	86.28	14.40	927.5			1.106	6592				

TABLE C-5--Continued

Run No: 042871-12-5-1 Fuel: Jet A Burner Dia, In: 12 Test Time, Min: 43.96 Water Flow, lb/hr: 28.6

Test Time Interval Minutes	Probe Surface Temperature, °F									Cylinder Flame Temp, °F	Air Temp °F	Fuel Temp °F
	1T	2T	3T	Mean T	1B	2B	3B	Mean B	Probe Mean			
14-19	1206	1251	1243	1233	1216	1222	1190	1209	1221	1343	76.0	76.5
19-24	1210	1247	1238	1232	1210	1215	1178	1201	1206	1353	77.5	76.5
24-29	1214	1244	1234	1231	1203	1208	1170	1194	1212	1353	77.5	76.5
29-34	1209	1239	1227	1225	1197	1196	1162	1185	1205	1349	78.0	76.5
34-39	1218	1237	1220	1225	1183	1186	1151	1173	1199	1341	79.0	76.5
39-44	1220	1233	1216	1223	1169	1180	1147	1165	1194	1335	79.0	76.0

Test Time Interval Minutes	Probe Water Temp, °F			q_w*	Radiometer 81510				Radiometer 72804 with 7° View			
	In	Out	Diff		Min mv	Max mv	Mean mv	Mean Flux*	Min mv	Max mv	Mean mv	Mean Flux*
14-19	71.29	86.74	15.45	912.2			1.090	6497				
19-24	71.53	87.27	15.74	929.3			1.098	6544				
24-29	71.77	87.48	15.71	927.6			1.122	6687				
29-34	71.92	87.66	15.74	929.3			1.090	6497				
34-39	72.05	87.71	15.66	924.6			1.132	6747				
39-44	72.19	87.85	15.66	924.6			1.134	6759				

TABLE C-5--Continued

Run No: 042871-12-5-2 Fuel: Jet A Burner Dia, In: 12 Test Time, Min: 40.81 Water Flow, lb/hr: 33.8

Test Time Interval Minutes	Probe Surface Temperature, °F									Cylinder Flame Temp, °F	Air Temp °F	Fuel Temp °F
	1T	2T	3T	Mean T	1B	2B	3B	Mean B	Probe Mean			
10.8-15.8	1116	1245	1128	1163	1222	1198	1237	1219	1191	1211	71.0	79.0
15.8-20.8	1121	1234	1103	1153	1221	1200	1233	1218	1185	1162	71.5	79.0
20.8-25.8	1111	1224	1099	1145	1218	1196	1228	1214	1179	1141	71.0	78.5
25.8-30.8	1102	1216	1115	1144	1213	1183	1222	1206	1175	1152	71.5	78.5
30.8-35.8	1097	1212	1112	1140	1213	1179	1221	1204	1172	1156	71.5	78.5
35.8-40.8	1083	1206	1108	1132	1212	1175	1218	1202	1167	1155	71.5	78.0

Test Time Interval Minutes	Probe Water Temp, °F			q_w*	Radiometer 81510				Radiometer 72804 with 7° View			
	In	Out	Diff		Min mv	Max mv	Mean mv	Mean Flux*	Min mv	Max mv	Mean mv	Mean Flux*
10.8-15.8	71.6	94.5	22.9	1600.3			.790	4709				
15.8-20.8	71.75	93.54	21.79	1520.4			.752	4482				
20.8-25.8	71.81	93.63	21.82	1731.9			.758	4518				
25.8-30.8	71.89	93.81	21.92	1529.5			.764	4554				
30.8-35.8	71.81	92.25	20.44	1426.2			.776	4625				
35.8-40.8	71.81	92.34	20.53	1432.5			.772	4601				

TABLE C-6

EXPERIMENTAL DATA FOR JP-4 FLAMES

Run No: 083171-24-6-1 Fuel: JP-4 Burner Dia, In: 24 Test Time, Min: 24.49 Water Flow, lb/hr: 52

Test Time Interval Minutes	Probe Surface Temperature, °F									Cylinder Flame Temp, °F	Air Temp °F	Fuel Temp °F
	1T	2T	3T	Mean T	1B	2B	3B	Mean B	Probe Mean			
9.5-14.5	1273	1267	1317	1286	1224	1236	1186	1215	1251	1431	99.8	83.1
14.5-19.5	1288	1255	1330	1291	1217	1250	1194	1220	1256	1440	99.8	83.0
19.5-24.5	1302	1267	1346	1305	1190	1254	1211	1218	1262	1453	99.8	83.0

Test Time Interval Minutes	Probe Water Temp, °F			q_w*	Radiometer 81510				Radiometer 72804 with 7° View			
	In	Out	Diff		Min mv	Max mv	Mean mv	Mean Flux*	Min mv	Max mv	Mean mv	Mean Flux*
9.5-14.5	86.13	95.03	8.90	946.1	1.600	2.640	2.120	12635.8	.526	.646	.586	24612
14.5-19.5	86.67	95.76	9.09	966.3	1.705	2.855	2.280	13589.4	.538	.656	.597	25074
19.5-24.5	87.07	96.36	9.29	987.6	1.715	2.825	2.270	13529.8	.554	.691	.623	26166

*Units: Btu/hr-ft^2.

TABLE C-6--Continued

Run No: 041771-24-6-1 Fuel: JP-4 Burner Dia, In: 24 Test Time, Min: 33.89 Water Flow, lb/hr: 33.8

Test Time Interval Minutes	Probe Surface Temperature, °F									Cylinder Flame Temp, °F	Air Temp °F	Fuel Temp °F
	1T	2T	3T	Mean T	1B	2B	3B	Mean B	Probe Mean			
13.9-18.9	1344	1401	1360	1368	1375	1382	1385	1381	1375	1360	73.5	67.0
18.9-23.9	1363	1373	1373	1370	1354	1350	1358	1354	1362	1422	75.0	67.0
23.9-28.9	1362	1365	1351	1359	1340	1318	1346	1335	1347	1389	75.5	67.0
28.9-33.9	1369	1367	1378	1371	1354	1354	1342	1350	1361	1440	76.0	67.0

Test Time Interval Minutes	Probe Water Temp, °F			q_w*	Radiometer 81510				Radiometer 72804 with 7° View			
	In	Out	Diff		Min mv	Max mv	Mean mv	Mean Flux*	Min mv	Max mv	Mean mv	Mean Flux*
13.9-18.9	73.20	93.78	20.58	1429.0			2.065	12308				
18.9-23.9	73.25	94.43	21.18	1470.6			2.015	12010				
23.9-28.9	73.01	94.09	21.08	1463.7			2.000	11921				
28.9-33.9	72.84	94.45	21.61	1500.5			2.045	12189				

TABLE C-6--Continued

Run No: 041771-24-6-2 Fuel: JP-4 Burner Dia, In: 24 Test Time, Min: 29.73 Water Flow, lb/hr: 32.5

Test Time Interval Minutes	Probe Surface Temperature, °F									Cylinder Flame Temp, °F	Air Temp °F	Fuel Temp °F
	1T	2T	3T	Mean T	1B	2B	3B	Mean B	Probe Mean			
9.7-14.7	1323	1243	1385	1317	1294	1290	1240	1275	1296	1496	78.0	67.0
14.7-19.7	1338	1278	1374	1330	1284	1297	1233	1271	1301	1483	78.0	67.0
19.7-24.7	1361	1306	1369	1345	1272	1296	1230	1266	1306	1465	78.0	67.0
24.7-29.7	1374	1340	1368	1361	1254	1290	1271	1272	1316	1463	78.5	67.0

Test Time Interval Minutes	Probe Water Temp, °F			q_w*	Radiometer 81510				Radiometer 72804 with 7° View			
	In	Out	Diff		Min mv	Max mv	Mean mv	Mean Flux*	Min mv	Max mv	Mean mv	Mean Flux*
9.7-14.7	71.41	87.14	15.73	1050.2			2.430	14483				
14.7-19.7	71.51	87.71	16.20	1081.6			2.315	13798				
19.7-24.7	71.90	88.46	16.56	1105.6			2.275	13560				
24.7-29.7	72.26	89.53	17.27	1153.0			2.190	13053				

TABLE C-6--Continued

Run No: 041771-24-6-3 Fuel: JP-4 Burner Dia, In: 24 Test Time, Min: 43.5 Water Flow, lb/hr: 31.2

Test Time Interval Minutes	Probe Surface Temperature, °F									Cylinder Flame Temp, °F	Air Temp °F	Fuel Temp °F
	1T	2T	3T	Mean T	1B	2B	3B	Mean B	Probe Mean			
13.5-18.5	1383	1371	1354	1369	1291	1311	1264	1289	1329	1462	78.0	68.0
18.5-23.5	1378	1364	1354	1365	1290	1316	1261	1289	1327	1441	78.5	68.0
23.5-28.5	1375	1358	1355	1363	1293	1317	1260	1290	1326	1436	79.0	68.0
28.5-33.5	1376	1363	1355	1365	1287	1311	1260	1286	1325	1423	79.5	68.0
33.5-38.5	1365	1339	1354	1353	1289	1316	1254	1286	1319	1413	80.5	68.0
38.5-43.5	1365	1339	1354	1353	1289	1310	1253	1284	1318	1409	81.0	68.0

Test Time Interval Minutes	Probe Water Temp, °F			q_w*	Radiometer 81510				Radiometer 72804 with 7° View			
	In	Out	Diff		Min mv	Max mv	Mean mv	Mean Flux*	Min mv	Max mv	Mean mv	Mean Flux*
13.5-18.5	71.84	91.03	19.19	1230.0			2.235	13321				
18.5-23.5	72.09	92.01	19.92	1276.8			2.175	12964				
23.5-28.5	72.36	93.05	20.69	1326.1			2.170	12934				
28.5-33.5	72.65	93.66	20.99	1345.4			2.105	12546				
33.5-38.5	72.89	94.28	21.39	1371.0			2.110	12576				
38.5-43.5	73.09	94.66	21.57	1382.5			2.100	12517				

TABLE C-6--Continued

Run No: 081071-18-6-1 Fuel: JP-4 Burner Dia, In: 18 Test Time, Min: 25.88 Water Flow, lb/hr: 39

Test Time Interval Minutes	Probe Surface Temperature, °F									Cylinder Flame Temp, °F	Air Temp °F	Fuel Temp °F
	1T	2T	3T	Mean T	1B	2B	3B	Mean B	Probe Mean			
10.3-15.3	1104	1130	1137	1124	1082	1071	1042	1065	1094		81.6	76.7
15.3-20.3	1146	1125	1153	1141	1048	1105	1065	1073	1107		83.6	76.6
20.3-25.3	1158	1117	1138	1138	1055	1128	1106	1098	1117		85.1	76.5
25.3-30.3	1166	1141	1167	1158	1078	1118	1088	1095	1126		85.1	76.4

Test Time Interval Minutes	Probe Water Temp, °F			q_w*	Radiometer 81510				Radiometer 72804 with 7° View			
	In	Out	Diff		Min mv	Max mv	Mean mv	Mean Flux*	Min mv	Max mv	Mean mv	Mean Flux*
10.3-15.3	82.75	91.46	8.71	697.8	.775	1.170	.973	5799.3	.434	.528	.481	20202
16.3-20.3	82.96	92.05	9.09	728.3	.880	1.320	1.100	6556.3	.409	.495	.452	18984
20.3-25.3	83.09	92.40	9.31	745.9	.830	1.240	1.035	6168.9	.390	.510	.450	18900
25.3-30.3	83.13	92.66	9.53	763.5	.930	1.540	1.235	7360.9	.405	.511	.458	19236

TABLE C-6--Continued

Run No: 042171-18-6-1 Fuel: JP-4 Burner Dia, In: 18 Test Time, Min: 34.71 Water Flow, lb/hr: 31.2

Test Time Interval Minutes	Probe Surface Temperature, °F									Cylinder Flame Temp, °F	Air Temp °F	Fuel Temp °F
	1T	2T	3T	Mean T	1B	2B	3B	Mean B	Probe Mean			
10-15	1230	1234	1202	1222	1123	1171	1186	1160	1191	1278	67.0	67.0
15-20	1188	1228	1232	1216	1144	1149	1117	1137	1176	1338	69.5	67.0
20-25	1151	1201	1233	1195	1157	1163	1117	1146	1170	1362	69.5	67.0
25-30	1218	1220	1234	1224	1120	1168	1158	1149	1186	1348	69.5	67.0
30-34.7	1206	1236	1233	1225	1110	1145	1132	1129	1177	1354	70.0	67.0

Test Time Interval Minutes	Probe Water Temp, °F			q_w*	Radiometer 81510				Radiometer 72804 with 7° View			
	In	Out	Diff		Min mv	Max mv	Mean mv	Mean Flux*	Min mv	Max mv	Mean mv	Mean Flux*
10-15	68.80	82.70	13.90	890.9			1.355	8076				
15-20	68.88	82.62	13.74	880.7			1.420	8464				
20-25	68.86	82.66	13.80	884.5			1.445	8613				
25-30	68.79	82.75	13.96	894.8			1.480	8821				
30-34.7	68.78	82.99	14.21	910.8			1.425	8493				

TABLE C-6--Continued

Run No: 042171-18-6-2 Fuel: JP-4 Burner Dia, In: 18 Test Time, Min: 34.28 Water Flow, lb/hr: 29.9

Test Time Interval Minutes	Probe Surface Temperature, °F									Cylinder Flame Temp, °F	Air Temp °F	Fuel Temp °F
	1T	2T	3T	Mean T	1B	2B	3B	Mean B	Probe Mean			
9.3-14.3	1203	1215	1215	1211	1131	1162	1152	1148	1180	1309	73.0	65.5
14.3-19.3	1192	1210	1236	1213	1141	-160	1132	1144	1179	1364	74.0	65.5
19.3-24.3	1185	1212	1232	1210	1143	1153	1124	1140	1175	1373	75.0	65.5
24.3-29.3	1168	1202	1232	1201	1158	1158	1117	1144	1173	1378	75.5	65.5
29.3-34.3	1162	1199	1228	1196	1157	1159	1115	1144	1170	1369	76.0	65.5

Test Time Interval Minutes	Probe Water Temp, °F			q_w*	Radiometer 81510				Radiometer 72804 with 7° View			
	In	Out	Diff		Min mv	Max mv	Mean mv	Mean Flux*	Min mv	Max mv	Mean mv	Mean Flux*
9.3-14.3	70.53	95.74	25.21	1548.5			1.510	9000				
14.3-19.3	71.17	96.97	25.80	1584.7			1.575	9387				
19.3-24.3	71.63	97.86	26.23	1611.2			1.535	9149				
24.3-29.3	72.04	98.69	26.65	1637.0			1.555	9268				
29.3-34.3	72.55	99.33	26.78	1644.9			1.465	8732				

TABLE C-6--Continued

Run No: 042171-18-6-3 Fuel: JP-4 Burner Dia, In: 18 Test Time, Min: 44.93 Water Flow, lb/hr: 31.2

Test Time Interval Minutes	Probe Surface Temperature, °F									Cylinder Flame Temp, °F	Air Temp °F	Fuel Temp °F
	1T	2T	3T	Mean T	1B	2B	3B	Mean B	Probe Mean			
9.9-14.9	1145	1213	1227	1195	1163	1163	1121	1149	1172	1360	77.0	69.0
14.9-19.9	1185	1219	1222	1209	1134	1158	1144	1145	1177	1348	77.5	69.0
19.9-24.9	1125	1203	1230	1186	1172	1171	1122	1155	1171	1363	79.0	68.5
24.9-29.9	1137	1200	1226	1188	1167	1162	1122	1150	1169	1359	79.0	68.5
29.9-34.9	1146	1208	1227	1194	1168	1158	1123	1150	1172	1351	80.5	68.5
34.9-39.9	1201	1220	1220	1214	1110	1148	1155	1138	1176	1325	80.5	68.5
39.9-44.9	1216	1199	1198	1204	1097	1169	1180	1149	1177	1272	81.0	68.5

Test Time Interval Minutes	Probe Water Temp, °F			q_w*	Radiometer 81510				Radiometer 72804 with 7° View			
	In	Out	Diff		Min mv	Max mv	Mean mv	Mean Flux*	Min mv	Max mv	Mean mv	Mean Flux*
9.9-14.9	69.89	84.28	14.39	922.3			1.450	8642				
14.9-19.9	70.22	84.81	14.69	941.6			1.450	8642				
19.9-24.9	70.36	84.67	14.31	917.2			1.420	8464				
24.9-29.9	70.70	85.24	14.54	931.9			1.415	8434				
29.9-34.9	71.08	85.71	14.63	937.7			1.405	8374				
34.9-39.9	71.13	85.60	14.47	927.4			1.355	8076				
39.9-44.9	71.38	85.77	14.39	922.3			1.315	7838				

TABLE C-6--Continued

Run No: 062271-12-6-1 Fuel: JP-4 Burner Dia, In: 12 Test Time, Min: 54.68 Water Flow, lb/hr: 52

Test Time Interval Minutes	Probe Surface Temperature, °F									Cylinder Flame Temp, °F	Air Temp °F	Fuel Temp °F
	1T	2T	3T	Mean T	1B	2B	3B	Mean B	Probe Mean			
34.7-39.7	999	1004	993	999	993	1010	989	997	998	--	87	74
39.7-44.7	1012	1031	1043	1027	1012	1022	987	1007	1017	--	87.5	74
44.7-49.7	993	1019	1064	1025	1016	1036	995	1016	1021	--	87.8	74
49.7-54.7	964	994	1074	1011	1028	1053	1019	1033	1022	1337	88.5	74.5

Test Time Interval Minutes	Probe Water Temp, °F			q_w*	Radiometer 81510				Radiometer 72804 with 7° View			
	In	Out	Diff		Min mv	Max mv	Mean mv	Mean Flux*	Min mv	Max mv	Mean mv	Mean Flux*
34.7-39.7	79.49	85.77	6.28	674.2	.428	.616	.522	3111.3	.183	.220	.202	8484
39.7-44.7	79.86	86.37	6.51	698.8	.506	.772	.639	3808.6	.164	.216	.190	7980
44.7-49.7	79.92	86.46	6.54	702.1	.546	.798	.672	4005.3	.170	.221	.196	8232
49.7-54.7	79.92	86.50	6.58	706.4	.592	.872	.732	4362.9	.155	.212	.184	7728

TABLE C-6--Continued

Run No: 042971-12-6-1 Fuel: JP-4 Burner Dia, In: 12 Test Time, Min: 40.37 Water Flow, lb/hr: 31.2

Test Time Interval Minutes	Probe Surface Temperature, °F									Cylinder Flame Temp, °F	Air Temp °F	Fuel Temp °F
	1T	2T	3T	Mean T	1B	2B	3B	Mean B	Probe Mean			
10-15	1162	1128	1174	1155	1133	1177	1130	1147	1151	1285	70	63
15-20	1182	1163	1186	1177	1142	1179	1123	1148	1163	1320	72	63
20-25	1179	1154	1176	1170	1131	1169	1109	1138	1153	1324	73	63
25-30	1173	1161	1175	1170	1124	1166	1109	1133	1151	1317	74	63
30-35	1174	1137	1175	1162	1128	1171	1119	1139	1151	1306	74	63
35-40	1174	1166	1175	1172	1105	1152	1114	1124	1148	1307	74	63

Test Time Interval Minutes	Probe Water Temp, °F			q_w*	Radiometer 81510				Radiometer 72804 with 7° View			
	In	Out	Diff		Min mv	Max mv	Mean mv	Mean Flux*	Min mv	Max mv	Mean mv	Mean Flux*
10-15	67.70	80.30	12.6	811.60			0.880	5245				
15-20	67.90	81.00	13.1	843.80			0.956	5698				
20-25	68.00	81.30	13.3	856.60			0.940	5603				
25-30	68.00	81.40	13.4	863.10			0.922	5495				
30-35	68.00	81.51	13.45	866.30			0.978	5829				
35-40	68.23	81.72	13.5	869.50			0.998	5948				

TABLE C-6--Continued

Run No: 042971-12-6-2 Fuel: JP-4 Burner Dia, In: 12 Test Time, Min: 36.33 Water Flow, lb/hr: 28.6

Test Time Interval Minutes	Probe Surface Temperature, °F									Cylinder Flame Temp, °F	Air Temp °F	Fuel Temp °F
	1T	2T	3T	Mean T	1B	2B	3B	Mean B	Probe Mean			
11.3-16.3	1164	1168	1178	1170	1121	1162	1108	1130	1150	1300	72.5	65
16.3-21.3	1161	1174	1176	1170	1113	1150	1110	1124	1147	1312	73.0	65
21.3-26.3	1156	1153	1169	1159	1110	1149	1100	1120	1140	1308	74.0	65
26.3-31.3	1171	1175	1180	1175	1108	1148	1105	1120	1148	1313	74.5	65
31.3-36.3	1170	1179	1187	1179	1091	1148	1122	1120	1150	1294	75.5	65

Test Time Interval Minutes	Probe Water Temp, °F			q_w*	Radiometer 81510				Radiometer 72804 with 7° View			
	In	Out	Diff		Min mv	Max mv	Mean mv	Mean Flux*	Min mv	Max mv	Mean mv	Mean Flux*
11.3-16.3	67.68	81.69	14.01	752.0			.906	5400				
16.3-21.3	67.98	82.47	14.49	777.7			.890	5305				
21.3-26.3	68.13	82.58	14.45	775.6			.866	5162				
26.3-31.3	68.44	83.07	14.63	785.3			.958	5710				
31.3-36.3	68.72	83.65	14.93	801.4			.960	5722				

TABLE C-6--Continued

Run No: 042971-12-6-3 Fuel: JP-4 Burner Dia, In: 12 Test Time, Min: 48.81 Water Flow, lb/hr: 26.2

Test Time Interval Minutes	Probe Surface Temperature, °F									Cylinder Flame Temp, °F	Air Temp °F	Fuel Temp °F
	1T	2T	3T	Mean T	1B	2B	3B	Mean B	Probe Mean			
13.8-18.8	1169	1161	1180	1170	1139	1177	1116	1144	1157	1305	75.0	66.0
18.8-23.8	1168	1165	1169	1167	1116	1163	1115	1131	1149	1307	75.5	66.0
23.8-33.8	1172	1110	1170	1151	1134	1177	1126	1146	1148	1306	76.0	66.0
28.8-33.8	1179	1140	1175	1165	1134	1182	1129	1148	1157	1301	76.5	66.0
33.8-38.8	1178	1159	1178	1172	1127	1167	1113	1136	1154	1302	77.0	66.0
38.8-43.8	1175	1156	1173	1168	1116	1163	1113	1131	1149	1300	77.5	66.0
43.8-48.8	1176	1141	1174	1164	1116	1167	1123	1135	1150	1301	78.0	66.0

Test Time Interval Minutes	Probe Water Temp, °F			q_w*	Radiometer 81510				Radiometer 72804 with 7° View			
	In	Out	Diff		Min mv	Max mv	Mean mv	Mean Flux*	Min mv	Max mv	Mean mv	Mean Flux*
13.8-18.8	68.63	8-.31	15.68	841.6			0.956	5698				
18.8-23.8	69.13	85.06	15.93	855.0			0.910	5424				
23.8-33.8	69.45	85.71	16.26	872.7			0.988	5889				
28.8-33.8	69.77	86.07	16.30	874.9			1.014	6044				
33.8-38.8	69.97	86.39	16.42	881.3			1.004	5984				
38.8-43.8	70.02	86.72	16.70	896.4			1.000	5960				
43.8-48.8	70.12	86.85	16.73	898.0			0.998	5948				

TABLE C-7

EXPERIMENTAL DATA FOR METHANOL FLAMES

Run No: 082771-24-7-1 Fuel: Methanol Burner Dia, In: 24 Test Time, Min: 33.02 Water Flow, lb/hr: 46.8

Test Time Interval Minutes	Probe Surface Temperature, °F									Cylinder Flame Temp, °F	Air Temp °F	Fuel Temp °F
	1T	2T	3T	Mean T	1B	2B	3B	Mean B	Probe Mean			
13-18	1110	1068	1003	1060	1131	1113	1091	1112	1086	--	96.7	87.7
18-23	1117	1063	972	1051	1138	1106	1074	1106	1078	973	97.2	87.5
23-28	1114	1064	986	1055	1137	1110	1085	1111	1083	973	96.9	87.1
28-33	1089	1057	982	1043	1134	1114	1084	1111	1077	973	97.8	86.7

Test Time Interval Minutes	Probe Water Temp, °F			q_w*	Radiometer 81510				Radiometer 72804 with 7° View			
	In	Out	Diff		Min mv	Max mv	Mean mv	Mean Flux*	Min mv	Max mv	Mean mv	Mean Flux*
13-18	86.63	94.05	7.42	709.9	.534	1.000	.767	4571.5	.0365	.0735	.0550	2310
18-23	86.88	94.34	7.46	713.7	.530	.960	.745	4440.4	.0330	.0665	.0498	2091.6
23-28	86.99	94.51	7.52	719.5	.534	.974	.754	4494.0	.0335	.0670	.0503	2112.6
28-33	87.13	94.71	7.58	725.2	.522	.974	.748	4458.3	.0295	.0623	.0459	1927.8

*Units: Btu/hr-ft^2.

TABLE C-7--Continued

Run No: 083071-24-7-1 Fuel: Methanol Burner Dia, In: 24 Test Time, Min: 34.13 Water Flow, lb/hr: 39

Test Time Interval Minutes	Probe Surface Temperature, °F									Cylinder Flame Temp, °F	Air Temp °F	Fuel Temp °F
	1T	2T	3T	Mean T	1B	2B	3B	Mean B	Probe Mean			
9.1-14.1	1068	1037	996	1034	1109	1111	1091	1104	1069	966	77.6	75.7
14.1-19.1	1080	1047	1007	1045	1114	1115	1093	1107	1076	959	77.9	75.7
19.1-24.1	1083	1054	1008	1048	1116	1120	1099	1112	1080	966	78.3	75.7
24.1-29.1	1097	1049	995	1047	1122	1117	1097	1112	1080	950	79.0	75.8
29.1-34.1	1090	1051	1006	1049	1119	1114	1095	1109	1079	947	79.6	75.8

Test Time Interval Minutes	Probe Water Temp, °F			q_w*	Radiometer 81510				Radiometer 72804 with 7° View			
	In	Out	Diff		Min mv	Max mv	Mean mv	Mean Flux*	Min mv	Max mv	Mean mv	Mean Flux*
9.1-14.1	81.83	90.19	8.36	666.5	.490	.938	.714	4255.6	.0382	.0667	.0525	2205
14.1-19.1	82.07	90.62	8.55	681.7	.490	.930	.710	4231.8	.0372	.0710	.0561	2356.2
19.1-24.1	82.18	90.90	8.72	695.2	.482	.906	.694	4136.4	.0417	.0696	.0557	2339.4
24.1-29.1	82.19	90.89	8.70	693.6	.472	.912	.692	4124.5	.0407	.0700	.0554	2326.8
29.1-34.1	82.10	90.81	8.71	694.4	.476	.916	.696	4148.3	.0395	.0685	.0540	2268

TABLE C-7--Continued

Run No: 083071-24-7-2 Fuel: Methanol Burner Dia, In: 24 Test Time, Min: 29.07 Water Flow, lb/hr: 39

Test Time Interval Minutes	Probe Surface Temperature, °F									Cylinder Flame Temp, °F	Air Temp °F	Fuel Temp °F
	1T	2T	3T	Mean T	1B	2B	3B	Mean B	Probe Mean			
9.6-14.6	1061	1056	1033	1050	1101	1120	1110	1110	1080	960	80.3	79.2
14.6-19.6	1069	1059	1028	1052	1111	1119	1108	1113	1082	971	80.5	79.2
19.6-24.6	1083	1063	1020	1055	1116	1122	1107	1115	1085	948	80.9	79.1
24.6-29.6	1091	1065	1025	1060	1118	1123	1111	1117	1089	951	81.6	79.1

Test Time Interval Minutes	Probe Water Temp, °F			q_w*	Radiometer 81510				Radiometer 72804 with 7° View			
	In	Out	Diff		Min mv	Max mv	Mean mv	Mean Flux*	Min mv	Max mv	Mean mv	Mean Flux*
9.6-14.6	81.55	90.23	8.68	692.0	.486	.918	.702	4184.1	.0365	.0665	.0515	2163
14.6-19.6	81.67	90.62	8.95	713.6	.480	.908	.694	4136.4	.0387	.0667	.0527	2213.4
19.6-24.6	81.84	90.79	8.95	713.6	.484	.906	.695	4142.4	.0402	.0645	.0524	2200.8
24.6-29.6	81.99	91.03	9.04	720.7	.470	.894	.682	4064.9	.0415	.0662	.0539	2263.8

TABLE C-7--Continued

Run No: 08307-24-7-3 Fuel: Methanol Burner Dia, In: 24 Test Time, Min: 36.4 Water Flow, lb/hr: 39

Test Time Interval Minutes	Probe Surface Temperature, °F									Cylinder Flame Temp, °F	Air Temp °F	Fuel Temp °F
	1T	2T	3T	Mean T	1B	2B	3B	Mean B	Probe Mean			
11.4-16.4	1082	1055	1005	1047	1122	1111	1099	1111	1079	952	82.9	84.1
16.4-21.4	1075	1061	1024	1053	1117	1121	1107	1115	1084	961	83.3	83.9
21.4-26.4	1080	1050	1007	1046	1118	1113	1097	1109	1078	964	83.1	83.6
26.4-31.4	1085	1052	1006	1048	1121	1114	1095	1110	1079	947	83.1	83.4
31.4-36.4	1084	1063	1016	1054	1121	1121	1106	1116	1085	959	84.8	83.2

Test Time Interval Minutes	Probe Water Temp, °F			q_w*	Radiometer 81510				Radiometer 72804 with 7° View			
	In	Out	Diff		Min mv	Max mv	Mean mv	Mean Flux*	Min mv	Max mv	Mean mv	Mean Flux*
11.4-16.4	82.03	90.73	8.73	696.0	.518	.938	.728	4339.1	.0422	.0700	.0561	2356.2
16.4-21.4	81.96	90.85	8.89	708.8	.520	.948	.734	4374.8	.0410	.0698	.0554	2326.8
21.4-26.4	82.19	91.02	8.83	704.0	.512	.936	.724	4315.2	.0398	.0655	.0527	2213.4
26.4-31.4	82.27	91.09	8.82	703.2	.516	.960	.738	4398.7	.0393	.0662	.0528	2217.6
31.4-36.4	82.26	91.18	8.92	711.2	.514	.926	.720	4291.4	.0370	.0678	.0524	2200.8

TABLE C-7--Continued

Run No: 081271-18-7-1 Fuel: Methanol Burner Dia, In: 18 Test Time, Min: 39.16 Water Flow, lb/hr: 39

Test Time Interval Minutes	Probe Surface Temperature, °F									Cylinder Flame Temp, °F	Air Temp °F	Fuel Temp °F
	1T	2T	3T	Mean T	1B	2B	3B	Mean B	Probe Mean			
9.2-14.2	987	965	1025	992	1065	1068	1088	1074	1033	959	90.5	80.3
14.2-19.2	970	961	1021	986	1058	1062	1086	1069	1028	959	91.6	80.3
19.2-24.2	963	972	1020	985	1058	1066	1090	1071	1028	957	91.6	80.3
24.2-29.2	961	968	1031	987	1054	1062	1089	1068	1028	969	92.0	80.3
29.2-34.2	975	962	1023	987	1058	1062	1089	1070	1028	961	91.0	80.3
34.2-39.2	959	960	1035	985	1055	1061	1086	1067	1026	980	92.0	80.2

Test Time Interval Minutes	Probe Water Temp, °F			q_w*	Radiometer 81510				Radiometer 72804 with 7° View			
	In	Out	Diff		Min mv	Max mv	Mean mv	Mean Flux*	Min mv	Max mv	Mean mv	Mean Flux*
9.2-14.2	83.89	92.01	8.12	650.6	.360	.614	.487	2902.7	.0372	.0776	.0574	2410.8
14.2-19.2	84.19	92.31	8.12	650.6	.348	.588	.468	2789.4	.0349	.0770	.0560	2352.0
19.2-24.2	84.39	92.49	8.10	649.0	.350	.594	.472	2813.2	.0353	.0797	.0575	2415.0
24.2-29.2	84.48	92.63	8.15	653.0	.350	.598	.474	2825.2	.0346	.0772	.0559	2347.8
29.2-34.2	84.56	92.75	8.19	656.2	.352	.598	.475	2831.1	.0334	.0763	.0549	2305.8
34.2-39.2	84.81	92.94	8.13	651.4	.348	.582	.465	2771.5	.0368	.0786	.0577	2423.4

TABLE C-7--Continued

Run No: 081271-18-7-2 Fuel: Methanol Burner Dia, In: 18 Test Time, Min: 50.11 Water Flow, lb/hr: 39.0

Test Time Interval Minutes	Probe Surface Temperature, °F									Cylinder Flame Temp, °F	Air Temp °F	Fuel Temp °F
	1T	2T	3T	Mean T	1B	2B	3B	Mean B	Probe Mean			
20.1-25.1	989	915	1000	968	1067	1042	1087	1065	1017	928	92.8	81.4
25.1-30.1	992	911	1000	968	1067	1040	1086	1064	1016	938	93.8	81.3
30.1-35.1	992	913	996	967	1067	1038	1090	1065	1016	933	93.2	81.3
35.1-40.1	1001	907	996	968	1073	1035	1084	1064	1016	933	93.7	81.3
40.1-45.1	997	899	986	961	1070	1030	1080	1060	1010	933	94.3	81.2
45.1-50.1	999	913	1000	971	1072	1041	1088	1067	1019	933	93.9	81.2

Test Time Interval Minutes	Probe Water Temp, °F			q_w*	Radiometer 81510				Radiometer 72804 with 7° View			
	In	Out	Diff		Min mv	Max mv	Mean mv	Mean Flux*	Min mv	Max mv	Mean mv	Mean Flux*
20.1-25.1	84.99	93.16	8.17	654.6	.394	.648	.521	3105.3	.0154	.0540	.0347	1457.4
25.1-30.1	85.14	93.43	8.29	664.2	.394	.662	.578	3147.0	.0126	.0570	.0348	1461.6
30.1-35.1	85.29	93.54	8.25	661.0	.398	.626	.512	3051.7	.0119	.0540	.0330	1386.0
35.1-40.1	85.40	93.67	8.27	662.6	.390	.642	.516	3075.5	.0114	.0502	.0308	1293.6
40.1-45.1	85.54	93.83	8.29	664.2	.386	.654	.520	3099.3	.0117	.0513	.0315	1323.0
45.1-50.1	85.72	93.97	8.25	661.0	.384	.652	.518	3087.4	.0129	.0516	.0323	1356.6

TABLE C-7--Continued

Run No: 081271-18-7-3 Fuel: Methanol Burner Dia, In: 18 Test Time, Min: 41.12 Water Flow, lb/hr: 39.0

Test Time Interval Minutes	Probe Surface Temperature, °F									Cylinder Flame Temp, °F	Air Temp °F	Fuel Temp °F
	1T	2T	3T	Mean T	1B	2B	3B	Mean B	Probe Mean			
11.1-16.1	1006	916	984	969	1075	1047	1076	1066	1017	961	91.7	82.8
16.1-21.1	1009	928	985	974	1075	1051	1073	1066	1020	959	91.9	82.7
21.1-26.1	1003	922	982	969	1072	1051	1073	1065	1017	956	91.4	82.7
26.1-31.1	1007	913	983	968	1071	1050	1076	1066	1017	961	90.9	82.6
31.1-36.1	1008	926	982	972	1071	1053	1076	1067	1019	958	91.0	82.6
36.1-41.1	1007	923	984	971	1074	1050	1073	1066	1019	955	91.0	82.5

Test Time Interval Minutes	Probe Water Temp, °F			q_w*	Radiometer 81510				Radiometer 72804 with 7° View			
	In	Out	Diff		Min mv	Max mv	Mean mv	Mean Flux*	Min mv	Max mv	Mean mv	Mean Flux*
11.1-16.1	85.66	93.31	7.65	612.9	.334	.556	.445	2652.3	.0128	.0491	.0310	1302
16.1-21.1	85.69	93.47	7.78	623.3	.328	.560	.444	2646.4	.0120	.0498	.0309	1297.8
21.1-26.1	85.72	93.50	7.78	623.3	.326	.554	.440	2622.5	.0116	.0494	.0305	1281
26.1-31.1	85.82	93.53	7.71	617.7	.330	.544	.435	2592.7	.0149	.0497	.0323	1356.6
31.1-36.1	85.83	93.60	7.77	622.5	.330	.534	.432	2574.8	.0114	.0460	.0287	1205.4
36.1-41.1	85.94	93.66	7.72	618.5	.320	.524	.422	2515.2	.0127	.0506	.0317	1331.4

TABLE C-7--Continued

Run No: 070871-12-7-1 Fuel: Methanol Burner Dia, In: 12 Test Time, Min: 52.1 Water Flow, lb/hr: 37.7

Test Time Interval Minutes	Probe Surface Temperature, °F									Cylinder Flame Temp, °F	Air Temp °F	Fuel Temp °F
	1T	2T	3T	Mean T	1B	2B	3B	Mean B	Probe Mean			
17.1-22.1	845	855	883	861	1012	1919	1028	1020	940	709	97.5	85
22.1-27.1	845	843	883	857	1015	1021	1029	1022	939	696	96	85
27.1-32.1	887	807	819	838	1023	1021	1019	1021	929	641	97.5	85
32.1-37.1	879	821	822	841	1023	1023	1026	1024	932	598	96	85
37.1-42.1	896	807	809	837	1024	1023	1020	1022	930	593	97	84.5
42.1-47.1	893	830	815	846	1022	1024	1021	1022	934	590	96	84.5
47.1-52.1	902	807	804	838	1023	1022	1021	1022	930	576	96.3	84.5

Test Time Interval Minutes	Probe Water Temp, °F			q_w*	Radiometer 81510				Radiometer 72804 with 7° View			
	In	Out	Diff		Min mv	Max mv	Mean mv	Mean Flux*	Min mv	Max mv	Mean mv	Mean Flux*
17.1-22.1	84.90	91.82	6.92	538.6	.159	.277	.218	1299.3		.0182		
22.1-27.1	84.98	91.93	6.95	540.9	.171	.267	.219	1305.3		.0135		
27.1-32.1	95.16	92.01	6.85	533.1	.146	.253	.200	1192.1		.0125		
32.1-37.1	85.32	92.06	6.64	516.8	.147	.255	.201	1198.0		.0133		
37.1-42.1	85.41	92.19	6.78	527.7	.143	.252	.198	1180.1		.0124		
42.1-47.1	85.66	92.46	6.80	529.2	.142	.259	.201	1198.0		.0140		
47.1-52.1	85.86	92.55	6.69	520.7	.141	.249	.195	1162.3		.0112		

TABLE C-7--Continued

Run No: 070871-12-7-2 Fuel: Methanol Burner Dia, In: 12 Test Time, Min: 48.67 Water Flow, lb/hr: 37.7

Test Time Interval Minutes	Probe Surface Temperature, °F									Cylinder Flame Temp, °F	Air Temp °F	Fuel Temp °F
	1T	2T	3T	Mean T	1B	2B	3B	Mean B	Probe Mean			
13.7-18.7	887	879	847	871	1030	1033	1027	1030	951	640	95.5	88.0
18.7-23.7	897	875	842	871	1032	1032	1022	1029	950	647	95.5	88.0
23.7-28.7	887	879	846	871	1033	1036	1026	1032	951	656	97.5	87.5
28.7-33.7	846	894	890	877	1008	1022	1031	1020	949	717	98.5	87.5
33.7-38.7	841	898	878	872	1012	1024	1029	1022	947	730	98.0	87.5
38.7-43.7	849	898	869	872	1017	1026	1029	1024	948	718	97.0	87.0
43.7-48.7	859	908	863	877	1018	1027	1024	1023	950	697	97.5	87.0

Test Time Interval Minutes	Probe Water Temp, °F			q_w*	Radiometer 81510				Radiometer 72804 with 7° View			
	In	Out	Diff		Min mv	Max mv	Mean mv	Mean Flux*	Min mv	Max mv	Mean mv	Mean Flux*
13.7-18.7	85.36	92.37	7.01	545.6	.143	.258	.201	1198.0				
18.7-23.7	85.60	92.67	7.07	550.2	.139	.257	.198	1180.1				
23.7-28.7	85.84	92.92	7.09	551.8	.142	.263	.203	1210.1				
28.7-33.7	85.93	93.04	7.11	553.4	.147	.271	.200	1245.7				
33.7-38.1	86.01	93.12	7.11	553.4	.143	.266	.205	1221.9				
38.7-43.7	86.23	93.36	7.13	559.9	.140	.263	.202	1204.0				
43.7-48.7	86.25	93.38	7.13	554.9	.138	.256	.197	1174.2				

TABLE C-7--Continued

Run No: 070871-12-7-3 Fuel: Methanol Burner Dia, In: 12 Test Time, Min: 67.25 Water Flow, lb/hr: 39.0

Test Time Interval Minutes	Probe Surface Temperature, °F									Cylinder Flame Temp, °F	Air Temp °F	Fuel Temp °F
	1T	2T	3T	Mean T	1B	2B	3B	Mean B	Probe Mean			
42.3-49.3	855	827	816	833	1016	1011	1007	1011	922	634	96.5	87
47.3-52.3	870	841	831	847	1024	1021	1017	1021	934	655	96.0	87
52.3-57.3	870	843	828	847	1024	1019	1015	1019	933	660	96.5	86.5
57.3-62.3	872	840	823	845	1025	1019	1009	1018	931	666	96.5	86
62.3-67.3	867	841	826	845	1025	1018	1016	1020	932	665	97.0	86

Test Time Interval Minutes	Probe Water Temp, °F			q_w*	Radiometer 81510				Radiometer 72804 with 7° View			
	In	Out	Diff		Min mv	Max mv	Mean mv	Mean Flux*	Min mv	Max mv	Mean mv	Mean Flux*
42.3-47.3	86.94	93.82	6.88	553.9	.142	.273	.208	1239.7				
47.3-52.3	86.99	93.95	6.96	560.4	.143	.275	.209	1245.7				
52.3-57.3	87.10	94.02	6.92	557.1	.146	.276	.211	1257.6				
57.3-67.3	87.14	94.13	6.99	562.8	.142	.267	.205	1221.9				
62.3-67.3	87.15	94.14	6.99	562.8	.142	.270	.206	1227.8				

APPENDIX D

CHARACTERISTICS OF FUEL SYSTEM

General

The burner fuel level control system described in Chapter IV is best suited for short distances between the fuel reservoir and the burner. The system is basically a constant head siphon which uses the fuel in the delivery lines as a liquid seal between the burner and fuel tank. The end of the breather tube is positioned at the static level desired for the fuel in the burner. When the valve on the bottom of the fuel tank is opened, fuel flows into the burner until the liquid head at the burner balances the head at the end of the breather tube. The liquid head above the end of the breather tube is balanced by the vacuum created by the initial removal of fuel from the sealed tank. As fuel is burned and the burner level starts to drop, air is sucked into the fuel tank through the breather tube and the pressure rises lightly in the vacuum space and more fuel flows out of the reservoir. When the fuel use rate is constant, accurate control can be established, and the fuel level maintained without much attention.

When the connecting line between the burner and fuel tank is long or has a number of fittings, then the fuel level

in the burner is lower than the level at the end of the breather tube due to the flowing pressure losses in the line.

Dimensional Information

Figure D-1 shows the pertinent dimensions of the fuel delivery system. The line between the fuel tank and the burner consists of the components listed in Table D-1. This table also lists the turbulent flow equivalent length to diameter ratio for fittings.

Table D-1. Fuel Line Components

Quantity	Description	L_1/D_1
1	1" sch. 40, Brass Pipe Nipple 2" long	--
1	1" Ball Valve	--
1	1" Gate Valve	13
3	1" Pipe x 1" c.w.t.* solder male adapter	--
8	1" c.w.t. 90° solder elbow	30
1	1" c.w.t. 45° solder elbow	16
2	1" c.w.t. solder tee branch	60
1	1" c.w.t. solder tee run	20
2	1" c.w.t. solder union	--
1	L' c.w.t. x 3/8" pipe solder female adapter	--
1	20.69' of 1" ridgid c.w.t.	--
1	1" x 1/2" pipe bushing	--
1	1/2" pipe 90° street elbow	3-
1	1/2" x 3/8" pipe 90° reducing elbow	50
1	1/2" sch. 40 pipe nipple, 3" long	--
1	16" of 5/8" c.w.t.	--
2	5/8" tube to 3/8" m.p.t. tube fitting	--

* c.w.t. = copper water tube

The diameter and depth of the fuel pans were measured at several locations and the results are shown in Tables D-2,

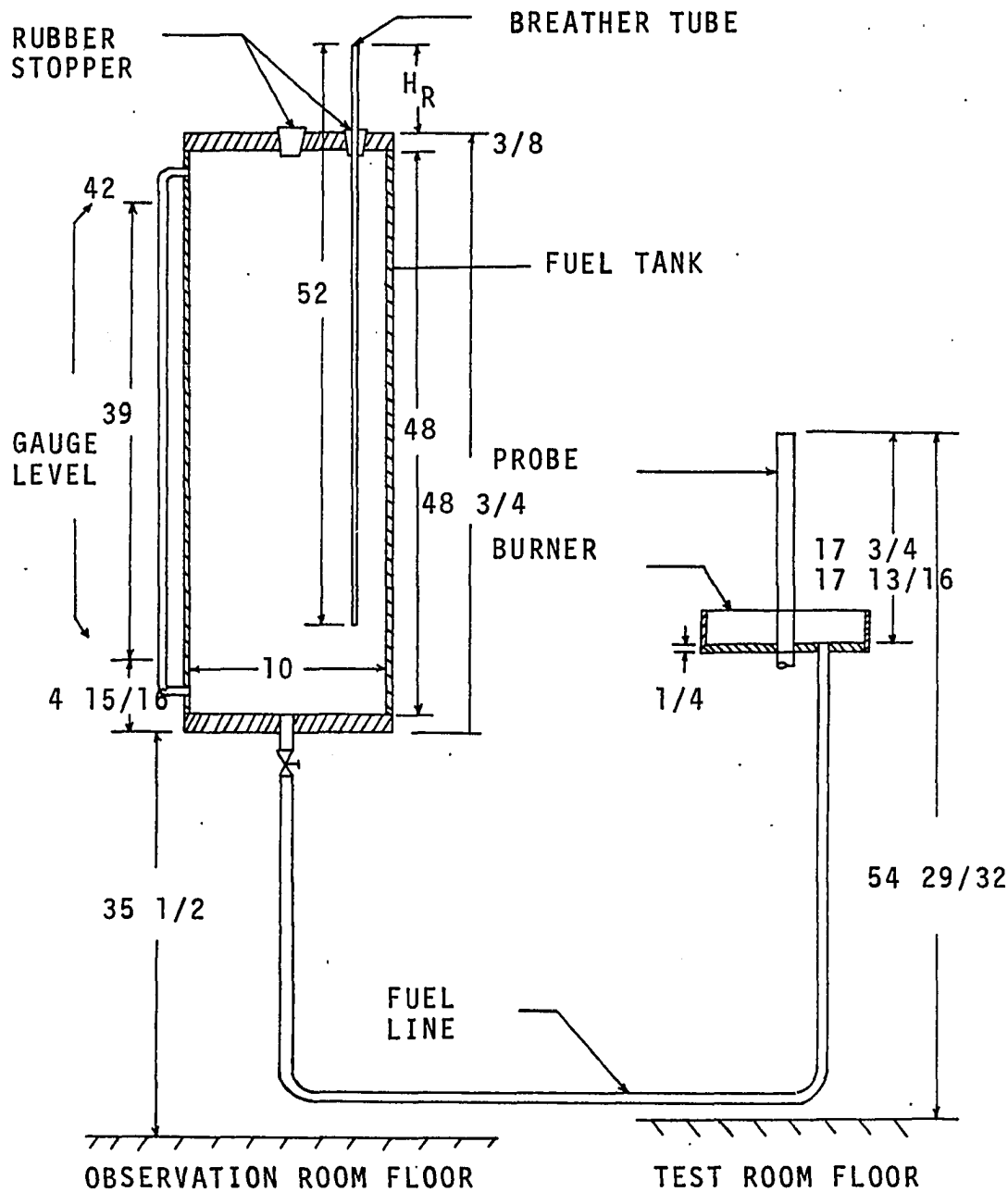


Figure D-1. Pertinent Dimensions of Fuel System.

D-3, and D-4. Measured volumes of water were added to the pans and the water depth was measured at 5 locations. These results along with the calculated depth of the water are also given in Tables D-2, D-3, and D-4. From these tables, it can be seen that the diameter of the fuel pan can be taken as 12", 18" and 24". For the 12" and 18" fuel pan the depth of the fuel can be calculated from the measured volume and the cross sectional area of the pan. For the 24" burner, the fuel depth, H_p, can be calculated by the equation

$$H_p = (ml-1150)(.13608)(10^{-3}) + .25 \qquad (D-1)$$

where ml is the measured volume in milliters. This equation accounts for the deformation of the fuel pan bottom.

Comparisons of the measured height of the fuel surface with that predicted by the breather rod height led to the conclusion that the test room floor was higher than the observation room floor. In order to predict fuel pan level from breather rod height, this difference in floor levels had to be determined. To do this, the fuel pan was replaced by a graduated burette because of the difficulty in obtaining accurate depth measurements with a large fuel pan. Nineteen readings of tank gauge level and burette level were used to obtain the following equation

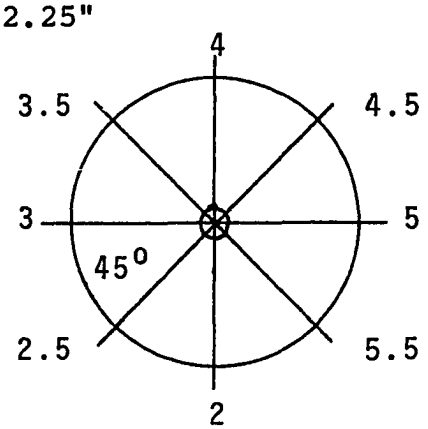
$$Z_t = 1.017 + 1.00054(Z_p) \qquad (D-2)$$

TABLE D-2

MEASURED DIMENSIONS AND VOLUME FOR THE
24-INCH DIAMETER FUEL PAN

Center Diameter = 2.25"

Position	Depth inches
1	2
2	2
3	2
4	2
5	2



Position	Inside Diameter inches
2-4	24.062
3-5	23.938
2.5-4.5	23.812
3.5-5.5	24.093

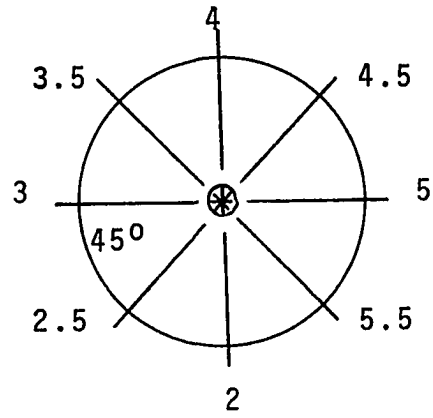
Water Volume ml	Water Depth, inches							Mean minus Calc.
	Measured at Position					Mean	Calc.	
	1	2	3	4	5			
1150	0.250	0.234	0.062	0.109	0.047	0.140	0.156	-0.016
3085	0.500	0.516	0.328	0.406	0.344	0.419	0.420	-0.001
4985	0.750	0.734	0.594	0.625	0.562	0.653	0.678	-0.025
6705	1.000	1.000	0.797	0.906	0.812	0.903	0.912	-0.009
8485	1.250	1.250	1.062	1.109	1.047	1.144	1.155	-0.011
10310	1.500	1.484	1.312	1.359	1.297	1.390	1.403	-0.013
12285	1.750	1.781	1.594	1.656	1.597	1.675	1.672	-0.003

TABLE D-3

MEASURED DIMENSIONS AND VOLUME FOR THE
18-INCH DIAMETER FUEL PAN

Center Diameter = 2.25"

Position	Depth inches
1	2.031
2	2.000
3	2.031
4	2.062
5	2.031



Position	Inside Diameter inches
2-4	18.031
3-5	18.000
2.5-4.5	18.016
3.5-5.5	17.984

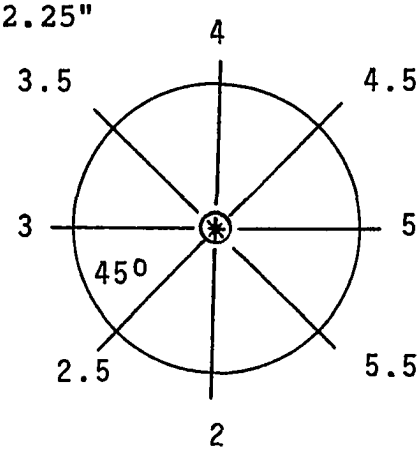
Water Volume ml	Water Depth, inches							
	Measured at Position					Mean	Calc.	Mean minus Calc.
	1	2	3	4	5			
1060	0.250	0.250	0.266	0.266	0.281	0.262	0.258	0.004
2110	0.500	0.484	0.500	0.500	0.547	0.506	0.514	-0.008
3220	0.750	0.750	0.766	0.766	0.797	0.766	0.784	-0.018
4220	1.000	1.000	1.031	1.031	1.047	1.022	1.028	-0.006
5260	1.250	1.234	1.281	1.281	1.297	1.269	1.281	-0.012
6355	1.500	1.531	1.562	1.531	1.562	1.540	1.548	-0.008
7366	1.750	1.750	1.812	1.781	1.812	1.784	1.792	-0.008

TABLE D-4

MEASURED DIMENSIONS AND VOLUME FOR THE
12-INCH DIAMETER FUEL PAN

Center Diameter = 2.25"

Position	Depth inches
1	2.125
2	2.094
3	2.125
4	2.094
5	2.125



Position	Inside Diameter inches
2-4	12.000
3-5	12.031
2.5-4.5	12.031
3.5-5.5	12.000

Water Volume ml	Water Depth, inches							Mean minus Calc.
	Measured at Position					Mean	Calc.	
	1	2	3	4	5			
475	0.250	0.250	0.281	0.219	0.281	0.256	0.266	-0.010
898	0.500	0.500	0.500	0.469	0.531	0.500	0.502	-0.002
1358	0.750	0.750	0.750	0.734	0.766	0.750	0.759	-0.009
1828	1.000	1.000	1.031	1.000	1.031	1.013	1.022	-0.009
2303	1.250	1.250	1.281	1.234	1.281	1.259	1.288	-0.029
2735	1.500	1.500	1.531	1.484	1.531	1.509	1.529	-0.020
3185	1.750	1.750	1.781	1.734	1.797	1.762	1.781	-0.019

For the 18 and 24" diameter fuel pans with no fuel, Z_p = 37.156" while Z_p = 37.094" for the 12" diameter pan. Using these values and Equation D-2 shows that the test room floor is 1.028" higher than the observation room floor. From the geometry of Figure D-1, it can be seen that the length of the fuel in the burner can be predicted by

$$H_p = 39.25 + H_R - Z_p \qquad \text{(D-3)}$$

Table D-4 shows the values of H_p predicted by Equation D-1, D-3, and values measured at position 1 defined in Table D-2. From Table D-5, it can be seen that the static depth of fuel in the burner can be adequately predicted by Equation D-3. The difference between values of H_p predicted by Equation D-1 and D-3 for values of H_R < 6 1/4 is due to the fact that the line between the tank and the fuel pan is full of liquid and a finite quantity of fluid has to flow out of the tank to produce the necessary vacuum to balance the liquid height above the bottom of the breather tube.

Fuel Pan Equilibrium Time

Now that the static depth of the fuel in the burner can be predicted, the time to reach this equilibrium depth is desirable. Starting with a full fuel line, when the ball valve below the fuel tank is suddenly opened, the liquid level in the tank decreases. Simultaneously a vacuum above the liquid is formed and the liquid in the breather tube begins to fall. In about 10 to 20 seconds, the breather tube is devoid of

TABLE D-5

COMPARISON OF PREDICTED AND MEASURED FUEL DEPTH FOR 24-INCH DIAMETER FUEL PAN

H_R inches	Tank Gage Reading, in		Volume Transferred ml	H_p, inches		
	Initial	Final		Eqn D-1	Eqn D-3	Measured
6	26.60	25.28	1643	0.317	0.056	0.312
6	19.50	18.25	1556	0.305	0.056	0.312
6	18.25	17.00	1556	0.305	0.056	0.312
6 1/8	27.68	26.35	1656	0.319	0.181	0.344
6 1/4	32.00	30.79	1506	0.299	0.306	0.312
6 1/4	25.25	23.92	1531	0.302	0.306	0.312
6 1/4	16.75	15.52	1531	0.302	0.306	0.312
6 1/4	29.00	27.68	1643	0.317	0.306	0.312
6 5/16	30.50	29.00	1868	0.348	0.368	0.375
6 5/16	20.63	18.92	2129	0.383	0.368	0.375
6 3/8	32.47	30.50	2453	0.427	0.431	0.438
6 7/16	23.12	20.63	3100	0.515	0.493	0.500
6/1/2	35.93	33.30	3274	0.539	0.556	0.562
6 1/2	33.30	30.60	3362	0.551	0.556	0.562
6 1/2	30.60	27.91	3349	0.549	0.556	0.562
6 1/2	27.91	25.25	3312	0.544	0.556	0.562
6 1/2	25.25	22.56	3349	0.549	0.556	0.562
6 1/2	22.56	19.90	3312	0.544	0.556	0.562
6 1/2	19.90	17.26	3287	0.541	0.556	0.562
6 1/2	17.26	14.60	3312	0.544	0.556	0.562
6 1/2	14.60	11.91	3349	0.549	0.556	0.562
6 1/2	34.05	31.40	3299	0.542	0.556	0.562
6 1/2	30.00	27.28	3386	0.554	0.556	0.562
6 1/2	37.98	35.13	3548	0.576	0.556	0.562
6 1/2	36.04	33.30	3411	0.558	0.556	0.562
6 17/32	34.00	31.02	3710	0.598	0.587	0.594
6 17/32	34.00	31.07	3648	0.590	0.587	0.594
6 9/16	26.34	23.12	4009	0.639	0.618	0.625
6 9/16	42.00	39.00	3735	0.602	0.618	0.625
6 9/16	39.00	35.93	3822	0.614	0.618	0.625
6 5/8	36.01	32.50	4370	0.688	0.681	0.688
6 3/4	25.15	20.92	5266	0.810	0.806	0.812
6 3/4	20.05	15.82	5266	0.810	0.806	0.812
6 7/8	25.27	20.26	6160	0.942	0.931	0.938
7	42.00	36.44	6922	1.306	1.056	1.062
7	36.43	30.75	7072	0.056	1.056	1.062
7	30.75	24.95	7221	0.076	1.056	1.062
7	24.95	19.25	7097	0.059	1.056	1.062

TABLE D-5--Continued

H_R inches	Tank Gage Reading, in		Volume Transferred ml	H_p, inches		
	Initial	Final		Eqn D-1	Eqn D-3	Measured
7	19.25	13.45	7221	1.076	1.056	1.062
7	13.45	7.65	7221	1.076	1.056	1.062
7	31.00	25.27	7134	1.064	1.056	1.062
7 1/4	31.70	24.36	9138	1.337	1.306	1.312
7 1/4	38.00	31.01	8703	1.278	1.306	1.312

of liquid and a bubbling sound can be heard. When the bubbling sound ceases the fuel pan equilibrium depth is reached.

The difference in tank fuel level versus time up to the equilibrium point is plotted in Figure D-2. This change in tank level cnn be predicted by the simultaneous solution of the following equations

$$A_T \frac{dH_T}{dt} = - \frac{H_T - H_p}{R_1} \qquad (D\text{-}4)$$

$$A_s \frac{dH_p}{dt} = \frac{H_T - H_p}{R_1} \qquad (D\text{-}5)$$

with the boundary conditions that $H_p = 0$ and $H_p = H_b$ at $t = \infty$ along with $A_T(\Delta H_T) = A_s(\Delta H_p)$ the following equation is obtained

$$\Delta H_T = \frac{A_s}{A_T} H_b \left[1 - \rho^{-(A_s+A_T)t/A_s A_T R_1}\right] \qquad (D\text{-}6)$$

If the curves in Figure D-2 are fitted to Equation D-6, the value of $A_s H_b/A_T$ and $(A_s+A_T)/A_s A_T R_1$ can be obtained. A non-linear curve fit program was used to obtain these values and the results are shown in Table D-6. Since A_s, A_T and H_b are known, then the value of $A_s H_b/A_T$ can be calculated, and these results are also shown in Table D-6. The difference in values is primarily caused by the warped bottom of the 24" diameter fuel pan which affects the volume time transfer of the fluid. Therefore, an effective value of A_s was calculated from the curve fitted values of $A_s H_b/A_T$. These effective areas were used to compute the value of $(A_s+A_T)/A_s A_T$, which has an actual

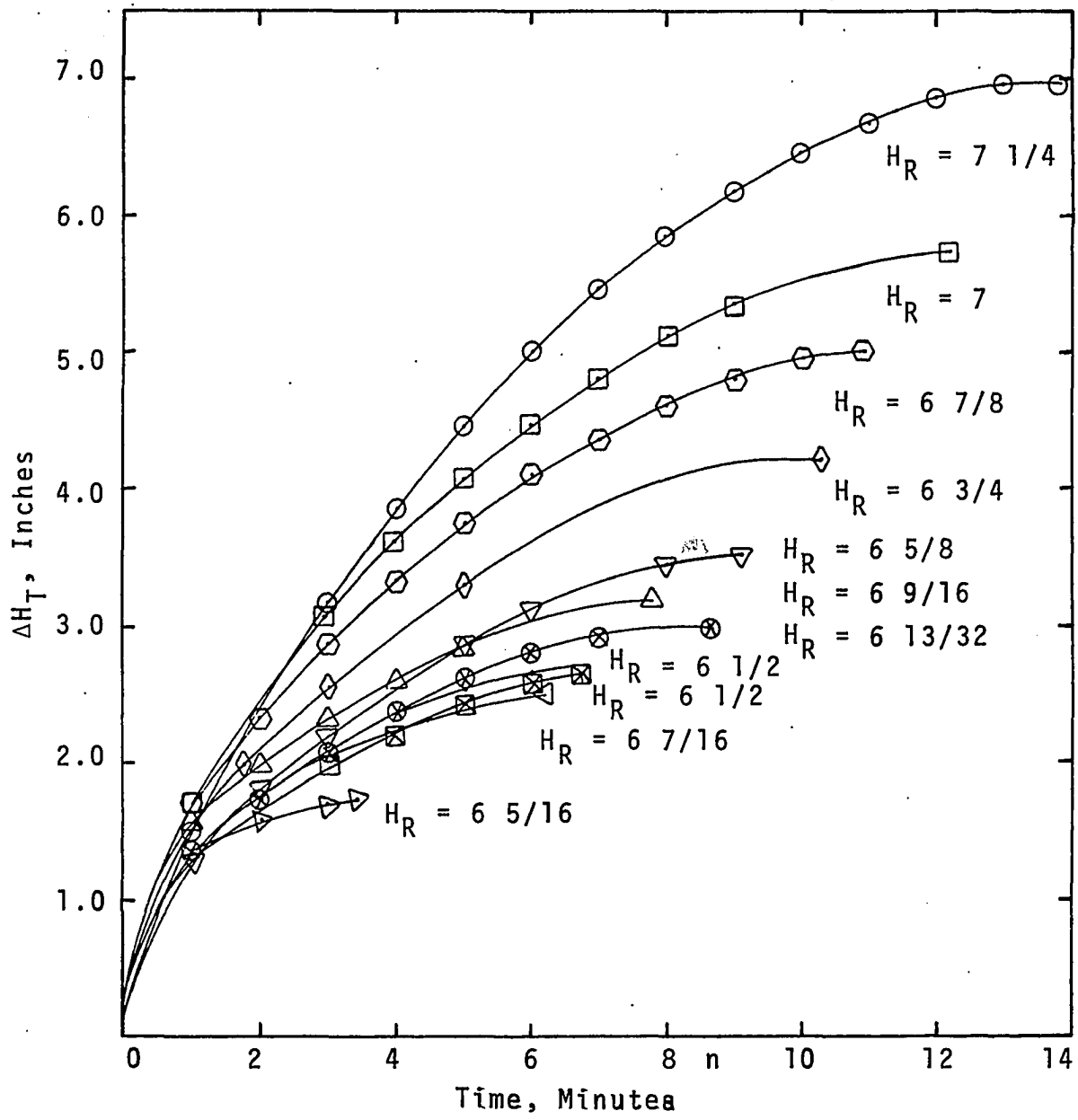


Figure D-2. Fuel Tank Level Difference as a Function of Time with H_R as a Parameter for the 24" Diameter Burner.

value of 0.015393 ft^{-2}. From these results, the line resistance, R_l, was calculated and these values are listed in Table D-6.

TABLE D-6

COEFFICIENTS FOR EQUATION D-6

H_R inches	H_b inches	$A_s H_b / A_T$ curve-fit	inches calculated	Effective A_s in^2	$\frac{A_s + A_T}{A_s A_T}$ ft^{-2}	$\frac{A_s + A_T}{A_s A_T R_l}$ min^{-1}	R_l $\frac{min}{ft^2}$
6 5/16	0.368	1.678	2.172	364.4	0.01605	1.6790	1.3765
6 7/16	0.494	2.503	2.916	384.9	0.01576	0.6048	3.7526
6 1/2	0.556	2.754	3.282	376.3	0.01582	0.5202	4.3794
6 1/2	0.556	2.657	3.282	363.0	0.01592	0.4791	4.7842
6 17/32	0.587	3.063	3.465	396.4	0.01569	0.3933	5.7431
6 9/16	0.618	3.222	3.648	396.1	0.01569	0.4476	5.0470
6 5/8	0.681	3.705	4.020	413.3	0.01558	0.3078	7.2901
6 3/4	0.806	4.217	4.757	397.5	0.01569	0.3331	6.7781
6 7/8	0.931	5.190	5.495	423.5	0.01552	0.2708	8.2555
7	1.056	5.878	6.233	422.9	0.01553	0.2470	9.0527
7 1/4	1.306	7.751	7.708	450.9	0.01538	0.1755	12.6203

Figure D-3 shows that R_l is a linear function of R_b. These results can be used with Equation D-6 to compute the fuel level equilibrium time for the 18 and 12 inch fuel pans.

Equivalent Length of Fuel and Dynamic Fuel Pan Level

For a steady flow of fuel from the tank to the burner, the pressure loss through the fuel line results in a decrease in the burner fuel level. This decrease can be calculated by the modified Bernoulli equation which is

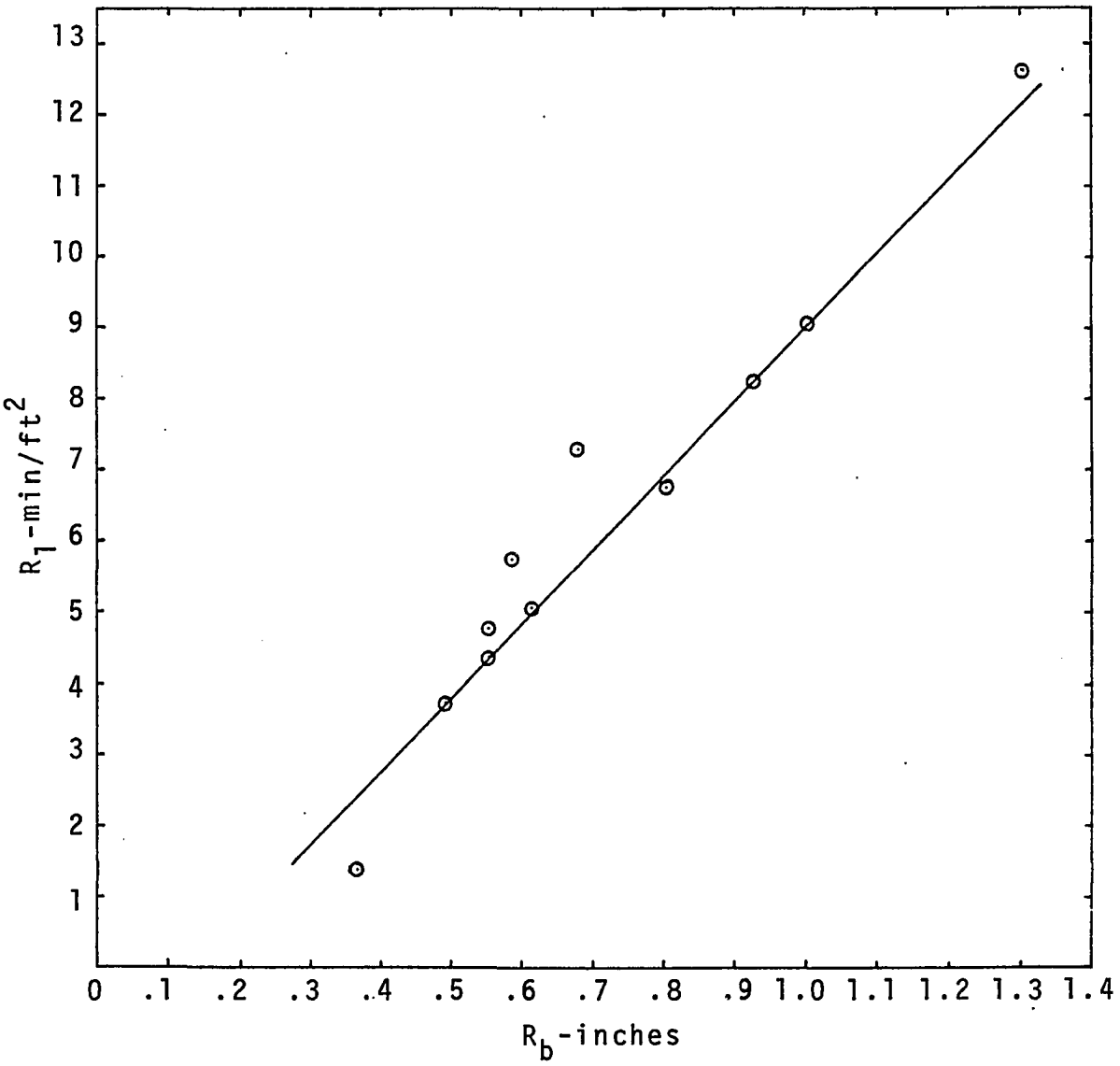


Figure D-3. Line Resistance as a Function of Breather Rod Height Above Bottom of Fuel Pan.

$$\Delta Z = 128\ Q_z \mu L_1 / (\pi D_1^4\ \rho_1 g) \qquad \text{(D-7)}$$

where D_1 = diameter of fuel line, ft

L_1 = length of fuel line, ft

Q_z = volume flow rate through fuel line, ft^3/hr

ΔZ = change in burner fuel level, ft

According to Reference 22, the turbulent flow (L_1/D_1) values given in Table D-1 must be reduced by 0.001 (Re) when the Reynolds number is less than 1000. The pressure loss through the line is a function of $L_1/(D_1)^4$. Utilizing this information the equivalent length of a 1 inch diameter fuel line can be approximated by

$$L_1 = 23.15 + 6.756\ Q_z\ \rho_1/\mu \qquad \text{(D-8)}$$

All the fuel flow rates in this study produce laminar flow Reynolds numbers less than 1000, so the equivalent line length and resulting fuel pan level are variable.

In order to check the validity of Equation D-8, several tests were conducted with water to measure the change in fuel pan level at various flow rates. The flow rate data are shown in Figure D-4, and the calculated line length using Equation D-7 and D-8 are given in Table D-7.

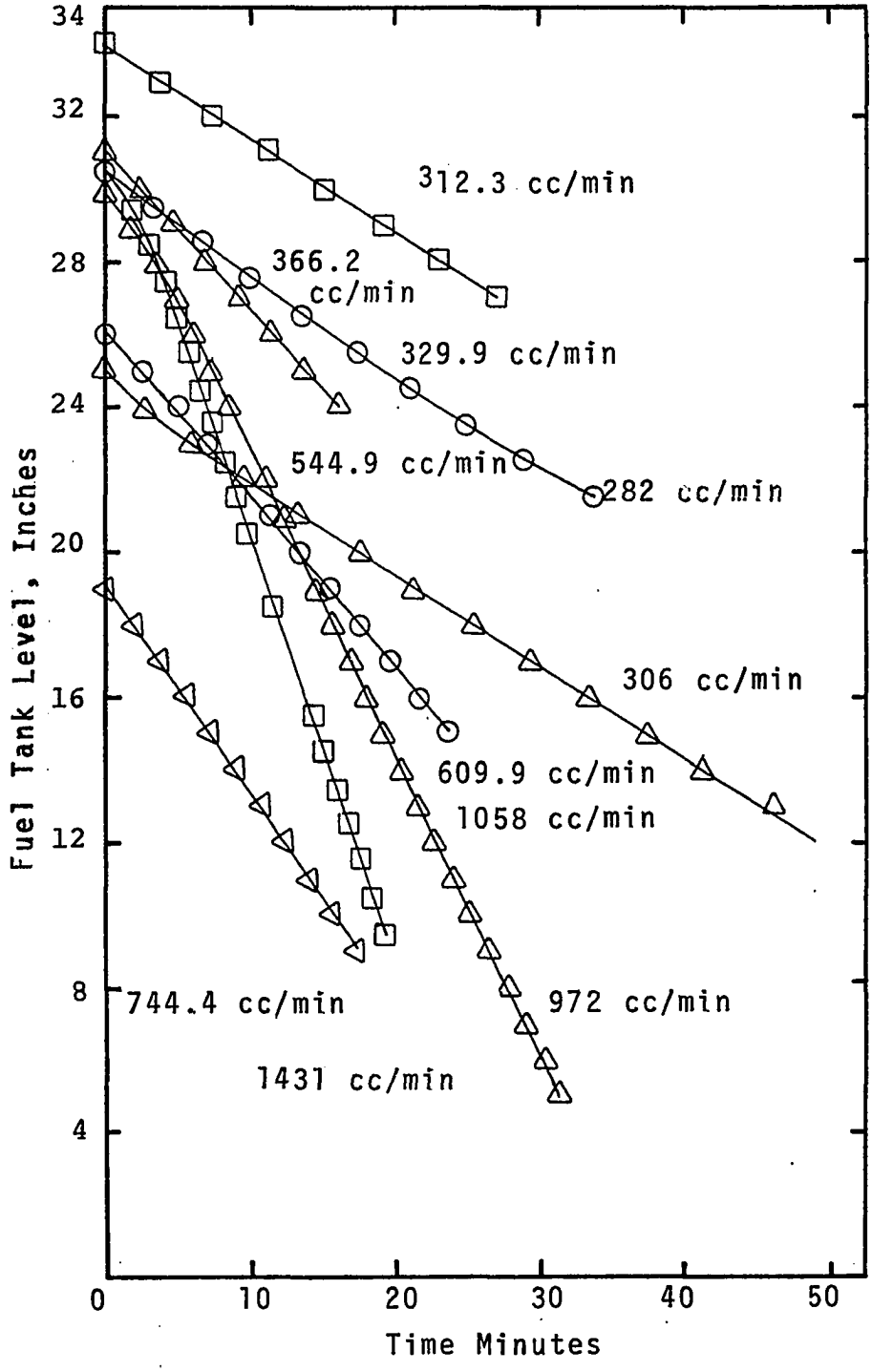


Figure D-4. Fuel Tank Level as a Function of Time.

TABLE D-7

COMPARISON OF MEASURED AND CALCULATED CHANGE IN FUEL PAN LEVEL

H_R inches	Q_z cc/min	ft^3/hr	R_1	Measured ΔZ inches	L_1, ft	
					Eqn D-7	Eqn D-8
6 1/2	306	0.645	284	0.0938	170	148
6 1/2	312.3	0.660	290	0.0625	111	150
6 17/32	329.9	0.696	304	0.0938	170	158
6 1/2	544.9	1.150	505	0.250	254	245
6 1/2	609.9	1.287	566	0.326	298	271
6 1/2	744.4	1.570	690	0.412	309	325
6 1/2	1058	2.23	981	7.556*	292	454
6 17/32	1431	3.02	1330	7.587*	228	608

*Fuel pan completely empty; pan drained.

From Table D-7, it can be seen that Equation D-8 adequately describes the effective fuel line length.

APPENDIX E

COMPUTER PROGRAMS

The programs primarily used in this study are written in BASIC language and are CYLIF, CONIF, CYLOF, and CONOF. Program CYLIF computes the heat flux to a target inside a cylindrical-shaped flame. Program CONIF computes the heat flux to a target inside a conical shaped flame. Program CYLOF computes the heat flux to a target outside a cylindrical-shaped flame. Program CONIF computes the heat flux to a target outside a conical-shaped flame.

PROGRAM CONOF

```
5 PRINT "HEAT FLUX TØ TARGET ØUTSIDE A CØNICAL FLAME"
10 PRINT "C. A. BLØMQUIST, JULY 30, 1972"
15 DIM F(90), B(90), E(90), A(90), S(90)
20 READ M, C1, C2, C3
25 FØR J=1 TØ M
30 READ F(J), B(J), E(J)
35 LET F(J)=F(J)*C1
40 LET B(J)=B(J)*C2
45 LET E(J)=E(J)*C3
50 NEXT J
55 FØR J=1 TØ M
60 READ S(J)
65 LET S(J)=S(J)*C2
70 NEXT J
75 LET H1=9.9375
80 LET R4=13
85 LET X(1)=.069432
90 LET X(2)=.330009
95 LET X(3)=.669991
100 LET X(4)=.930568
105 LET W(1)=.173927
110 LET W(2)=.326073
115 LET W(3)=.326073
120 LET W(4)=.173927
125 READ D2, H2
130 LET R2=D2/2
135 LET L1=-ATN(H1/(R4+R2))
140 LET L2=ATN((H2-H1)/(R4+R2))
145 LET M2=0
146 IF L2 < 1.309 THEN 150
147 LET L2=1.309
150 PRINT
155 PRINT
160 PRINT "FLAME DIA", D2, "FLAME HEIGHT", H2
165 PRINT
170 PRINT "HEIGHT", "          HEAT FLUX, BTU/HR-FT↑2"
175 PRINT "INCHES", "SIDE", "BØTTØM", "TØTAL"
180 LET Q3=0
185 FØR J=1 TØ (M-1)
190 LET Q1=0
192 LET D3=0
193 LET Q2=0
195 FØR K=1 TØ 4
200 LET M1=-1
205 LET G(K)=(L2-L1)*X(K)+L1
206 IF M2 < 1 THEN 210
207 LET R7=-H1/TAN(G(K))
208 LET R6=ATN(SQR((2*R4*R7/(R7↑2+R4↑2-R2↑2))↑2-1))
209 GØ TØ 225
210 LET R=R2*(H2-H1-R4*TAN(G(K)))/(H2*R4)
215 LET R5=1.5707288-.2121144*R+.074261*R↑2-.013729 3*R↑3
```

PROGRAM CONOF (continued)

```
220 LET R6=1.570796-R5*SQR(1-R)
225 LET C(K)=W(K)*COS(G(K))↑2*R6
230 FOR I=1 TO 4
235 LET P(I)=R6*X(I)
240 LET U(I)=R4↑2*SIN(P(I))↑2
245 LET V(I)=-H2+H1+R4*TAN(G(K))*COS(P(I))
250 LET N(I)=TAN(G(K))*SQR(V(I)↑2-U(I)*((H2/R2)↑2-TAN(G(K))↑2))
255 LET R3=((H2/R2)*V(I)+M1*N(I))/((H2/R2)↑2-TAN(G(K))↑2)
270 LET R0=(-(H2/R2)*V(I)+M1*N(I))/((H2/R2)↑2-TAN(G(K))↑2)
275 LET Z(I)=EXP(-S(J)*(R4*COS(P(I))-SQR(R3↑2-U(I)))/COS(G(K)))
277 IF M2 < 1 THEN 280
278 LET Y(I)=-H1/SIN(G(K))-(R4*COS(P(I))-SQR(R3↑2-U(I)))/COS(G(K))
279 GO TO 290
280 LET Y(I)=SIN(ATN(H2/R2))*(SQR(R3↑2-U(I))+SQR(R0↑2-U(I)))
285 LET Y(I)=Y(I)/SIN(3.141592-G(K)-ATN(H2/R2))
290 LET M(I)=1-EXP(-B(J)*Y(I))
295 LET Q1=Q1+C(K)*W(I)*COS(P(I))*Z(I)*M(I)
300 LET Q2=Q2+C(K)*W(I)*COS(P(I))
305 LET D3=D3+Y(I)
310 NEXT I
315 NEXT K
320 LET A(J)=(E(J)/B(J)+E(J+1)/B(J+1))*(F(J+1)-F(J))/2
325 LET Q3=Q3+Q1*A(J)
330 NEXT J
335 IF M2 >0 THEN 370
340 LET Q9=Q3*2*(L2-L1)
345 LET D9=D3/16
347 LET Q7=Q2
350 LET L2=-ATN(H1/(R4+R2))
355 LET L1=-ATN(H1/(R4-R2))
360 LET M2=1
365 GO TO 180
370 LET Q6=Q3*2*(L2-L1)
375 LET D6=D3/16
376 LET Q8=Q9
378 LET D3=D9
380 LET Q=Q3+Q6
382 LET Q5=Q2
383 LET Q2=Q7
385 LET D=(D3+D6)/2
390 PRINT H1, Q3, Q6, Q
395 PRINT
400 PRINT "MEAN PATH LENGTH, INCHES"
405 PRINT "SIDE","BOTTOM","TOTAL"
410 PRINT D3, D6, D
415 PRINT
420 PRINT "PRE-MULTIPLIER","SIDE =", Q2,"BOTTOM =", Q5
425 LET C5=Q3/Q
430 LET C6=Q6/Q
435 PRINT "Q3/Q =", C5,"Q6/Q =", C6
440 GO TO 125
999 END
```

PROGRAM CYLOF

```
5 PRINT "HEAT FLUX TØ TARGET 3UTSIDE A CYLINDRICAL FLAME"
10 PRINT "C. A. BLØMQUIST, JULY 19,1972"
15 DIM F(90),B(90),E(90),S(90),A(90)
20 READ M,C1,C2,C3
25 FØR J=1 TØ M
30 READ F(J),B(J),E(J)
35 LET F(J)=F(J)*C1
40 LET B(J)=B(J)*C2
45 LET E(J)=E(J)*C3
50 NEXT J
55 FØR J=1 TØ M
60 READ S(J)
65 LET S(J)=S(J)*C2
70 NEXT J
75 LET H1=9.9375
80 LET R4=13
85 LET X(1)=.069432
90 LET X(2)=.330009
95 LET X(3)=.669991
100 LET X(4)=.930568
105 LET W(1)=.173927
110 LET W(2)=.326073
115 LET W(3)=.326073
120 LET W(4)=.173927
125 READ D2,H2
130 LET R2=D2/2
135 LET R=R2/R4
140 LET R5=1.5707288-.2121144*R+.074261*R↑2-.0137293*R↑3
145 LET R6=1.570796-R5*SØR(1-R)
150 PRINT
155 PRINT
160 PRINT "FLAME DIA",D2,"FLAME HEIGHT",H2
165 PRINT
170 PRINT "HEIGHT","          HEAT FLUX,BTU/HR-FT↑2"
175 PRINT "INCHES","SIDE","BØTTØM","TØP","TØTAL"
180 LET Q3=0
185 FØR J=1 TØ (M-1)
190 LET Q1=0
192 LET D3=0
193 LET Q2=0
195 FØR I=1 TØ 4
200 LET P(I)=R6*X(I)
205 LET Y(I)=SQR(R2↑2-R4↑2*SIN(P(I))↑2)
210 LET L(I)=-ATN(H1/(R4+R2))
215 LET U(I)=ATN((H2-H1)/(R4+R2))
216 IF U(I)<1.309 THEN 220
217 LET U(I)=1.309
220 LET C(I)=W(I)*COS(P(I))*(U(I)-L(I))
225 FØR K=1 TØ 4
230 LET G(K)=(U(I)-L(I))*X(K)+L(I)
235 LET Z(K)=EXP(-S(J)*(R4*COS(P(I))-Y(I))/COS(G(K)))
```

PROGRAM CYLOF (continued)

```
240 LET M(K)=1-EXP(-B(J)*2*Y(I)/C0S(G(K)))
242 LET 02=02+C(I)*W(K)*C0S(G(K))↑2
245 LET 01=01+C(I)*W(K)*C0S(G(K))↑2*Z(K)*M(K)
247 LET D3=D3+2*Y(I)/C0S(G(K))
250 NEXT K
255 NEXT I
260 LET A(J)=(E(J)/B(J)+E(J+1)/B(J+1))*(F(J+1)-F(J))/2
265 LET 03=03+01*A(J)
267 LET D3=D3/16
270 NEXT J
275 LET 03=03*2*R6
278 LET 02=02*R6
280 LET 06=0
285 FØR J=1 TØ (M-1)
287 LET D4=0
290 LET 04=0
293 LET 05=0
295 FØR I=1 TØ 4
300 LET Ø(I)=-ATN(H1/(R4-R2))
310 FØR K=1 TØ 4
315 LET T(K)=(L(I)-Ø(I))*X(K)+Ø(I)
316 LET R5=-H1/TAN(T(K))
317 LET R6=ATN(SQR((2*R4*R5/(R5↑2+R4↑2-R2↑2))↑2-1))
318 LET P(I)=R6*X(I)
319 LET C(I)=(L(I)-Ø(I))*W(I)*C0S(P(I))
320 LET Y(I)=SQR(R2↑2-R4↑2*SIN(P(I))↑2)
321 LET N(K)=EXP(-B(J)*(-H1/SIN(T(K))-(R4*C0S(P(I))-Y(I))/C0S(T(K))))
322 LET 05=05+C(I)*W(K)*C0S(T(K))↑2*R6
325 LET 04=04+C(I)*W(K)*C0S(T(K))↑2*Z(K)*(1-N(K))*R6
327 LET D4=D4-H1/SIN(T(K))-(R4*C0S(P(I))-Y(I))/C0S(T(K))
330 NEXT K
335 NEXT I
340 LET 06=06+04*A(J)
342 LET D4=D4/16
345 NEXT J
350 LET 06=06*2
355 LET 09=0
360 FØR J=1 TØ (M-1)
362 LET D5=0
363 LET 08=0
365 LET 07=0
370 FØR I=1 TØ 4
375 LET 9(I)=ATN((H2-H1)/(R4-R2))
380 IF U(I)<1.309 THEN 390
385 GØ TØ 435
390 IF 9(I)<1.309 THEN 400
395 LET Ø(I)=1.309
400 FØR K=1 TØ 4
410 LET V(K)=(9(I)-U(I))*X(K)+U(I)
411 LET R5=(H2-H1)/TAN(V(K))
412 LET R6=ATN(SQR((2*R4*R5/(R5↑2+R4↑2-R2↑2))↑2-1))
```

PROGRAM CYLOF (continued)

```
413 LET P(I)=R6*X(I)
414 LET C(I)=(U(I)-U(I))*W(I)*COS(P(I))
415 LET Y(I)=SQR(R2↑2-R4↑2*SIN(P(I))↑2)
416 LET N(K)=EXP(-B(J)*((H2-H1)/SIN(V(K))-(R4*COS(P(I))-Y(I))/COS(V(K))))
417 LET Q8=Q8+C(I)*W(K)*COS(V(K))↑2*R6
420 LET Q7=Q7+C(I)*W(K)*COS(V(K))↑2*Z(K)*(1-N(K))*R6
422 LET D5=D5+(H2-H1)/SIN(V(K))-(R4*COS(P(I))-Y(I))/COS(V(K))
425 NEXT K
430 NEXT I
435 LET Q9=Q9+Q7*A(J)
437 LET D5=D5/16
440 NEXT J
445 LET Q9=2*Q9
450 LET Q=Q3+Q6+Q9
455 LET D=(D4+D5+D6)/3
460 PRINT H1, Q3, Q6, Q9, Q
465 PRINT
470 PRINT "MEAN PATH LENGTH, INCHES"
475 PRINT "SIDE","BOTTOM","TOP","TOTAL"
480 PRINT D3, D4, D5, D
485 PRINT
490 PRINT "PRE-MULTIPLIER, SIDE, BOTTOM, TOP"
495 PRINT Q2, Q5, Q8
500 LET R5=Q3/Q
505 LET R6=Q6/Q
510 LET R7=Q9/Q
515 PRINT
520 PRINT "Q3/Q","Q6/Q","Q9/Q"
525 PRINT R5, R6, R7
530 GO TO 125
999 END
```

PROGRAM CONIF

```
5 PRINT "HEAT FLUX TO TARGET INSIDE A CONICAL FLAME"
6 PRINT "C. A. BLOMQUIST, JULY 16, 1972"
10 DIM F(90), B(90), E(90), A(90)
15 READ M, C1, C2, C3
20 FOR J=1 TO M
25 READ F(J), B(J), E(J)
30 LET F(J)=F(J)*C1
35 LET B(J)=B(J)*C2
40 LET E(J)=E(J)*C3
45 NEXT J
50 LET R1=.875
55 LET X(1)=.069432
60 LET X(2)=.330009
65 LET X(3)=.669991
70 LET X(4)=.930568
75 LET W(1)=.173927
80 LET W(2)=.326073
85 LET W(3)=.326073
90 LET W(4)=.173927
91 READ H3, H4, H5
92 READ D2, H2
93 LET R2=D2/2
94 PRINT
95 PRINT
96 PRINT "FLAME DIA", D2, "FLAME HEIGHT", H2
97 PRINT
98 PRINT "TARGET HEIGHT","      HEAT FLUX, BTU/HR-FT↑2"
99 PRINT "INCHES", "SIDE", "BOTTOM", "TOTAL"
100 LET V=ATN(H2/R2)
102 LET V1=3.141592-V
105 FOR H1=H3 TO H4 STEP H5
106 LET Q3=0
107 LET R3=R2*(1-H1/H2)
110 FOR J=1 TO (M-1)
112 LET Q1=0
113 LET Q2=0
115 FOR I=1 TO 4
120 LET P(I)=1.570796*X(I)
125 LET Y(I)=-R1*COS(P(I))+SQR(R3↑2-R1↑2*SIN(P(I))↑2)
130 LET L(I)=-ATN(H1/(R2-R1))
140 LET Z(I)=1.570796-L(I)
142 LET C(I)= W(I)*COS(P(I))
145 LET Q1=Q1+W(I)*(2*Z(I)-SIN(2*L(I)))*COS(P(I))
150 FOR K=1 TO 4
155 LET G(K)=Z(I)*X(K)+L(I)
157 LET N(K)=EXP(-B(J)*Y(I)*SIN(V)/SIN(V1-G(K)))
160 LET Q2=Q2+Z(I)*C(I)*W(K)*COS(G(K))↑2*N(K)
```

PROGRAM CONIF (continued)

```
165 NEXT K
170 NEXT I
177 LET A(J) = (E(J)/B(J)+E(J+1)/B(J+1))*(F(J+1)-F(J))/2
180 LET Q3=Q3+(Q1/4-Q2)*A(J)
185 NEXT J
190 LET Q3=-3.141592*Q3
205 LET Q6=0
207 FØR J=1 TØ (M-1)
208 LET Q4=0
209 LET Q5=0
210 FØR I=1 TØ 4
215 LET Q4=Q4+W(I)*CØS(P(I))*(2*L(I)+SIN(2*L(I))+3.141592)
220 FØR K=1 TØ 4
225 LET T(K)=(L(I)+1.570796)*X(K)-1.570796
230LETQ5=Q5+(1.570796+L(I))*C(I)*W(K)*CØS(T(K))↑2*EXP(B(J)*H1/SIN(T(K)))
235 NEXT K
240 NEXT I
250 LET Q6=Q6+(Q4/4-Q5)*A(J)
255NEXT J
260 LET Q6=-3.141592*Q6
265 LET Q=Q3+Q6
270 PRINT H1, Q3, Q6, Q
275 NEXT H1
280 GØ TØ 92
999 END
```

PROGRAM CYLIF

```
5 PRINT "HEAT FLUX TØ TARGET INSIDE A CYLINDRICAL FLAME"
6 PRINT "C. A. BLØMQUIST, JULY 11, 1972"
10 DIM F(90),B(90),E(90),A(90)
15 READ M,C1,C2,C3
20 FØR J=1 TØ M
25 READ F(J),B(J),E(J)
30 LET F(J)=F(J)*C1
35 LET B(J)=B(J)*C2
40 LET E(J)=E(J)*C3
45 NEXT J
50 LET R1=.875
55 LET X(1)=.069432
60 LET X(2)=.330009
65 LET X(3)=.669991
70 LET X(4)=.930568
75 LET W(1)=.173927
80 LET W(2)=.326073
85 LET W(3)=.326073
90 LET W(4)=.173927
91 READ H3,H4,H5
92 READ D2,H2
93 LET R2=D2/2
94 PRINT
95 PRINT
96 PRINT "FLAME DIA",D2,"FLAME HEIGHT",H2
97 PRINT
98 PRINT "TARGET HEIGHT","     HEAT FLUX, BTU/HR-FT↑2"
99 PRINT "INCHES", "SIDE", "BØTTØM", "TØP", "TØTAL"
100 FØR H1=H3 TØ H4 STEP H5
106 LET Q3=0
110 FØR J=1 TØ (M-1)
112 LET Q1=0
113 LET Q2=0
115 FØR I=1 TØ 4
120 LET P(I)=1.570796*X(I)
125 LET Y(I)=-R1*CØS(P(I))+SQR(R2↑2-R1↑2*SIN(P(I))↑2)
130 LET L(I)=-ATN(H1/(R2-R1))
135 LET U(I)=ATN((H2-H1)/(R2-R1))
140 LET Z(I)=U(I)-L(I)
142 LET C(I)= W(I)*CØS(P(I))
145 LET Q1=Q1+W(I)*(2*Z(I)+SIN(2*U(I))-SIN(2*L(I)))*CØS(P(I))
150 FØR K=1 TØ 4
155 LET G(K)=Z(I)*X(K)+L(I)
160 LET Q2=Q2+Z(I)*C(I)*W(K)*CØS(G(K))↑2*EXP(-B(J)*Y(I)/CØS(G(K)))
165 NEXT K
170 NEXT I
177 LET A(J) = (E(J)/B(J)+E(J+1)/B(J+1))*(F(J+1)-F(J))/2
180 LET Q3=Q3+(Q1/4-Q2)*A(J)
185 NEXT J
```

PROGRAM CYLIF (continued)

```
190 LET Q3=-3.141592*Q3
205 LET Q6=0
207 FOR J=1 TO (M-1)
208 LET Q4=0
209 LET Q5=0
210 FOR I=1 TO 4
215 LET Q4=Q4+W(I)*COS(P(I))*(2*L(I)+SIN(2*L(I))+3.141592)
220 FOR K=1 TO 4
225 LET T(K)=(L(I)+1.570796)*X(K)-1.570796
230LETQ5=Q5+(1.570796+L(I))*C(I)*W(K)*COS(T(K))↑2*EXP(B(J)*H1/SIN(T(K)))
235 NEXT K
240 NEXT I
250 LET Q6=Q6+(Q4/4-Q5)*A(J)
255NEXT J
260 LET Q6=-3.141592*Q6
275LET Q9=0
277 FOR J=1 TO (M-1)
278 LET Q8=0
279 LET Q7=0
280 FOR I=1 TO 4
285 LET Q7=Q7+C(I)*(3.141592-2*U(I)-SIN(2*U(I)))
290 FOR K=1 TO 4
295 LET V(K)=(1.570796-U(I))*X(K)+U(I)
297 LET N(I)=C(I)*(1.570796-U(I))
300 LET Q8=Q8+N(I)*W(K)*COS(V(K))↑2*EXP(-B(J)*(H2-H1)/SIN(V(K)))
305 NEXT K
310 NEXT I
320 LET Q9=Q9+(Q7/4-Q8)*A(J)
325 NEXT J
330 LET Q9=-3.141592*Q9
335 LET Q=Q3+Q6+Q9
345 PRINT H1, Q3, Q6, Q9, Q
350 NEXT H1
355 GO TO 92
999 END
```